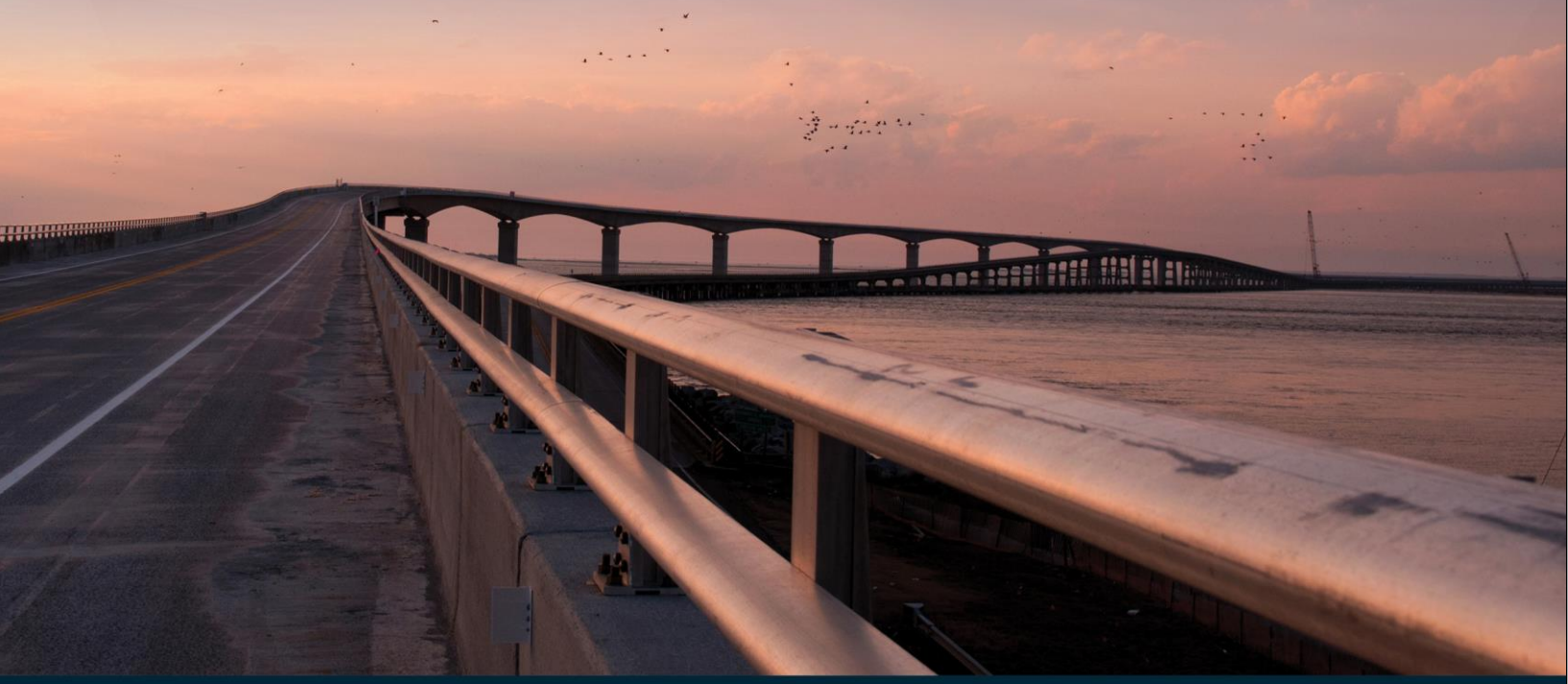
Evaluation of Four Bridge Rail Systems for Compliance with the 2016 Edition of Manual for Assessing Safety Hardware (MASH)



Vehicle trajectories of 2007 Chevy Silverado impacting the 2BMR.
(a) With expansion splice as reference; and
(b) with the post as reference



NCDOT Project 2019-23
FHWA/NC/2019-23
August 20, 2021

Howie Fang, Ph.D. et al.
Department of Mechanical Engineering & Engineering Science
University of North Carolina at Charlotte

RESEARCH & DEVELOPMENT

Technical Report Documentation Page

1. Report No. **FHWA/NC/2019-23**	2. Government Accession No.	3. Recipient's Catalog No.
4. Title and Subtitle ***Evaluation of Four Bridge Rail Systems for Compliance with the 2016 Edition of Manual for Assessing Safety Hardware (MASH)***		5. Report Date **March 09, 2022** 6. Performing Organization Code
7. Author(s) **Howie Fang, Zheng Li, Joshua Fatoki, Cody Stolle**		8. Performing Organization Report No.
9. Performing Organization Name and Address The University of North Carolina at Charlotte 9201 University City Boulevard Charlotte, NC 28223-0001		10. Work Unit No. (TRAIS) 11. Contract or Grant No.
12. Sponsoring Agency Name and Address North Carolina Department of Transportation Research and Analysis Group 1 South Wilmington Street Raleigh, North Carolina 27601		13. Type of Report and Period Covered **Final Report** **August 1, 2018 – July 31, 2021** 14. Sponsoring Agency Code **RP 2019-23**
Supplementary Notes:		

16. Abstract

In this project, the NC Two-bar Metal Rail (2BMR) was evaluated for compliance with the 2016 edition of Manual for Assessing Safety Hardware (MASH) under Test Level 3 (TL-3) conditions. Two full-scale crash tests, MASH Tests 3-10 and 3-11, were performed on a 90-ft section of the 2BMR and successfully passed all MASH evaluation criteria. A finite element (FE) model of the test section was created and used in simulations to determine the critical impact points and to predict the 2BMR performance under MASH TL-3 conditions. The simulation results were shown to agree well with test data and all the performance metrics met the MASH requirements. An application was submitted to FHWA to obtain a letter of eligibility for federal-aid reimbursement and the application was approved in August 2021.

In addition to the work on 2BMR, the FE models of three additional bridge rails were created: the Oregon Rail, the Three-bar Metal Rail, and the Classic Rail. Finite element simulations were performed to evaluate their performance under different MASH test conditions: the Oregon Rail under MASH TL-4 conditions, the Three-bar Metal Rail under MASH TL-2 and TL-3 conditions, and the Classic Rail under MASH TL-2 and TL-3 conditions. The simulation results demonstrated the performance trends of these three bridge rails as well as indicated some potential issues or safety concerns.

Finite element modeling and simulation were shown to be a powerful tool for assisting roadside safety research. The FE models of the vehicles and bridge rails from this project are readily available for use in other investigations.

17. Key Words	18. Distribution Statement		
19. Security Classify. (of this report) Unclassified	20. Security classify. (of this page) Unclassified	21. No. of Pages 311	22. Price

Form DOT F 1700.7 (8-72) **Reproduction of completed page authorized**

Disclaimer

The contents of this report reflect the views of the authors and not necessarily the views of the university. The authors are responsible for the facts and the accuracy of the data presented herein. The contents do not necessarily reflect the official views or policies of either the North Carolina Department of Transportation or the Federal Highway Administration. This report does not constitute a standard, specification, or regulation.

Acknowledgements

This study was supported by the North Carolina Department of Transportation (NCDOT) under Project No. 2019-23. The authors would like to thank NCDOT personnel from the *Structures Management Unit*, *Construction Unit*, *Manufactured Products*, *Materials & Tests Unit*, and the *Research and Development Unit* for their support and cooperation during the grant period.

Executive Summary

The main objective of this research was to evaluate the NC Two-bar Metal Rail (2BMR) for compliance with the 2016 edition of Manual for Assessing Safety Hardware (MASH) under Test Level 3 (TL-3) conditions. Two full-scale crash tests, MASH Tests 3-10 and 3-11, were performed at Midwest Roadside Safety Facility (MwRSF) on a 90-ft section of the 2BMR and successfully passed all MASH evaluation criteria. A finite element (FE) model of the test section was created and used in simulations to determine the critical impact points and to predict the 2BMR performance under MASH TL-3 conditions. The simulation results were shown to agree well with test data and all the performance metrics met the MASH requirements. An application was submitted to FHWA to obtain a letter of eligibility for federal-aid reimbursement and the application was approved in August 2021.

In addition to the work on 2BMR, the FE models of three additional bridge rails were created: the Oregon Rail, the Three-bar Metal Rail (3BMR), and the Classic Rail. Finite element simulations were performed to evaluate their performance under different MASH test conditions. The Oregon Rail was evaluated under MASH TL-4 conditions with two impact locations. The simulation results showed that it passed all MASH evaluation criteria under TL-4 conditions at both impact locations. The 3BMR was evaluated under MASH TL-2 and TL-3 conditions with two impact locations. Based on the simulation results, this bridge rail met all MASH TL-2 requirement, but it failed the exit box criterion under TL-3 conditions when impacted by a small passenger car. The Classic Rail was evaluated under MASH TL-2 and TL-3 conditions but could not pass the exit box criterion under impacts of the small passenger car. It should be noted that both the 3BMR and Classic Rail were evaluated on a flat terrain based on MASH test conditions. Under in-service conditions, both rails require a minimum of 5-ft wide sidewalk in front of them and their performance could be different from the simulation results of this project. Further simulations are suggested by NCDOT officials and will be conducted after including a 5-ft sidewalk in the FE models of the 3BMR and Classic Rail.

The full-scale crash tests were extremely useful in validating the vehicle models, particularly the FE models of the 2007 and 2014 Chevy Silverado models. By comparing to test data, the 2014 Silverado model was determined to have higher fidelity than the 2007 Silverado model. Overall, the simulation results demonstrated the performance trends of these four bridge rails and indicated some potential issues or safety concerns. Without denial of the extremely high value of physical testing, particularly full-scale crash tests, FE modeling and simulation were shown to be a powerful tool for assisting roadside safety research. The FE models of the vehicles and bridge rails from this project are readily available for use in other investigations.

Table of Contents

Disclaimer ii
Acknowledgements iii
Executive Summary iv
Table of Contents v
List of Figures vii
List of Tables x

1. Introduction 1
   1.1 Background 1
   1.2 Research Objectives and Tasks 2
2. Literature Review 5
   2.1 Performance Evaluation of Bridge Rails 5
   2.2 Finite Element Modeling and Simulations of Vehicular Crashes 12
3. Finite Element Modeling of Vehicles and Bridge Rails 18
   3.1 Finite Element Modeling of MASH-compliant Test Vehicles 18
   3.2 Finite Element Modeling of NC Two-bar Metal Rail 20
   3.3 Finite Element Modeling of Oregon Rail 22
   3.4 Finite Element Modeling of Three-bar Metal Rail 24
   3.5 Finite Element Modeling of Classic Rail 28
   3.6 Simulation Setup 30
      3.6.1 2BMR under MASH TL-3 conditions 30
      3.6.2 The Oregon Rail under MASH TL-4 conditions 32
      3.6.3 3BMR under MASH TL-2 and TL-3 conditions 33
      3.6.4 Classic Rail under MASH TL-2 and TL-3 conditions 34
4. Simulation Results and Analysis 36
   4.1 Evaluation of NC Two-bar Metal Rail under MASH TL-3 Conditions 37
      4.1.1 The 2BMR Impacted by 2010 Toyota Yaris 37
      4.1.2 The 2BMR Impacted by 2007 Chevy Silverado 42
      4.1.3 The 2BMR Impacted by 2014 Chevy Silverado 46
   4.2 Evaluation of the Oregon Rail under MASH TL-4 Conditions 50
      4.2.1 The Oregon Rail Impacted by 2010 Toyota Yaris 51
      4.2.2 The Oregon Rail Impacted by 2007 Chevy Silverado 53
      4.2.3 The Oregon Rail Impacted by 2014 Chevy Silverado 55
      4.2.4 The Oregon Rail Impacted by 1996 Ford F800 57
   4.3 Evaluation of the Three-Bar Metal Rail under MASH TL-2 and TL-3 Conditions 59
      4.3.1 Evaluation of 3BMR-1 under TL-2 conditions 59
      4.3.2 Evaluation of 3BMR-1 under TL-3 conditions 65
      4.3.3 Evaluation of 3BMR-2 under TL-3 conditions 72
   4.4 Evaluation of Classic Rail under MASH TL-2 and TL-3 Conditions 78

4.4.1 Evaluation of Classic Rail under TL-2 conditions 78
4.4.2 Evaluation of Classic Rail under TL-3 conditions 84
5. Research Findings and Conclusions 91
5.1 Performance of Bridge Rails 91
5.2 Effect of Concrete Reinforcement on Occupant Safety Factors 92
5.3 Structural Differences Between Two Silverado Models 94
5.4 Concluding Remarks 95
References 96
Appendix. Full-Scale Crash Test of a Two-Bar Metal Rail 100

List of Figures

Figure 1.1: An NC two-bar metal rail. 1
Figure 1.2: Finite element models of two MASH-compliant test vehicles. 3
Figure 1.3: MASH-compliant test vehicles for this project. 4
Figure 3.1: FE models of four test vehicles. 18
Figure 3.2: Finite element model of the 2BMR. 20
Figure 3.3: The FE model of a post assembly of the 2BMR. 21
Figure 3.4: Steel reinforcement bars in the concrete parapet of 2BMR. 22
Figure 3.5: Cross-sectional view of the concrete parapet with horizontal and vertical steel reinforcement. 22
Figure 3.6: Finite element model of the Oregon Rail. 23
Figure 3.7: Close-up view of a post assembly and cross-section profiles of the rails in the Oregon Rail. 23
Figure 3.8: Steel reinforcement bars in the concrete foundation and end parapets of the Oregon Rail. 24
Figure 3.9: Finite element model of the Three-bar Metal Rail. 25
Figure 3.10: Post assembly of the 3BMR. 25
Figure 3.11: Cross-sectional profiles of aluminum rails of the 3BMR. 26
Figure 3.12: Close-up view of expansion bars at the expansion joint of the 3BMR. 26
Figure 3.13: Close-up view of rail connections at the terminal of the 3BMR. 27
Figure 3.14: Steel reinforcement bars in the end parapet of the 3BMR. 27
Figure 3.15: Steel reinforcement bars inside the concrete foundation of the 3BMR. 28
Figure 3.16: Finite element model of a 90-ft Classic Rail. 29
Figure 3.17: Close-up view of a subsection of the Classic Rail. 29
Figure 3.18: Steel reinforcement bars inside the Classic Rail. 30
Figure 3.19: Reference posts and expansion splices for impact locations on the 2BMR. 30
Figure 3.20: Full simulation models for the three impact cases with posts as the reference points. 31
Figure 3.21: Reference points for the CIPs on the Oregon Rail. 32
Figure 3.22: Full simulation models for the Oregon Rail using expansion joints as the reference points. 32
Figure 3.23: Reference points for the CIPs on the 3BMR. 33
Figure 3.24: Full simulation models for Group 1 simulations using expansion joint as reference point. 34
Figure 3.25: Full simulation models for simulations of Classic Rail under MASH TL-2 conditions. 35
Figure 4.1: Illustration of the MASH exit box criterion. 36
Figure 4.2: Vehicle trajectories of 2010 Toyota Yaris impacting the 2BMR. 37
Figure 4.3: Time histories of accelerations of 2010 Toyota Yaris impacting the 2BMR. 38
Figure 4.4: Time histories of angular motions of 2010 Toyota Yaris impacting the 2BMR. 38
Figure 4.5: Comparison of responses of the 1100C test vehicles impacting the 2BMR (Left: a 2010 Hyundai Assent used in field test. Right: a 2010 Toyota Yaris used in simulation). 40
Figure 4.6: Comparison of accelerations of 2010 Hyundai Assent (test) and 2010 Toyota Yaris (model). 41
Figure 4.7: Comparison of angular motions of the 2010 Hyundai Assent (test) and 2010 Toyota Yaris (model). 41
Figure 4.8: Vehicle trajectories of 2007 Chevy Silverado impacting the 2BMR. 42
Figure 4.9: Time histories of accelerations of 2007 Chevy Silverado impacting the 2BMR. 42
Figure 4.10: Time histories of angular motions of 2007 Chevy Silverado impacting the 2BMR. 43
Figure 4.11: Comparison of responses of the 2270P test vehicles impacting the 2BMR (Left: a 2015 Chevy Silverado used in field test. Right: a 2007 Chevy Silverado used in simulation). 44
Figure 4.12: Comparison of angular motions of 2015 Chevy Silverado (test) and 2007 Chevy Silverado (model). 45
Figure 4.13: Comparison of accelerations of 2015 Chevy Silverado (test) and 2007 Chevy Silverado (model). 45
Figure 4.14: Vehicle trajectories of 2014 Chevy Silverado impacting the 2BMR. 46
Figure 4.15: Time histories of accelerations of the 2014 Chevy Silverado impacting the 2BMR. 47
Figure 4.16: Time histories of angular motions of 2014 Chevy Silverado impacting the 2BMR. 47
Figure 4.17: Comparison of angular motions of the 2015 Chevy Silverado (test) and 2014 Chevy Silverado (model). 48
Figure 4.18: Comparison of responses of the 2270P test vehicles impacting the 2BMR (Left: a 2015 Chevy Silverado used in field test. Right: a 2014 Chevy Silverado used in simulation). 49
Figure 4.19: Comparison of longitudinal and lateral accelerations of 2015 Chevy Silverado (test) and 2014 Chevy Silverado (model) impacting the 2BMR. 50
Figure 4.20: Vehicle trajectories of 2010 Toyota Yaris impacting the Oregon Rail. 51

Figure 4.21: Time histories of accelerations of 2010 Toyota Yaris impacting the Oregon Rail. 51
Figure 4.22: Time histories of angular motions of 2010 Toyota Yaris impacting the Oregon Rail. 52
Figure 4.23: Vehicle trajectories of 2007 Chevy Silverado impacting the Oregon Rail. 53
Figure 4.24: Time histories of accelerations of 2007 Chevy Silverado impacting the Oregon Rail. 53
Figure 4.25: Time histories of angular motions of 2007 Chevy Silverado impacting the Oregon Rail. 54
Figure 4.26: Vehicle trajectories of 2014 Chevy Silverado impacting the Oregon Rail. 55
Figure 4.27: Time histories of accelerations of 2014 Chevy Silverado impacting the Oregon Rail. 55
Figure 4.28: Time histories of angular motions of 2014 Chevy Silverado impacting the Oregon Rail. 56
Figure 4.29: Vehicle trajectories of 1996 Ford F800 impacting the Oregon Rail. 57
Figure 4.30: Time histories of accelerations of 1996 Ford F800 impacting the Oregon Rail. 57
Figure 4.31: Time histories of angular motions of 1996 Ford F800 impacting the Oregon Rail. 58
Figure 4.32: Top view of the Oregon Rail with permanent deformation impacted by 1996 Ford F800. 59
Figure 4.33: Vehicle trajectories of 2010 Toyota Yaris impacting 3BMR-1 under TL-2 conditions. 60
Figure 4.34: Time histories of accelerations of 2010 Toyota Yaris impacting 3BMR-1 under TL-2 conditions. 60
Figure 4.35: Time histories of angular motions of 2010 Toyota Yaris impacting 3BMR-1 under TL-2 conditions. 61
Figure 4.36: Vehicle trajectories of 2007 Chevy Silverado impacting 3BMR-1 under TL-2 conditions. 62
Figure 4.37: Time histories of accelerations of 2007 Chevy Silverado impacting 3BMR-1 under TL-2 conditions. 62
Figure 4.38: Time histories of angular motions of 2007 Chevy Silverado impacting 3BMR-1 under TL-2 conditions. 63
Figure 4.39: Vehicle trajectories of 2014 Chevy Silverado impacting 3BMR-1 under TL-2 conditions. 64
Figure 4.40: Time histories of accelerations of 2014 Chevy Silverado impacting 3BMR-1 under TL-2 conditions. 64
Figure 4.41: Time histories of angular motions of 2014 Chevy Silverado impacting 3BMR-1 under TL-2 conditions. 65
Figure 4.42: Vehicle trajectories of 2010 Toyota Yaris impacting 3BMR-1 under TL-3 conditions. 66
Figure 4.43: Time histories of accelerations of 2010 Toyota Yaris impacting 3BMR-1 under TL-3 conditions. 66
Figure 4.44: Time histories of angular motions of the 2010 Toyota Yaris impacting 3BMR-1 under TL-3 conditions. 67
Figure 4.45: Vehicle trajectories of 2007 Chevy Silverado impacting 3BMR-1 under TL-3 conditions. 68
Figure 4.46: Time histories of accelerations of 2007 Chevy Silverado impacting 3BMR-1 under TL-3 conditions. 68
Figure 4.47: Time histories of angular motions of 2007 Chevy Silverado impacting 3BMR-1 under TL-3 conditions. 69
Figure 4.48: Vehicle trajectories of 2014 Chevy Silverado impacting 3BMR-1 under TL-3 conditions. 70
Figure 4.49: Time histories of accelerations of 2014 Chevy Silverado impacting 3BMR-1 under TL-3 conditions. 71
Figure 4.50: Time histories of angular motions of 2014 Chevy Silverado impacting 3BMR-1 under TL-3 conditions. 71
Figure 4.51: Vehicle trajectories of 2010 Toyota Yaris impacting 3BMR-2 under TL-3 conditions. 72
Figure 4.52: Time histories of accelerations of 2010 Toyota Yaris impacting 3BMR-2 under TL-3 conditions. 73
Figure 4.53: Time histories of angular motions of 2010 Toyota Yaris impacting 3BMR-2 under TL-3 conditions. 73
Figure 4.54: Vehicle trajectories of the 2007 Chevy Silverado impacting 3BMR-2 under TL-3 conditions. 74
Figure 4.55: Time histories of accelerations of 2007 Chevy Silverado impacting 3BMR-2 under TL-3 conditions. 75
Figure 4.56: Time histories of angular motions of 2007 Chevy Silverado impacting 3BMR-2 under TL-3 conditions. 75
Figure 4.57: Vehicle trajectories of 2014 Chevy Silverado impacting 3BMR-2 under TL-3 conditions. 76
Figure 4.58: Time histories of accelerations of 2014 Chevy Silverado impacting 3BMR-2 under TL-3 conditions. 77
Figure 4.59: Time histories of angular motions of 2014 Chevy Silverado impacting 3BMR-2 under TL-3 conditions. 77
Figure 4.60: Vehicle trajectories of 2010 Toyota Yaris impacting Classic Rail under TL-2 conditions. 79
Figure 4.61: Damage on the Classic Rail under impact by 2010 Toyota Yaris under TL-2 conditions. 79
Figure 4.62: Time histories of angular motions of 2010 Toyota Yaris impacting Classic Rail under TL-2 conditions. 79
Figure 4.63: Time histories of accelerations of 2010 Toyota Yaris impacting Classic Rail under TL-2 conditions. 80
Figure 4.64: Vehicle trajectories of 2007 Chevy Silverado impacting Classic Rail under TL-2 conditions. 81
Figure 4.65: Damage on the Classic Rail under impact by 2007 Chevy Silverado under TL-2 conditions. 81
Figure 4.66: Time histories of angular motions of 2007 Chevy Silverado impacting Classic Rail under TL-2 conditions. 81

Figure 4.67: Time histories of accelerations of 2007 Chevy Silverado impacting Classic Rail under TL-2 conditions. 82
Figure 4.68: Vehicle trajectories of 2014 Chevy Silverado impacting Classic Rail under TL-2 conditions. 83
Figure 4.69: Damage on the Classic Rail under impact by 2014 Chevy Silverado under TL-2 conditions.....83
Figure 4.70: Time histories of angular motions of 2014 Chevy Silverado impacting Classic Rail under TL-2 conditions. 83
Figure 4.71: Time histories of accelerations of 2014 Chevy Silverado impacting Classic Rail under TL-2 conditions. 84
Figure 4.72: Vehicle trajectories of 2010 Toyota Yaris impacting Classic Rail under TL-3 conditions. 85
Figure 4.73: Damage on the Classic Rail under impact by 2010 Toyota Yaris under TL-3 conditions. 85
Figure 4.74: Time histories of angular motions of 2010 Toyota Yaris impacting Classic Rail under TL-3 conditions. 85
Figure 4.75: Time histories of accelerations of 2010 Toyota Yaris impacting Classic Rail under TL-3 conditions. ..86
Figure 4.76: Vehicle trajectories of 2007 Chevy Silverado impacting Classic Rail under TL-3 conditions. 87
Figure 4.77: Damage on the Classic Rail under impact by 2007 Chevy Silverado under TL-3 conditions.....87
Figure 4.78: Time histories of angular motions of 2007 Chevy Silverado impacting Classic Rail under TL-3 conditions. 87
Figure 4.79: Time histories of accelerations of 2007 Chevy Silverado impacting Classic Rail under TL-3 conditions. 88
Figure 4.80: Vehicle trajectories of 2014 Chevy Silverado impacting Classic Rail under TL-3 conditions. 89
Figure 4.81: Damage on the Classic Rail under impact by 2014 Chevy Silverado under TL-3 conditions.....89
Figure 4.82: Time histories of angular motions of 2014 Chevy Silverado impacting Classic Rail under TL-3 conditions. 89
Figure 4.83: Time histories of accelerations of 2014 Chevy Silverado impacting Classic Rail under TL-3 conditions. 90
Figure 5.1: Time histories of relative velocities of the 2010 Toyota Yaris impacting the 3BMR-1 (no rebar) and 3BMR-2 (with Φ-16mm rebars) under TL-3 conditions. 93
Figure 5.2: Time histories of accelerations of the 2010 Toyota Yaris impacting the 3BMR-1 (no rebar) and 3BMR-2 (with Φ-16mm rebars) under TL-3 conditions. 94
Figure 5.3: FE models of the front wheels on the 2007 and 2014 Chevy Silverado. 94

List of Tables

Table 1.1: Major changes of TL-3 conditions from NCHRP Report 350 to MASH 2016. 2
Table 2.1: Bridge rail test level equivalencies. 7
Table 2.2: Impact conditions for Test Levels 1, 2, 3 and 4 of NCHRP Report 350. 7
Table 3.1: Finite element model information of the test vehicles used in crash simulations. 19
Table 3.2: Simulation matrix for Two-bar Metal Rail under MASH TL-3 conditions. 31
Table 3.3: Simulation matrix for the Oregon Rail under MASH TL-4 conditions. 32
Table 3.4: Group 1 cases: TL-2 conditions with reinforcement bars only in end parapets. 33
Table 3.5: Group 2 cases: TL-3 conditions with reinforcement bars only in end parapets. 34
Table 3.6: Group 3 cases: TL-3 conditions with reinforcement bars in end parapets and foundation. 34
Table 3.7: Simulation cases for Classic Rail under TL-2 conditions. 35
Table 3.8: Simulation cases for Classic Rail under TL-3 conditions. 35
Table 4.1: Dimensions of exit boxes for test vehicles based on MASH specifications. 37
Table 4.2: Evaluation factors of 2BMR impacted by 2010 Toyota Yaris with expansion splice as reference. 39
Table 4.3: Evaluation factors of 2BMR impacted by 2010 Toyota Yaris with post as reference. 39
Table 4.4: Comparison of occupant safety factors from simulation and test for impacts by the 1100C vehicles. 41
Table 4.5: Evaluation factors of 2BMR impacted by 2007 Chevy Silverado with expansion splice as reference. 43
Table 4.6: Evaluation factors of 2BMR impacted by 2007 Chevy Silverado with post as reference. 43
Table 4.7: Comparison of occupant safety factors from simulation and test for impacts by the 2270P vehicles. 46
Table 4.8: Evaluation factors of 2BMR impacted by 2014 Chevy Silverado with expansion splice as reference. 48
Table 4.9: Evaluation factors of 2BMR impacted by 2014 Chevy Silverado with post as reference. 48
Table 4.10: Comparison of occupant safety factors from simulation and test for impacts by the 2270P vehicles. 50
Table 4.11: Evaluation factors of Oregon Rail impacted by 2010 Toyota Yaris with expansion joint as reference. ..52
Table 4.12: Evaluation factors of Oregon Rail impacted by 2010 Toyota Yaris with post as reference. 52
Table 4.13: Evaluation factors of Oregon Rail impacted by 2007 Chevy Silverado with expansion joint as reference. 54
Table 4.14: Evaluation factors of Oregon Rail impacted by 2007 Chevy Silverado with post as reference. 54
Table 4.15: Evaluation factors of Oregon Rail impacted by 2014 Chevy Silverado with expansion joint as reference. 56
Table 4.16: Evaluation factors of Oregon Rail impacted by 2014 Chevy Silverado with post as reference. 56
Table 4.17: Evaluation factors of Oregon Rail impacted by 1996 Ford F800 with expansion joint as reference. 58
Table 4.18: Evaluation factors of Oregon Rail impacted by 1996 Ford F800 with post as reference. 58
Table 4.19: Evaluation factors of 3BMR-1 impacted by 2010 Toyota Yaris (TL-2) with expansion joint as reference. 61
Table 4.20: Evaluation factors of 3BMR-1 impacted by 2010 Toyota Yaris (TL-2) with post as reference. 61
Table 4.21: Evaluation factors of 3BMR-1 impacted by 2007 Chevy Silverado (TL-2) with expansion joint as reference. 63
Table 4.22: Evaluation factors of 3BMR-1 impacted by 2007 Chevy Silverado (TL-2) with post as reference. 63
Table 4.23: Evaluation factors of 3BMR-1 impacted by 2014 Chevy Silverado (TL-2) with expansion joint as reference. 65
Table 4.24: Evaluation factors of 3BMR-1 impacted by 2014 Chevy Silverado (TL-2) with post as reference. 65
Table 4.25: Evaluation factors of 3BMR-1 impacted by 2010 Toyota Yaris (TL-3) with expansion joint as reference. 67
Table 4.26: Evaluation factors of 3BMR-1 impacted by 2010 Toyota Yaris (TL-3) with post as reference. 67
Table 4.27: Evaluation factors of 3BMR-1 impacted by 2007 Chevy Silverado (TL-3) with expansion joint as reference. 69
Table 4.28: Evaluation factors of 3BMR-1 impacted by 2007 Chevy Silverado (TL-3) with post as reference. 70
Table 4.29: Evaluation factors of 3BMR-1 impacted by 2014 Chevy Silverado (TL-3) with expansion joint as reference. 72
Table 4.30: Evaluation factors of 3BMR-1 impacted by 2014 Chevy Silverado (TL-3) with post as reference. 72
Table 4.31: Evaluation factors of 3BMR-2 impacted by 2010 Toyota Yaris (TL-3) with expansion joint as reference. 74
Table 4.32: Evaluation factors of 3BMR-2 impacted by 2010 Toyota Yaris (TL-3) with post as reference. 74

Table 4.33: Evaluation factors of 3BMR-2 impacted by 2007 Chevy Silverado (TL-3) with expansion joint as reference. 76
Table 4.34: Evaluation factors of 3BMR-2 impacted by 2007 Chevy Silverado (TL-3) with post as reference. 76
Table 4.35: Evaluation factors of 3BMR-2 impacted by 2014 Chevy Silverado (TL-3) with expansion joint as reference. 78
Table 4.36: Evaluation factors of 3BMR-2 impacted by 2014 Chevy Silverado (TL-3) with post as reference. 78
Table 4.37: Evaluation factors of Classic Rail impacted by 2010 Toyota Yaris under TL-2 conditions.....80
Table 4.38: Evaluation factors of Classic Rail impacted by 2007 Chevy Silverado under TL-2 conditions. 82
Table 4.39: Evaluation factors of Classic Rail impacted by 2014 Chevy Silverado under TL-2 conditions. 84
Table 4.40: Evaluation factors of Classic Rail impacted by 2010 Toyota Yaris under TL-3 conditions.....86
Table 4.41: Evaluation factors of Classic Rail impacted by 2007 Chevy Silverado under TL-3 conditions. 88
Table 4.42: Evaluation factors of Classic Rail impacted by 2014 Chevy Silverado under TL-3 conditions. 90
Table 5.1: Summary of performance of the four bridge rails at different MASH test levels. 91

1. Introduction

Roadside safety systems are important devices to ensure transportation safety. Different types of roadside safety devices such as longitudinal barriers, terminals, and crash cushions have been developed over the years to improve transportation safety. Currently, all safety devices used on U.S. highways must be tested to meet the safety criteria specified by the Manual for Assessing Safety Hardware (MASH) issued by the American Association of State Highway and Transportation Officials (AASHTO).

1.1 Background

Longitudinal barriers are generally categorized into flexible, semi-rigid and rigid barriers. Semi-rigid barriers such as the two-bar metal rail are more forgiving in severe crashes than rigid barriers and are relatively easy to maintain. Figure 1.1 shows the two-bar metal rail (2BMR) developed by the North Carolina Department of Transportation (NCDOT). It is a commonly used bridge rail in North Carolina and is recognized for its performance and aesthetics. This bridge rail consists of aluminum or steel posts, elliptical rails, and base plates mounted on a concrete parapet.



Figure 1.1: An NC two-bar metal rail.

NCDOT has had a long-term success with the two-bar metal rail including its use in scenic and historic areas and intends to continue its use in the future. In January 2016, AASHTO and Federal Highway Administration (FHWA) issued a Joint Implementation Agreement that required all new installations of safety hardware on the national highway system be evaluated using the 2016 edition of MASH (MASH 2016). The requirement applies to bridge railings with contract letting dates after December 31, 2019. MASH 2016 supersedes the old standard, NCHRP Report 350, and requires bridge rails to be tested to ensure safety performance. Table 1.1 shows the major changes on crash test conditions of Test Level 3 (TL-3) from NCHRP Report 350 to MASH 2016.

Table 1.1: Major changes of TL-3 conditions from NCHRP Report 350 to MASH 2016.

Safety Standard	Mass of Small Sedan	Mass of Pickup Truck	Impact Angle	Limits of Roll and Pitch Angles
NCHRP Report 350	1,800 lb (820 kg)	4,400 lb (2,000 kg)	20º *	No requirement
2016 ed. of MASH	2,420 lb (1,100 kg)	5,000 lb (2,270 kg)	25º	75º

* This change only applies to the small sedan. The impact angle for pickup truck was also 25° in NCHRP Report 350.

The current NC 2BMR was recognized as meeting the TL-3 requirements of NCHRP Report 350, but no crash tests for MASH compliance had been performed on this specific rail type as of December 2018. Research was needed to evaluate the performance of the 2BMR, determine its compliance with MASH 2016, and obtain approval for the FHWA Eligibility Letter.

1.2 Research Objectives and Tasks

The main objective of this research was to conduct full-scale crash tests and perform finite element (FE) analysis to evaluate the performance of the 2BMR under TL-3 conditions specified by MASH 2016. The test data and FE simulation results were synthesized and submitted to FHWA for approval of using 2BMR on the national highway system. Additionally, FE models of three other bridge rails were created and simulations were performed to evaluate their performance under MASH test conditions. The major tasks of this research project are as follows.

Task 1: Literature Review and Data Collection

In this task, literature on crash testing and modeling of bridge rails, particularly those based on MASH 2016 and with FHWA approvals, was collected and reviewed to assist with the testing and modeling work of this project.

Task 2: Crash Test Preparation and Finite Element Model Development

In this task, a detailed plan to conduct the full-scale crash tests of the 2BMR was developed, including designing and building the test section, purchasing MASH-compliant test vehicles, developing the FE model of the 2BMR test section, and integrating the FE models of the 2BMR and vehicles based on MASH TL-3 conditions. The test section and test vehicles for the crash tests were prepared by researchers at the Midwest Roadside Safety Facility (MwRSF), The University of Nebraska, Lincoln, and the FE model development was conducted at The University of North Carolina at Charlotte.

The test vehicles required for MASH TL-3 are a small passenger car (1100C) and a pickup truck (2270P) with masses of 2,420 lb (1,100 kg) and 5,000 lb (2,270 kg), respectively. Figure 1.2 shows the FE models of two MASH-compliant vehicles, a 2010 Toyota Yaris and a 2007 Chevy Silverado pickup truck, that were available for this project. Although it would be ideal to use the exact same vehicles (years and makes) in the crash tests as the FE vehicle models, the research team could not obtain the same vehicles for crash tests. The two vehicles for the crash tests in this project were a 2010 Hyundai Accent passenger car (1100C) and a 2015 Chevy Silverado quad cab pickup truck (2270P), both were MASH-compliant and similar/comparable in sizes and shapes to the respective FE vehicle models. During the project, the research team obtained the FE model of a 2014 Chevy Silverado quad cap that was also used in the simulations and compared to the 2007 Chevy

Silverado model. These vehicle models were combined with the FE model of the 2BMR test section to simulate the two full-scale crash tests under MASH TL-3 conditions. More details of the FE models of the three vehicles and the 2BMR are presented in Chapter 3. Details about the two test vehicles and full-scale crash tests are given in the Appendix of this report.



(a) (b)

Figure 1.2: Finite element models of two MASH-compliant test vehicles.
(a) 2010 Toyota Yaris; and (b) 2007 Chevy Silverado quad cab.

In addition to the work on 2BMR, the research team also developed the FE models of three other bridge rails and conducted simulations to evaluate their performance under different MASH test conditions.

1. Oregon Rail under MASH TL-4 conditions.
2. Three-bar Metal Rail (3BMR) under MASH TL-2 and TL-3 conditions.
3. Classic Rail under MASH TL-2 and TL-3 conditions.

Task 3: Finite Element Analysis of Bridge Rails under MASH Test Conditions

In this task, the 2BMR was first evaluated using FE simulations under MASH TL-3 conditions. Before the full-scale crash tests were conducted, FE simulations were conducted for 2BMR to determine the critical impact points (CIPs) that would be used in the crash tests. Two reference points for determining the CIPs were selected, one being the expansion splice and the other being the post closest to the expansion splice. For the 1100C test vehicle, the CIP was determined to be 3.6 ft (1.1 m ± 0.3 m) from a post closest to an expansion splice between two consecutive longitudinal rail elements. For impact by the 2270P test vehicle, the CIP was determined to be 4.3 ft (1.3 m ± 0.3 m) from a post closest to an expansion splice between two consecutive longitudinal rail elements. These CIPs were used in the full-scale crash tests conducted by MwRSF researchers.

After the full-scale crash tests were carried out, FE simulations were conducted using the exact impact conditions (i.e., impact velocities, angles, and locations) as those from the two crash tests of this study. The simulation results were compared with test data to further validate the FE models, particularly the vehicle models. The simulation results were also used to assess occupant risk based on MASH criteria.

Finally, the validated vehicle models of the 2010 Toyota Yaris, 2007 Chevy Silverado, and 2014 Chevy Silverado were used in the FE simulations of the three additional bridge rails to evaluate their performance under different MASH test conditions, as defined in Task 2.

Task 4: Full-scale Crash Testing of NC Two-bar Metal Rail

In this task, a 90-ft test section of the 2BMR was constructed at MwRSF and tested under MASH TL-3 conditions. Figure 1.3 shows the stock pictures of two MASH-compliant test vehicles obtained for this project, a 2010 Hyundai Accent (1100C) and a 2015 Chevy Silverado quad cab (2270P). Detailed information about the 2BMR test section and test vehicles are included in the Appendix of this report.



(a) (b)

Figure 1.3: MASH-compliant test vehicles for this project.
(a) 2010 Hyundai Accent; and (b) 2015 Chevy Silverado quad cab.

Two MASH TL-3 crash tests, Tests 3-10 and 3-11, were successfully conducted at MwRSF, and a detailed test report was prepared by MwRSF researchers as attached in the Appendix. Since both test vehicles were similar/comparable in sizes and shapes to the respective FE vehicle models, the crash test data were used to further validate the FE vehicle models in terms of vehicular responses and occupant safety parameters.

Task 5: Synthesis of Test Data and Simulation Results

In this task, the full-scale crash test data and FE simulation results for the 2BMR under MASH TL-3 conditions were synthesized and summarized. An application document was prepared and submitted for approval of the FHWA eligibility letter, and the application was approved by FHWA in August 2021. The simulation results for the three bridge rails were also analyzed and summarized.

Task 6: Final Report

This final report provides a comprehensive summary of research activities, findings, and outcomes for this project. It synthesizes literature review, full-scale crash testing, FE modeling, simulation results, and research findings on the performance of the 2BMR under MASH TL-3 conditions. This report also includes FE analysis of the performance of three additional bridge rails under different MASH test conditions.

2. Literature Review

Roadside safety systems are important devices to ensure transportation safety. Different types of roadside safety devices such as longitudinal barriers, terminals, and crash cushions have been developed over the years to improve transportation safety. Longitudinal barriers are generally categorized into flexible, semi-rigid and rigid barriers. Semi-rigid barriers such as W-beam guardrails and metal rails are more forgiving in severe crashes than rigid barriers. The two-bar metal rail is a commonly used semi-rigid barrier in North Carolina. In this section, a comprehensive summary is provided on studies related to bridge rails and other barrier systems. The topics cover performance evaluation of bridge rails and barriers, crash testing and the application of FE modeling and simulations in highway safety research.

2.1 Performance Evaluation of Bridge Rails

Since the creation of Standard Specifications for Highway Bridges and Incidental Structures by AASHTO in 1931, bridge rails have been required to follow design specifications. Prior to 1953, performance evaluation of bridge rails was primarily conducted onsite after a vehicle collision occurred. In 1955, the state of California pioneered several full-scale dynamic impact tests of bridge rail systems as an alternative means of onsite performance evaluation on bridge rails from vehicular crashes. During these tests, it was observed that there was an extremely high probability of vehicle snagging in the existing baluster-type rail designs. Consequently, the baluster-type rail designs were replaced by the solid, non-yielding smooth-wall barriers that were deemed more effective. Additionally, the Type 1 bridge rail design, which utilized extruded metal rails and posts mounted on a reinforced concrete parapet, was adopted by the California Division of Highways as a result of these impact tests.

In the early 1960s, Nordlin et al. (1965) evaluated the impact performance of three different bridge rail designs, the standard California Type 1, standard California Type 2, and experimentally modified Type 1 bridge rails. Five full-scale crash tests were conducted to evaluate the overall effectiveness and structural adequacy of the three bridge rail designs based on four criteria: the ability to retain the striking vehicle, structural integrity of the bridge rail after an impact, potential of vehicle snagging, and ease of repair. The results of these full-scale crash tests led to several significant conclusions on the performance of bridge rail systems. Although all four evaluation criteria were met, it was observed that the test vehicles exhibited various post-impact behaviors for different barrier heights. For instance, there was no tendency for the test vehicle to climb up the barrier when the parapet was sufficiently high to absorb a significant portion of the impact energy. However, at these elevated barrier heights, severe deformations were observed on the body and frame of the test vehicles. In addition, the test results indicated that when a significant portion of the impact load was taken by the metal rail, the rail had excessive deflections and the vehicle nearly vaulted over the rail. It was concluded that the modified Type 1 bridge rail with a 28-inch high parapet (36-inch overall barrier height) was the most effective design among the three tested bridge rails.

An analysis performed in the late 1960s indicated that the New Jersey concrete barrier could mitigate the severity of deformations sustained by an errant vehicle due to the barrier's lower slope. Consequently, the Bridge Department of the California Division of Highways designed a bridge rail that incorporated the New Jersey type of concrete parapet and the tubular steel rails used in

the California Type 1 bridge rail design (Nordlin et al., 1970). This new design was named the California Type 20 bridge rail and was evaluated using full-scale crash tests to determine its ability to safely redirect a vehicle and minimize deformations sustained by an impacting vehicle during the collision. Analysis of the test results indicated that the sloped lower face of the parapet minimized the collision severity. However, the Type 20 bridge rail had limited see-through properties when compared to older designs.

Michie et al. (1981) conducted research funded by the National Cooperative Highway Research Program (NCHRP) and provided guidelines for the safety evaluation of highway appurtenances in NCHRP Report 230. In 1986, FHWA issued a policy memorandum requiring bridge railings installed on federal interstates and state highways to meet or exceed the full-scale crash test criteria of NCHRP Report 230 in order to receive federal funding. Mak et al. (1990) evaluated the performance of the Wyoming tube-type bridge rail and a box-beam guardrail transition using four full-scale tests based on the guidelines of NCHRP Report 230. Two crash tests were performed on the tube-type bridge rail: a 1,800-lb (816-kg) vehicle striking the bridge rail at 60 mph (96.6 km/h) and 20 degrees, and a 4,500-lb (2,041-kg) vehicle striking the bridge rail at 60 mph (96.6 km/h) and 25 degrees. The box-beam guardrail transition was tested at two transition points using two 4,500-lb (2,041-kg) vehicles, both at 60 mph (96.6 km/h) and 25 degrees. The test results showed that the bridge rail and guardrail transition met the safety requirements of NCHRP Report 230.

Jewell et al. (1993) evaluated the performance of the California Type 115 bridge rail using three full-crash tests: two on the bridge rail by a 1,786-b (810-kg) small car and a 5,401-lb (2450-kg) pickup truck at 59 mph (95 km/h) and 20 degrees, and one on the transition by a 5,401-lb (2450-kg) pickup truck at 59 mph (95 km/h) and 20 degrees. These tests were performed at the AASHTO PL-2 level, but due to wheel snagging in the two tests on the bridge rail, the Type 115 was recommended for use as a PL-1 bridge rail on low-speed narrow bridges where impact angles were expected to be less. In the work of Buth et al. (1993), they designed and tested three PL-1 railings, seven PL-2 railings, three PL-3 railings, one PL-1 transition, and one PL-2 transition based on the AASHTO bridge railing specifications. They recommended design criteria for each of the three performance levels, including magnitude, distribution, and location of collision forces in addition to geometric requirements for various impact conditions. It was concluded that railings designed by the recommended procedure were found to be generally adequate and show little or no structural distress in full-scale crash tests.

Bligh et al. (1994) analyzed and evaluated the impact performance of various designs of bridge rails, guardrails, transitions, and end treatments used by the Tennessee Department of Transportation. The study included theoretical analyses and computer simulations on six bridge railings, and full-scale crash tests on an open concrete beam-and-post bridge rail. The results showed that the open concrete beam-and-post bridge rail could safely contain and redirect a 4,500-lb (2,041-kg) pickup truck, but it failed to meet the NCHRP Report 230 criteria for the small-car severity test due to wheel snagging on the interior face of a concrete post. Design modifications were suggested to remedy this problem for both new construction and retrofit applications.

In 1993, Ross et al. published their research in NCHRP Report 350, “Recommended Procedures for the Safety Performance Evaluation of Highway Features,” which was adopted by researchers in the field of roadside safety to replace NCHRP Report 230. NCHRP Report 350 differed from

NCHRP Report 230 in that it defined six test levels for testing highway barriers including bridge rails and specified a small passenger sedan and a pickup truck as the standard test vehicles in all test levels. It also provided guidelines for selecting the CIPs for crash tests on redirecting-type safety hardware. NCHRP Report 350 provided information on enhanced measurement techniques related to occupant risk and reflected a critical review of methods and technologies for safety performance evaluation. Periodically, FHWA published lists of bridge rails that were successfully crash tested. In 1997, FHWA issued a memorandum summarizing 68 crash-tested bridge rails and established the tentative equivalency of previous test level ratings for bridge rails in comparison to NCHRP Report 350, as summarized in Table 2.1. The impact conditions for Test Levels 1 to 4 in NCHRP Report 350, which are relevant to the work of this project based on MASH, are shown in Table 2.2.

Table 2.1: Bridge rail test level equivalencies.

Bridge Rail Testing Criteria	Acceptance Equivalencies					
NCHRP Report 350	TL-1	TL-2	TL-3	TL-4	TL-5	TL-6
NCHRP Report 230		MSL-1 MSL-2		MSL-3		
AASHTO Guide Specifications for Bridge Railings		PL-1		PL-2	PL-3	
AASHTO LRFD Bridge Specifications		PL-1		PL-2	PL-3	

Table 2.2: Impact conditions for Test Levels 1, 2, 3 and 4 of NCHRP Report 350.

Test level	Impact Conditions		
	Vehicle Mass	Speed	Angle
TL-1	Passenger car: 1,808 lb (820 kg) Pick-up Truck: 4,409 lb (2000 kg)	31 mph (50 km/h) 31 mph (50 km/h)	20° 25°
TL-2	Passenger car: 1,808 lb (820 kg) Pick-up Truck: 4,409 lb (2000 kg)	43.5 mph (70 km/h) 43.5 mph (70 km/h)	20° 25°
TL-3	Passenger car: 1,808 lb (820 kg) Pick-up Truck: 4,409 lb (2000 kg)	62 mph (100 km/h) 62 mph (100 km/h)	20° 25°
TL-4	Passenger car: 1,808 lb (820 kg) Pick-up Truck: 4,409 lb (2000 kg) Single-unit Truck: 17,637 lb (8000 kg)	62 mph (100 km/h) 62 mph (100 km/h) 50 mph (80 km/h)	20° 25° 15°

In 1997, an additional FHWA memorandum was published, requiring all highway safety hardware installed on or after October 1, 1998 be crash tested and in compliance with NCHRP Report 350. This memorandum allowed exceptions on some bridge rails tested and found acceptable for use on the National Highway System. In 2000, transportation agencies could request FHWA approval from state-specific bridge railings without full-scale crash testing by providing an in-depth structural analysis of all possible failure modes and assumed responses of all rail elements and connections in compliance with the requirements of NCHRP Report 350. In addition to the structural analysis, bridge railings were also required to meet the dimensional and design requirements by the AASTHO LRFD Bridge Specifications.

In the work by Polivka et al. (1998), they developed and tested a combination traffic/bicycle bridge rail that consisted of a standard New Jersey concrete barrier and steel panels formed by tubular posts and rails, and square vertical spindle bars. Two full-scale crash tests were conducted on the

combination bridge rail using a pickup truck and a single-unit truck. The test results showed that the combination bridge rail met the TL-4 requirements of NCHRP Report 350 under impacts of the two test vehicles. Note that under TL-4 conditions of NCHRP Report 350, a small passenger car was also required for the crash test. Since the TL-4 impact conditions for the small passenger car were the same as those under TL-3 conditions at which the New Jersey barrier had been tested and met the requirements, it was assumed that the steel panel on top of the New Jersey barrier would not change its overall performance; therefore, it was safe to assume the combination bridge rail would meet all the TL-4 requirements of NCHRP Report 350.

To evaluate the performance of bridge rails on non-concrete bridge decks, Faller et al. (2000) studied the performance of railing systems constructed on transverse timber decks. In this work, two bridge rails and guardrail transitions for use on timber-deck bridges were developed. The first bridge rail was constructed with glulam timber components, whereas the second one was built with steel hardware. It was observed from crash test results that the bridge rails and transition systems met the TL-4 requirements of NCHRP Report 350. In addition, the test results indicated that bridge rails constructed on timber decks had similar performance to those constructed on concrete decks.

Shankar et al. (2000) performed an empirical study on the safety performance of in-service bridge rails under vehicular impacts from data collected in Washington State. Based on a statistical analysis of vehicular accident severity, it was determined that concrete balusters and metal rails underperformed in comparison with the average bridge rail type, whereas Thrie-beam guardrails and safety shape barriers had superior performance.

In 2001, the Texas Department of Transportation (TxDOT) contracted with the Texas Transportation Institute (TTI) to develop two crashworthy and aesthetically pleasing bridge rails for use on selected bridges and roadways. Several designs were conceptualized resulting from this work. The two final designs chosen were the Texas Type F411 and Type T77 aesthetic bridge rails. The Type F411 was a concrete bridge rail consisting of two six-inch (152-mm) wide concrete rails atop a 42-inch (1.07-m) high parapet, with vertical reinforcements in both the concrete rails and parapet. The parapet was secured to the bridge deck utilizing “U” Bars. The Texas T77 bridge rail consisted of two elliptical-shaped steel rails welded to steel posts, which were anchored to a concrete curb. The total height of the T77 bridge rail was 33 inches (0.8 m). The two bridge rails were crash tested under TL-3 conditions of NCHRP Report 350 (Bullard et al., 2002). The test results showed that Type F411 design meet the evaluation criteria of Test 3-11, and that there was a potential for an errant vehicle to intrude into adjacent traffic lanes after a collision. The Type T77 bridge rail was found to meet the evaluation criteria of Test 3-10, but it failed to pass the evaluation criteria of Test 3-11 due to vehicle snagging at a rail splice joint and consequently causing excessive deformations of the occupant compartment.

To mitigate the cost of construction and repair of bridge rails, TxDOT sponsored another project to design, develop, and crash test a cost-effective and crashworthy bridge rail that would meet the TL-3 requirements of NCHRP Report 350. As a result of this work, Williams et al. (2008) designed the Texas Type T1F bridge rail with aesthetic features and ease of constructing. Elliptical-shaped aluminum rails were mechanically attached to the posts without welding and could be adjusted after installation, thus making it easy to construct and repair the bridge rail. The T1F bridge rail was crash tested and shown to meet the TL-3 requirements of NCHRP Report 350. Although the

T1F bridge rail exhibited a potential for wheel snagging on rail splices, the low yield strength of the aluminum rails and posts might prevent excessive vehicular snagging and thus greatly reduce the deformations of the vehicle compartment.

Buth et al. (2003) investigated the performance of the TxDOT T202 (MOD) bridge rail under impacts of a 4,502-lb (2,044 kg) pickup truck under TL-3 conditions of NCHRP Report 350. The T202 was a concrete bridge rail with fiber-reinforced-polymer reinforcement that would have a reduced strength after deterioration due to long-term exposure to the environment. Two full-scale crash tests were performed on the T202 bridge rail, one on the strong section that had the strength immediately after construction and the other on a weak section with reduced strength. The test results on the stronger section showed that the structural performance of the bridge rail was good, but the safety performance was unacceptable due to vehicle rollover. For the test on the weak section, the height of the rail was increased to 30 inches (0.762 m) and both structural and safety performance of the rail were acceptable.

Alberson et al. (2004) evaluated the performance of the Florida Jersey safety shaped bridge rail under impacts of a pickup truck and single-unit truck under TL-4 conditions of NCHRP Report 350. In both tests, the Florida bridge rail contained and redirected the test vehicles, which remained upright during and after the collision period and did not penetrate, underride, or override the installation. Although the Florida bridge rail performed acceptably in both tests according to the requirements of NCHRP Report 350, it failed the subsequent static load test at the impact location; the parapet failed at 45.1 kips (201 kN) and it did not meet the 54-kip (240-kN) design load for single-unit trucks according to the AASHTO LRFD Bridge Design Specifications. Further research was suggested to account for the reduced loading capacity imparted by the impacting single-unit truck.

Faller et al. (2004) reviewed tractor-trailer impacts into rigid barrier systems to study the dynamic lateral vehicular loads imparted into common barrier systems. Based on two linear regression analyses on a selected number of crash tests, they determined the ranges of peak lateral design loads for the AASHTO PL-3 and NCHRP Report 350 TL-5 impact conditions, respectively. Using the existing yield-line analysis procedures, they designed two single-faced, F-Shape concrete barrier systems, which had 42-in. (1.067-m) and 51-in. (1.295-m) top-mounting heights, to meet the TL-5 safety requirements. The study concluded that the barrier and foundation systems were based on a conservative design approach and thus full-scale vehicle crash testing would not be required.

In late 1990s, California DOT funded a project to develop and crash test two bridge rails, Type 80 and Type 80SW, for use on scenic highways. Both designs were made of concrete that incorporated a continuous square railing between the two end posts of the bridge. Analysis of crash test results showed that both Type 80 and Type 80SW bridge rails met the TL-4 requirements of NCHRP Report 350. However, these designs had limited “see through” capabilities and exhibited a potential for vehicle snagging. In a subsequent project also funded by California DOT, a one-bar bridge rail, Type 90, was designed to replace the previous Type 80 and Type 80SW bridge rails (Whitesel et al., 2008). The Type 90 design had adequate “see through” capabilities and required low maintenance. In this bridge rail design, steel posts and beams were connected to a concrete parapet using anchor bolts. The steel-beam railing was securely attached to steel posts that were

spaced three meters apart. Three crash tests were carried out on the Type 90 bridge rail for its compliance with NCHRP report 350 under TL-4 conditions, i.e., impacts by an 1,808-lb (820-kg) small car, a 4,409-lb (2,000-kg) pickup truck, and an 17,637-lb (8,000-kg) single-unit truck. The test results showed that there was minimal lateral deflection and negligible permanent damage to the concrete parapet. The barrier successfully contained and redirected all three test vehicles. More importantly, the results showed that structural adequacy, vehicle trajectory as well as occupant safety criteria were all within the acceptable limits specified by NCHRP Report 350.

In 2009, AASHTO published the Manual for Accessing Safety Hardware (MASH 2009), which superseded NCHRP Report 350 for evaluating new safety hardware devices. AASHTO and FHWA jointly adopted an implementation plan for MASH such that all highway safety hardware accepted based on criteria of NCHRP Report 350 prior to the adoption of MASH could remain in use and continue to be manufactured and installed. In addition, highway safety hardware accepted using NCHRP Report 350 criteria was not required to be retested using MASH criteria. However, new highway safety hardware not previously evaluated must be tested and evaluated using MASH. MASH represents an update to crash testing requirements primarily on the test vehicles. In 2016, AASHTO published the second version of MASH (MASH 2016), which ended the approval of roadside safety hardware that was compliant with NCHRP Report 350. In addition, AASHTO and FHWA issued a Joint Implementation Agreement that required all hardware previously approved based on NCHRP Report 350 be replaced or retested to meet the MASH 2016 evaluation criteria before being installed on the National Highway System. As a response to the AASHTO/FHWA Joint Implementation Agreement for MASH 2016, NCDOT funded this project to determine the compliance of 2BMR with MASH 2016 requirements.

In the work by Williams et al. (2010), they evaluated the TxDOT single-slope bridge rail (Type SSTR) with 36-in. height on a pan-formed deck using a full-scale crash test with a 5,000-lb (2,268-kg) pickup truck. The test results showed that the performance of the single-slope bridge rail under impact of the pickup truck was acceptable based on MASH TL-3 requirements. In the work by Sheikh et al. (2011), the 36-in. Type SSTR bridge rail was further evaluated to determine its minimum height under MASH TL-4 conditions using a 22,046-lb (10,000-kg) single-unit truck. The test results showed that the 36-in. bridge rail performed acceptably and met all relevant MASH criteria. The vehicle was successfully contained and redirected without any significant damage to the barrier. Note that the 36-in. Type SSTR bridge rail was already tested using a pickup truck by Williams et al. (2010) and found to meet all MASH TL-3 requirements that were the same as MASH TL-4 requirements for pickup truck. In reference to the test results on a 32-in. New Jersey concrete barrier impacted by a small car, Sheikh et al. believed that the 36-in. TxDOT SSTR should perform acceptably under impact by a small passenger car under MASH TL-4 conditions. Based on these considerations, Sheikh et al. believe the Type SSTR bridge rail met all the MASH TL-4 requirements.

Williams et al. (2013) conducted full-scale crash tests to evaluate the performance of a transition design for the TxDOT T131RC bridge rail under MASH TL-3 conditions. The performance was evaluated on structural adequacy, occupant risk, and post-impact vehicle trajectories. Each test vehicle was instrumented with data acquisition systems to measure accelerations and rotations (yaw, pitch, and roll angles). Based on test results, the T131RC bridge rail was shown to meet the strength and safety performance criteria under MASH TL-3 conditions. In another work by

Williams et al. (2015), a low-cost bridge rail system was designed that would minimize or eliminate bridge deck damage (observed from crash testing of prior designs) when impacted by errant vehicles. The newly developed bridge rail, named Texas Type T631, consisted of W-beam rails securely bolted to steel posts that were welded to steel base plates. The bridge rail was crash tested to evaluate its compliance with MASH and was found to perform exceptionally well under TL-2 conditions. Subsequently, the Texas Type T631 bridge rail was revised with reduced post spacing (from 75 inches to 37½ inches) and was evaluated under MASH TL-3 conditions. The test results showed that the bridge rail with reduced post spacing met the MASH TL-3 requirements.

In a recent work by Williams et al. (2018), they evaluated the impact performance of the TxDOT T224 bridge rail using full-scale crash tests under MASH TL-5 conditions. The T224 was an open concrete bridge rail and had an overall height of 42 inches (1.067 m) above the bridge deck, with the bottom of the rail at 21 inches (0.533 m) above the deck. The rail was 16½-in. (419 mm) wide and supported on integral posts every 15 feet (4.57 m) with a 10-ft (3.05-m) clear opening between adjacent posts. The posts were installed on a 9-in. (229-mm) tall steel reinforced concrete curb. The deck, curb, posts, and beam had a 2-in. (51-mm) wide expansion joint at 65 feet (19.8 m) from the upstream end of the installation. Under impacts of the three MASH TL-5 vehicles, the T224 bridge rail was found to meet all the MASH TL-5 safety criteria and performance requirements.

Thiele et al. (2010) designed a low-cost bridge rail that was compatible with the Midwest Guardrail System (MGS) such that an approach transition was not required between the two barriers. The bridge rail was composed of a W-beam section mounted by bolts to S3x5.7 (S76x8.5) steel posts that were housed in sockets placed at the vertical edge of the deck and anchored to the deck with one through-deck bolt. Two full-scale crash tests were performed under MASH TL-3 conditions in which the system was shown to meet all the safety performance criteria. Rosenbaugh et al. (2012) used FE simulations and component testing to develop a precast concrete bridge rail system that would meet the MASH TL-4 safety requirements. In this phase of the research, the focus was on designing the joint component that would be used to connect adjacent rail segments and meet the design criteria of load capacity. Connection details for attaching the rail to the bridge deck as well as the CAD details of a complete set of prototype precast concrete bridge rail system were developed.

In the early 2000s, the California DOT initiated a project to test the Type 26 bridge rail under TL-3 conditions of NCHRP report 350, but failed to meet the FHWA's deadline for testing based on NCHRP Report 350. The Type 26 bridge rail was subsequently redesigned to be tested according to the requirements of MASH 2009 (Whitesel, et al., 2016). The redesigned version was named Type 732SW, which was taller and stronger than the Type 26 bridge rail. The Type 732SW bridge rail included a concrete parapet, steel handrails for pedestrian, and a sidewalk. Crash tests were conducted on the Type 732SW bridge rail for compliance with MASH 2009 requirements under TL-3 conditions. It was concluded that the Type 732SW bridge rail met all the requirements of MASH 2009 for Test 3-11 (i.e., using a 2270P pickup truck), but failed to meet the occupant risk criteria for Test 3-10 (i.e., using a 1100C passenger car). Analysis of the Test 3-10 results showed that the ridedown acceleration was too high, because the initial impact between the tire and the sidewalk edge was significant enough to reduce the lateral flail space before impacting the concrete parapet and caused the hypothetical occupant impact to occur sooner than that for a narrower sidewalk. The Type 732SW bride rail was subsequently crash tested for Test 2-10, i.e., impacted

by a 1100C passenger car at 44 mph (70 km/h), and was found to pass the Test 2-10 requirements of MASH 2009 and thus was recommended for approval on California highways requiring TL-2 bridge rails with pedestrian traffic.

Ecklund and Sritharan (2018) studied the connections for precast concrete barriers used in accelerated bridge construction. Two barrier-to-deck connections were considered, one with inclined reinforcing bars with threaded ends and the other using U-shaped bars. The barrier-to-barrier connection was headed reinforcement in both the longitudinal and transverse directions. The connections were designed to meet MASH TL-4 requirements and LRFD Bridge Design Specifications and were tested using quasi-static loads on full-scale precast barriers. The results suggested that all tested connections were viable for accelerated construction of concrete barriers.

In the work of Rasmussen et al. (2020) and Pena et al. (2020), they designed a steel, side-mounted, beam-and-post bridge rail that was evaluated using full-scale crash tests under MASH TL-4 conditions. The bridge rail was designed to be compatible with multiple concrete bridge decks utilized by the States of Illinois and Ohio, and optimized for weight per foot, constructability, and safety. The bridge rail consisted of three tubular steel rail elements supported by W6x15 (W150x22.5) steel posts mounted to the vertical edge of concrete deck and spaced at 8 ft (2.4 m) on centers. Full-scale crash testing was performed with MASH-compliant vehicles, a single-unit truck (SUT), a pickup truck, and a small car. In all the TL-4 crash tests, the vehicles were successfully contained and redirected, and all occupant risk measures and evaluation criteria were within the MASH 2016 limits. In a recent work by Rosenbaugh et al. (2020, 2021), a new concrete bridge rail was developed based on MASH TL-4 design loads, and optimized for vehicle stability, installation costs, and loads transferred to the deck. The bridge rail was designed with a 39-in. installation height to remain crashworthy after future roadway overlays up to three inches thick. A full-scale crash test was conducted on the concrete bridge rail under MASH TL-4 conditions: a 22,198-lb (10,069-kg) single-unit truck was used to impact the bridge rail at a speed of 57.6 mph (92.7 km/h) and an angle of 16 degrees. The test results showed that the single-unit truck was successfully contained and redirected, and all MASH safety criteria were met.

2.2 Finite Element Modeling and Simulations of Vehicular Crashes

Historically, the safety performance of vehicles and roadside safety devices were evaluated through full-scale crash testing. While it is a valid means for evaluating the safety performance of vehicles and roadway structures, physical crash testing is very expensive, time-consuming, and difficult to perform. Consequently, only a limited number of representative crash scenarios can be evaluated based on regulations given by MASH for roadside safety hardware designs. With the rapid development of computing hardware and commercial software for high performance computing, computer simulations have been increasingly used in highway safety designs. Full-scale FE simulations have been widely accepted as a powerful tool to investigate various roadside safety issues. Compared to full-scale crash testing, FE simulations are particularly useful in assessing the performance of roadside structures under various impact and site conditions that would be either impossible or impractical to conduct physical experiments. In recent decades, various FE models of vehicles and roadside safety devices have been developed.

Wekezer et al. (1993) developed the first FE model for simulations of a whole vehicle impacting roadside hardware. Prior to this, simulations of a vehicle impacting roadside hardware were only

performed using some deformable components of a vehicle and a rigid part representing the safety hardware. This research was one of the several projects funded by FHWA with the aim of developing better FE models that could predict vehicle and barrier responses during impacts. In this research, a simple FE model of a 1991 GM Saturn was developed to demonstrate the capabilities of FE modeling for crash simulations. Two impact scenarios were examined: the vehicle impacting a rigid wall and impacting a luminaire pole. The simulation results were compared with data from crash tests performed by the National Highway Traffic Safety Administration (NHTSA). The simulation results were found to match well to test data and the FE modeling technique was shown to be effective in predicting vehicular responses in impacts. In a similar project also funded by FHWA, Mendis et al. (1995) developed an FE model of a 1981 Honda Civic to evaluate the crash performance in a frontal impact with a highway sign post and barriers. Because the scope of this research was limited to frontal impact conditions, the rear half of the vehicle was assumed to be rigid and only the front half was modeled as deformable. The simulation results were compared with test data from a previous crash test and were shown to predict similar deformation patterns to those observed in the actual crash test. Although the overall responses predicted by the FE model were considered satisfactory, this model was limited to frontal impacts with narrow object and rigid walls. Cofie et al. (1995), developed a simple FE model of a 1989 Ford Festiva, with improvements over some of the limitations observed in previous vehicle models. For instance, an accelerometer model was incorporated in this FE model at the center of gravity (CG) of the vehicle. Consequently, the vehicle's accelerations, velocities and displacements could be obtained from simulations and compared directly with actual test data. The test conditions used in this study were frontal impacts and the simulation results were shown to agree with the actual test results.

Over the years, NHTSA and FHWA funded several projects on the development of FE models that could be used in roadside safety research to advance knowledge of highway/vehicle safety issues and to assist mitigating the severity of highway crashes. In one of these projects, researchers at George Washington University developed the FE model of a 1994 Chevrolet C-1500 pickup truck for impact simulations of roadside hardware (Zaouk et al., 1997). Since previous vehicle models were developed for only frontal impacts, the accuracy of simulation results obtained using these models for other impact conditions were questionable. The C1500 was the first FE model developed for both frontal and side impact scenarios. The approach taken by the researchers involved creating a detailed and a simplified vehicle model. The simplified model was used to test various components of the detailed model. In addition, tensile and shear tests were conducted on several components of the vehicle such as the fender, bumper, and door frames to obtain their material properties. Two crash tests, a frontal impact with a rigid wall and a side impact with a vertical concrete barrier, were used to validate the vehicle models. It was shown from simulation results that the vehicle trajectories were similar to those from the actual crash tests. In addition, the deformations observed from frontal and side impact simulations agreed with test results. It was concluded that the simulation results generally had good agreement with test data, and that it was also necessary to further improve the fidelity of the models.

Over the past decades, FE simulations have been increasingly used to determine if a safety barrier would meet the requirements of safety guidelines before conducting full-scale crash tests. Ray et al. (2004) used FE simulations to design an F-shape aluminum bridge railing and analyze its performance under TL-3 and TL-4 conditions of NCHRP Report 350. The FE model of a C2500

pickup truck, which included fully functioning suspension, steering and tire models, was used in the simulation of the vehicle impacting the F-shape aluminum bridge rail under TL-3 conditions. The FE model of an 800S single-unit truck was used in the simulation of the TL-4 test. The simulation results showed that the bridge rail mainly remained intact, with only minor deformations and reasonable local deformations at both test levels. Furthermore, the FE simulation results were shown to have good agreement with crash test data on the predicted characteristics and crash responses of the bridge rail. It was concluded that the performance of the F-shape aluminum bridge rail was acceptable under TL-3 and TL-4 conditions of NCHRP Report 350.

In the work by William et al. (2008), FE analysis was utilized in the design of the Texas T-1F bridge rail to determine the overall stiffness, thickness and ultimate force that could be applied to the proposed T-1F posts and ultimately to the 7/8-inch diameter anchor bolts. In addition, FE analysis was used to investigate several failure modes in the posts due to impact loading. Based on the analysis, the thickness of the posts and base plates were determined. Subsequent simulation results showed that the proposed bridge rail design met the minimum strength requirement of the AASHTO LRFD TL-3 loading conditions.

In the work by Mohan et al. (2009), they conducted several full-scale crash tests to generate data for validating the FE model of the steering and suspension system of a 2007 Chevrolet Silverado pickup truck that was being developed. In the first series of tests, low-speed, non-destructive tests were conducted to measure suspension deflections when the vehicle went through speed bumps and sloped terrains. In the second series of tests, the front and rear suspensions were subjected to vertical and lateral loading from a swinging rigid pendulum. Subsequently, a detailed FE model of the 2007 Chevrolet Silverado pickup truck was developed that incorporated all structural components of the vehicle and emulated the functionality of steering and suspension systems. The accuracy of this model was accessed using several impact scenarios, including frontal impact into a rigid wall, centerline pole impact, and side impacts at varying speeds. The vehicular responses and damage profiles predicted by the FE model were found consistent with actual tests for all impact conditions investigated. It was concluded that the FE model was suitable for various impact conditions and satisfied the requirements for a MASH compliant 2270P test vehicle.

Fang et al. (2009) used FE analysis to evaluate two retrofit options to enhance the performance of cable median barriers (CMBs). In their work, several CMB designs for each retrofit option were evaluated using full-scale FE simulations of vehicles crashing into the CMB. The safety performance of these retrofit designs was evaluated for both front-side and backside impacts at different impact speeds and angles. The simulation results showed that some retrofit options could enhance the CMB performance for backside impacts without compromising the performance for front-side impacts. Two retrofit designs, one with three cables and the other with four cables, were identified as the best options and subsequently evaluated using FE analysis under MASH TL-3 conditions (Fang et al. 2019).

In the work by Marzougui et al. (2012), they developed an FE model of a 2010 Toyota Yaris passenger sedan. This vehicle was selected to reflect automotive designs and technology advancements at the time for an important segment of the vehicle fleet. In addition, this vehicle conformed to the MASH requirements for a 1100C test vehicle. Similar to the 2007 Chevrolet Silverado, the 2010 Toyota Yaris model incorporated functional suspension and steering systems.

The model was subsequently validated using crash test data from NHTSA and was found to have consistent overall responses with those from the actual test. Both the kinematics and accelerations of the vehicle from simulations were shown to have a good correlation with test data.

In roadside safety research, the commercial FE program, LS-Dyna, is widely used in analysis of impact responses of various structures. Much work has been done over the years since its pioneer version to improve the program's capability of accurately simulating vehicular impacts. Abu-Odeh (2008) evaluated the suitability of three concrete material models in LS-Dyna, i.e., material types 72R3, 84 and 159, for modeling the deformations and damages of concrete barriers under impact loading. In addition, the research work provided methods of modeling concrete materials with minimum user inputs. To compare the damages of a concrete barrier predicted by the material models with actual test data, a Texas F-shaped barrier (TxDOT T501) was used in the simulation of impacts by a 5000-lb bogie. The simulation results showed that all three material models performed reasonably well. It was also suggested that the accuracy of these models could be improved by calibrating the models' input parameters.

In another study by Abu-Odeh (2007), the FE model of a Texas T4 bridge rail was created to evaluate the suitability of a concrete material model in LS-Dyna, MAT 159, for analyzing concrete roadside safety features. LS-Dyna offers two input formats for MAT 159: a short format that utilizes built-in values for numerous variables, and a long format for which the user must supply values for all the required input parameters. The T4 bridge rail consisted of steel elliptical rails, posts, and base plates attached to a reinforced concrete parapet. The study focused on evaluating the capability of the material model in capturing concrete deformations. Additionally, the short and long input formats were compared to determine the better one in capturing concrete damage. For the long input format, a sensitivity study was performed to evaluate the parapet's response to different combinations of the required parameter inputs. Finite element simulations were also conducted on the concrete barrier impacted by two different pendulums. The simulation results showed that the FE model with long input format could capture the deformation patterns observed in the actual test and thus was deemed better than the one with short format. It was also concluded that the long-format model was suitable for modeling concrete bridge rails.

Several methods exist in literature addressing issues of modeling steel reinforcements in concrete materials in FE analysis. Schwer (2014) evaluated three methods of modeling rebars in reinforced concrete slabs. The first approach involved homogenizing the material properties of the concrete and rebars by combining the volume-fraction ratios of the steel and concrete materials. This approach for modeling reinforced concrete is commonly known as the smeared reinforcement. The second method evaluated by Schwer, known as the constraint method, was to couple the rebars with the surrounding concrete continuum using internally generated constraints in LS-Dyna. The third method, known as the node-sharing method, involved constructing the mesh of the rebars such that the nodes would coincide with nodes on the mesh of the surrounding concrete. The effectiveness of these methods for modeling rebars in reinforced concrete slabs was evaluated under three loading conditions: axial extension, self-weight, and blast loading. The simulation results showed that under axial extension loading, the constraint method was unable to predict the effect of the steel reinforcement in the concrete because the deformation profile of the concrete was the same as the case with no rebars. For the self-weight loading condition, the smeared reinforcement technique failed to accurately predict the deflection of the concrete. As a result, the

smeared reinforcement technique was deemed only suitable for small displacement when the reinforcement remains elastic. Results from the blast loading condition showed that the node-sharing and constraint methods could predict the displacements of the concrete. Conversely, the smeared reinforcement approach failed to accurately represent the reinforcement in the concrete or predict the deflections of the concrete. It was observed that only the node-sharing approach of modeling reinforced concrete performed well in all three loading conditions.

For crash simulations involving bolted joints or connections, there exists extensive literature on the representations in FE models. Narkhede et al. (2010) examined two approaches for modeling bolted joints in LS-Dyna with bolt pre-stresses and bolt failure characteristics in crash simulations. The first approach involved modeling the bolt shank with beam elements and modeling its connection to surrounding plate with discrete spring elements. In addition, the bolt head and nut were modeled using rigid shells. In the second approach, the bolt shank, bolt head and nut were modeled using solid elements. The bolt responses were compared to analytical solutions for shear, compressive, and tensile loading conditions. It was concluded that the bolted joint responses predicted by both modeling techniques had good agreements with analytical solutions as well as physical test data under shear and tensile loading conditions.

Atahan (2016) used nonlinear FE simulations to analyze the performance of a bridge rail to guardrail transition under impact of a 17,637-lb (8000-kg) single-unit truck at 50 mph (80 km/h) and 15 degrees based on the TL-4 conditions of NCHRP Report 350. The simulation results showed that the transition structure could adequately contain and redirect the vehicle. The post-impact trajectory of the truck, occupant risk values, test article deflections, and exit conditions were also found similar to those obtained from a similar transition structure that was crash-tested under TL-4 conditions of NCHRP Report 350. It was concluded that the FE model of the bridge rail to guardrail transition was fairly accurate for used in other studies, such as crash simulations under MASH TL-4 conditions.

In a project sponsored by the United States Marine Corps, Hadjioannou et al. (2016) investigated different approaches for modeling bolted connections using both numerical simulations and physical experiments. The study focused on developing computationally efficient methods to represent bolted joints under static and dynamic loading conditions. Simplified FE models of bolted connections were developed utilizing a combination of beam and shell elements. The simulation results of the simplified model were compared to static and dynamic test data. It was concluded that the simplified model could simulate the responses of bolted connections with reasonable accuracy.

Most of the FE vehicle models in the public domain were originally developed at the National Crash Analysis Center (NCAC), George Washington University. These vehicle models were validated using standard crash tests specified in Federal Motor Vehicle Safety Standards (FMVSS) including full-frontal, offset-frontal, and side impacts. The impact speeds of the FMVSS crash tests are much lower than those specified in MASH, for example, the impact speed for the 40% offset-frontal crash is 35 mph (56 km/h), while the impact speed for sedans and pickup trucks is 62.1 mph (100 km/h) as specified in MASH. When these vehicle models are used in simulations of vehicular crashes into roadside safety systems, they may experience issues such as large deformations and numerical instability that must be fixed by the researchers using these models.

For the FE models used in this project, i.e., a 2010 Toyota Yaris, a 2007 Chevy Silverado, and a 2014 Chevy Silverado, some components were re-meshed and hourglass controls were added to handle large deformations and improving numerical stability. In addition, new contact definitions were added between components that might be in contact during a roadside crash simulation and initial penetrations on some components were removed. Detailed information about the vehicle models used in this project is presented in Chapter 3.

3. Finite Element Modeling of Vehicles and Bridge Rails

In this section, details of the FE models of MASH-compliant vehicles and four bridge rails are presented. For the performance evaluation of this project, three test vehicles were needed: a small passenger car (1100C), a pickup truck (2270P), and a single-unit truck (10000S). For the 2270P test vehicle, two FE models were available in this project, and both were used in the simulations to compare the vehicular responses predicted by the two models. The FE model of 2BMR was created to match exactly to the actual test section. For the three additional bridge rails, the FE models were created similarly to that of 2BMR. Simulation setup for the MASH tests of the four bridge rails are also presented along with the FE models.

3.1 Finite Element Modeling of MASH-compliant Test Vehicles

The FE models of the vehicles used in this project were a 2010 Toyota Yaris (1100C), a 2007 Chevy Silverado (2270P), a 2014 Chevy Silverado (2270P), and a 1996 Ford F800 (10000S). Figure 3.1 shows the four vehicle models and Table 3.1 gives the model information.

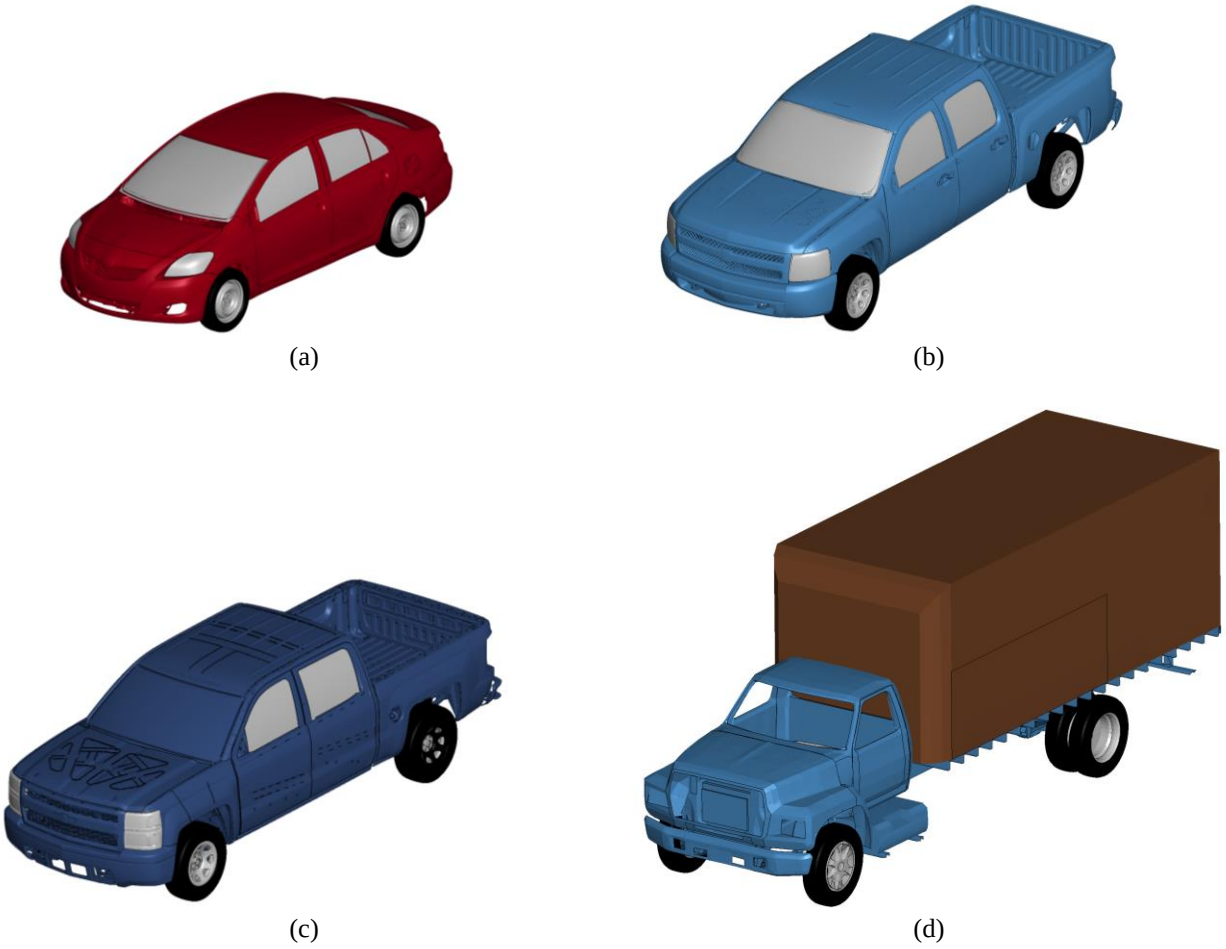


Figure 3.1: FE models of four test vehicles.
(a) 2010 Toyota Yaris; (b) 2007 Chevy Silverado; (c) 2014 Chevy Silverado; and (d) 1996 Ford F800.

Table 3.1: Finite element model information of the test vehicles used in crash simulations.

Specification	Test Vehicle			
	2010 Toyota Yaris	2007 Chevy Silverado	2014 Chevy Silverado	1996 Ford F800
Mass (kg)	1,101.7	2,271.8	2,277.6	9,990.8
Number of parts	941	721	1,498	142
Number of nodes	1,488,671	979,598	2,809,787	63,093
Number of solid elements	259,803	53,294	284,286	886
Number of shell elements	1,254,993	907,067	2,654,053	58,427
Number of beam elements	4,802	3,113	22,403	548
Number of discrete elements	19	34	36	52

The FE model of the 2010 Toyota Yaris was originally developed at NCAC and validated with frontal impact test (Marzougui et al. 2012). This model had a total of 1,519,587 elements with an average mesh size of 0.2 inch (6 mm) and included fully functional suspension and steering systems. An accelerometer (model) was positioned at the CG point of the vehicle to obtain time histories of vehicle accelerations during an impact. A total of ten different constitutive models were used to model the different materials of the components in the vehicle, including

- Piecewise linear plasticity model used to model most steel components,
- Rigid model for mounting hardware and accelerometer,
- Elastic model for rubber components,
- Viscous damping model for the shock absorbers,
- Low-density foam model for the radiator core,
- Spot-weld model for sheet metal connections,
- Null material model defined for contact purposes, and
- Nonlinear elastic spring model for the spring-damper connection of the front suspension.

The FE model of the 2007 Silverado was originally developed at NCAC and validated with frontal impact test (Mohan et al. 2009; Marzougui et al. 2012). This model had a total of 963,474 elements with an average mesh size of 0.3 inch (8 mm) and ten constitutive models, same as those used in the FE model of the 2010 Toyota Yaris. An accelerometer was positioned at the CG point of the vehicle to obtain acceleration histories. Hourglass control was used on components that could potentially experience large deformations. The FE model of the 2014 Silverado was developed and validated with frontal impact test at the Center for Collision Safety and Analysis, George Mason University (CCSA 2018). This model had a total of 2,960,778 elements with an average mesh size of 0.2 inch (6 mm) and eleven constitutive models, most of which were the same as those of the 2010 Toyota Yaris. This vehicle model also included fully functional suspension and steering systems.

The FE model of the 1996 Ford F800 was originally developed at NCAC and further improved at the National Transportation Research Center Inc. and Oak Ridge National Laboratory and validated using TTI's Test 471470-17. This model had a total of 142 components that were meshed into 63,093 nodes and 59,913 elements. Hourglass control was used on various components that could potentially experience large deformations. Seven different constitutive models were used, including

- Piecewise linear plasticity model defined for most steel components,
- Rigid model for mounting hardware,
- Elastic model for the tires and other rubber components,
- Linear elastic spring model for the steering springs,
- Nonlinear elastic spring model for the suspension springs,
- Nonlinear viscous damping model for the shock absorbers, and
- Null material model for contact purposes.

3.2 Finite Element Modeling of NC Two-bar Metal Rail

A detailed FE model of a 90-ft (27.4-m) 2BMR section, which was used in the full-scale crash tests, was developed to evaluate its performance under MASH TL-3 conditions. The 2BMR model, as shown in Figure 3.2, consisted of aluminum posts, elliptical rails, and base plates on top of a concrete parapet. The geometry of the bridge rail was determined according to the NCDOT specifications. The 2BMR entailed sixteen posts with two splices. The bridge rail model was discretized into 4,856,352 elements with an average mesh size of 0.5 inches (12.7 mm).

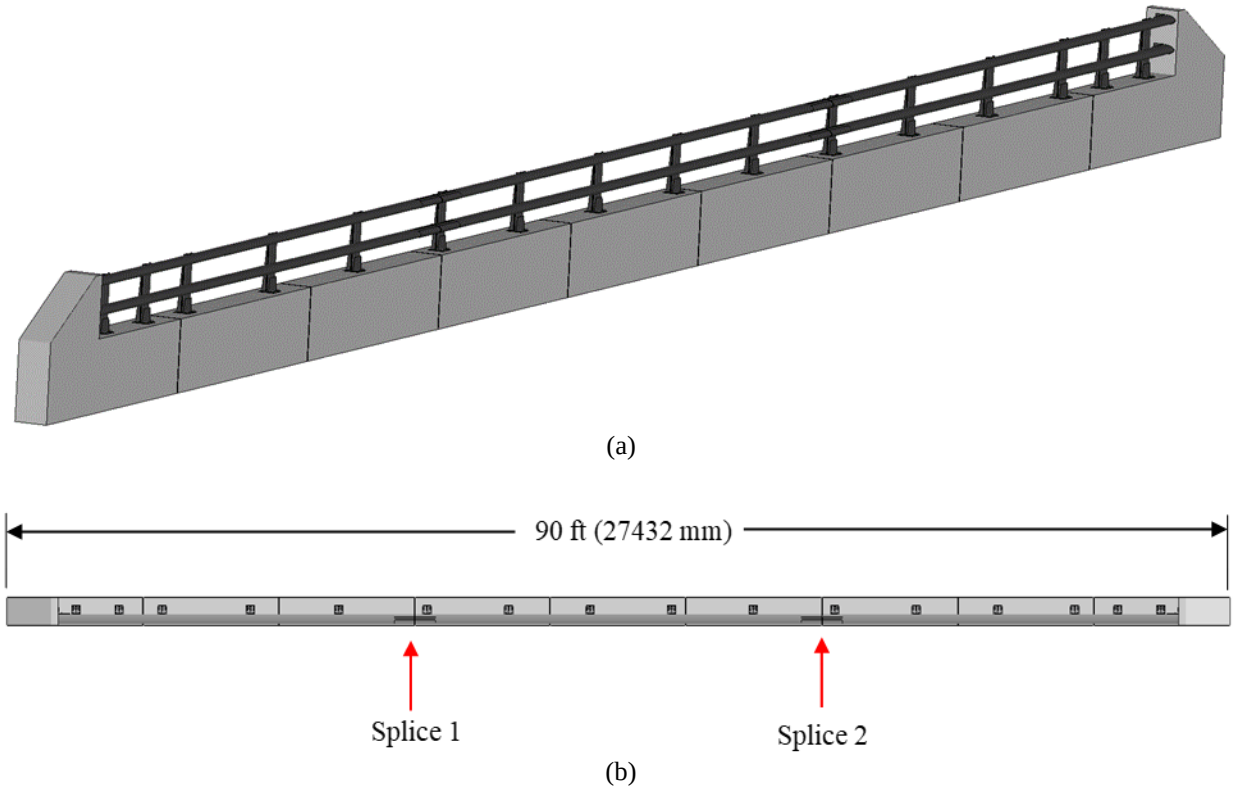


Figure 3.2: Finite element model of the 2BMR.
(a) Isometric view; and (b) top view.

Figure 3.3 shows a detailed post assembly of the 2BMR that includes an aluminum post, clamp bar base plate, and anchor bolts assembly. The aluminum post was meshed using a combination of shell and solid elements: the front face and mid-section of the post were meshed using shell

elements and the rear support section was meshed with solid elements. Null shells were used on the surface of the solid elements that were on the interface between the mid-section of the post and the rear support section. The base plate was meshed using fully integrated shell elements and the clamp bars were meshed using solid elements. Beam elements were used to model the anchor bolts as well as the anchor assembly. Node-sharing technique was used to model the bolts embedded in the concrete parapet, i.e., nodes of the anchor bolts would coincide with nodes of the concrete parapet. Pre-tensioning of bolted joints was achieved by adding discrete linear spring elements: one node of the spring was constrained to the nut and the other shared a node with the concrete parapet. An initial tensile force was applied to the spring to achieve a tightened bolted joint at the beginning of the simulation. The elliptical rails, which were mounted to clamp bars, were meshed using fully integrated shell elements. The extension bars, which were used to connect elliptical rails, were modelled using solid elements. The piecewise linear plasticity constitutive model was defined for the elliptical rails, aluminum posts, clamp bars, expansion bars, and steel bolts.

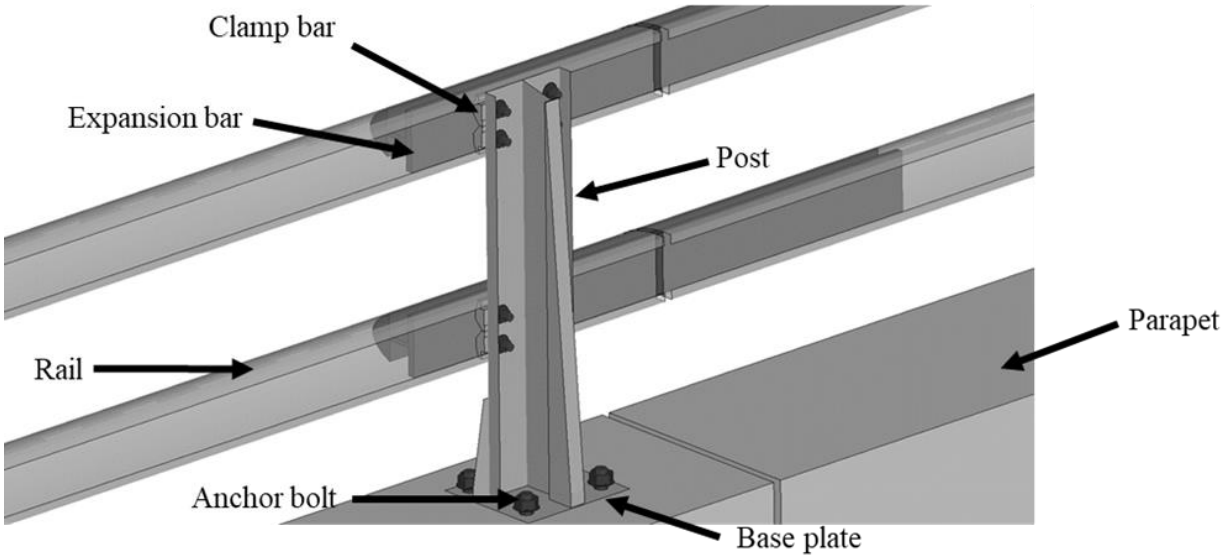


Figure 3.3: The FE model of a post assembly of the 2BMR.

The concrete parapet was meshed using solid elements with reduced integration (i.e., Type 1 in LS-Dyna) and Flanagan-Belytschko hourglass control (i.e., using the exact volume integration formulation). An elastoplastic constitutive model with damage and rate effects was utilized to model the concrete parapet. The concrete parapet consisted of both horizontal and vertical steel reinforcements that were explicitly modeled using beam elements throughout the entire length of the parapet, as shown in Figure 3.4. Node-sharing technique was used to model the steel reinforcement bars in the parapet, i.e., the nodes of the steel bars were aligned with nodes of the solid elements for the parapet. Figure 3.5 shows the cross-sectional view of the concrete parapet with the embedded horizontal and vertical steel bars sharing nodes with the solid elements for the parapet. The steel bars were modeled using Hughes-Liu beam elements with an average mesh size of 0.5 inches (12.7 mm) and a piecewise linear plasticity material model. The boundary conditions for the bridge rail were applied by fixing the nodes at the bottom of the parapet, including nodes

on the vertical reinforcement. The ground was modeled using shell element and was assigned with a rigid material model (i.e., no deformation of the ground).

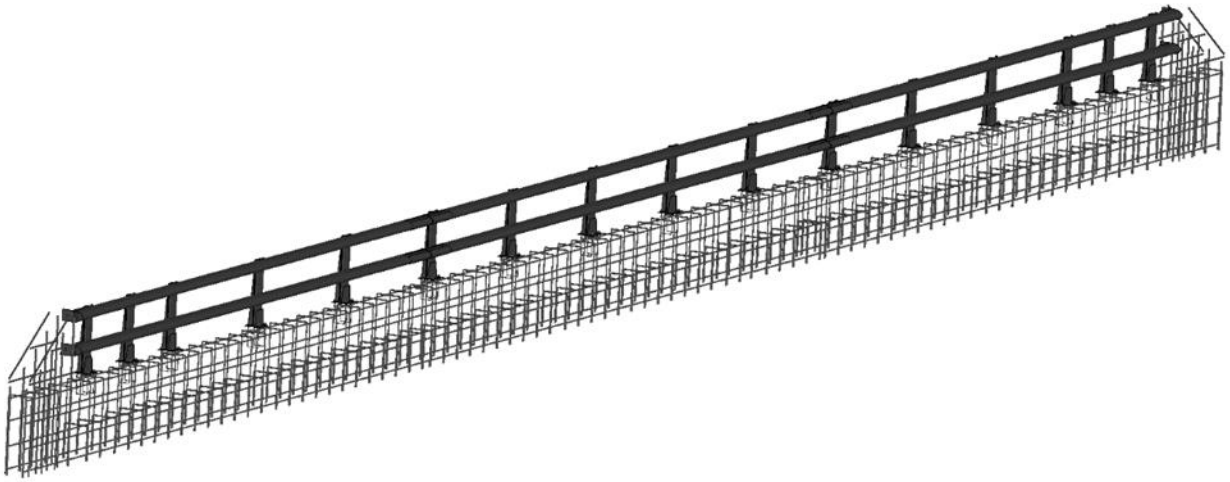


Figure 3.4: Steel reinforcement bars in the concrete parapet of 2BMR.

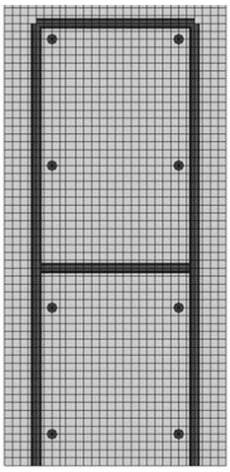
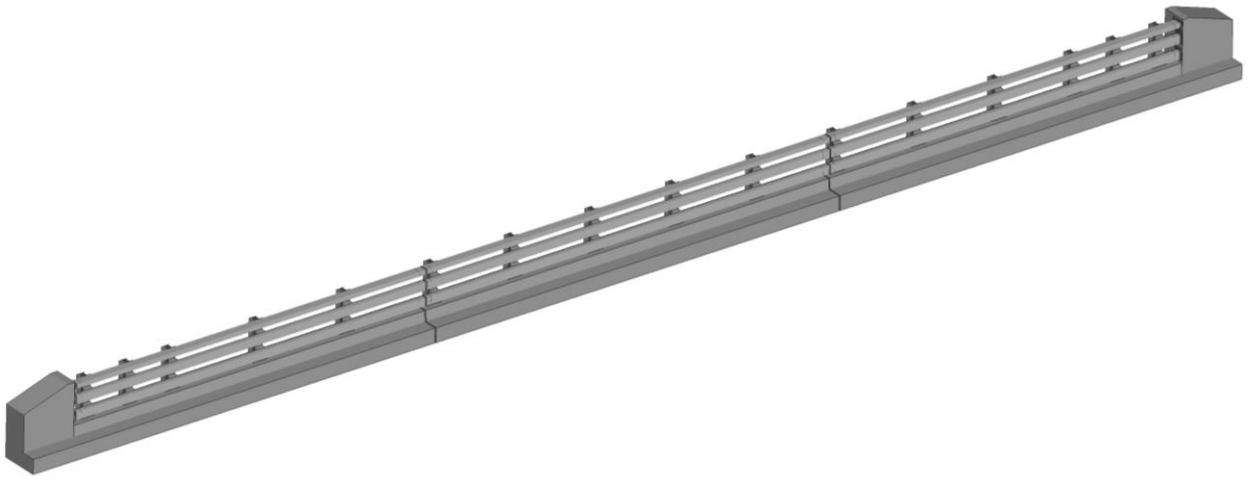


Figure 3.5: Cross-sectional view of the concrete parapet with horizontal and vertical steel reinforcement.

3.3 Finite Element Modeling of Oregon Rail

The FE model of a 90-ft (27.4-m) long Oregon Rail was developed to evaluate its performance under MASH TL-4 conditions. The Oregon Rail consisted of three aluminum rails with rectangular cross-sections, I-beam posts, rail attachment brackets, and concrete foundation. Figure 3.6 shows the FE model of the 90-ft (27.4-m) Oregon Rail, which had three 30-ft (9.14-m) sections separated by two expansion joints. The Oregon Rail consisted of three horizontal rails (top, middle, and bottom rails) that were constrained to the aluminum I-beam posts. Figure 3.7 shows a close-up view of a single post assembly and the cross-section profiles of three aluminum rails. On each post assembly, three attachment brackets were fastened to the front face of the I-beam post by two ø-0.75” studs. The I-beam post was welded to a base plate, which was fixed to the concrete foundation by four 7/8" anchor bolts. Inside the concrete foundation, the steel reinforcement bars

were modeled using beam elements that shared nodes with the solid elements for the concrete foundation. Figure 3.8 shows the steel reinforcement bars inside the concrete foundation and the end parapets.

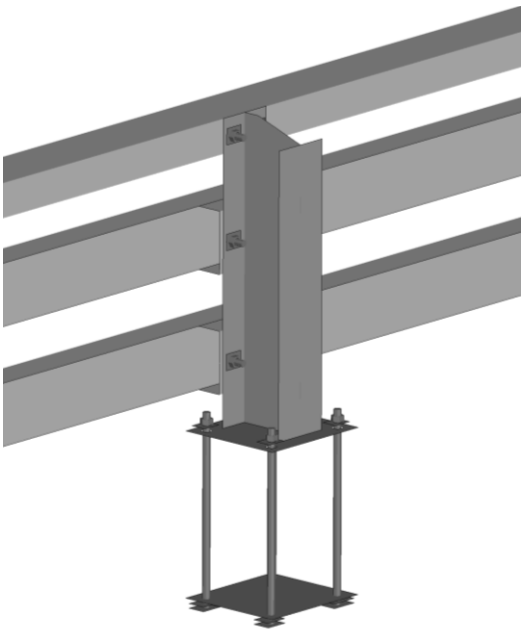


(a)

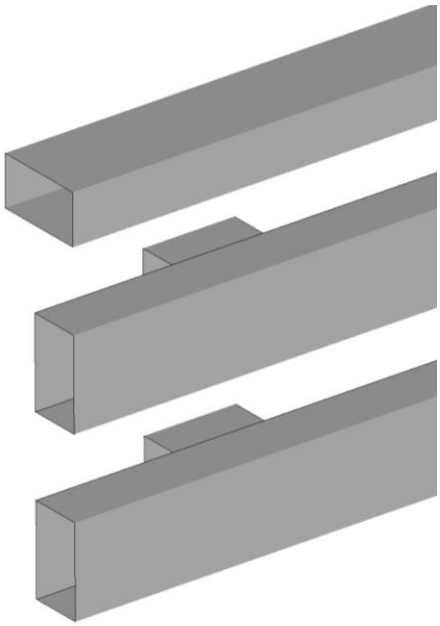


(b)

Figure 3.6: Finite element model of the Oregon Rail.
(a) Isometric view; and (b) top view.



(a)



(b)

Figure 3.7: Close-up view of a post assembly and cross-section profiles of the rails in the Oregon Rail.
(a) Post assembly; and (b) cross-section profiles of the three rails.

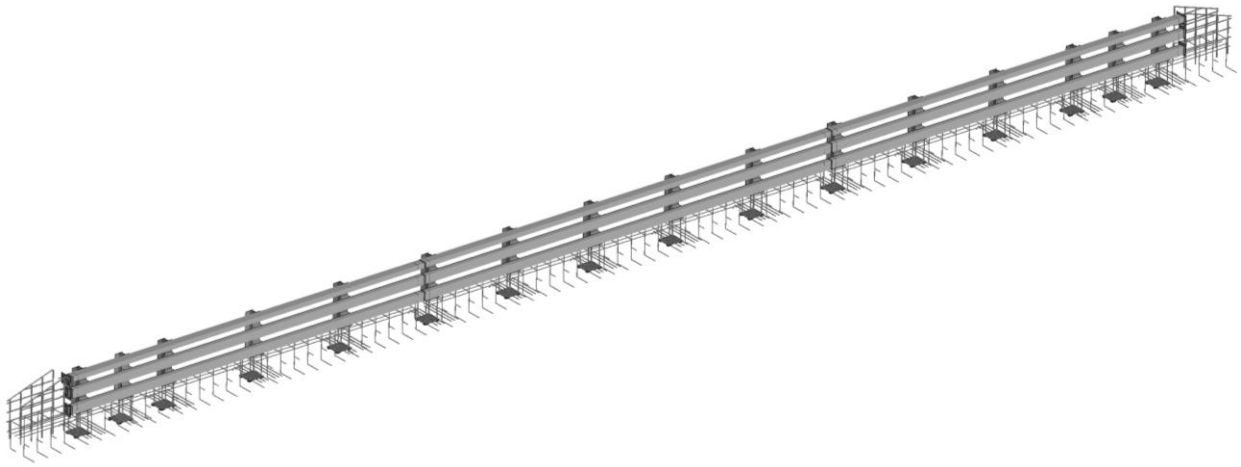


Figure 3.8: Steel reinforcement bars in the concrete foundation and end parapets of the Oregon Rail.

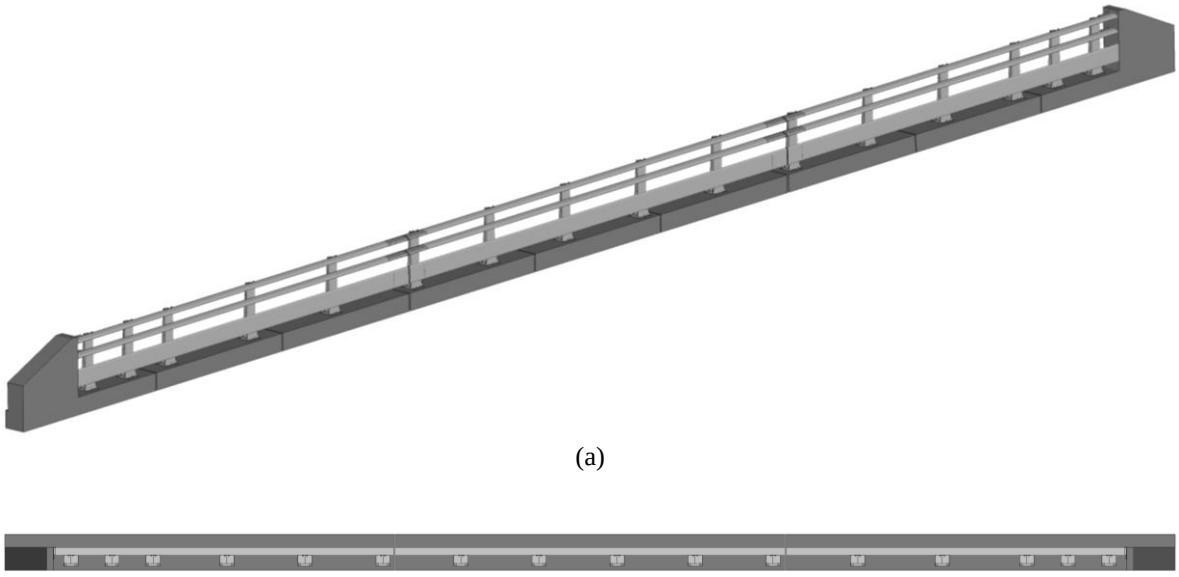
The FE model of the Oregon Rail had a total of 625 components that were discretized into 5,717,298 nodes and 5,497,546 elements (4,877,668 solid, 580,709 shell, 38,997 beams, and 172 discrete elements). Seven constitutive models were used to model the different components:

- Piecewise linear plasticity model for aluminum rails and brackets.
- CSCM model for concrete foundation.
- Plastic kinematic model for steel reinforcements.
- Elastic spring model for discrete components.
- Rigid model for nuts and washers.
- Null material model for contact purpose definition, and
- Elastic model for road surface.

3.4 Finite Element Modeling of Three-bar Metal Rail

A detailed FE model of the 3BMR was created according to NCDOT specifications to evaluate its performance under MASH TL-2 and TL-3 conditions. Figure 3.9 shows the FE model of a 90-ft (27.4-m) section of the 3BMR that were composed of three 30-ft (9.14-m) sections separated by two expansion joints.

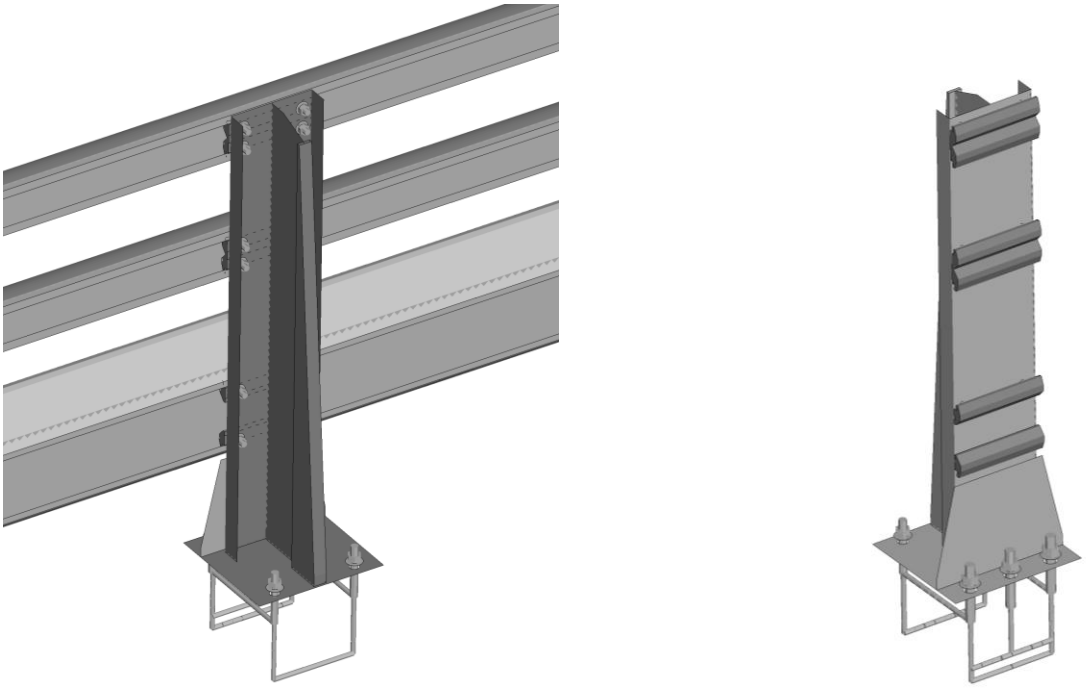
Each section of the 3BMR consisted of three horizontal rails (top, middle, and bottom rails) that were constrained to aluminum posts. The post of the 3BMR, as shown in Figure 3.10, was composed of a T-shaped front post and a rear trapezoidal solid support, both constrained together and welded to the base plate. Three pairs of standard clamping bars were constrained to the T-shaped front post by twelve ø-0.5" bolts and nuts. Three ø-0.75" and two ø-0.625" bolts were used to fix the post plate to the concrete foundation. These bolts were tied with wire struts below the base plate to form the anchor assembly. The actual posts could be made of either Aluminum alloy 6061-T6 or galvanized steel. In the FE model of this project, Aluminum alloy 6061-T6 was selected as the material of the posts. Bolts, nuts, and washers as well as reinforcement bars were modeled as carbon steels. The modeling of bolt-and-nut fastening mechanism was the same as that in the 2BMR system.



(a)

(b)

Figure 3.9: Finite element model of the Three-bar Metal Rail.
(a) Isometric view; and (b) top view.



(a) (b)

Figure 3.10: Post assembly of the 3BMR.
(a) Backside view; and (b) front view.

Figure 3.11 shows the cross-sectional profiles of three horizontal rails, which were all meshed with shell elements. The top and middle rails were the same oval cross-section and the bottom rail had a trapezoidal cross-section with round corners. Expansion bars were used to connect two adjacent rail sections, as shown in Figure 3.12, to maintain structural integrity along the entire span of the bridge rail.

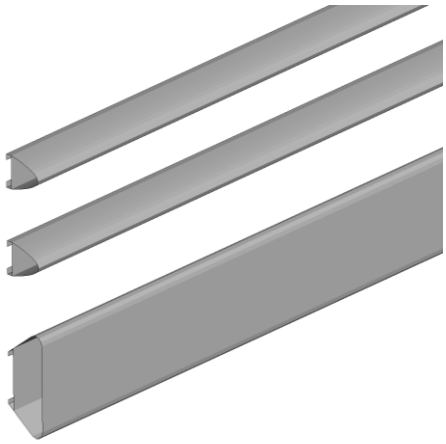


Figure 3.11: Cross-sectional profiles of aluminum rails of the 3BMR.

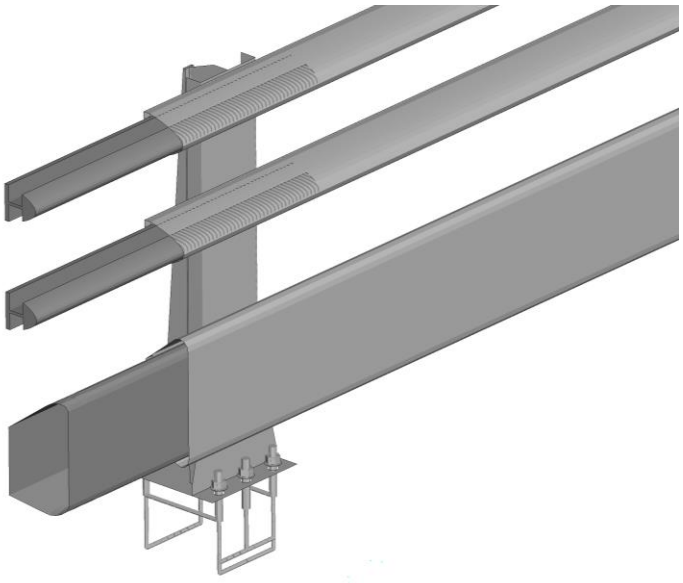


Figure 3.12: Close-up view of expansion bars at the expansion joint of the 3BMR.

At each terminal, the aluminum rails were fastened to the end concrete parapet by brackets and bolt-and-nut connections, as shown in Figure 3.13. Four bolts and nuts were used to fasten each bracket to the back of the rail, and the bracket is fastened to the end parapet using one or two bolt connections with a hook insert to provide enhanced constraint. All these brackets were modeled using shell elements.

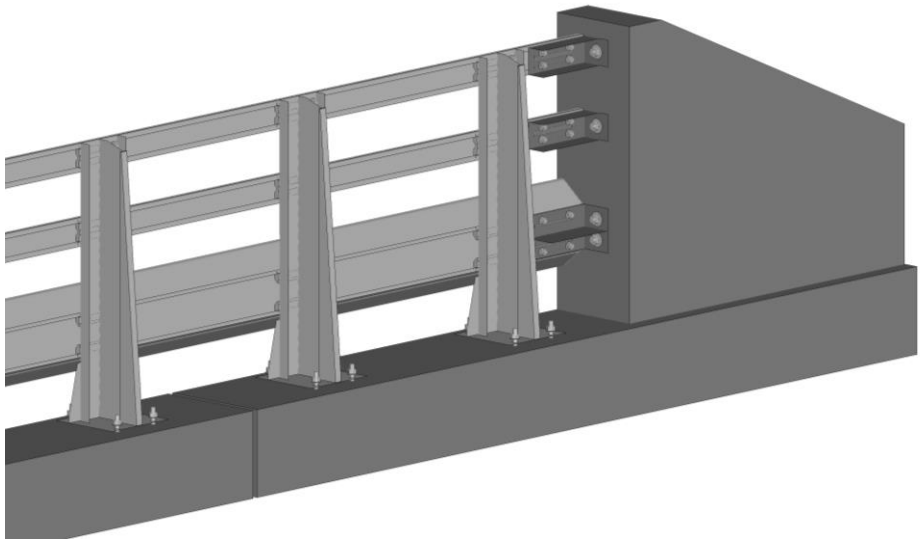


Figure 3.13: Close-up view of rail connections at the terminal of the 3BMR.

The steel reinforcement bars inside the end concrete parapets were modeled in the FE model of the 3BMR, as shown by the detailed view in Figure 3.14. The steel reinforcement bars inside the concrete foundation were not modeled in the simulations under TL-2 conditions due to the anticipated low impact severity; however, they were explicitly modeled using beam elements in the FE models for simulations under TL-3 conditions, as shown in Figure 3.15. The FE models without steel reinforcement in the concrete foundation were also used in TL-3 simulations to compare with those with full steel reinforcement in the concrete foundation.

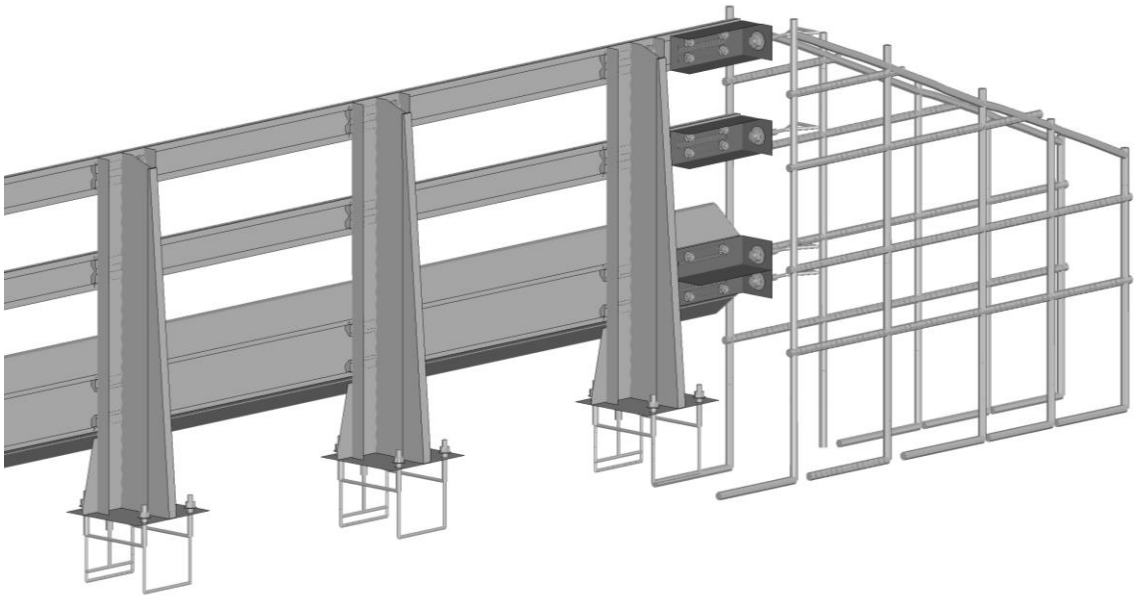


Figure 3.14: Steel reinforcement bars in the end parapet of the 3BMR.

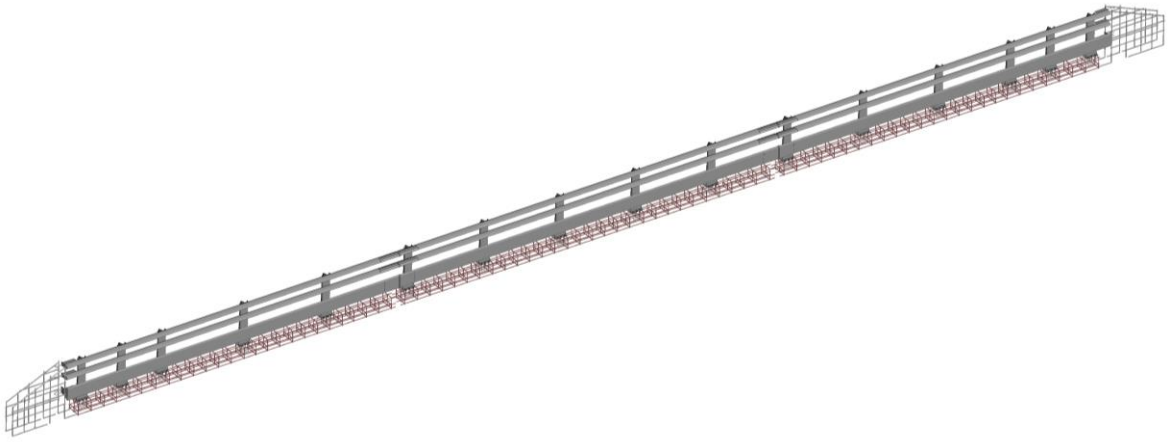


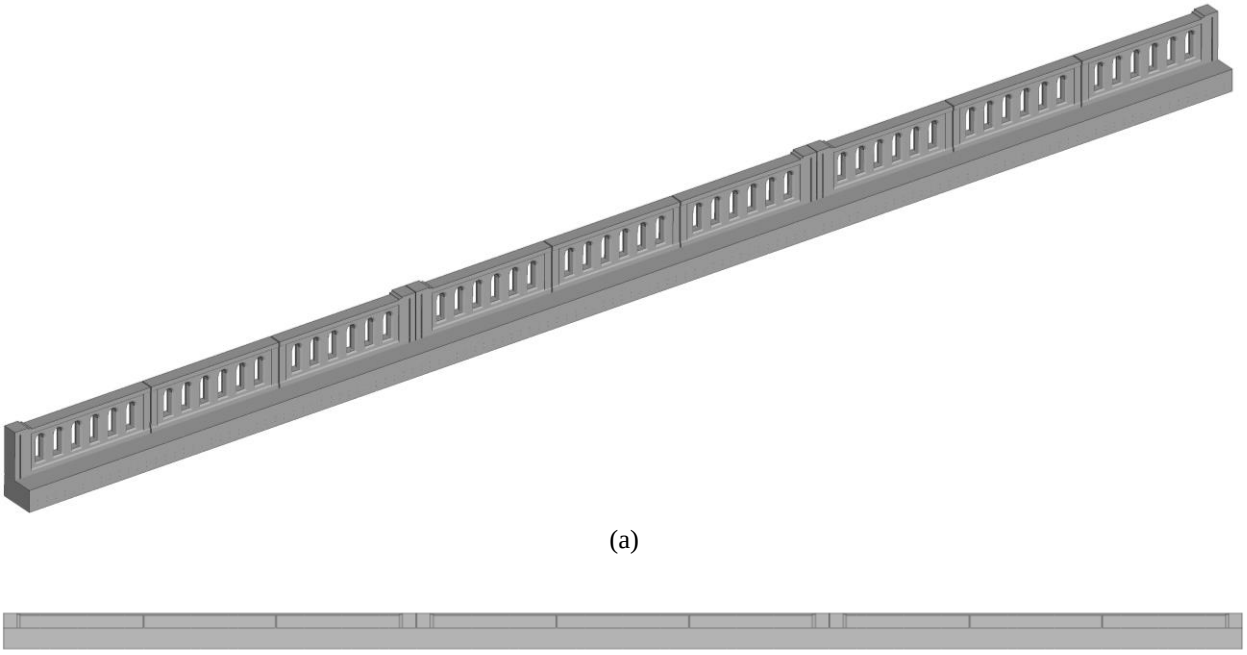
Figure 3.15: Steel reinforcement bars inside the concrete foundation of the 3BMR.

The FE model of the 3BMR had a total of 1,530 components that were discretized into 1,244,441 nodes and 1,111,527 elements (680,653 solid, 416,056 shell, 14,514 beams, and 304 discrete elements). Seven constitutive models were used for the different materials in the bridge rail, including:

- Piecewise linear plasticity model for aluminum rails and brackets,
- CSCM model for concrete foundation,
- Plastic kinematic model for steel reinforcements,
- Elastic spring model for discrete components,
- Rigid model for nuts and washers
- Null material model for contact purpose definition, and
- Elastic model for road surface.

3.5 Finite Element Modeling of Classic Rail

The FE model of Classic Rail (known as Traffic Railing Type C411) was developed to evaluate its safety performance under MASH TL-2 and TL-3 conditions. It should be noted that the Classic Rail has been successfully crashed tested under MASH TL-2 conditions. The evaluation under MASH TL-3 conditions would provide insights on its performance limit. Figure 3.16 shows the FE model of a 90-ft (27.4-m) Classic Rail that had a nominal height of 42 inches (1.07 m) and was consisted of three 30-ft (9.14-m) sections separated by two expansion joints. Each section was composed by three subsections separated by span pilasters. On each subsection, an 8-inch (203-mm) wide window was periodically placed at a 10-inch (254-mm) spacing (see Figure 3.17). A 1.5-inch (38-mm) chamfer was designed along the edge of window to provide smooth transition and a one-inch reinforcement draft was built on the side surface of the window. The main concrete body of Classic Rail were modeled using solid elements with average element size of one inch. The steel reinforcement bars were modeled using beam elements that shared nodes with the solid elements of the concrete. Figure 3.18 shows the detailed reinforcement bars inside the concrete bridge rail.



(a)

(b)

Figure 3.16: Finite element model of a 90-ft Classic Rail.
(a) Isometric view; and (b) top view.

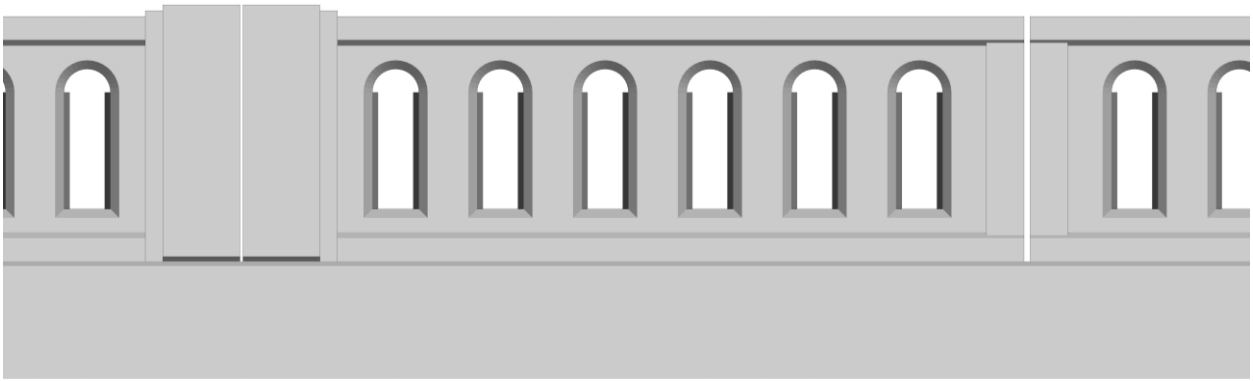


Figure 3.17: Close-up view of a subsection of the Classic Rail.

The FE model of the Classic Rail had a total of 1,630,233 nodes and 1,530,189 elements (1,488,450 solid, 1 shell, and 41,738 beam elements). The Flanagan-Belytschko stiffness form hourglass control was used on solid elements that could potentially experience large deformations. Three different constitutive material models were used, including

- CSCM model for concrete material,
- Plastic kinematic model for the steel reinforcement bars, and
- Elastic model for the road surface.

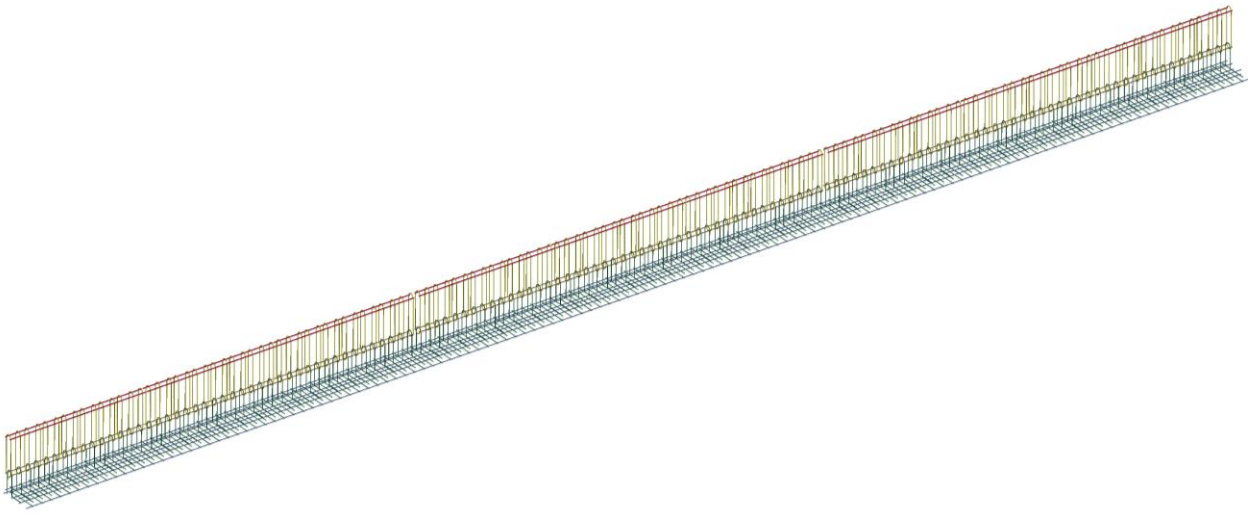


Figure 3.18: Steel reinforcement bars inside the Classic Rail.

3.6 Simulation Setup

3.6.1 2BMR under MASH TL-3 conditions

In the FE simulations for 2BMR, the bridge rail model was combined with each model of the three test vehicles to perform crash simulations. Note that two 2270P vehicle, a 2007 and a 2014 Chevy Silverado pickup truck, were used in the simulations to compare vehicular responses and further validate the vehicle models. Two impact locations were considered to determine the CIP: (1) at a specified distance by MASH from a reference expansion splice, and (2) at a specified distance from a reference post near an expansion splice. For the 2010 Toyota Yaris, the two reference points of the CIPs were at the mid-point of splice #2 and at the mid-point of the aluminum post closest to splice #2, respectively (see Figure 3.19). For the 2007 and 2014 Chevy Silverado models, the two reference points of the CIPs were at the mid-point of splice #2 and at the mid-point of the aluminum post closest to splice #1, respectively. Figure 3.20 shows the full models for the three impact cases with posts as the reference points. The other three simulation models were similar except for using different reference points. In all the simulations, the vehicles impacted the 2BMR section at a speed of 62 mph (100 km/h) and a 25-degree angle. Table 3.2 give a summary of all the impact cases along with the impact conditions.

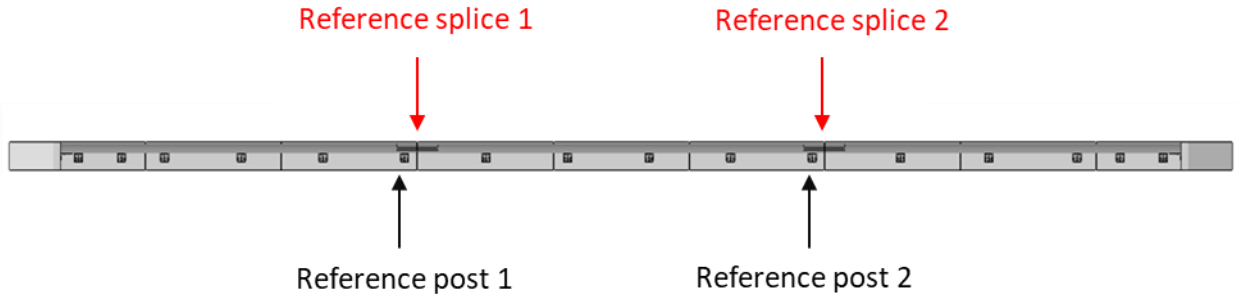
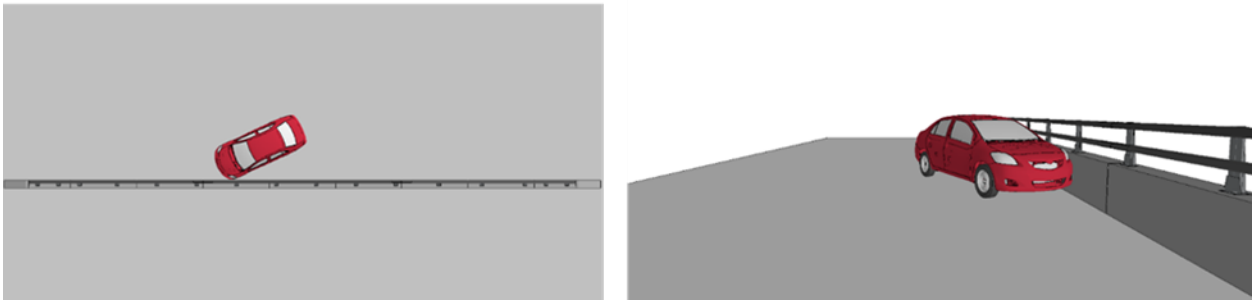
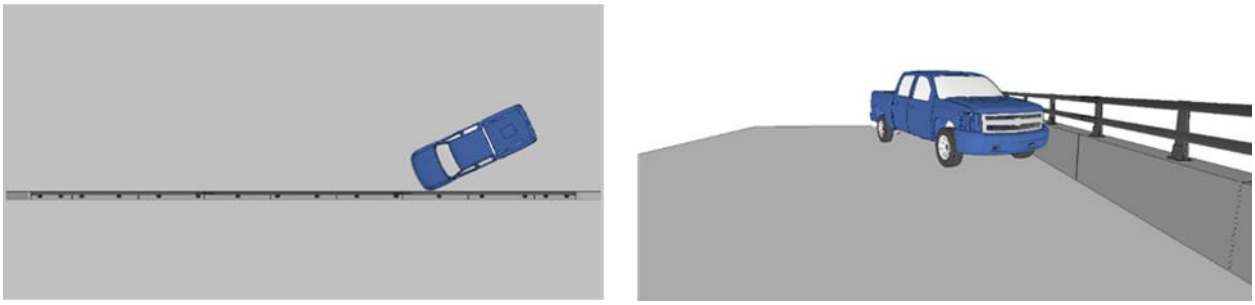


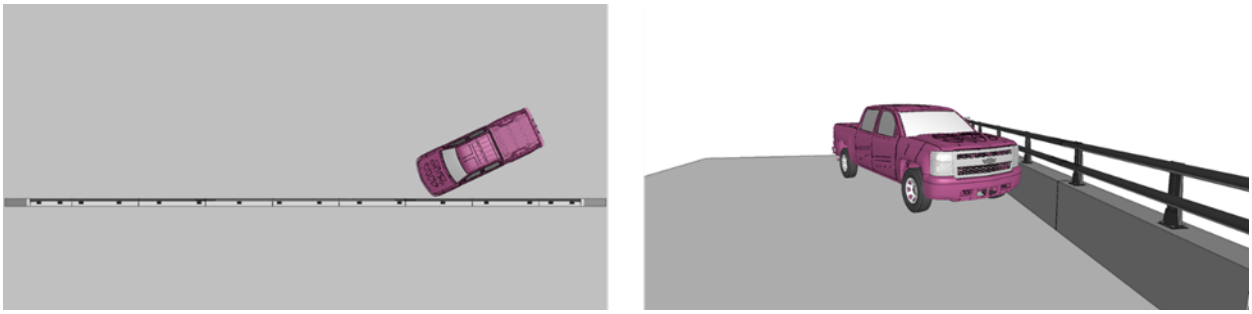
Figure 3.19: Reference posts and expansion splices for impact locations on the 2BMR.



(a)



(b)



(c)

Figure 3.20: Full simulation models for the three impact cases with posts as the reference points. (a) 2010 Toyota Yaris; (b) 2007 Chevy Silverado; and (c) 2014 Chevy Silverado.

Table 3.2: Simulation matrix for Two-bar Metal Rail under MASH TL-3 conditions.

Test Vehicle	Impact Location	Impact Speed	Impact Angle
2010 Toyota Yaris	Post as reference point Expansion splice as reference point	62 mph (100km/h)	25°
2007 Chevy Silverado	Post as reference point Expansion splice as reference point	62 mph (100km/h)	25°
2014 Chevy Silverado	Post as reference point Expansion splice as reference point	62 mph (100km/h)	25°

3.6.2 The Oregon Rail under MASH TL-4 conditions

The safety performance of the Oregon Rail was evaluated under MASH TL-4 conditions, which involved four test vehicles: a 2010 Toyota Yaris, a 2007 Chevy Silverado, a 2014 Chevy Silverado, and a 1996 Ford F800. Two reference points were used to determine the CIPs: the expansion joint and a post closest to the expansion joint, as shown in Figure 3.21. A total of eight crash simulations were required for the Oregon Rail and the simulation matrix is given in Table 3.3. Figure 3.22 shows the full simulation models of the four impact cases using the expansion joint as the reference point.

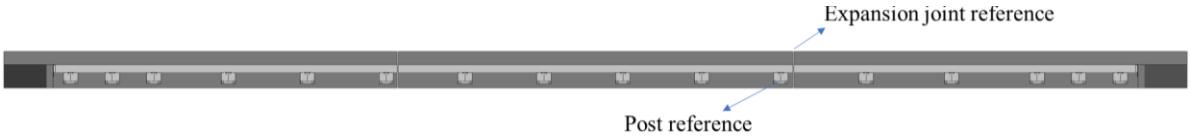


Figure 3.21: Reference points for the CIPs on the Oregon Rail.

Table 3.3: Simulation matrix for the Oregon Rail under MASH TL-4 conditions.

Test vehicle	Impact speed	Impact angle	Reference distance for CIP	Reference point for CIP
2010 Toyota Yaris	62 mph (100 km/h)	25°	3.6 ft (1.1 m)	Expansion joint Post
2007 Chevy Silverado	62 mph (100 km/h)	25°	4.3 ft (1.3 m)	Expansion joint Post
2014 Chevy Silverado	62 mph (100 km/h)	25°	4.3 ft (1.3 m)	Expansion joint Post
1996 Ford F800	56 mph (90 km/h)	25°	5.0 ft (1.5 m)	Expansion joint Post

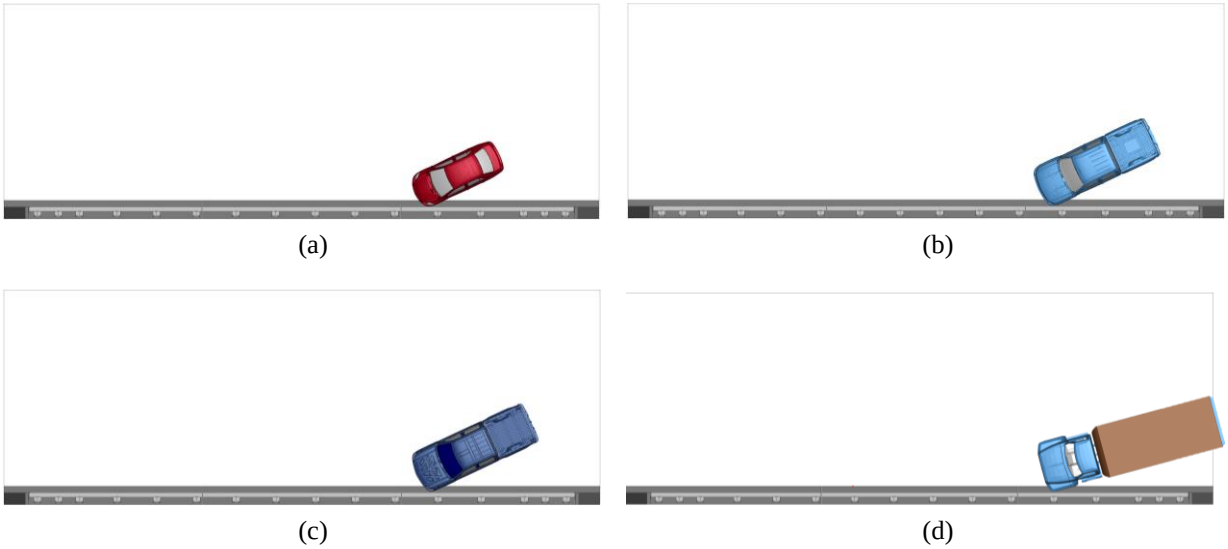


Figure 3.22: Full simulation models for the Oregon Rail using expansion joints as the reference points. (a) 2010 Toyota Yairs; (b) 2007 Chevy Silverado; (c) 2014 Chevy Silverado; and (d) 1996 Ford F800.

3.6.3 3BMR under MASH TL-2 and TL-3 conditions

The 3BMR was evaluated under MASH TL-2 and TL-3 conditions with three test vehicles: a 2010 Toyota Yaris, a 2007 Chevy Silverado, and a 2014 Chevy Silverado. Two reference points for the CIPs were used: the expansion joint and a post closest to the expansion joint, as shown in Figure 3.23.

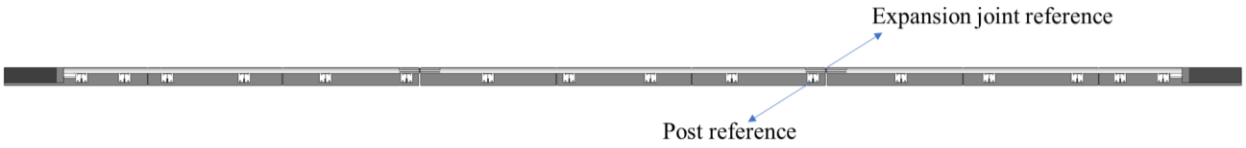


Figure 3.23: Reference points for the CIPs on the 3BMR.

For the 3BMR, two FE models were developed: a simplified model (3BMR-1) without modeling the rebars in the concrete foundation, and a full model (3BMR-2) with rebars in the concrete foundation (based on the 3BMR design specifications). The 3BMR-1 model was developed to reduce the computational cost, but it was shown to work only under MASH TL-2 conditions (no significant failure in the concrete foundation) and did not work well under MASH TL-3 conditions (due to unrealistic concrete failure, see section 3.6.3.2 for details). Therefore, the 3BMR-2 model was also used to determine the performance of 3BMR under MASH TL-3 conditions. It should be noted that since the 3BMR-2 model is the full model, it can be used in simulations at both MASH TL-2 and TL-3 conditions, while the 3BMR-1 model is only appropriate for simulations under MASH TL-2 conditions where no significant concrete failure would occur due to the low impact severity. For the 3BMR, a total of 18 simulations were performed and the simulation cases were divided into three groups as follows.

1. 3BMR under TL-2 conditions using the 3BMR-1 model,
2. 3BMR under TL-3 conditions using the 3BMR-1 model, and
3. 3BMR under TL-3 conditions using the 3BMR-2 model.

Each group consisted of six simulation cases and the simulation conditions were summarized in Tables 3.4, 3.5, and 3.6. Figure 3.24 shows the model setups for the three cases of Group 1 using expansion joint as the reference point. All other cases were similar to the cases of Group 1 except for the impact velocities and/or reference points and CIPs.

Table 3.4: Group 1 cases: TL-2 conditions with reinforcement bars only in end parapets.

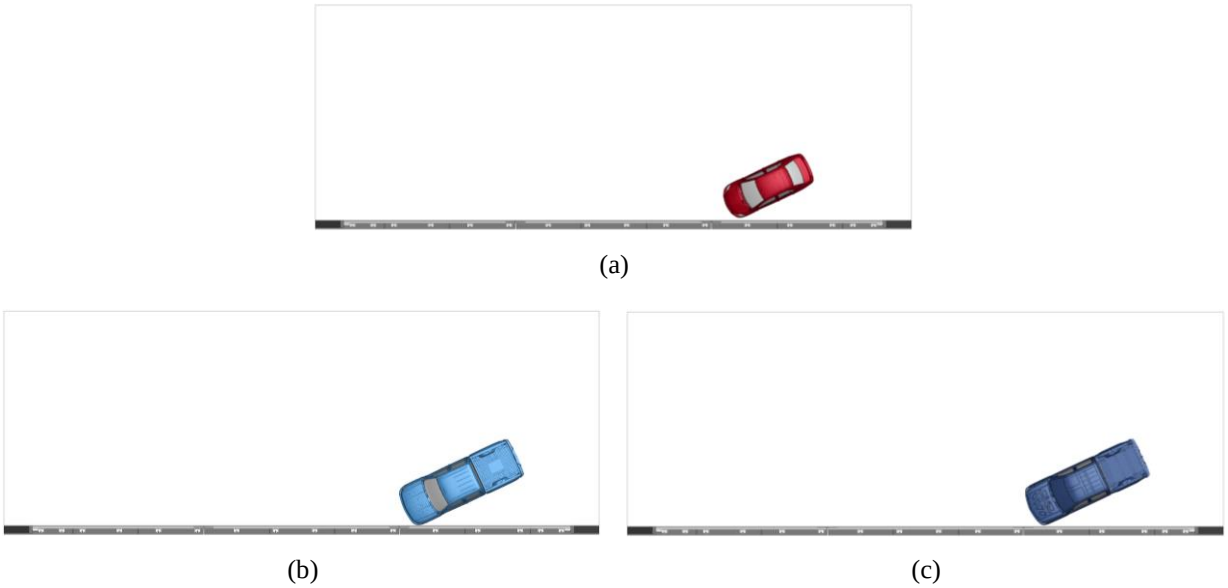
Test vehicle	Impact speed	Impact angle	Reference distance for CIP	Reference point for CIP
2010 Toyota Yaris	44 mph (70 km/h)	25°	3.3 ft (1.0 m)	Expansion joint Post
2007 Chevy Silverado	44 mph (70 km/h)	25°	2.6 ft (0.8 m)	Expansion joint Post
2014 Chevy Silverado	44 mph (70 km/h)	25°	2.6 ft (0.8 m)	Expansion joint Post

Table 3.5: Group 2 cases: TL-3 conditions with reinforcement bars only in end parapets.

Test vehicle	Impact speed	Impact angle	Reference distance for CIP	Reference point for CIP
2010 Toyota Yaris	62 mph (100 km/h)	25°	3.6 ft (1.1 m)	Expansion joint Post
2007 Chevy Silverado	62 mph (100 km/h)	25°	4.3 ft (1.3 m)	Expansion joint Post
2014 Chevy Silverado	62 mph (100 km/h)	25°	4.3 ft (1.3m)	Expansion joint Post

Table 3.6: Group 3 cases: TL-3 conditions with reinforcement bars in end parapets and foundation.

Test vehicle	Impact speed	Impact angle	Reference distance for CIP	Reference point for CIP
2010 Toyota Yaris	62 mph (100 km/h)	25°	3.6 ft (1.1 m)	Expansion joint Post
2007 Chevy Silverado	62 mph (100 km/h)	25°	4.3 ft (1.3 m)	Expansion joint Post
2014 Chevy Silverado	62 mph (100 km/h)	25°	4.3 ft (1.3m)	Expansion joint Post



(a)

(b) (c)

Figure 3.24: Full simulation models for Group 1 simulations using expansion joint as reference point. (a) 2010 Toyota Yaris; (b) 2007 Chevy Silverado; and (c) 2014 Chevy Silverado.

3.6.4 Classic Rail under MASH TL-2 and TL-3 conditions

The Classic Rail was evaluated under MASH TL-2 and TL-3 conditions with three test vehicles: a 2010 Toyota Yaris, a 2007 and a 2014 Chevy Silverado. The reference point of the CIPs for both

the passenger car and pickup trucks was at the expansion joint. Tables 3.7 and 3.8 give the simulation cases for the Classic Rail under MASH TL-2 and TL-3 conditions, respectively. Figure 3.25 shows the model setups for the three cases under MASH TL-2 conditions. Model setup for the cases under MASH TL-3 conditions was the same as those shown in Figure 3.25 except for the impact velocity and distances of the CIPs from the reference point.

Table 3.7: Simulation cases for Classic Rail under TL-2 conditions.

Test vehicle	Impact speed	Impact angle	Reference distance for CIP
2010 Toyota Yaris	44 mph (70 km/h)	25°	3.3 ft (1.0 m)
2007 Chevy Silverado	44 mph (70 km/h)	25°	2.6 ft (0.8 m)
2014 Chevy Silverado	44 mph (70 km/h)	25°	2.6 ft (0.8 m)

Table 3.8: Simulation cases for Classic Rail under TL-3 conditions.

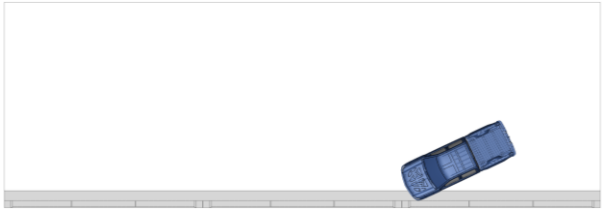
Test vehicle	Impact speed	Impact angle	Reference distance for CIP
2010 Toyota Yaris	62 mph (100 km/h)	25°	3.6 ft (1.1 m)
2007 Chevy Silverado	62 mph (100 km/h)	25°	4.3 ft (1.3 m)
2014 Chevy Silverado	62 mph (100 km/h)	25°	4.3 ft (1.3 m)



(a)



(b)



(c)

Figure 3.25: Full simulation models for simulations of Classic Rail under MASH TL-2 conditions. (a) 2010 Toyota Yaris; (b) 2007 Chevy Silverado; and (c) 2014 Chevy Silverado.

4. Simulation Results and Analysis

The performance of the four bridge rails were evaluated on structural adequacy, occupant risk, and post-impact trajectory of the test vehicle. The structural adequacy was assessed using MASH evaluation criterion *A*, which requires a barrier to contain and redirect the vehicles. In addition, the vehicle should not override, underride or penetrate the barrier. Occupant risk was assessed using MASH evaluation criteria *D*, *F*, *H*, *I* and *N*. MASH evaluation criterion *D* specifies that debris from the barrier as a result of the crash should not intrude into the occupant compartment or pose hazard to pedestrians. MASH evaluation criterion *F* requires the vehicle to remain upright during the entire impact and not to exceed a maximum of 75° roll and pitch angles. MASH evaluation criteria *H* and *I* specify two occupant risk parameters, Occupant Impact Velocity (OIV) and the Occupant Ridedown Acceleration (ORA), that are calculated in both longitudinal and lateral directions. According to MASH, the preferred and acceptable limits for OIV are 9.1 m/s and 12.20 m/s, respectively, and the preferred and acceptable limits for ORA are 15.0 G and 20.49 G, respectively.

The post-impact trajectory of an impacting vehicle can be evaluated to determine the possibility of the vehicle getting involved in a secondary collision with other vehicles. Excessive pocketing or snagging of the vehicle into the barrier could lead to unsafe post-impact trajectories such as spinouts or large exit angles. Ideally, the barrier should contain and smoothly redirect the vehicle without any penetration of the vehicle behind the barrier. In this study, the MASH exit box criterion *N* was used to assess the post-impact responses of the vehicles. The exit box is defined as a rectangle with its length parallel to the traffic side of the barrier and starting at the final point of contact of the wheel track with the initial, undeformed face of the barrier. Figure 4.1 gives a graphical illustration of the exit box and exit angle. Table 4.1 gives the dimensions of exit boxes for the 2010 Toyota Yaris, 2007 Chevy Silverado, 2014 Chevy Silverado, and 1996 Ford F800. According to MASH, dimension "*A*" is calculated using the length (V_L) and width (V_W) of the vehicle and dimension "*B*" has a fixed length for a given type of vehicle, i.e., a small car, pickup truck, or single-unit truck. The exit box criterion is satisfied if the vehicle's wheel tracks are within the exit box before the vehicle pass through the entire length of the exit box. In addition to the exit box criterion, the longitudinal and lateral accelerations were also obtained from the accelerometer placed at the vehicle's CG point and filtered using an SAE Class 60 filter.

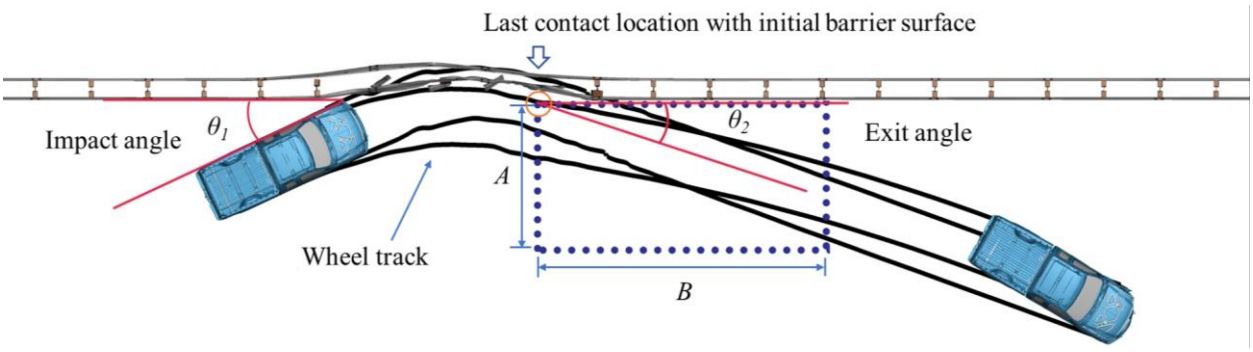


Figure 4.1: Illustration of the MASH exit box criterion.

Table 4.1: Dimensions of exit boxes for test vehicles based on MASH specifications.

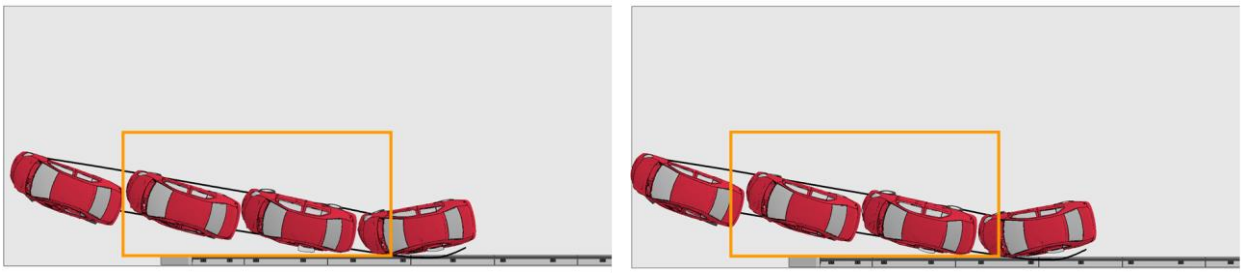
Vehicle type	Dimension of exit box	
	A	*B*
2010 Toyota Yaris	(7.2 + V_W + 0.16V_L) ft = 15.02 ft (4.58 m)	32.8 ft (10 m)
2007 Chevy Silverado	(7.2 + V_W + 0.16V_L) ft = 16.92 ft (5.16 m)	32.8 ft (10 m)
2014 Chevy Silverado	(7.2 + V_W + 0.16V_L) ft = 16.92 ft (5.16 m)	32.8 ft (10 m)
1996 Ford F800	(14.4 + V_W + 0.16V_L) ft = 26.93 ft (8.21 m)	65.6 ft (20 m)

4.1 Evaluation of NC Two-bar Metal Rail under MASH TL-3 Conditions

The FE simulations for the 2BMR included six impact cases, with three impacting vehicles and two impact locations. The two impact locations for the 1100C vehicle were at 54.5 ft (1.39 m) from the expansion splice and from the post closest to the expansion splice. The impact locations for the two 2270P vehicles were at 61.1 ft (1.6 m) from the expansion splice and from the post closest to the expansion splice. It should be noted that in the full-scale crash tests of the 2BMR, only the posts closest to the expansion splices were used to determine the impact location. Therefore, only the simulation results with the same impact locations were compared to test data. Note that in the full-scale crash tests, the 1100C vehicle was a 2010 Hyundai Accent and the 2270P vehicle was a 2015 Chevy Silverado. These are different makes and/or years from the vehicles used in the simulations. Although vehicles in the simulations had similar sizes and structures to their respective ones in the actual crash tests, some discrepancies would be expected and acceptable in the comparison. The focus of the comparison was on the overall vehicular responses and bridge rail deformations and damages.

4.1.1 The 2BMR Impacted by 2010 Toyota Yaris

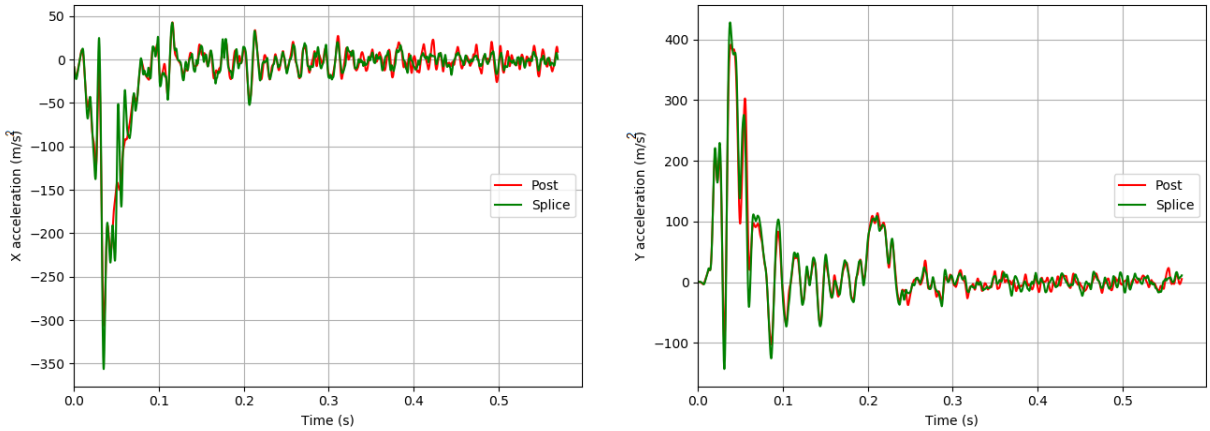
Figure 4.2 shows the top-view vehicle trajectories of the 2010 Toyota Yaris impacting the 2BMR at 62 mph (100 km/h) and a 25° impact angle. Tire tracks of the vehicle and the exit box were also shown in the figure. For both impact cases, the vehicle was redirected by the bridge rail with small exit angles and passed the MASH exit box criterion. The post-impact trajectories of the vehicle in both cases were considered as safe redirections.



(a) (b)

Figure 4.2: Vehicle trajectories of 2010 Toyota Yaris impacting the 2BMR.
(a) With expansion splice as reference; and (b) with the post as reference.

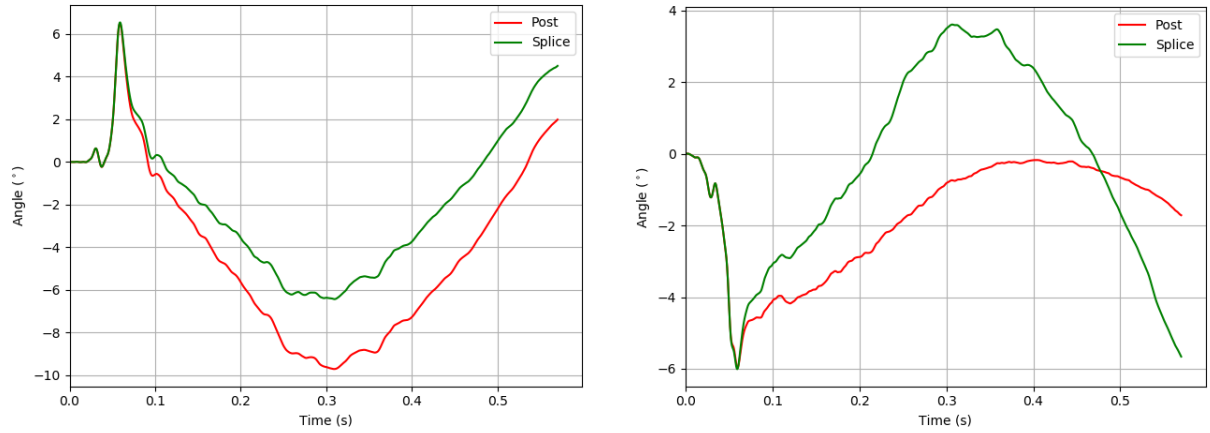
Figure 4.3 shows the time histories of vehicle accelerations in both longitudinal and lateral directions. No significant difference in vehicle accelerations was observed between the two impact locations.



(a) (b)

Figure 4.3: Time histories of accelerations of 2010 Toyota Yaris impacting the 2BMR.
(a) Longitudinal direction; and (b) lateral direction.

Figure 4.4 shows the time history of the vehicle's row and pitch angles. The maximum roll angles for the two impact cases were 6.4° and 9.5°, and the maximum pitch angles were 6.0° for both impact cases. In both cases, the 2BMR passed the MASH evaluation criterion *F*, which specified a maximum 75° roll and pitch angles.



(a) (b)

Figure 4.4: Time histories of angular motions of 2010 Toyota Yaris impacting the 2BMR.
(a) Roll angle; and (b) pitch angle.

The occupant safety factors, i.e., the OIVs and ORAs, were calculated using the time histories of vehicle accelerations in both longitudinal and lateral directions. The OIV and ORA values for both

impact cases are summarized in Tables 4.2 and 4.3, along with the vehicle's roll, pitch, and exit angles. It can be seen from the results that all the OIV and ORA values were below the limit values specified in MASH. Note that the OIV and ORA values were even lower than the preferred values suggested by MASH, i.e., 9.1 m/s for OIVs and 15.0G for ORAs. Based on the simulation results, the 2BMR passed all the MASH evaluation criteria under impacts by the 2010 Toyota Yaris at the two impact locations.

Table 4.2: Evaluation factors of 2BMR impacted by 2010 Toyota Yaris with expansion splice as reference.

Criteria	MASH criterion *H*		MASH criterion *I*		MASH criterion *F*		MASH criterion *N*
Factors	OIV_x	OIV_y	ORA_x	ORA_y	Max roll angle	Max pitch angle	Exit angle
Value	7.32 m/s	9.84 m/s	2.01G	10.58G	6.4°	6.0°	6.8°
Limit	12.2 m/s	12.2 m/s	20.49G	20.49G	75°	75°	/
Evaluation	Pass	Pass	Pass	Pass	Pass	Pass	Pass

Table 4.3: Evaluation factors of 2BMR impacted by 2010 Toyota Yaris with post as reference.

Criteria	MASH criterion *H*		MASH criterion *I*		MASH criterion *F*		MASH criterion *N*
Factors	OIV_x	OIV_y	ORA_x	ORA_y	Max roll angle	Max pitch angle	Exit angle
Value	7.33 m/s	9.84 m/s	2.31G	10.25G	9.5°	6.0°	6.1°
Limit	12.2 m/s	12.2 m/s	20.49G	20.49G	75°	75°	/
Evaluation	Pass	Pass	Pass	Pass	Pass	Pass	Pass

A full-scale crash test was conducted on the 2BMR using a 2010 Hyundai Accent (1100C) to check its compliance with MASH requirements. The test results were also used to further validate the FE models. Despite the different makes of the test vehicle and simulation model, both vehicles had comparable sizes and body structures. Note that the impact location in the crash test was determined using the post closest to the expansion splice as the reference point; therefore, only the simulation case with the same impact location was compared to test results. Figure 4.5 shows the comparison of the vehicle model with test vehicle in the crash test at six instants during the impact. Both vehicles exhibited similar overall responses.

Figure 4.6 shows the comparison of longitudinal and lateral accelerations from simulation results and test data. Similar trends in the acceleration histories were observed. Figure 4.7 shows the time histories of roll, pitch, and yaw angles from both actual testing and simulation results. The yaw angles from simulation results matched well to test data, indicating similar vehicle responses and redirection characteristics. There were discrepancies between the simulation results and test data on roll and pitch angles. These discrepancies could be caused by structural differences of the two vehicles, particularly the stiffness of suspensions and the types of steering systems, even though both vehicles had similar sizes and masses. Nevertheless, the overall trends of roll and pitch angles from simulation results were similar to those from the actual test.

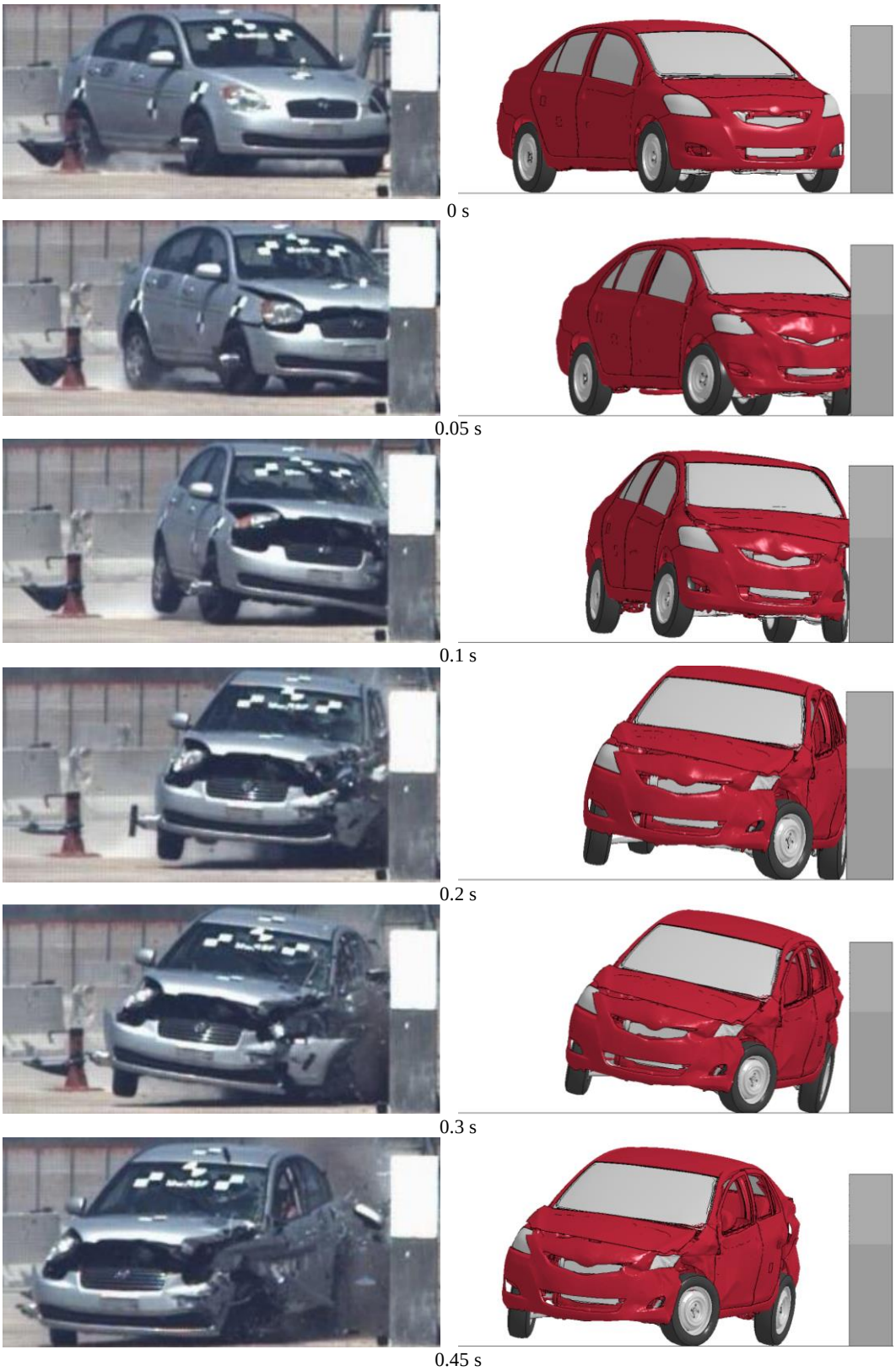
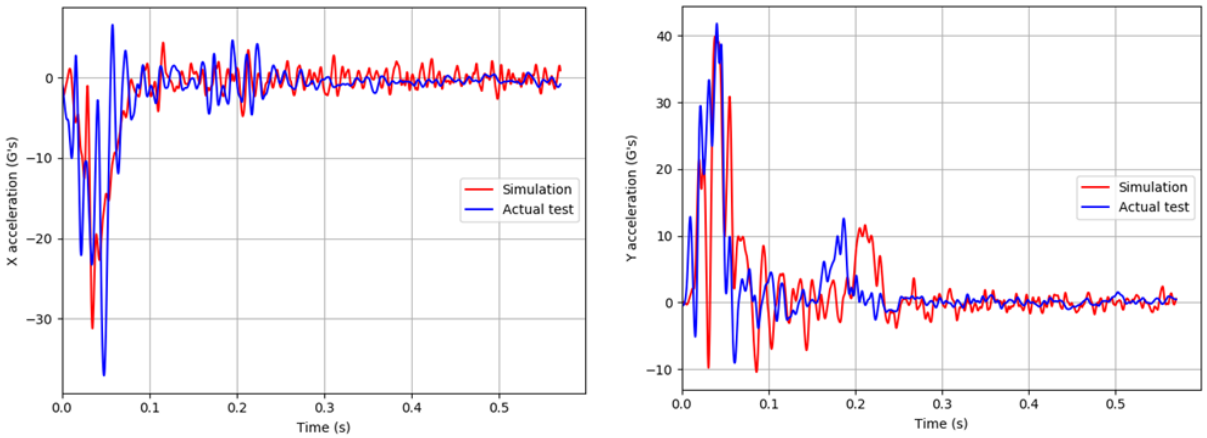
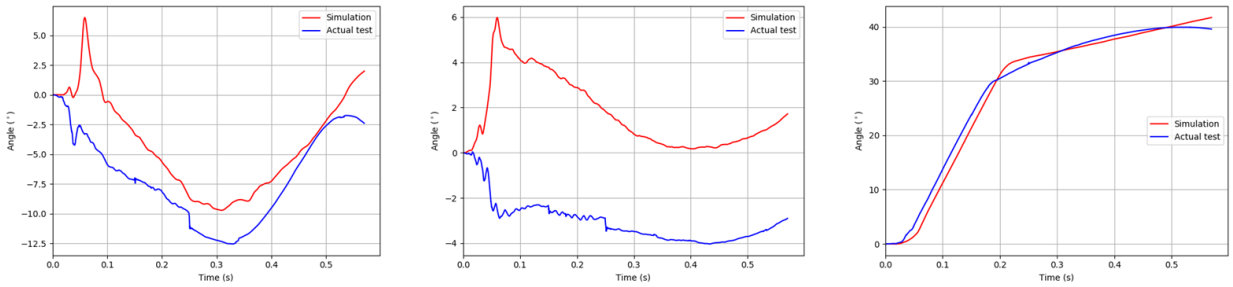


Figure 4.5: Comparison of responses of the 1100C test vehicles impacting the 2BMR (Left: a 2010 Hyundai Assent used in field test. Right: a 2010 Toyota Yaris used in simulation).



(a) (b)

Figure 4.6: Comparison of accelerations of 2010 Hyundai Assent (test) and 2010 Toyota Yaris (model). (a) Longitudinal direction; and (b) lateral direction.



(a) (b) (c)

Figure 4.7: Comparison of angular motions of the 2010 Hyundai Assent (test) and 2010 Toyota Yaris (model). (a) Roll angles; (b) pitch angles; and (c) yaw angles.

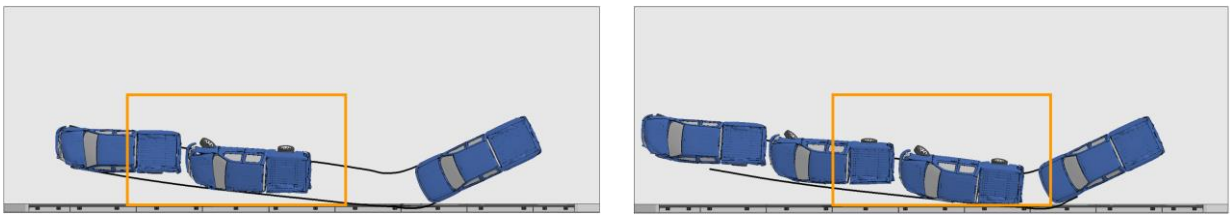
Table 4.4 gives a comparison of occupant safety factors from simulation results and test data for impacts by the 1100C vehicles. Note that in both the simulation and actual test, the impact point was determined using the post closest to the expansion splice as the reference point. The simulation results were shown to agree well with test data. Details of the full-scale crash test using the 1100C test vehicle can be found in the Appendix.

Table 4.4: Comparison of occupant safety factors from simulation and test for impacts by the 1100C vehicles.

Criteria	MASH criterion *H*		MASH criterion *I*	
Factors	OIV_x	OIV_y	ORA_x	ORA_y
Simulation	7.33 m/s	9.84 m/s	2.31G	10.25G
Crash test	7.45 m/s	9.38 m/s	3.65G	10.20G
Difference	1.6%	4.9%	36.7%	0.5%

4.1.2 The 2BMR Impacted by 2007 Chevy Silverado

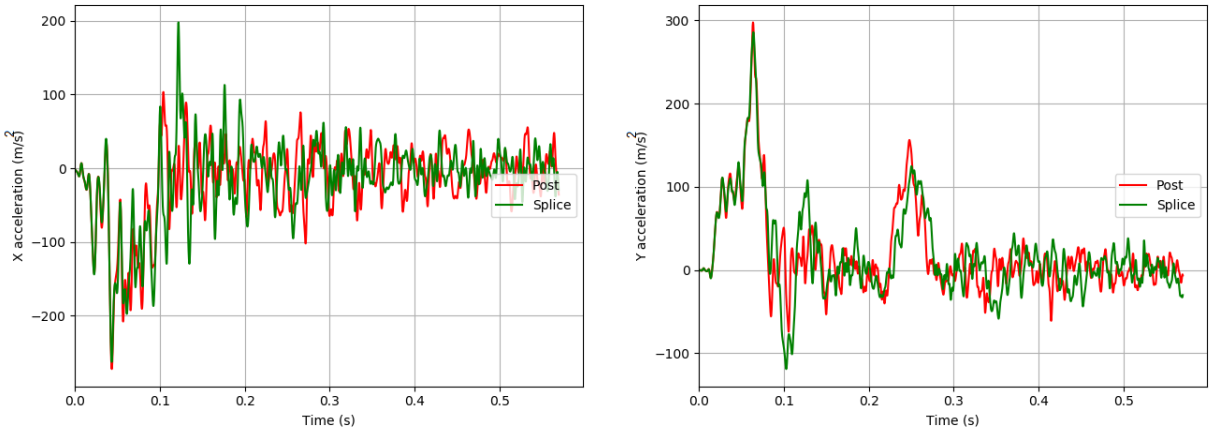
Figure 4.8 shows the top-view vehicle trajectories of the 2007 Chevy Silverado impacting the 2BMR at 62 mph (100 km/h) and a 25° impact angle. Tire tracks of the vehicle and the exit box were also shown in the figure. For both impact cases, the vehicle was redirected by the bridge rail with small exit angles and passed the MASH exit box criterion. The post-impact trajectories of the vehicle in both cases were considered as safe redirections.



(a) (b)

Figure 4.8: Vehicle trajectories of 2007 Chevy Silverado impacting the 2BMR.
(a) With expansion splice as reference; and (b) with the post as reference.

Figure 4.9 shows the time histories of vehicle accelerations in both longitudinal and lateral directions. No significant difference in vehicle accelerations was observed between the two impact locations.



(a) (b)

Figure 4.9: Time histories of accelerations of 2007 Chevy Silverado impacting the 2BMR.
(a) Longitudinal direction; and (b) lateral direction.

Figure 4.10 shows the time history of the vehicle's row and pitch angles. The maximum roll angles for the two impact cases were 24.9° and 23.5°, respectively, and the maximum pitch angles were 8.0° and 8.5°, respectively, for the two impact cases. In both cases, the 2BMR passed the MASH evaluation criterion *F*, which specified a maximum 75° roll and pitch angles.

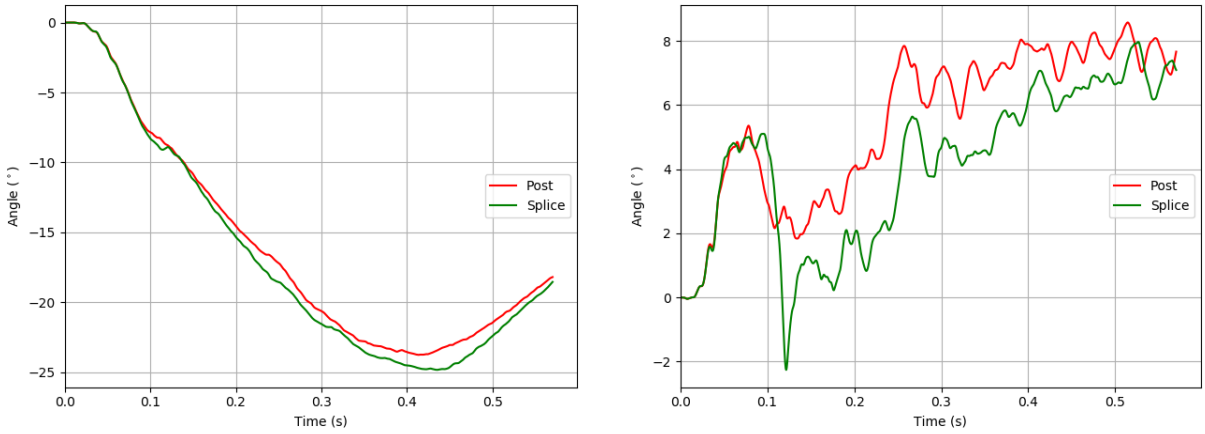


Figure 4.10: Time histories of angular motions of 2007 Chevy Silverado impacting the 2BMR. (a) Roll angle; and (b) pitch angle.

The occupant safety factors, the OIVs and ORAs, were calculated using the time histories of vehicle accelerations in both longitudinal and lateral directions. The OIV and ORA values for both impact cases are summarized in Tables 4.5 and 4.6, along with the vehicle's roll, pitch, and exit angles. It can be seen from the results that all the OIV and ORA values were below the limit values specified in MASH. Note that the OIV and ORA values were even lower than the preferred values suggested by MASH, i.e., 9.1 m/s for OIVs and 15.0G for ORAs. Based on the simulation results, the 2BMR passed all the MASH evaluation criteria under impacts by the 2007 Chevy Silverado at the two impact locations.

Table 4.5: Evaluation factors of 2BMR impacted by 2007 Chevy Silverado with expansion splice as reference.

Criteria	MASH criterion *H*		MASH criterion *I*		MASH criterion *F*		MASH criterion *N*
Factors	OIV_x	OIV_y	ORA_x	ORA_y	Max roll angle	Max pitch angle	Exit angle
Value	8.06 m/s	8.30 m/s	10.31G	11.34G	24.9°	8.0°	6.0°
Limit	12.2 m/s	12.2 m/s	20.49G	20.49G	75°	75°	/
Evaluation	Pass	Pass	Pass	Pass	Pass	Pass	Pass

Table 4.6: Evaluation factors of 2BMR impacted by 2007 Chevy Silverado with post as reference.

Criteria	MASH criterion *H*		MASH criterion *I*		MASH criterion *F*		MASH criterion *N*
Factors	OIV_x	OIV_y	ORA_x	ORA_y	Max roll angle	Max pitch angle	Exit angle
Value	8.21 m/s	7.72 m/s	5.87G	13.26G	23.5°	8.5°	5.9°
Limit	12.2 m/s	12.2 m/s	20.49G	20.49G	75°	75°	/
Evaluation	Pass	Pass	Pass	Pass	Pass	Pass	Pass

A full-scale crash test was conducted on the 2BMR using a 2015 Chevy Silverado (2270P) to check its compliance with MASH requirements. The test results were also used to further validate the FE models. Figure 4.11 shows the comparison of the vehicle model with the test vehicle in crash test at six instants during the impact.

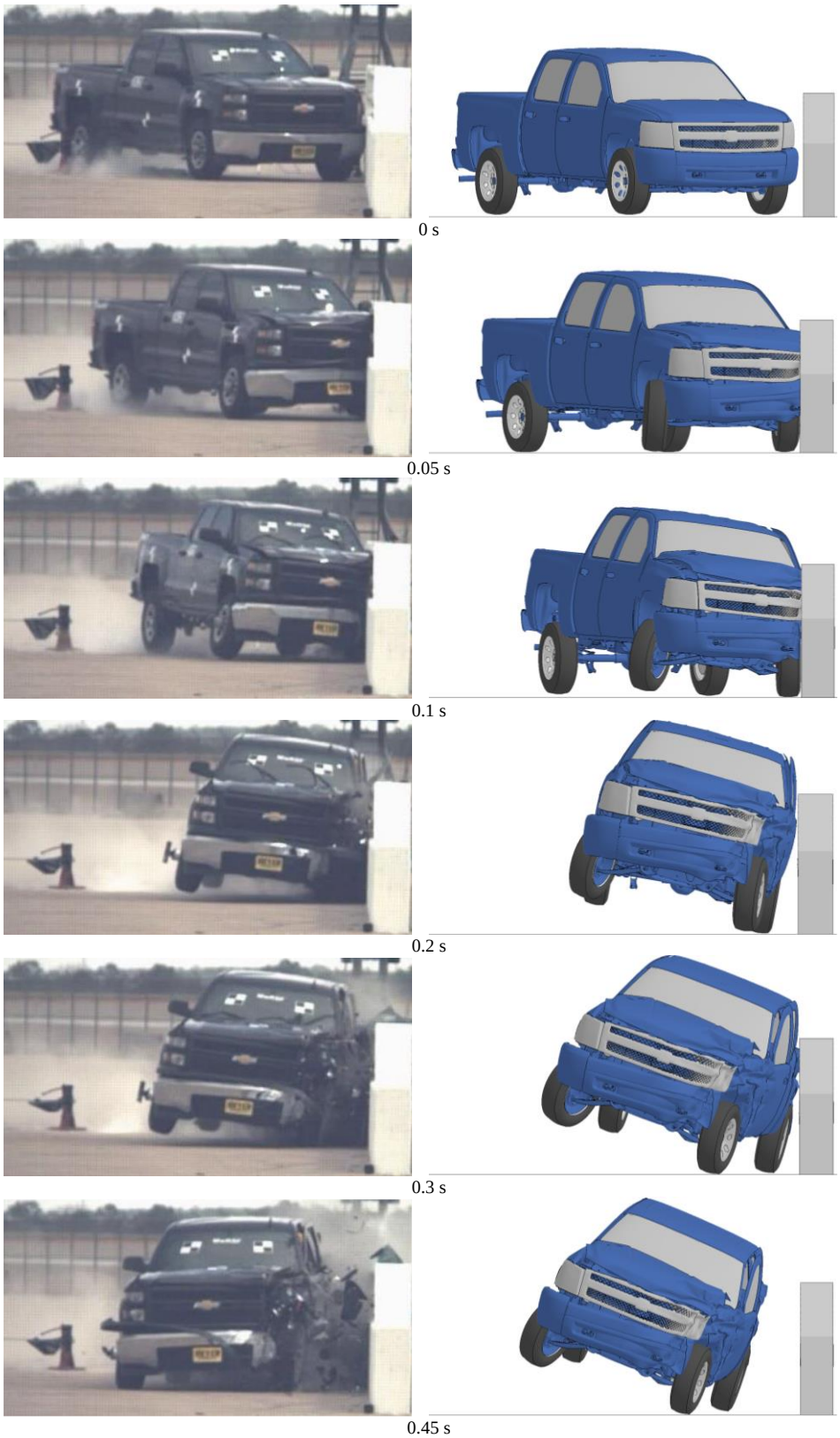
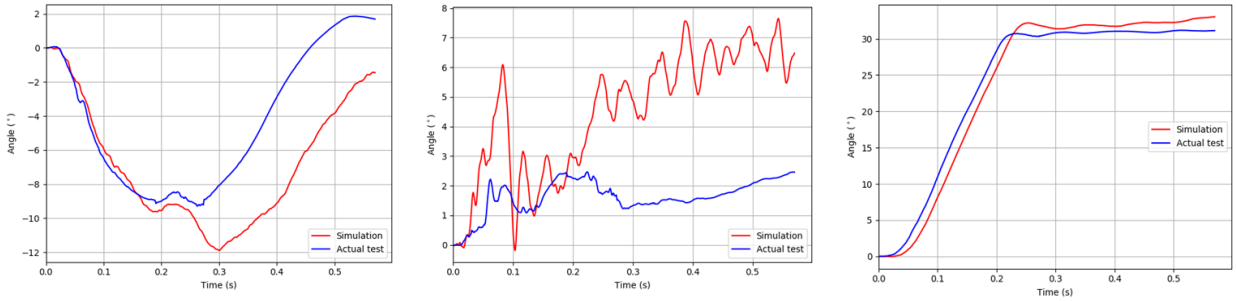


Figure 4.11: Comparison of responses of the 2270P test vehicles impacting the 2BMR (Left: a 2015 Chevy Silverado used in field test. Right: a 2007 Chevy Silverado used in simulation).

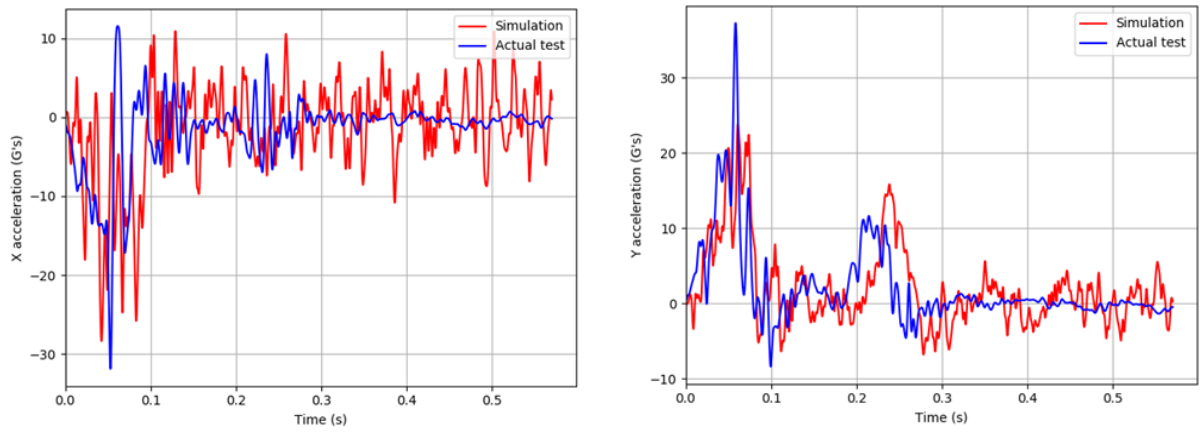
Figure 4.12 shows the time histories of angular motions of the vehicle from simulation results compared to test data. There were some discrepancies in roll and pitch angles between the test vehicle and the simulation model, as shown in Figure 4.12(a) and Figure 4.12(b). This could be caused by the difference in suspension systems and/or other structures due to the different years of the two vehicles as well as simplifications in the modeling work. The maximum roll and pitch angles of the test vehicle in the crash test were all below the 75° limit specified by MASH criterion *F*. Despite the different years of the test vehicle and simulation model, the vehicles exhibited similar redirection characteristics, as seen from the yaw angles in Figure 4.12(c).



(a) (b) (c)

Figure 4.12: Comparison of angular motions of 2015 Chevy Silverado (test) and 2007 Chevy Silverado (model). (a) Roll angles; (b) pitch angles; and (c) yaw angles.

The longitudinal and lateral accelerations from simulation results were compared to test data, as shown in Figure 4.13. The trends of accelerations from simulation results generally matched those from test data in both directions, with some discrepancies in the peak values and noises in the simulation results.



(a) (b)

Figure 4.13: Comparison of accelerations of 2015 Chevy Silverado (test) and 2007 Chevy Silverado (model). (a) Longitudinal direction; and (b) lateral direction.

Table 4.7 gives a comparison of occupant safety factors from simulation results (using the 2007 Chevy Silverado) and test data (using the 2015 Chevy Silverado). Note that in both the simulation and actual test, the impact point was determined using the post closest to the expansion splice as the reference point. Although the discrepancies between simulation results and test data were larger than those for the 1100C vehicles, the occupant safety factors predicted by simulation results were below the MASH limit and preferred values, reaching the same conclusion as the actual test. Details of the full-scale crash test using the 2270P test vehicle can be found in the Appendix.

Table 4.7: Comparison of occupant safety factors from simulation and test for impacts by the 2270P vehicles.

Criteria	MASH criterion *H*		MASH criterion *I*	
Factors	OIV_x	OIV_y	ORA_x	ORA_y
Simulation (2007 Chevy Silverado)	8.21 m/s	7.72 m/s	5.87G	13.26G
Test (2015 Chevy Silverado)	6.55 m/s	8.50 m/s	5.09G	10.78G
Difference	25.3%	9.2%	15.3%	23%

4.1.3 The 2BMR Impacted by 2014 Chevy Silverado

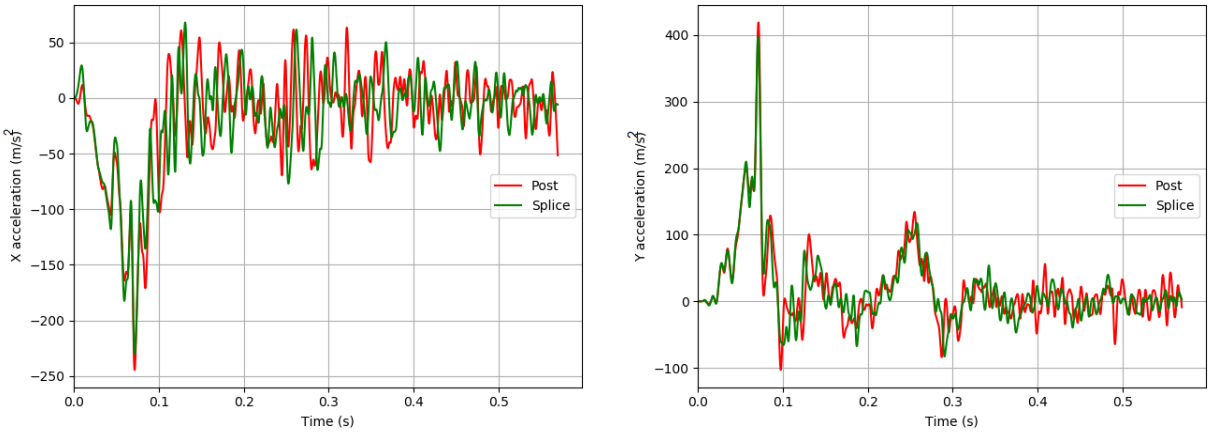
Figure 4.14 shows the top-view vehicle trajectories of the 2014 Chevy Silverado impacting the 2BMR at 62 mph (100 km/h) and a 25° impact angle. Tire tracks of the vehicle and the exit box were also shown in the figure. For both impact cases, the vehicle was redirected by the bridge rail with small exit angles and passed MASH exit box criterion. The post-impact trajectories of the vehicle in both cases were considered as safe redirections.



(a) (b)

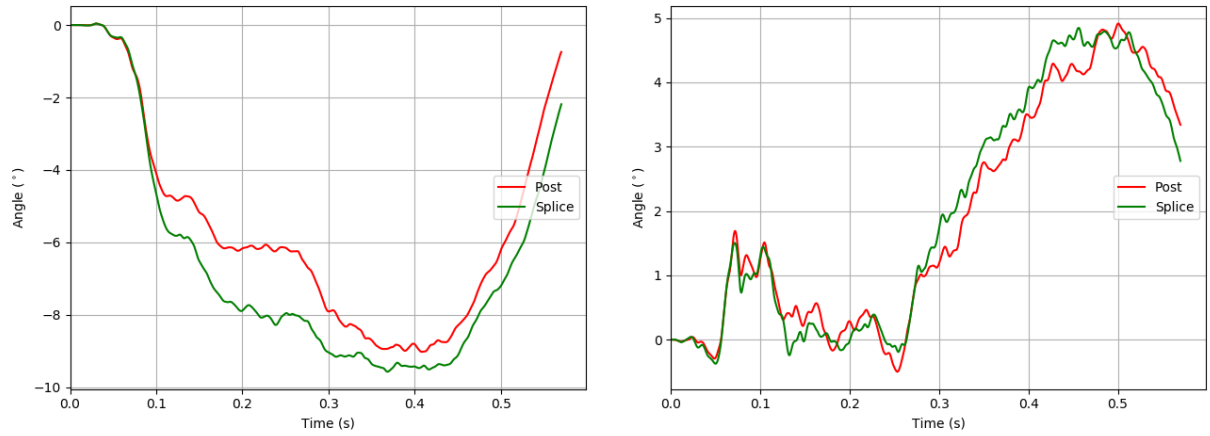
Figure 4.14: Vehicle trajectories of 2014 Chevy Silverado impacting the 2BMR.
(a) With expansion splice as reference; and (b) with the post as reference.

Figure 4.15 shows the time histories of vehicle accelerations in both longitudinal and lateral directions. No significant difference in vehicle accelerations was observed between the two impact locations. Figure 4.16 shows the time history of the vehicle's row and pitch angles. The maximum roll angles for the two impact cases were 9.3° and 9.0°, respectively, and the maximum pitch angles were 4.9° and 5.0°, respectively, for the two impact cases. In both cases, the 2BMR passed the MASH evaluation criterion *F*, which specified a maximum 75° roll and pitch angles.



(a) (b)

Figure 4.15: Time histories of accelerations of the 2014 Chevy Silverado impacting the 2BMR. (a) Longitudinal direction; and (b) lateral direction.



(a) (b)

Figure 4.16: Time histories of angular motions of 2014 Chevy Silverado impacting the 2BMR. (a) Roll angle; and (b) pitch angle.

The occupant safety factors, the OIVs and ORAs, were calculated using the time histories of vehicle accelerations in both longitudinal and lateral directions. The OIV and ORA values for both impact cases are summarized in Tables 4.8 and 4.9, along with the vehicle's roll, pitch, and exit angles. It can be seen from the results that all the OIV and ORA values were below the limit and preferred values specified in MASH. Based on the simulation results, the 2BMR passed all the MASH evaluation criteria under impacts by the 2014 Chevy Silverado at the two impact locations.

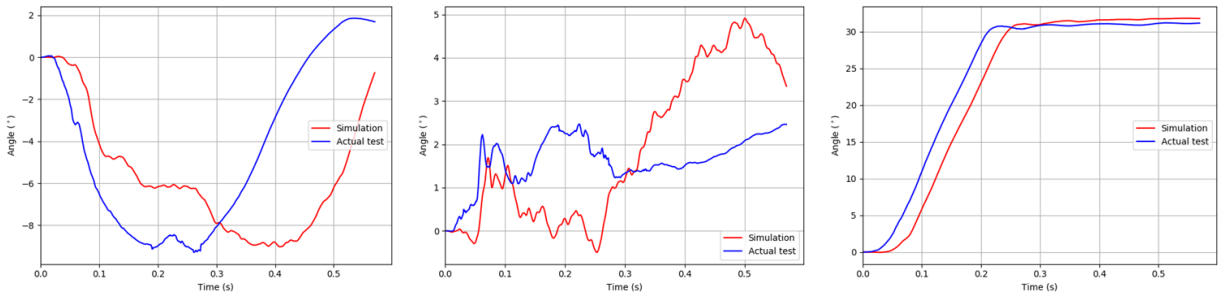
Table 4.8: Evaluation factors of 2BMR impacted by 2014 Chevy Silverado with expansion splice as reference.

Criteria	MASH criterion *H*		MASH criterion *I*		MASH criterion *F*		MASH criterion *N*
Factors	OIV_x	OIV_y	ORA_x	ORA_y	Max roll angle	Max pitch angle	Exit angle
Value	7.74 m/s	8.16 m/s	4.78G	10.64G	9.3°	4.9°	6.1°
Limit	12.2 m/s	12.2 m/s	20.49G	20.49G	75°	75°	/
Evaluation	Pass	Pass	Pass	Pass	Pass	Pass	Pass

Table 4.9: Evaluation factors of 2BMR impacted by 2014 Chevy Silverado with post as reference.

Criteria	MASH criterion *H*		MASH criterion *I*		MASH criterion *F*		MASH criterion *N*
Factors	OIV_x	OIV_y	ORA_x	ORA_y	Max roll angle	Max pitch angle	Exit angle
Value	7.78 m/s	8.19 m/s	7.45G	11.06G	9.0°	5.0°	6.3°
Limit	12.2 m/s	12.2 m/s	20.49G	20.49G	75°	75°	/
Evaluation	Pass	Pass	Pass	Pass	Pass	Pass	Pass

The vehicular responses of the 2014 Chevy Silverado impacting the 2BMR were also compared to the 2015 Chevy Silverado that was used in the crash test. Figure 4.17 shows the time histories of angular motions of the vehicle from simulation results compared to test data. The trends of roll angles were similar but with a delay in the simulated responses. The largest discrepancy was on the pitch angles, which could be caused by the difference in suspension systems and/or other structures, and more likely due to modeling of the vehicle structure, particularly the suspension system. The maximum roll and pitch angles of the test vehicle in the crash test were all below the 75° limit specified by MASH criterion *F*. Despite the different years of the test vehicle and simulation model, the vehicles exhibited similar redirection characteristics, as seen from the yaw angles in Figure 4.17(c).



(a) (b) (c)

Figure 4.17: Comparison of angular motions of the 2015 Chevy Silverado (test) and 2014 Chevy Silverado (model). (a) Roll angles; (b) pitch angles; and (c) yaw angles.

Figure 4.18 shows the comparison of the vehicle model with the test vehicle in crash test at six instants during the impact. It can be seen that the responses of the 2014 Silverado model were similar to the test vehicle. The excessive vaulting of the vehicle in the simulation, as seen on the 2007 Silverado model, did not happen on the 2014 Silverado model, an improvement of vehicular responses by the new model.

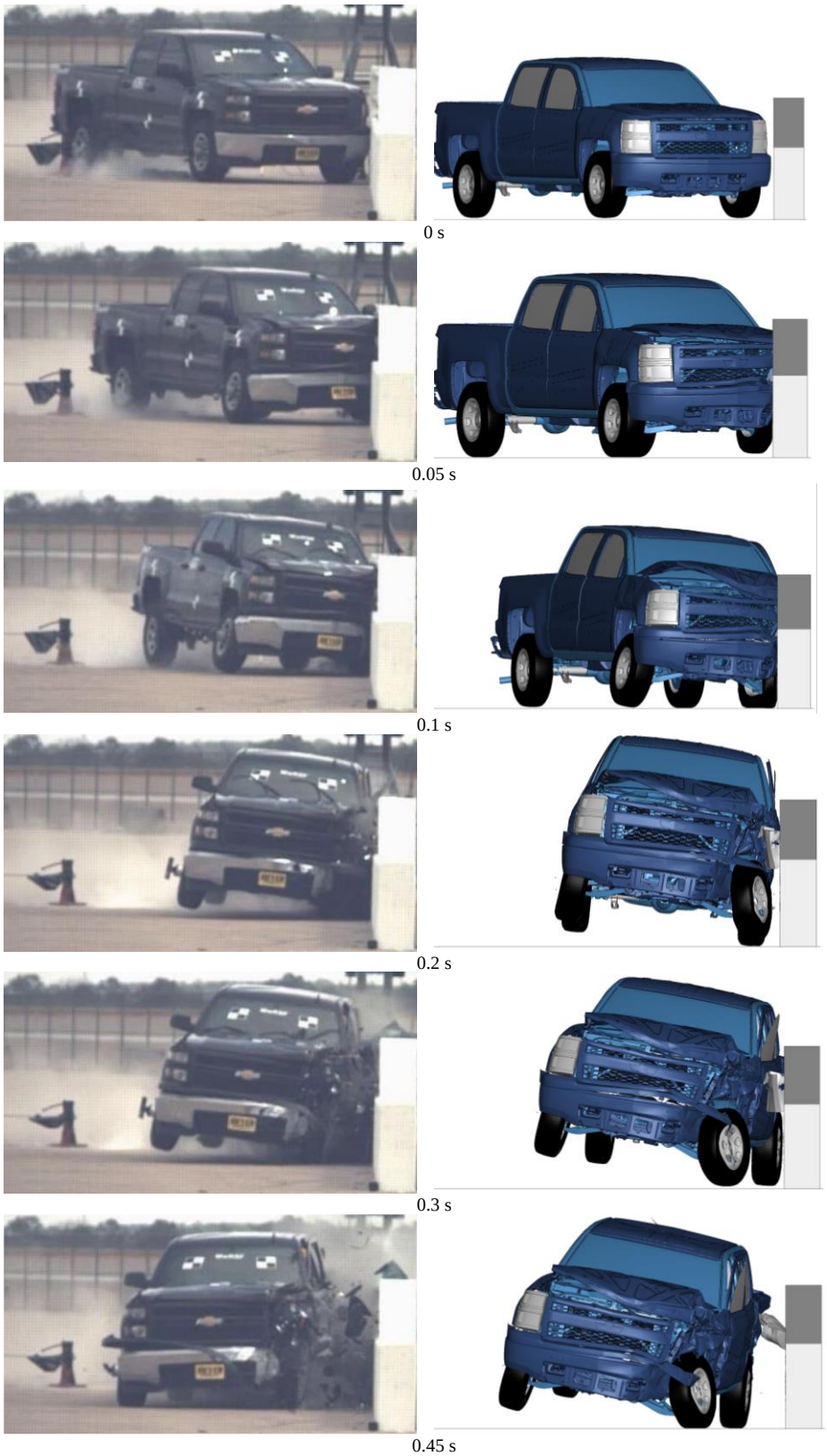
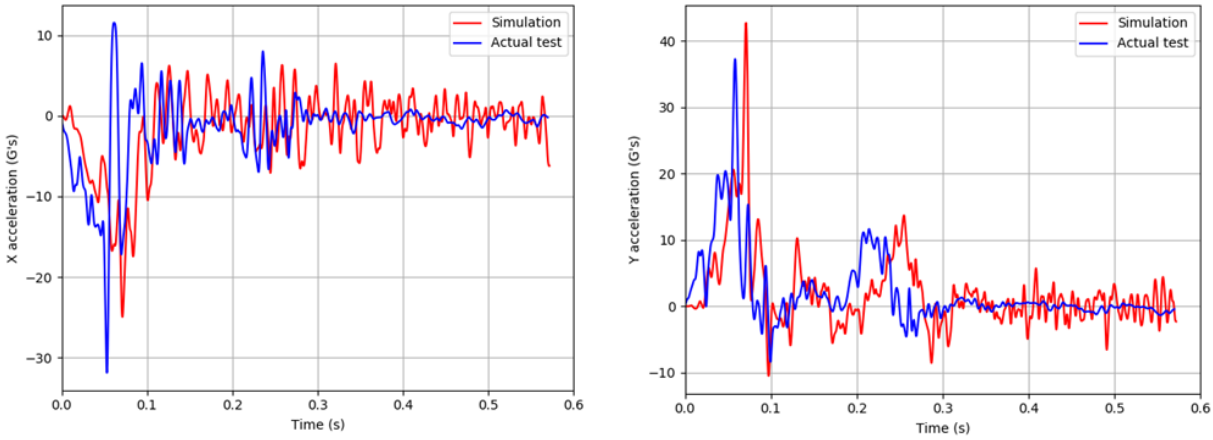


Figure 4.18: Comparison of responses of the 2270P test vehicles impacting the 2BMR (Left: a 2015 Chevy Silverado used in field test. Right: a 2014 Chevy Silverado used in simulation).

The longitudinal and lateral accelerations from simulation results were compared to test data, as shown in Figure 4.19. The trends of accelerations in both directions generally matched those from test data, with some discrepancies in the peak values and noises in the simulation results.



(a) (b)

Figure 4.19: Comparison of longitudinal and lateral accelerations of 2015 Chevy Silverado (test) and 2014 Chevy Silverado (model) impacting the 2BMR.
(a) Longitudinal direction; and (b) lateral direction.

Table 4.10 gives a comparison of the occupant safety factors from simulation results (using the 2014 Chevy Silverado) and test data (using the 2015 Chevy Silverado), both with the post closest to the expansion splice as the reference point. Occupant safety factors predicted by the 2014 Chevy Silverado had generally better agreement with test data than those by the 2007 Chevy Silverado, except for the ORA value in the longitudinal direction. The OIV and ORA values predicted by the simulation were all below the MASH limit and preferred values, reaching the same conclusion as the actual test.

Table 4.10: Comparison of occupant safety factors from simulation and test for impacts by the 2270P vehicles.

Criteria	MASH criterion *H*		MASH criterion *I*	
Factors	OIV_x	OIV_y	ORA_x	ORA_y
Simulation (2014 Chevy Silverado)	7.78 m/s	8.19 m/s	7.45G	11.06G
Test (2015 Chevy Silverado)	6.55 m/s	8.50 m/s	5.09G	10.78G
Difference	18.8%	3.6%	46.4%	2.6%

4.2 Evaluation of the Oregon Rail under MASH TL-4 Conditions

The Oregon Rail (see Figure 3.6) was evaluated under MASH TL-4 conditions using FE simulations, i.e., impacted by a 2010 Toyota Yaris, a 2007 Chevy Silverado, and a 2014 Chevy Silverado at 62 mph (100 km/h) and 25°, and by a 1996 Ford F800 at 56 mph (90 km/h) and 25°. For each impacting vehicle, two impact locations were used: one with an expansion joint as the reference point and the other with the post closest to the expansion joint as the reference point.

4.2.1 The Oregon Rail Impacted by 2010 Toyota Yaris

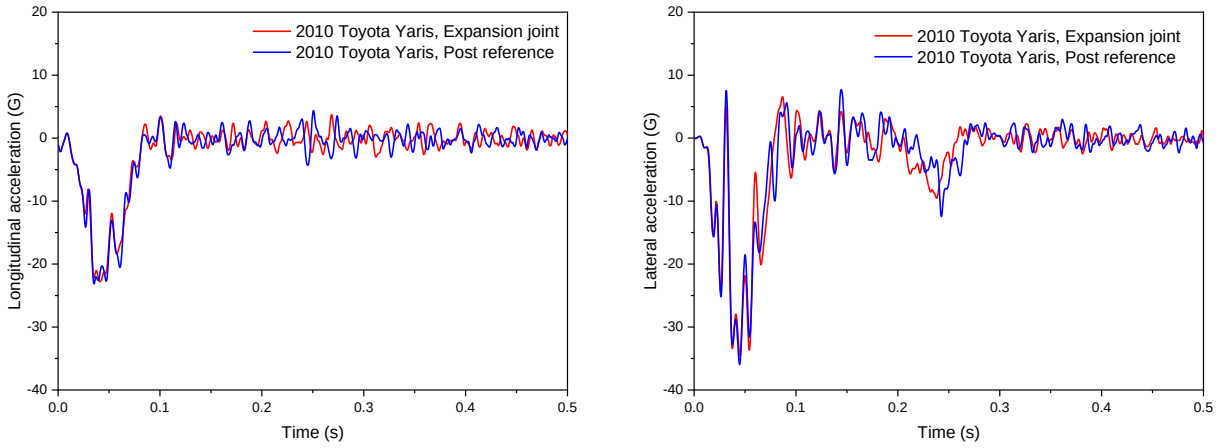
Figure 4.20 shows the top-view vehicle trajectories of the 2010 Toyota Yaris impacting the Oregon Rail at 62 mph (100 km/h) and a 25° impact angle. Tire tracks of the vehicle and the exit box were also shown in the figure. For both impact cases, the vehicle was redirected by the bridge rail with small exit angles (11.5° and 11°) and passed MASH exit box criterion. Although the vehicle exhibited some counterclockwise rotations after leaving the exit box, the post-impact trajectories of the vehicle in both cases were considered as safe redirections.



(a) (b)

Figure 4.20: Vehicle trajectories of 2010 Toyota Yaris impacting the Oregon Rail.
(a) With expansion joint as reference; and (b) with the post as reference.

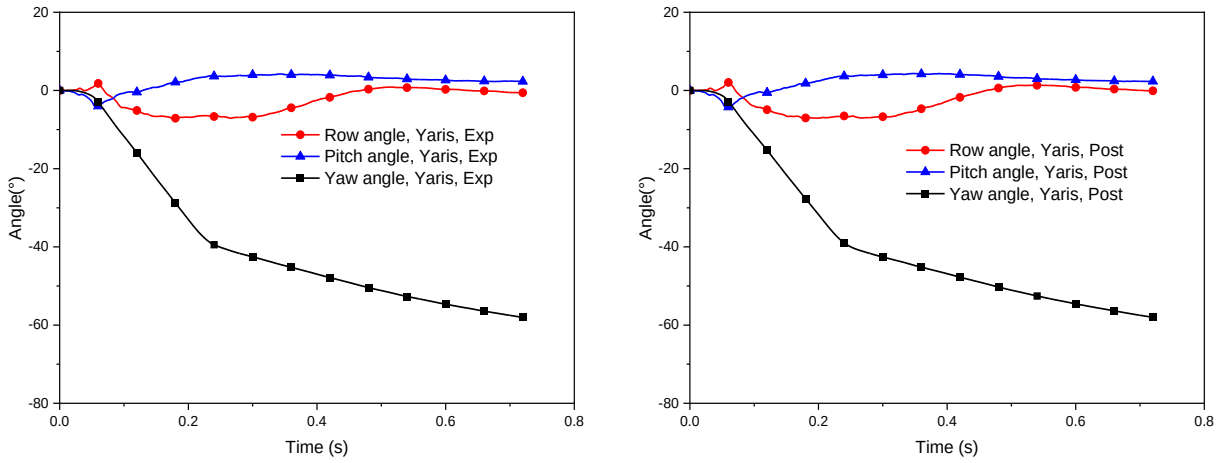
Figure 4.21 shows the time histories of vehicle accelerations in both longitudinal and lateral directions. No significant difference in vehicle accelerations was observed between the two impact locations.



(a) (b)

Figure 4.21: Time histories of accelerations of 2010 Toyota Yaris impacting the Oregon Rail.
(a) Longitudinal direction; and (b) lateral direction.

Figure 4.22 shows the time history of the vehicle's row, pitch, and yaw angles. The maximum roll angles for the two impact cases were both 7.1°, and the maximum pitch angles were 4.3° and 4.4°, respectively. In both cases, the Oregon Rail passed the MASH evaluation criterion *F*, which specified a maximum 75° roll and pitch angles.



(a) (b)

Figure 4.22: Time histories of angular motions of 2010 Toyota Yaris impacting the Oregon Rail. (a) With expansion joint as reference; and (b) with the post as reference.

The occupant safety factors, the OIVs and ORAs, were calculated using the time histories of vehicle accelerations in both longitudinal and lateral directions. The OIV and ORA values for both impact cases are summarized in Tables 4.11 and 4.12, along with the vehicle's roll, pitch, and exit angles. It can be seen from the results that all the OIV and ORA values were below the limit values specified in MASH. The maximum dynamic and permanent deflections of the bridge rail were also calculated and found insignificant in both cases, as shown in Tables 4.11 and 4.12. Based on the simulation results, the Oregon Rail passed all the evaluation criteria of MASH TL-4 under impacts by the 2010 Toyota Yaris at the two impact locations.

Table 4.11: Evaluation factors of Oregon Rail impacted by 2010 Toyota Yaris with expansion joint as reference.

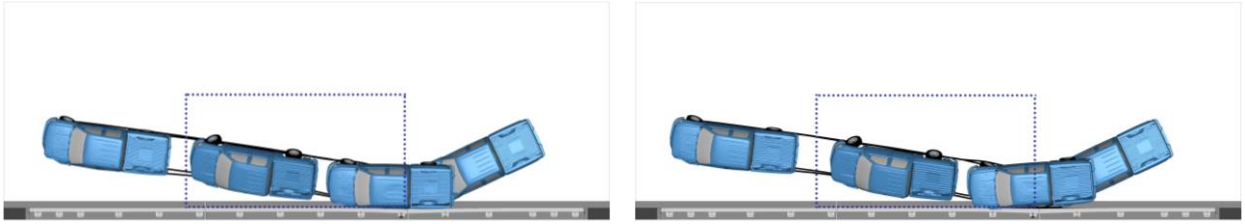
Criteria	MASH criterion *H*		MASH criterion *I*		MASH criterion *F*		MASH criterion *N*	MASH criterion *A*	
Factors	OIV_x	OIV_y	ORA_x	ORA_y	Max roll angle	Max pitch angle	Exit angle	Permanent deflection	Dynamic deflection
Value	8.19 m/s	10.76 m/s	3.137G	8.631G	7.1°	4.3°	11.5°	23.8 mm	53.1 mm
Limit	12.2 m/s	12.2 m/s	20.49G	20.49G	75°	75°	/	/	
Evaluation	Pass	Pass	Pass	Pass	Pass	Pass	Pass	/	

Table 4.12: Evaluation factors of Oregon Rail impacted by 2010 Toyota Yaris with post as reference.

Criteria	MASH criterion *H*		MASH criterion *I*		MASH criterion *F*		MASH criterion *N*	MASH criterion *A*	
Factors	OIV_x	OIV_y	ORA_x	ORA_y	Max roll angle	Max pitch angle	Exit angle	Permanent deflection	Dynamic deflection
Value	8.39 m/s	10.54 m/s	3.662G	9.089G	7.1°	4.4°	11°	26.2 mm	53.4 mm
Limit	12.2 m/s	12.2 m/s	20.49G	20.49G	75°	75°	/	/	
Evaluation	Pass	Pass	Pass	Pass	Pass	Pass	Pass	/	

4.2.2 The Oregon Rail Impacted by 2007 Chevy Silverado

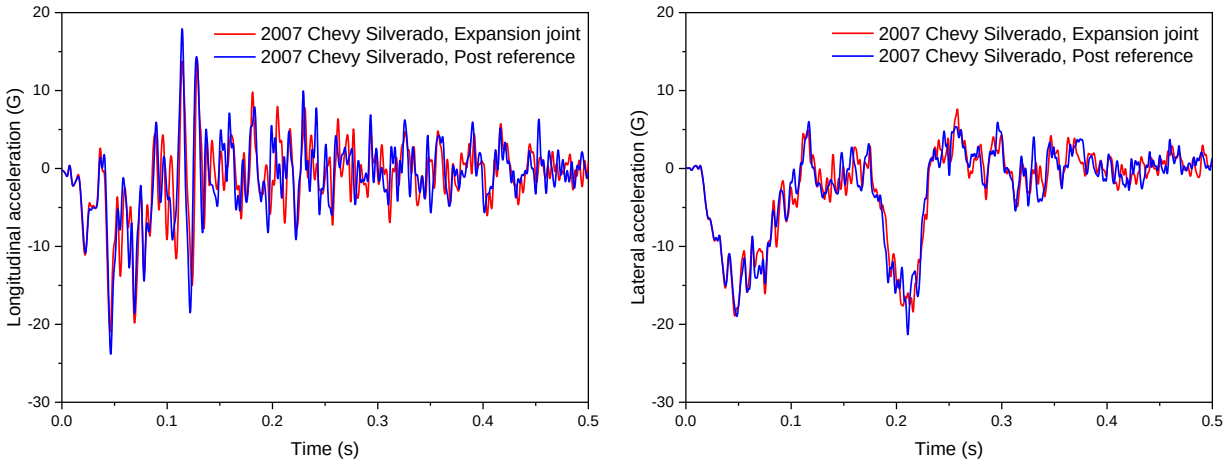
Figure 4.23 shows the top-view vehicle trajectories of the 2007 Chevy Silverado impacting the Oregon Rail at 62 mph (100 km/h) and a 25° impact angle. Tire tracks of the vehicle and the exit box were also shown in the figure. For both impact cases, the vehicle was redirected by the bridge rail with small exit angles and passed MASH exit box criterion. The post-impact trajectories of the vehicle in both cases were considered as safe redirections.



(a) (b)

Figure 4.23: Vehicle trajectories of 2007 Chevy Silverado impacting the Oregon Rail.
(a) With expansion joint as reference; and (b) with the post as reference.

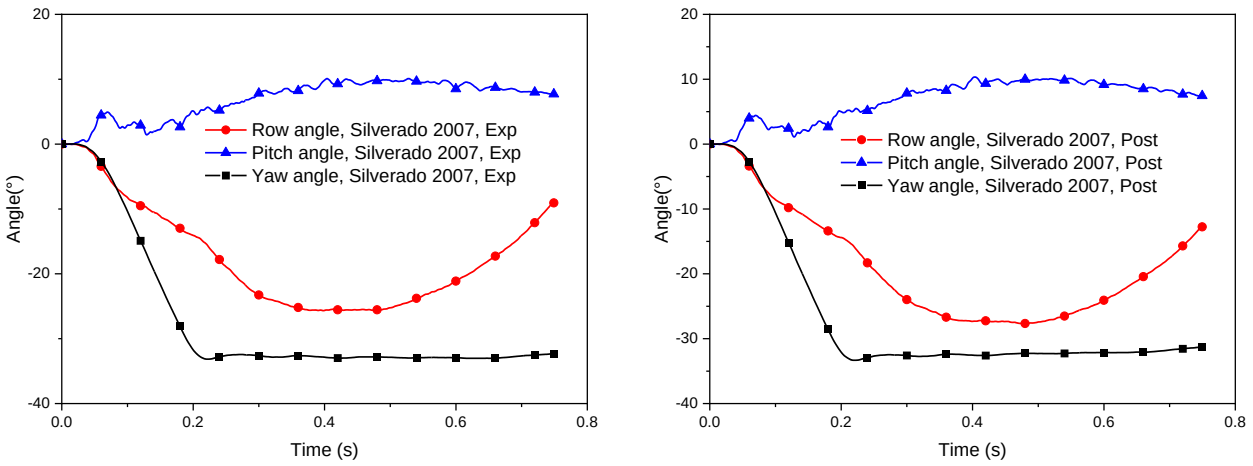
Figure 4.24 shows the time histories of vehicle accelerations in both longitudinal and lateral directions. No significant difference in vehicle accelerations was observed between the two impact locations.



(a) (b)

Figure 4.24: Time histories of accelerations of 2007 Chevy Silverado impacting the Oregon Rail.
(a) Longitudinal direction; and (b) lateral direction.

Figure 4.25 shows the time history of the vehicle's row, pitch, and yaw angles. The maximum roll angles for the two impact cases were 25.7° and 27.7°, respectively, and the maximum pitch angles were 10.1° and 10.3°, respectively, for the two cases. In both cases, the Oregon Rail passed the MASH evaluation criterion *F*, which specified a maximum 75° roll and pitch angles.



(a) (b)

Figure 4.25: Time histories of angular motions of 2007 Chevy Silverado impacting the Oregon Rail. (a) With expansion joint as reference; and (b) with the post as reference.

The occupant safety factors, the OIVs and ORAs, were calculated using the time histories of vehicle accelerations in both longitudinal and lateral directions. The OIV and ORA values for both impact cases are summarized in Tables 4.13 and 4.14, along with the vehicle's roll, pitch, and exit angles. It can be seen that all the OIV and ORA values were below the MASH limit values. The maximum dynamic and permanent deflections of the bridge rail were found insignificant in both cases (see Tables 4.13 and 4.14), though they were much larger than those in the cases of 2010 Toyota Yaris. Based on the simulation results, the Oregon Rail passed all the evaluation criteria of MASH TL-4 under impacts by the 2007 Chevy Silverado at the two impact locations.

Table 4.13: Evaluation factors of Oregon Rail impacted by 2007 Chevy Silverado with expansion joint as reference.

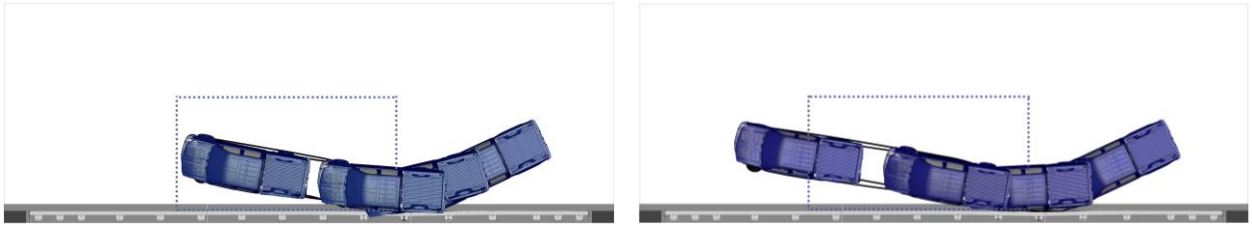
Criteria	MASH criterion *H*		MASH criterion *I*		MASH criterion *F*		MASH criterion *N*	MASH criterion *A*	
Factors	OIV_x	OIV_y	ORA_x	ORA_y	Max roll angle	Max pitch angle	Exit angle	Permanent deflection	Dynamic deflection
Value	5.25 m/s	7.93 m/s	5.514G	16.989G	25.7°	10.1°	12°	79.2 mm	132.6 mm
Limit	12.2 m/s	12.2 m/s	20.49G	20.49G	75°	75°	/	/	
Evaluation	Pass	Pass	Pass	Pass	Pass	Pass	Pass	/	

Table 4.14: Evaluation factors of Oregon Rail impacted by 2007 Chevy Silverado with post as reference.

Criteria	MASH criterion *H*		MASH criterion *I*		MASH criterion *F*		MASH criterion *N*	MASH criterion *A*	
Factors	OIV_x	OIV_y	ORA_x	ORA_y	Max roll angle	Max pitch angle	Exit angle	Permanent deflection	Dynamic deflection
Value	5.17 m/s	8.02 m/s	6.639G	16.802G	27.7°	10.3°	11.5°	78.6 mm	133.6 mm
Limit	12.2 m/s	12.2 m/s	20.49G	20.49G	75°	75°	/	/	
Evaluation	Pass	Pass	Pass	Pass	Pass	Pass	Pass	/	

4.2.3 The Oregon Rail Impacted by 2014 Chevy Silverado

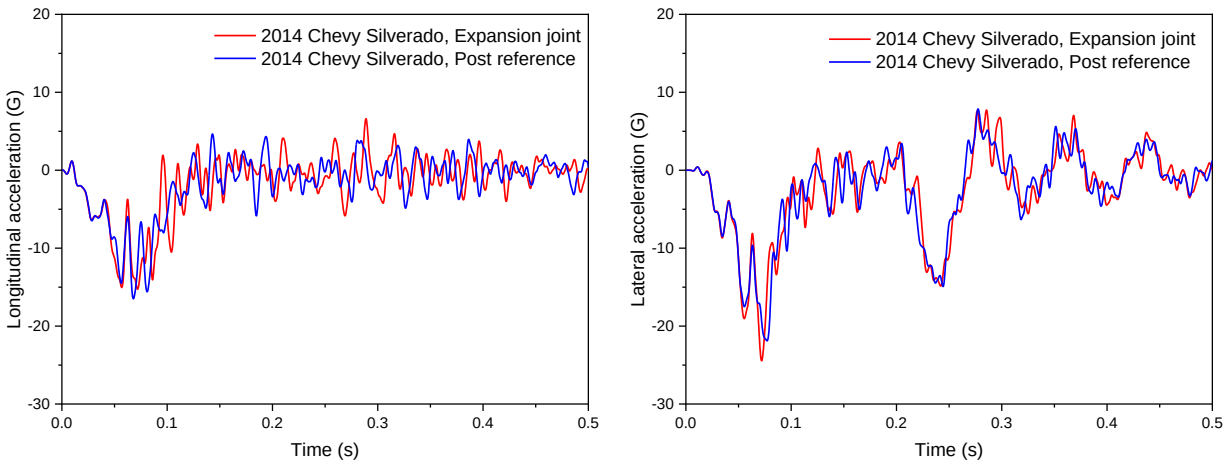
Figure 4.26 shows the top-view vehicle trajectories of the 2014 Chevy Silverado impacting the Oregon Rail at 62 mph (100 km/h) and a 25° impact angle. Tire tracks of the vehicle and the exit box were also shown in the figure. For both impact cases, the vehicle was redirected by the bridge rail with small exit angles and passed MASH exit box criterion. The post-impact trajectories of the vehicle in both cases were considered as safe redirections.



(a) (b)

Figure 4.26: Vehicle trajectories of 2014 Chevy Silverado impacting the Oregon Rail.
(a) With expansion joint as reference; and (b) with the post as reference.

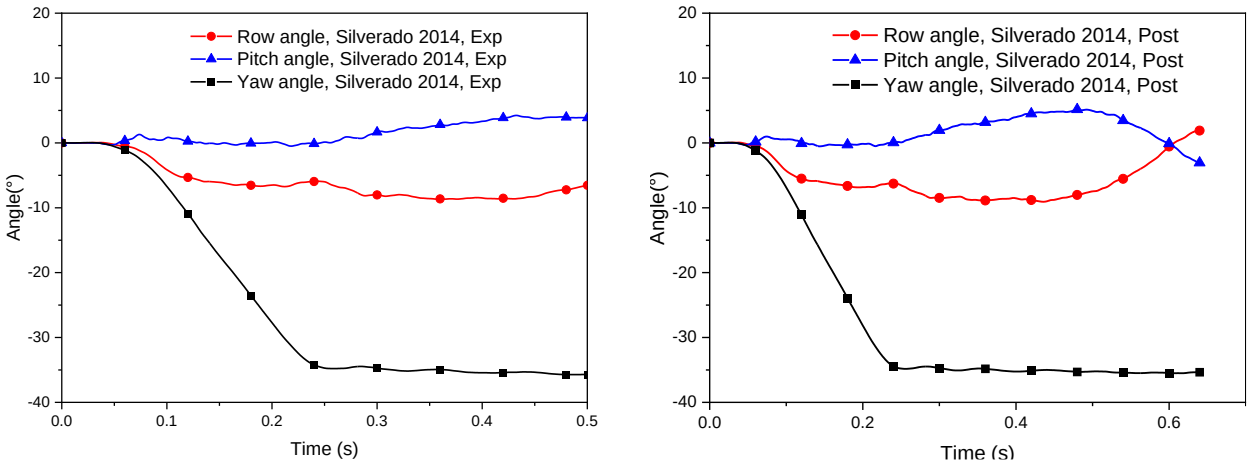
Figure 4.27 shows the time histories of vehicle accelerations in both longitudinal and lateral directions. No significant difference in vehicle accelerations was observed between the two impact locations.



(a) (b)

Figure 4.27: Time histories of accelerations of 2014 Chevy Silverado impacting the Oregon Rail.
(a) Longitudinal direction; and (b) lateral direction.

Figure 4.28 shows the time history of the vehicle's row, pitch, and yaw angles. The maximum roll angles for the two impact cases were 8.7° and 9.1°, respectively, and the maximum pitch angles were 4.2° and 5.1°, respectively, for the two cases. These values were much smaller than those of the 2007 Chevy Silverado, indicating a more robust suspension system (model) of the 2014 Chevy Silverado. In both cases, the Oregon Rail passed the MASH evaluation criterion *F*.



(a) (b)

Figure 4.28: Time histories of angular motions of 2014 Chevy Silverado impacting the Oregon Rail. (a) With expansion joint as reference; and (b) with the post as reference.

The occupant safety factors, the OIVs and ORAs, were calculated using the time histories of vehicle accelerations in both longitudinal and lateral directions. The OIV and ORA values for both impact cases are summarized in Tables 4.15 and 4.16, along with the vehicle's roll, pitch, and exit angles. It can be seen from the results that all the OIV and ORA values were below the MASH limit values. The maximum dynamic and permanent deflections of the bridge rail were comparable to, but slightly larger than, those in the cases of 2007 Chevy Silverado. Based on the simulation results, the Oregon Rail passed all the evaluation criteria of MASH TL-4 under impacts by the 2014 Chevy Silverado at the two impact locations.

Table 4.15: Evaluation factors of Oregon Rail impacted by 2014 Chevy Silverado with expansion joint as reference.

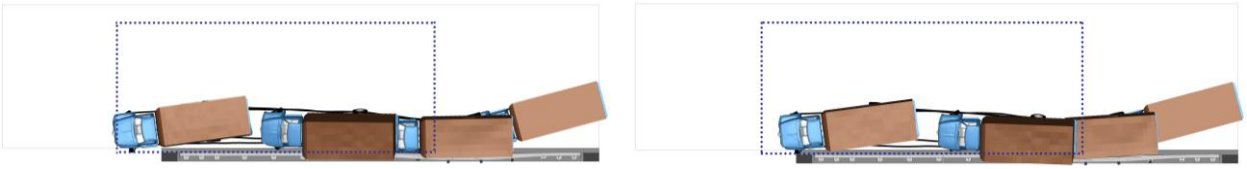
Criteria	MASH criterion *H*		MASH criterion *I*		MASH criterion *F*		MASH criterion *N*	MASH criterion *A*	
Factors	OIV_x	OIV_y	ORA_x	ORA_y	Max roll angle	Max pitch angle	Exit angle	Permanent deflection	Dynamic deflection
Value	6.75 m/s	8.16 m/s	5.423G	14.168G	8.7°	4.2°	14.5°	94.6 mm	164.8 mm
Limit	12.2 m/s	12.2 m/s	20.49G	20.49G	75°	75°	/	/	
Evaluation	Pass	Pass	Pass	Pass	Pass	Pass	Pass	/	

Table 4.16: Evaluation factors of Oregon Rail impacted by 2014 Chevy Silverado with post as reference.

Criteria	MASH criterion *H*		MASH criterion *I*		MASH criterion *F*		MASH criterion *N*	MASH criterion *A*	
Factors	OIV_x	OIV_y	ORA_x	ORA_y	Max roll angle	Max pitch angle	Exit angle	Permanent deflection	Dynamic deflection
Value	6.92 m/s	8.20 m/s	3.422G	14.170G	9.1°	5.1°	14.5°	80.2 mm	168.0 mm
Limit	12.2 m/s	12.2 m/s	20.49G	20.49G	75°	75°	/	/	
Evaluation	Pass	Pass	Pass	Pass	Pass	Pass	Pass	/	

4.2.4 The Oregon Rail Impacted by 1996 Ford F800

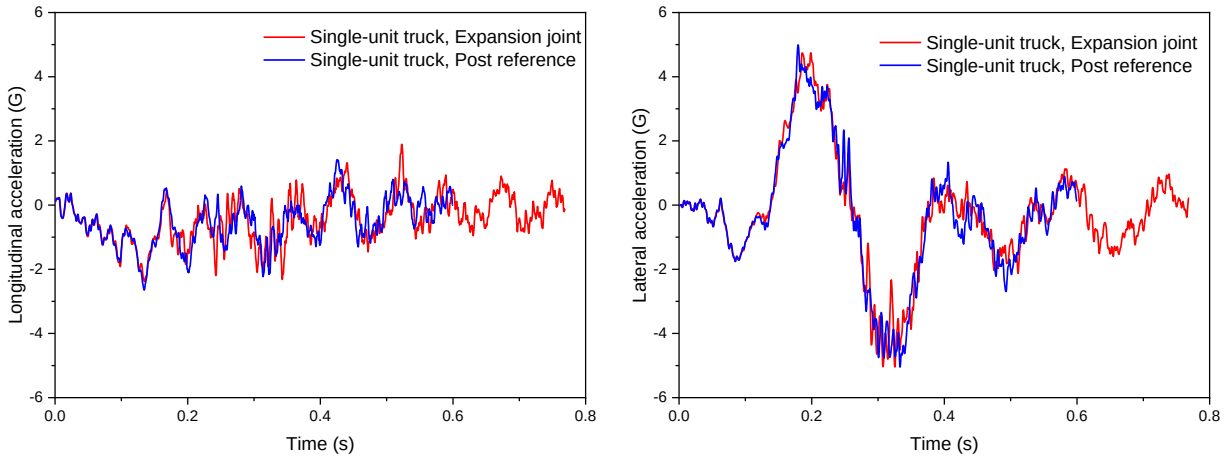
Figure 4.29 shows the top-view vehicle trajectories of the 1996 Ford F800 single-unit truck impacting the Oregon Rail at 56 mph (90 km/h) with a 25° impact angle. Tire tracks of the vehicle and the exit box were also shown in the figure. For both impact cases, the vehicle was redirected by the bridge rail with small exit angles and passed MASH exit box criterion. Due to the small exit angle, the vehicle maintained an upright position during the entire course of impact, though this was not required by MASH for single-unit trucks. The post-impact trajectories of the vehicle in both cases were considered as safe redirections.



(a) (b)

Figure 4.29: Vehicle trajectories of 1996 Ford F800 impacting the Oregon Rail.
(a) With expansion joint as reference; and (b) with the post as reference.

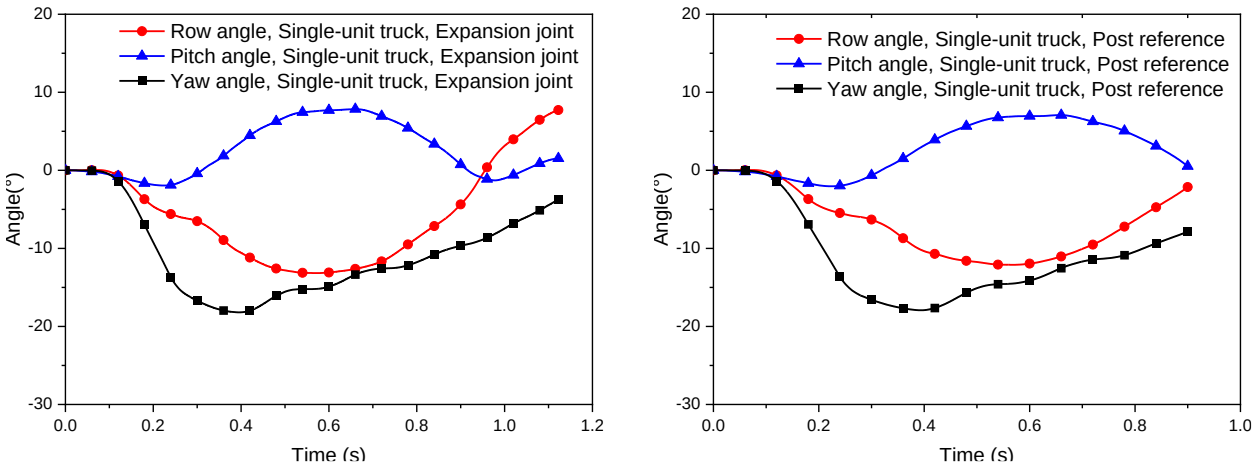
Figure 4.30 shows the time histories of vehicle accelerations in both longitudinal and lateral directions. No significant difference in vehicle accelerations was observed between the two impact locations.



(a) (b)

Figure 4.30: Time histories of accelerations of 1996 Ford F800 impacting the Oregon Rail.
(a) Longitudinal direction; and (b) lateral direction.

Figure 4.31 shows the time history of the vehicle's row, pitch, and yaw angles. The maximum roll angles for the two impact cases were 13.2° and 12.1°, respectively, and the maximum pitch angles were 7.8° and 7.1°, respectively. These results showed that the Oregon Rail passed the MASH evaluation criterion *F* in both cases under impacts by the 1996 Ford F800.



(a) (b)

Figure 4.31: Time histories of angular motions of 1996 Ford F800 impacting the Oregon Rail. (a) With expansion joint as reference; and (b) with the post as reference.

The occupant safety factors, the OIVs and ORAs, were calculated using the time histories of vehicle accelerations in both longitudinal and lateral directions. The OIV and ORA values for both impact cases are summarized in Tables 4.17 and 4.18, along with the vehicle's roll, pitch, and exit angles. It can be seen from the results that all the OIV and ORA values were much lower than the preferred values recommended by MASH, indicating extremely low potential of causing occupant injuries.

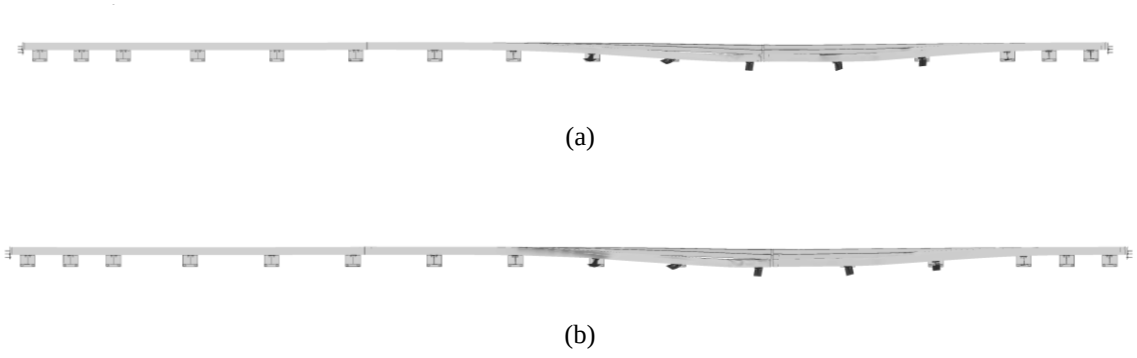
Table 4.17: Evaluation factors of Oregon Rail impacted by 1996 Ford F800 with expansion joint as reference.

Criteria	MASH criterion *H*		MASH criterion *I*		MASH criterion *F*		MASH criterion *N*	MASH criterion *A*	
Factors	OIV_x	OIV_y	ORA_x	ORA_y	Max roll angle	Max pitch angle	Exit angle	Permanent deflection	Dynamic deflection
Value	3.00 m/s	0.72 m/s	1.194G	1.866G	13.2°	7.8°	7°	292.9 mm	388.9 mm
Limit	12.2 m/s	12.2 m/s	20.49G	20.49G	75°	75°	/	/	
Evaluation	Pass	Pass	Pass	Pass	Pass	Pass	Pass	/	

Table 4.18: Evaluation factors of Oregon Rail impacted by 1996 Ford F800 with post as reference.

Criteria	MASH criterion *H*		MASH criterion *I*		MASH criterion *F*		MASH criterion *N*	MASH criterion *A*	
Factors	OIV_x	OIV_y	ORA_x	ORA_y	Max roll angle	Max pitch angle	Exit angle	Permanent deflection	Dynamic deflection
Value	3.06 m/s	0.86 m/s	1.195G	2.197G	12.1°	7.1°	5.5°	277.9 mm	382.0 mm
Limit	12.2 m/s	12.2 m/s	20.49G	20.49G	75°	75°	/	/	
Evaluation	Pass	Pass	Pass	Pass	Pass	Pass	Pass	/	

The maximum dynamic and permanent deflections of the bridge rail under impacts of the single-unit truck were moderate and normal but much larger than those in the cases of the pickup trucks, as shown by the results in Tables 4.15 to 4.18. Figure 4.32 shows the top view of the bridge rail with permanent deformations in both impact cases. Based on the simulation results, the Oregon Rail passed all the evaluation criteria of MASH TL-4 under impacts by the 1996 Ford F800 at the two impact locations.



(a)

(b)

Figure 4.32: Top view of the Oregon Rail with permanent deformation impacted by 1996 Ford F800. (a) With expansion joint as reference; and (b) with the post as reference.

4.3 Evaluation of the Three-Bar Metal Rail under MASH TL-2 and TL-3 Conditions

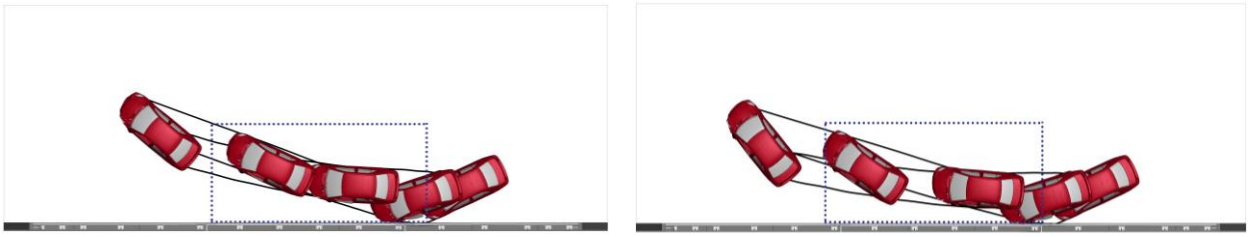
The 3BMR was evaluated under MASH TL-2 and TL-3 conditions with three test vehicles (a 2010 Toyota Yaris, a 2007 Chevy Silverado, and a 2014 Chevy Silverado) and two impact locations (determined by reference points at the expansion joint and at a post closest to the expansion joint, see Figure 3.23).

For simulations under TL-2 conditions, the FE model of the 3BMR had only reinforcement bars in the end parapet. Under TL-3 conditions, this model was shown to be inappropriate due to the increased impact severity; therefore, a new FE model was developed, with full reinforcement bars in the concrete foundation, and used in simulations under TL-3 conditions. For ease of presentation, the two 3BMR models are referred to as 3BMR-1 (with reinforcement bars only in end parapets) and 3BMR-2 (with reinforcement bars in both end parapets and concrete foundation). The simulation results for the 3BMR are presented in three subsections as 3BMR-1 under TL-2 conditions, 3BMR-1 under TL-3 conditions, and 3BMR-2 under TL-3 conditions.

4.3.1 Evaluation of 3BMR-1 under TL-2 conditions

4.3.1.1 The 3BMR-1 impacted by 2010 Toyota Yaris under TL-2 conditions

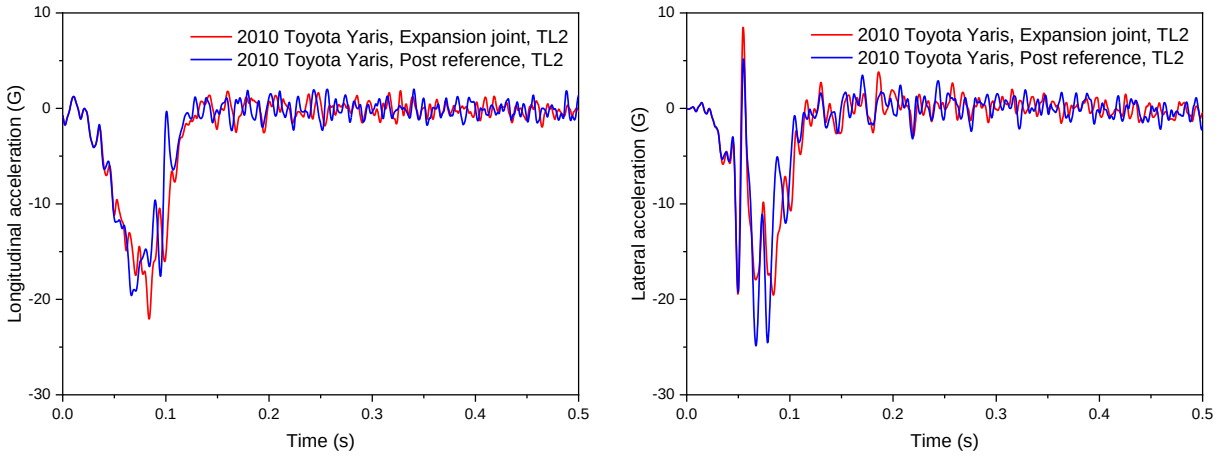
Figure 4.33 shows the top-view vehicle trajectories of the 2010 Toyota Yaris impacting the 3BMR-1 at 44 mph (70 km/h) and a 25° impact angle. Tire tracks of the vehicle and the exit box were also shown in the figure. For both impact cases, the vehicle was redirected by the bridge rail with exit angles 20° and 17.5° and passed MASH exit box criterion. Although the vehicle exhibited counterclockwise rotations after leaving the exit box, the post-impact trajectories of the vehicle in both cases were considered as safe redirections.



(a) (b)

Figure 4.33: Vehicle trajectories of 2010 Toyota Yaris impacting 3BMR-1 under TL-2 conditions. (a) With expansion joint as reference; and (b) with the post as reference.

Figure 4.34 shows the time histories of vehicle accelerations in both longitudinal and lateral directions. No significant difference in vehicle accelerations was observed between the two impact locations.

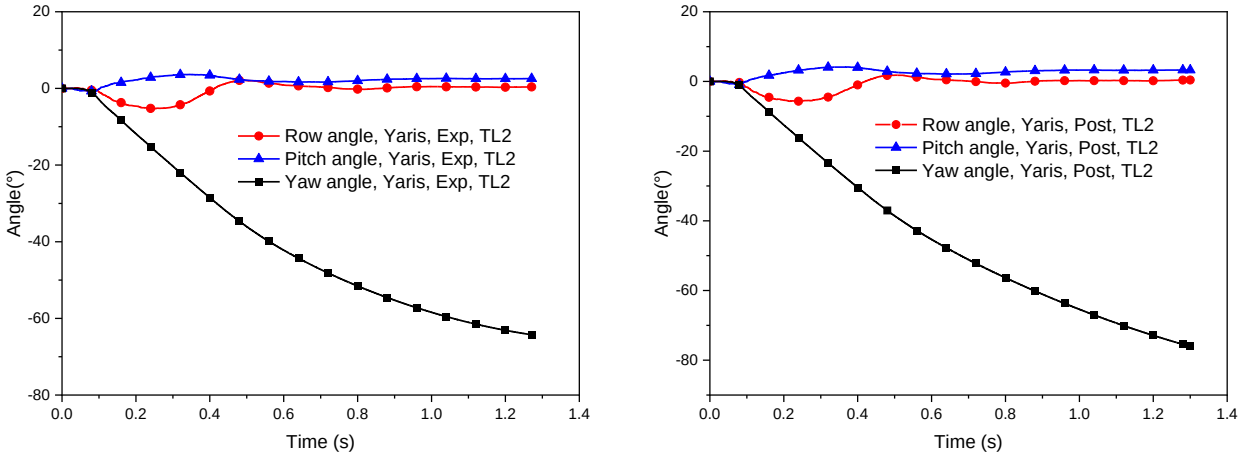


(a) (b)

Figure 4.34: Time histories of accelerations of 2010 Toyota Yaris impacting 3BMR-1 under TL-2 conditions. (a) Longitudinal direction; and (b) lateral direction.

Figure 4.35 shows the time history of the vehicle's row, pitch, and yaw angles. The maximum roll angles for the two impact cases were 5.3° and 5.7°, respectively, and the maximum pitch angles were 3.6° and 4.1°, respectively, for the two cases. In both cases, the 3BMR-1 passed the MASH evaluation criterion *F*, which specified a maximum 75° roll and pitch angles.

The occupant safety factors, the OIVs and ORAs, were calculated using the time histories of vehicle accelerations in both longitudinal and lateral directions. The OIV and ORA values for both impact cases are summarized in Tables 4.19 and 4.20, along with the vehicle's roll, pitch, and exit angles. It can be seen from the results that all the OIV and ORA values were below the limit values specified in MASH. The maximum dynamic and permanent deflections of the bridge rail were calculated and found insignificant in both cases, as shown in Tables 4.19 and 4.20. Based on the simulation results, the 3BMR-1 passed all the evaluation criteria of MASH TL-2 under impacts by the 2010 Toyota Yaris at the two impact locations.



(a) (b)

Figure 4.35: Time histories of angular motions of 2010 Toyota Yaris impacting 3BMR-1 under TL-2 conditions. (a) With expansion joint as reference; and (b) with the post as reference.

Table 4.19: Evaluation factors of 3BMR-1 impacted by 2010 Toyota Yaris (TL-2) with expansion joint as reference.

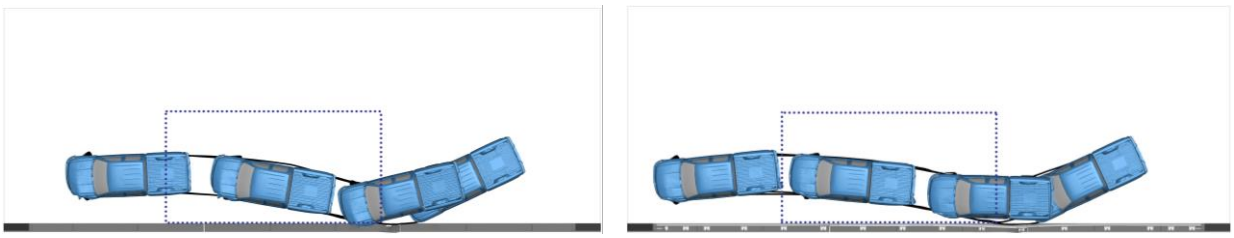
Criteria	MASH criterion *H*		MASH criterion *I*		MASH criterion *F*		MASH criterion *N*	MASH criterion *A*	
Factors	OIV_x	OIV_y	ORA_x	ORA_y	Max roll angle	Max pitch angle	Exit angle	Permanent deflection	Dynamic deflection
Value	9.57 m/s	7.73 m/s	2.443G	2.150G	5.3°	3.6°	20°	74.0 mm	122.9 mm
Limit	12.2 m/s	12.2 m/s	20.49G	20.49G	75°	75°	/	/	
Evaluation	Pass	Pass	Pass	Pass	Pass	Pass	Pass	/	

Table 4.20: Evaluation factors of 3BMR-1 impacted by 2010 Toyota Yaris (TL-2) with post as reference.

Criteria	MASH criterion *H*		MASH criterion *I*		MASH criterion *F*		MASH criterion *N*	MASH criterion *A*	
Factors	OIV_x	OIV_y	ORA_x	ORA_y	Max roll angle	Max pitch angle	Exit angle	Permanent deflection	Dynamic deflection
Value	8.77 m/s	7.47 m/s	1.797G	1.701G	5.7°	4.1°	17.5°	54.6 mm	98.3 mm
Limit	12.2 m/s	12.2 m/s	20.49G	20.49G	75°	75°	/	/	
Evaluation	Pass	Pass	Pass	Pass	Pass	Pass	Pass	/	

4.3.1.2 The 3BMR-1 impacted by 2007 Chevy Silverado under TL-2 conditions

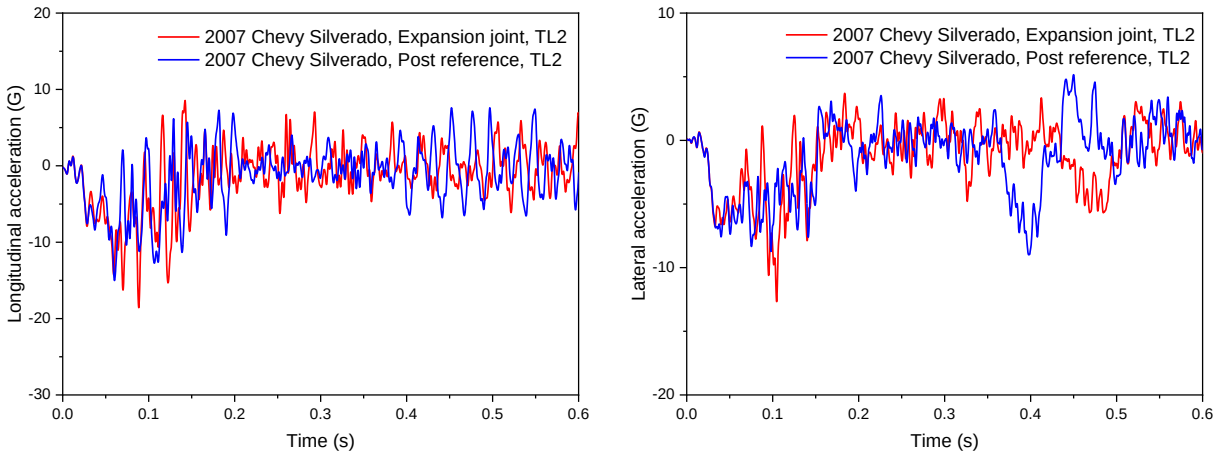
Figure 4.36 shows the top-view vehicle trajectories of the 2007 Chevy Silverado impacting the 3BMR-1 at 44 mph (70 km/h) and a 25° impact angle. Tire tracks of the vehicle and the exit box were also shown in the figure. For both impact cases, the vehicle was smoothly redirected by the bridge rail with small exit angles and passed MASH exit box criterion. The post-impact trajectories of the vehicle in both cases were considered as safe redirections.



(a) (b)

Figure 4.36: Vehicle trajectories of 2007 Chevy Silverado impacting 3BMR-1 under TL-2 conditions. (a) With expansion joint as reference; and (b) with the post as reference.

Figure 4.37 shows the time histories of vehicle accelerations in both longitudinal and lateral directions. No significant difference in vehicle accelerations was observed between the two impact locations.



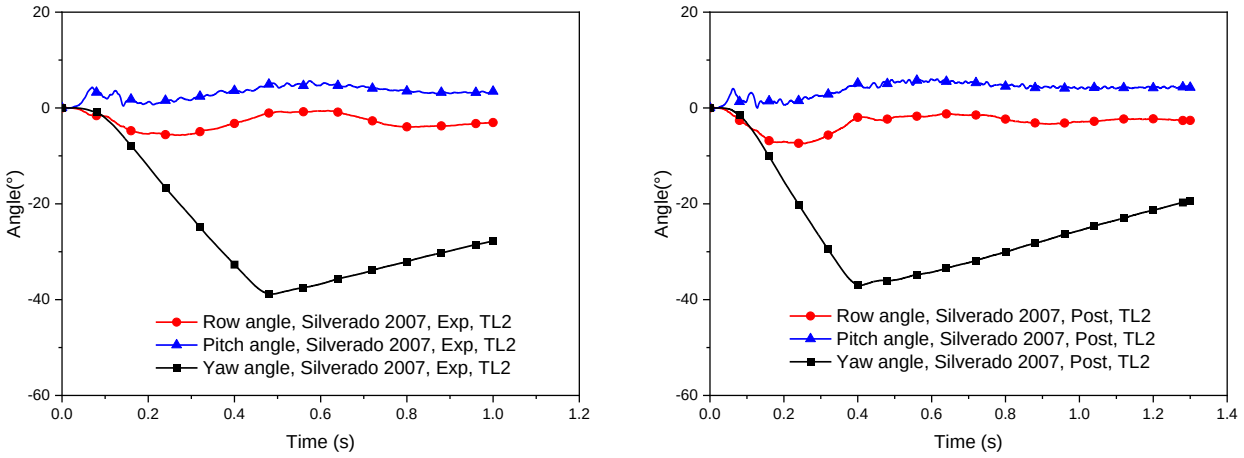
(a) (b)

Figure 4.37: Time histories of accelerations of 2007 Chevy Silverado impacting 3BMR-1 under TL-2 conditions. (a) Longitudinal direction; and (b) lateral direction.

Figure 4.38 shows the time history of the vehicle's row, pitch, and yaw angles. The maximum roll angles for the two impact cases were 5.7° and 7.4°, respectively, and the maximum pitch angles were 5.7° and 6.0°, respectively. In both cases, the 3BMR-1 passed the MASH evaluation criterion *F*, which specified a maximum 75° roll and pitch angles.

The occupant safety factors, the OIVs and ORAs, were calculated using the time histories of vehicle accelerations in both longitudinal and lateral directions. The OIV and ORA values for both impact cases are summarized in Tables 4.21 and 4.22, along with the vehicle's roll, pitch, and exit angles. It can be seen from the results that all the OIV and ORA values were below the MASH limit values. The maximum dynamic and permanent deflections of the bridge rail were found insignificant in both cases (see Tables 4.21 and 4.22), though they were much larger than those in the cases of 2010 Toyota Yaris. Based on the simulation results, the 3BMR-1 passed all the

evaluation criteria of MASH TL-2 under impacts by the 2007 Chevy Silverado at the two impact locations.



(a) (b)

Figure 4.38: Time histories of angular motions of 2007 Chevy Silverado impacting 3BMR-1 under TL-2 conditions. (a) With expansion joint as reference; and (b) with the post as reference.

Table 4.21: Evaluation factors of 3BMR-1 impacted by 2007 Chevy Silverado (TL-2) with expansion joint as reference.

Criteria	MASH criterion *H*		MASH criterion *I*		MASH criterion *F*		MASH criterion *N*	MASH criterion *A*	
Factors	OIV_x	OIV_y	ORA_x	ORA_y	Max roll angle	Max pitch angle	Exit angle	Permanent deflection	Dynamic deflection
Value	7.78 m/s	5.25 m/s	3.764G	5.108G	5.7°	5.7°	15°	97.8 mm	231.1 mm
Limit	12.2 m/s	12.2 m/s	20.49G	20.49G	75°	75°	/	/	
Evaluation	Pass	Pass	Pass	Pass	Pass	Pass	Pass	/	

Table 4.22: Evaluation factors of 3BMR-1 impacted by 2007 Chevy Silverado (TL-2) with post as reference.

Criteria	MASH criterion *H*		MASH criterion *I*		MASH criterion *F*		MASH criterion *N*	MASH criterion *A*	
Factors	OIV_x	OIV_y	ORA_x	ORA_y	Max roll angle	Max pitch angle	Exit angle	Permanent deflection	Dynamic deflection
Value	6.15 m/s	5.39 m/s	6.588G	7.873G	7.4°	6.0°	15°	103.9 mm	227.1 mm
Limit	12.2 m/s	12.2 m/s	20.49G	20.49G	75°	75°	/	/	
Evaluation	Pass	Pass	Pass	Pass	Pass	Pass	Pass	/	

4.3.1.3 The 3BMR-1 impacted by 2014 Chevy Silverado under TL-2 conditions

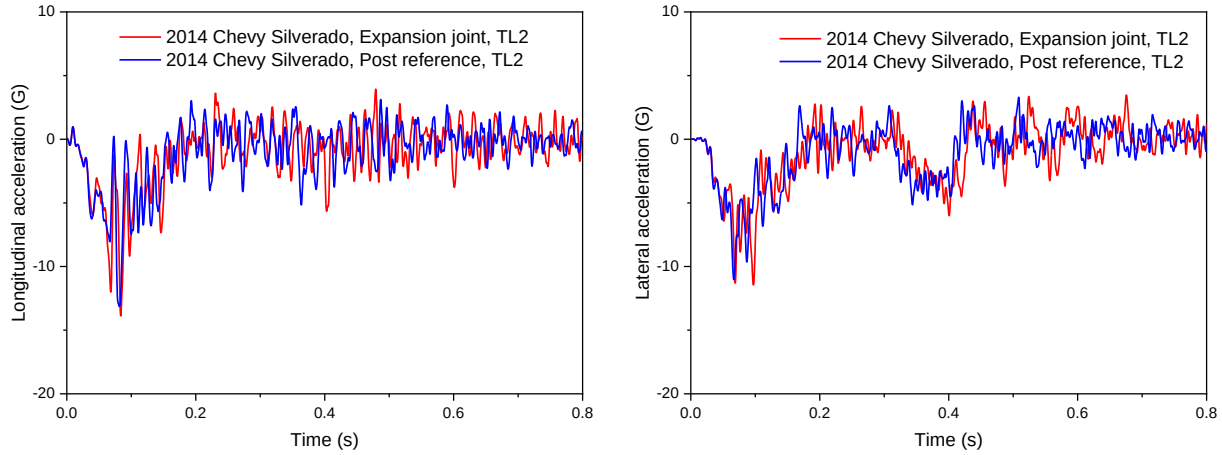
Figure 4.39 shows the top-view vehicle trajectories of the 2014 Chevy Silverado impacting the 3BMR-1 at 44 mph (70 km/h) and a 25° impact angle. For both impact cases, the vehicle passed MASH exit box criterion and the post-impact trajectories were considered as safe redirections.



(a) (b)

Figure 4.39: Vehicle trajectories of 2014 Chevy Silverado impacting 3BMR-1 under TL-2 conditions. (a) With expansion joint as reference; and (b) with the post as reference.

Figure 4.40 shows the time histories of vehicle accelerations in both longitudinal and lateral directions. No significant difference in vehicle accelerations was observed between the two impact locations.

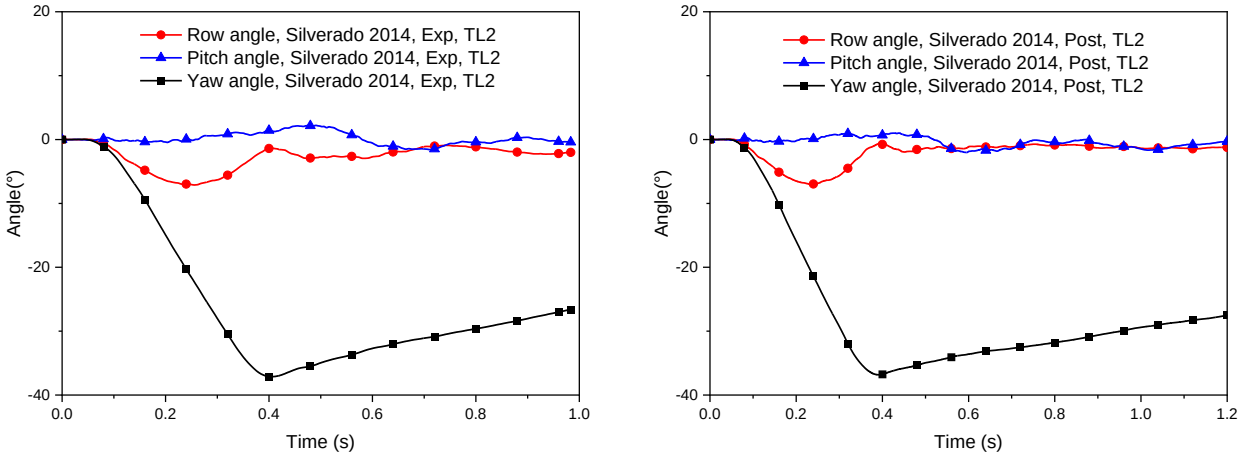


(a) (b)

Figure 4.40: Time histories of accelerations of 2014 Chevy Silverado impacting 3BMR-1 under TL-2 conditions. (a) Longitudinal direction; and (b) lateral direction.

Figure 4.41 shows the time history of the vehicle's row, pitch, and yaw angles. The maximum roll angles for the two impact cases were 7.1° and 7.0°, respectively, and the maximum pitch angles were 2.2° and 2.0°, respectively. In both cases, the 3BMR-1 passed the MASH evaluation criterion *F*, which specified a maximum 75° roll and pitch angles.

The occupant safety factors, the OIVs and ORAs, were calculated using the time histories of vehicle accelerations in both longitudinal and lateral directions. The OIV and ORA values for both impact cases are summarized in Tables 4.23 and 4.24, along with the vehicle's roll, pitch, and exit angles. It can be seen that all the OIV and ORA values were below the MASH limit values. The maximum dynamic and permanent deflections of the bridge rail were comparable to those in the cases of 2007 Chevy Silverado. Based on the simulation results, the 3BMR-1 passed all the evaluation criteria of MASH TL-2 under impacts by the 2014 Chevy Silverado at the two impact locations.



(a) (b)

Figure 4.41: Time histories of angular motions of 2014 Chevy Silverado impacting 3BMR-1 under TL-2 conditions. (a) With expansion joint as reference; and (b) with the post as reference.

Table 4.23: Evaluation factors of 3BMR-1 impacted by 2014 Chevy Silverado (TL-2) with expansion joint as reference.

Criteria	MASH criterion *H*		MASH criterion *I*		MASH criterion *F*		MASH criterion *N*	MASH criterion *A*	
Factors	OIV_x	OIV_y	ORA_x	ORA_y	Max roll angle	Max pitch angle	Exit angle	Permanent deflection	Dynamic deflection
Value	5.65 m/s	5.37 m/s	-5.175G	-4.863G	7.1°	2.2°	14°	122.8 mm	250.7 mm
Limit	12.2 m/s	12.2 m/s	20.49G	20.49G	75°	75°	/	/	
Evaluation	Pass	Pass	Pass	Pass	Pass	Pass	Pass	/	

Table 4.24: Evaluation factors of 3BMR-1 impacted by 2014 Chevy Silverado (TL-2) with post as reference.

Criteria	MASH criterion *H*		MASH criterion *I*		MASH criterion *F*		MASH criterion *N*	MASH criterion *A*	
Factors	OIV_x	OIV_y	ORA_x	ORA_y	Max roll angle	Max pitch angle	Exit angle	Permanent deflection	Dynamic deflection
Value	5.69 m/s	5.51 m/s	4.537G	4.092G	7.0°	2.0°	16°	119.1 mm	221.5 mm
Limit	12.2 m/s	12.2 m/s	20.49G	20.49G	75°	75°	/	/	
Evaluation	Pass	Pass	Pass	Pass	Pass	Pass	Pass	/	

4.3.2 Evaluation of 3BMR-1 under TL-3 conditions

4.3.2.1 The 3BMR-1 impacted by 2010 Toyota Yaris under TL-3 conditions

Figure 4.42 shows the top-view vehicle trajectories of the 2010 Toyota Yaris impacting the 3BMR-1 at 62 mph (100 km/h) and a 25° impact angle. Tire tracks of the vehicle and the exit box were also shown in the figure. Under TL-3 conditions, the post-impact vehicular responses were different in the two impact cases. For impact with the expansion joint as the reference point, as shown in Figure 4.42(a), the vehicle was bounced back without being redirected. In this case, the

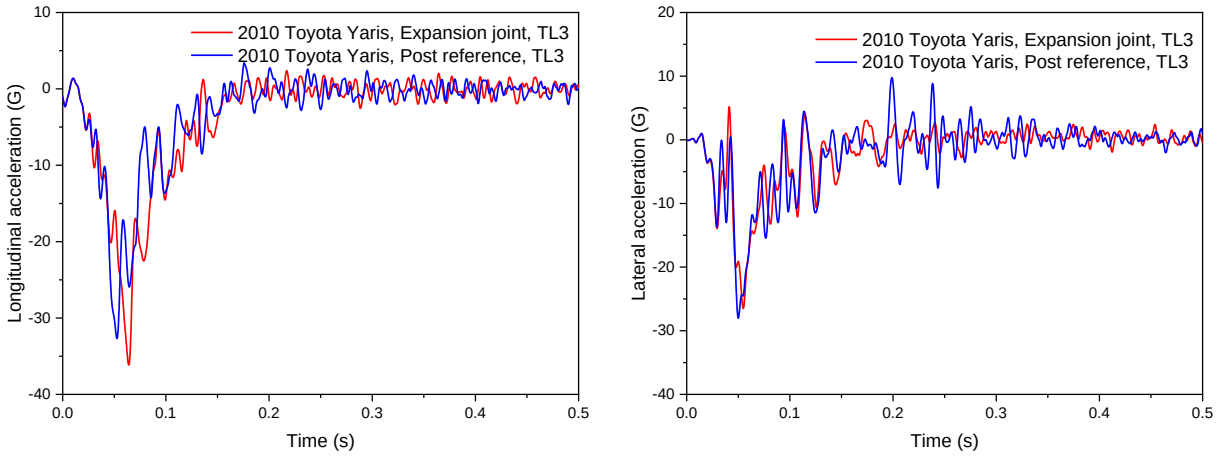
MASH exit box criterion was not met because the vehicle left the rectangular box with wheel tracks on both the left side (i.e., the short side) and the top side (i.e., the long side) of the rectangular box. To pass the exit box criterion, the vehicle must leave the rectangular box from the left side with wheel tracks not going over the top, long side. For the case with the post as reference point, the vehicle was redirected and passed the MASH exit box criterion, because the vehicle's wheel tracks were below the top side before leaving the rectangular box from the left side. Based on the post-impact trajectories of the vehicle, only the case with the post as reference point was considered as a safe redirection.



(a) (b)

Figure 4.42: Vehicle trajectories of 2010 Toyota Yaris impacting 3BMR-1 under TL-3 conditions.
(a) With expansion joint as reference; and (b) with the post as reference.

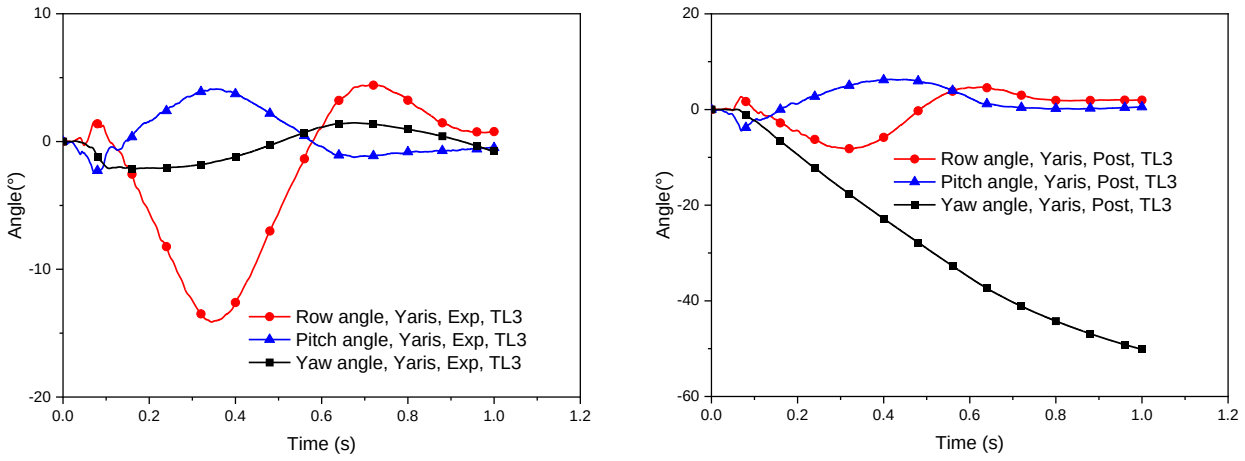
Figure 4.43 shows the time histories of vehicle accelerations in both longitudinal and lateral directions. No significant difference in vehicle accelerations was observed between the two impact locations even though the vehicular responses were different in the two cases.



(a) (b)

Figure 4.43: Time histories of accelerations of 2010 Toyota Yaris impacting 3BMR-1 under TL-3 conditions.
(a) Longitudinal direction; and (b) lateral direction.

Figure 4.44 shows the time history of the vehicle's row, pitch, and yaw angles. The maximum roll angles for the two impact cases were 14.1° and 8.2°, respectively, and the maximum pitch angles were 4.1° and 6.3°, respectively, for the two impact cases. In both cases, the 3BMR-1 passed the MASH evaluation criterion *F*, which specified a maximum 75° roll and pitch angles.



(a) (b)

Figure 4.44: Time histories of angular motions of the 2010 Toyota Yaris impacting 3BMR-1 under TL-3 conditions. (a) With expansion joint as reference; and (b) with the post as reference.

The occupant safety factors, the OIVs and ORAs, were calculated using the time histories of vehicle accelerations in both longitudinal and lateral directions. The OIV and ORA values for both impact cases are summarized in Tables 4.25 and 4.26, along with the vehicle's roll, pitch, and exit angles. It can be seen that all the OIV and ORA values were below the limit values specified in MASH, except for OIV_x in the case with expansion joint as the reference point. The maximum dynamic and permanent deflections of the bridge rail were calculated and found insignificant in both cases (see Tables 4.25 and 4.26). Based on the simulation results, the 3BMR-1 passed all the MASH evaluation criteria under impacts by the 2010 Toyota Yaris with the post as reference point but exceeded the OIV limit in the case with expansion joint as the reference point.

Table 4.25: Evaluation factors of 3BMR-1 impacted by 2010 Toyota Yaris (TL-3) with expansion joint as reference.

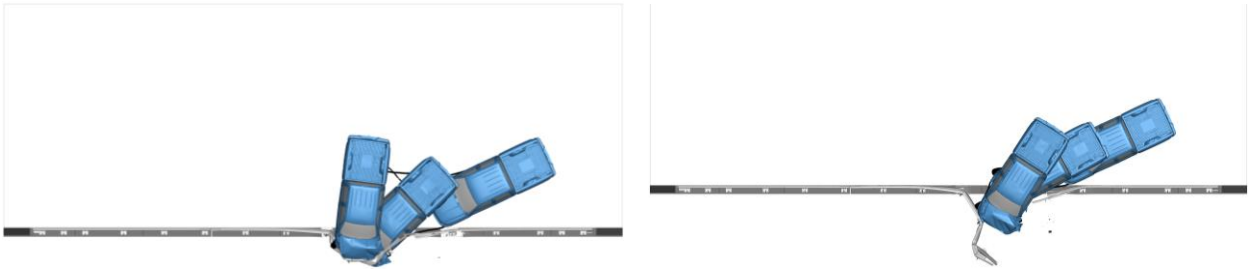
Criteria	MASH criterion *H*		MASH criterion *I*		MASH criterion *F*		MASH criterion *N*	MASH criterion *A*	
Factors	OIV_x	OIV_y	ORA_x	ORA_y	Max roll angle	Max pitch angle	Exit angle	Permanent deflection	Dynamic deflection
Value	12.27 m/s	7.62 m/s	12.310G	7.822G	14.1°	4.1°	15°	181.4 mm	271.2 mm
Limit	12.2 m/s	12.2 m/s	20.49G	20.49G	75°	75°	/	/	
Evaluation	Fail	Pass	Pass	Pass	Pass	Pass	Fail	/	

Table 4.26: Evaluation factors of 3BMR-1 impacted by 2010 Toyota Yaris (TL-3) with post as reference.

Criteria	MASH criterion *H*		MASH criterion *I*		MASH criterion *F*		MASH criterion *N*	MASH criterion *A*	
Factors	OIV_x	OIV_y	ORA_x	ORA_y	Max roll angle	Max pitch angle	Exit angle	Permanent deflection	Dynamic deflection
Value	10.74 m/s	7.94 m/s	12.292G	8.864G	8.2°	6.3°	9.5°	118.9 mm	226.5 mm
Limit	12.2 m/s	12.2 m/s	20.49G	20.49G	75°	75°	/	/	
Evaluation	Pass	Pass	Pass	Pass	Pass	Pass	Pass	/	

4.3.2.2 The 3BMR-1 impacted by 2007 Chevy Silverado under TL-3 conditions

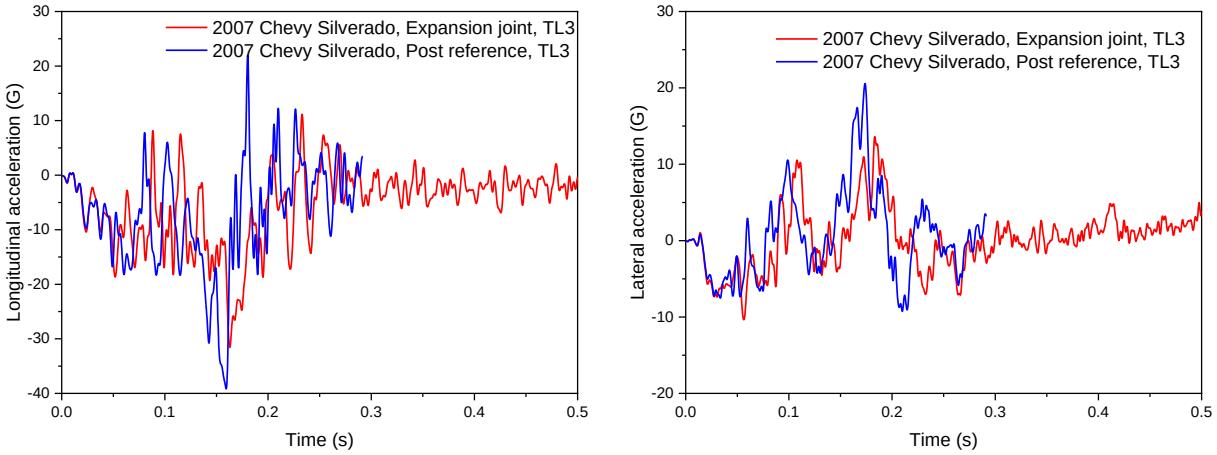
Figure 4.45 shows the top-view vehicle trajectories of the 2007 Chevy Silverado impacting the 3BMR-1 at 62 mph (100 km/h) and a 25° impact angle. In both cases, the vehicle stuck on the bridge rail without being redirected and the metal rails experienced large displacement and deformations. In the case with the post as reference point, the vehicle penetrated through the bridge rail due to metal rail failure. Since the vehicle did not leave the bridge rail in both cases, the MASH exit box criterion was not applicable, and both cases were not considered as safe redirections. A close examination showed that the bridge rail failure originated from the concrete foundation under the post hit by the vehicle. This was due to the low strength of the concrete foundation without steel reinforcement bars in the 3BMR-1 model. It became necessary to run the impact simulations with the 3BMR-2 models, which had full reinforcement in the concrete foundation, to determine if the 3BMR could meet MASH TL-3 requirements.



(a) (b)

Figure 4.45: Vehicle trajectories of 2007 Chevy Silverado impacting 3BMR-1 under TL-3 conditions. (a) With expansion joint as reference; and (b) with the post as reference.

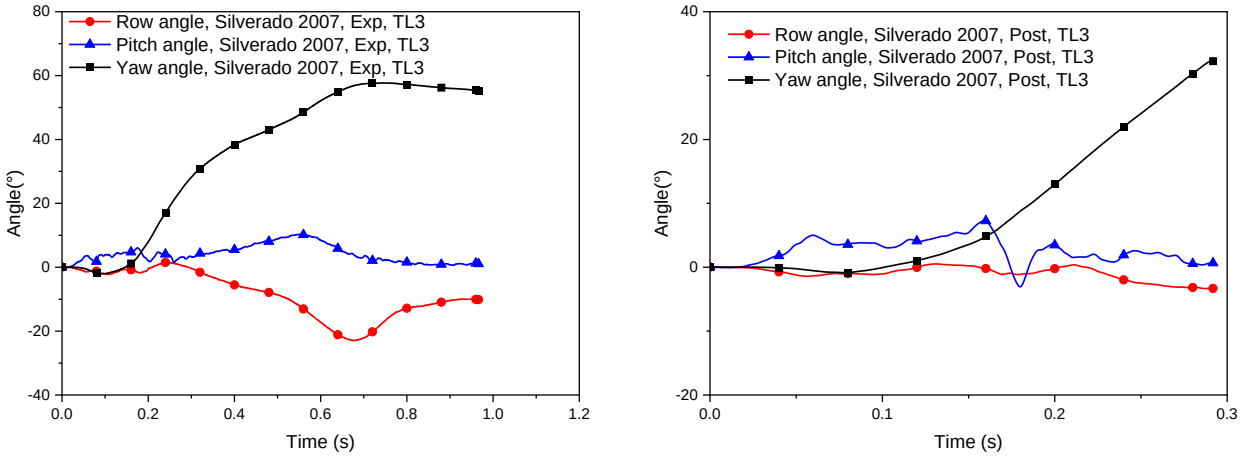
Figure 4.46 shows the time histories of vehicle accelerations in both longitudinal and lateral directions. No significant difference in vehicle accelerations was observed between the two impact locations.



(a) (b)

Figure 4.46: Time histories of accelerations of 2007 Chevy Silverado impacting 3BMR-1 under TL-3 conditions. (a) Longitudinal direction; and (b) lateral direction.

Figure 4.47 shows the time history of the vehicle's row, pitch, and yaw angles. The maximum roll angles for the two impact cases were 22.9° and 3.3°, respectively, and the maximum pitch angles were 10.3° and 7.3°, respectively. In both cases, the 3BMR-1 passed the MASH evaluation criterion *F*, which specified a maximum 75° roll and pitch angles.



(a) (b)

Figure 4.47: Time histories of angular motions of 2007 Chevy Silverado impacting 3BMR-1 under TL-3 conditions. (a) With expansion joint as reference; and (b) with the post as reference.

The occupant safety factors, the OIVs and ORAs, were calculated using the time histories of vehicle accelerations in both longitudinal and lateral directions. The OIV and ORA values for both impact cases are summarized in Tables 4.27 and 4.28, along with the vehicle's roll, pitch, and exit angles. It was observed that the ORA values in the longitudinal direction exceeded the MASH limit value due to severe vehicle snagging. Based on the simulation results, the 3BMR-1 could not pass all the evaluation criteria of MASH TL-3 under impacts by the 2007 Chevy Silverado at the two impact locations. The 3BMR-2 model was needed to evaluate the performance of this bridge rail under MASH TL-3 conditions.

Table 4.27: Evaluation factors of 3BMR-1 impacted by 2007 Chevy Silverado (TL-3) with expansion joint as reference.

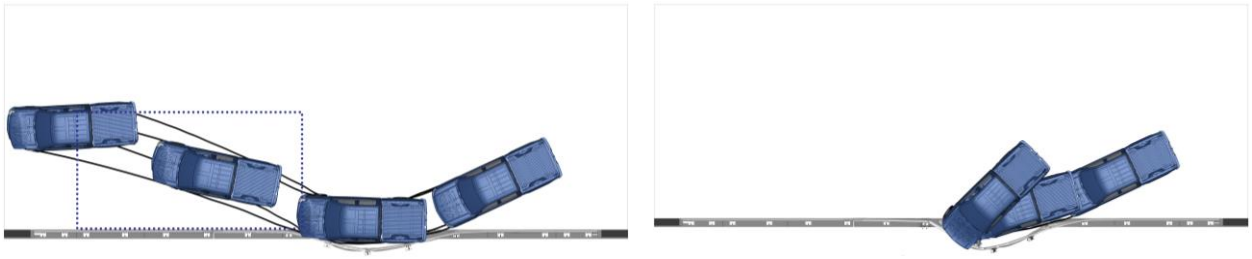
Criteria	MASH criterion *H*		MASH criterion *I*		MASH criterion *F*		MASH criterion *N*	MASH criterion *A*	
Factors	OIV_x	OIV_y	ORA_x	ORA_y	Max roll angle	Max pitch angle	Exit angle	Permanent deflection	Dynamic deflection
Value	9.83 m/s	2.44 m/s	27.030G	11.145G	22.9°	10.3°	N/A	N/A	N/A
Limit	12.2 m/s	12.2 m/s	20.49G	20.49G	75°	75°	/	/	
Evaluation	Pass	Pass	Fail	Pass	Pass	Pass	N/A	/	

Table 4.28: Evaluation factors of 3BMR-1 impacted by 2007 Chevy Silverado (TL-3) with post as reference.

Criteria	MASH criterion *H*		MASH criterion *I*		MASH criterion *F*		MASH criterion *N*	MASH criterion *A*	
Factors	OIV_x	OIV_y	ORA_x	ORA_y	Max roll angle	Max pitch angle	Exit angle	Permanent deflection	Dynamic deflection
Value	10.31 m/s	1.79 m/s	34.963G	16.626G	3.3°	7.3°	N/A	N/A	N/A
Limit	12.2 m/s	12.2 m/s	20.49G	20.49G	75°	75°	/	/	
Evaluation	Pass	Pass	Fail	Pass	Pass	Pass	N/A	/	

4.3.2.3 The 3BMR-1 impacted by 2014 Chevy Silverado under TL-3 conditions

Figure 4.48 shows the top-view vehicle trajectories of the 2014 Chevy Silverado impacting the 3BMR-1 at 62 mph (100 km/h) and a 25° impact angle. In the case with the expansion joint as reference point, the vehicle was redirected but failed to pass the MASH exit box criterion. In the case with the post as reference point, the vehicle stuck on the bridge rail without being redirected, causing a large deflection of the bridge rail. Both cases were not considered as safe redirections. Failures of the concrete footing were observed in both cases, similar to the cases of 2007 Chevy Silverado impacting the 3BMR-1 under TL-3 conditions. To this end, the 3BMR-2 models were used to determine if the 3BMR could meet MASH TL-3 requirements, with details given in Section 4.3.3.



(a) (b)

Figure 4.48: Vehicle trajectories of 2014 Chevy Silverado impacting 3BMR-1 under TL-3 conditions. (a) With expansion joint as reference; and (b) with the post as reference.

Figure 4.49 shows the time histories of vehicle accelerations in both longitudinal and lateral directions. No significant difference in vehicle accelerations was observed between the two impact locations.

Figure 4.50 shows the time history of the vehicle's row, pitch, and yaw angles. The maximum roll angles for the two impact cases were 5.9° and 8.4°, respectively, and the maximum pitch angles were 3.5° and 2.7°, respectively, for the two impact cases. In both cases, the 3BMR-1 passed the MASH evaluation criterion *F*, which specified a maximum 75° roll and pitch angles.

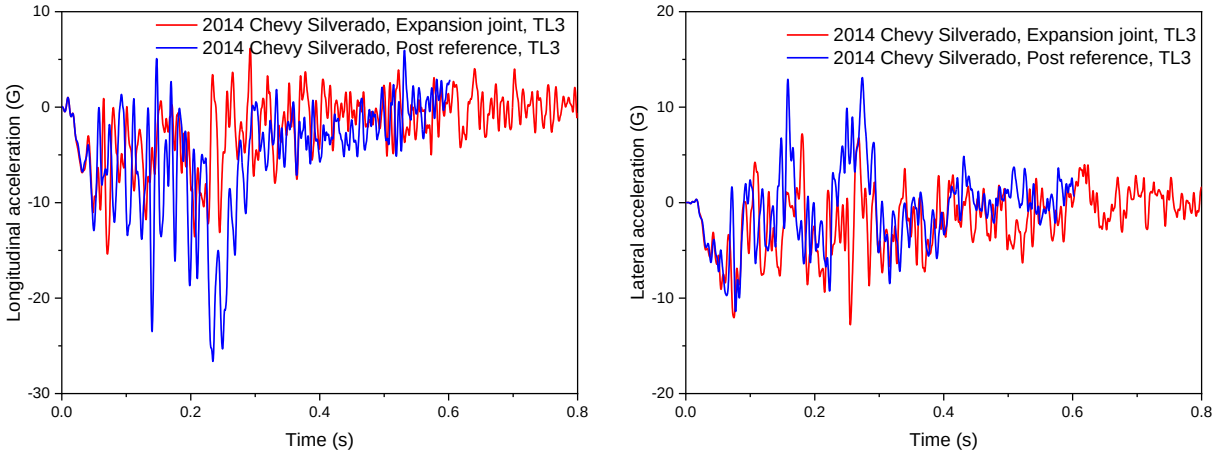


Figure 4.49: Time histories of accelerations of 2014 Chevy Silverado impacting 3BMR-1 under TL-3 conditions. (a) Longitudinal direction; and (b) lateral direction.

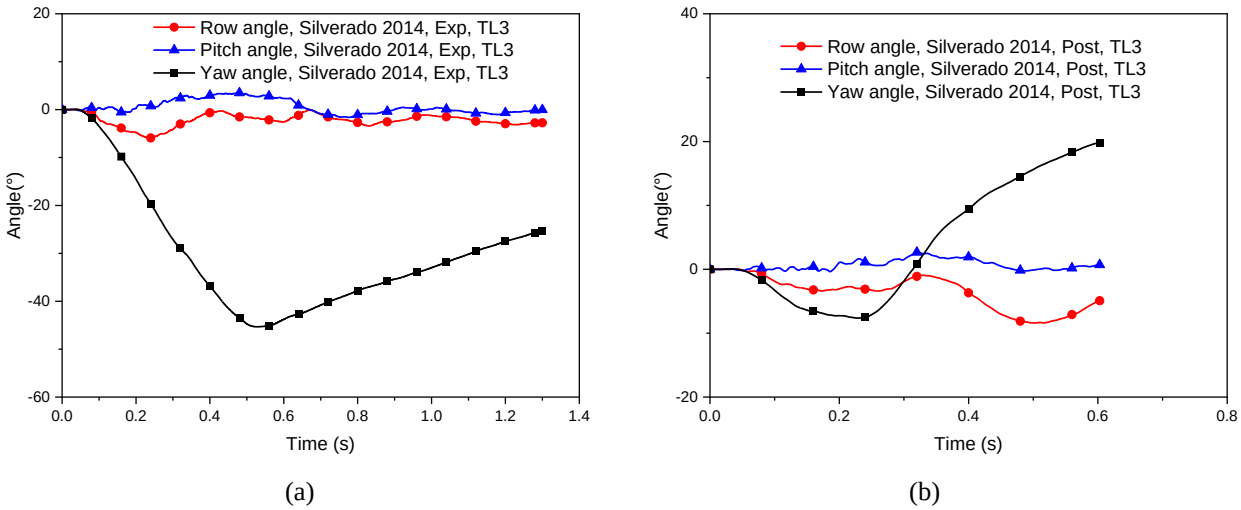


Figure 4.50: Time histories of angular motions of 2014 Chevy Silverado impacting 3BMR-1 under TL-3 conditions. (a) With expansion joint as reference; and (b) with the post as reference.

The occupant safety factors, the OIVs and ORAs, were calculated using the time histories of vehicle accelerations in both longitudinal and lateral directions. The OIV and ORA values for both impact cases are summarized in Tables 4.29 and 4.30, along with the vehicle's roll, pitch, and exit angles. Under impacts of the 2014 Chevy Silverado, only the ORA value in the longitudinal direction exceeded the MASH limit value in the case with the post as reference point. Similar to the cases of the 2007 Chevy Silverado, the bridge rail experienced large deflections in both cases due to failure in the concrete foundation. Based on the simulation results, the 3BMR-1 could not pass all the MASH TL-3 evaluation criteria under impacts by the 2014 Chevy Silverado at the two impact locations. The 3BMR-2 model was needed to evaluate the performance of this bridge rail under MASH TL-3 conditions.

Table 4.29: Evaluation factors of 3BMR-1 impacted by 2014 Chevy Silverado (TL-3) with expansion joint as reference.

Criteria	MASH criterion *H*		MASH criterion *I*		MASH criterion *F*		MASH criterion *N*	MASH criterion *A*	
Factors	OIV_x	OIV_y	ORA_x	ORA_y	Max roll angle	Max pitch angle	Exit angle	Permanent deflection	Dynamic deflection
Value	6.70 m/s	4.72 m/s	10.251G	7.708G	5.9°	3.5°	25°	907.5 mm	946.0 mm
Limit	12.2 m/s	12.2 m/s	20.49G	20.49G	75°	75°	/	/	
Evaluation	Pass	Pass	Pass	Pass	Pass	Pass	Fail	/	

Table 4.30: Evaluation factors of 3BMR-1 impacted by 2014 Chevy Silverado (TL-3) with post as reference.

Criteria	MASH criterion *H*		MASH criterion *I*		MASH criterion *F*		MASH criterion *N*	MASH criterion *A*	
Factors	OIV_x	OIV_y	ORA_x	ORA_y	Max roll angle	Max pitch angle	Exit angle	Permanent deflection	Dynamic deflection
Value	7.42 m/s	4.37 m/s	23.863G	10.485G	8.4°	2.7°	N/A	1433.2 mm	1569.4 mm
Limit	12.2 m/s	12.2 m/s	20.49G	20.49G	75°	75°	/	/	
Evaluation	Pass	Pass	Fail	Pass	Pass	Pass	N/A	/	

4.3.3 Evaluation of 3BMR-2 under TL-3 conditions

Under TL-3 conditions, the 3BMR-1 model exhibited unrealistically large rail deflections due to failure in the concrete foundation (without steel reinforcement) under impacts of the three test vehicles. To this end, the 3BMR-2 model, which included steel reinforcement bars in the concrete foundation, was developed and used in the evaluation of this bridge rail under TL-3 conditions.

4.3.3.1 The 3BMR-2 impacted by 2010 Toyota Yaris under TL-3 conditions

Figure 4.51 shows the top-view vehicle trajectories of the 2010 Toyota Yaris impacting the 3BMR-2 at 62 mph (100 km/h) and a 25° impact angle. The post-impact vehicular responses for the two impact cases were similar to those using the 3BMR-1 model (see Figure 4.42). These responses were expected, since no significant failure was found in the concrete foundation under impacts of the 2010 Toyota Yaris using the 3BMR-1 model. Only in the case with the post as reference point, the vehicle was redirected and passed the MASH exit box criterion.



(a) (b)

Figure 4.51: Vehicle trajectories of 2010 Toyota Yaris impacting 3BMR-2 under TL-3 conditions. (a) With expansion joint as reference; and (b) with the post as reference.

Figure 4.52 shows the time histories of vehicle accelerations in both longitudinal and lateral directions. No significant difference in vehicle accelerations was observed between the two impact locations.

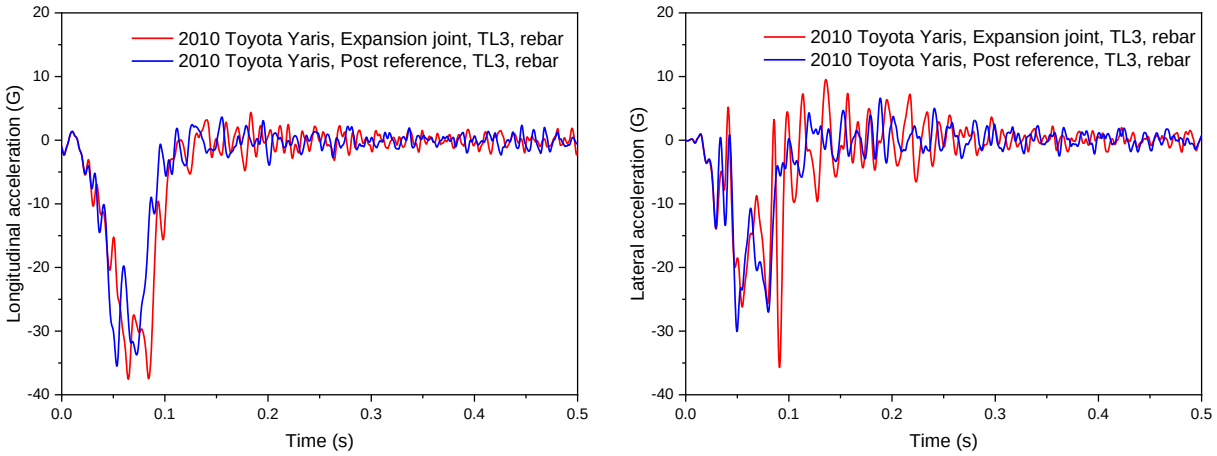


Figure 4.52: Time histories of accelerations of 2010 Toyota Yaris impacting 3BMR-2 under TL-3 conditions. (a) Longitudinal direction; and (b) lateral direction.

Figure 4.53 shows the time history of the vehicle's row, pitch, and yaw angles. The maximum roll angles for the two impact cases were 6.0° and 7.4°, respectively, and the maximum pitch angles were 10.8° and 6.6°, respectively, for the two impact cases. In both cases, the 3BMR-2 passed the MASH evaluation criterion *F*, which specified a maximum 75° roll and pitch angles.

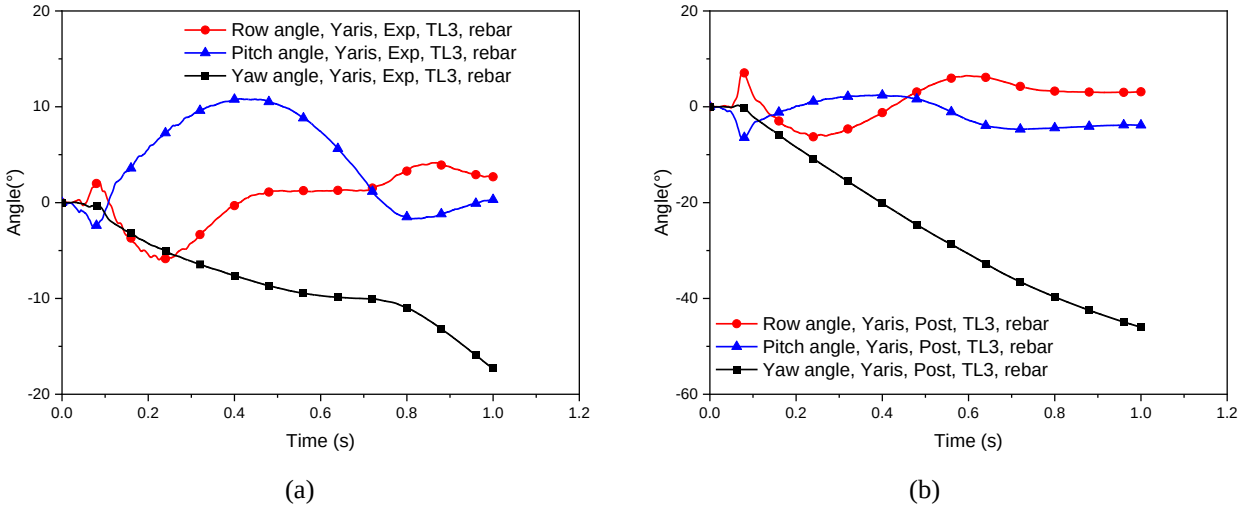


Figure 4.53: Time histories of angular motions of 2010 Toyota Yaris impacting 3BMR-2 under TL-3 conditions. (a) With expansion joint as reference; and (b) with the post as reference.

The occupant safety factors, the OIVs and ORAs, were calculated using the time histories of vehicle accelerations in both longitudinal and lateral directions. The OIV and ORA values for both

impact cases are summarized in Tables 4.31 and 4.32, along with the vehicle's roll, pitch, and exit angles. It can be seen that all the OIV and ORA values were below the MASH limit values except for the OIVs in the longitudinal direction in both cases. When impacting the 3BMR, the Yaris engaged with the aluminum rails with several components on the impact side: the front wheel (including the rim) on the driver side, frame rails, fender, hood, and bumper cover. This engagement caused large impact forces in the longitudinal direction of the vehicle and resulted in the OIV values exceeding the MASH limit. The maximum dynamic and permanent deflections of the bridge rail were calculated and found insignificant in both cases, as shown in Tables 4.31 and 4.32. Based on the simulation results, the 3BMR-2 could not pass all the MASH TL-3 evaluation criteria under impacts by the 2010 Toyota Yaris at both impact locations.

Table 4.31: Evaluation factors of 3BMR-2 impacted by 2010 Toyota Yaris (TL-3) with expansion joint as reference.

Criteria	MASH criterion *H*		MASH criterion *I*		MASH criterion *F*		MASH criterion *N*	MASH criterion *A*	
Factors	OIV_x	OIV_y	ORA_x	ORA_y	Max roll angle	Max pitch angle	Exit angle	Permanent deflection	Dynamic deflection
Value	15.28 m/s	9.87 m/s	11.042G	5.754G	6.0°	10.8°	18°	137.9 mm	208.9 mm
Limit	12.2 m/s	12.2 m/s	20.49G	20.49G	75°	75°	/	/	
Evaluation	Fail	Pass	Pass	Pass	Pass	Pass	Fail	/	

Table 4.32: Evaluation factors of 3BMR-2 impacted by 2010 Toyota Yaris (TL-3) with post as reference.

Criteria	MASH criterion *H*		MASH criterion *I*		MASH criterion *F*		MASH criterion *N*	MASH criterion *A*	
Factors	OIV_x	OIV_y	ORA_x	ORA_y	Max roll angle	Max pitch angle	Exit angle	Permanent deflection	Dynamic deflection
Value	13.59 m/s	9.81 m/s	4.307G	4.437G	7.4°	6.6°	11°	95.8 mm	149.6 mm
Limit	12.2 m/s	12.2 m/s	20.49G	20.49G	75°	75°	/	/	
Evaluation	Fail	Pass	Pass	Pass	Pass	Pass	Pass	/	

4.3.3.2 The 3BMR-2 impacted by 2007 Chevy Silverado under TL-3 conditions

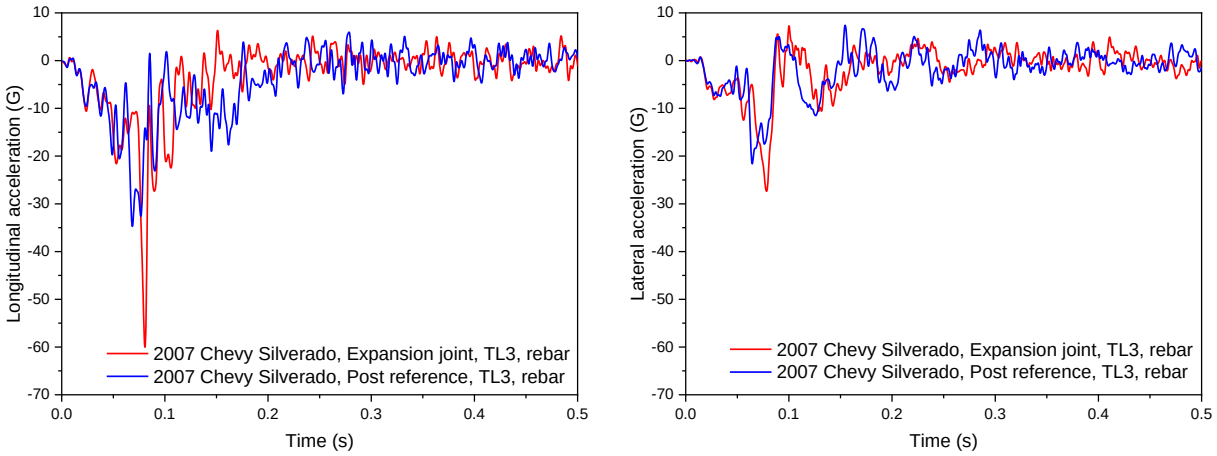
Figure 4.54 shows the top-view vehicle trajectories of the 2007 Chevy Silverado impacting the 3BMR-2 at 62 mph (100 km/h) and a 25° impact angle. In both cases, the vehicle was redirected and passed the MASH exit box criterion. Unlike the cases using the 3BMR-1 models, no unrealistic failure was observed in the concrete foundation using the 3BMR-2 models as a result of the added reinforcement bars. In the case with the expansion joint as reference point, the vehicle exhibited some clockwise rotation after being redirected.



(a) (b)

Figure 4.54: Vehicle trajectories of the 2007 Chevy Silverado impacting 3BMR-2 under TL-3 conditions. (a) With expansion joint as reference; and (b) with the post as reference.

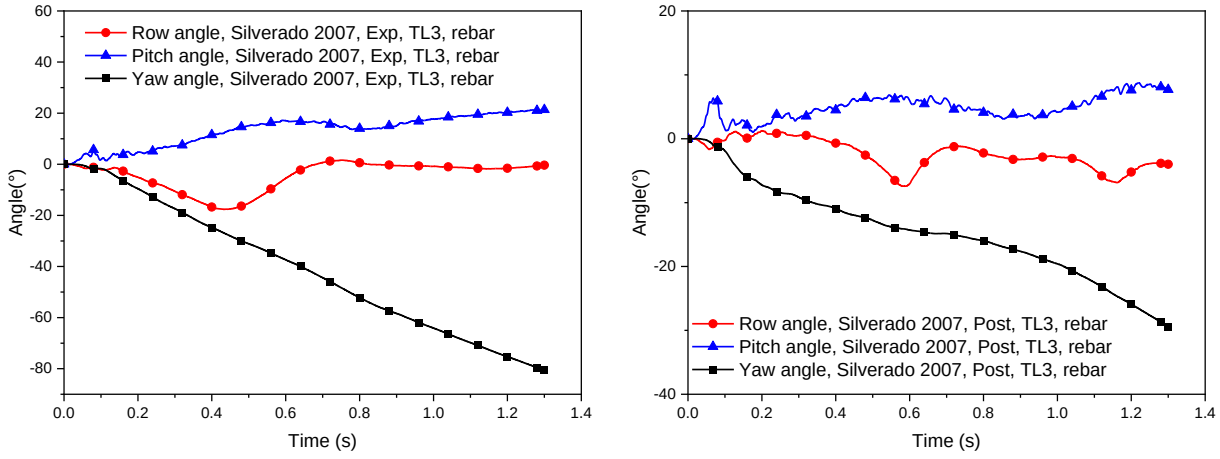
Figure 4.55 shows the time histories of vehicle accelerations in both longitudinal and lateral directions. The trends of vehicle accelerations were similar in both cases but the peak accelerations in the longitudinal direction had some significant difference.



(a) (b)

Figure 4.55: Time histories of accelerations of 2007 Chevy Silverado impacting 3BMR-2 under TL-3 conditions. (a) Longitudinal direction; and (b) lateral direction.

Figure 4.56 shows the time history of the vehicle's row, pitch, and yaw angles. The maximum roll angles for the two impact cases were 17.6° and 7.4°, respectively, and the maximum pitch angles were 21.4° and 8.8°, respectively. In both cases, the 3BMR-2 passed the MASH evaluation criterion *F*, which specified a maximum 75° roll and pitch angles.



(a) (b)

Figure 4.56: Time histories of angular motions of 2007 Chevy Silverado impacting 3BMR-2 under TL-3 conditions. (a) With expansion joint as reference; and (b) with the post as reference.

The occupant safety factors, the OIVs and ORAs, were calculated using the time histories of vehicle accelerations in both longitudinal and lateral directions. The OIV and ORA values for both

impact cases are summarized in Tables 4.33 and 4.34, along with the vehicle's roll, pitch, and exit angles. It was observed in the case with expansion joint as reference point that the OIV value in the longitudinal direction exceeded the MASH limit. In this case, the front wheel on the driver side of the 2007 Silverado twisted inward upon hitting the curb, and the vehicle climbed up the curb and engaged with the aluminum rails, resulting in an increased impact forces and OIV values in the longitudinal direction. All other MASH evaluation criteria were met in both cases. The bridge rail deflections were calculated and found to be insignificant. This indicated that the 3BMR-2 model should be used for impact under the pickup truck under MASH TL-3 conditions. Based on the simulation results, the 3BMR-2 passed all the MASH evaluation criteria under impacts by the 2007 Chevy Silverado with the post as reference point but exceeded the OIV limit in the case with the expansion joint as reference point.

Table 4.33: Evaluation factors of 3BMR-2 impacted by 2007 Chevy Silverado (TL-3) with expansion joint as reference.

Criteria	MASH criterion *H*		MASH criterion *I*		MASH criterion *F*		MASH criterion *N*	MASH criterion *A*	
Factors	OIV_x	OIV_y	ORA_x	ORA_y	Max roll angle	Max pitch angle	Exit angle	Permanent deflection	Dynamic deflection
Value	13.60 m/s	6.32 m/s	8.329G	8.668G	17.6°	21.4°	11.5°	235.9 mm	259.0 mm
Limit	12.2 m/s	12.2 m/s	20.49G	20.49G	75°	75°	/	/	
Evaluation	Fail	Pass	Pass	Pass	Pass	Pass	Pass	/	

Table 4.34: Evaluation factors of 3BMR-2 impacted by 2007 Chevy Silverado (TL-3) with post as reference.

Criteria	MASH criterion *H*		MASH criterion *I*		MASH criterion *F*		MASH criterion *N*	MASH criterion *A*	
Factors	OIV_x	OIV_y	ORA_x	ORA_y	Max roll angle	Max pitch angle	Exit angle	Permanent deflection	Dynamic deflection
Value	11.92 m/s	5.52 m/s	13.596G	10.383G	7.4°	8.8°	18°	304.0 mm	393.8 mm
Limit	12.2 m/s	12.2 m/s	20.49G	20.49G	75°	75°	/	/	
Evaluation	Pass	Pass	Pass	Pass	Pass	Pass	Pass	/	

4.3.3.3 The 3BMR-2 impacted by 2014 Chevy Silverado under TL-3 conditions

Figure 4.57 shows the top-view vehicle trajectories of the 2014 Chevy Silverado impacting the 3BMR-2 at 62 mph (100 km/h) and a 25° impact angle. For both impact cases, the vehicle passed MASH exit box criterion and the post-impact trajectories were considered as safe redirections.



(a) (b)

Figure 4.57: Vehicle trajectories of 2014 Chevy Silverado impacting 3BMR-2 under TL-3 conditions. (a) With expansion joint as reference; and (b) with the post as reference.

Figure 4.58 shows the time histories of vehicle accelerations in both longitudinal and lateral directions. No significant difference in vehicle accelerations was observed between the two impact locations.

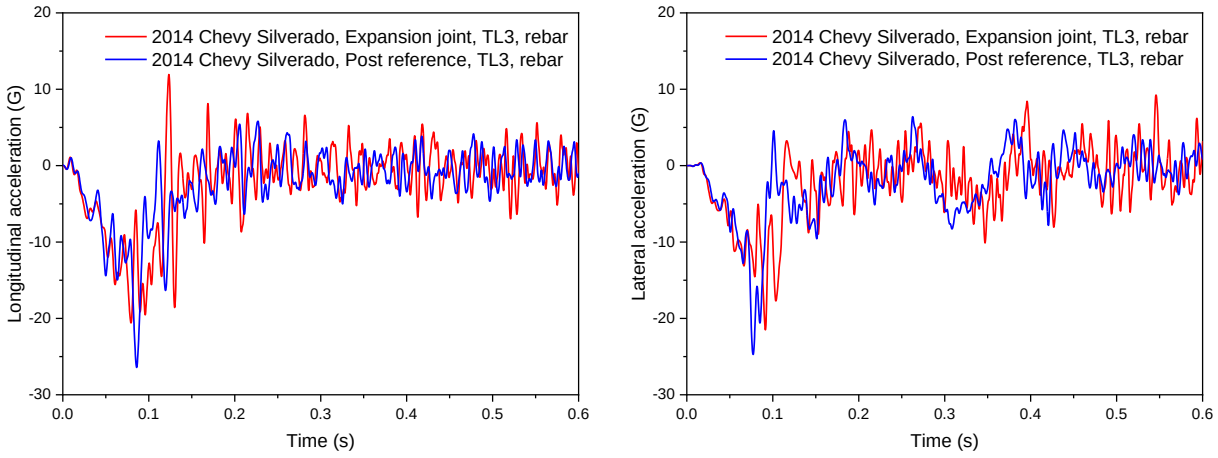


Figure 4.58: Time histories of accelerations of 2014 Chevy Silverado impacting 3BMR-2 under TL-3 conditions. (a) Longitudinal direction; and (b) lateral direction.

Figure 4.59 shows the time history of the vehicle's row, pitch, and yaw angles. The maximum roll angles for the two impact cases were 5.0° and 9.8°, respectively, and the maximum pitch angles were 4.1° and 9.5°, respectively. In both cases, the 3BMR-2 passed the MASH evaluation criterion *F*, which specified a maximum 75° roll and pitch angles.

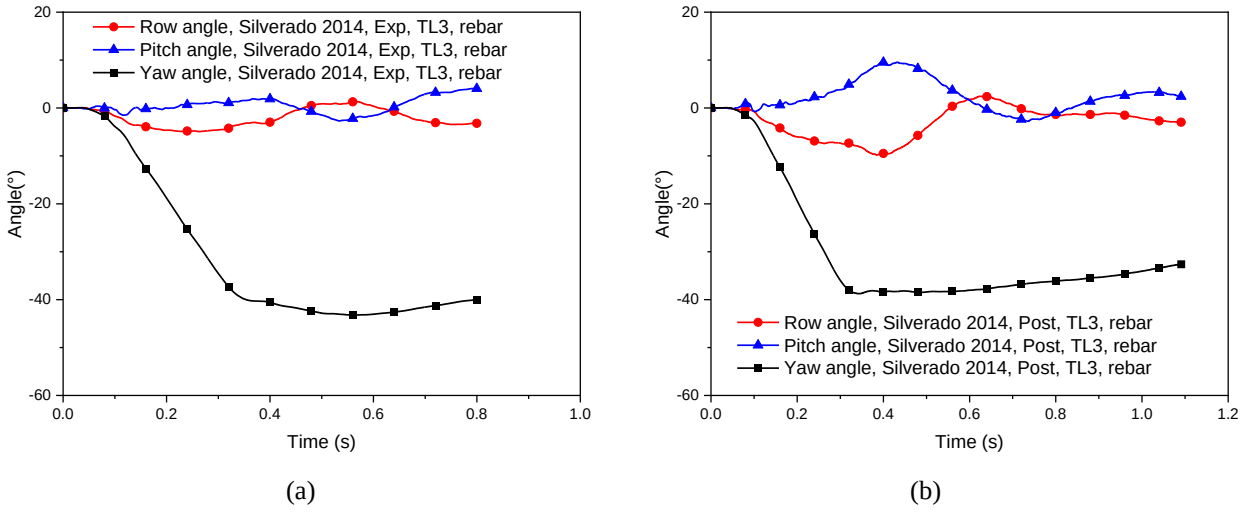


Figure 4.59: Time histories of angular motions of 2014 Chevy Silverado impacting 3BMR-2 under TL-3 conditions. (a) With expansion joint as reference; and (b) with the post as reference.

The occupant safety factors, i.e., OIVs and ORAs were calculated using the time histories of vehicle accelerations in both longitudinal and lateral directions. The OIV and ORA values for both

impact cases are summarized in Tables 4.35 and 4.36, along with the vehicle's roll, pitch, and exit angles. It can be seen that all the OIV and ORA values were below the MASH limit values. The maximum dynamic and permanent deflections of the bridge rail were calculated and found to be insignificant, also comparable to those in the cases of 2007 Chevy Silverado. Based on the simulation results, the 3BMR-2 passed all the evaluation criteria of MASH TL-3 under impacts by the 2014 Chevy Silverado at both impact locations.

Table 4.35: Evaluation factors of 3BMR-2 impacted by 2014 Chevy Silverado (TL-3) with expansion joint as reference.

Criteria	MASH criterion *H*		MASH criterion *I*		MASH criterion *F*		MASH criterion *N*	MASH criterion *A*	
Factors	OIV_x	OIV_y	ORA_x	ORA_y	Max roll angle	Max pitch angle	Exit angle	Permanent deflection	Dynamic deflection
Value	9.93 m/s	8.25 m/s	8.545G	6.279G	5.0°	4.1°	16°	204.6 mm	283.0 mm
Limit	12.2 m/s	12.2 m/s	20.49G	20.49G	75°	75°	/	/	
Evaluation	Pass	Pass	Pass	Pass	Pass	Pass	Pass	/	

Table 4.36: Evaluation factors of 3BMR-2 impacted by 2014 Chevy Silverado (TL-3) with post as reference.

Criteria	MASH criterion *H*		MASH criterion *I*		MASH criterion *F*		MASH criterion *N*	MASH criterion *A*	
Factors	OIV_x	OIV_y	ORA_x	ORA_y	Max roll angle	Max pitch angle	Exit angle	Permanent deflection	Dynamic deflection
Value	8.60 m/s	6.88 m/s	10.817G	7.990G	9.8°	9.5°	14°	208.2 mm	314.0 mm
Limit	12.2 m/s	12.2 m/s	20.49G	20.49G	75°	75°	/	/	
Evaluation	Pass	Pass	Pass	Pass	Pass	Pass	Pass	/	

4.4 Evaluation of Classic Rail under MASH TL-2 and TL-3 Conditions

The Classic Rail was evaluated under MASH TL-2 and TL-3 conditions with three test vehicles (a 2010 Toyota Yaris, a 2007 Chevy Silverado, and a 2014 Chevy Silverado) and one impact location (using an expansion joint as the reference point, see Figure 3.25).

4.4.1 Evaluation of Classic Rail under TL-2 conditions

4.4.1.1 The Classic Rail impacted by 2010 Toyota Yaris under TL-2 conditions

Figure 4.60 shows the top-view vehicle trajectories of the 2010 Toyota Yaris impacting the Classic Rail at 44 mph (70 km/h) and a 25° impact angle. Tire tracks of the vehicle and the exit box were also shown in the figure. In this case, the vehicle was bounced back without being redirected and failed to pass the MASH exit box criterion. The bridge rail had only minor damages around the initial impact location (see Figure 4.61), but the vehicle experienced severe damage on the driver side windows and the bumper cover.

Figure 4.62 shows the time history of the vehicle's row, pitch, and yaw angles. With a maximum roll angle of 3.1° and a maximum pitch angle of 3.4°, the Classic Rail passed the MASH evaluation criterion *F*, which specified a maximum 75° roll and pitch angles.

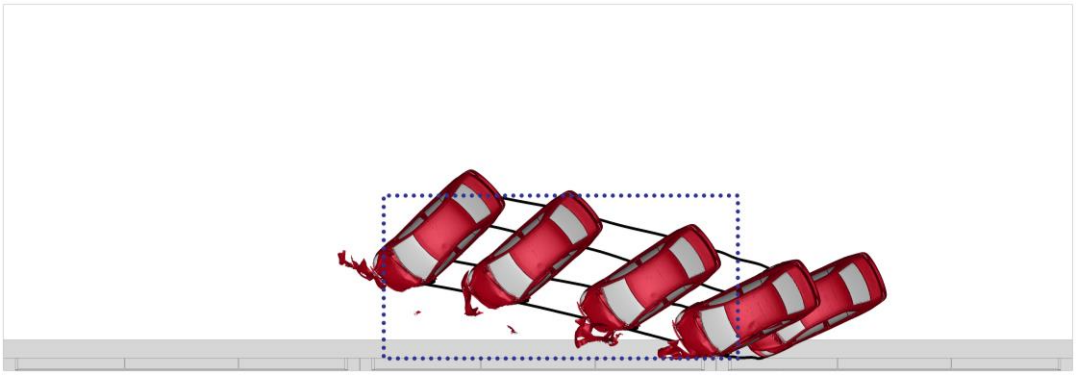


Figure 4.60: Vehicle trajectories of 2010 Toyota Yaris impacting Classic Rail under TL-2 conditions.

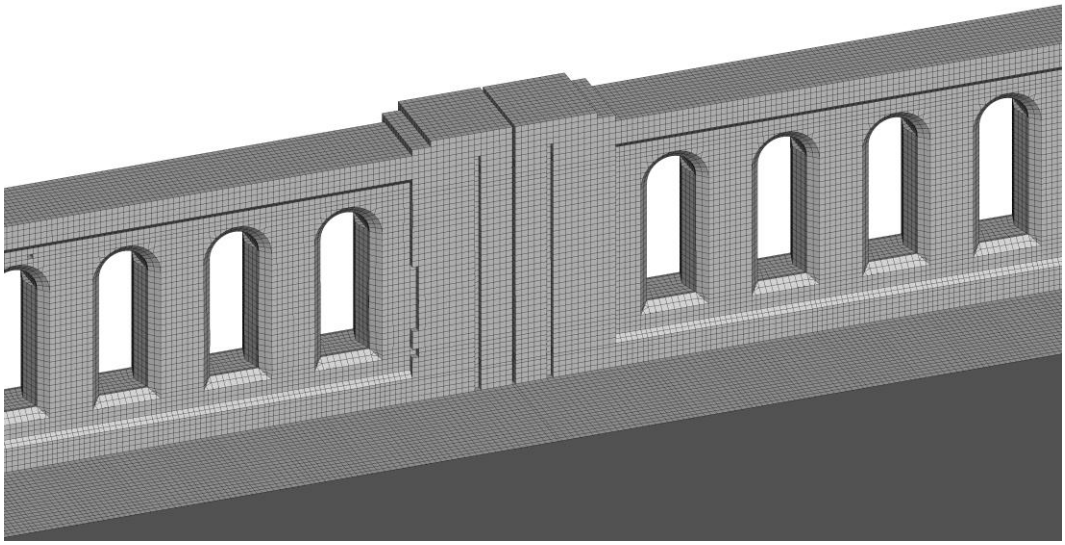


Figure 4.61: Damage on the Classic Rail under impact by 2010 Toyota Yaris under TL-2 conditions.

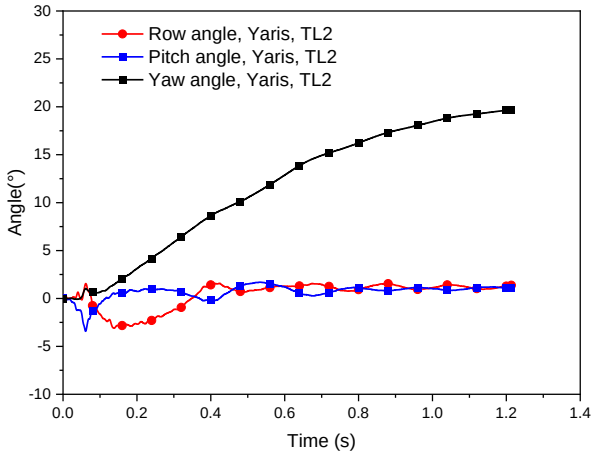
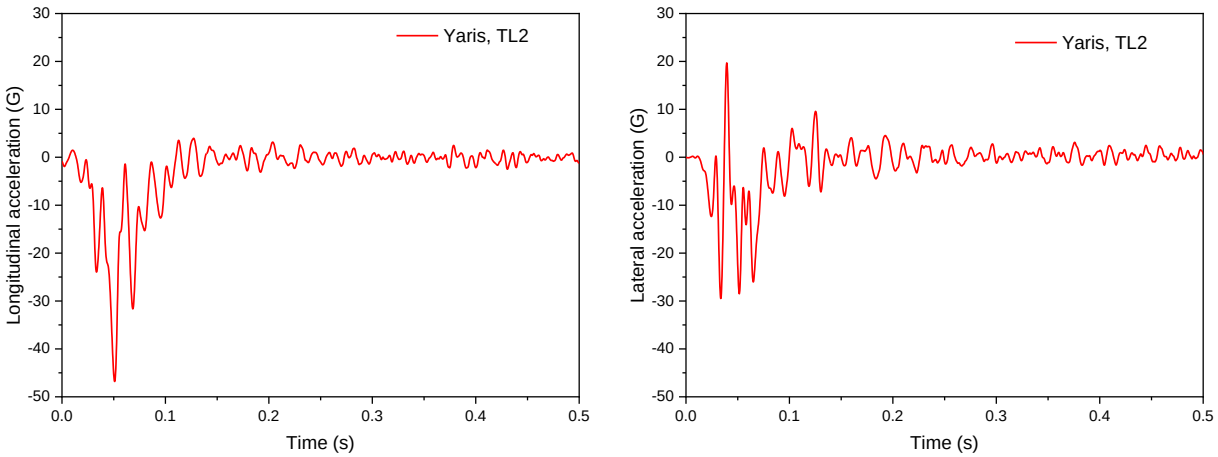


Figure 4.62: Time histories of angular motions of 2010 Toyota Yaris impacting Classic Rail under TL-2 conditions.

Figure 4.63 shows the time histories of vehicle accelerations in longitudinal and lateral directions, which were used to calculate the occupant safety factors, i.e., OIVs and ORAs in both directions, as given in Table 4.37. It can be seen that all the OIV and ORA values were below the MASH limit values. Based on the simulation results, the Classic Rail passed all the evaluation criteria of MASH TL-2 under impacts by the 2010 Toyota Yaris, except for the MASH exit box criterion.



(a) (b)

Figure 4.63: Time histories of accelerations of 2010 Toyota Yaris impacting Classic Rail under TL-2 conditions. (a) Longitudinal direction; and (b) lateral direction.

Table 4.37: Evaluation factors of Classic Rail impacted by 2010 Toyota Yaris under TL-2 conditions.

Criteria	MASH criterion *H*		MASH criterion *I*		MASH criterion *F*		MASH criterion *N*	MASH criterion *A*	
Factors	OIV_x	OIV_y	ORA_x	ORA_y	Max roll angle	Max pitch angle	Exit angle	Permanent deflection	Dynamic deflection
Value	11.80 m/s	6.77 m/s	3.763G	3.341G	3.1°	3.4°	15.1°	N/A	N/A
Limit	12.2 m/s	12.2 m/s	20.49G	20.49G	75°	75°	/	/	
Evaluation	Pass	Pass	Pass	Pass	Pass	Pass	Fail	/	

4.4.1.2 The Classic Rail impacted by 2007 Chevy Silverado under TL-2 conditions

Figure 4.64 shows the top-view vehicle trajectories of the 2007 Chevy Silverado impacting the Classic Rail at 44 mph (70 km/h) and a 25° impact angle. The vehicle was redirected and passed the MASH exit box criterion. The bridge rail experienced more damage around the initial impact location (see Figure 4.65) than that in the case of 2010 Toyota Yaris.

Figure 4.66 shows the time history of the vehicle's row, pitch, and yaw angles. With a maximum roll angle of 6.9° and a maximum pitch angle of 8.8°, the Classic Rail passed the MASH evaluation criterion *F*, which specified a maximum 75° roll and pitch angles.

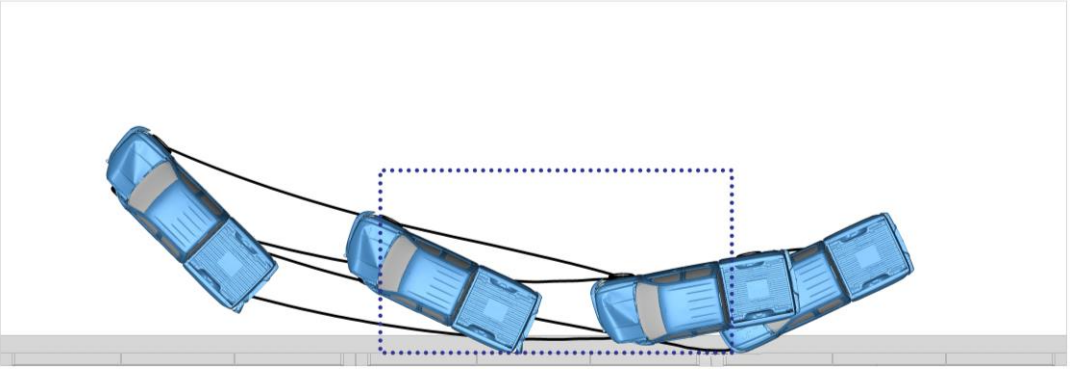


Figure 4.64: Vehicle trajectories of 2007 Chevy Silverado impacting Classic Rail under TL-2 conditions.

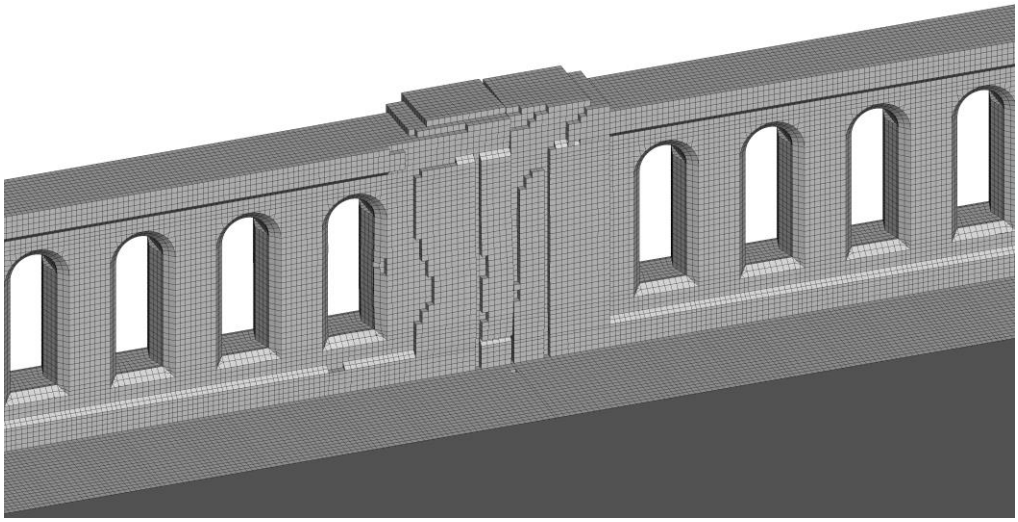


Figure 4.65: Damage on the Classic Rail under impact by 2007 Chevy Silverado under TL-2 conditions.

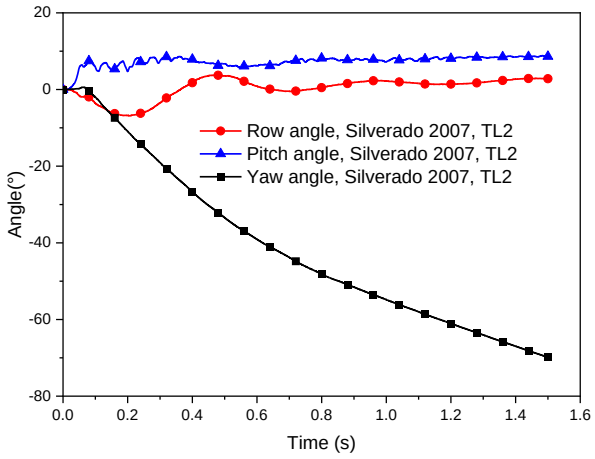
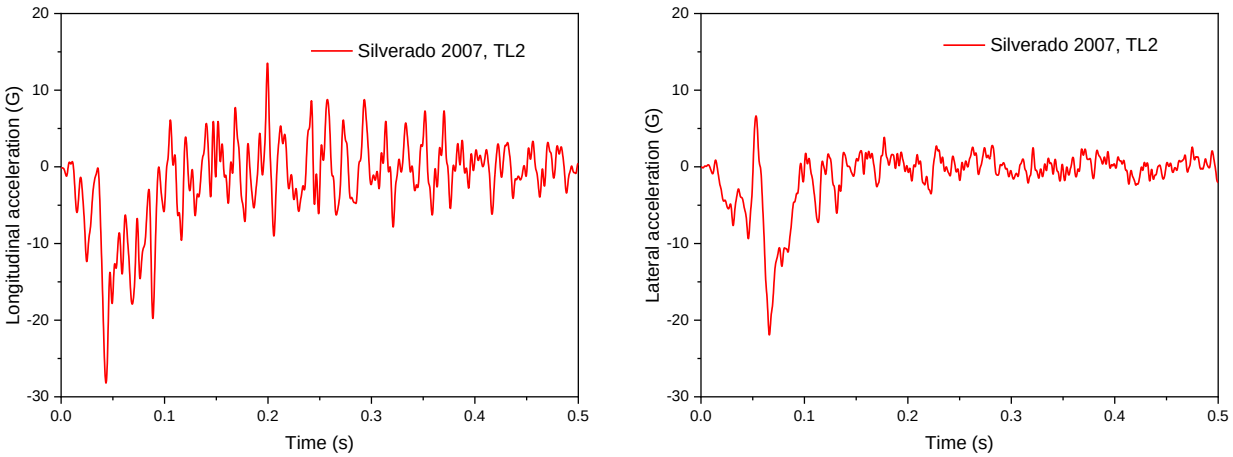


Figure 4.66: Time histories of angular motions of 2007 Chevy Silverado impacting Classic Rail under TL-2 conditions.

Figure 4.67 shows the time histories of vehicle accelerations in longitudinal and lateral directions, which were used to calculate the occupant safety factors, i.e., OIVs and ORAs in both directions, as given in Table 4.38. It can be seen that all the OIV and ORA values were below the MASH limit values. Based on the simulation results, the Classic Rail passed all the evaluation criteria of MASH TL-2 under impacts by the 2007 Chevy Silverado.



(a) (b)

Figure 4.67: Time histories of accelerations of 2007 Chevy Silverado impacting Classic Rail under TL-2 conditions. (a) Longitudinal direction; and (b) lateral direction.

Table 4.38: Evaluation factors of Classic Rail impacted by 2007 Chevy Silverado under TL-2 conditions.

Criteria	MASH criterion *H*		MASH criterion *I*		MASH criterion *F*		MASH criterion *N*	MASH criterion *A*	
Factors	OIV_x	OIV_y	ORA_x	ORA_y	Max roll angle	Max pitch angle	Exit angle	Permanent deflection	Dynamic deflection
Value	8.75 m/s	5.73 m/s	4.875G	3.112G	6.9°	8.8°	11.1°	N/A	N/A
Limit	12.2 m/s	12.2 m/s	20.49G	20.49G	75°	75°	/	/	
Evaluation	Pass	Pass	Pass	Pass	Pass	Pass	Pass	/	

4.4.1.3 The Classic Rail impacted by 2014 Chevy Silverado under TL-2 conditions

Figure 4.68 shows the top-view vehicle trajectories of the 2014 Chevy Silverado impacting the Classic Rail at 44 mph (70 km/h) and a 25° impact angle. The vehicle was smoothly redirected and passed the MASH exit box criterion. The damage on bridge rail was localized around the initial impact location (see Figure 4.69) and was similar to that in the case of the 2007 Chevy Silverado.

Figure 4.70 shows the time history of the vehicle's row, pitch, and yaw angles. With a maximum roll angle of 4.8° and a maximum pitch angle of 3.0°, the Classic Rail passed the MASH evaluation criterion *F*, which specified a maximum 75° roll and pitch angles.

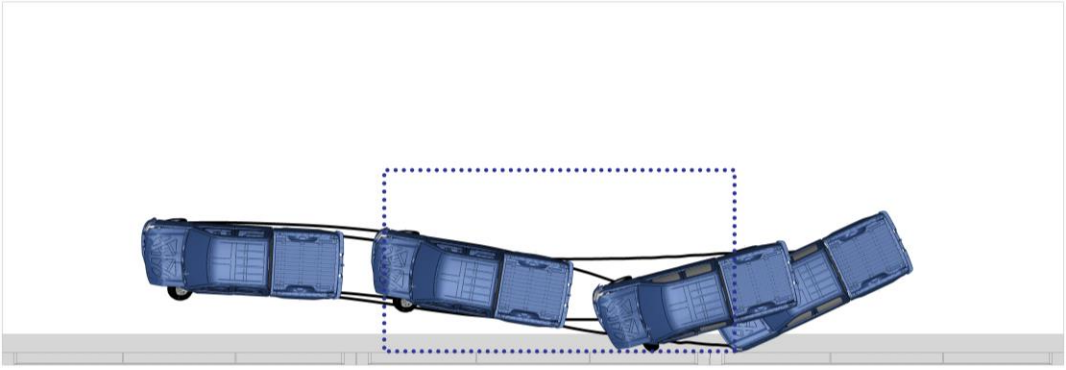


Figure 4.68: Vehicle trajectories of 2014 Chevy Silverado impacting Classic Rail under TL-2 conditions.

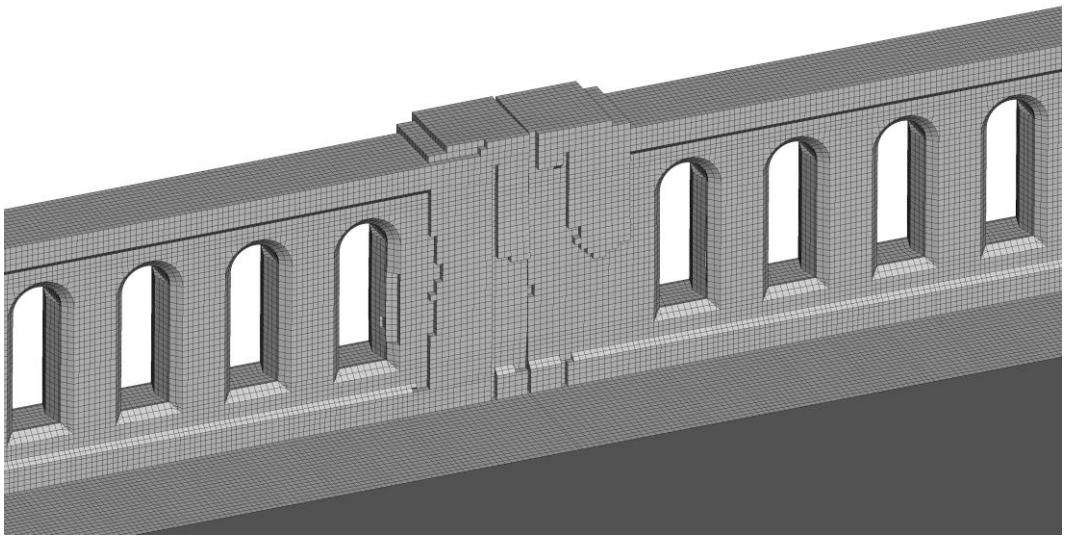


Figure 4.69: Damage on the Classic Rail under impact by 2014 Chevy Silverado under TL-2 conditions.

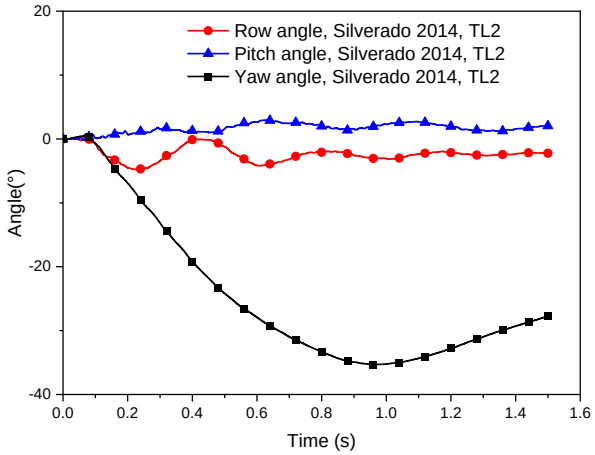
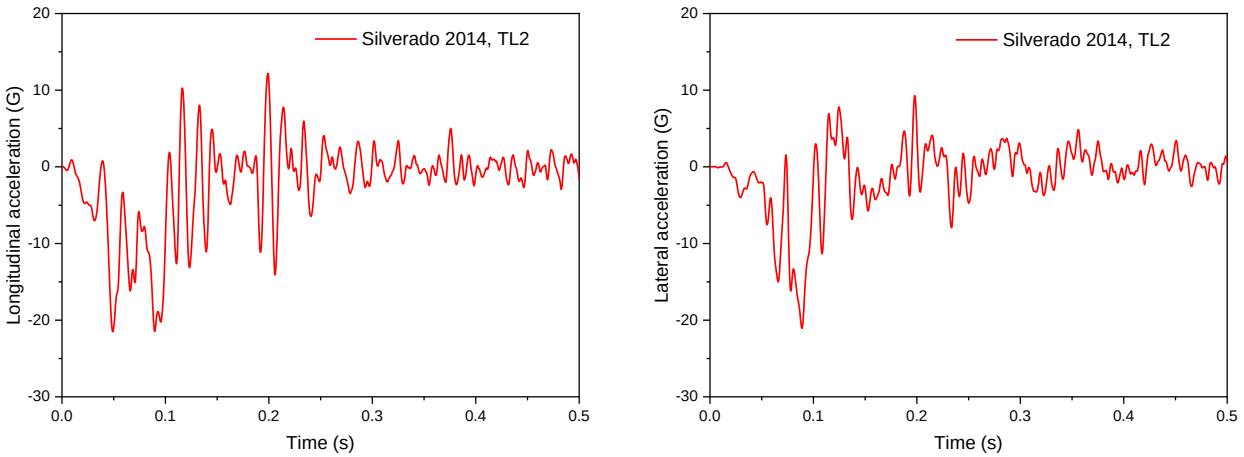


Figure 4.70: Time histories of angular motions of 2014 Chevy Silverado impacting Classic Rail under TL-2 conditions.

Figure 4.71 shows the time histories of vehicle accelerations in longitudinal and lateral directions, which were used to calculate the occupant safety factors, i.e., OIVs and ORAs in both directions, as given in Table 4.39. It can be seen that all the OIV and ORA values were below the limit values specified in MASH. Based on the simulation results, the Classic Rail passed all the evaluation criteria of MASH TL-2 under impacts by the 2014 Chevy Silverado.



(a) (b)

Figure 4.71: Time histories of accelerations of 2014 Chevy Silverado impacting Classic Rail under TL-2 conditions. (a) Longitudinal direction; and (b) lateral direction.

Table 4.39: Evaluation factors of Classic Rail impacted by 2014 Chevy Silverado under TL-2 conditions.

Criteria	MASH criterion *H*		MASH criterion *I*		MASH criterion *F*		MASH criterion *N*	MASH criterion *A*	
Factors	OIV_x	OIV_y	ORA_x	ORA_y	Max roll angle	Max pitch angle	Exit angle	Permanent deflection	Dynamic deflection
Value	9.35 m/s	5.50 m/s	5.125G	4.166G	4.8°	3.0°	2.7°	N/A	N/A
Limit	12.2 m/s	12.2 m/s	20.49G	20.49G	75°	75°	/	/	
Evaluation	Pass	Pass	Pass	Pass	Pass	Pass	Pass	/	

4.4.2 Evaluation of Classic Rail under TL-3 conditions

4.4.2.1 The Classic Rail impacted by 2010 Toyota Yaris under TL-3 conditions

Figure 4.72 shows the top-view vehicle trajectories of the 2010 Toyota Yaris impacting the Classic Rail at 62 mph (100 km/h) and a 25° impact angle. In this case, the vehicle was stuck on the barrier before it was bounced back; therefore, the vehicle was not redirected and failed to pass the MASH exit box criterion. The damage on the bridge rail was localized around the initial impact location (see Figure 4.73), and it was much more severe than the case by 2010 Toyota Yaris under TL-2 conditions.

Figure 4.74 shows the time history of the vehicle's row, pitch, and yaw angles. With a maximum roll angle of 7.4° and a maximum pitch angle of 6.9°, the Classic Rail passed the MASH evaluation criterion *F*, which specified a maximum 75° roll and pitch angles.

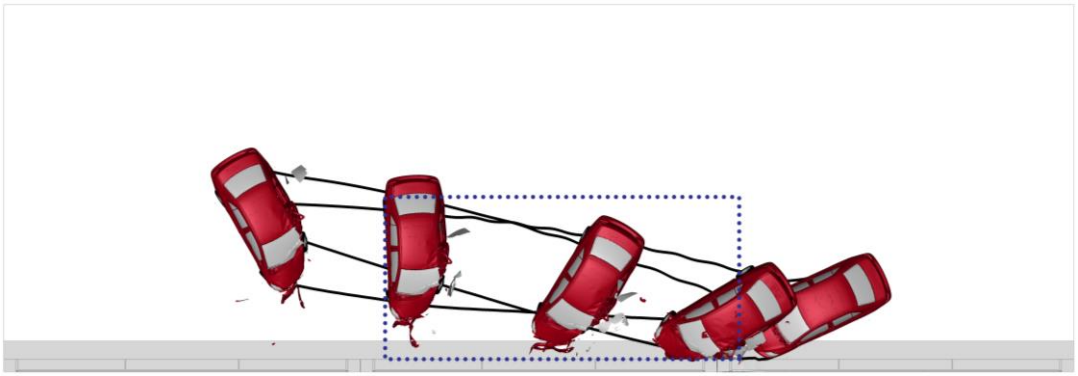


Figure 4.72: Vehicle trajectories of 2010 Toyota Yaris impacting Classic Rail under TL-3 conditions.

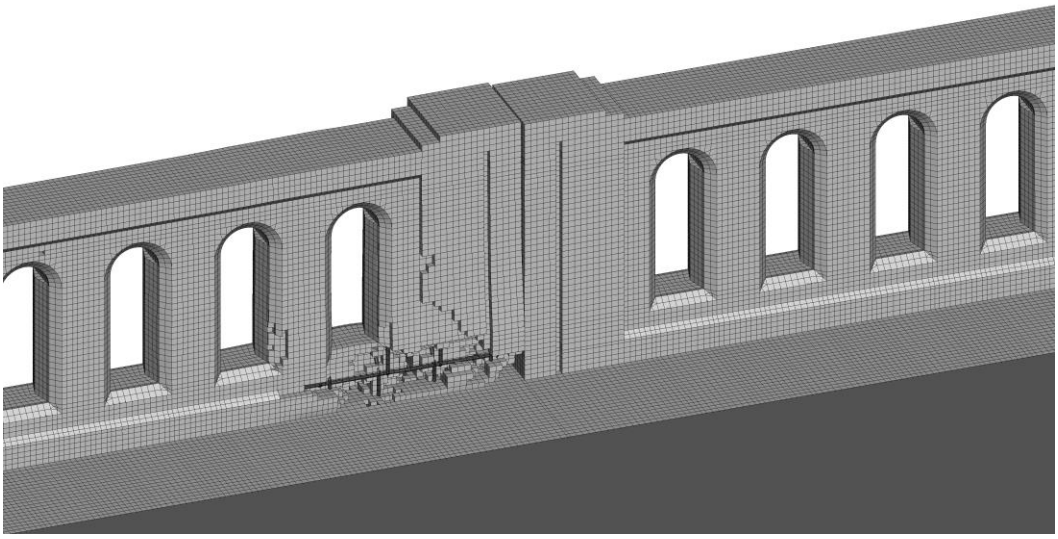


Figure 4.73: Damage on the Classic Rail under impact by 2010 Toyota Yaris under TL-3 conditions.

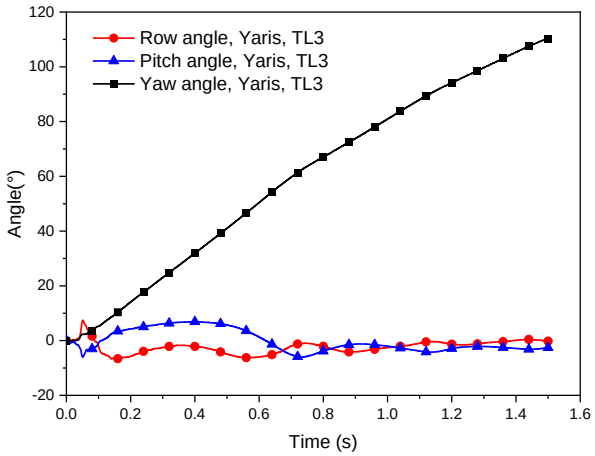
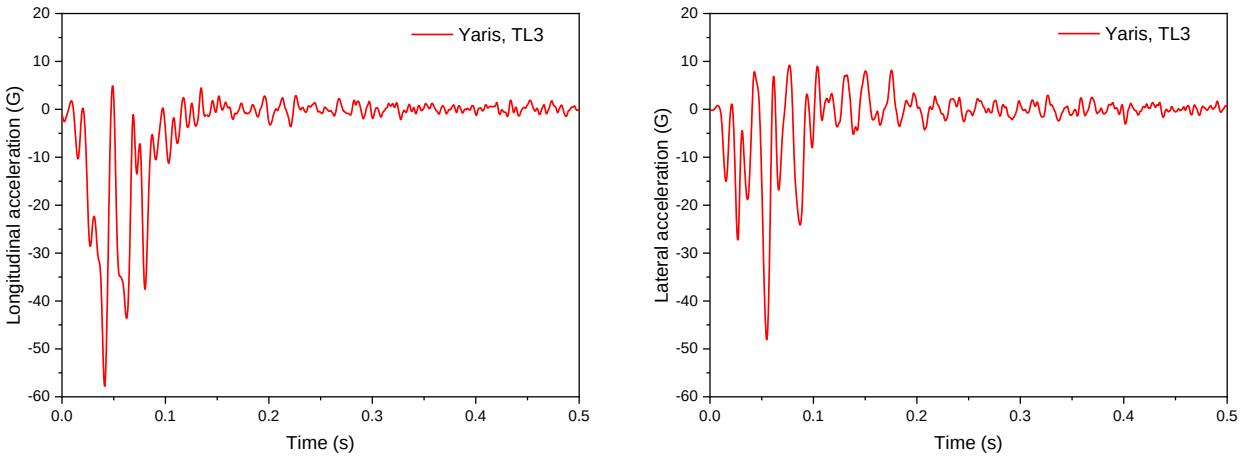


Figure 4.74: Time histories of angular motions of 2010 Toyota Yaris impacting Classic Rail under TL-3 conditions.

Figure 4.75 shows the time histories of vehicle accelerations in longitudinal and lateral directions, which were used to calculate the occupant safety factors, i.e., OIVs and ORAs in both directions, as given in Table 4.40. All the OIV and ORA values were below the MASH limit values except for the OIV in the longitudinal direction. Based on the simulation results, the Classic Rail could not pass all the evaluation criteria of MASH TL-3 under impact of the 2010 Toyota Yaris.



(a) (b)

Figure 4.75: Time histories of accelerations of 2010 Toyota Yaris impacting Classic Rail under TL-3 conditions. (a) Longitudinal direction; and (b) lateral direction.

Table 4.40: Evaluation factors of Classic Rail impacted by 2010 Toyota Yaris under TL-3 conditions.

Criteria	MASH criterion *H*		MASH criterion *I*		MASH criterion *F*		MASH criterion *N*	MASH criterion *A*	
Factors	OIV_x	OIV_y	ORA_x	ORA_y	Max roll angle	Max pitch angle	Exit angle	Permanent deflection	Dynamic deflection
Value	16.05 m/s	7.69 m/s	6.554G	5.438G	7.4°	6.9°	14.0°	N/A	N/A
Limit	12.2 m/s	12.2 m/s	20.49G	20.49G	75°	75°	/	/	
Evaluation	Fail	Pass	Pass	Pass	Pass	Pass	Fail	/	

4.4.2.2 The Classic Rail impacted by 2007 Chevy Silverado under TL-3 conditions

Figure 4.76 shows the top-view vehicle trajectories of the 2007 Chevy Silverado impacting the Classic Rail at 62 mph (100 km/h) and a 25° impact angle. The vehicle was redirected and passed the MASH exit box criterion, leaving some damage on the bridge rail around the initial impact location (see Figure 4.77).

Figure 4.78 shows the time history of the vehicle's row, pitch, and yaw angles. With a maximum roll angle of 8.1° and a maximum pitch angle of 18.4°, the Classic Rail passed the MASH evaluation criterion *F*, which specified a maximum 75° roll and pitch angles.

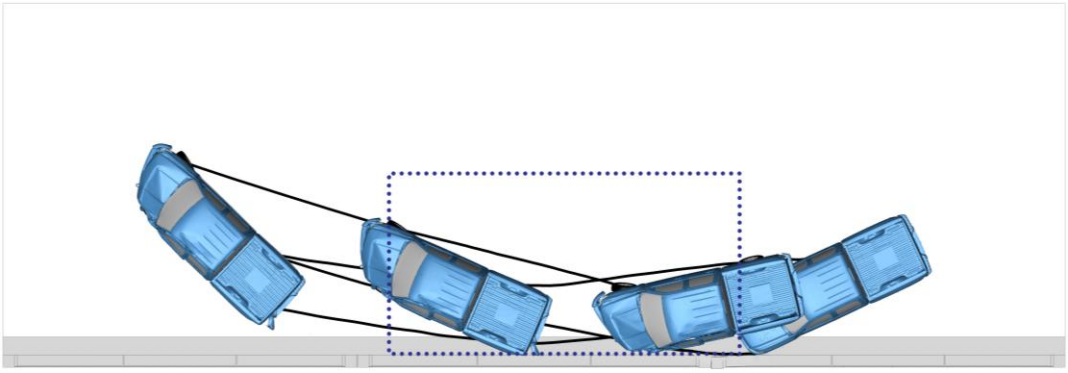


Figure 4.76: Vehicle trajectories of 2007 Chevy Silverado impacting Classic Rail under TL-3 conditions.

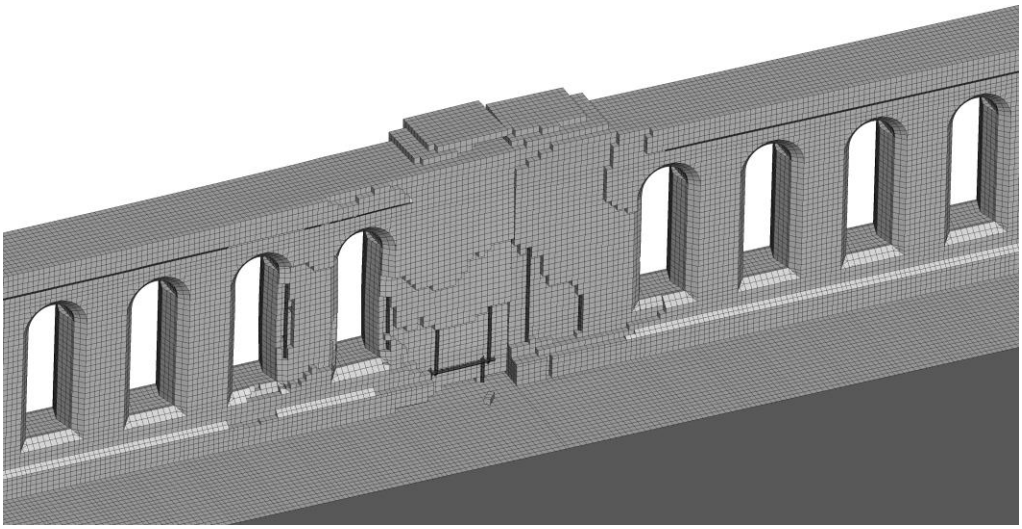


Figure 4.77: Damage on the Classic Rail under impact by 2007 Chevy Silverado under TL-3 conditions.

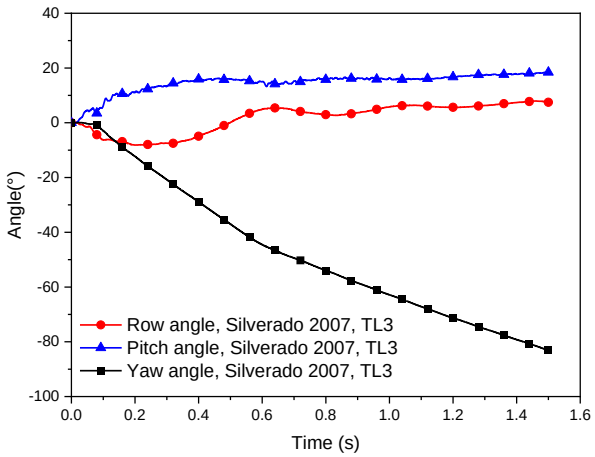
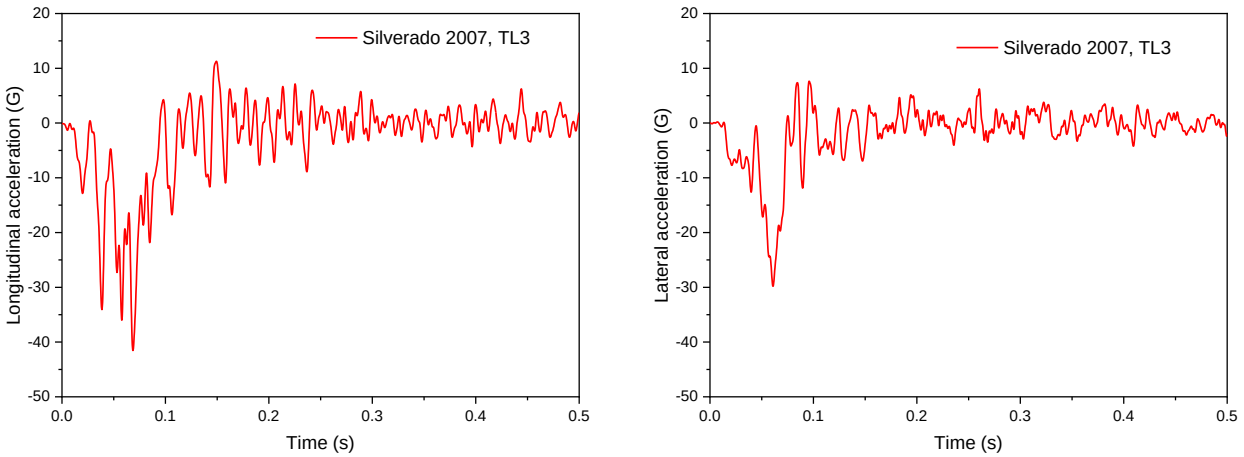


Figure 4.78: Time histories of angular motions of 2007 Chevy Silverado impacting Classic Rail under TL-3 conditions.

Figure 4.79 shows the time histories of vehicle accelerations in longitudinal and lateral directions, which were used to calculate the occupant safety factors, i.e., OIVs and ORAs in both directions, as given in Table 4.41. Except for the OIV in the longitudinal direction, all other OIV and ORA values were below the MASH limits. Based on the simulation results, the Classic Rail could not pass all the evaluation criteria of MASH TL-3 under impact of the 2007 Chevy Silverado.



(a) (b)

Figure 4.79: Time histories of accelerations of 2007 Chevy Silverado impacting Classic Rail under TL-3 conditions. (a) Longitudinal direction; and (b) lateral direction.

Table 4.41: Evaluation factors of Classic Rail impacted by 2007 Chevy Silverado under TL-3 conditions.

Criteria	MASH criterion *H*		MASH criterion *I*		MASH criterion *F*		MASH criterion *N*	MASH criterion *A*	
Factors	OIV_x	OIV_y	ORA_x	ORA_y	Max roll angle	Max pitch angle	Exit angle	Permanent deflection	Dynamic deflection
Value	12.75 m/s	7.33 m/s	11.269G	4.283G	8.1°	18.4°	1.0°	N/A	N/A
Limit	12.2 m/s	12.2 m/s	20.49G	20.49G	75°	75°	/	/	
Evaluation	Fail	Pass	Pass	Pass	Pass	Pass	Pass	/	

4.4.2.3 The Classic Rail impacted by 2014 Chevy Silverado under TL-3 conditions

Figure 4.80 shows the top-view vehicle trajectories of the 2014 Chevy Silverado impacting the Classic Rail at 62 mph (100 km/h) and a 25° impact angle. The vehicle was smoothly redirected and passed the MASH exit box criterion. The damage on bridge rail was localized around the initial impact location (see Figure 4.81) but much larger than that in the case under TL-2 conditions.

Figure 4.82 shows the time history of the vehicle's row, pitch, and yaw angles. With a maximum roll angle of 10.7° and a maximum pitch angle of 10.2°, the Classic Rail passed the MASH evaluation criterion *F*, which specified a maximum 75° roll and pitch angles.

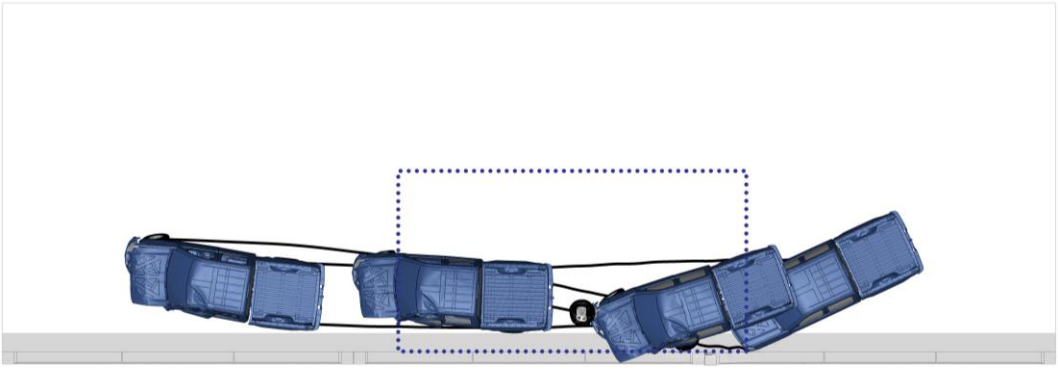


Figure 4.80: Vehicle trajectories of 2014 Chevy Silverado impacting Classic Rail under TL-3 conditions.

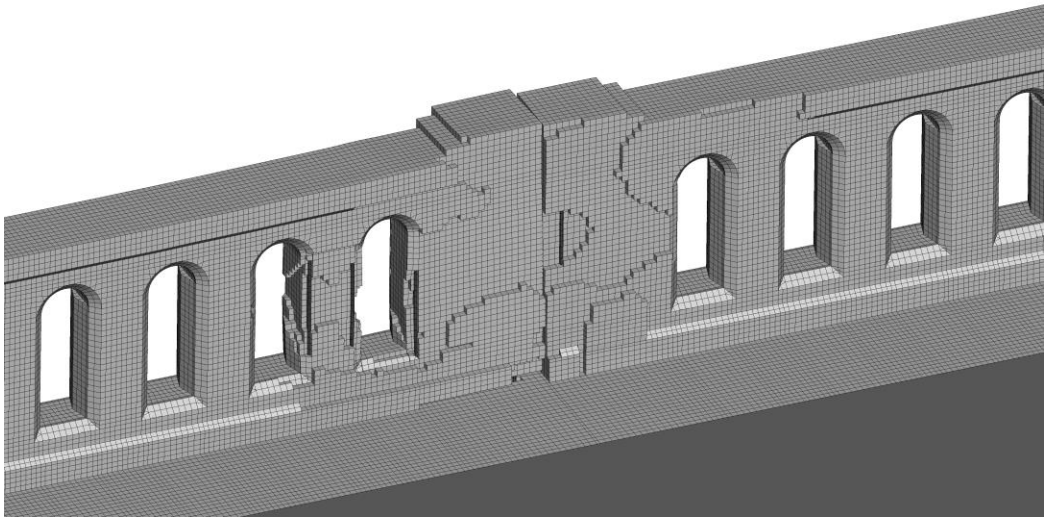


Figure 4.81: Damage on the Classic Rail under impact by 2014 Chevy Silverado under TL-3 conditions.

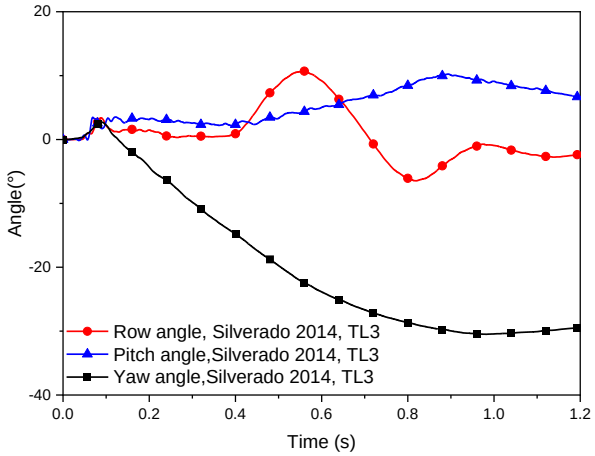
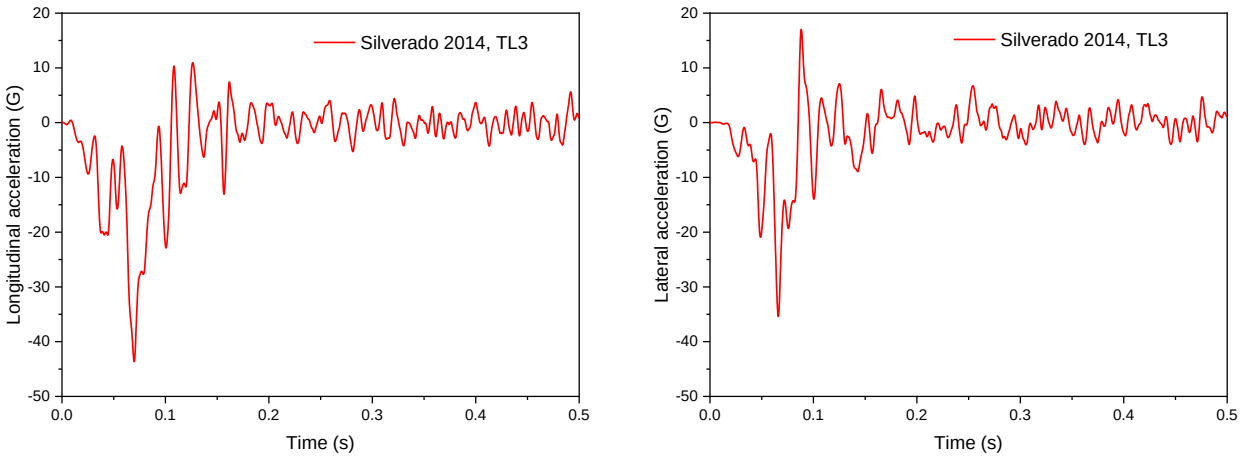


Figure 4.82: Time histories of angular motions of 2014 Chevy Silverado impacting Classic Rail under TL-3 conditions.

Figure 4.83 shows the time histories of vehicle accelerations in longitudinal and lateral directions, which were used to calculate the occupant safety factors, i.e., OIVs and ORAs in both directions, as given in Table 4.42. Similar to the case of 2007 Chevy Silverado under TL-3 conditions, the OIV in the longitudinal direction exceeded the MASH limit value and all other OIV and ORA values were below the MASH limits. Based on the simulation results, the Classic Rail could not pass all the evaluation criteria of MASH TL-3 under impact of the 2014 Chevy Silverado.



(a) (b)

Figure 4.83: Time histories of accelerations of 2014 Chevy Silverado impacting Classic Rail under TL-3 conditions. (a) Longitudinal direction; and (b) lateral direction.

Table 4.42: Evaluation factors of Classic Rail impacted by 2014 Chevy Silverado under TL-3 conditions.

Criteria	MASH criterion *H*		MASH criterion *I*		MASH criterion *F*		MASH criterion *N*	MASH criterion *A*	
Factors	OIV_x	OIV_y	ORA_x	ORA_y	Max roll angle	Max pitch angle	Exit angle	Permanent deflection	Dynamic deflection
Value	13.63 m/s	6.94 m/s	10.534G	7.461G	10.7°	10.2°	5.6°	N/A	N/A
Limit	12.2 m/s	12.2 m/s	20.49G	20.49G	75°	75°	/	/	
Evaluation	Fail	Pass	Pass	Pass	Pass	Pass	Pass	/	

5. Research Findings and Conclusions

In this research, full-scale crash tests and finite element (FE) simulations were performed on the NC two-bar metal bridge rail (2BMR) under MASH TL-3 conditions. The test results were used in the application for FHWA Eligibility Letter, which was approved in August 2021. The test data were also used to validate the FE models, particularly the vehicle models, to improve the accuracy and fidelity of the models. Additionally, FE modeling and simulations were utilized to evaluate the performance of three bridge rail systems: 1) the Oregon Rail under MASH TL-4 conditions; 2) the Three-bar Metal Rail (3BMR) under MASH TL-2 and TL-3 conditions; and 3) the Classic Rail under MASH TL-2 and TL-3 conditions. Table 5.1 gives a summary of the performance of the four bridge rails at different MASH test levels. The following sections give some major research findings from this project.

Table 5.1: Summary of performance of the four bridge rails at different MASH test levels.

Bridge Rail	MASH TL-2		MASH TL-3		MASH TL-4		
	1100C	2270P	1100C	2270P	1100C	2270P	10000S
2BMR	–	–	Pass	Pass	–	–	–
Oregon Rail	–	–	–	–	Pass	Pass	Pass
3BMR	Pass	Pass	Fail (OIV_x)	Pass	–	–	–
Classic Rail	Fail (exit box)	Pass	Fail (exit box and OIV_x)	Fail (OIV_x)	–	–	–

5.1 Performance of Bridge Rails

The 2BMR was crash tested using a 2010 Hyundai Assent passenger car (1100C vehicle) and a 2015 Chevy Silverado pickup truck (2270P vehicle) under MASH TL-3 conditions. Full-scale FE simulations were performed on the 2BMR using a 2010 Toyota Yaris passenger car (1100C), a 2007 Chevy Silverado pickup truck (2270P), and a 2014 Chevy Silverado pickup truck (2270P). In the FE simulations, two impact locations were selected, one with the expansion splice as the reference point and the other with the post closest to the expansion splice as the reference point. Based on simulation results, the critical impact point was selected with the post as the reference point and used in the full-scale crash tests (Tests 3-10 and 3-11). Despite the differences in the makes and/or years of the test vehicles and simulation models, the simulation results were shown to generally agree well with test data in overall responses of the vehicle and bridge rail. Both simulation and test results showed that the 2BMR passed the safety requirements specified in MASH under TL-3 conditions.

The Oregon Rail was evaluated using FE simulations under MASH TL-4 conditions, i.e., under impacts of a 2010 Toyota Yaris (1100C), a 2007 Chevy Silverado (2270P), a 2014 Chevy Silverado (2270P), and a 1996 Ford F800 single-unit truck (10000S). Two impact locations was selected to evaluate the performance of the bridge rail, one with the expansion joint as the reference point and the other with the post closest to the expansion joint as the reference point. Based on the simulation results, the Oregon Rail successfully passed all MASH evaluation criteria under TL-4 conditions at both impact locations.

The 3BMR was evaluated using FE simulations under MASH TL-2 and TL-3 conditions in which three test vehicles were used, a 2010 Toyota Yaris (1100C), a 2007 Chevy Silverado (2270P), and a 2014 Chevy Silverado (2270P). Two impact locations were selected to evaluate the performance of the bridge rail, one with the expansion joint as the reference point and the other with the post closest to the expansion joint as the reference point. Based on the simulation results, the 3BMR successfully passed all MASH evaluation criteria under TL-2 conditions at both impact locations. It was observed in the cases of 2010 Toyota Yaris that the vehicle exhibited clockwise rotations after being redirected. This could cause some safety concerns and may be further investigated for performance enhancement. Under MASH TL-3 conditions, the 3BMR failed to pass the MASH exit box criterion under impact of the 2010 Toyota Yaris with expansion joint as the reference point. In this impact case, the OIV value in the longitudinal direction also exceed the MASH limit, and the same was true with the 2007 Chevy Silverado with expansion joint as the reference point. For all other impact cases, the 3BMR passed all MASH evaluation criteria. Since the 2014 Silverado model has higher fidelity than the 2007 Silverado model and the 3BMR passed all MASH requirements under impacts by the 2014 Silverado, the concern was left only on the case of 2010 Toyota Yaris impacting the 3BMR with the expansion joint as reference point.

The Classic Rail was evaluated using full-scale FE simulations under MASH TL-2 and TL-3 conditions in which three test vehicles were used, a 2010 Toyota Yaris (1100C), a 2007 Chevy Silverado (2270P), and a 2014 Chevy Silverado (2270P). The impact location was selected with the expansion joint as the reference point. Under TL-2 conditions, the Classic Rail met all MASH requirements under impacts of the 2270P vehicles (i.e., both the 2007 and 2014 Chevy Silverado), but failed to meet the MASH exit box criterion under impact of the 2010 Toyota Yaris. Under TL-3 conditions, the Classic Rail failed to pass the MASH exit box criterion under impact of 2010 Toyota Yaris and exceeded the MASH OIV limit in the longitudinal direction. Under impacts of the two 2270P vehicles, the Classic Rail passed all MASH evaluation criteria except for the OIV values in the longitudinal direction. The simulation results suggested that the window design of the Classic Rail could potentially cause vehicle snagging, particularly for small passenger cars, and thus increase the impact severity as reflected by occupant safety factors in the longitudinal direction.

It should be noted that both the 3BMR and Classic Rail were evaluated on a flat terrain based on MASH test conditions. Under in-service conditions, both rails require a minimum of 5-ft (1.52-m) wide sidewalk in front of them and their performance could be different from the simulation results of this project. Further simulations are suggested by NCDOT officials and will be conducted after including a 5-ft (1.52-m) sidewalk in the FE models of the 3BMR and Classic Rail.

5.2 Effect of Concrete Reinforcement on Occupant Safety Factors

Two FE models were developed and used in the evaluation of 3BMR, one without steel reinforcement bars in the concrete foundation (3BMR-1) and the other with full steel reinforcement (3BMR-2). The 3BMR-1 model worked well under TL-2 conditions but produced unrealistic results under TL-3 conditions due to the lack of steel reinforcement and increased impact severity. By comparing 3BMR-1 and 3BMR-2 under TL-3 conditions, it was observed that the reinforcement bars increased the stiffness of the concrete foundation and also affected the safety factors, i.e., OIVs and ORAs.

It was observed from the simulation results of 3BMR under TL-3 conditions that the OIVs in both longitudinal and lateral directions were increased and the ORAs were decreased after introducing full steel reinforcement bars inside concrete foundation. Using the results of the 2010 Toyota Yaris, this was further investigated on the 3BMR-1 (no reinforcement bars) and 3BMR2 models (with Φ-16mm reinforcement bars).

Figure 5.1 and 5.2 show the time histories of velocities and accelerations at the CG point of 2010 Toyota Yaris in the longitudinal and lateral directions. The time instant at which the vehicle moved 0.6 m in the longitudinal direction or 0.3 m in the lateral direction, whichever happened first, was the time for OIVs (the velocities at this time) in both longitudinal and lateral directions. The corresponding vehicle's velocity at this time is considered as occupant impact velocity. It can be seen from Figure 5.1(a) and 5.1(b) that the velocities in both directions were larger in the case of 3BMR-2 than those in the case of 3BMR-1. The reason for increased velocities was that the reinforced concrete foundation caused larger deacceleration of the vehicle at the beginning of impact than that in the case without reinforcement bars, resulting in increased velocities.

Starting from the time instant for OIV values, a 10-ms moving window was applied to the acceleration curve to calculate the average acceleration within each window and the maximum average acceleration was chosen as the ORA, as demonstrated in Figure 5.2(a) and 5.2(b). The ORAs are shown by the rectangular bars with horizontal sides being the 10-ms window and the vertical sides giving the ORA values. Although the accelerations from 0.06 to 0.09 seconds by 3BMR-2 model were generally higher than those by the 3BMR-1 model, the 10-ms moving windows were after 0.09 seconds and the maximum moving average was higher by the 3BMR-1 model than that by the 3BMR-2 model. This was the same reason that in the cases with Chevy Silverado, the OIVs were higher and the ORAs were lower in the 3BMR-1 model than those in the 3BMR-2 model under MASH TL-3 conditions.

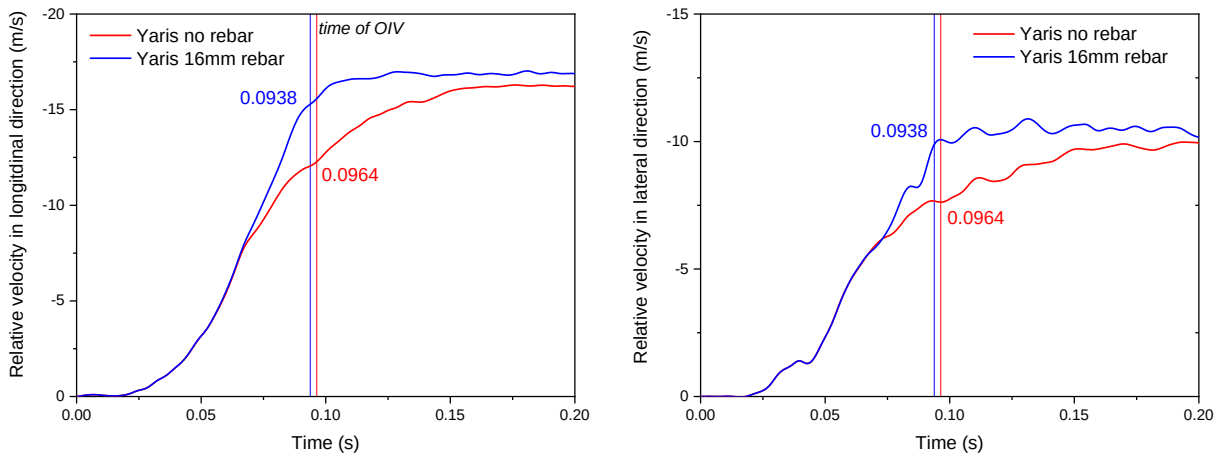


Figure 5.1: Time histories of relative velocities of the 2010 Toyota Yaris impacting the 3BMR-1 (no rebar) and 3BMR-2 (with Φ-16mm rebars) under TL-3 conditions.
(a) Longitudinal; and (b) lateral.

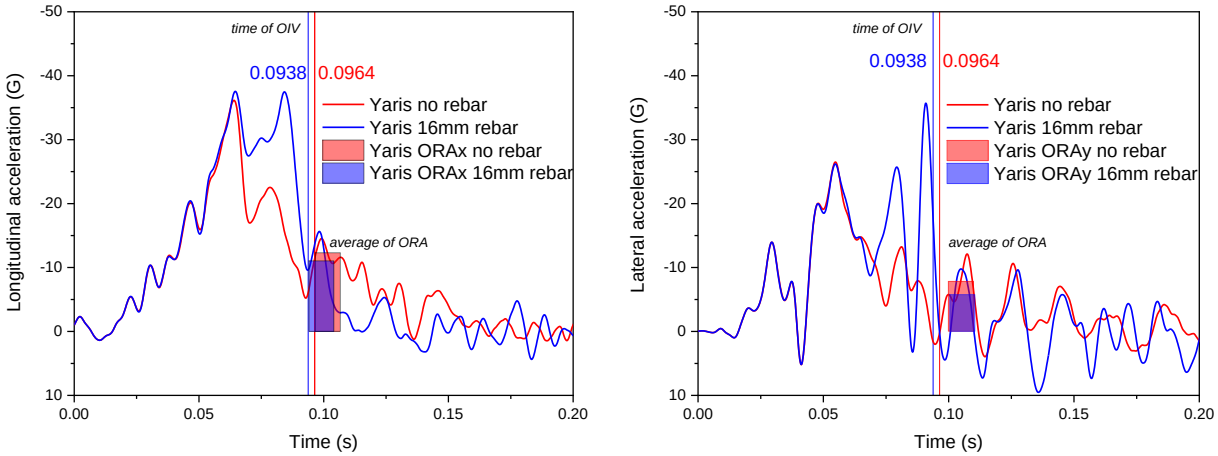
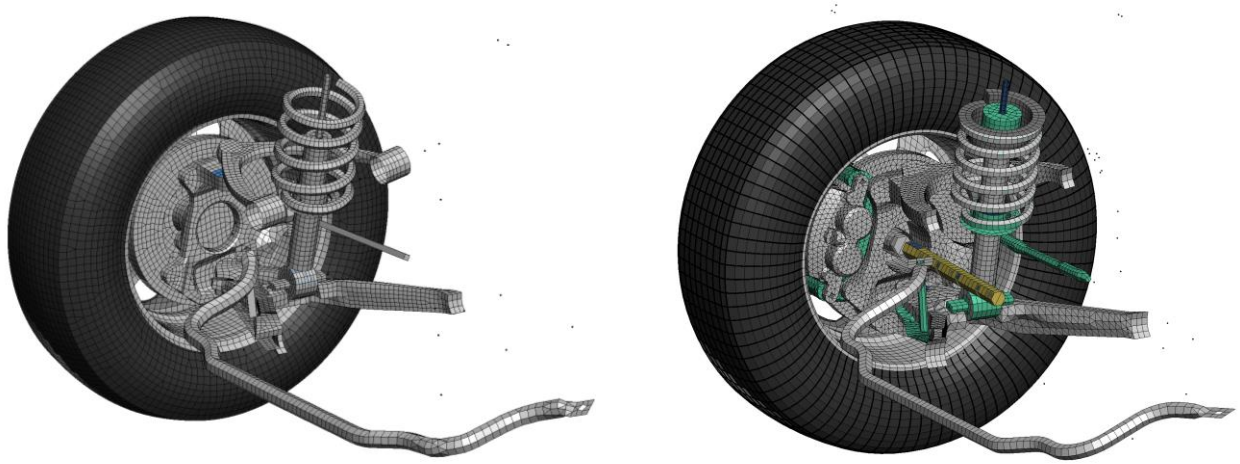


Figure 5.2: Time histories of accelerations of the 2010 Toyota Yaris impacting the 3BMR-1 (no rebar) and 3BMR-2 (with Φ-16mm rebars) under TL-3 conditions.
(a) Longitudinal; and (b) lateral.

5.3 Structural Differences Between Two Silverado Models

In this study, two FE models of the 2270P test vehicle were used in crash simulations, a 2007 and a 2014 Chevy Silverado pickup truck. It was observed from simulation results that there existed noticeable differences in the vehicular responses of the two FE models, such as vehicle redirection characteristics, angular motions (roll, yaw, and pitch), and occupant safety factors (OIVs and ORAs). Since the front wheels of the vehicles played an important role in vehicular responses, the front wheel structures in the two vehicle models were closely examined and compared, as shown in Figure 5.3.



(a) (b)

Figure 5.3: FE models of the front wheels on the 2007 and 2014 Chevy Silverado.
(a) 2007 Chevy Silverado; and (b) 2014 Chevy Silverado.

Compared to the FE model of 2007 Chevy Silverado, the 2014 Silverado model included some major components that were not present in the 2007 Silverado model, e.g., the horizontal control shaft (highlighted in yellow in Figure 5.3(b) that was connected to the center of wheel and the braking caliper. This could be due to the structure difference of the two vehicles, but more likely due to model construction and simplification. This horizontal control shaft helped to stabilize the wheel with increased stiffness and maintain structural integrity of the wheel system when impacting a barrier. It was observed from simulation results that the wheel of the 2007 Chevy Silverado was easily twisted and separated from the vehicle underbody, while the wheel of the 2014 Silverado helped the vehicle to maintain an upright position and be redirected smoothly. Compared to the full-scale crash test, which was conducted using a 2015 Chevy Silverado, the 2014 Silverado model was shown to outperform the 2007 Silverado model and thus recommended in future research work for its high fidelity and good quality of mesh.

5.4 Concluding Remarks

In this project, the NC two-bar metal rail (2BMR) was evaluated using full-scale crash tests coupled with FE simulations for its compliance with MASH under TL-3 conditions. Both test and simulation results showed that the 2BMR met all the MASH TL-3 requirements and an application for the FHWA Eligibility Letter was submitted and approved in August 2021. Another important outcome of this research was the validation of vehicle models, particularly the 2014 Chevy Silverado pickup truck, using the full-scale crash tests of this project. With the validated vehicle models, the Oregon Rail, 3BMR, and Classic Rail were evaluated using FE simulations for their performance at different test levels specified by MASH. The simulation results demonstrated the general performance trends of these four bridge rails and indicated some potential issues or safety concerns. However, for the three bridge rails that were not physically tested in this project, the simulation results should not be used to draw definitive conclusions regarding their performance for a specific impact scenario. Without denial of the extremely high value of physical testing, particularly full-scale crash tests, FE modeling and simulations were shown to be a powerful tool for assisting roadside safety research. The FE models of the vehicles and bridge rails from this project are readily available for use in other investigations.

References

AASHTO (1989). *Guide Specifications for Bridge Railings*. Washington, DC.

AASHTO (2009). *Manual for assessing safety hardware (MASH)*. Washington, DC.

AASHTO (2016). *Manual for Assessing Safety Hardware (MASH), 2nd Ed*. Washington, D.C.

Abu-Odeh, A. (2008). Modeling and simulation of bogie impacts on concrete bridge rails using LS-DYNA. *The 10th International LS-DYNA Users Conference*, Detroit, MI.

Alberson, D.C., Williams, W.F., Menges, W.L., and Haug, R.R. (2004) Testing and evaluation of the Florida Jersey safety shaped bridge rail. *Texas Transportation Institute (TTI)*, FHWA/TX-04/9-8132-1.

Atahan, A.O. (2016) Crashworthiness analysis of a bridge rail-to-guardrail transition. *International Journal of Crashworthiness*, 21(5), 423-434.

Bligh, R.P., Mak, K.K., and Hirsch, T.J. (1994) Evaluation of Tennessee bridge rail designs. *Texas Transportation Institute (TTI)*, RF 7199.

Buth, C.E., Williams, W.F., Bligh, R.P., Menges, W.L., and Haug, R.R. (2003) Performance of the TxDOT T202 (MOD) bridge rail reinforced with fiber reinforced polymer bars. *Texas Transportation Institute (TTI)*, FHWA/TX-03/0-4138-3.

Buth, E.C., Hirsch, T.J., and Menges, W.L. (1993) Testing of new bridge rail and transition designs. *Texas Transportation Institute (TTI)*, FHWA-RD-93-058.

CCSA (2018) 2014 Chevrolet Silverado 1500 Detailed Finite Element Model. *Center for Collision Safety and Analysis, George Mason University*, doi:10.13021/p6mn-hp79.

Cofie, E. (1995). Finite element model of a small automobile impacting a rigid pole. *Federal Highway Administration*, FHWA-RD-94-151.

Ecklund, A. and Sritharan, S. (2018) Precast Concrete Bridge Barriers for Accelerated Bridge Construction. *Iowa State University*, Final Report, October 2018.

Faller, R.K., Ritter, M.A., Rosson, B.T., Fowler, M.D., and Duwadi, S.R. (2000). Two test level 4 bridge railing and transition systems for transverse timber deck bridges. *Transportation Research Record*, 1696(1), 334-351.

Faller, R.K., Sicking, D.L., Larsen, J., Rohde, J.R., Bielenberg, R.W., and Polivka, K.A. (2004) TL-5 development of 42 and 51-inch tall single-faced, F-shape concrete barriers. *Midwest Roadside Safety Facility (MwRSF)*, TRP-03-149-04.

Fang, H., Palta, E., Li, Z., and Fatoki, O. (2019). Performance evaluation of cable barriers on a 6:1 sloped median under MASH TL-3 conditions. *North Carolina Department of Transportation*, FHWA/NC/2017-13.

Fang, H., Weggel, D.C., Bi, J., and Martin, M.E. (2009). Finite element evaluation of two retrofit options to enhance the performance of cable media barriers. *North Carolina Department of Transportation*, FHWA/NC/2008-10.

Hadjioannou, M., Stevens, D., and Barsotti, M. (2016). Development and validation of bolted connection modeling in LS-DYNA for large vehicle models. *The 14th International LS-DYNA Users Conference*, Detroit, MI.

Horne, D.A. (1997). Action: Crash Testing of Bridge Railings. *Federal Highway Administration*, Memorandum, May 30.

Jewell, J., Stoughton, R.L., and Glauz, D. (1993) Vehicle crash tests of Type 115 barrier rail systems for use on secondary highways. *Transportation Research Record*, 1419, 86-94.

Mak, K.K., Bligh, R.P., and Pope, D.H. (1990) Wyoming tube-type bridge rail and box-beam guardrail transition. *Transportation Research Record*, 1258, 61-70.

Marzougui, D., Kan, C.D., Samaha, R.R., Cui, C., and Nix, L. (2012). Extended validation of the finite element model for the 2007 Chevrolet Silverado pick-up truck (MASH 2270kg vehicle). *National Crash Analysis Center*, NCAC 2012-W-003.

Marzougui, D., Samaha, R.R., Cui, C., Kan, C.D., and Opiela, K.S. (2012). Extended validation of the finite element model for the 2010 Toyota Yaris Passenger Sedan (MASH 1100kg vehicle). *National Crash Analysis Center*, NCAC-2012-W-005.

Meline, R., Jewell, J., and Peter, R. (1999). Vehicle crash tests of the Type 80 bridge rail. *California Department of Transportation*, FHWA/CA/ESC-98/06.

Mendis, K., Mani, A., and Shyu, S. C. (1995). Finite element crash models of motor vehicles. *Federal Highway Administration*, FHWA-RD-016.

Michie, J.D. (1981). Recommended procedures for the safety performance evaluation of highway appurtenances. *NCHRP Report 230*.

Mohan, P., Marzougui, D., Arispe, E., and Story, C. (2009). Component and full-scale tests of the 2007 Chevrolet Silverado Suspension System. *National Crash Analysis Center*, NCAC-2009-R-004.

Murray, Y.D., Abu-Odeh, A., and Bligh, R.P. (2007). Evaluation of concrete material model 159. *Federal Highway Administration*, FHWA-HRT-05-063.

Narkhede, S., Lokhande, N., Gangani, B., and Gadekar, G. (2010). Bolted joint representation in LS-DYNA to model bolt pre-stress and bolt failure characteristics in crash simulations. *The 11th International LS-DYNA Users Conference*, Detroit, MI.

Nordlin, E.F., Field, R.N., and Hackett, R.P. (1965). Dynamic Full-Scale Impact Tests of Bridge Barrier Rails. *The 43rdTransportation Research Board Annual Meeting*. Washington, DC.

Nordlin, E.F., Hackett, R.P., and Folsom, J.J. (1970). Dynamic tests of California Type 9 bridge barrier rail and Type 8 bridge approach guardrail. *The 49thTransportation Research Board Annual Meeting*. Washington, DC.

Pena, O., Faller, R. K., Rasmussen, J.D., Steelman, J.S., Rosenbaugh, S.K., Bielenberg, R.W., Mauricio, P., and Duren, J.T. (2020) Development of a MASH Test Level 4 steel, side-mounted, beam-and-post, bridge rail. *Midwest Roadside Safety Facility (MwRSF)*, TRP-03-410-20.

Polivka, K.A., Faller, R.K., Keller, E.A., Sicking, D.L., Rohde, J.R., and Holloway, J.C. (1998) Design and evaluation of the TL-4 Minnesota combination traffic/bicycle bridge rail. *Midwest Roadside Safety Facility (MwRSF)*, SPR-3(017).

Rails, A.B., Bullard Jr, D.L., Williams, W.F., Menges, W.L., and Haug, R.R. (2002). Design and evaluation of the TxDOT F411 and T77 aesthetic bridge rails. *Texas Department of Transportation*, FHWA/TX-03/4288-1.

Rasmussen, J.D., Rosenbaugh, S.K., Faller, R.K., Bielenberg, R.W., Steelman, J.S., Pena, O., and Mauricio, P. (2020) Development of a Test Level 4, side-mounted, steel tube bridge rail. *Transportation Research Record*, 2674(9) 525-537.

Ray, M.H., Oldani, E., and Plaxico, C.A. (2004). Design and analysis of an aluminum F-shape bridge railing. *International Journal of Crashworthiness*, 9(4), 349-363.

Rentz, H.H. (1998). Action: National Cooperative Highway Research Program (NCHRP) Report 350 Hardware Compliance Dates. *Federal Highway Administration*, Memorandum, August 18.

Rosenbaugh, S.K., Faller, R.K., Bielenberg, R.W., Sicking, D.L., and Reid, J.D. (2012) Phase I Development of an aesthetic, precast concrete bridge rail. *Midwest Roadside Safety Facility (MwRSF)*, TRP-03-239-12.

Rosenbaugh, S.K., Faller, R.K., Dixon, J., Loken, A., Rasmussen, J.D., and Flores, J. (2021) Development and testing of an optimized MASH TL-4 bridge rail. *Midwest Roadside Safety Facility (MwRSF),* TRP-03-415-21.

Rosenbaugh, S.K., Rasmussen, J.D., and Faller, R.K. (2020) Development and testing of a Test Level 4 concrete bridge rail and deck overhang. *Transportation Research Record*, 2674(8) 455-465.

Ross Jr, H.E., Sicking, D.L., Zimmer, R.A., and Michie, J.D. (1993). Recommended procedures for the safety performance evaluation of highway features. *NCHRP Report 350.*

Schwer, L. (2014). Modeling rebar: the forgotten sister in reinforced concrete modeling. *The 13th International LS-DYNA Users Conference*, Detroit, MI.

Shankar, V.N., Albin, R.B., Milton, J.C., and Nebergall, M. (2000) In-service, performance-based roadside design policy - preliminary insights from Washington State's bridge rail study. *Transportation Research Record*, 1720, 72-79.

Sheikh, N.M., Bligh, R.P., and Menges, W.L. (2011) Determination of minimum height and lateral design load for MASH Test Level 4 bridge rails. *Texas Transportation Institute (TTI)*, FHWA/TX-12/9-1002-5.

Thiele, J.C., Sicking, D.L., Faller, R.K., Bielenberg, R.W., Lechtenberg, K.A., Reid, J.D., and Rosenbaugh, S.K. (2010) Development of a low-cost, energy-absorbing bridge rail. *Midwest Roadside Safety Facility (MwRSF)*, TRP-03-226-10.

Weintrob, L.H. (1997). Action: Management advisory memorandum on relocation of utilities, Central Artery/Third Harbor Tunnel, FHWA region 1. *U.S. Department of Transportation*, Memorandum, September 25.

Wekezer, J.W., Oskard, M.S., Logan, R.W., and Zywicz, E. (1993). Vehicle impact simulation. *Journal of transportation engineering*, 119(4), 598-617.

Whitesel, D. and Jewell, J.R. (2008). Development and crash testing of an aesthetic, see-through bridge rail, Type 90. *California Department of Transportation*, December 2008.

Whitesel, D., Jewell, J., and Meline, R. (2016). Compliance crash testing of the Type 732SW bridge rail. *California Department of Transportation*, FHWA/CA15-2181.

Williams, W. (2008). New Aesthetic Type T-1F Bridge Rail from the Texas Department of Transportation: Design and Test Level 3 Crash Testing. *Transportation Research Record*, 2050(1), 39-46.

Williams, W.F. and Holt, J. (2013). Design and Full-Scale Testing of Texas Department of Transportation Type T131RC Bridge Rail. *Texas Department of Transportation*, FHWA/TX-12/9-1002-12-1.

Williams, W.F., Bligh, R.P., and Menges, W.L. (2010) MASH Test 3-11 of the TxDOT single slope bridge rail (Type SSTR) on pan-formed bridge deck. *Texas Transportation Institute (TTI)*, FHWA/TX-11/9-1002-3.

Williams, W.F., Bligh, R.P., Menges, W.L., and Kuhn, D.L. (2018) Crash test and evaluation of the TxDOT T224 bridge rail. *Texas Transportation Institute (TTI)*, FHWA/TX-15/9-1002-15-5.

Williams, W.F., Bligh, R.P., Odell, W., Smith, A., and Holt, J. (2015). Design and Full-Scale Testing of Low-Cost Texas Department of Transportation Type T631 Bridge Rail for MASH Test Level 2 and 3 Applications. *Transportation Research Record*, 2521(1), 117-127.

Zaouk, A. K., Bedewi, N.E., Kan, C.D., and Marzougui, D. (1997). Development and evaluation of a C-1500 pick-up truck model for roadside hardware impact simulation. *Proceedings of FHWA Vehicle Crash Analysis Conference*, FHWA-RD-96-212.

Appendix. Full-Scale Crash Test of a Two-Bar Metal Rail

Research Project Number 20180380-01-NEB

FULL-SCALE CRASH TEST OF A TWO-BAR METAL BRIDGE RAIL

Submitted by

Nathan T. Dowler, B.S.M.E.
Graduate Research Assistant

Cody S. Stolle, Ph.D., E.I.T.
Research Assistant Professor

Miguel A. Hinojosa, B.S.M.E.
Graduate Research Assistant

Howie Fang, Ph.D.
Professor and ISOL Director

MIDWEST ROADSIDE SAFETY FACILITY
Nebraska Transportation Center
University of Nebraska–Lincoln

Main Office
Prem S. Paul Research Center at Whittier School
Room 130, 2200 Vine Street
Lincoln, Nebraska 68583-0853
(402) 472-0965

Outdoor Test Site
4630 N.W. 36th Street
Lincoln, Nebraska 68524

UNIVERSITY OF NORTH CAROLINA-CHARLOTTE
University of North Carolina at Charlotte
9201 University City Blvd.
Charlotte, NC 28223-0001

Submitted to

NORTH CAROLINA DEPARTMENT OF TRANSPORTATION
1501 Mail Service Center
Raleigh, North Carolina 27699-1501

MwRSF Research Report No. TRP-03-419-19

November 27, 2019

TECHNICAL REPORT DOCUMENTATION PAGE

1. Report No. TRP-03-419-19	2.	3. Recipient's Accession No.
4. Title and Subtitle Full-Scale Crash Test of a Two-Bar Metal Bridge Rail		5. Report Date November 27, 2019
		6.
7. Authors Dowler, N.T., Stolle, C.S., Hinojosa, M.A, and Fang, H.		8. Performing Organization Report No. TRP-03-419-19
9. Performing Organization Name and Address Midwest Roadside Safety Facility (MwRSF) Nebraska Transportation Center University of Nebraska–Lincoln Main Office: Prem S. Paul Research Center at Whittier School Room 130, 2200 Vine Street Lincoln, Nebraska 68583-0853 Outdoor Test Site: 4630 N.W. 36th Street Lincoln, Nebraska 68524		10. Project/Task/Work Unit No. 11. Contract (C) or Grant (G) No. 20180380-01-NEB
12. Sponsoring Organization Name and Address North Carolina Department of Transportation 1501 Mail Service Center Raleigh, North Carolina 27699-1501		13. Type of Report and Period Covered Final Report: 2017 – 2019 14. Sponsoring Agency Code
15. Supplementary Notes Prepared in cooperation with U.S. Department of Transportation, Federal Highway Administration.		

16. Abstract

The North Carolina Department of Transportation (NCDOT) frequently uses a two-bar metal bridge rail in scenic locations to preserve observational integrity. NCDOT had previously evaluated this system under National Cooperative Highway Research Program (NCHRP) Report No. 350 safety performance criteria, but recent updates to the American Association of State Highway Transportation Officials' *Manual for Assessing Safety Hardware (MASH)* necessitated further testing to ensure continued compliance with the latest safety standards. A 90-ft long, 30-in. tall vertical concrete parapet was constructed at Midwest Roadside Safety Facility's Outdoor Test Site. The top face of the parapet supported posts attached to two longitudinal elliptical rails offset from the front face of the parapet by 1 in.

The bridge rail was evaluated through two full-scale crash tests in accordance with Test Level 3 (TL-3) of MASH 2016. In test no. NCBR-1 (test designation no. 3-10), an 1100C small car impacted the downstream end of the barrier at 63.2 mph and an angle of 25.2 deg. In test no. NCBR-2 (test designation no. 3-11), a 2270P quad cab pickup truck impacted the upstream end of the barrier at 61.9 mph and an angle of 24.9 deg. In both tests, the two-bar metal bridge rail successfully contained and redirected the vehicle and did not penetrate or show potential for debris to penetrate the occupant compartment. All occupant risk measurements were below the maximum threshold. Thus, the NCDOT two-bar metal bridge rail was determined to be crashworthy according to MASH 2016 TL-3 standards.

17. Document Analysis/Descriptors Highway Safety, Crash Test, Compliance Test, MASH 2016, TL-3, Bridge Rail, Concrete Parapet, Combination Rail		18. Availability Statement No restrictions. Document available from: National Technical Information Services, Springfield, Virginia 22161	
19. Security Class (this report) Unclassified	20. Security Class (this page) Unclassified	21. No. of Pages 188	22. Price

DISCLAIMER STATEMENT

This report was completed with funding from the North Carolina Department of Transportation. The contents of this report reflect the views and opinions of the authors who are responsible for the facts and the accuracy of the data presented herein. The contents do not necessarily reflect the official views or policies of the North Carolina Department of Transportation nor the Federal Highway Administration, U.S. Department of Transportation. This report does not constitute a standard, specification, regulation, product endorsement, or an endorsement of manufacturers.

UNCERTAINTY OF MEASUREMENT STATEMENT

The Midwest Roadside Safety Facility (MwRSF) has determined the uncertainty of measurements for several parameters involved in standard full-scale crash testing and non-standard testing of roadside safety features. Information regarding the uncertainty of measurements for critical parameters is available upon request by the sponsor and the Federal Highway Administration.

INDEPENDENT APPROVING AUTHORITY

The Independent Approving Authority (IAA) for the data contained herein was Dr. Jennifer Rasmussen, Research Assistant Professor.

ACKNOWLEDGEMENTS

The authors wish to acknowledge several sources that made a contribution to this project: (1) North Carolina Department of Transportation for sponsoring this project; and (2) MwRSF personnel for constructing the bridge rail system and conducting the crash tests. Acknowledgement is also given to the following individuals who made a contribution to the completion of this research project.

University of North Carolina – Charlotte
UNCC Staff & students

Midwest Roadside Safety Facility
R.K. Faller, Ph.D., P.E., Research Professor & MwRSF Director
J.D. Reid, Ph.D., Professor
J.C. Holloway, M.S.C.E., E.I.T., Assistant Director –Physical Testing Division
K.A. Lechtenberg, M.S.M.E., E.I.T., Research Engineer
R.W. Bielenberg, M.S.M.E., E.I.T., Research Engineer
S.K. Rosenbaugh, M.S.C.E., E.I.T., Research Engineer
A.T. Russell, B.S.B.A., Testing and Maintenance Technician II
E.W. Krier, B.S., Construction and Testing Technician II
S.M. Tighe, Construction and Testing Technician I
D.S. Charroin, Construction and Testing Technician I
R.M. Novak, Construction and Testing Technician I
T.C. Donahoo, Construction and Testing Technician I
J.T. Jones, Construction and Testing Technician I
C.I. Sims, Construction and Testing Technician I
J.E. Kohtz, B.S.M.E., CAD Technician
E.L. Urbank, B.A., Research Communication Specialist
Z.Z. Jabr, Engineering Technician
Undergraduate and Graduate Research Assistants

North Carolina Department of Transportation
Gichuru Muchane, P.E., Structures Management Unit

TABLE OF CONTENTS

TECHNICAL REPORT DOCUMENTATION PAGE i

DISCLAIMER STATEMENT ii

UNCERTAINTY OF MEASUREMENT STATEMENT ii

INDEPENDENT APPROVING AUTHORITY ii

ACKNOWLEDGEMENTS iii

TABLE OF CONTENTS iv

LIST OF FIGURES vi

LIST OF TABLES x

1 INTRODUCTION 1
- 1.1 Background 1
- 1.2 Objectives 1
- 1.3 Scope 2

2 TEST REQUIREMENTS AND EVALUATION CRITERIA 3
- 2.1 Test Requirements 3
- 2.2 Evaluation Criteria 3

3 DESIGN DETAILS 5

4 TEST CONDITIONS 40
- 4.1 Test Facility 40
- 4.2 Vehicle Tow and Guidance System 40
- 4.3 Test Vehicles 40
- 4.4 Simulated Occupant 50
- 4.5 Data Acquisition Systems 50
  - 4.5.1 Accelerometers 50
  - 4.5.2 Rate Transducers 50
  - 4.5.3 Retroreflective Optic Speed Trap 50
  - 4.5.4 Digital Photography 51

5 FULL-SCALE CRASH TEST NO. NCBR-1 54
- 5.1 Weather Conditions 54
- 5.2 Test Description 54
- 5.3 Barrier Damage 64
- 5.4 Vehicle Damage 69
- 5.5 Occupant Risk 76
- 5.6 Barrier Loads 77
- 5.7 Discussion 78

6 FULL-SCALE CRASH TEST NO. NCBR-2 80
6.1 Weather Conditions 80
6.2 Test Description 80
6.3 Barrier Damage 90
6.4 Vehicle Damage 96
6.5 Occupant Risk 103
6.6 Barrier Loads 104
6.7 Discussion 105

7 HEAD EJECTION ANALYSIS 107

8 SUMMARY AND CONCLUSIONS 114

9 MASH EVALUATION 116

10 REFERENCES 117

11 APPENDICES 118
Appendix A. NCDOT Standard Plans 119
Appendix B. Material Specifications 122
Appendix C. Vehicle Center of Gravity Determination 142
Appendix D. Vehicle Deformation Record 145
Appendix E. Accelerometer and Rate Transducer Data Plots, Test No. NCBR-1 154
Appendix F. Accelerometer and Rate Transducer Data Plots, Test No. NCBR-2 171

LIST OF FIGURES

Figure 1. NCDOT Two-Bar Metal Bridge Rail Installation 1
Figure 2. System Layout, Test Nos. NCBR-1 and NCBR-2 7
Figure 3. Section Detail, Test Nos. NCBR-1 and NCBR-2 8
Figure 4. Rail and Concrete Parapet Details, Test Nos. NCBR-1 and NCBR-2 9
Figure 5. Post Assembly, Test Nos. NCBR-1 and NCBR-2 10
Figure 6. Post Detail, Test Nos. NCBR-1 and NCBR-2 11
Figure 7. Post Base Assembly, Test Nos. NCBR-1 and NCBR-2 12
Figure 8. Post Base Components, Test Nos. NCBR-1 and NCBR-2 13
Figure 9. Clamp Bar Detail, Test Nos. NCBR-1 and NCBR-2 14
Figure 10. Shim Details, Test Nos. NCBR-1 and NCBR-2 15
Figure 11. Expansion Bar Detail, Test Nos. NCBR-1 and NCBR-2 16
Figure 12. Rail Components, Test Nos. NCBR-1 and NCBR-2 17
Figure 13. Rail Bracket Assembly, Test Nos. NCBR-1 and NCBR-2 18
Figure 14. Rail Bracket Components, Test Nos. NCBR-1 and NCBR-2 19
Figure 15. Post Anchor Assembly, Test Nos. NCBR-1 and NCBR-2 20
Figure 16. Concrete Anchor and Insert Components, Test Nos. NCBR-1 and NCBR-2 21
Figure 17. Upstream Concrete Parapet Assembly, Test Nos. NCBR-1 and NCBR-2 22
Figure 18. Upstream Concrete Parapet Assembly Detail, Test Nos. NCBR-1 and NCBR-2 23
Figure 19. Center Concrete Parapet Assembly, Test Nos. NCBR-1 and NCBR-2 24
Figure 20. Downstream Concrete Parapet Assembly, Test Nos. NCBR-1 and NCBR-2 25
Figure 21. Downstream Concrete Parapet Assembly, Test Nos. NCBR-1 and NCBR-2 26
Figure 22. System Rebar, Test Nos. NCBR-1 and NCBR-2 27
Figure 23. System Rebar, Test Nos. NCBR-1 and NCBR-2 28
Figure 24. Hardware, Test Nos. NCBR-1 and NCBR-2 29
Figure 25. Bill of Materials, Test Nos. NCBR-1 and NCBR-2 30
Figure 26. Bill of Materials, Test Nos. NCBR-1 and NCBR-2 31
Figure 27. Test No. NCBR-1 with Vehicle Detail 32
Figure 28. Test No. NCBR-2 with Vehicle Detail 33
Figure 29. Construction Photographs, Test Nos. NCBR-1 and NCBR-2 34
Figure 30. System Installation Photographs, Test Nos. NCBR-1 and NCBR-2 35
Figure 31. Post and Rail Assembly, Test Nos. NCBR-1 and NCBR-2 36
Figure 32. Post-to-Parapet and Post-to-Rail Attachment Details, Test Nos. NCBR-1 and NCBR-2 37
Figure 33. Rail End Anchorage Details, Test Nos. NCBR-1 and NCBR-2 38
Figure 34. Load-Time Plot for Threaded Rod Proof Testing, Test Nos. NCBR-1 and NCBR-2 39
Figure 35. Test Vehicle, Test No. NCBR-1 42
Figure 36. Test Vehicle's Interior Floorboards and Undercarriage, Test No. NCBR-1 43
Figure 37. Vehicle Dimensions, Test No. NCBR-1 44
Figure 38. Test Vehicle, Test No. NCBR-2 45
Figure 39. Test Vehicle's Interior Floorboards and Undercarriage, Test No. NCBR-2 46
Figure 40. Vehicle Dimensions, Test No. NCBR-2 47
Figure 41. Target Geometry, Test No. NCBR-1 48
Figure 42. Target Geometry, Test No. NCBR-2 49
Figure 43. Camera Locations, Speeds, and Lens Settings, Test No. NCBR-1 52

Figure 44. Camera Locations, Speeds, and Lens Settings, Test No. NCBR-2 53
Figure 45. Impact Location, Test No. NCBR-1 55
Figure 46. Downstream High-Speed Footage, Test No. NCBR-1 57
Figure 47. Overhead High-Speed Footage, Test No. NCBR-1 57
Figure 48. Sequential Photographs, Test No. NCBR-1 58
Figure 49. Sequential Photographs, Test No. NCBR-1 59
Figure 50. Documentary Photographs, Test No. NCBR-1 60
Figure 51. Documentary Photographs, Test No. NCBR-1 61
Figure 52. Documentary Photographs, Test No. NCBR-1 62
Figure 53. Vehicle Final Position and Trajectory Marks, Test No. NCBR-1 63
Figure 54. System Damage, Test No. NCBR-1 65
Figure 55. System Damage, Test No. NCBR-1 66
Figure 56. Concrete Gouging, Test No. NCBR-1 67
Figure 57. Rail and Post No. 11 Damage, Test No. NCBR-1 68
Figure 58. Barrier Deflections, Test No. NCBR-1 69
Figure 59. Vehicle Damage, Test No. NCBR-1 71
Figure 60. Vehicle Damage, Test No. NCBR-1 72
Figure 61. Occupant Compartment Damage, Test No. NCBR-1 73
Figure 62. Undercarriage Damage, Test No. NCBR-1 74
Figure 63. Windshield Damage (Pre- and Post-Test), Test No. NCBR-1 75
Figure 64. Estimated Barrier Impact and Friction Loads, Test No. NCBR-1 78
Figure 65. Summary of Test Results and Sequential Photographs, Test No. NCBR-1 79
Figure 66. Impact Location, Test No. NCBR-2 81
Figure 67. Downstream High-Speed Footage, Test No. NCBR-2 83
Figure 68. Overhead High-Speed Footage, Test No. NCBR-2 83
Figure 69. Sequential Photographs, Test No. NCBR-2 84
Figure 70. Sequential Photographs, Test No. NCBR-2 85
Figure 71. Documentary Photographs, Test No. NCBR-2 86
Figure 72. Documentary Photographs, Test No. NCBR-2 87
Figure 73. Documentary Photographs, Test No. NCBR-2 88
Figure 74. Vehicle Final Position and Trajectory Marks, Test No. NCBR-2 89
Figure 75. System Damage, Test No. NCBR-2 91
Figure 76. System Damage, Test No. NCBR-2 92
Figure 77. Concrete Gouging, Test No. NCBR-2 93
Figure 78. Post No. 6 Backside Damage, Test No. NCBR-2 94
Figure 79. Rail and Post No. 6 Damage, Test No. NCBR-2 95
Figure 80. Barrier Deflections, Test No. NCBR-2 96
Figure 81. Vehicle Damage, Test No. NCBR-2 98
Figure 82. Vehicle Damage, Test No. NCBR-2 99
Figure 83. Occupant Compartment Damage, Test No. NCBR-2 100
Figure 84. Undercarriage Damage, Test No. NCBR-2 101
Figure 85. Windshield Damage (Pre- and Post-Test), Test No. NCBR-2 102
Figure 86. Estimated Barrier Impact and Friction Loads, Test No. NCBR-2 105
Figure 87. Summary of Test Results and Sequential Photographs, Test No. NCBR-2 106
Figure 88. Onboard High-Speed Footage, Test No. NCBR-1 108
Figure 89. Onboard High-Speed Footage, Test No. NCBR-1 108
Figure 90. Onboard High-Speed Footage, Test No. NCBR-2 109

Figure 91. Onboard High-Speed Footage, Test No. NCBR-2 109
Figure 92. Occupant Head Movement, Test No. NCBR-1 110
Figure 93. Occupant Head Movement, Test No. NCBR-2 111
Figure 94. Maximum Occupant Head Protrusion, Test No. NCBR-1 112
Figure 95. Maximum Occupant Head Protrusion, Test No. NCBR-2 112
Figure 96. Vehicle Position and Dummy Head Protrusion at Maximum Dummy Movement, Test Nos. NCBR-1 and NCBR-2 113
Figure A-1. NCDOT Design Standards of Two-Bar Metal Bridge Rail 120
Figure A-2. NCDOT Design Standards of Two-Bar Metal Bridge Rail 121
Figure B-1. Aluminum Parts, Test Nos. NCBR-1 and NCBR-2 125
Figure B-2. Additional Aluminum Parts, Test Nos. NCBR-1 and NCBR-2 126
Figure B-3. ¾ in. Threaded Ferrule, Test Nos. NCBR-1 and NCBR-2 127
Figure B-4. Longitudinal Elliptical Rails, Test Nos. NCBR-1 and NCBR-2 128
Figure B-5. Concrete, Test Nos. NCBR-1 and NCBR-2 129
Figure B-6. Concrete, Test Nos. NCBR-1 and NCBR-2 130
Figure B-7. #5 Bar, Test Nos. NCBR-1 and NCBR-2 131
Figure B-8. #5 Bar, 36 in. Long, Test Nos. NCBR-1 and NCBR-2 132
Figure B-9. #6 Bar, Test Nos. NCBR-1 and NCBR-2 133
Figure B-10. #7 Bar, Test Nos. NCBR-1 and NCBR-2 134
Figure B-11. ¾ in.-Diameter, $1^{3}/_{8}$-in. Long Rivet, Test Nos. NCBR-1 and NCBR-2 135
Figure B-12. ¾-in. Diameter, 6½-in. Long Hex Head Drill-In Anchor, Test Nos. NCBR-1 and NCBR-2 136
Figure B-13. ¾ in.-10 UNC, 2½ in. Long Hex Bolt, Test Nos. NCBR-1 and NCBR-2 137
Figure B-14. ½ in.-13 UNC, 1¼ in. Long Hex Head Cap Screw, Test Nos. NCBR-1 and NCBR-2 138
Figure B-15. ½ in.-13 UNC, 1 in. Long Hex Head Cap Screw, Test Nos. NCBR-1 and NCBR-2 139
Figure B-16. ¾ in. Dia. Plain Washers, Test Nos. NCBR-1 and NCBR-2 140
Figure B-17. ½ in. Dia. Plain SAE Washer, Test Nos. NCBR-1 and NCBR-2 141
Figure C-1. Vehicle Mass Distribution, Test No. NCBR-1 143
Figure C-2. Vehicle Mass Distribution, Test No. NCBR-2 144
Figure D-1. Occupant Compartment Deformation Data – Set 1, Test No. NCBR-1 146
Figure D-2. Floor Pan Deformation Data – Set 1, Test No. NCBR-1 147
Figure D-3. Occupant Compartment Deformation Data – Set 2, Test No. NCBR-1 148
Figure D-4. Exterior Vehicle Crush (NASS) - Front, Test No. NCBR-1 149
Figure D-5. Exterior Vehicle Crush (NASS) - Side, Test No. NCBR-1 150
Figure D-6. Windshield Deformation, Test No. NCBR-1 151
Figure D-7. Occupant Compartment Deformation Data – Set 1, Test No. NCBR-2 152
Figure D-8. Floor Pan Deformation Data – Set 2, Test No. NCBR-2 153
Figure E-1. 10-ms Average Longitudinal Deceleration (SLICE-1), Test No. NCBR-1 155
Figure E-2. Longitudinal Occupant Impact Velocity (SLICE-1), Test No. NCBR-1 156
Figure E-3. Longitudinal Occupant Displacement (SLICE-1), Test No. NCBR-1 157
Figure E-4. 10-ms Average Lateral Deceleration (SLICE-1), Test No. NCBR-1 158
Figure E-5. Lateral Occupant Impact Velocity (SLICE-1), Test No. NCBR-1 159
Figure E-6. Lateral Occupant Displacement (SLICE-1), Test No. NCBR-1 160
Figure E-7. Vehicle Angular Displacements (SLICE-1), Test No. NCBR-1 161
Figure E-8. Acceleration Severity Index (SLICE-1), Test No. NCBR-1 162

Figure E-9. 10-ms Average Longitudinal Deceleration (SLICE-2), Test No. NCBR-1.....163
Figure E-10. Longitudinal Occupant Impact Velocity (SLICE-2), Test No. NCBR-1 164
Figure E-11. Longitudinal Occupant Displacement (SLICE-2), Test No. NCBR-1 165
Figure E-12. 10-ms Average Lateral Deceleration (SLICE-2), Test No. NCBR-1.....166
Figure E-13. Lateral Occupant Impact Velocity (SLICE-2), Test No. NCBR-1.....167
Figure E-14. Lateral Occupant Displacement (SLICE-2), Test No. NCBR-1.....168
Figure E-15. Vehicle Angular Displacements (SLICE-2), Test No. NCBR-1 169
Figure E-16. Acceleration Severity Index (SLICE-2), Test No. NCBR-1 170
Figure F-1. 10-ms Average Longitudinal Deceleration (SLICE-1), Test No. NCBR-2.....172
Figure F-2. Longitudinal Occupant Impact Velocity (SLICE-1), Test No. NCBR-2.....173
Figure F-3. Longitudinal Occupant Displacement (SLICE-1), Test No. NCBR-2 174
Figure F-4. 10-ms Average Lateral Deceleration (SLICE-1), Test No. NCBR-2 175
Figure F-5. Lateral Occupant Impact Velocity (SLICE-1), Test No. NCBR-2.....176
Figure F-6. Lateral Occupant Displacement (SLICE-1), Test No. NCBR-2.....177
Figure F-7. Vehicle Angular Displacements (SLICE-1), Test No. NCBR-2 178
Figure F-8. Acceleration Severity Index (SLICE-1), Test No. NCBR-2.....179
Figure F-9. 10-ms Average Longitudinal Deceleration (SLICE-2), Test No. NCBR-2.....180
Figure F-10. Longitudinal Occupant Impact Velocity (SLICE-2), Test No. NCBR-2.....181
Figure F-11. Longitudinal Occupant Displacement (SLICE-2), Test No. NCBR-2 182
Figure F-12. 10-ms Average Lateral Deceleration (SLICE-2), Test No. NCBR-2 183
Figure F-13. Lateral Occupant Impact Velocity (SLICE-2), Test No. NCBR-2.....184
Figure F-14. Lateral Occupant Displacement (SLICE-2), Test No. NCBR-2.....185
Figure F-15. Vehicle Angular Displacements (SLICE-2), Test No. NCBR-2 186
Figure F-16. Acceleration Severity Index (SLICE-2), Test No. NCBR-2.....187

LIST OF TABLES

Table 1. MASH 2016 TL-3 Crash Test Conditions for Longitudinal Barriers....3
Table 2. MASH 2016 Evaluation Criteria for Longitudinal Barrier....4
Table 3. Weather Conditions, Test No. NCBR-1 54
Table 4. Sequential Description of Impact Events, Test No. NCBR-1....56
Table 5. Maximum Occupant Compartment Intrusions by Location, Test No. NCBR-1 76
Table 6. Summary of OIV, ORA, THIV, PHD, and ASI Values, Test No. NCBR-1 77
Table 7. Weather Conditions, Test No. NCBR-2 80
Table 8. Sequential Description of Impact Events, Test No. NCBR-2....82
Table 9. Maximum Occupant Compartment Intrusions by Location, Test No. NCBR-2 103
Table 10. Summary of OIV, ORA, THIV, PHD, and ASI Values, Test No. NCBR-2 104
Table 11. Summary of Safety Performance Evaluation....115
Table B-1. Bill of Materials, Test Nos. NCBR-1 and NCBR-2 123
Table B-1. Bill of Materials, Test Nos. NCBR-1 and NCBR-2, Cont....124

1 INTRODUCTION

1.1 Background

The North Carolina Department of Transportation's (NCDOT) two-bar metal bridge rail was developed for use on scenic bridges to allow for enhanced viewing of the surroundings. An example of an installed configuration is shown in Figure 1. NCDOT's standard drawings of the two-bar metal bridge rail are shown in Appendix A.



Figure 1. NCDOT Two-Bar Metal Bridge Rail Installation

The crashworthiness of this bridge rail was previously recognized as meeting National Cooperative Highway Research Program (NCHRP) Report No. 350, *Recommended Procedures for the Safety Performance Evaluation of Highway Features* [1] safety performance standards. NCHRP Report No. 350 has since been superseded by the American Association of State Highway and Transportation Officials' (AASHTO) *Manual for Assessing Safety Hardware* (MASH 2016) [2]. Thus, it was desired to evaluate the bridge rail to MASH 2016 standards.

NCDOT solicited the help of researchers at the University of North Carolina–Charlotte (UNCC) and the Midwest Roadside Safety Facility (MwRSF) to evaluate the crashworthiness of the NCDOT two-bar combination bridge rail system. The research study consisted of an investigation of critical impact points (CIPs), evaluation of vehicle snag and occupant interaction with roadside structures, and barrier capacity and impact loading using finite element analysis (FEA) and full-scale crash testing according to MASH Test-Level (TL-3) test designation nos. 3-10 and 3-11 impact conditions.

1.2 Objectives

The objective of this study was to evaluate the NCDOT two-bar metal bridge rail according to the TL-3 safety performance criteria set forth in MASH 2016.

1.3 Scope

In order to complete the research objective, researchers conducted the following tasks:

1. Developed NCDOT-approved CAD drawings of the NCDOT two-bar metal bridge rail, and constructed the system at the MwRSF Outdoor Test Site.

2. Conducted two full-scale crash tests at the MwRSF Outdoor Test Site, according to MASH 2016 test designation nos. 3-10 and 3-11.

2 TEST REQUIREMENTS AND EVALUATION CRITERIA

2.1 Test Requirements

Longitudinal barriers, such as the NCDOT two-bar metal bridge rail, must satisfy impact safety standards in order to be declared eligible for federal reimbursement by the FHWA for use on the National Highway System (NHS). For new hardware, these safety standards consist of the guidelines and procedures published in MASH 2016. Note that there is no difference between MASH 2009 [3] and MASH 2016 for longitudinal barriers, such as the system tested in this project, except additional occupant compartment deformation measurements, photographs, and documentation are required by MASH 2016. According to TL-3 of MASH 2016, longitudinal barrier systems must be subjected to two full-scale vehicle crash tests, as summarized in Table 1.

Table 1. MASH 2016 TL-3 Crash Test Conditions for Longitudinal Barriers

Test Article	Test Designation No.	Test Vehicle	Vehicle Weight lb	Impact Conditions		Evaluation Criteria [1]
				Speed mph	Angle deg.	
Longitudinal Barrier	3-10	1100C	2,420	62	25	A,D,F,H,I
	3-11	2270P	5,000	62	25	A,D,F,H,I

[1] Evaluation criteria explained in Table 2

2.2 Evaluation Criteria

Evaluation criteria for full-scale vehicle crash testing are based on three appraisal areas: (1) structural adequacy, (2) occupant risk, and (3) vehicle trajectory after collision. Criteria for structural adequacy are intended to evaluate the ability of the system to contain and redirect impacting vehicles. In addition, controlled lateral deflection of the test article is acceptable. Occupant risk evaluates the degree of hazard to occupants in the impacting vehicle. Post-impact vehicle trajectory is a measure of the potential of the vehicle to result in a secondary collision with other vehicles and/or fixed objects, thereby increasing the risk of injury to the occupants of the impacting vehicle and/or other vehicles. These evaluation criteria, summarized in Table 2, are defined in greater detail in MASH 2016. The full-scale vehicle crash tests documented herein were conducted and reported in accordance with the procedures provided in MASH 2016.

In addition to the standard occupant risk measures, the Post-Impact Head Deceleration (PHD), Theoretical Head Impact Velocity (THIV), and Acceleration Severity Index (ASI) were determined and reported. Additional discussion on PHD, THIV and ASI is provided in MASH 2016.

Table 2. MASH 2016 Evaluation Criteria for Longitudinal Barrier

<table>
<tr><td>Structural Adequacy</td><td>A.</td><td colspan="3">Test article should contain and redirect the vehicle or bring the vehicle to a controlled stop; the vehicle should not penetrate, underride, or override the installation, although controlled lateral deflection of the test article is acceptable.</td></tr>
<tr><td rowspan="4">Occupant Risk</td><td>D.</td><td colspan="3">Detached elements, fragments, or other debris from the test article should not penetrate or show potential for penetrating the occupant compartment, or present an undue hazard to other traffic, pedestrians, or personnel in a work zone. Deformations of, or intrusions into, the occupant compartment should not exceed limits set forth in Section 5.2.2 and Appendix E of MASH 2016.</td></tr>
<tr><td>F.</td><td colspan="3">The vehicle should remain upright during and after collision. The maximum roll and pitch angles are not to exceed 75 deg.</td></tr>
<tr><td>H.</td><td colspan="3">Occupant Impact Velocity (OIV) (see Appendix A, Section A5.2.2 of MASH 2016 for calculation procedure) should satisfy the following limits:
<table>
<tr><td colspan="3">Occupant Impact Velocity Limits</td></tr>
<tr><td>Component</td><td>Preferred</td><td>Maximum</td></tr>
<tr><td>Longitudinal and Lateral</td><td>30 ft/s</td><td>40 ft/s</td></tr>
</table></td></tr>
<tr><td>I.</td><td colspan="3">The Occupant Ridedown Acceleration (ORA) (see Appendix A, Section A5.2.2 of MASH 2016 for calculation procedure) should satisfy the following limits:
<table>
<tr><td colspan="3">Occupant Ridedown Acceleration Limits</td></tr>
<tr><td>Component</td><td>Preferred</td><td>Maximum</td></tr>
<tr><td>Longitudinal and Lateral</td><td>15.0 g’s</td><td>20.49 g’s</td></tr>
</table></td></tr>
</table>

3 DESIGN DETAILS

The test installation consisted of a 90-ft long concrete parapet with top-mounted aluminum posts and elliptical rails. Schematics of the test installation are shown in Figures 2 through 28. Photographs of the test installation are shown in Figures 29 through 33. Material specifications, mill certifications, and certificates of conformity for the system materials are shown in Appendix B.

The concrete parapet consisted of three 30-ft long concrete barrier segments with 1-in. long, unfilled gaps to replicate bridge expansion joints in between segments. NCDOT typically installs a joint filler between expansion joints, but this material erodes over time. Thus, this material was omitted in construction to ensure a "worst practical case" impact scenario, maximizing the risk that snag could occur. The overall length and width of the concrete parapet were 90 ft and 14 in., respectively. The concrete parapets consisted of tapered buttress ends at the upstream and downstream end of the system, and 30-in. tall prismatic concrete parapet segments. The concrete end buttresses were 56 in. tall and were vertically tapered to 32¾ in. above the roadway at the outer faces over a longitudinal distance of 39 in. All edges of the concrete faces had ½-in. x ½-in. chamfers. Construction joints, consisting of ½-in. wide, saw-cut grooves extending on the front, back, and top faces, were installed in equally-spaced, 10-ft increments and at the interior faces of the concrete buttresses. Photos of the rail parapet construction are shown in Figure 29, and the parapet is shown in Figure 30.

Typical internal concrete reinforcement consisted of two vertically-staggered, #5 U-shaped stirrups tied together and spaced 12 in. apart on center, with eight #5 longitudinal rebar extending from end to end of each parapet segment. The internal rebar cages for the buttress ends consisted of a mesh of vertical #7 bars which followed the contour of the vertically-tapered ends, diagonal #7 bars parallel to the surface of the taper, and #6 longitudinal bars above the typical #5 longitudinal bars. All rebar were Grade 60 and had a minimum clear cover of 2 in. Concrete reinforcement details are shown in Figures 16 through 23.

The rail system consisted of 16 vertical post and base plate assemblies attached to two elliptical rail segments, as shown in Figures 5 through 8. Posts consisted of welded aluminum plates measuring 23½ in. tall, 5¾ in. wide, and 4¼ in. deep at the base, mounted to the top of a two-piece, cast aluminum base plate assembly, as shown in Figures 6 through 8. The posts were riveted through the front face of the base plate assembly with ¾-in. diameter, 1-in. long aluminum rivets. The posts were installed with the front flange offset 5¾ in. from the traffic-side face of the rail. As a result, there was a 1-in. lateral offset between the front face of the concrete parapet and the leading edge of the aluminum rail.

Post nos. 1 and 16 were spaced 16 in. from the upstream and downstream edges of the parapet, respectively, in compliance with NCDOT design specifications [4]. Post nos. 1 through 3 and 14 through 16 were spaced 38 in. apart. Post nos. 3 through 6, where impact for test no. NCBR-2 occurred, were spaced 78 in. apart. Post nos. 6 through 13, where impact for test no. NCBR-1 occurred, were spaced 72 in. apart. Post nos. 13 and 14 were spaced 68 in. apart. NCDOT state standards permit the post spacing for the two-bar bridge rail system to be up to 6 ft – 6 in. apart. In addition, there are minimum allowable distances between the expansion gaps and the vertical post-to-parapet connections. The tested post configuration was selected to maximize the loading on the rail splices by placing posts on the downstream sides of the expansion joints, and the post

spacing was selected to be consistent with NCDOT standards for rail end sections and expansion joint offsets. This was deemed a critical construction scenario to maximize the likelihood of a vehicle stiff element, such as a hood or quarter panel, protruding above the top surface of the concrete parapet and engaging with the upstream vertical edge of a post flange, and also to increase the possibility of vehicle snag at the expansion gap. Real-world installations of the NCBR 2-bar bridge rail were examined and the test setup was determined to be comparable to rail spacings for previously-constructed systems.

Two elliptical rail segments were mounted on the front side of each aluminum post, as shown in Figures 3, 4, and 31. The elliptical rails were 4¾ in. wide and 4 in. tall, with a grooved back slot, as shown in Figure 12. At each post location, clamp bars and shim plates (as needed for alignment) were bolted to the posts with ½-in.-13 UNC, 1-in. long, ASTM F593 stainless steel cap screws, as shown in Figures 3, 9, and 10. Shaped splice bars measuring 36 in. long with dimpled back plates were inserted into the elliptical rails at every expansion joint, which provided rail shear and bending connectivity. Post-to-rail attachment details are shown in Figure 32.

The post base assemblies were attached to the top surface of the concrete parapet using four ¾-in. diameter by 2½-in. long, ASTM A3125 bolts threaded into steel ferrules, as shown in Figures 3, 15, and 16. The ferrules were welded to a wire cage and cast into the concrete parapets. The upstream and downstream ends of the aluminum rail were bolted to ½-in. thick, L-angle brackets which connected the back side of the elliptical aluminum rails to the interior vertical face of the concrete buttress, as shown in Figures 13 and 14. The L-angle brackets were bolted to the concrete buttress ends using a ¾-in. diameter, 7-in. long threaded rod with washer and nut epoxied into the buttress face to a minimum depth of 5 in., as shown in Figure 4. The epoxy was Adhesive Technologies (ATC) Ultrabond 1 with a minimum bond strength of 1,100 psi. Post-to-parapet and rail end anchorage attachment details are shown in Figures 32 and 33.

The NCDOT two-bar bridge rail system is typically installed on a reinforced box girder bridge deck system, but based on feedback from NCDOT, the strengths of the barrier-to-deck connection and the stiffness of the bridge deck were deemed sufficient to install the parapet directly to the top surface of the concrete tarmac at the MwRSF Outdoor Test Site to represent typical installation on an NCDOT bridge deck. Vertical attachment of the concrete parapet to the concrete tarmac surface consisted of #5 rebar embedded 6 in. into the tarmac on the front and back sides of the system and spaced 12 in. apart on centers, as shown in Figures 16 through 23. The end buttresses were anchored to the concrete tarmac using #7 bars epoxied to the tarmac surface, also with an embedment depth of 6 in. to ensure full development of the bars.

A field test of a threaded anchor rod epoxied into the barrier was conducted prior to full-scale testing. The 6.4 kip achieved exceeded the 5 kip requirement. The load-force plot for the test is shown in Figure 34. The critical impact point for test no. NCBR-1 was $54^{9}/_{16}$ in. upstream from post no. 11, 43.2 in. upstream from the expansion joint between post nos. 10 and 11. The critical impact point for test no. NCBR-2 was $61^{15}/_{16}$ in. upstream from post no. 6, 51.6 in. upstream from the expansion joint between post nos. 5 and 6. Both critical impact points were selected based on CIP simulation results from UNCC and verified by NCDOT. The impact side of the rail was painted white to clearly delineate marks produced during impact. Impact points for test nos. NCBR-1 and NCBR-2 are shown in Figures 27 and 28, respectively. Photographs of the constructed system are shown in Figures 30 through 33.

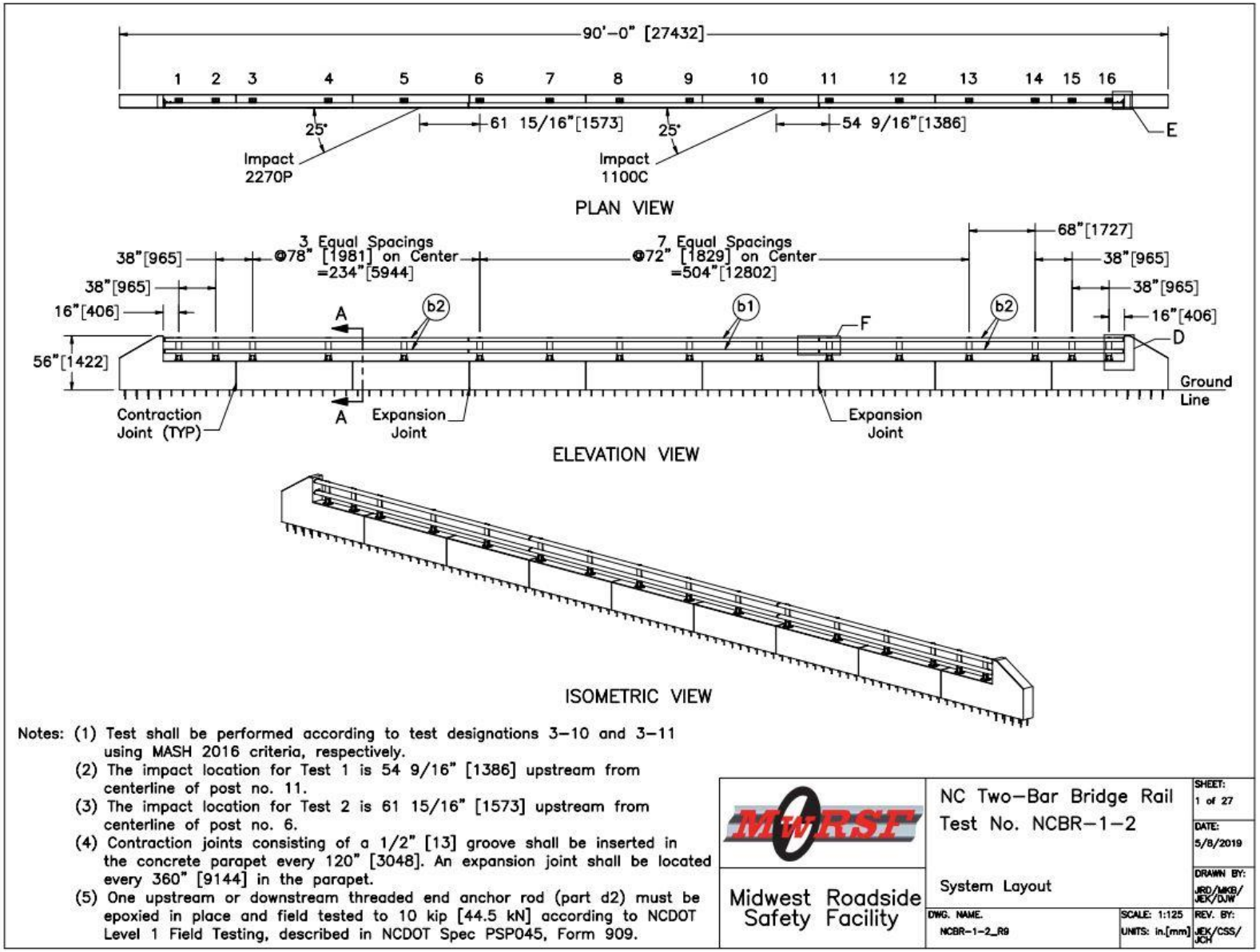


Figure 2. System Layout, Test Nos. NCBR-1 and NCBR-2

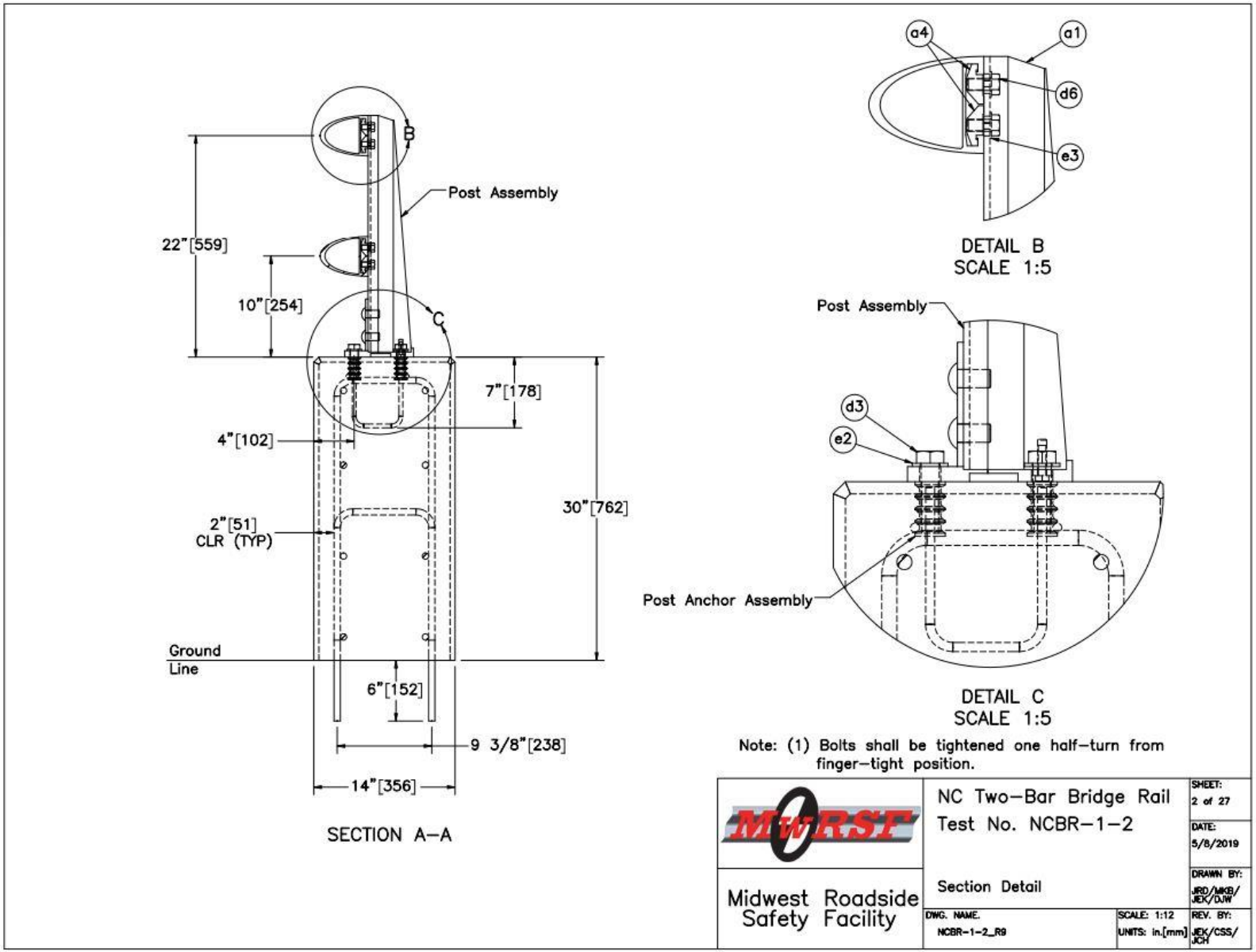


Figure 3. Section Detail, Test Nos. NCBR-1 and NCBR-2

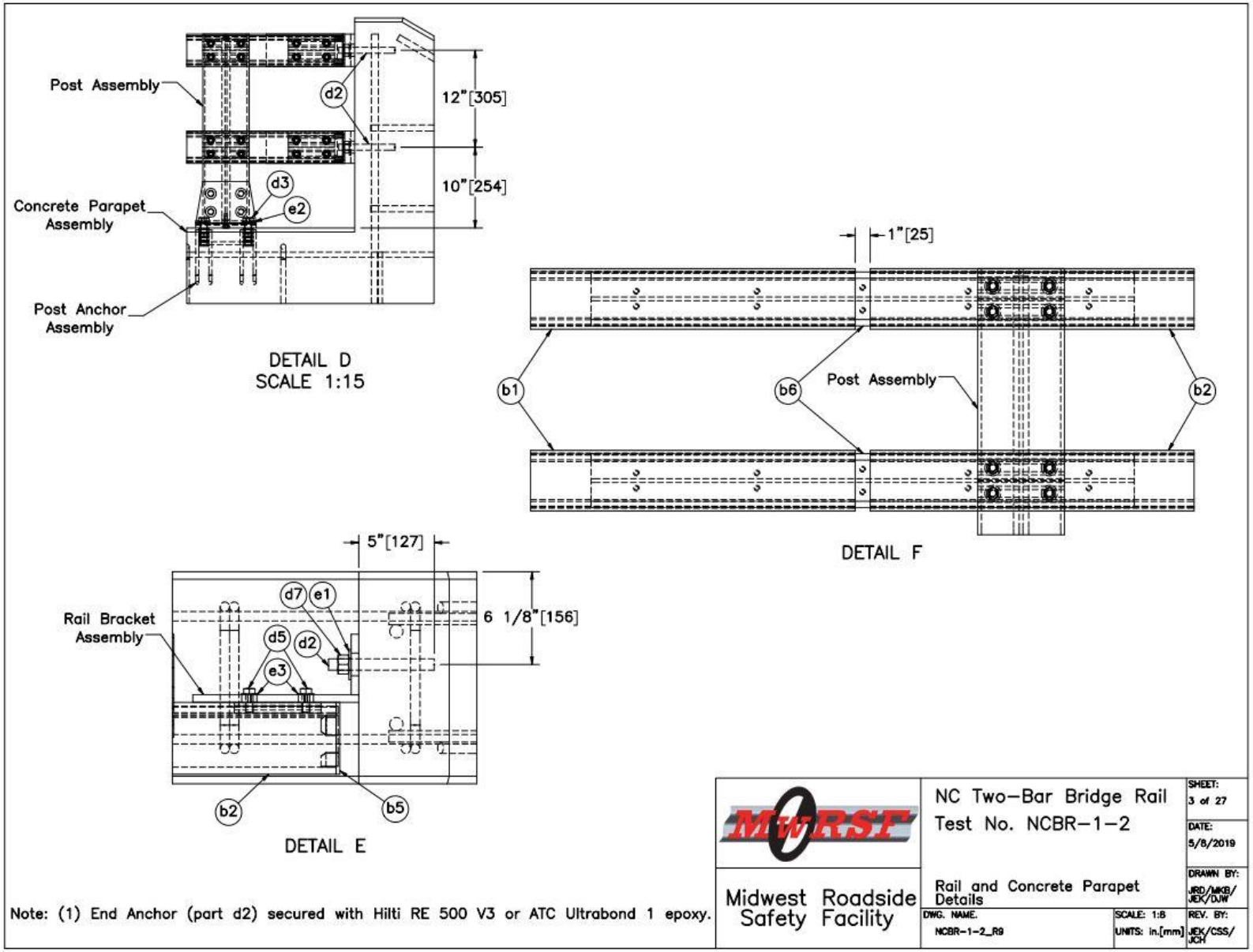
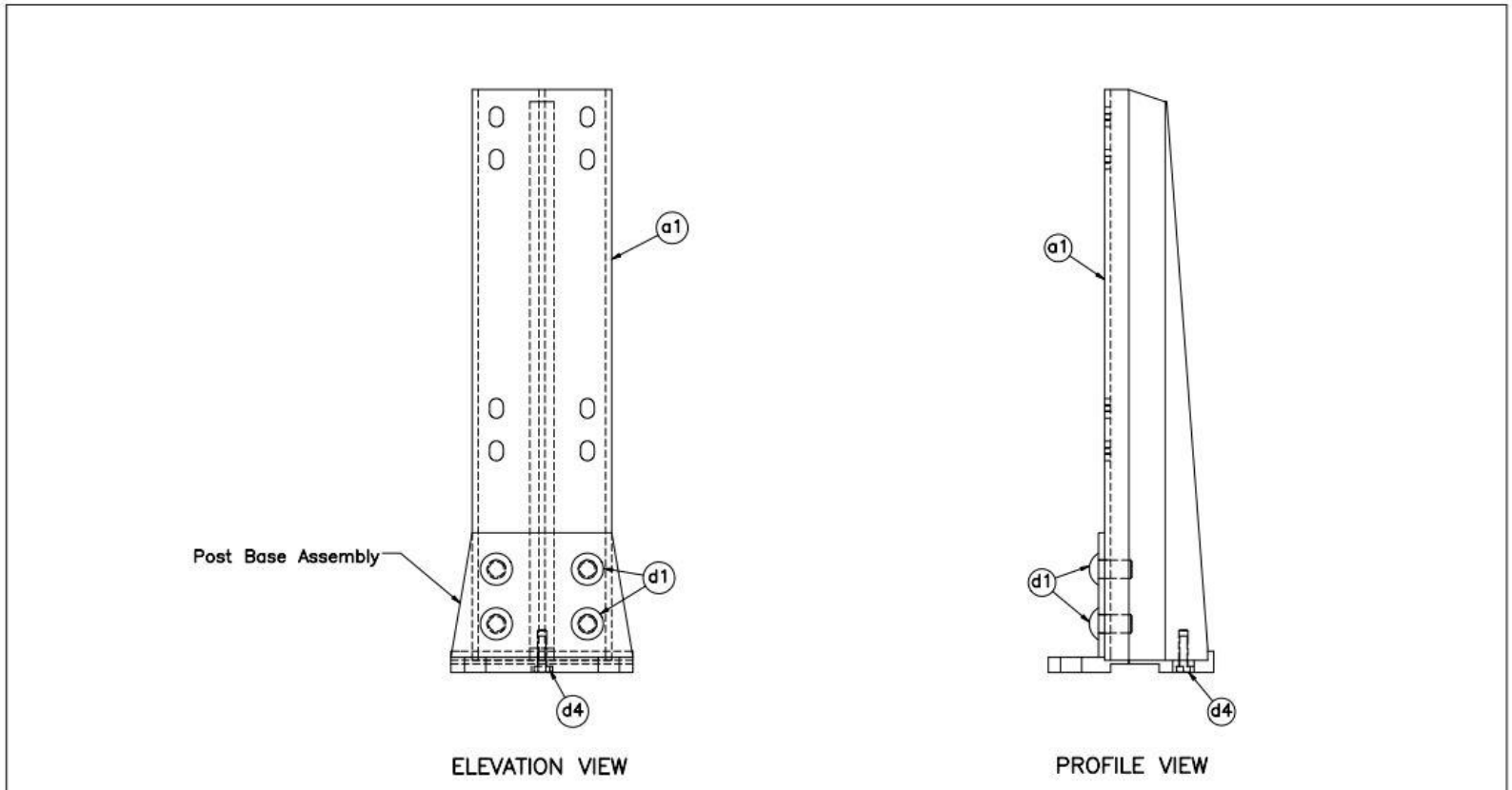


Figure 4. Rail and Concrete Parapet Details, Test Nos. NCBR-1 and NCBR-2



Item No.	QTY.	Description	Material Specification	Treatment Specification
–	16	Post Assembly	–	–
–	1	Post Base Assembly	–	–
a1	1	5 3/4"x 4 1/4" [146x108], 23 1/2" [597] Long Post	ASTM B221 Alloy 6061–T6	–
d1	4	3/4" [19] Dia., 1 3/8" Long Rivet	ASTM B316 Alloy 6061–T6	–
d4	1	3/8"–16 UNC [M10x1.5], 1 1/2" [38] Long Cap Screw	ASTM F593 Alloy 305 Stainless Steel	–

MwRSF

Midwest Roadside Safety Facility

NC Two–Bar Bridge Rail
Test No. NCBR–1–2

Post Assembly

DWG. NAME. NCBR–1–2_R9
SCALE: 1:6
UNITS: in.[mm]

SHEET: 4 of 27
DATE: 5/8/2019
DRAWN BY: JRD/MKB/JEK/DJW
REV. BY: JEK/CSS/JCH

Figure 5. Post Assembly, Test Nos. NCBR-1 and NCBR-2

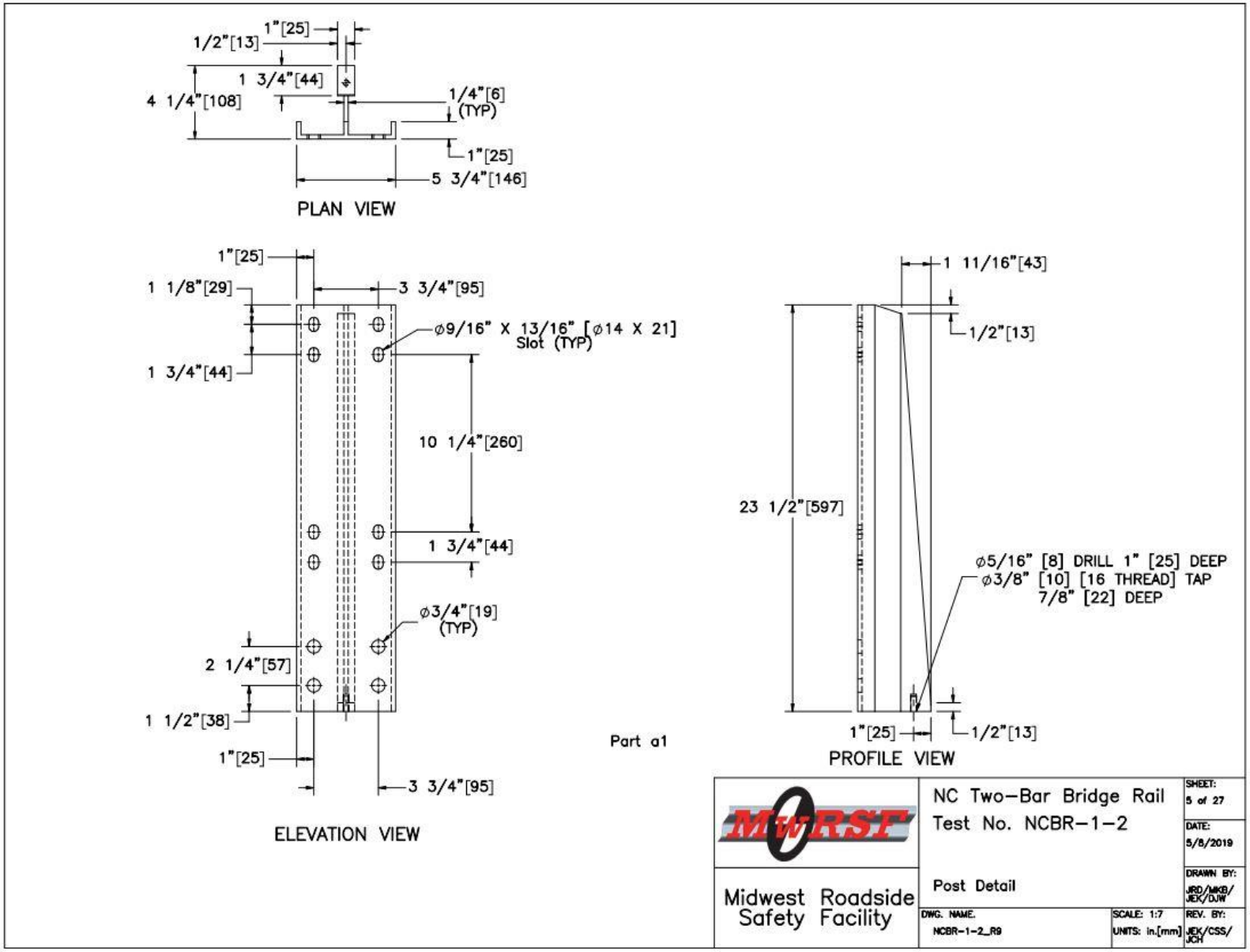
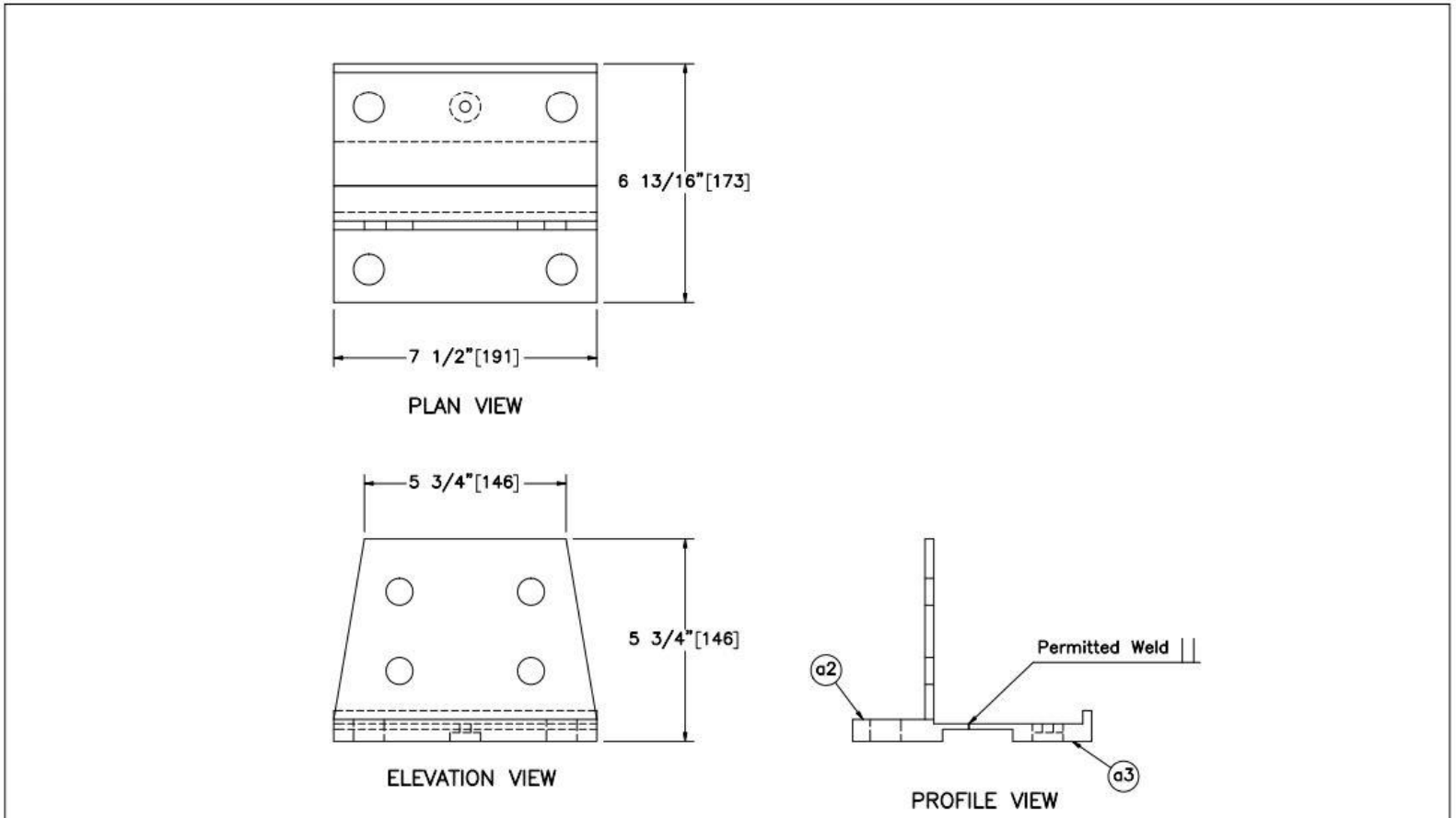


Figure 6. Post Detail, Test Nos. NCBR-1 and NCBR-2



Item No.	QTY.	Description	Material Specification	Treatment Specification
–	16	Post Base Assembly	–	–
a2	1	7 1/2"x3 5/16"x5 3/4" [191x84x146] Post Plate	ASTM B221 Alloy 6061–T6	-
a3	1	7 1/2"x3 1/4"x7/8" [181x83x22] Post Plate	ASTM B221 Alloy 6061–T6	-

Midwest Roadside Safety Facility

NC Two–Bar Bridge Rail
Test No. NCBR–1–2

Post Base Assembly

DWG. NAME. NCBR–1–2_R9
SCALE: 1:4
UNITS: in.[mm]
SHEET: 6 of 27
DATE: 5/8/2019
DRAWN BY: JRD/MKB/JEK/DJW
REV. BY: JEK/CSS/JCH

Figure 7. Post Base Assembly, Test Nos. NCBR-1 and NCBR-2

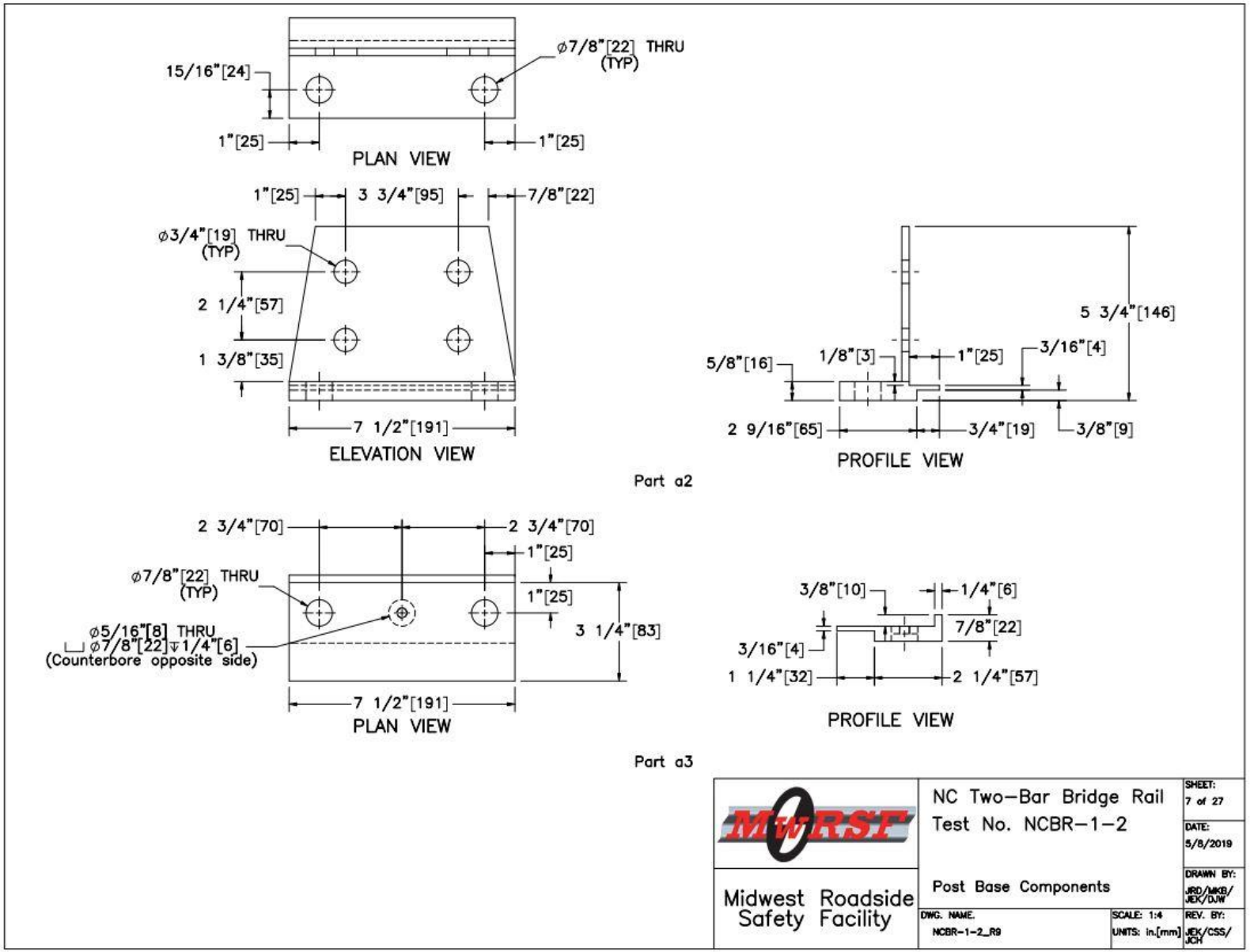


Figure 8. Post Base Components, Test Nos. NCBR-1 and NCBR-2

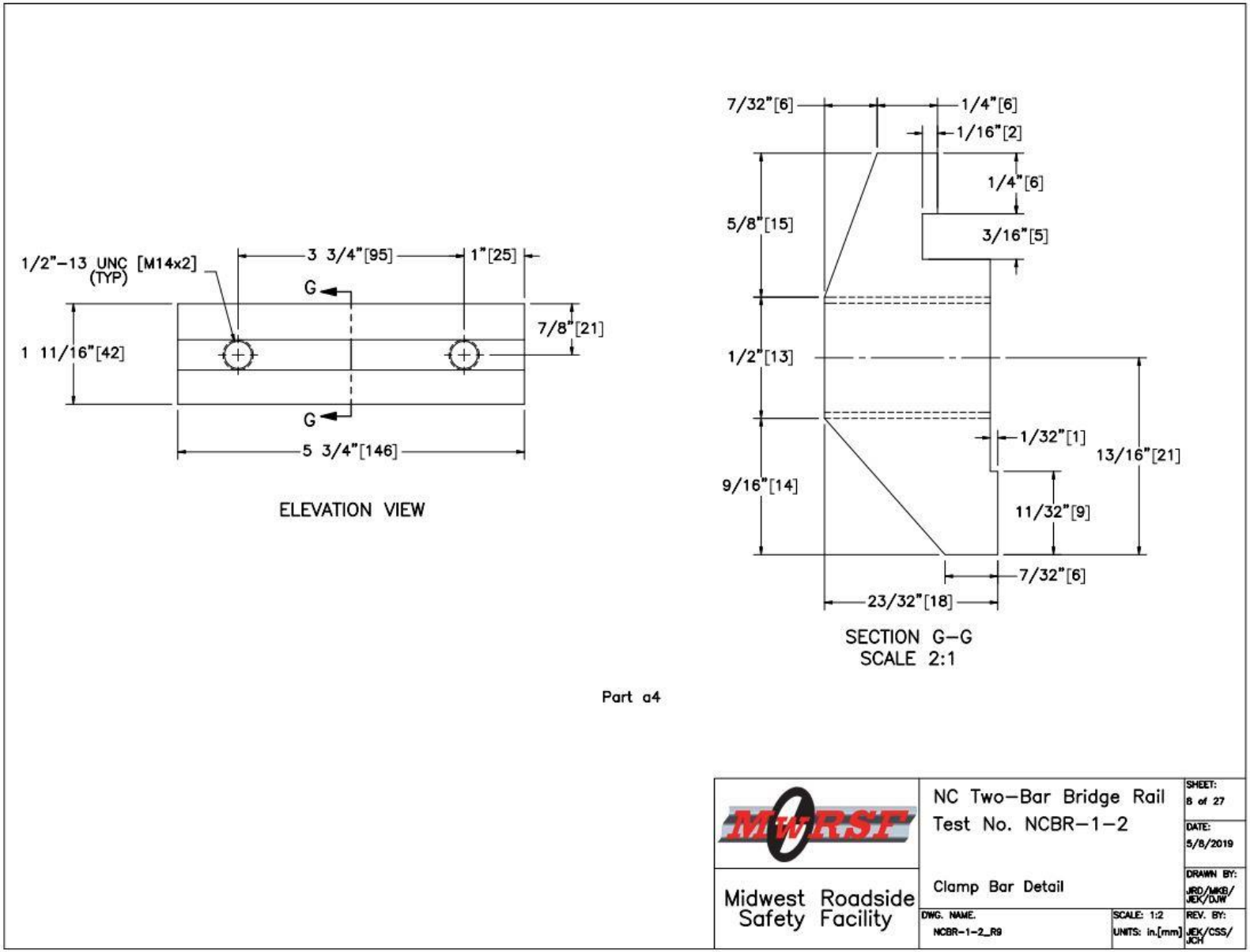


Figure 9. Clamp Bar Detail, Test Nos. NCBR-1 and NCBR-2

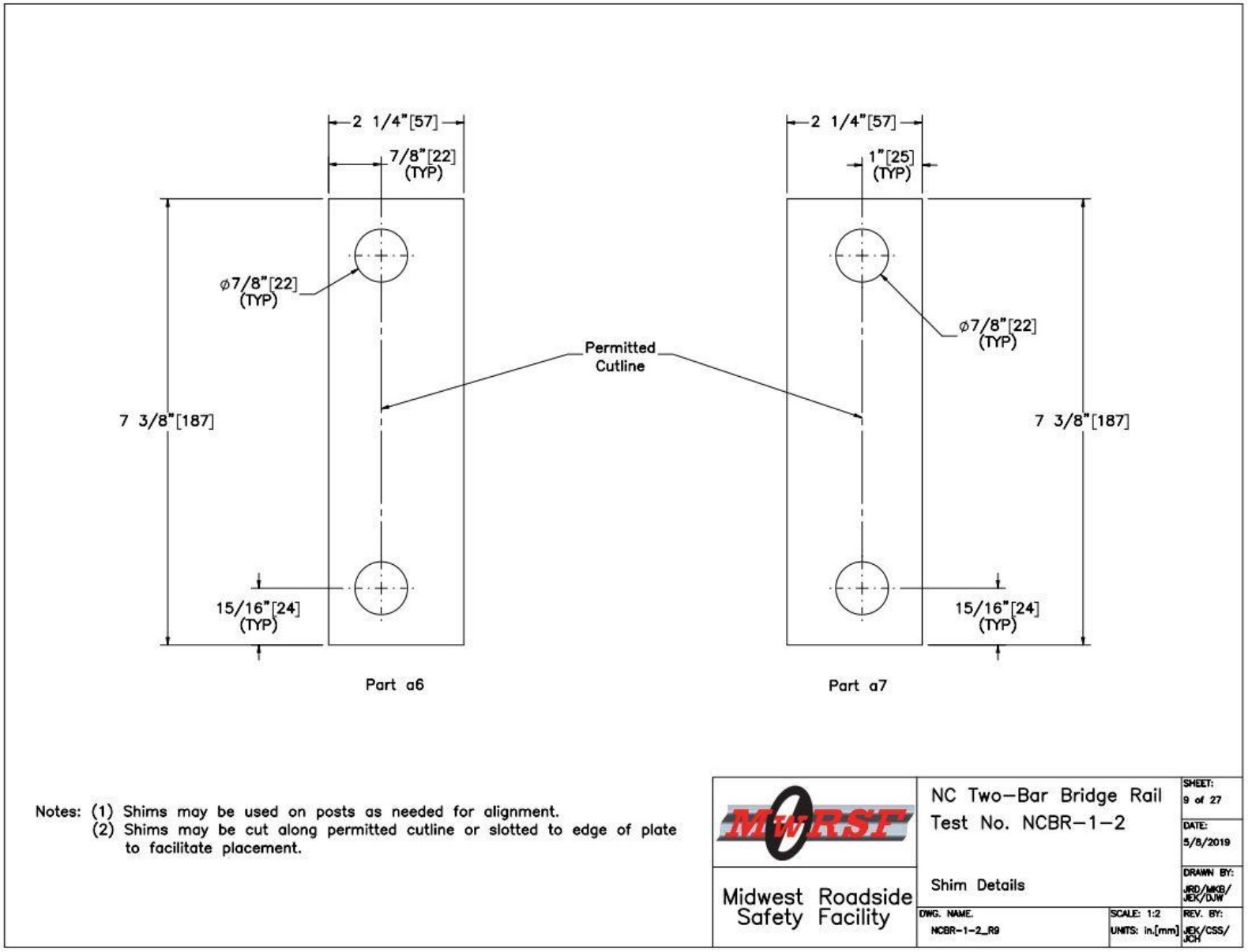


Figure 10. Shim Details, Test Nos. NCBR-1 and NCBR-2

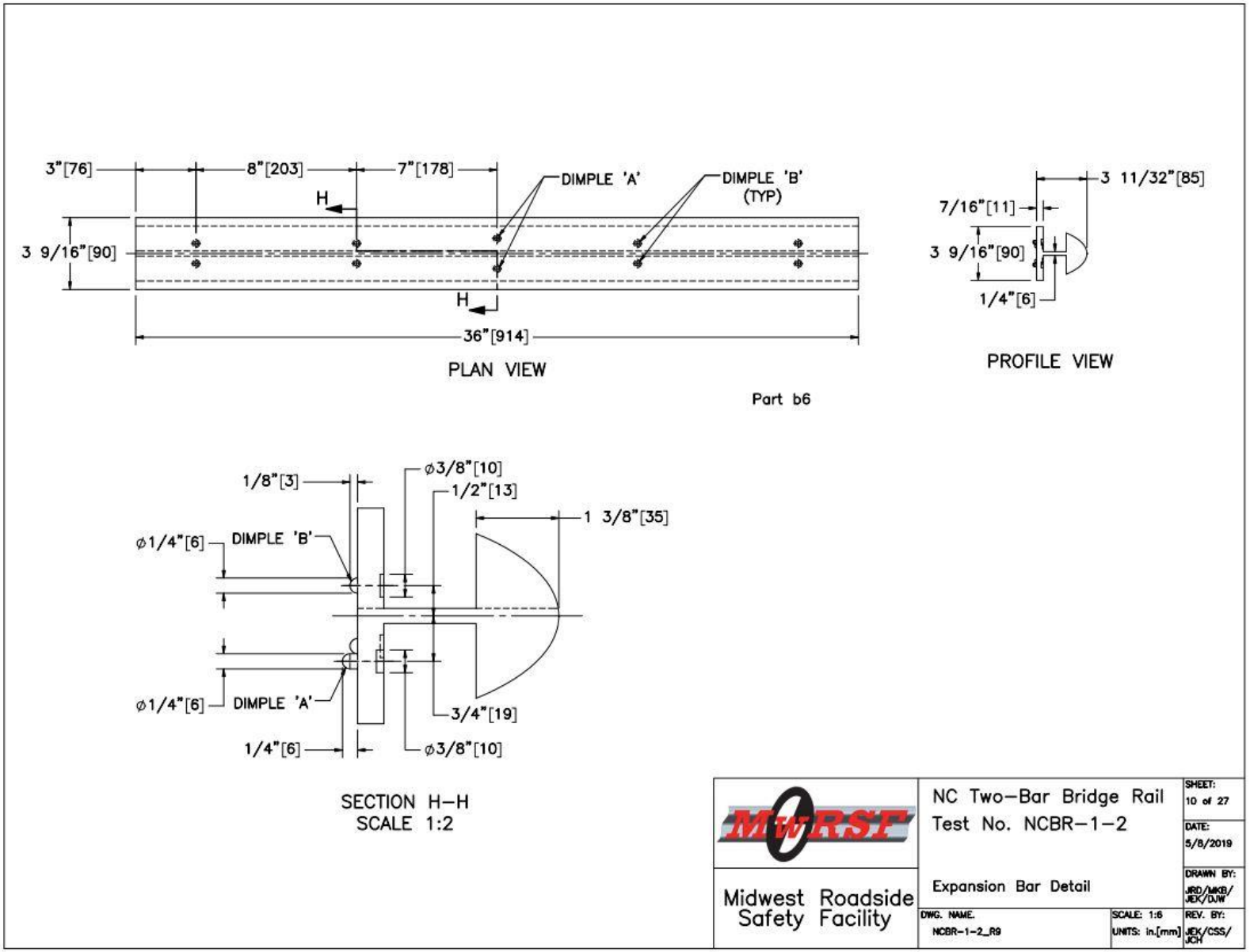


Figure 11. Expansion Bar Detail, Test Nos. NCBR-1 and NCBR-2

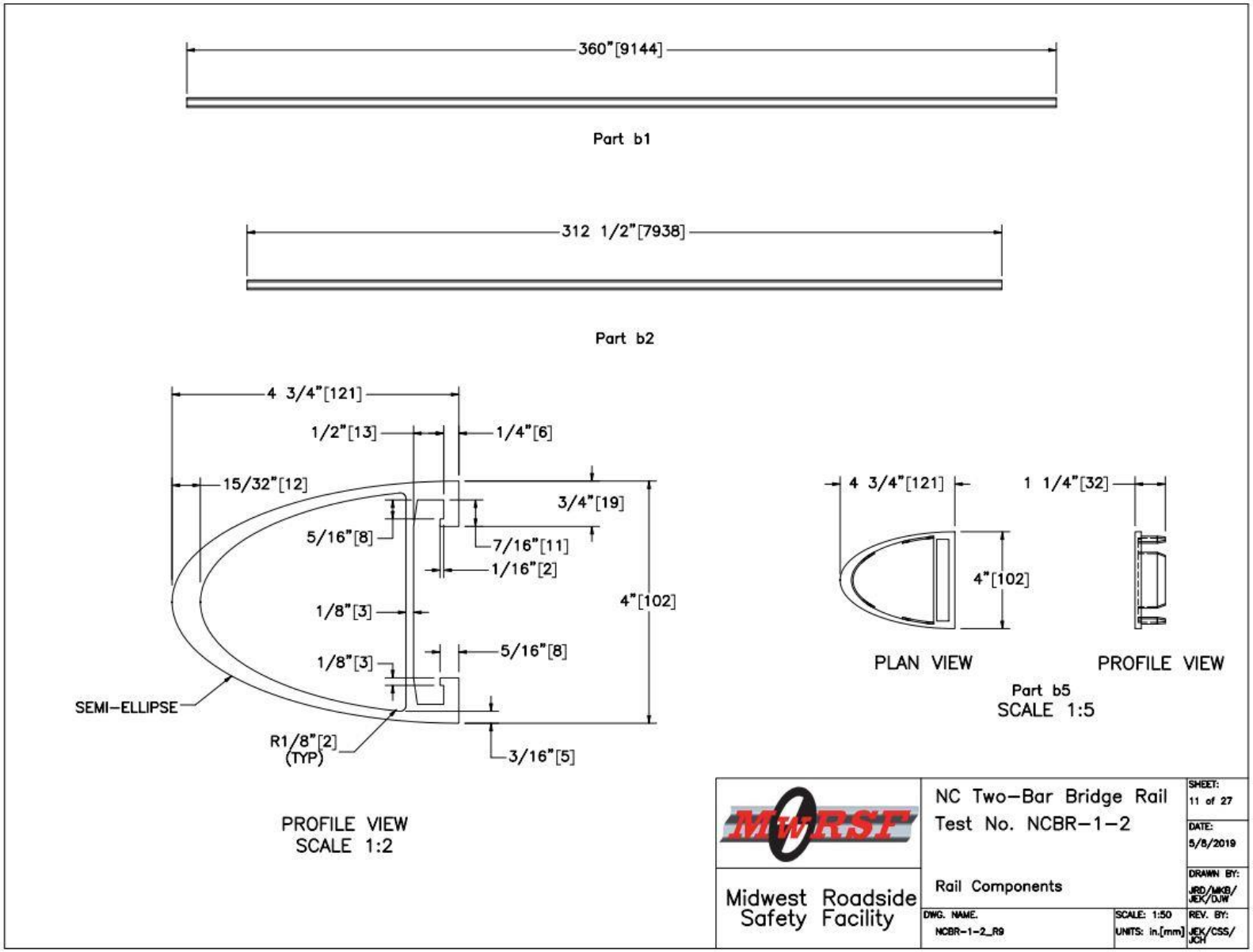
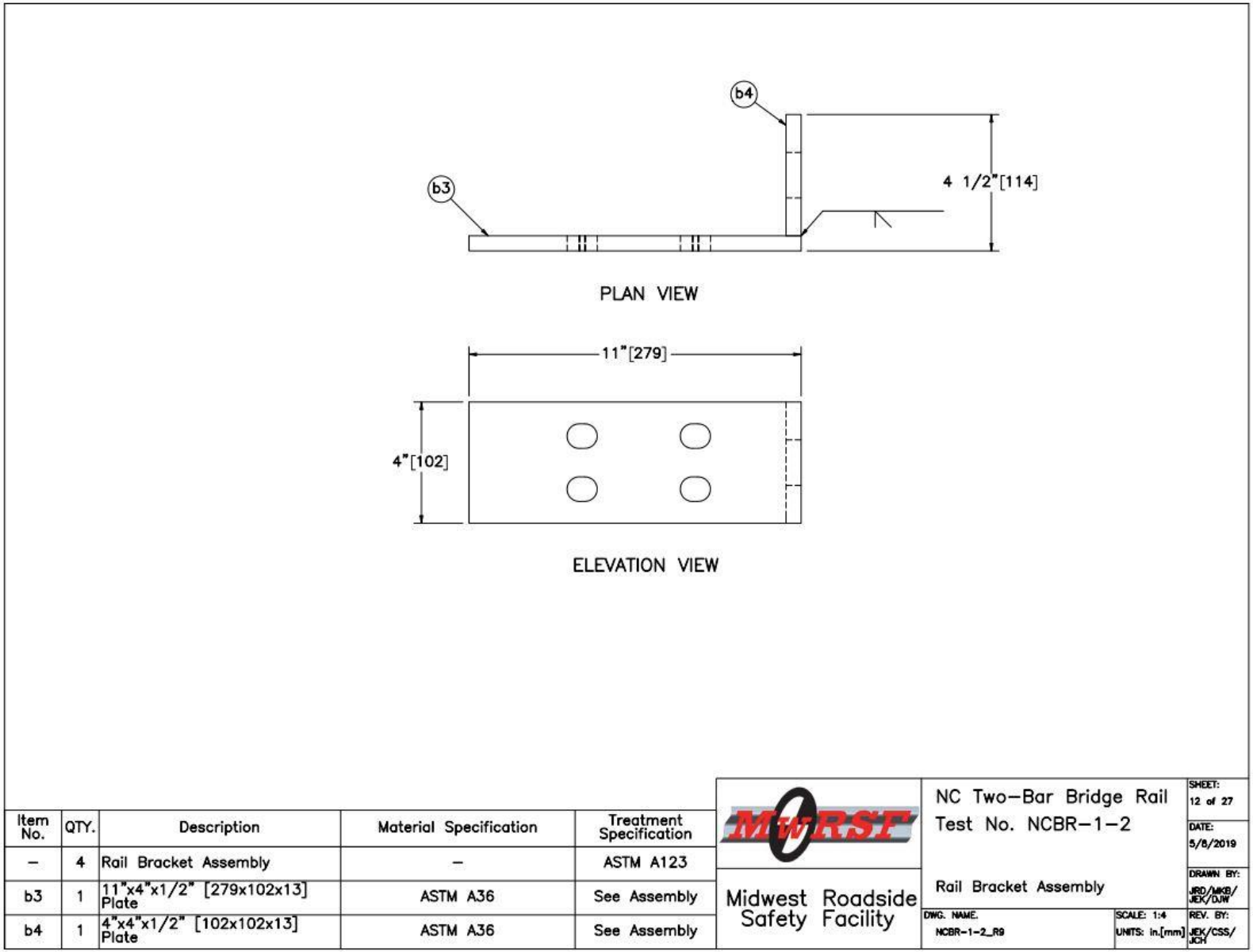


Figure 12. Rail Components, Test Nos. NCBR-1 and NCBR-2



Item No.	QTY.	Description	Material Specification	Treatment Specification
–	4	Rail Bracket Assembly	–	ASTM A123
b3	1	11"x4"x1/2" [279x102x13] Plate	ASTM A36	See Assembly
b4	1	4"x4"x1/2" [102x102x13] Plate	ASTM A36	See Assembly

Midwest Roadside Safety Facility

NC Two–Bar Bridge Rail
Test No. NCBR–1–2

Rail Bracket Assembly

DWG. NAME. NCBR–1–2_R9
SCALE: 1:4
UNITS: in.[mm]

SHEET: 12 of 27
DATE: 5/8/2019
DRAWN BY: JRD/MKB/JEK/DJW
REV. BY: JEK/CSS/JCH

Figure 13. Rail Bracket Assembly, Test Nos. NCBR-1 and NCBR-2

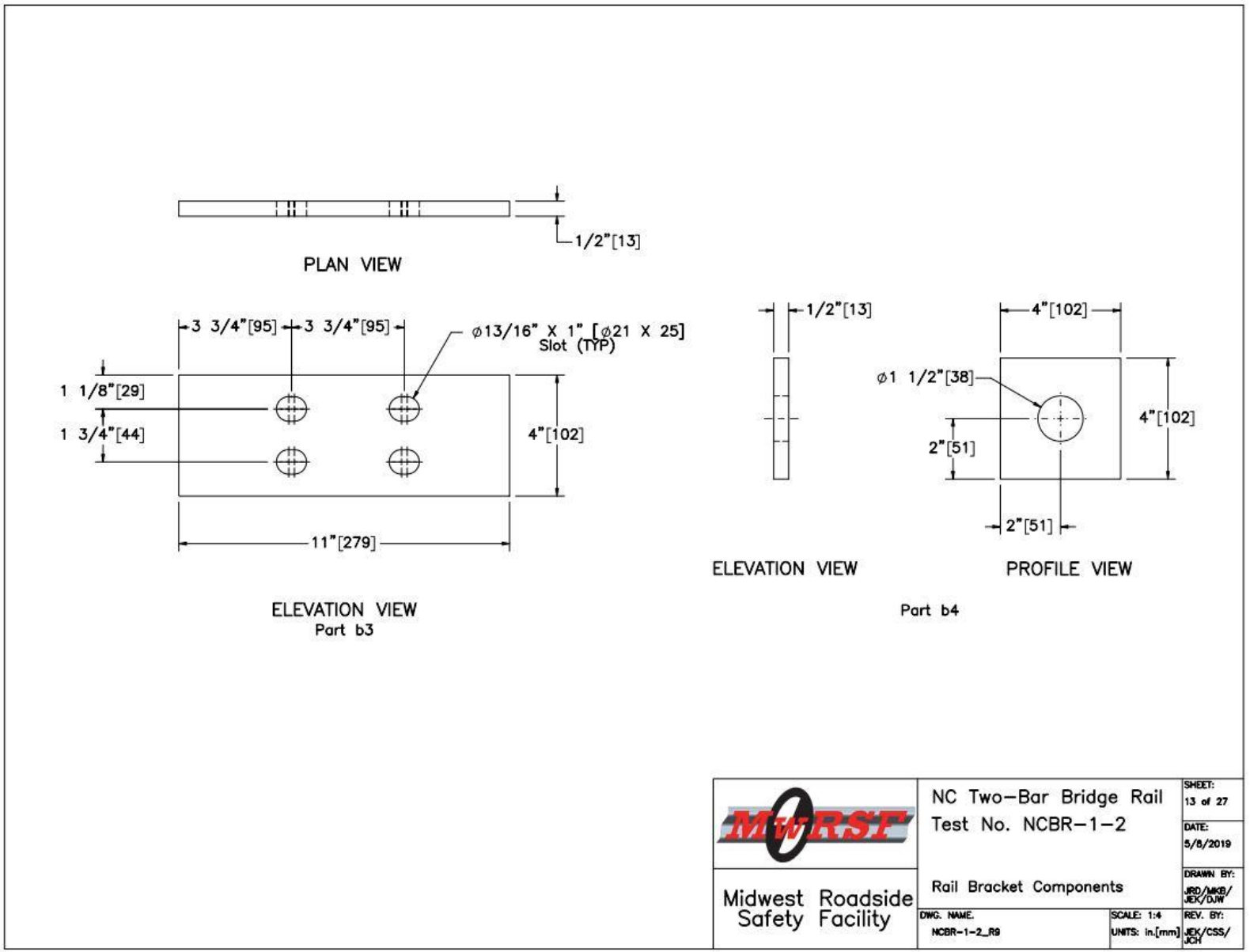
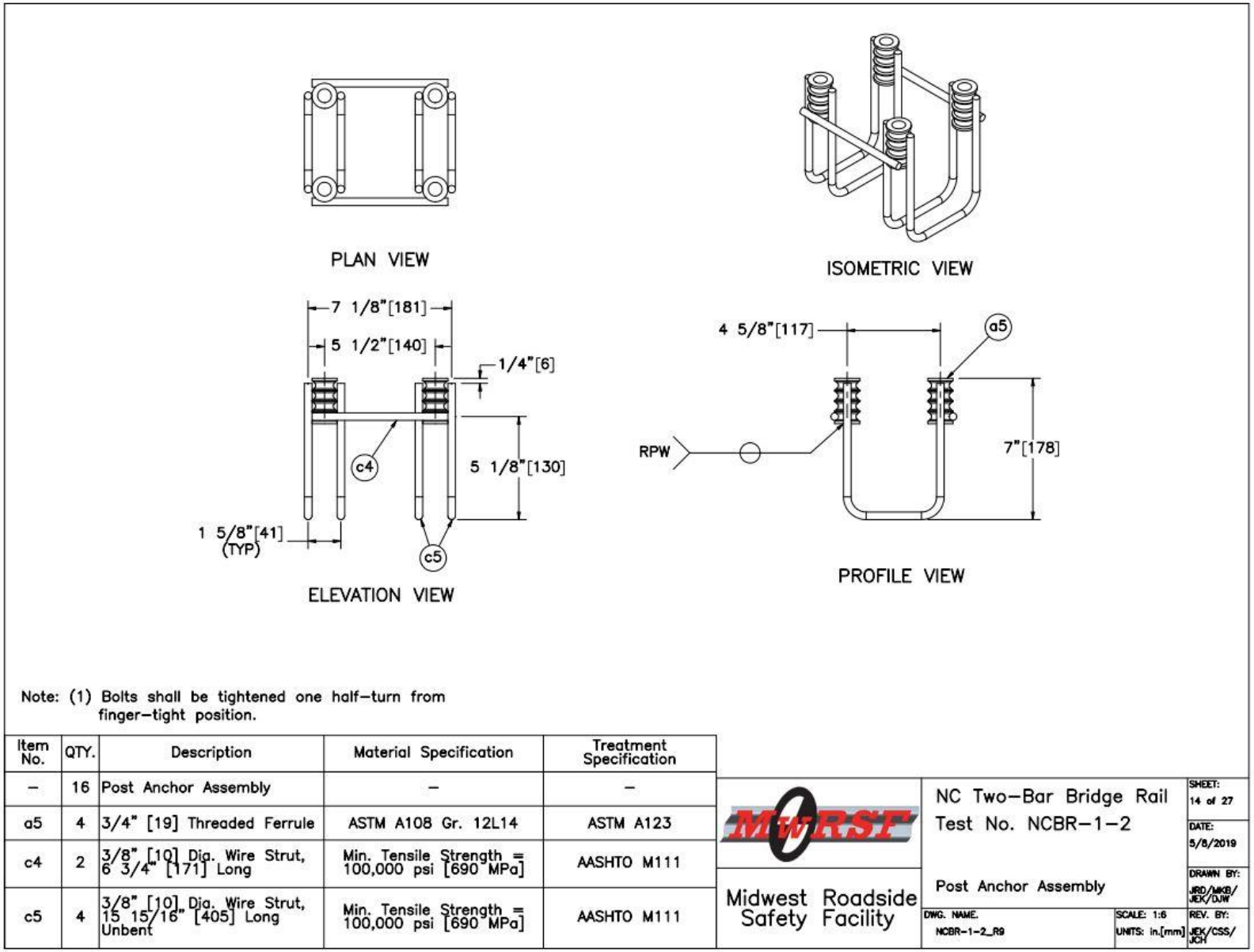


Figure 14. Rail Bracket Components, Test Nos. NCBR-1 and NCBR-2



Item No.	QTY.	Description	Material Specification	Treatment Specification
–	16	Post Anchor Assembly	–	–
a5	4	3/4" [19] Threaded Ferrule	ASTM A108 Gr. 12L14	ASTM A123
c4	2	3/8" [10] Dia. Wire Strut, 6 3/4" [171] Long	Min. Tensile Strength = 100,000 psi [690 MPa]	AASHTO M111
c5	4	3/8" [10] Dia. Wire Strut, 15 15/16" [405] Long Unbent	Min. Tensile Strength = 100,000 psi [690 MPa]	AASHTO M111

Midwest Roadside Safety Facility

NC Two-Bar Bridge Rail
Test No. NCBR-1-2

Post Anchor Assembly

SHEET: 14 of 27
DATE: 5/8/2019
DRAWN BY: JRD/MKB/JEK/DJW
REV. BY: JEK/CSS/JCH
DWG. NAME. NCBR-1-2_R9
SCALE: 1:6
UNITS: in.[mm]

Figure 15. Post Anchor Assembly, Test Nos. NCBR-1 and NCBR-2

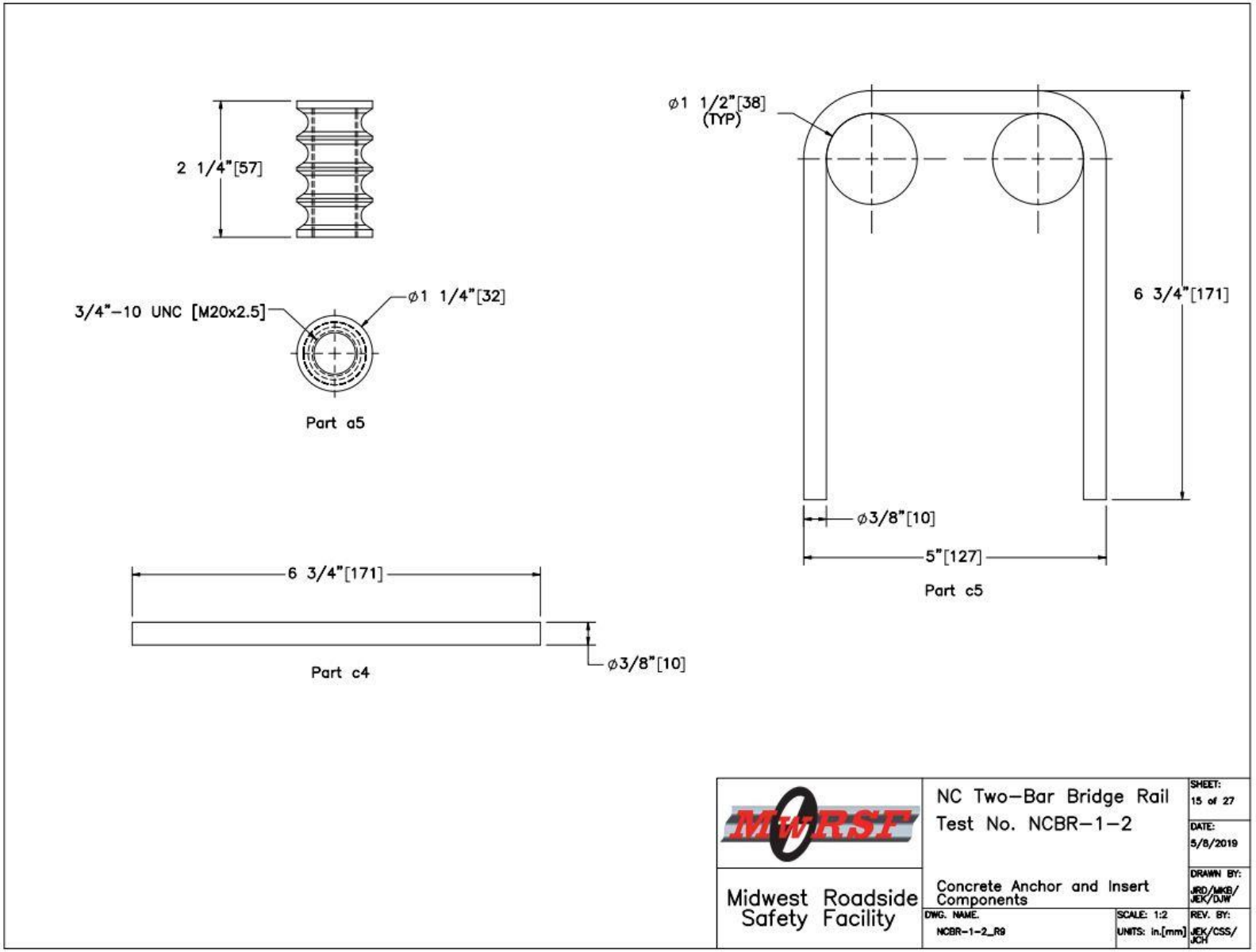
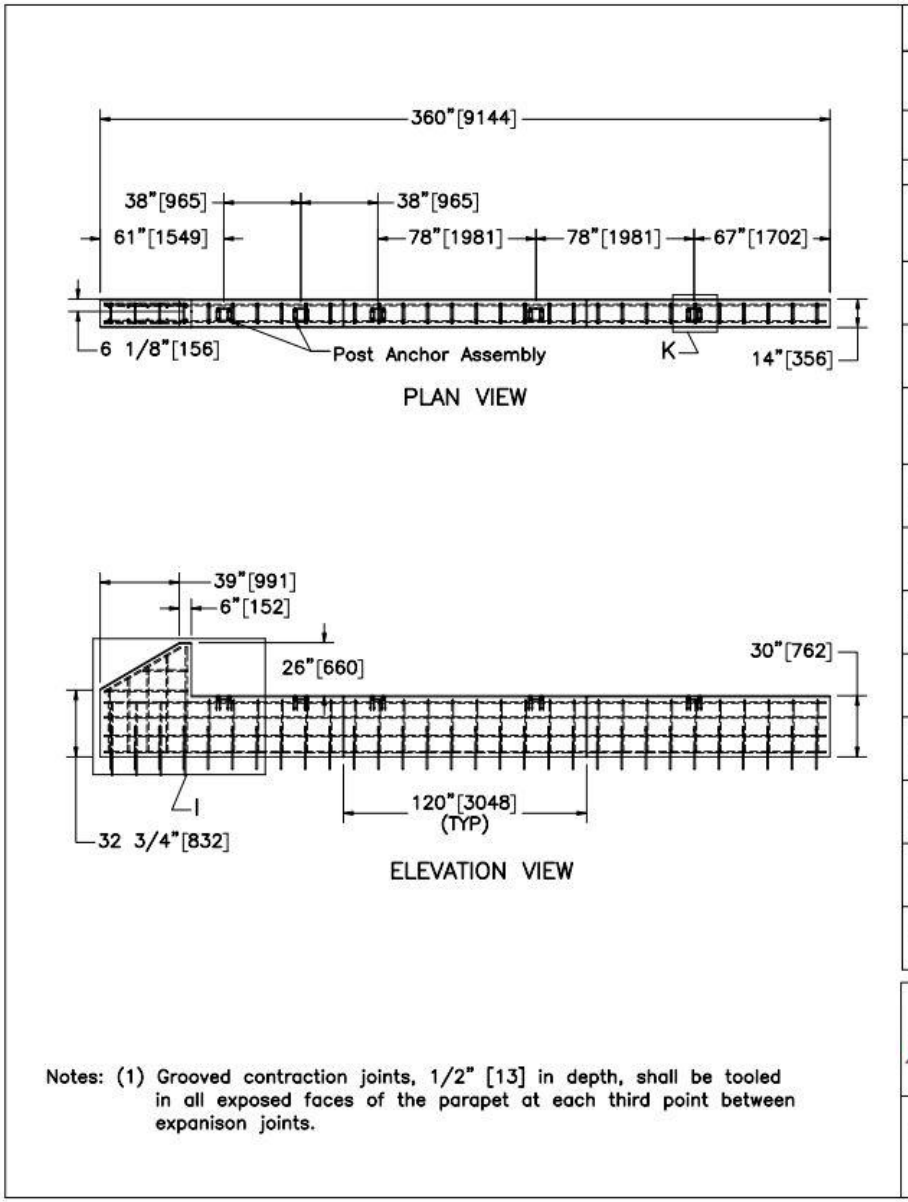


Figure 16. Concrete Anchor and Insert Components, Test Nos. NCBR-1 and NCBR-2



Item No.	QTY.	Description	Material Specification	Treatment Specification
–	1	Upstream Parapet Assembly	–	–
–	5	Post Anchor Assembly		
c1	1	Concrete	–	–
c6	26	#5 [16] Bar, 59 1/2" [1,511] Long Unbent	ASTM A615 Gr. 60	Epoxy–Coated (ASTM A775 or A934)
c8	8	#5 [16] Bar, 356" [9,042] Long	ASTM A615 Gr. 60	Epoxy–Coated (ASTM A775 or A934)
c9	8	#5 [16] Bar, 36" [914] Long	ASTM A615 Gr. 60	Epoxy–Coated (ASTM A775 or A934)
c10	30	#5 [16] Bar, 49 1/2" [1,257] Long Unbent	ASTM A615 Gr. 60	Epoxy–Coated (ASTM A775 or A934)
c11	2	#6 [19] Bar, 22" [559] Long	ASTM A615 Gr. 60	Epoxy–Coated (ASTM A775 or A934)
c12	2	#6 [19] Bar, 40" [1,016] Long	ASTM A615 Gr. 60	Epoxy–Coated (ASTM A775 or A934)
c13	2	#6 [19] Bar, 43 1/4" [1,099] Long	ASTM A615 Gr. 60	Epoxy–Coated (ASTM A775 or A934)
c14	2	#7 [22] Bar, 31" [787] Long	ASTM A615 Gr. 60	Epoxy–Coated (ASTM A775 or A934)
c15	2	#7 [22] Bar, 36 1/2" [927] Long	ASTM A615 Gr. 60	Epoxy–Coated (ASTM A775 or A934)
c16	2	#7 [22] Bar, 42" [1,067] Long	ASTM A615 Gr. 60	Epoxy–Coated (ASTM A775 or A934)
c17	2	#7 [22] Bar, 47 1/2" [1,207] Long	ASTM A615 Gr. 60	Epoxy–Coated (ASTM A775 or A934)
c18	2	#7 [22] Bar, 52" [1,321] Long	ASTM A615 Gr. 60	Epoxy–Coated (ASTM A775 or A934)

Notes: (1) Grooved contraction joints, 1/2" [13] in depth, shall be tooled in all exposed faces of the parapet at each third point between expanison joints.

MwRSF	NC Two–Bar Bridge Rail Test No. NCBR–1–2	SHEET: 16 of 27
		DATE: 5/8/2019
Midwest Roadside Safety Facility	Upstream Concrete Parapet Assembly	DRAWN BY: JRD/MKB/ JEK/DJW
	DWG. NAME. NCBR–1–2_R9 / SCALE: 1:75 / UNITS: in.[mm]	REV. BY: JEK/CSS/ JCH

Figure 17. Upstream Concrete Parapet Assembly, Test Nos. NCBR-1 and NCBR-2

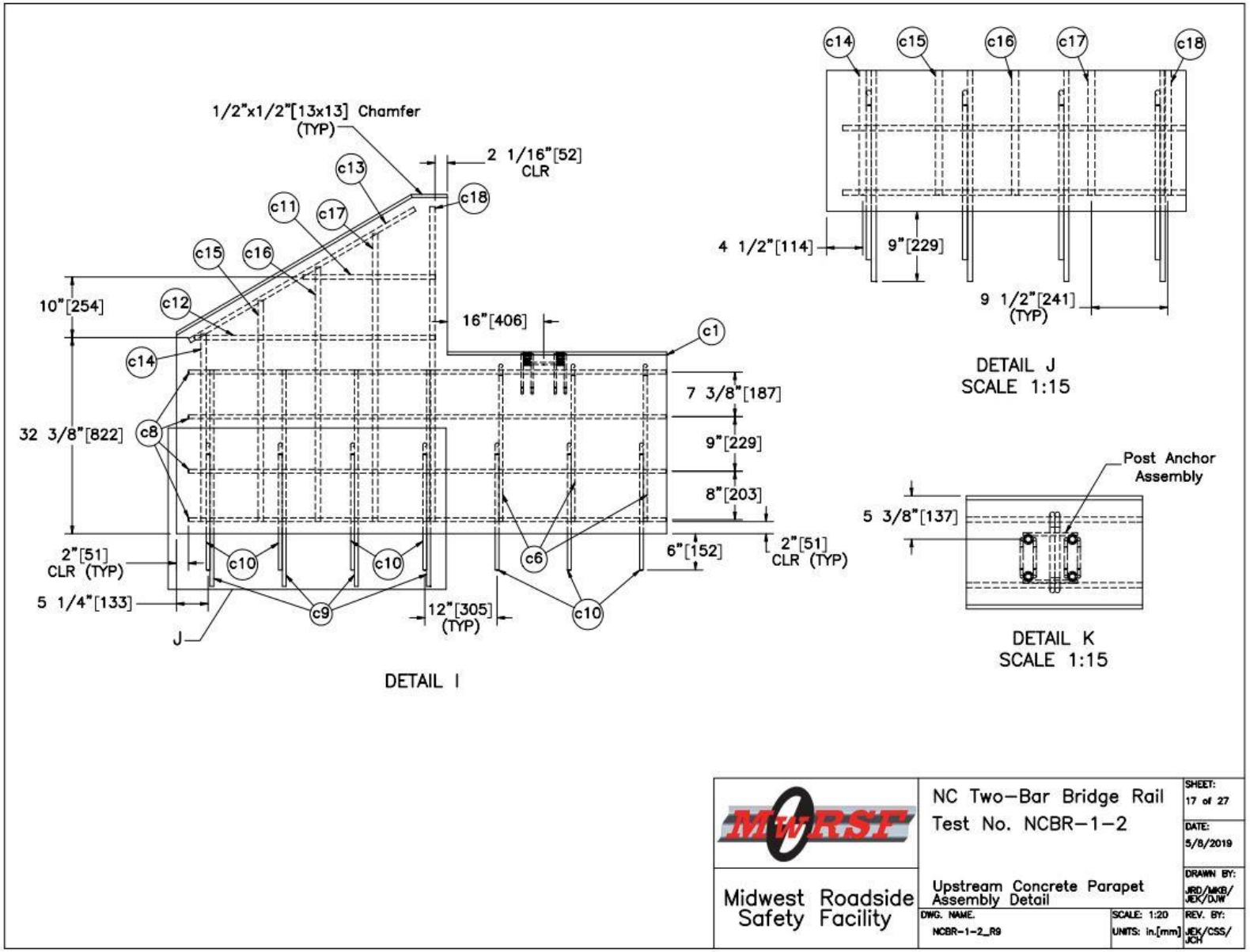
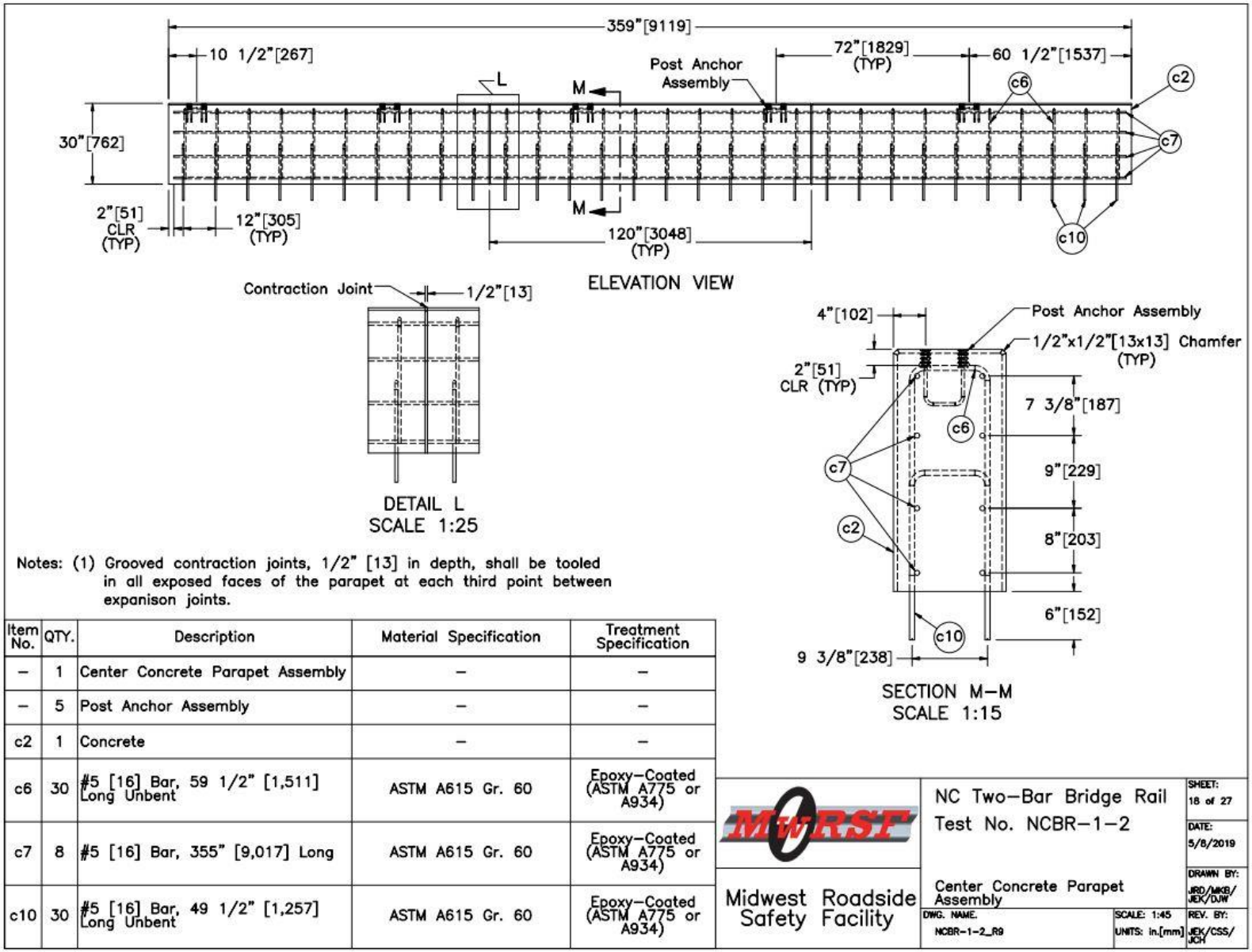
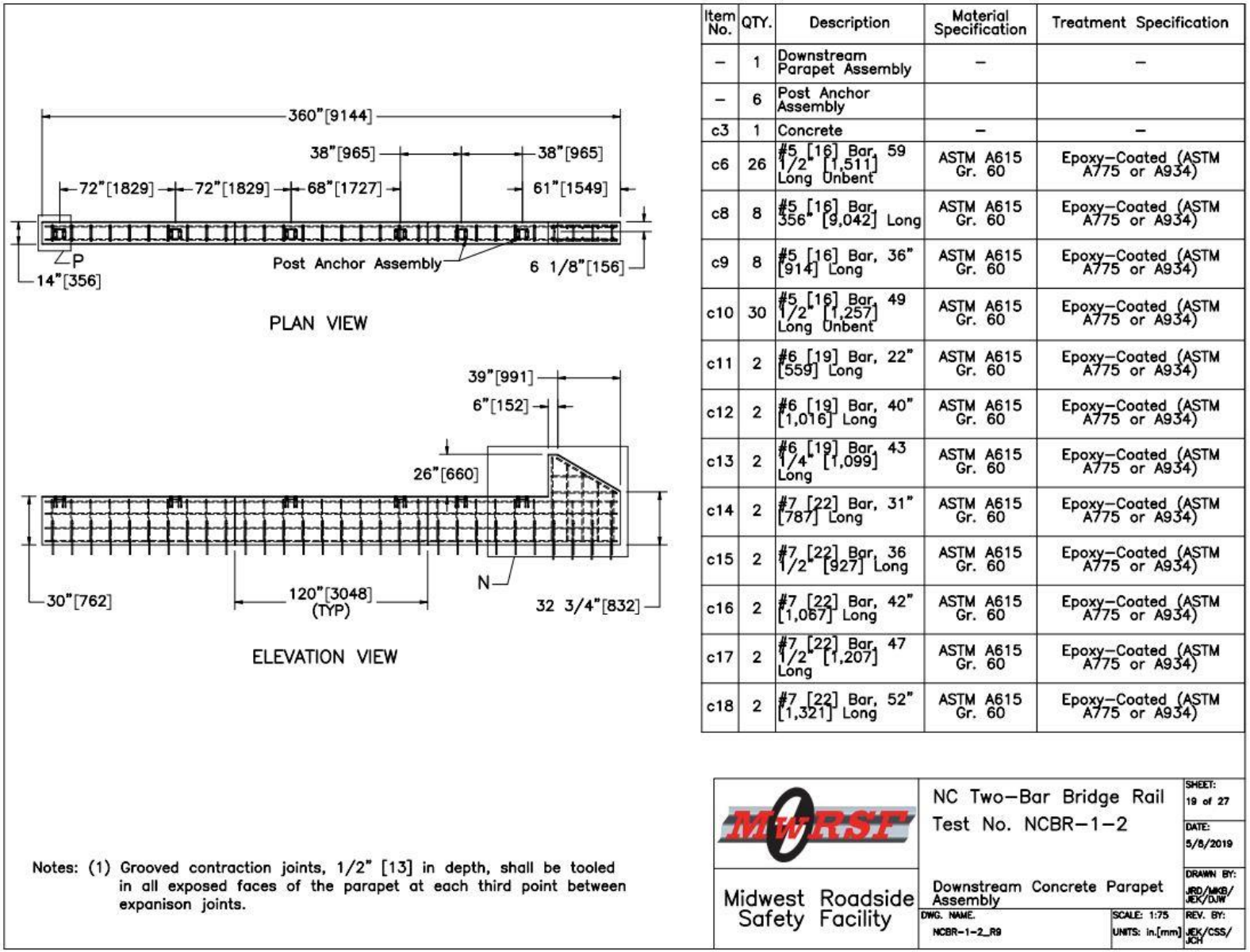


Figure 18. Upstream Concrete Parapet Assembly Detail, Test Nos. NCBR-1 and NCBR-2



Item No.	QTY.	Description	Material Specification	Treatment Specification
–	1	Center Concrete Parapet Assembly	–	–
–	5	Post Anchor Assembly	–	–
c2	1	Concrete	–	–
c6	30	#5 [16] Bar, 59 1/2" [1,511] Long Unbent	ASTM A615 Gr. 60	Epoxy-Coated (ASTM A775 or A934)
c7	8	#5 [16] Bar, 355" [9,017] Long	ASTM A615 Gr. 60	Epoxy-Coated (ASTM A775 or A934)
c10	30	#5 [16] Bar, 49 1/2" [1,257] Long Unbent	ASTM A615 Gr. 60	Epoxy-Coated (ASTM A775 or A934)

Figure 19. Center Concrete Parapet Assembly, Test Nos. NCBR-1 and NCBR-2



Item No.	QTY.	Description	Material Specification	Treatment Specification
–	1	Downstream Parapet Assembly	–	–
–	6	Post Anchor Assembly		
c3	1	Concrete	–	–
c6	26	#5 [16] Bar, 59 1/2" [1,511] Long Unbent	ASTM A615 Gr. 60	Epoxy–Coated (ASTM A775 or A934)
c8	8	#5 [16] Bar, 356" [9,042] Long	ASTM A615 Gr. 60	Epoxy–Coated (ASTM A775 or A934)
c9	8	#5 [16] Bar, 36" [914] Long	ASTM A615 Gr. 60	Epoxy–Coated (ASTM A775 or A934)
c10	30	#5 [16] Bar, 49 1/2" [1,257] Long Unbent	ASTM A615 Gr. 60	Epoxy–Coated (ASTM A775 or A934)
c11	2	#6 [19] Bar, 22" [559] Long	ASTM A615 Gr. 60	Epoxy–Coated (ASTM A775 or A934)
c12	2	#6 [19] Bar, 40" [1,016] Long	ASTM A615 Gr. 60	Epoxy–Coated (ASTM A775 or A934)
c13	2	#6 [19] Bar, 43 1/4" [1,099] Long	ASTM A615 Gr. 60	Epoxy–Coated (ASTM A775 or A934)
c14	2	#7 [22] Bar, 31" [787] Long	ASTM A615 Gr. 60	Epoxy–Coated (ASTM A775 or A934)
c15	2	#7 [22] Bar, 36 1/2" [927] Long	ASTM A615 Gr. 60	Epoxy–Coated (ASTM A775 or A934)
c16	2	#7 [22] Bar, 42" [1,067] Long	ASTM A615 Gr. 60	Epoxy–Coated (ASTM A775 or A934)
c17	2	#7 [22] Bar, 47 1/2" [1,207] Long	ASTM A615 Gr. 60	Epoxy–Coated (ASTM A775 or A934)
c18	2	#7 [22] Bar, 52" [1,321] Long	ASTM A615 Gr. 60	Epoxy–Coated (ASTM A775 or A934)

MwRSF	NC Two–Bar Bridge Rail Test No. NCBR–1–2	SHEET: 19 of 27
		DATE: 5/8/2019
Midwest Roadside Safety Facility	Downstream Concrete Parapet Assembly	DRAWN BY: JRD/MKB/ JEK/DJW
	DWG. NAME. NCBR–1–2_R9 SCALE: 1:75 UNITS: in.[mm]	REV. BY: JEK/CSS/ JCH

Figure 20. Downstream Concrete Parapet Assembly, Test Nos. NCBR-1 and NCBR-2

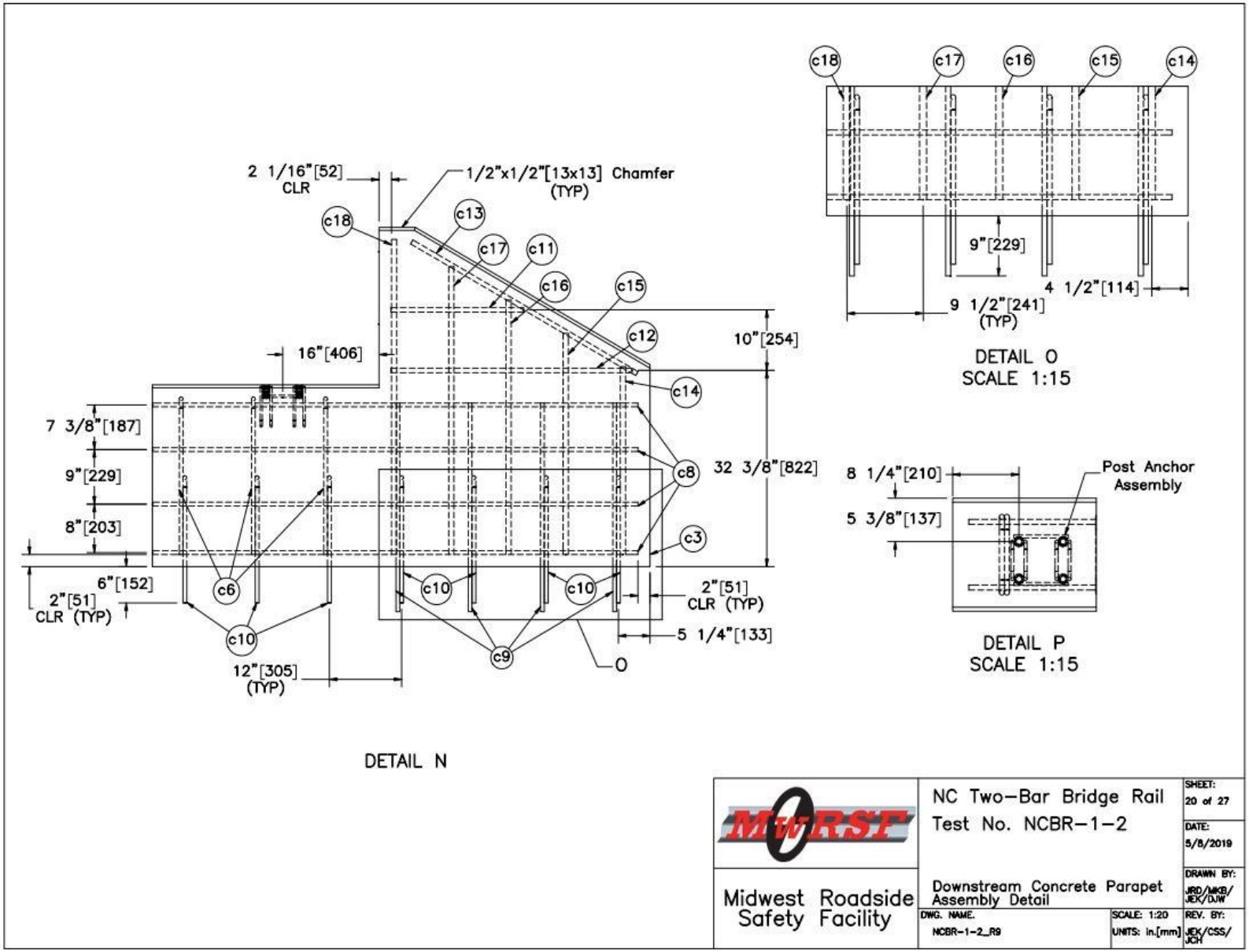
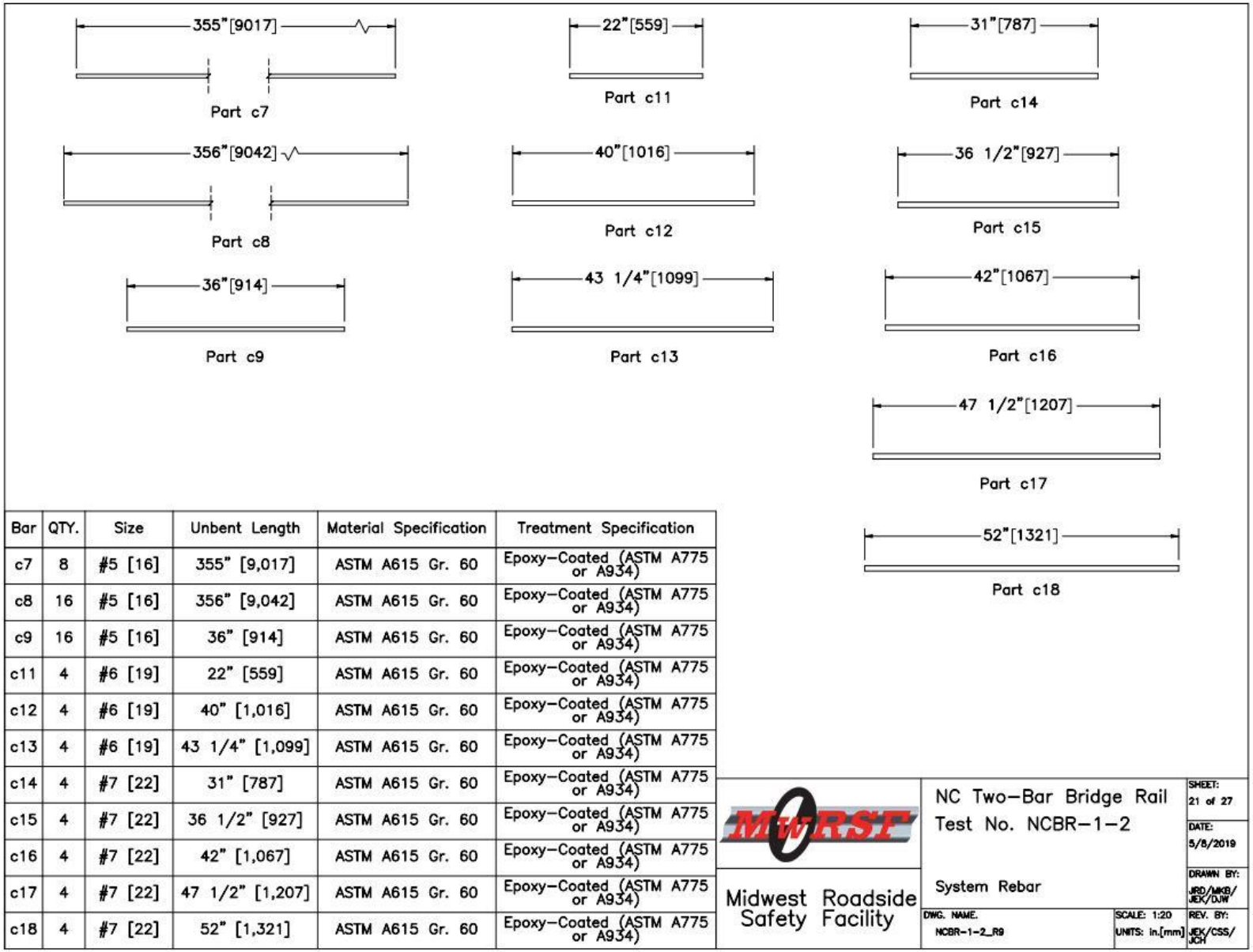


Figure 21. Downstream Concrete Parapet Assembly, Test Nos. NCBR-1 and NCBR-2



Bar	QTY.	Size	Unbent Length	Material Specification	Treatment Specification
c7	8	#5 [16]	355" [9,017]	ASTM A615 Gr. 60	Epoxy-Coated (ASTM A775 or A934)
c8	16	#5 [16]	356" [9,042]	ASTM A615 Gr. 60	Epoxy-Coated (ASTM A775 or A934)
c9	16	#5 [16]	36" [914]	ASTM A615 Gr. 60	Epoxy-Coated (ASTM A775 or A934)
c11	4	#6 [19]	22" [559]	ASTM A615 Gr. 60	Epoxy-Coated (ASTM A775 or A934)
c12	4	#6 [19]	40" [1,016]	ASTM A615 Gr. 60	Epoxy-Coated (ASTM A775 or A934)
c13	4	#6 [19]	43 1/4" [1,099]	ASTM A615 Gr. 60	Epoxy-Coated (ASTM A775 or A934)
c14	4	#7 [22]	31" [787]	ASTM A615 Gr. 60	Epoxy-Coated (ASTM A775 or A934)
c15	4	#7 [22]	36 1/2" [927]	ASTM A615 Gr. 60	Epoxy-Coated (ASTM A775 or A934)
c16	4	#7 [22]	42" [1,067]	ASTM A615 Gr. 60	Epoxy-Coated (ASTM A775 or A934)
c17	4	#7 [22]	47 1/2" [1,207]	ASTM A615 Gr. 60	Epoxy-Coated (ASTM A775 or A934)
c18	4	#7 [22]	52" [1,321]	ASTM A615 Gr. 60	Epoxy-Coated (ASTM A775 or A934)

MwRSF

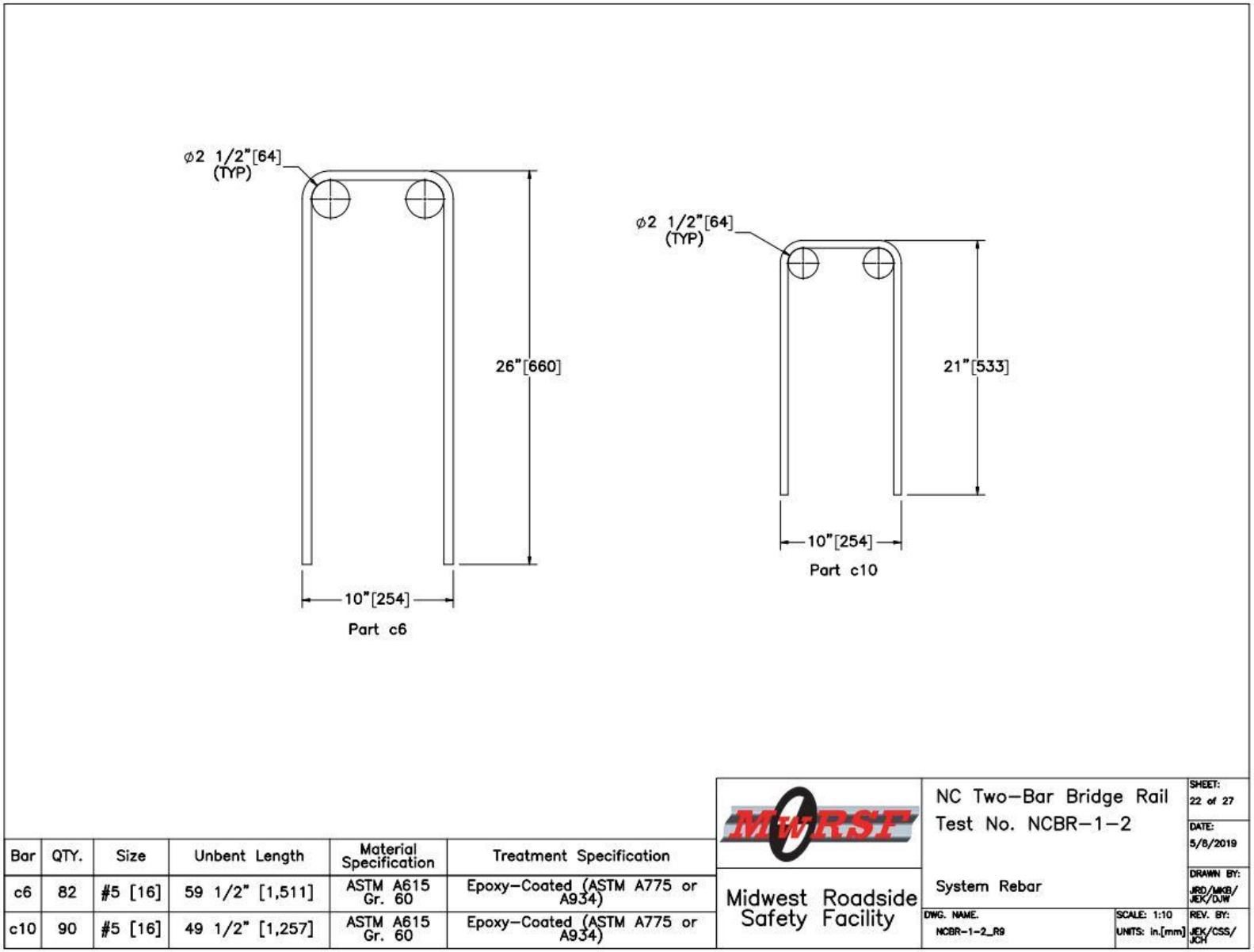
Midwest Roadside Safety Facility

NC Two-Bar Bridge Rail
Test No. NCBR-1-2

System Rebar

SHEET: 21 of 27
DATE: 5/8/2019
DRAWN BY: JRD/MKB/JEK/DJW
REV. BY: JEK/CSS/JCH
DWG. NAME. NCBR-1-2_R9
SCALE: 1:20
UNITS: in.[mm]

Figure 22. System Rebar, Test Nos. NCBR-1 and NCBR-2



Bar	QTY.	Size	Unbent Length	Material Specification	Treatment Specification
c6	82	#5 [16]	59 1/2" [1,511]	ASTM A615 Gr. 60	Epoxy-Coated (ASTM A775 or A934)
c10	90	#5 [16]	49 1/2" [1,257]	ASTM A615 Gr. 60	Epoxy-Coated (ASTM A775 or A934)

Midwest Roadside Safety Facility

NC Two-Bar Bridge Rail
Test No. NCBR-1-2

System Rebar

DWG. NAME. NCBR-1-2_R9
SCALE: 1:10
UNITS: in.[mm]

SHEET: 22 of 27
DATE: 5/8/2019
DRAWN BY: JRD/MKB/JEK/DJW
REV. BY: JEK/CSS/JCH

Figure 23. System Rebar, Test Nos. NCBR-1 and NCBR-2

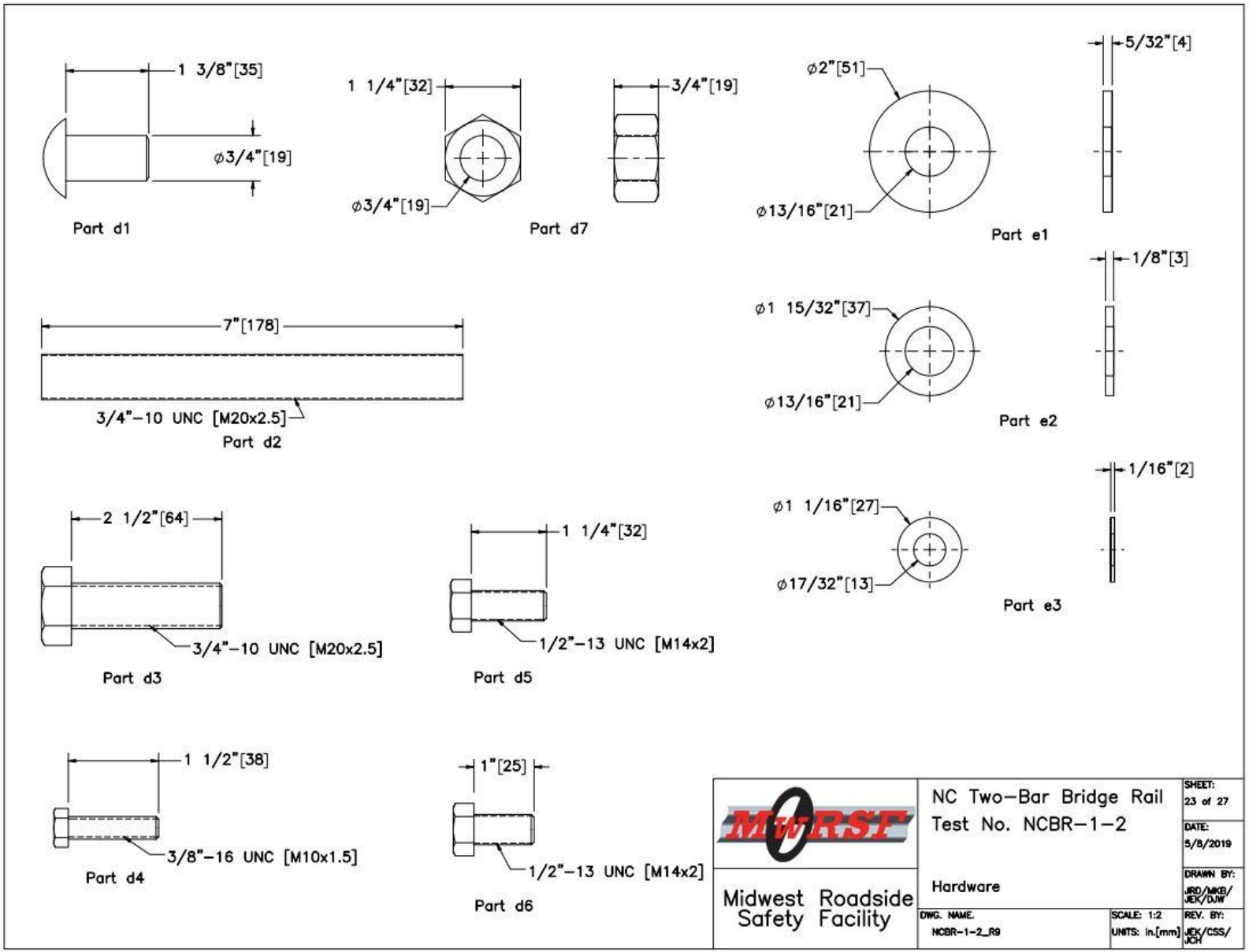


Figure 24. Hardware, Test Nos. NCBR-1 and NCBR-2

Item No.	QTY.	Description	Material Specification	Treatment Specification	Hardware Guide
a1	17	5 3/4"x 4 1/4" [146x108], 23 1/2" [597] Long Post	ASTM B221 Alloy 6061–T6	–	–
a2	17	7 1/2"x3 5/16"x5 3/4" [191x84x146] Post Plate	ASTM B221 Alloy 6061–T6	–	PAB02
a3	17	7 1/2"x3 1/4"x7/8" [181x83x22] Post Plate	ASTM B221 Alloy 6061–T6	–	PAB02
a4	76	5 3/4"x1 11/16"x3/4" [146x43x19] Clamp Bar	ASTM B221 Alloy 6061–T6	–	FPC01–02
a5	64	3/4" [19] Threaded Ferrule	ASTM A108 Gr. 12L14	ASTM A123	–
a6	–	7 3/8"x2 1/4" [187x57] Front Shim	ASTM B209 Alloy 6061–T6	–	–
a7	–	7 3/8"x2 1/4" [187x57] Rear Shim	ASTM B209 Alloy 6061–T6	–	–
b1	2	360" [9,144] Long Elliptical Rail	ASTM B221 Alloy 6061–T6	–	RAM06
b2	4	312 1/2" [7,938] Long Elliptical Rail	ASTM B221 Alloy 6061–T6	–	RAM06
b3	4	11"x4"x1/2" [279x102x13] Plate	ASTM A36	See Assembly	–
b4	4	4"x4"x1/2" [102x102x13] Plate	ASTM A36	See Assembly	–
b5	4	4 1/4"x4"x1 1/4" [108x102x32] Rail Cap	ASTM B221 Alloy 6061–T6	–	–
b6	4	36"x3 9/16"x3 5/8" [914x90x92] Expansion Bar	ASTM B221 Alloy 6061–T6	–	RAS06
c1	1	Concrete	–	–	–
c2	1	Concrete	–	–	–
c3	1	Concrete	–	–	–
c4	32	3/8" [10] Dia. Wire Strut, 6 3/4" [171] Long	Min. Tensile Strength = 100,000 psi [690 MPa]*	AASHTO M111	–
c5	64	3/8" [10] Dia. Wire Strut, 15 15/16" [405] Long Unbent	Min. Tensile Strength = 100,000 psi [690 MPa]*	AASHTO M111	–
c6	82	#5 [16] Bar, 59 1/2" [1,511] Long Unbent	ASTM A615 Gr. 60	Epoxy–Coated (ASTM A775 or A934)	–
c7	8	#5 [16] Bar, 355" [9,017] Long	ASTM A615 Gr. 60	Epoxy–Coated (ASTM A775 or A934)	–
c8	16	#5 [16] Bar, 356" [9,042] Long	ASTM A615 Gr. 60	Epoxy–Coated (ASTM A775 or A934)	–
c9	16	#5 [16] Bar, 36" [914] Long	ASTM A615 Gr. 60	Epoxy–Coated (ASTM A775 or A934)	–

Notes: (1) Alloy 6351–T5 may be substituted for alloy 6061–T6 where applicable.

*A 7/16" [11] wire strut with a minimum tensile strength of 90,000 psi [621 MPa] is acceptable.

Midwest Roadside Safety Facility

NC Two–Bar Bridge Rail
Test No. NCBR–1–2

Bill of Materials

SHEET: 24 of 27
DATE: 5/8/2019
DRAWN BY: JRD/MKB/JEK/DJW
REV. BY: JEK/CSS/JCH
DWG. NAME. NCBR–1–2_R9
SCALE: NONE
UNITS: in.[mm]

Figure 25. Bill of Materials, Test Nos. NCBR-1 and NCBR-2

Item No.	QTY.	Description	Material Specification	Treatment Specification	Hardware Guide
c10	90	#5 [16] Bar, 49 1/2" [1,257] Long Unbent	ASTM A615 Gr. 60	Epoxy-Coated (ASTM A775 or A934)	–
c11	4	#6 [19] Bar, 22" [559] Long	ASTM A615 Gr. 60	Epoxy-Coated (ASTM A775 or A934)	–
c12	4	#6 [19] Bar, 40" [1,016] Long	ASTM A615 Gr. 60	Epoxy-Coated (ASTM A775 or A934)	–
c13	4	#6 [19] Bar, 43 1/4" [1,099] Long	ASTM A615 Gr. 60	Epoxy-Coated (ASTM A775 or A934)	–
c14	4	#7 [22] Bar, 31" [787] Long	ASTM A615 Gr. 60	Epoxy-Coated (ASTM A775 or A934)	–
c15	4	#7 [22] Bar, 36 1/2" [927] Long	ASTM A615 Gr. 60	Epoxy-Coated (ASTM A775 or A934)	–
c16	4	#7 [22] Bar, 42" [1,067] Long	ASTM A615 Gr. 60	Epoxy-Coated (ASTM A775 or A934)	–
c17	4	#7 [22] Bar, 47 1/2" [1,207] Long	ASTM A615 Gr. 60	Epoxy-Coated (ASTM A775 or A934)	–
c18	4	#7 [22] Bar, 52" [1,321] Long	ASTM A615 Gr. 60	Epoxy-Coated (ASTM A775 or A934)	–
d1	68	3/4" [19] Dia., 1 3/8" Long Rivet	ASTM B316 Alloy 6061-T6	–	–
d2	4	3/4"-10 UNC [M20x2.5], 7" [178] Long Fully Threaded Rod	Alloy 304 Stainless Steel	–	FRR20b
d3	68	3/4"-10 UNC [M20x2.5], 2 1/2" [64] Long Hex Bolt	ASTM F3125 Gr. A325 Type I	ASTM A153 or B695 Class 55 or F1941 or F2329 or F1136 Gr. 3 or F2833 Gr. 1	FBX20b
d4	17	3/8"-16 UNC [M10x1.5], 1 1/2" [38] Long Cap Screw	ASTM F593 Alloy 305 Stainless Steel	–	–
d5	16	1/2"-13 UNC [M14x2], 1 1/4" [32] Long Hex Head Cap Screw	ASTM F593 Alloy 305 Stainless Steel	–	FBS14
d6	136	1/2"-13 UNC [M14x2], 1" [25] Long Hex Head Cap Screw	ASTM F593 Alloy 305 Stainless Steel	–	FBS14
d7	4	3/4"-10 UNC [M20x2.5] Heavy Hex Nut	Alloy 304 Stainless Steel	–	FNX20b
e1	4	3/4" [19] Dia. Plain USS Washer	Alloy 304 Stainless Steel	–	–
e2	68	3/4" [19] Dia. Plain SAE Washer	ASTM F436*	ASTM A153 or B695 Class 55 or F1136 Gr. 3 or F2329	FWC20b
e3	152	1/2" [13] Dia. Plain SAE Washer	ASTM F844 Alloy 304 Stainless Steel	–	–
–**	–	Hilti RE 500 V3 or ATC Ultrabond 1 Epoxy	ASTM C881 Type I, II, IV & V Gr. 3, Class A, B & C	–	–

*At the contractor's option, stainless steel bolt and washer may be used as an alternative.
**Epoxy for part d2 must have a minimum bond strength of 1,100 psi [7.6 MPa]. Bond strength of 1,300 psi [9.0 Mpa] or greater is preferred.

MwRSF

Midwest Roadside Safety Facility

NC Two-Bar Bridge Rail
Test No. NCBR-1-2

Bill of Materials

SHEET: 25 of 27
DATE: 5/8/2019
DRAWN BY: JRD/MKB/JEK/DJW
REV. BY: JEK/CSS/JCH
DWG. NAME. NCBR-1-2_R9
SCALE: NONE
UNITS: in.[mm]

Figure 26. Bill of Materials, Test Nos. NCBR-1 and NCBR-2

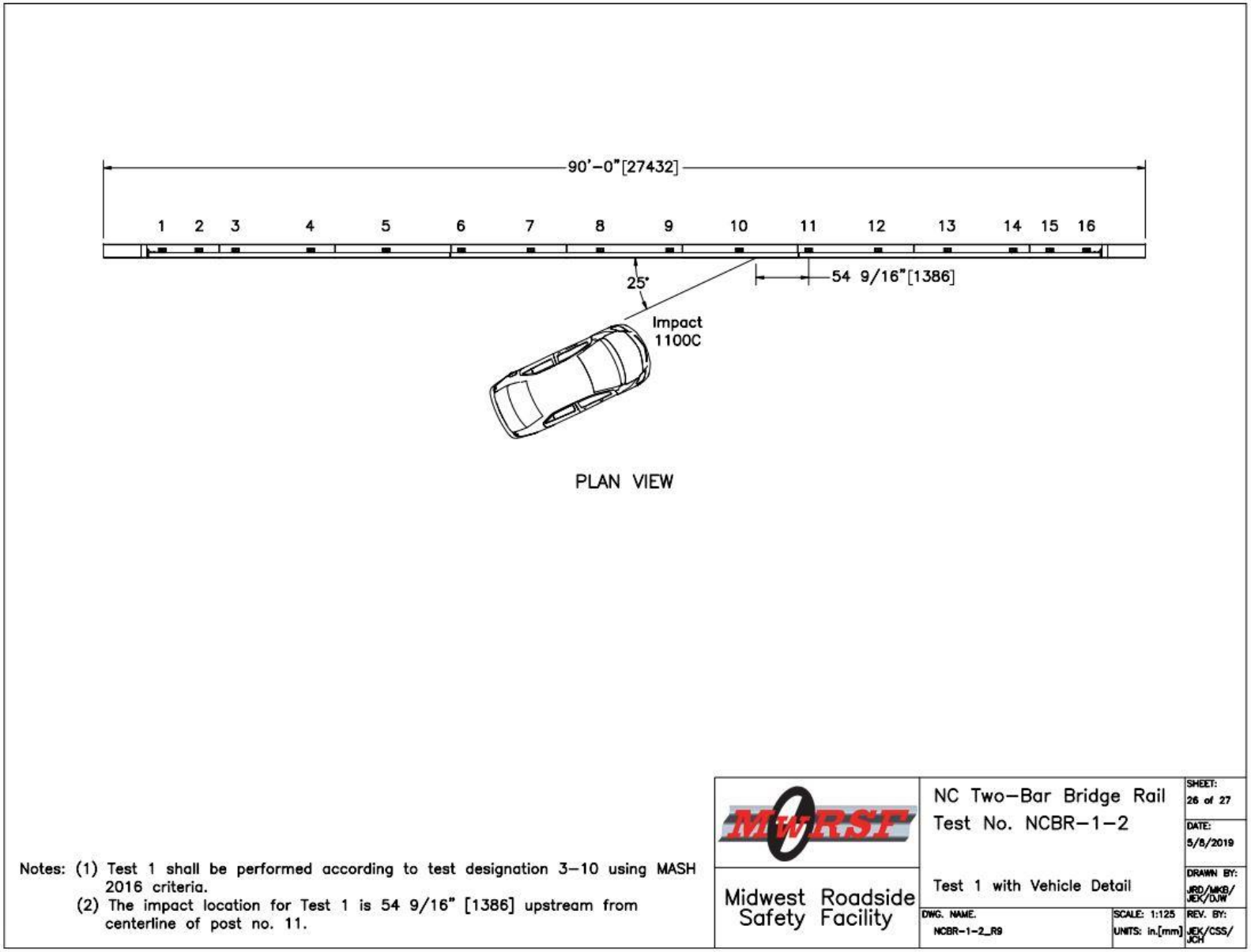


Figure 27. Test No. NCBR-1 with Vehicle Detail

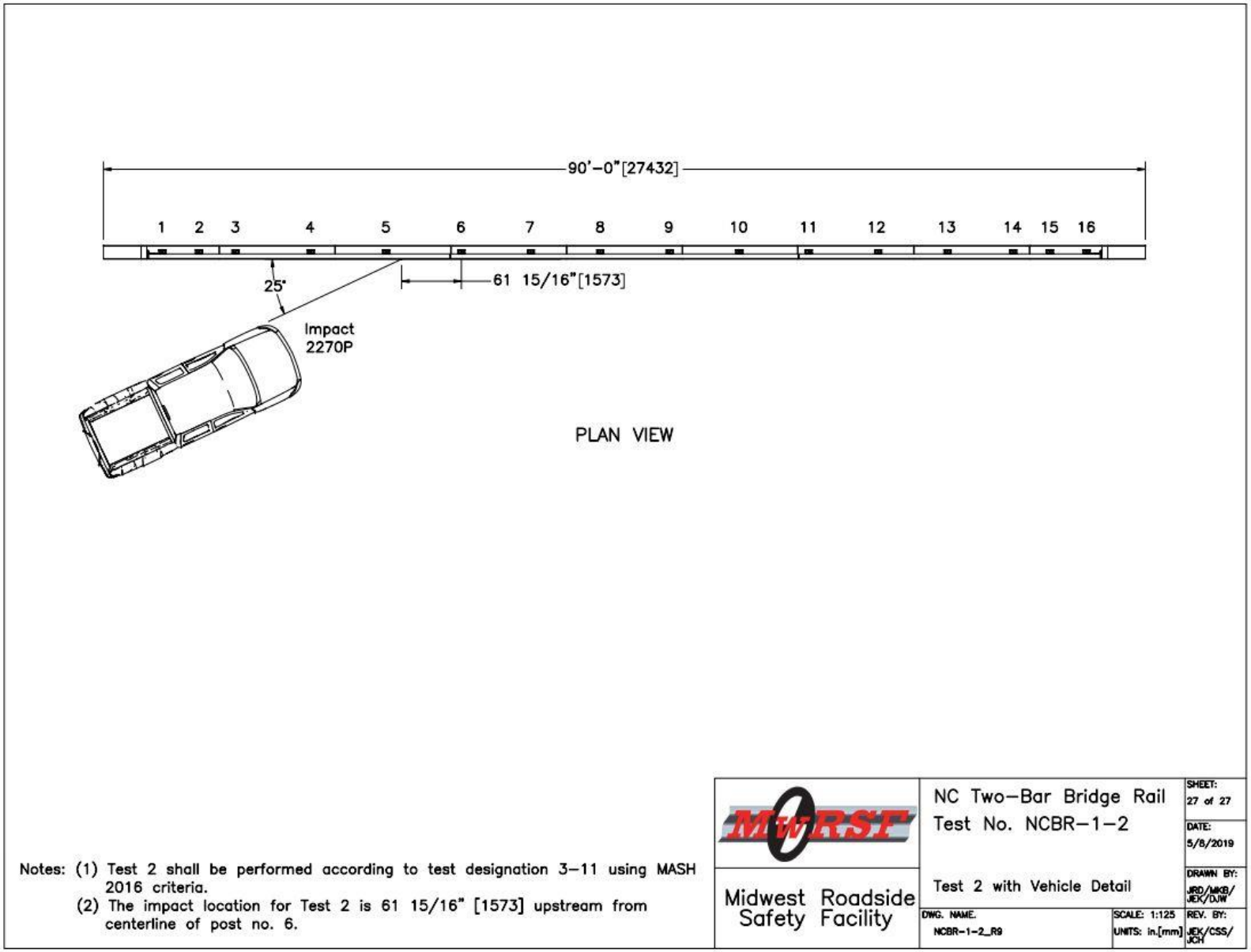


Figure 28. Test No. NCBR-2 with Vehicle Detail





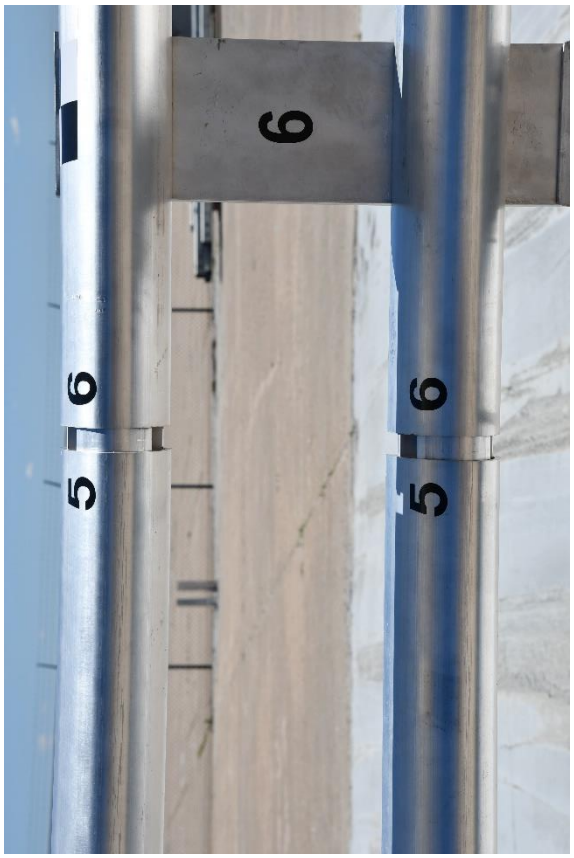




Figure 29. Construction Photographs, Test Nos. NCBR-1 and NCBR-2



Figure 30. System Installation Photographs, Test Nos. NCBR-1 and NCBR-2





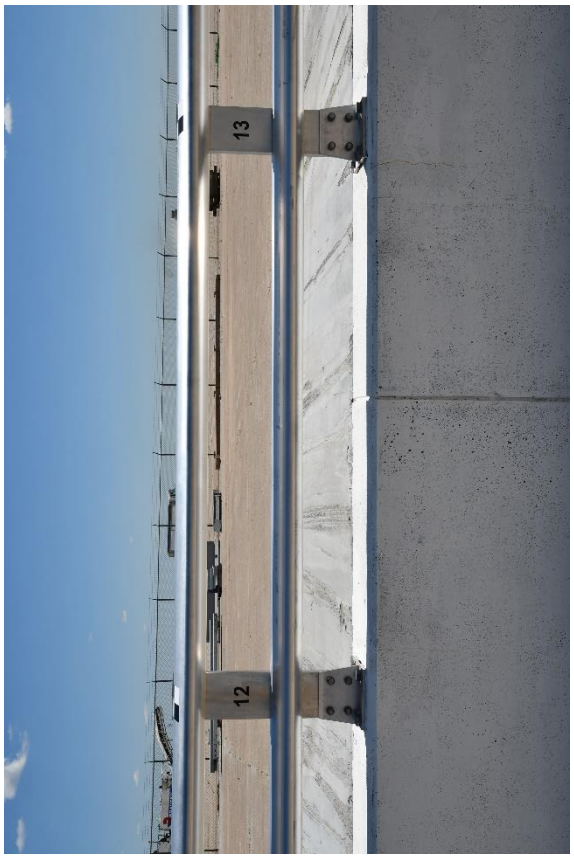




Figure 31. Post and Rail Assembly, Test Nos. NCBR-1 and NCBR-2









Figure 32. Post-to-Parapet and Post-to-Rail Attachment Details, Test Nos. NCBR-1 and NCBR-2









Figure 33. Rail End Anchorage Details, Test Nos. NCBR-1 and NCBR-2

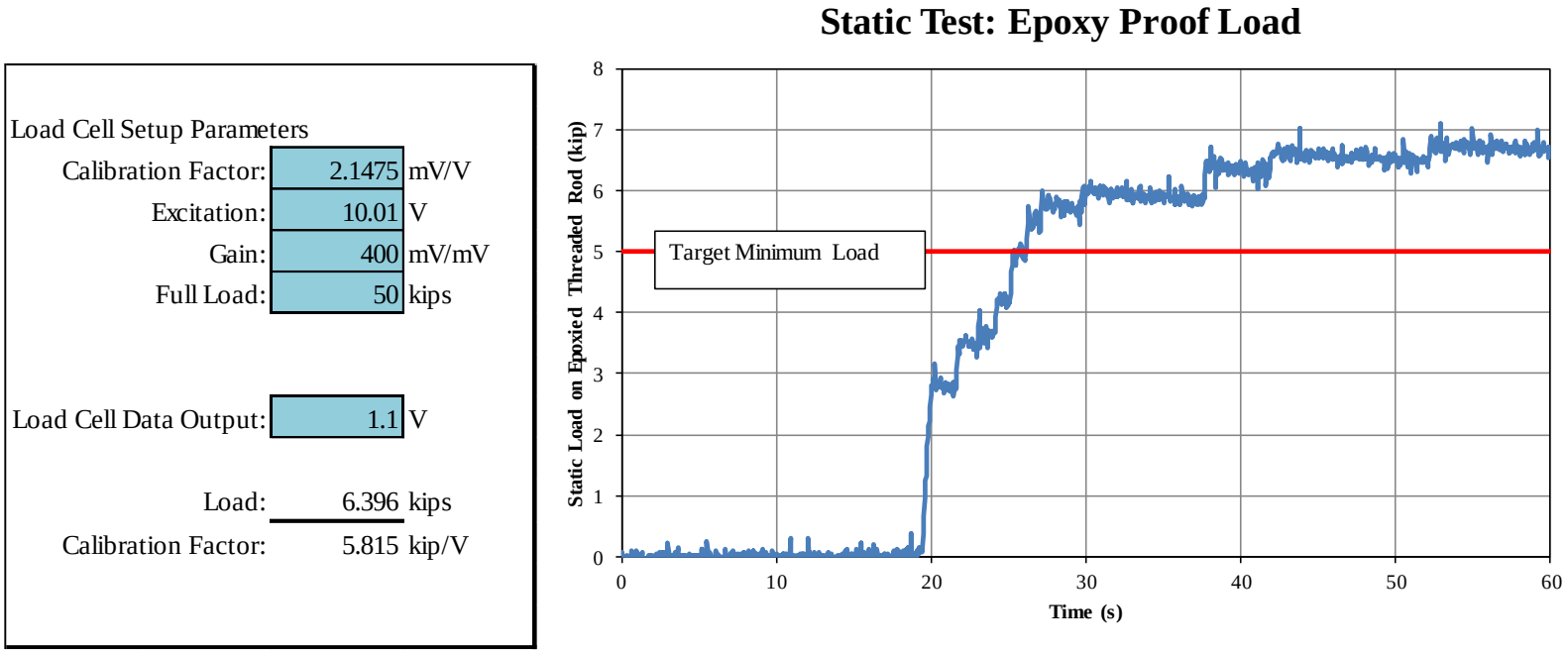


Figure 34. Load-Time Plot for Threaded Rod Proof Testing, Test Nos. NCBR-1 and NCBR-2

4 TEST CONDITIONS

4.1 Test Facility

Both full-scale crash test nos. NCBR-1 and NCBR-2 were conducted at the MwRSF Outdoor Test Site. The MwRSF Outdoor Test Site is located at the Lincoln Air Park on the northwest side of the Lincoln Municipal Airport and is approximately five miles northwest of the University of Nebraska–Lincoln.

4.2 Vehicle Tow and Guidance System

A reverse-cable tow system with a 1:2 mechanical advantage was used to propel the test vehicle. The distance traveled and the speed of the tow vehicle were one-half that of the test vehicle. The test vehicle was released from the tow cable before impact with the barrier system. A digital speedometer on the tow vehicle increased the accuracy of the test vehicle impact speed.

A vehicle guidance system developed by Hinch [5] was used to steer the test vehicle. A guide flag, attached to the right-front wheel and the guide cable, was sheared off before impact with the barrier system. The ⅜-in. diameter guide cable was tensioned to approximately 3,500 lb and supported both laterally and vertically every 100 ft by hinged stanchions. The hinged stanchions stood upright while holding up the guide cable, but as the vehicle was towed down the line, the guide flag struck and knocked each stanchion to the ground.

4.3 Test Vehicles

For test no. NCBR-1, a 2010 Hyundai Accent was used as the test vehicle. The curb, test inertial, and gross static vehicle weights were 2,505 lb, 2,425 lb, and 2,585 lb, respectively. The test vehicle is shown in Figures 35 and 36, and vehicle dimensions are shown in Figure 37. MASH 2016 requires that test vehicles used in crash testing be no more than six model years old. However, a 2010 model was used for test no. NCBR-1 per a joint agreement with NCDOT to select a small car with geometry that complied with recommended vehicle dimension ranges specified in Table 4.1 of MASH 2016. Note that the computer simulation vehicle used to predict the vehicle engagement with the system during test no. NCBR-1 was a Toyota Yaris produced by the National Crash Analysis Center (NCAC) [6], but no Toyota Yaris test vehicles were found which could be purchased and shipped to the MwRSF Outdoor Test Site within the specified contract time and budget limits.

For test no. NCBR-2, a 2015 Chevrolet Silverado quad cab pickup truck was used as the test vehicle. The curb, test inertial, and gross static vehicle weights were 5,015 lb, 5,018 lb, and 5,183 lb, respectively. The test vehicle is shown in Figures 38 and 39 and vehicle dimensions are shown in Figure 40. The 2015 Chevrolet Silverado was selected for testing because it was believed to have similar properties to the simulation vehicle model, a 2007 Silverado C1500 quad cab initially developed at NCAC [6] and modified at UNCC.

The longitudinal components of the center of gravity (c.g.) were determined using the measured axle weights. The vertical component of the c.g. for the 1100C vehicle was determined using a procedure published by SAE [7]. The location of the final c.g. is shown in Figure 41. The Suspension Method [8] was used to determine the vertical component of the c.g. for the 2270P

vehicle. This method is based on the principle that the c.g. of any freely suspended body is in the vertical plane through the point of suspension. The pickup truck was suspended successively in three positions, and the respective planes containing the c.g. were established. The intersection of these planes pinpointed the final c.g. location for the test inertial condition. The location of the final c.g. is shown in Figure 42. Data used to calculate the locations of the c.g. and ballast information are shown in Appendix C.

Square, black- and white-checkered targets were placed on the vehicles for reference to be viewed from the high-speed digital video cameras and aid in video analysis, as shown in Figures 41 and 42. Round, checkered targets were placed at the c.g. on the left-side door, the right-side door, and the roof of the vehicles.

The front wheels of the test vehicles were aligned to vehicle standards, and wheel toe-in values was adjusted to zero such that the vehicles would track properly along the guide cable. A 5B flash bulb was mounted under the vehicles' left-side windshield wiper and fired by a pressure tape switch mounted at the impact corner of the bumper. The flash bulb was fired upon initial impact with the test article to create a visual indicator of the precise time of impact on the high-speed digital videos. A remote-controlled brake system was installed in the test vehicles so the vehicle could be brought to a safe stop after impacting the system.



Figure 35. Test Vehicle, Test No. NCBR-1







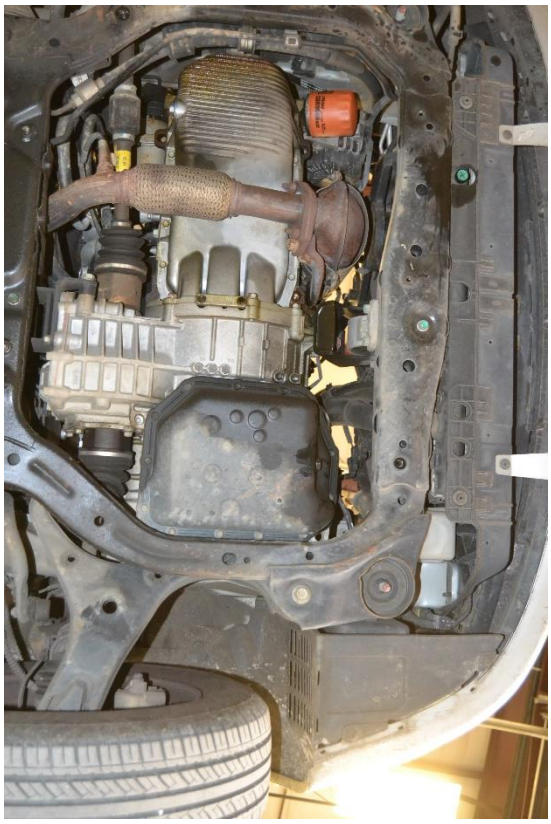
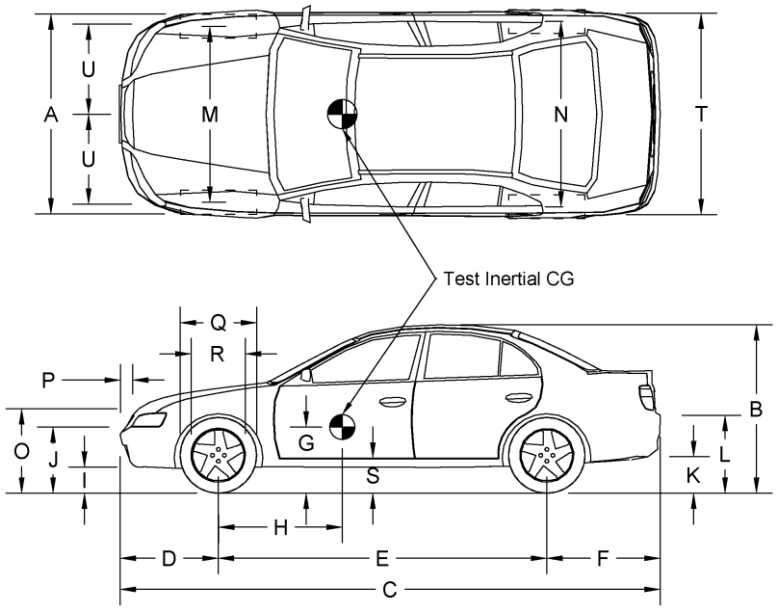


Figure 36. Test Vehicle's Interior Floorboards and Undercarriage, Test No. NCBR-1

Date:	5/13/2019	**Test Name:**	NCBR-1	**VIN No:**	kmhcn4ac1au467917
Year:	2010	**Make:**	Hyundai	**Model:**	Accent
Tire Size:	185/65 r14	**Tire Inflation Pressure:**	32 psi	**Odometer:**	195823



Vehicle Geometry - in. (mm)
Target Ranges listed below

A:	66 7/8 (1699) 65±3 (1650±75)	**B:**	57 5/8 (1464)
C:	168 4/9 (4278) 169±8 (4300±200)	**D:**	32 3/8 (822) 35±4 (900±100)
E:	99 (2515) 98±5 (2500±125)	**F:**	37 (940)
G:	22 5/8 (575)	**H:**	35 1/2 (902) 39±4 (990±100)
I:	8 (203)	**J:**	21 1/2 (546)
K:	12 3/4 (324)	**L:**	23 1/4 (591)
M:	57 7/8 (1470) 56±2 (1425±50)	**N:**	57 1/4 (1454) 56±2 (1425±50)
O:	27 1/2 (699) 24±4 (600±100)	**P:**	3 1/2 (89)
Q:	15 3/8 (391)	**R:**	23 (584)
S:	6 (152)	**T:**	64 7/8 (1648)
		U (impact width):	29 1/4 (743)

Mass Distribution - lb (kg)

Gross Static	**LF**	845 (383)	**RF**	793 (360)
	LR	478 (217)	**RR**	469 (213)

Weights lb (kg)	**Curb**	**Test Inertial**	**Gross Static**
W-front	1596 (724)	1555 (705)	1638 (743)
W-rear	909 (412)	870 (395)	947 (430)
W-total	2505 (1136)	2425 (1100) 2420±55 (1100±25)	2585 (1173) 2585±55 (1175±50)

Top of radiator core support:	29 1/2 (749)
Wheel Center Height (Front):	10 2/3 (271)
Wheel Center Height (Rear):	11 (279)
Wheel Well Clearance (Front):	25 3/4 (654)
Wheel Well Clearance (Rear):	25 5/8 (651)
Bottom Frame Height (Front):	8 (203)
Bottom Frame Height (Rear):	16 (406)
Engine Type:	Gasoline
Engine Size:	1.4L 4 Cyl
Transmission Type:	Automatic
Drive Type:	FWD

GVWR Ratings lb

Front	1918
Rear	1874
Total	3638

Surrogate Occupant Data

Type:	Hybrid II
Mass:	160 lb
Seat Position:	Left/Driver

Note any damage prior to test:

Figure 37. Vehicle Dimensions, Test No. NCBR-1







Figure 38. Test Vehicle, Test No. NCBR-2

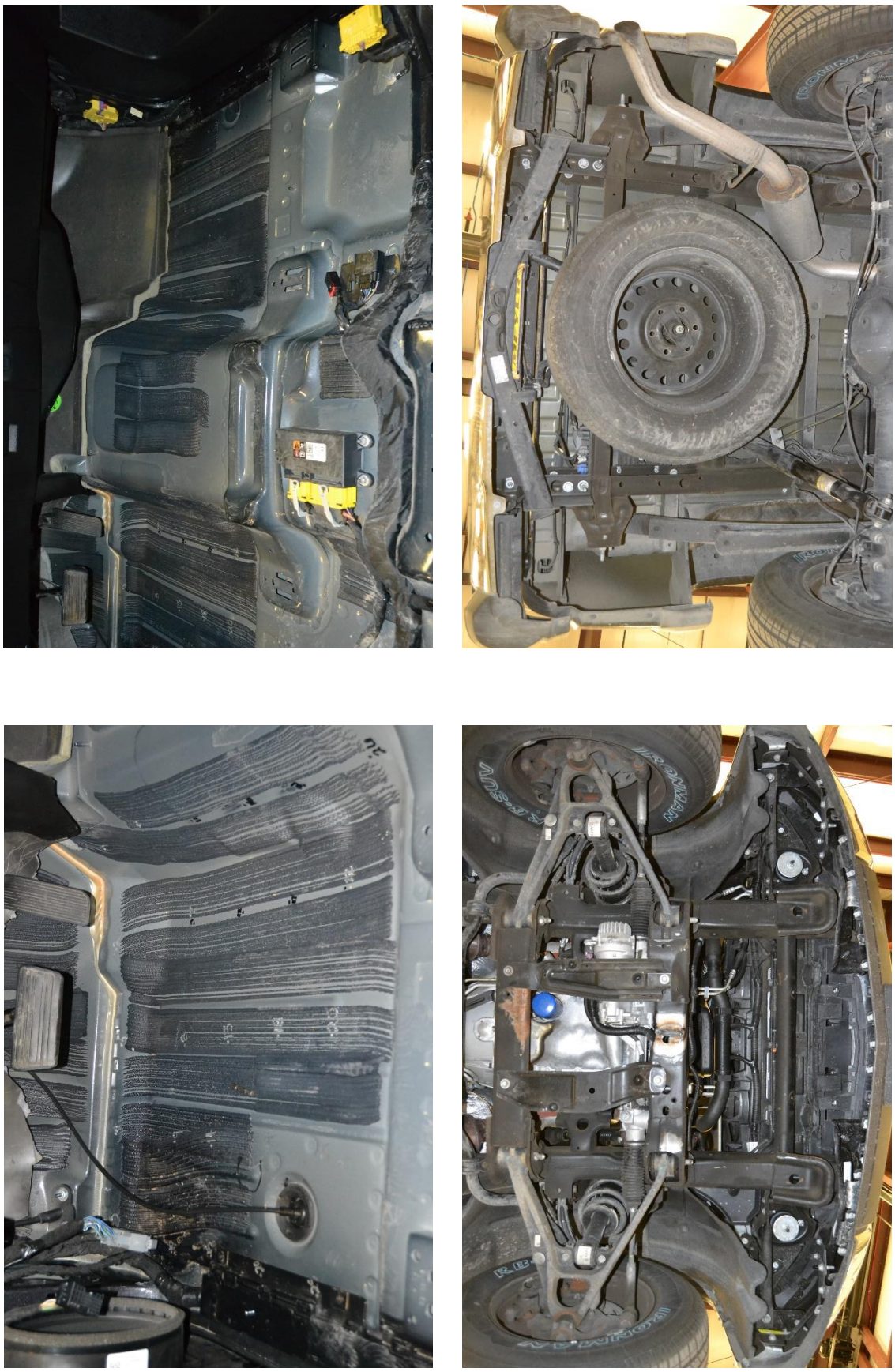
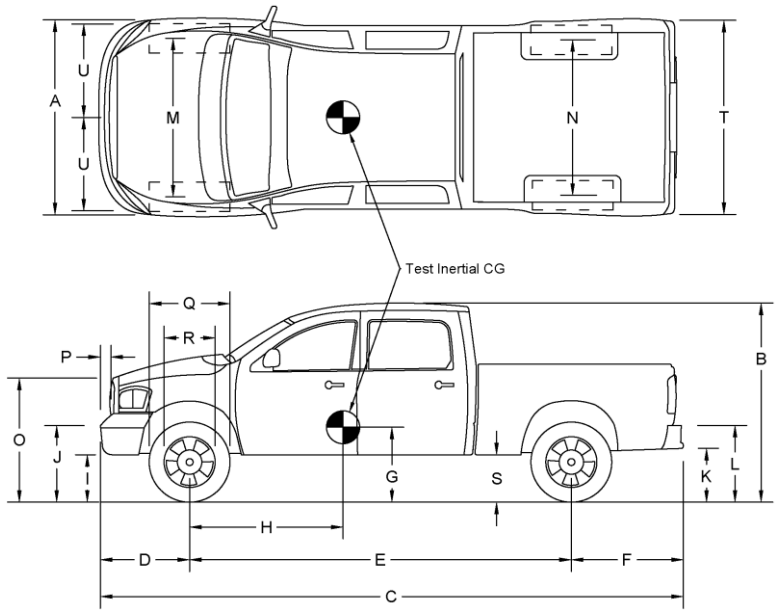


Figure 39. Test Vehicle's Interior Floorboards and Undercarriage, Test No. NCBR-2

Date:	6/11//2019	**Test Name:**	NCBR-2	**VIN No:**	1GCRCPEH6FZ173614
Year:	2015	**Make:**	Chevrolet	**Model:**	Silverado
Tire Size:	255/70R17	**Tire Inflation Pressure:**	35 psi	**Odometer:**	83730



Vehicle Geometry - in. (mm)
Target Ranges listed below

A:	79 3/4 (2026) 78±2 (1950±50)	**B:**	73 (1854)
C:	229 (5817) 237±13 (6020±325)	**D:**	38 (965) 39±3 (1000±75)
E:	144 (3658) 148±12 (3760±300)	**F:**	47 (1194)
G:	28 5/16 (719) min: 28 (710)	**H:**	61 3/8 (1559) 63±4 (1575±100)
I:	18 3/4 (476)	**J:**	25 (635)
K:	20 1/4 (514)	**L:**	28 1/2 (724)
M:	68 (1727) 67±1.5 (1700±38)	**N:**	67 1/2 (1715) 67±1.5 (1700±38)
O:	44 3/8 (1127) 43±4 (1100±75)	**P:**	1 3/4 (44)
Q:	30 1/2 (775)	**R:**	18 5/8 (473)
S:	16 (406)	**T:**	77 1/2 (1969)

U (impact width): 38 1/8 (968)

Mass Distribution - lb (kg)

Gross Static	**LF**	1519 (689)	**RF**	1464 (664)
	LR	1095 (497)	**RR**	1105 (501)

Weights lb (kg)	**Curb**	**Test Inertial**	**Gross Static**
W-front	2931 (1329)	2879 (1306)	2983 (1353)
W-rear	2084 (945)	2139 (970)	2200 (998)
W-total	5015 (2275)	5018 (2276) 5000±110 (2270±50)	5183 (2351) 5165±110 (2343±50)

Wheel Center Height (Front):	14 1/2 (368)
Wheel Center Height (Rear):	14 5/8 (371)
Wheel Well Clearance (Front):	35 3/4 (908)
Wheel Well Clearance (Rear):	38 (965)
Bottom Frame Height (Front):	9 1/2 (241)
Bottom Frame Height (Rear):	12 (305)
Engine Type:	Gasoline
Engine Size:	4.3L
Transmission Type:	Auto
Drive Type:	RWD
Cab Style:	Quad Cab
Bed Length:	67"

GVWR Ratings - lb

Front	3600
Rear	3950
Total	6900

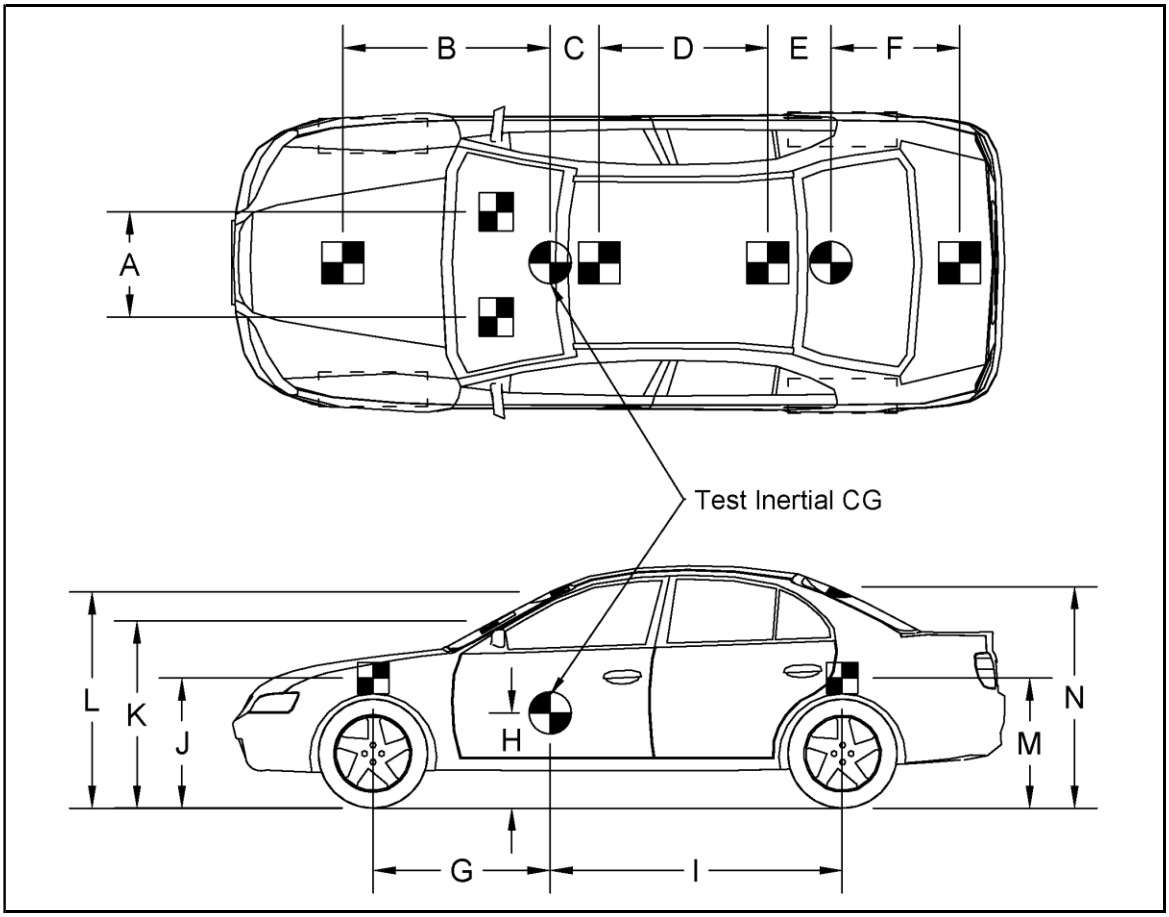
Surrogate Occupant Data

Type:	Hybrid II
Mass:	165 lb
Seat Position:	Left/Driver

Note any damage prior to test: None

Figure 40. Vehicle Dimensions, Test No. NCBR-2

Date: 5/13/2019	**Test Name:** NCBR-1	**VIN:** kmhcn4ac1au467917
Year: 2010	**Make:** Hyundai	**Model:** Accent

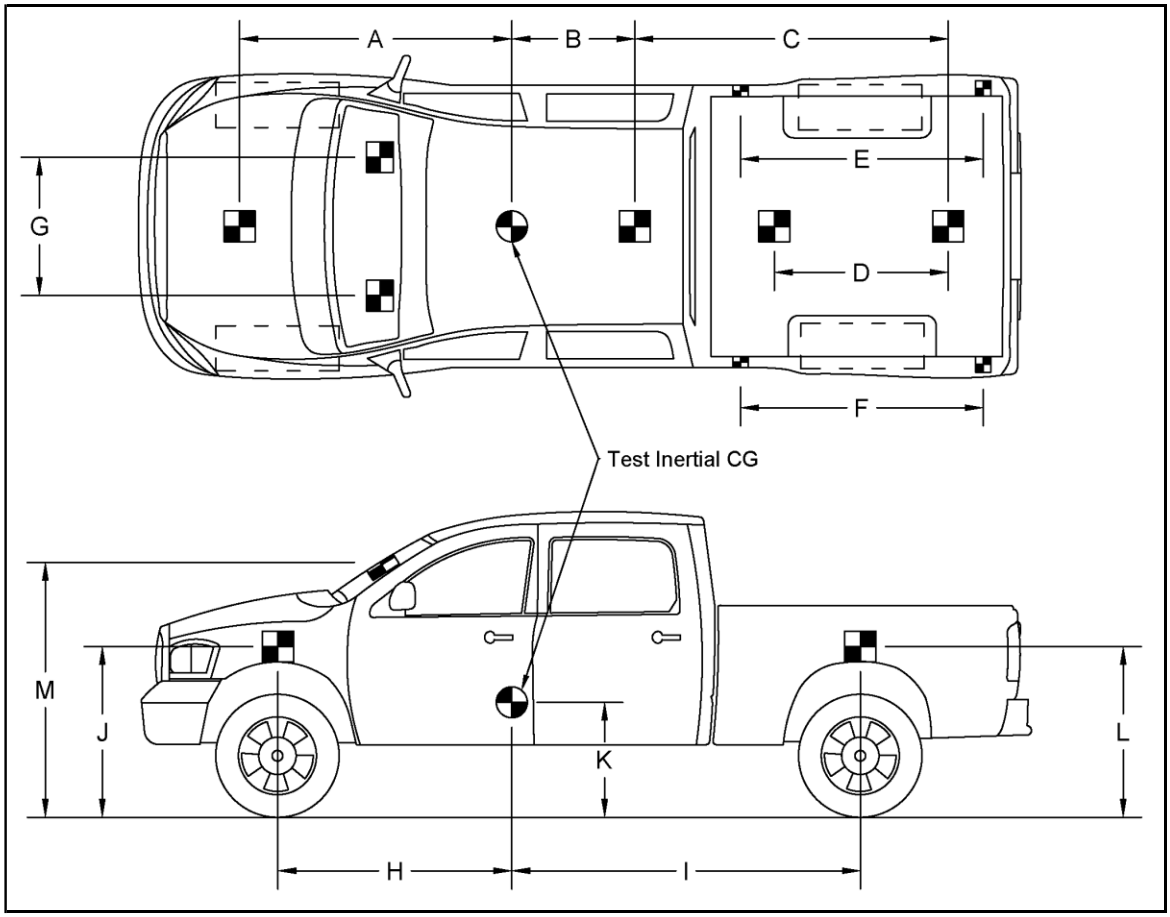


TARGET GEOMETRY-- in. (mm)

A: 24 7/8 (632)	**F:** 21 1/2 (546)	**K:** 48 15/16 (1243) Windshield Target
B: 46 1/4 (1175)	**G:** 35 5/8 (905)	**L:** 52 1/4 (1327) Front round CG target
C: 14 15/16 (379)	**H:** 22 9/16 (573)	**M:** 29 (737)
D: 34 1/4 (870)	**I:** 63 7/16 (1611)	**N:** 52 3/16 (1326) Rear Round target
E: 15 1/8 (384)	**J:** 28 3/4 (730)	

Figure 41. Target Geometry, Test No. NCBR-1

Date: 6/11//2019 **Test Name:** NCBR-2 **VIN:** 1GCRCPEH6FZ173614
Year: 2015 **Make:** Chevrolet **Model:** Silverado



TARGET GEOMETRY-- in. (mm)

A:	73 1/2	(1867)	**E:**	67 3/8	(1711)	**J:**	39 3/4	(1010)
B:	25 3/8	(645)	**F:**	67 3/8	(1711)	**K:**	28	(711)
C:	83 1/2	(2121)	**G:**	31 3/8	(797)	**L:**	42	(1067)
D:	46	(1168)	**H:**	61 3/8	(1559)	**M:**	60 1/2	(1537)
			I:	83 1/4	(2115)			

Figure 42. Target Geometry, Test No. NCBR-2

4.4 Simulated Occupant

For test nos. NCBR-1 and NCBR-2, a Hybrid II 50th-Percentile, Adult Male Dummy, equipped with clothing and footwear, was placed in the left-front seat of the test vehicle with the seat belt fastened. The dummy had a final weight of 160 lb for test no. NCBR-1 and 165 for test no. NCBR-2. As recommended by MASH 2016, the dummy was not included when calculating c.g. locations.

4.5 Data Acquisition Systems

4.5.1 Accelerometers

Two environmental shock and vibration sensor/recorder systems were used to measure the accelerations in the longitudinal, lateral, and vertical directions. Both accelerometer systems were mounted near the c.g. of the test vehicles. The electronic accelerometer data obtained in dynamic testing was filtered using the SAE Class 60 and the SAE Class 180 Butterworth filter conforming to the SAE J211/1 specifications [9].

The SLICE-1 and SLICE-2 units were modular data acquisition systems manufactured by Diversified Technical Systems, Inc. (DTS) of Seal Beach, California. The SLICE-1 unit was designated as the primary system for both tests. The acceleration sensors were mounted inside the bodies of custom-built, SLICE 6DX event data recorders and recorded data at 10,000 Hz to the onboard microprocessor. Both SLICE 6DX systems were configured with 7 GB of non-volatile flash memory, a range of ±500 g's, a sample rate of 10,000 Hz, and a 1,650 Hz (CFC 1000) anti-aliasing filter. The SLICEWare computer software program and a customized Microsoft Excel worksheet were used to analyze and plot the accelerometer data.

4.5.2 Rate Transducers

Two identical angular rate sensor systems mounted inside the bodies of the SLICE-1 and SLICE-2 event data recorders were used to measure the rates of rotation of the test vehicles. Each SLICE MICRO Triax ARS had a range of 1,500 deg./sec in each of the three directions (roll, pitch, and yaw) and recorded data at 10,000 Hz to the onboard microprocessors. The raw data measurements were then downloaded, converted to the proper Euler angles for analysis, and plotted. The SLICEWare computer software program and a customized Microsoft Excel worksheet were used to analyze and plot the angular rate sensor data.

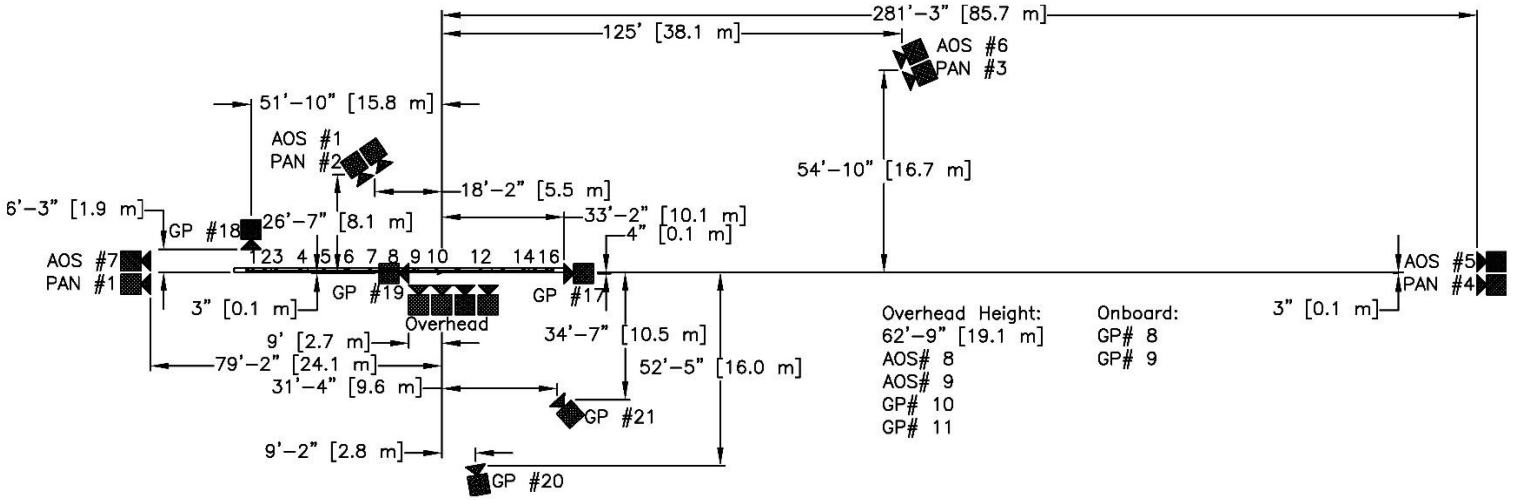
4.5.3 Retroreflective Optic Speed Trap

The retroreflective optic speed trap was used to determine the speed of the test vehicles before impact. Five retroreflective targets, spaced at approximately 18-in. intervals, were applied to the side of the vehicles. When the emitted beam of light was reflected by the targets and returned to the emitter/receiver, a signal was sent to the data acquisition computer, recording at 10,000 Hz, as well as the external LED box activating the LED flashes. The speed was then calculated using the spacing between the retroreflective targets and the time between the signals. LED lights and high-speed digital video analysis are only used if vehicle speeds cannot be determined from the electronic data.

4.5.4 Digital Photography

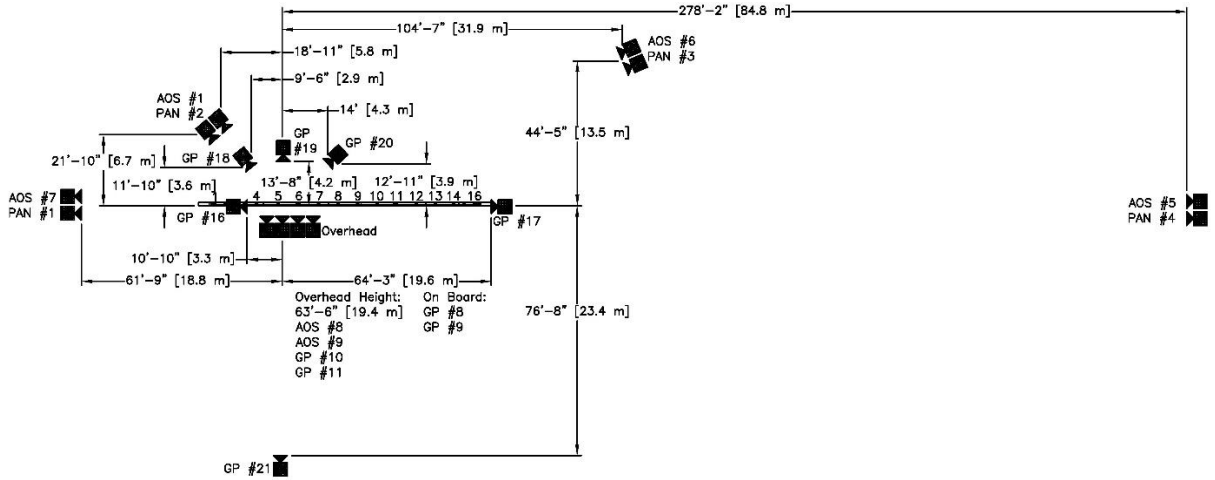
Six AOS high-speed digital video cameras, nine GoPro digital video cameras, and four Panasonic digital video cameras were used to film test no. NCBR-1. Six AOS high-speed digital video cameras, ten GoPro digital video cameras, and four Panasonic digital video cameras were used to film test no. NCBR-2. Camera details and operating speeds, lens information, and a schematic of the camera locations relative to the system are shown in Figures 43 and 44.

The high-speed videos were analyzed using TEMA Motion and Redlake MotionScope software programs. Actual camera speed and camera divergence factors were considered in the analysis of the high-speed videos. A Nikon digital still camera was used to document pre- and post-test conditions for the tests.



No.	Type	Operating Speed (frames/sec)	Lens	Lens Setting
AOS-1	AOS Vitcam	500	Kowa 25 mm	
AOS-5	AOS X-PRI	500	100 mm	
AOS-6	AOS X-PRI	500	Fujinon 35 mm	
AOS-7	AOS X-PRI	500	Fujinon 50 mm	
AOS-8	AOS S-VIT 1531	500	Kowa 16 mm	
AOS-9	AOS TRI-VIT 2236	500	Kowa 12 mm	
GP-8	GoPro Hero 4	120		
GP-9	GoPro Hero 4	120		
GP-10	GoPro Hero 4	120		
GP-11	GoPro Hero 4	240		
GP-17	GoPro Hero 4	240		
GP-18	GoPro Hero 6	240		
GP-19	GoPro Hero 6	240		
GP-20	GoPro Hero 6	240		
GP-21	GoPro Hero 6	240		
PAN-1	Panasonic HC-V770	120		
PAN-2	Panasonic HC-V770	120		
PAN-3	Panasonic HC-V770	120		
PAN-4	Panasonic HC-V770	120		

Figure 43. Camera Locations, Speeds, and Lens Settings, Test No. NCBR-1



No.	Type	Operating Speed (frames/sec)	Lens	Lens Setting
AOS-1	AOS Vitcam	500	Kowa 25 mm	
AOS-5	AOS X-PRI	500	100 mm fixed	
AOS-6	AOS X-PRI	500	Fujinon 35 mm fixed	
AOS-7	AOS X-PRI	500	Fujinon 50 mm fixed	
AOS-8	AOS S-VIT 1531	500	Kowa 16 mm	
AOS-9	AOS TRI-VIT 2236	500	Kowa 12 mm	
GP-8	GoPro Hero 4	120		
GP-9	GoPro Hero 4	120		
GP-10	GoPro Hero 4	120		
GP-11	GoPro Hero 4	240		
GP-16	GoPro Hero 4	240		
GP-17	GoPro Hero 4	240		
GP-18	GoPro Hero 6	240		
GP-19	GoPro Hero 6	240		
GP-20	GoPro Hero 6	240		
GP-21	GoPro Hero 6	240		
PAN-1	Panasonic HC-V770	120		
PAN-2	Panasonic HC-V770	120		
PAN-3	Panasonic HC-V770	120		
PAN-4	Panasonic HC-V770	120		

Figure 44. Camera Locations, Speeds, and Lens Settings, Test No. NCBR-2

5 FULL-SCALE CRASH TEST NO. NCBR-1

5.1 Weather Conditions

Test no. NCBR-1 was conducted on May 13, 2019 at approximately 2:00 p.m. The weather conditions as per the National Oceanic and Atmospheric Administration (station 14939/LNK) were reported and are shown in Table 3.

Table 3. Weather Conditions, Test No. NCBR-1

Temperature	72 deg. F
Humidity	46 percent
Wind Speed	13 mph
Wind Direction	180 deg. from True North
Sky Conditions	Clear
Visibility	10 Statute Miles
Pavement Surface	Dry
Previous 3-Day Precipitation	0.33 in.
Previous 7-Day Precipitation	1.68 in.

5.2 Test Description

Initial vehicle impact was to occur $54^{9}/_{16}$ in. upstream from post no. 11, as shown in Figure 45, which was selected by UNCC from simulation results and verified by NCDOT as the point that maximized the loading on the rail splices. The 2,425-lb small car impacted the NCDOT two-bar metal bridge rail at a speed of 63.2 mph and an angle of 25.2 deg. The actual point of impact was 51.1 in. upstream from post no. 11. The vehicle came to rest 164 ft – 8 in. downstream and 60 ft – 7 in. laterally behind the traffic side of the barrier after the brakes were applied.

A detailed description of the sequential impact events is contained in Table 4. High-speed footage of the test is shown in Figures 46 and 47. Sequential photographs are shown in Figures 48 and 49. Documentary photographs of the crash test are shown in Figures 50 through 52. The vehicle trajectory and final position are shown in Figure 53.



Figure 45. Impact Location, Test No. NCBR-1

Table 4. Sequential Description of Impact Events, Test No. NCBR-1

TIME (sec)	EVENT
0.000	Vehicle's front bumper contacted concrete parapet 51.1 in. upstream from post no. 11.
0.004	Vehicle's left headlight contacted concrete parapet.
0.006	Vehicle's left-front tire and left-front fender contacted concrete parapet.
0.008	Vehicle's left headlight shattered. Vehicle's hood contacted concrete parapet.
0.028	Vehicle's left-side mirror contacted rail.
0.034	Vehicle's left-front door contacted concrete parapet.
0.044	Vehicle's hood contacted post no. 11.
0.046	Vehicle's windshield cracked.
0.074	Vehicle’s left-front window shattered due to contact from simulated occupant's head.
0.078	Simulated occupant head passed through left-front window.
0.088	Vehicle's right-rear tire became airborne.
0.128	Simulated occupant head reentered through left-front window.
0.134	Vehicle's left-rear door contacted concrete parapet.
0.138	Vehicle's right-front tire became airborne.
0.162	Vehicle's left quarter panel contacted concrete parapet. Vehicle became parallel to system at 44.8 mph.
0.170	Vehicle's rear bumper contacted concrete parapet.
0.178	Vehicle's left quarter panel contacted rail.
0.182	Vehicle's left taillight contacted rail.
0.200	Vehicle's left-side mirror became disengaged.
0.330	Vehicle exited system at 42.8 mph and an 8.5 deg. angle.
0.372	Vehicle's right-front tire regained contact with ground.
0.446	Vehicle's right-rear tire regained contact with ground.



Figure 46. Downstream High-Speed Footage, Test No. NCBR-1

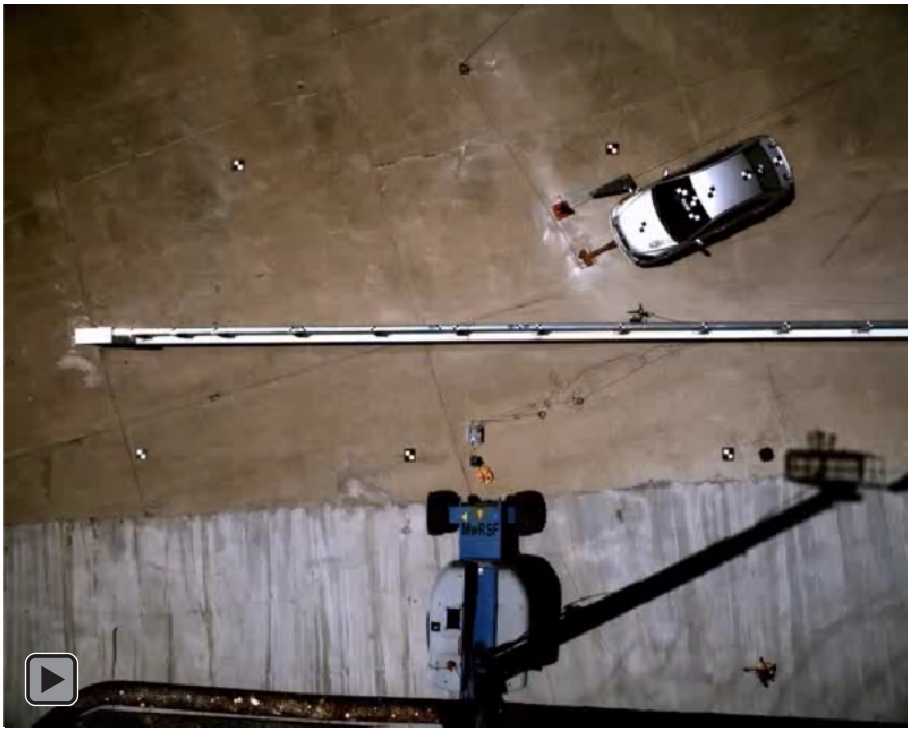
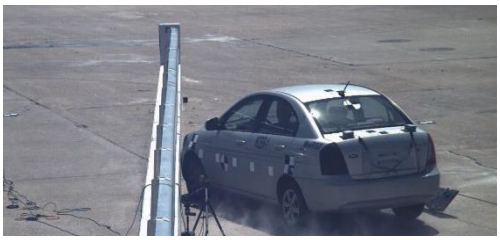
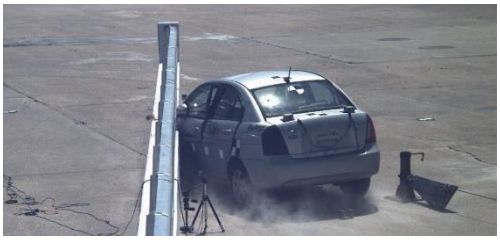


Figure 47. Overhead High-Speed Footage, Test No. NCBR-1


0.000 sec


0.000 sec

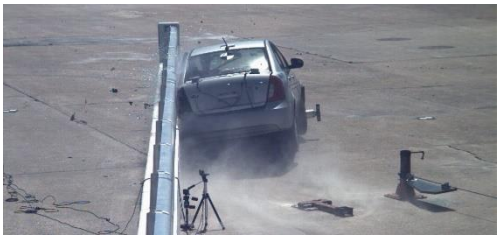

0.050 sec


0.050 sec

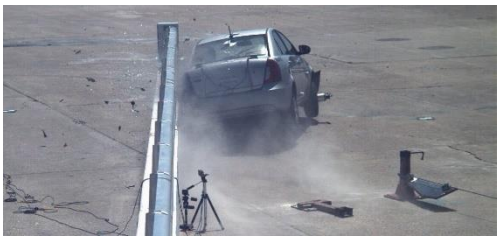

0.100 sec


0.100 sec


0.200 sec


0.200 sec


0.300 sec


0.300 sec


0.450 sec

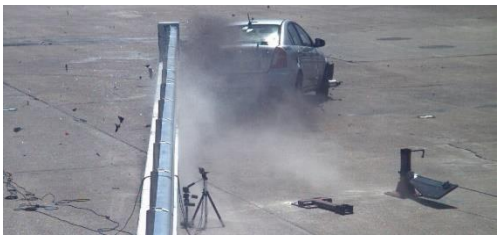
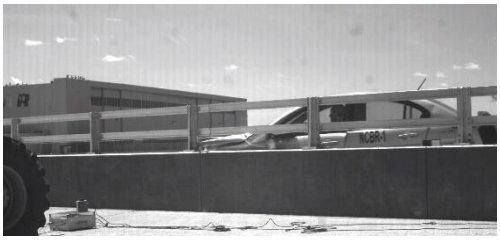

0.450 sec

Figure 48. Sequential Photographs, Test No. NCBR-1


0.000 sec


0.000 sec


0.050 sec


0.050 sec

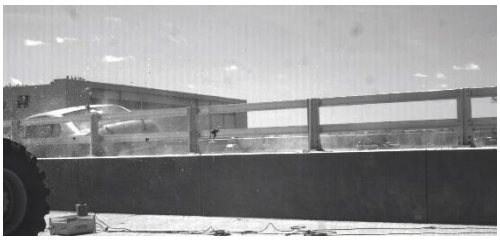

0.100 sec


0.100 sec


0.200 sec


0.200 sec


0.300 sec


0.300 sec


0.450 sec

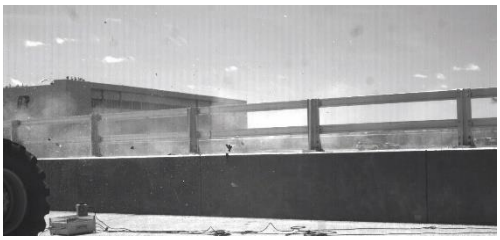

0.450 sec

Figure 49. Sequential Photographs, Test No. NCBR-1



Figure 50. Documentary Photographs, Test No. NCBR-1



Figure 51. Documentary Photographs, Test No. NCBR-1

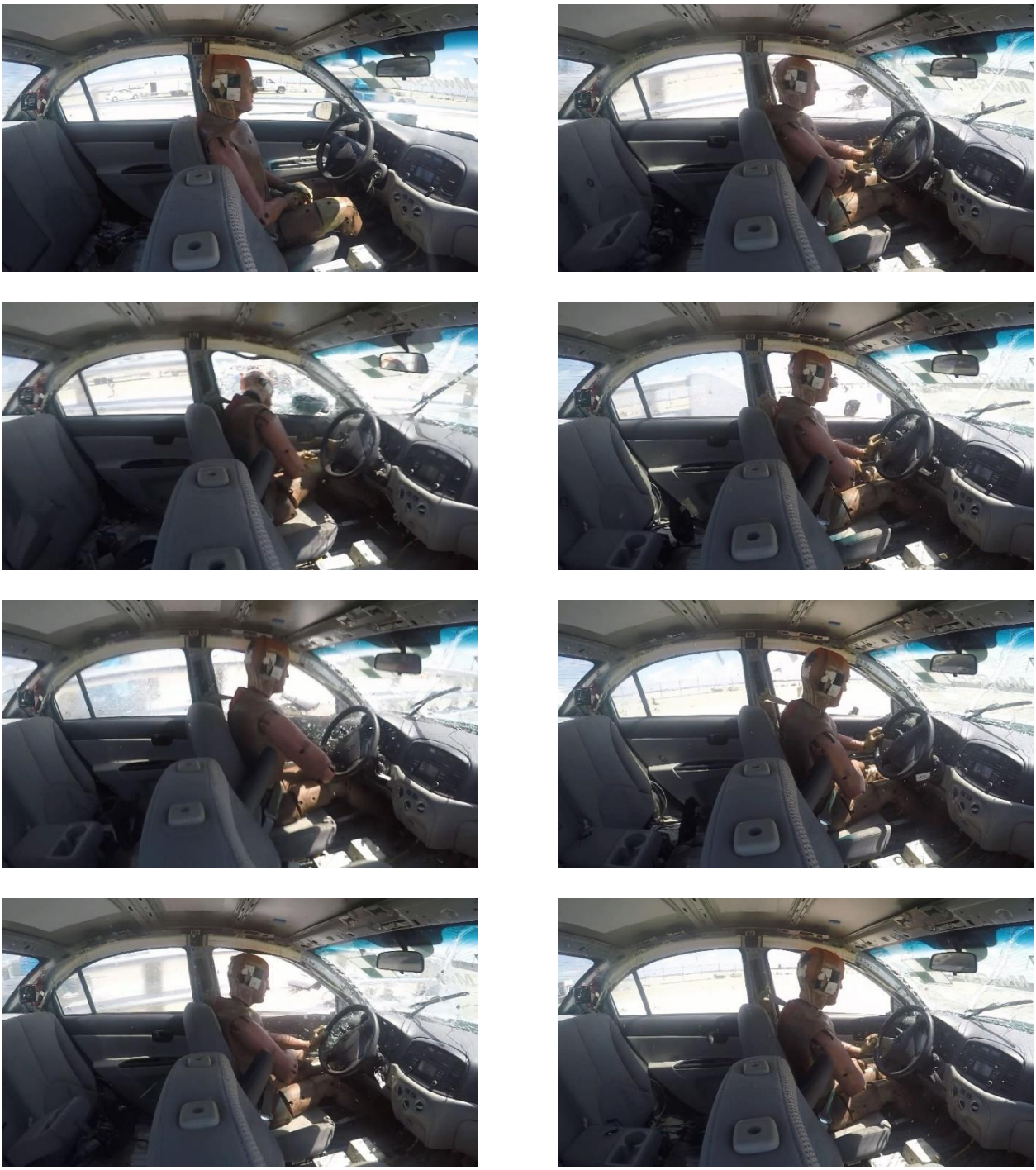


Figure 52. Documentary Photographs, Test No. NCBR-1



Figure 53. Vehicle Final Position and Trajectory Marks, Test No. NCBR-1

5.3 Barrier Damage

Damage to the barrier was minimal, as shown in Figures 54 through 57. Barrier damage consisted of contact marks and concrete gouging across the front face of the parapet. Note that all cracking visible in the system photographs was documented beforehand and not a result of test no. NCBR-1. The length of vehicle contact along the concrete parapet was 134¾ in., which spanned from 53¾ in. upstream from the splice between post nos. 10 and 11 to 71 in. downstream from the splice.

Tire marks were visible on the front face of the parapet. Scuff marks were on the front and top faces of the barrier. A ½-in. wide x 1-in. tall x ½-in. deep piece of concrete was removed from the top corner of the upstream edge of the expansion gap between post nos. 10 and 11.

Two small, parallel gouges beginning 14½ and 16 in. upstream from the expansion gap on parapet segment no. 2 extended to the expansion gap. A 3½-in. long, ¼-in. tall gouge was centered 27½ in. upstream from the expansion gap and 19¼ in. above the tarmac. A 1-in. wide x 1-in. tall x ¼-in. deep rounded gouge was located 16 in. upstream from the expansion gap and 14 in. above the tarmac. Gouging occurred on the top edge of the front face of the parapet, starting 44 in. upstream from the expansion gap, extending downstream for 14 in., and measuring 1¼ in. thick. A gouge occurred in the surface of the parapet 4¼ in. downstream from the expansion gap, measuring ¾ in. in both height and width.

A contact mark on the front face of the lower rail began 67½ in. upstream from and extended to the splice between post nos. 10 and 11. An additional 51½-in. long, 1¼-in. wide contact mark on the front face of the lower rail began 1½ in. upstream from the splice. A 32¼-in. long contact mark was located on the bottom face of the lower rail, beginning 1¾ in. upstream from the splice. Surface scratches, likely from the shattered left-front window, were located across the front face of both rails, beginning 16 in. upstream from the splice and extending to 53 in. downstream.

A 5½-in. long contact mark was observed on the upstream edge of the base plate of post no. 11, and contact was observed on the base plate and bolts extending 6½ in. downstream along the traffic-side face. Minor splice movement was observed between post nos. 10 and 11, such that the traffic-side gap was $^{13}/_{16}$ in. and the back-side gap was ¾ in. for the lower rail. Both front- and back-side gaps were ¾ in. for the upper rail between all posts.

Orange paint splatter was observed on post no. 11 and both rails, beginning 9½ in. upstream from the splice and extending to 16½ in. downstream, as seen in Figure 57. Paint splatter was also found on the front face and upstream edge of post no. 11. Note that the dummy had recently been painted, and the wet paint caused splatter when the dummy's head contacted the side window. The dummy's head did not contact the system. Surface scratches were found across the entire width of the front face of post no. 11 between both rails.



Figure 54. System Damage, Test No. NCBR-1



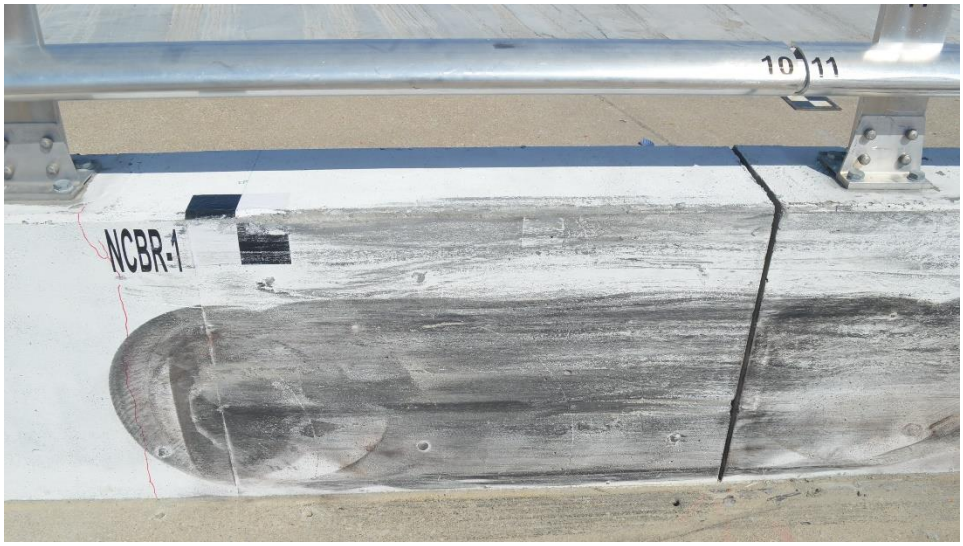




Figure 55. System Damage, Test No. NCBR-1

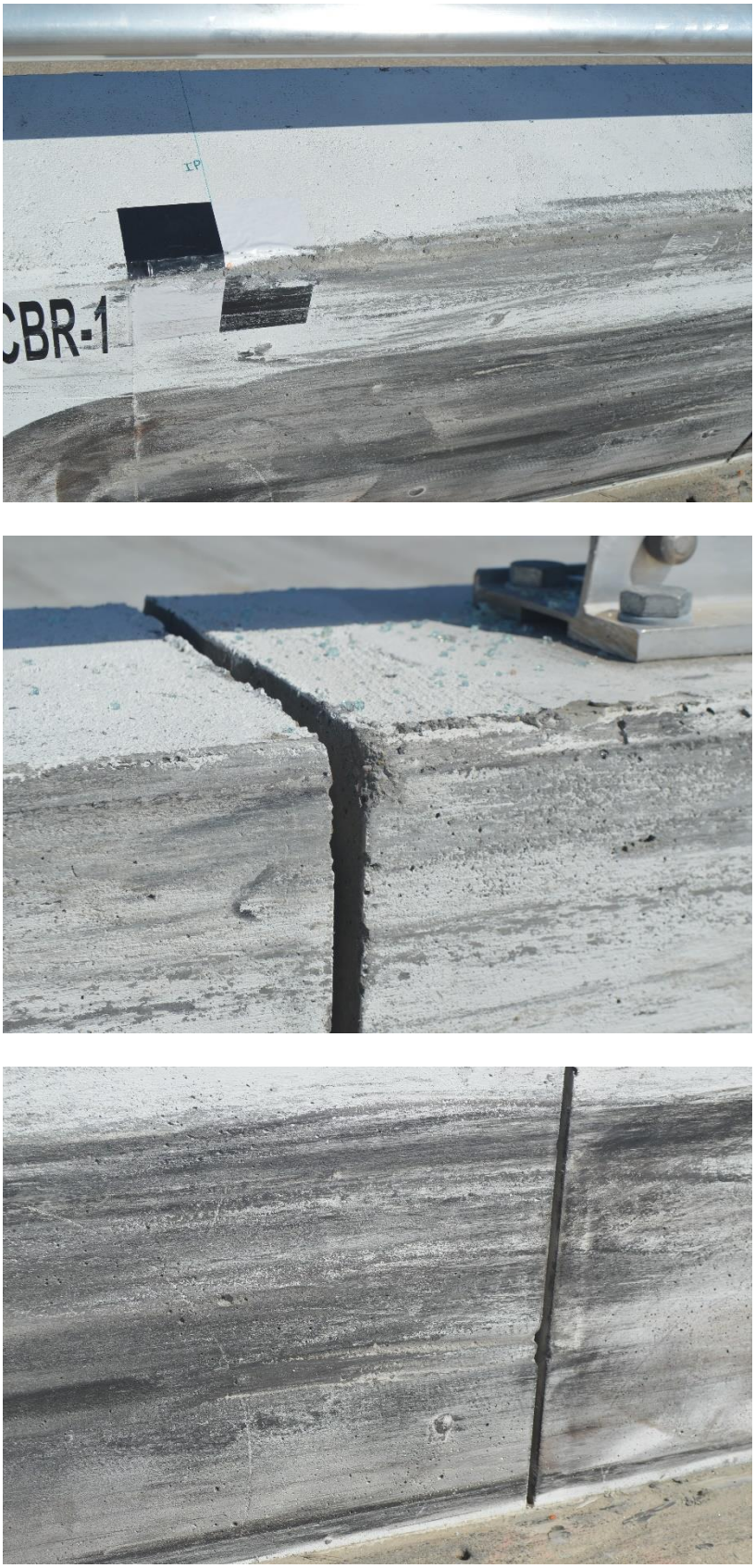


Figure 56. Concrete Gouging, Test No. NCBR-1

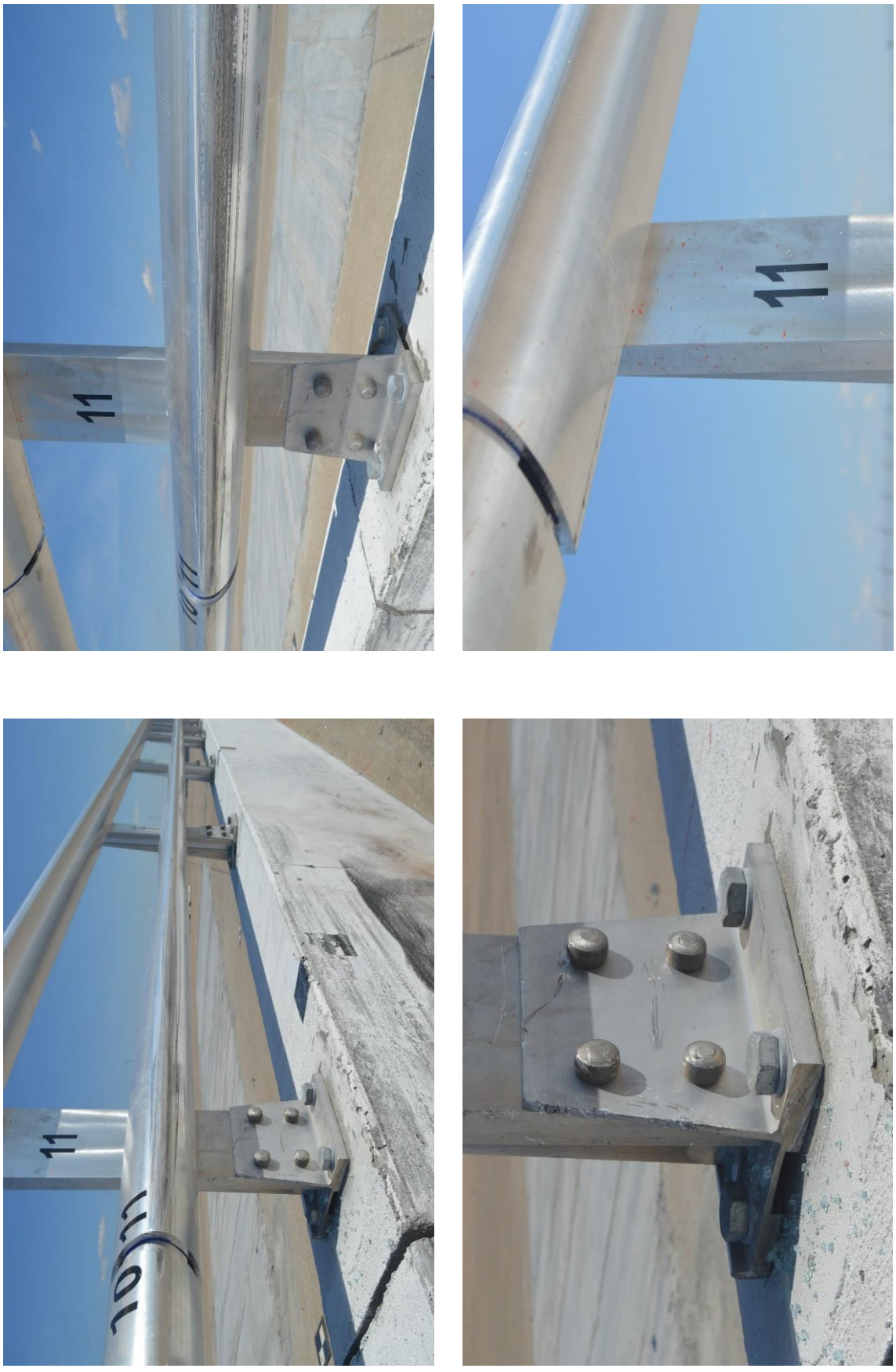


Figure 57. Rail and Post No. 11 Damage, Test No. NCBR-1

The maximum lateral permanent set of the barrier system was -0.2 in., as measured in the field, which was 0.2 in. forward from its initial position. The maximum lateral dynamic barrier deflection, including tipping of the barrier along the top surface, was 0.3 in. at post no. 15, as determined from high-speed digital video analysis. The working width of the system was found to be 14.0 in., also determined from high-speed digital video analysis. Barrier deflections are shown schematically in Figure 58.

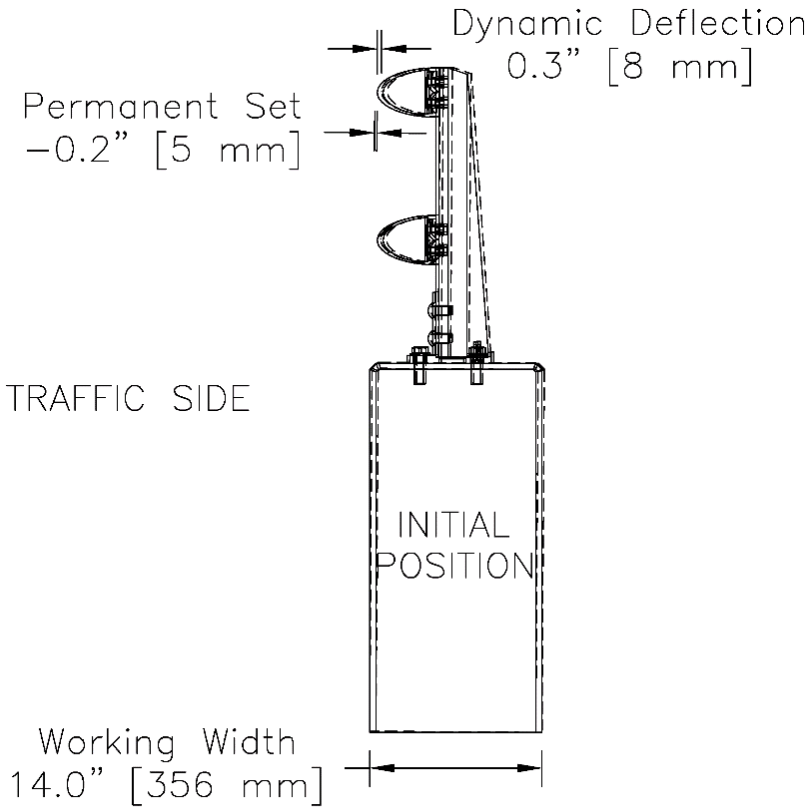


Figure 58. Barrier Deflections, Test No. NCBR-1

5.4 Vehicle Damage

Damage to the vehicle was moderate, as shown in Figures 59 through 63. The majority of the damage was concentrated on the left-front corner and left side of the vehicle where impact had occurred. The left side of the bumper was deformed and torn in front of the wheel. The left-front fender was pushed inward near the door panel and torn around the left-front wheel. The left-front steel rim was deformed with tears and crushing. The left-front tire was torn and deformed. The left-side headlight and fog light were disengaged from the vehicle. The left side of the radiator was pushed backward. Denting and scraping were observed across the entire left side. The top of the left-front door was slightly ajar and the bottom was pushed inward. The bottom of the left-rear door was dented and scuffed. The fuel hatch was ajar. The left-rear wheel assembly was deformed inward. The left-rear steel rim and tire were scuffed. The left side of the rear bumper was dented and scuffed. The hood was crushed inward, separated from the bumper entirely, and the left edge was torn. The right side of the bumper was pushed downward. The left side of the windshield was cracked and deformed, and the upper-right side had minor cracking. The left-front side window

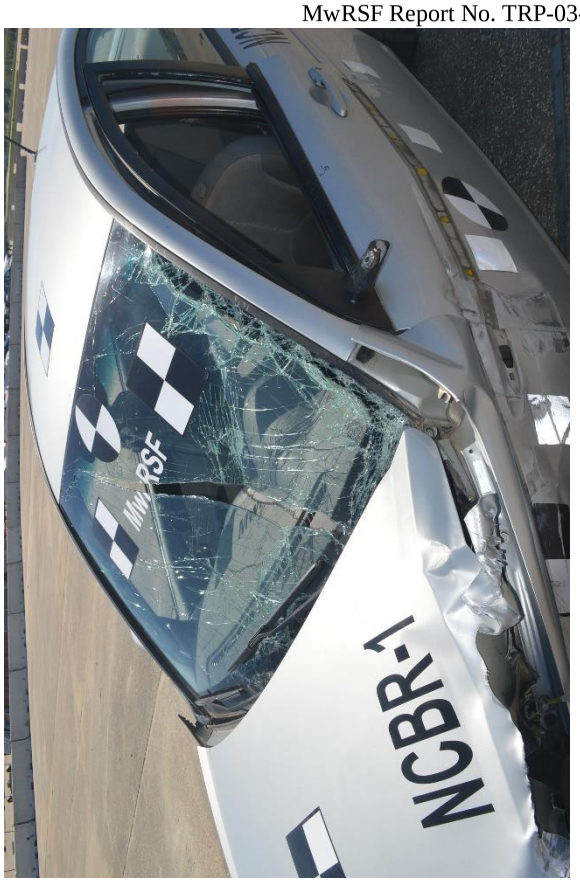
disengaged from the vehicle after contact with the dummy's head. The remaining window glass was undamaged. The spring perch on the left side was cracked. The left-side control arm was bent backward. The transmission mounts shifted toward the right side. The left-side frame rail compressed and bent upward. The rear cross member bent inward on both ends. The front cross member was bent and crushed upward. The frame horn was bent upward on the left side. The floor pan was opened at the seam across the whole left side. The front exhaust mount folded inward.

The maximum occupant compartment intrusions are listed in Table 5, along with the intrusion limits established in MASH 2016 for various areas of the occupant compartment. MASH 2016 defines intrusion or deformation as the occupant compartment being deformed and reduced in size with no observed penetration. There were no penetrations into the occupant compartment and none of the established MASH 2016 deformation limits were violated. Complete occupant compartment and vehicle deformations and the corresponding locations are provided in Appendix D. It should be noted that a large tear was visible in the vehicle windshield. Review of the high-speed video revealed that tearing of the windshield was formed due to crushing of the back left corner of the hood, resulting in a vertical crack which propagated through the windshield to the roof. Neither the barrier nor any vehicle component contacted the windshield except at the bottom left corner. The displacement of the vehicle's "A"-pillar and hood were minimal. No deformations occurred to the roof panel. After the test, the windshield displacements were measured and compared against an exemplary vehicle. However, windshield deformations were artificially high due to settling that occurred in between testing and measurement. Therefore, windshield displacements were deemed acceptable according to MASH, and none of the MASH criteria for windshield contact, protrusion, or deformation were violated.



Figure 59. Vehicle Damage, Test No. NCBR-1





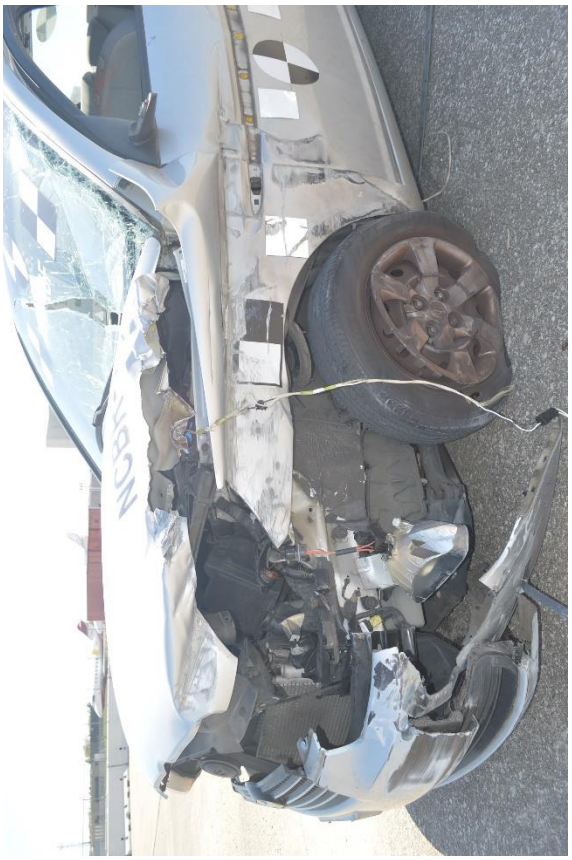




Figure 60. Vehicle Damage, Test No. NCBR-1

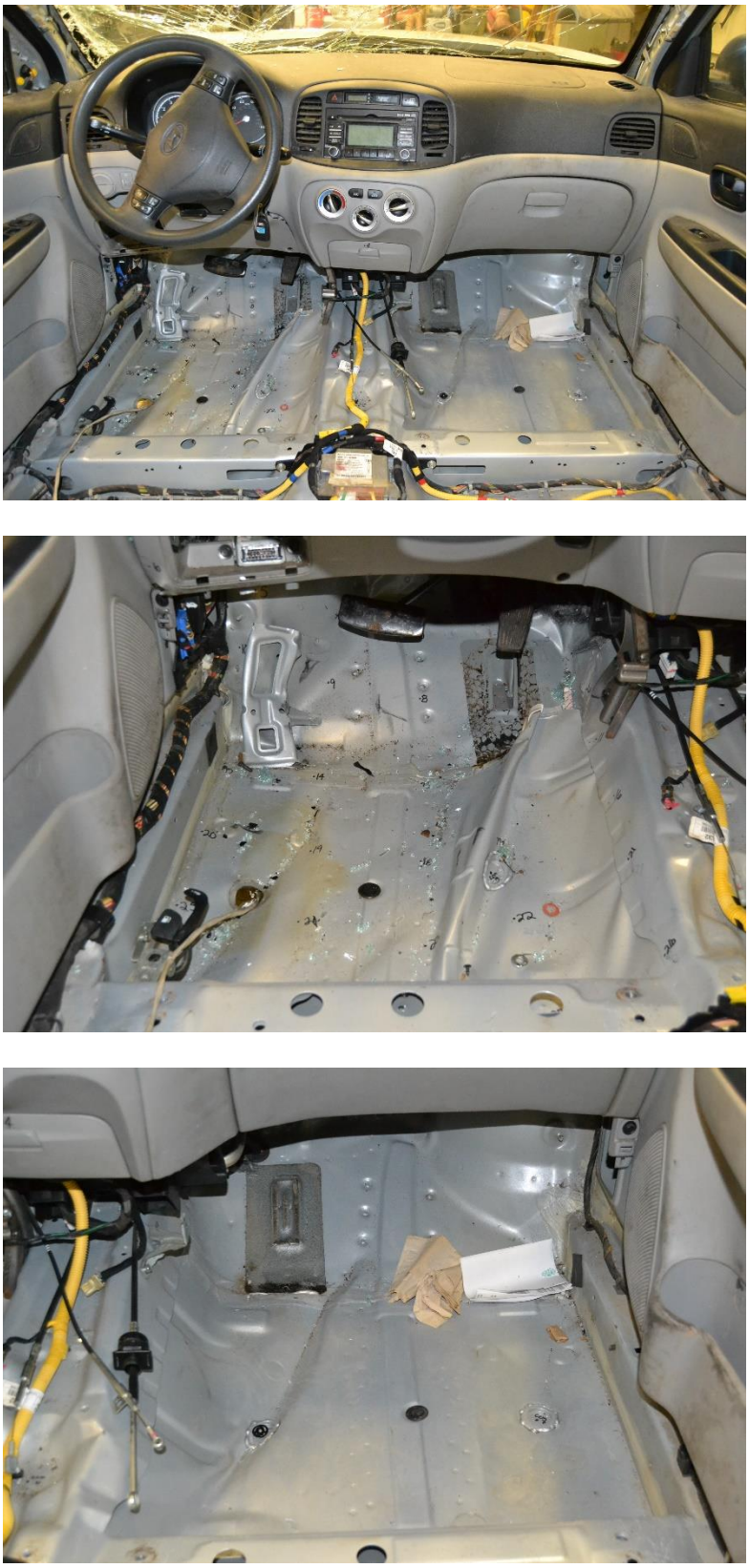


Figure 61. Occupant Compartment Damage, Test No. NCBR-1







Figure 62. Undercarriage Damage, Test No. NCBR-1



Figure 63. Windshield Damage (Pre- and Post-Test), Test No. NCBR-1

Table 5. Maximum Occupant Compartment Intrusions by Location, Test No. NCBR-1

LOCATION	MAXIMUM INTRUSION in.	MASH 2016 ALLOWABLE INTRUSION in.
Toe Pan – Wheel Well	2.7	≤ 9
Floor Pan	1.9	≤ 12
A-Pillar	1.0	≤ 5
B-Pillar	0.4	≤ 5
A-Pillars (lateral)	1.0	≤ 3
B-Pillar (lateral)	1.0	≤ 3
Side Front Panel	2.9	≤ 12
Side Door (above seat)	0.8	≤ 9
Side Door (below seat)	0.5	≤ 12
Roof	–0.3	N/A[2]
Windshield	5.0*	≤ 3
Side Window	Shattered due to contact with dummy's head	Test article did not cause window shatter
Dash	1.5	N/A[1]

Note: Negative values denote outward deformation
* Windshield crush was measured three days after the test and during that time frame settling of the damaged windshield occurred. Thus, the measured value is not believed to be realistic
N/A[1] – Not applicable
N/A[2] – MASH 2016 criteria is not applicable when deformation is outward

5.5 Occupant Risk

The calculated occupant impact velocities (OIVs) and maximum 0.010-sec average occupant ridedown accelerations (ORAs) in both the longitudinal and lateral directions, as determined from the accelerometer data, are shown in Table 6. Note that the OIVs and ORAs were within the suggested limits provided in MASH 2016. The calculated THIV, PHD, and ASI values are also shown in Table 6. Recorded data from the accelerometers and rate transducers are shown graphically in Appendix E.

Table 6. Summary of OIV, ORA, THIV, PHD, and ASI Values, Test No. NCBR-1

Evaluation Criteria		Transducer		MASH 2016 Limits
		SLICE-1 (primary)	SLICE-2	
OIV ft/s	Longitudinal	-24.46	-24.49	±40
	Lateral	30.78	28.60	±40
ORA g's	Longitudinal	-3.65	-2.86	±20.49
	Lateral	10.20	12.79	±20.49
MAX. ANGULAR DISPL. deg.	Roll	-12.6	-8.2	±75
	Pitch	-4.0	-5.0	±75
	Yaw	39.9	39.3	not required
THIV ft/s		38.74	35.75	not required
PHD g's		10.39	12.99	not required
ASI		2.51	2.34	not required

5.6 Barrier Loads

The longitudinal and lateral vehicle accelerations, as measured at the vehicle's c.g., were processed using an SAE CFC-60 filter and a 50-msec moving average. The 50-msec moving average vehicle accelerations were then combined with the uncoupled yaw angle versus time data in order to estimate the vehicular loading applied to the barrier system. The results of the barrier load estimate are shown in Figure 64. A peak load of 57.7 kip was noted at 0.031 s after impact, with a peak longitudinal wall force of approximately 14.8 kip. The average overall estimated vehicle-barrier sliding friction coefficient was 0.547 over the first 0.1 s of impact. The vehicle exhibited a "tail slap" effect in which two separate peaks were observed, the first corresponding to the redirection of the front of the vehicle, and the second corresponding to the tail end of the vehicle contacting the barrier system. The initial redirection load was approximately five times as large as the tail slap load.

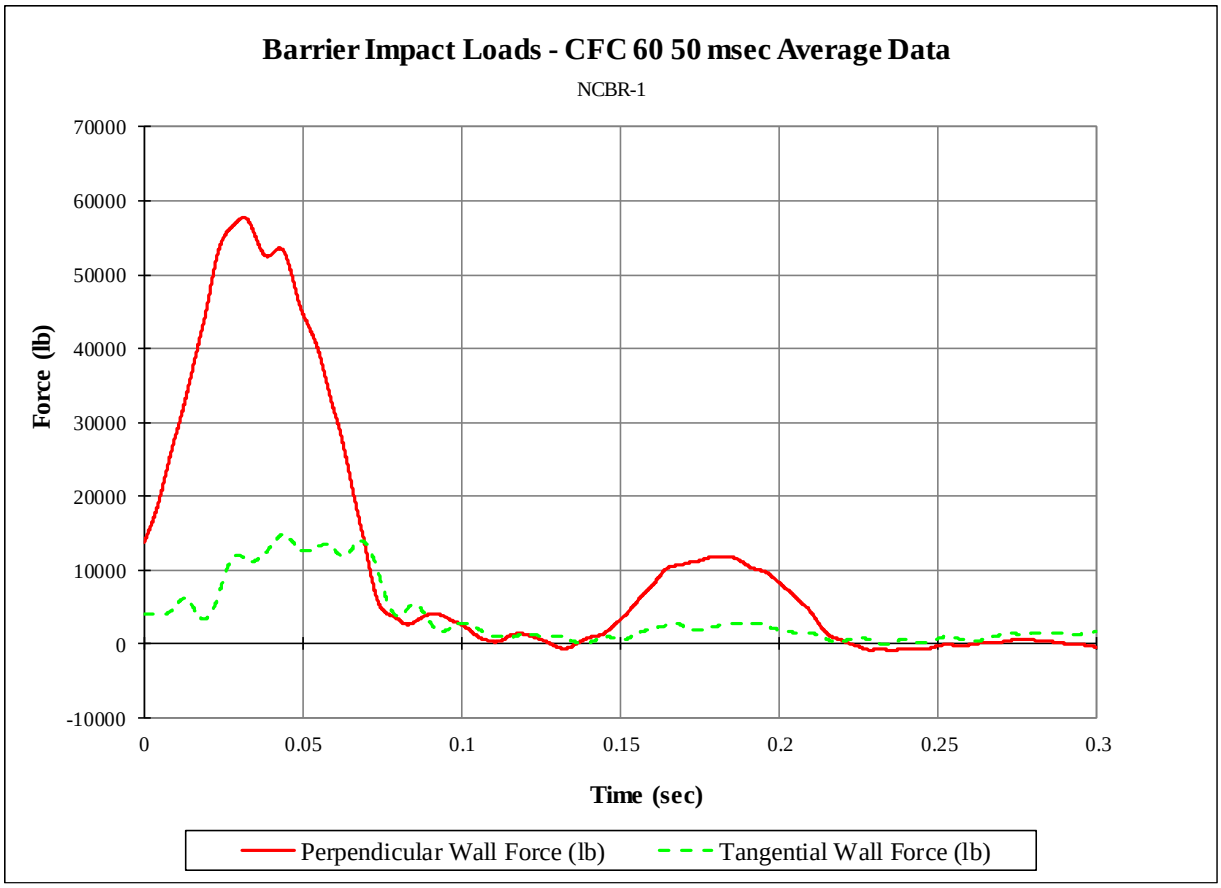


Figure 64. Estimated Barrier Impact and Friction Loads, Test No. NCBR-1

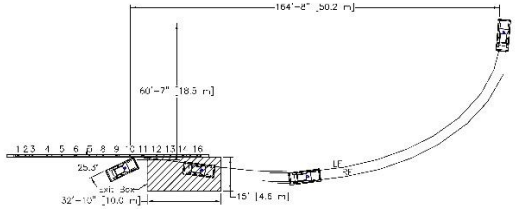
5.7 Discussion

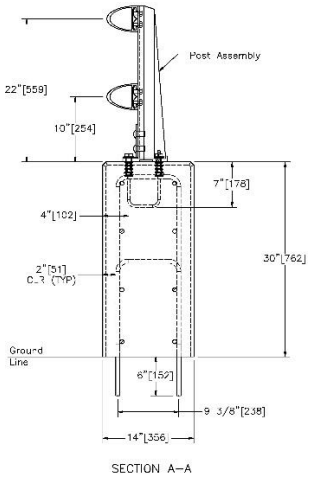
Analysis of the test results for test no. NCBR-1 showed that the system adequately contained and redirected the 1100C vehicle with minimal barrier damage and displacement. A summary of the test results and sequential photographs are shown in Figure 65. Detached elements, fragments, or other debris from the test article did not penetrate or show potential for penetrating the occupant compartment, or present an undue hazard to other traffic, pedestrians, or work-zone personnel. Deformations of, or intrusions into, the occupant compartment that could have caused serious injury did not occur. Windshield deformation was measured three days after testing, and in that time settling and buckling of the windshield occurred. The measured deformation of 5.0 in. is not believed to be realistic, and is therefore not considered a violation of MASH 2016 safety performance criteria. The test vehicle did not penetrate nor ride over the barrier and remained upright during and after impact. Vehicle roll, pitch, and yaw angular displacements, as shown in Appendix E, were deemed acceptable, because they did not adversely influence occupant risk nor cause rollover. After impact, the vehicle exited the barrier at an angle of 8.5 deg., and its trajectory did not violate the bounds of the exit box. Therefore, test no. NCBR-1 was determined to be acceptable according to the MASH 2016 safety performance criteria for test designation no. 3-10.

During the test, the dummy's head protruded out of the left-side window and nearly entered the ZOI without contacting the system. This behavior is associated with an increased occupant risk. Further evaluation of dummy movement is provided in Chapter 7.



0.000 sec 0.050 sec 0.100 sec 0.200 sec 0.300 sec





Test Agency ..... MwRSF

- Test Number NCBR-1
- Date ..... May 13, 2019
- MASH 2016 Test Designation No. 3-10
- Test Article ..... NCDOT Two-Bar Metal Bridge Rail
- Total Length ..... 90 ft
- Key Component – Elliptical Aluminum Rail
  - Length ..... 30 ft
  - Width ..... 4 in.
  - Depth ..... 4¾ in.
- Key Component – Aluminum Post
  - Height ..... 23½ in.
  - Length ..... 5¾ in.
  - Width ..... 4¼ in.
  - Spacing ..... 72 in.
- Vehicle Make / Model ..... 2010 Hyundai Accent
  - Curb ..... 2,505 lb
  - Test Inertial ..... 2,425 lb
  - Gross Static ..... 2,585 lb
- Impact Conditions
  - Speed ..... 63.2 mph
  - Angle ..... 25.2 deg.
  - Impact Location ..... 51.1 in. upstream from post no. 11
- Impact Severity ..... 59.0 kip-ft > 51 kip-ft limit from MASH 2016
- Exit Conditions
  - Speed ..... 42.8 mph
  - Angle ..... 8.5 deg.
- Exit Box Criterion ..... Pass
- Vehicle Stability ..... Satisfactory
- Vehicle Stopping Distance ..... 164 ft – 8 in. downstream, 60 ft – 7 in. laterally behind
- Vehicle Damage ..... Moderate
  - VDS [10] 11-LFQ-4
  - CDC [11] 11-LFEW-3
  - Maximum Interior Deformation ..... 2.9 in.
- Test Article Damage ..... Minimal
- Maximum Test Article Deflections
  - Permanent Set ..... -0.2 in.
  - Dynamic ..... 0.3 in.
  - Working Width ..... 14.0 in.
- Transducer Data

Evaluation Criteria		Transducer		MASH 2016 Limit
		SLICE-1 (primary)	SLICE-2	
OIV ft/s	Longitudinal	-24.46	-24.49	±40
	Lateral	30.78	28.60	±40
ORA g's	Longitudinal	-3.65	-2.86	±20.49
	Lateral	10.20	12.79	±20.49
MAX ANGULAR DISP. deg.	Roll	-12.6	-8.2	±75
	Pitch	-4.0	-5.0	±75
	Yaw	39.9	39.3	not required
THIV – ft/s		38.74	35.75	not required
PHD – g's		10.39	12.99	not required
ASI		2.51	2.34	not required

Figure 65. Summary of Test Results and Sequential Photographs, Test No. NCBR-1

6 FULL-SCALE CRASH TEST NO. NCBR-2

6.1 Weather Conditions

Test no. NCBR-2 was conducted on June 11, 2019 at approximately 12:00 p.m. The weather conditions as per the National Oceanic and Atmospheric Administration (station 14939/LNK) were reported and are shown in Table 7.

Table 7. Weather Conditions, Test No. NCBR-2

Temperature	75 deg. F
Humidity	37 percent
Wind Speed	11 mph
Wind Direction	230 deg. from True North
Sky Conditions	Overcast
Visibility	10 Statute Miles
Pavement Surface	Dry
Previous 3-Day Precipitation	0.15 in.
Previous 7-Day Precipitation	0.43 in.

6.2 Test Description

Initial vehicle impact was to occur $61^{15}/_{16}$ in. upstream from post no. 6, as shown in Figure 66, which was selected by UNCC from simulation results and verified by NCDOT as the point that maximized loading on the rail splices. The 5,018-lb quad cab pickup truck impacted the NCDOT two-bar metal bridge rail at a speed of 61.9 mph and an angle of 24.9 deg. The actual point of impact was $61^{7}/_{8}$ in. upstream from post no. 6. The vehicle came to rest 200 ft – 2 in. downstream and 25 ft – 10 in. laterally in front of the traffic side of the barrier after the brakes were applied.

A detailed description of the sequential impact events is contained in Table 8. High-speed footage of the test is shown in Figure 67. Sequential photographs are shown in Figures 69 and 70. Documentary photographs of the crash test are shown in Figures 71 through 73. The vehicle trajectory and final position are shown in Figure 74.



Figure 66. Impact Location, Test No. NCBR-2

Table 8. Sequential Description of Impact Events, Test No. NCBR-2

TIME (msec)	EVENT
0.0	Vehicle's front bumper contacted the parapet $61^{7}/_{8}$ in. upstream from post no. 6.
6.0	Vehicle's left headlight contacted rail.
8.0	Vehicle's left headlight deformed, vehicle's right fender contacted rail.
10.0	Vehicle's left fender deformed, vehicle's left-front tire contacted the parapet.
24.0	Vehicle's hood contacted post no. 6 and deformed.
30.0	Vehicle's left-front door deformed, vehicle's left headlight shattered.
34.0	Vehicle yawed away from system.
36.0	Vehicle's left-front tire became airborne.
38.0	Vehicle pitched downward.
42.0	Vehicle's left-front tire deformed.
46.0	Post no. 6 deflected downstream.
48.0	Vehicle's left-front door contacted the parapet and opened.
58.0	Vehicle rolled toward system.
62.0	Vehicle’s left-side mirror shattered.
68.0	Vehicle's left-front tire regained contact with ground.
70.0	Post no. 6 deflected backward.
72.0	Post no. 7 deflected backward.
92.0	Vehicle's left fender became disengaged.
94.0	Vehicle’s left-front window shattered.
104.0	Vehicle's right-front tire became airborne.
114.0	Vehicle's left-rear door deformed.
140.0	Vehicle's right-rear tire became airborne.
186.0	Vehicle's left-rear door contacted the parapet.
192.0	Vehicle’s left quarter panel contacted the parapet and vehicle became parallel to system at 49.9 mph.
194.0	Vehicle's left quarter panel deformed.
202.0	Vehicle's rear bumper contacted the parapet.
206.0	Vehicle's rear bumper deformed.
208.0	Post no. 5 deflected backward.
212.0	Post no. 5 deflected forward, vehicle's left taillight contacted rail.
214.0	Vehicle's left taillight deformed.
218.0	Vehicle's left taillight shattered.
222.0	Post no. 6 deflected backward.
306.0	Vehicle exited system at 46.6 mph and an 8.83 deg. angle.
376.0	Vehicle's right-front tire regained contact with ground.
430.0	Vehicle's right-rear tire regained contact with ground.



Figure 67. Downstream High-Speed Footage, Test No. NCBR-2

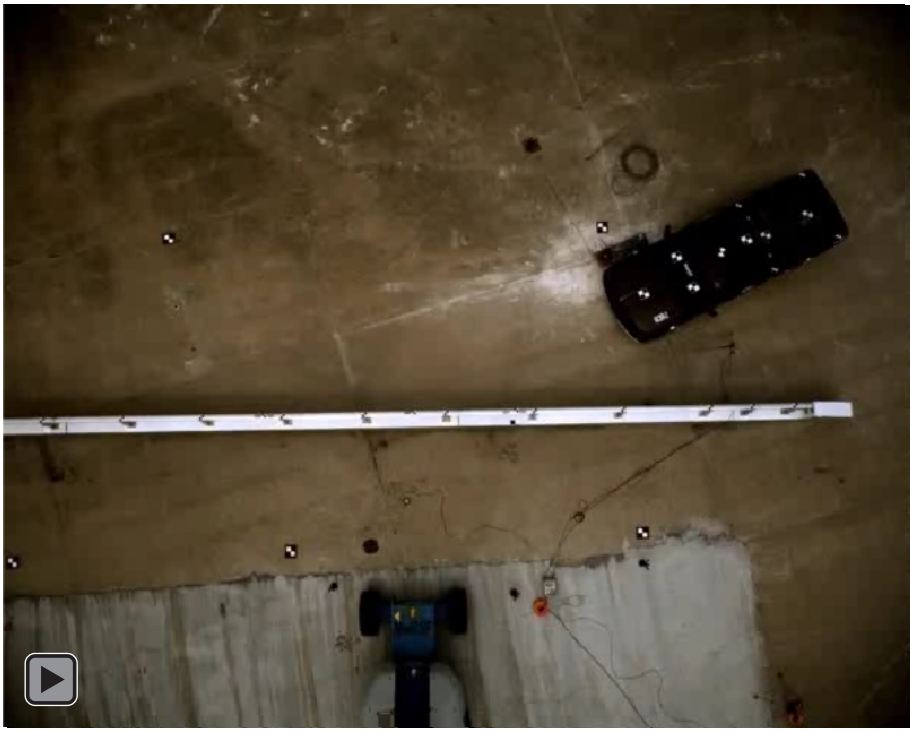


Figure 68. Overhead High-Speed Footage, Test No. NCBR-2

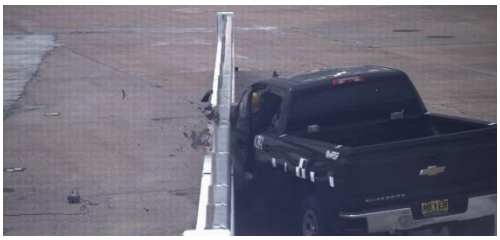

0.000 sec


0.000 sec


0.050 sec


0.050 sec


0.100 sec


0.100 sec


0.200 sec


0.200 sec


0.300 sec


0.300 sec


0.450 sec


0.450 sec

Figure 69. Sequential Photographs, Test No. NCBR-2


0.000 sec


0.000 sec


0.025 sec


0.025 sec


0.050 sec


0.050 sec


0.100 sec


0.100 sec


0.150 sec


0.150 sec


0.225 sec


0.225 sec

Figure 70. Sequential Photographs, Test No. NCBR-2

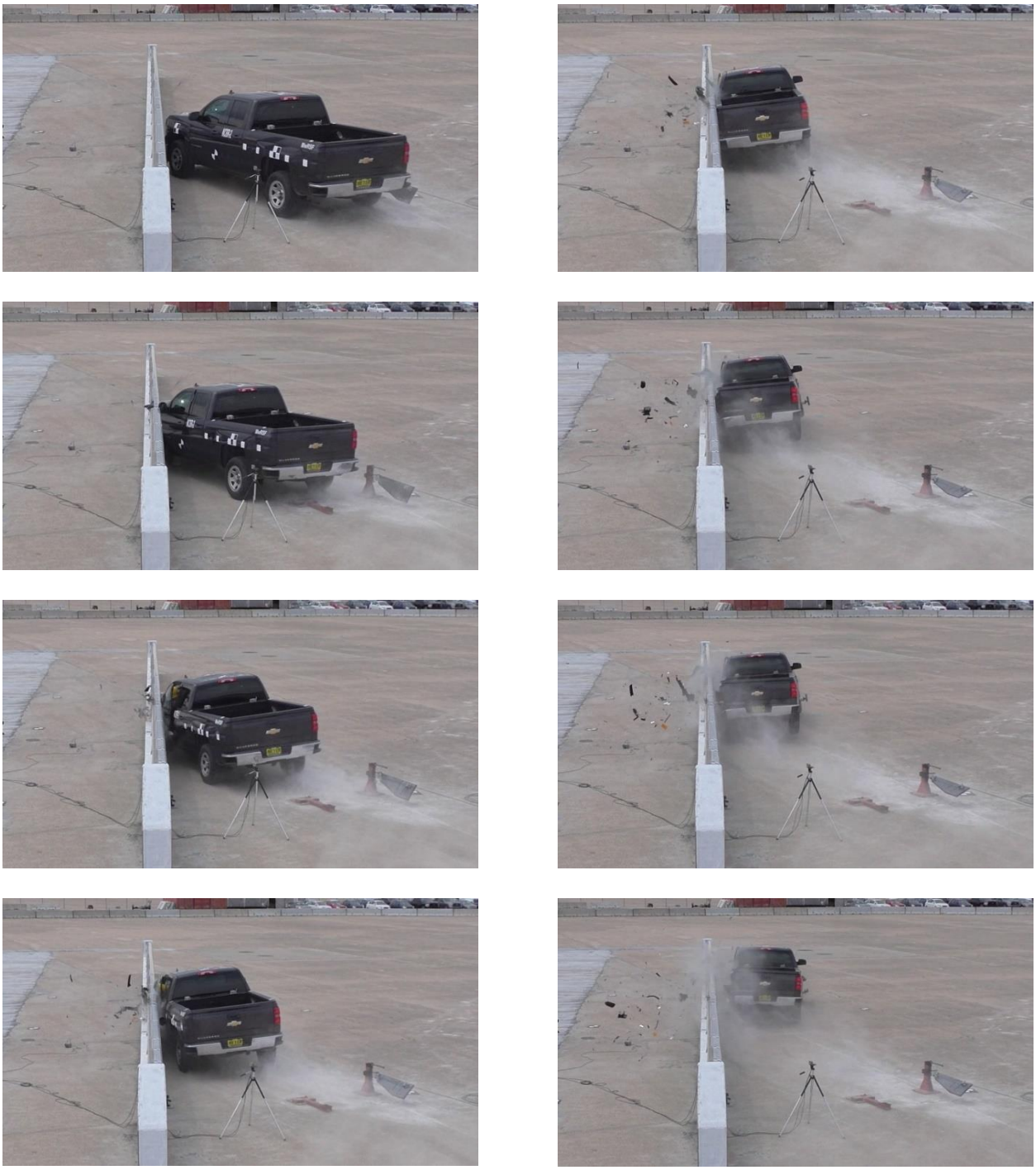


Figure 71. Documentary Photographs, Test No. NCBR-2



Figure 72. Documentary Photographs, Test No. NCBR-2



Figure 73. Documentary Photographs, Test No. NCBR-2



Figure 74. Vehicle Final Position and Trajectory Marks, Test No. NCBR-2

6.3 Barrier Damage

Damage to the barrier was minimal, as shown in Figures 75 through 79. Barrier damage consisted of contact marks and concrete gouging across the front face of the parapet, and minor concrete breakout on the upstream edge of the second parapet segment at the expansion joint. Note that any cracking visible in the system photographs was documented beforehand and not a result of test no. NCBR-2.

Contact marks on the lower rail were observed 16 in. downstream from post no. 5 and extending 150½ in. downstream. Contact marks on the upper rail were observed starting 10 in. downstream of the impact point and extending 164 in. downstream. A separate contact mark was observed on the underside of the upper rail, starting 33 in. upstream from post no. 8, measuring 21 in. long and ½ in. wide. The splices between the first and second rail segments experienced minor elongation, measuring $^{7}/_{8}$ in. at both the front and back of both rails.

Minor concrete breakout measuring up to 3 in. wide x 15 in. long x 1½ in. deep, extending vertically between 9 and 24 in. above the ground line, occurred on the upstream edge of the second concrete parapet at the expansion gap between post nos. 5 and 6. Gouging was observed 20 in. downstream from post no. 5 and 14 in. below the top surface of the parapet, measuring 16 in. long and 7 in. tall. Gouging also occurred along the top edge of the front face of the parapet, located 13 in. downstream from the impact point and measuring 22 in. long and 1 in. wide. A 17-in. circular gouge occurred 17½ in. downstream from post no. 5. Small scratches were located throughout the impact region across the front face of the parapet.

An 8¼-in. contact mark began 4¼ in. from the top of post no. 6 on its upstream flange. An additional 1½-in. contact mark, beginning 5¼ in. from the bottom of post no. 6, was observed on the upstream flange. Contact marks extended 2¾ in. downstream from the upstream edge of the post-mounting bracket at post no. 6. Contact marks were observed on the back side of the upstream flange beginning 3 in. from the top of the flange and extending down 5 in. downstream. Contact marks were also observed along the entire upstream front flange edge, front post-to-parapet attachment bolts, and front edge of the base plate at post no. 6. A ¼-in. contact mark began 4¾ in. from the top of post no. 7 on its upstream flange. Minor contact marks, measuring 7 in. in height, began 2 in. from the bottom of the upstream flange of post no. 7 and along the front edge and top surface of the base plate and the front post-to-parapet attachment bolts.



Figure 75. System Damage, Test No. NCBR-2



Figure 76. System Damage, Test No. NCBR-2



Figure 77. Concrete Gouging, Test No. NCBR-2



Figure 78. Post No. 6 Backside Damage, Test No. NCBR-2

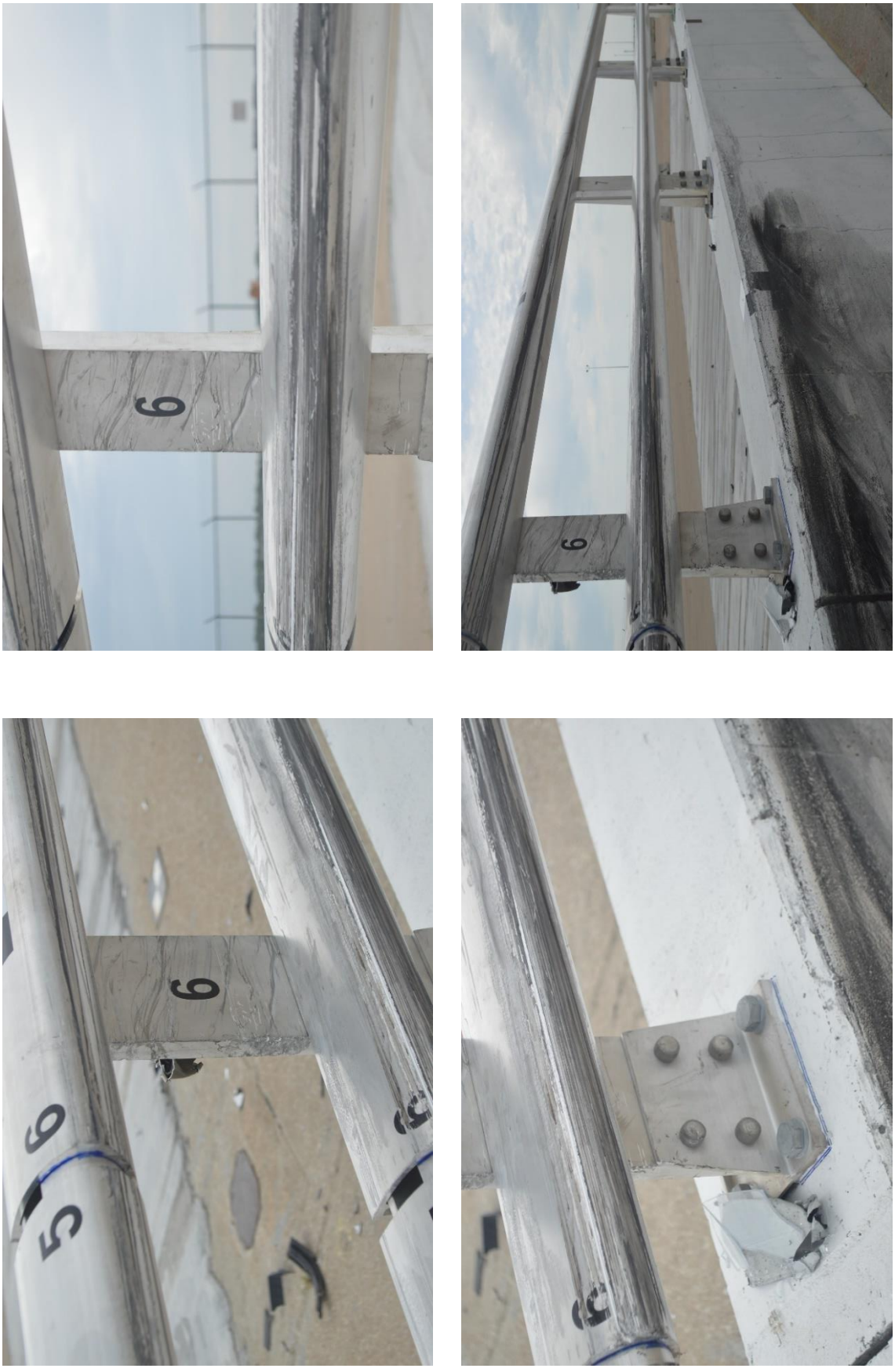


Figure 79. Rail and Post No. 6 Damage, Test No. NCBR-2

The maximum lateral permanent set of the barrier system was 0.7 in. between post nos. 5 and 6, as measured in the field. The maximum lateral dynamic barrier deflection, including tipping of the barrier along the top surface, was 0.8 in. on the upper rail, as determined from high-speed digital video analysis. The working width of the system was found to be 15.5 in., also determined from high-speed digital video analysis. Barrier deflections are shown schematically in Figure 80.

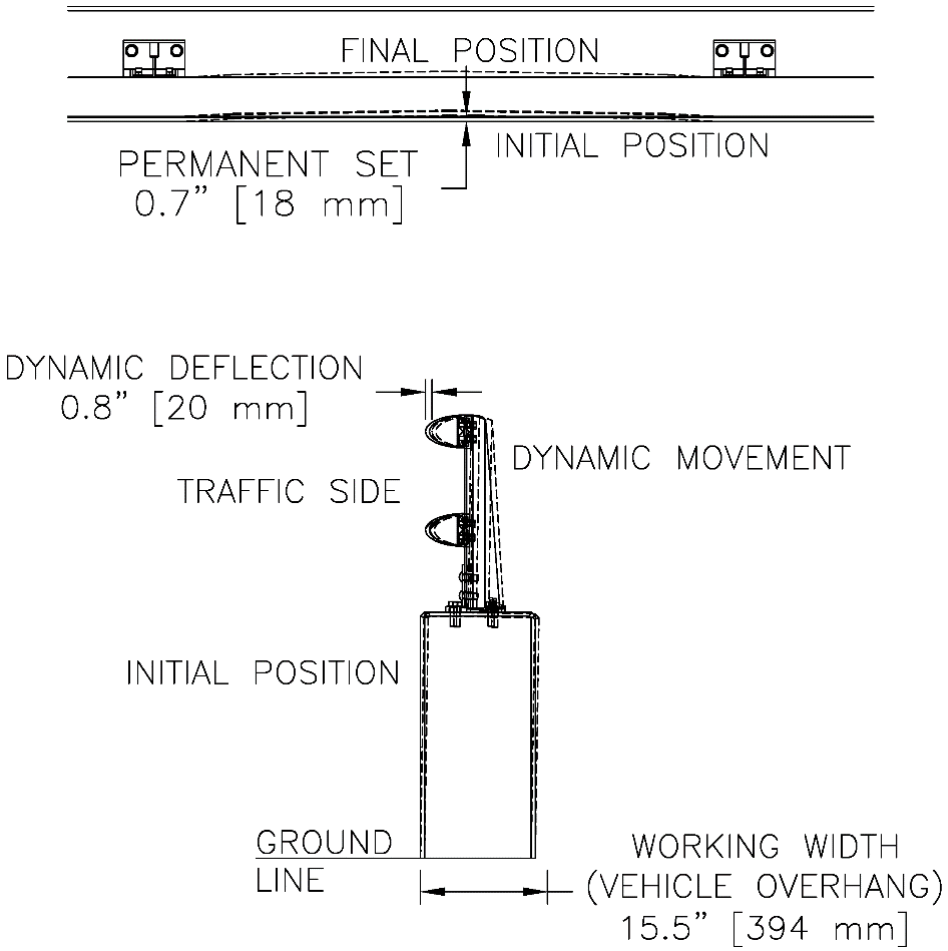


Figure 80. Barrier Deflections, Test No. NCBR-2

6.4 Vehicle Damage

Damage to the vehicle was moderate, as shown in Figures 81 through 85. The majority of the damage was concentrated on the left-front corner and left side of the vehicle where the impact occurred. The left side of the bumper was crushed inward. The left-front fender was pushed upward near the door panel and dented and torn behind the left-front wheel. The left-front steel rim and tire were scuffed and deformed. The grille was pushed backward around the left-side headlight assembly. The left-side headlight and fog light were disengaged from the vehicle. Denting and scraping were observed across the entire left side. The left-front door was slightly ajar and deformed inward at the bottom. The left-rear door was dented. The left side of the truck bed was dented and the fuel hatch was ajar. The left-rear tire was scuffed. The left taillight was disengaged from the vehicle. The left side of the rear bumper was torn and pushed downward. The right side of the front bumper was pushed downward. The vehicle's aluminum hood was deformed across

its entirety and the left edge was torn from front to back. A piece of the hood was torn off the left side. The left side window was ejected from the vehicle after impact with the dummy's head. The remaining window glass remained undamaged. The anti-roll bar shifted toward the right side and the left-side end link connector was bent. The left-side bottom control arm joint was torn out of the frame. The left-side outer tie rod was bent and the left-side upper mount of the steering rack was dented. The front left side of the oil pan had a 2.5 in. x 3.5 in. puncture. The left side of the frame at the impact point was caved inward and bent at the middle of the left-front door. The right side of the frame bent inward at the midpoint of the right-front door. The middle cross member bent where it connected to the frame. The left-side frame horn bent inward. The right-front passenger cab mount was disengaged. The floor pan was wrinkled. The tail pipe came out of the rear hanging mount.

The maximum occupant compartment intrusions are listed in Table 9 along with the intrusion limits established in MASH 2016 for various areas of the occupant compartment. MASH 2016 defines intrusion or deformation as the occupant compartment being deformed and reduced in size with no observed penetration. There were no penetrations into the occupant compartment and none of the established MASH 2016 deformation limits were violated. Complete occupant compartment and vehicle deformations and the corresponding locations are provided in Appendix D. Note that set 1 interior and floor pan deformation data was compromised and is not listed in Appendix D. Note there is no NASS crush information due to incomplete pretest profile information.



Figure 81. Vehicle Damage, Test No. NCBR-2

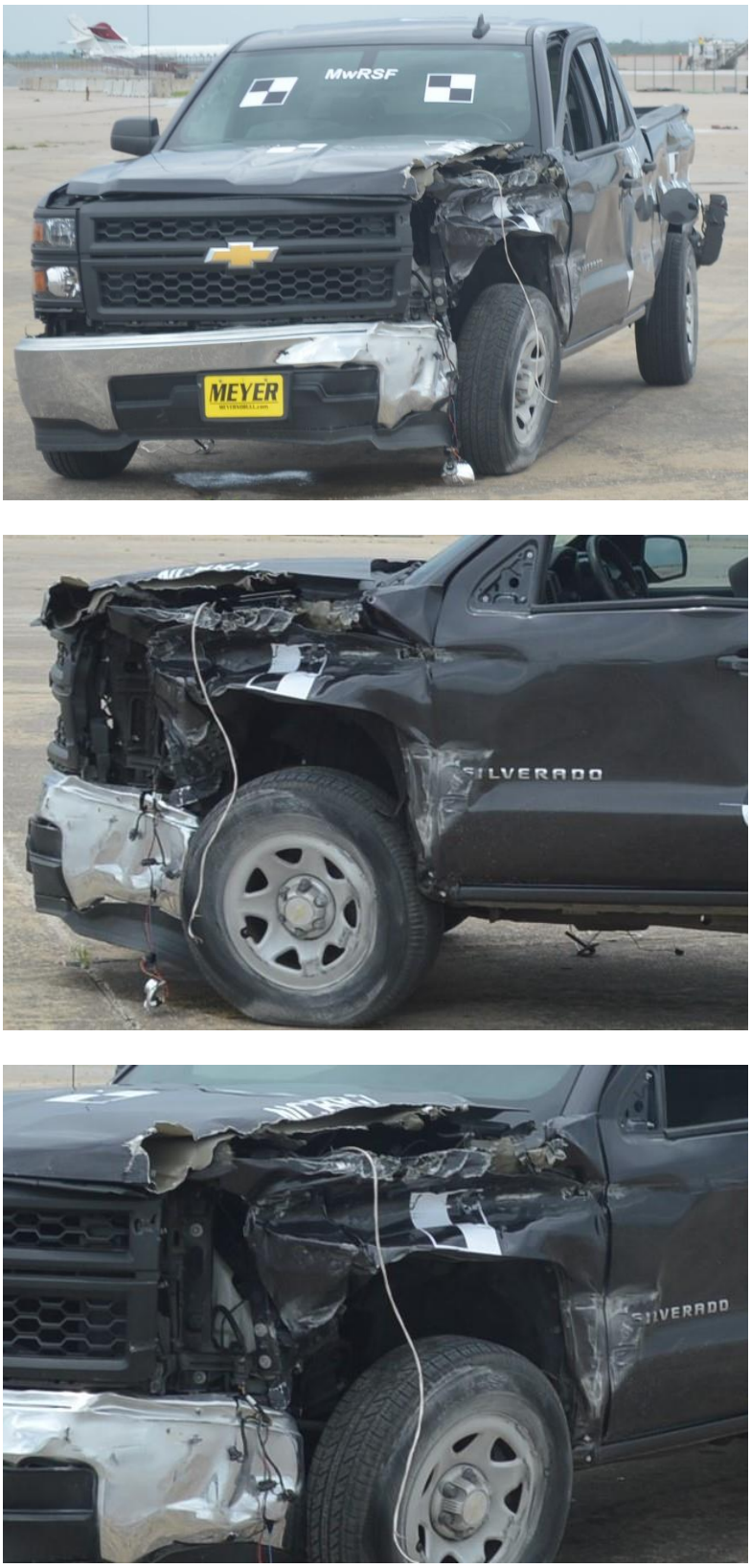


Figure 82. Vehicle Damage, Test No. NCBR-2







Figure 83. Occupant Compartment Damage, Test No. NCBR-2





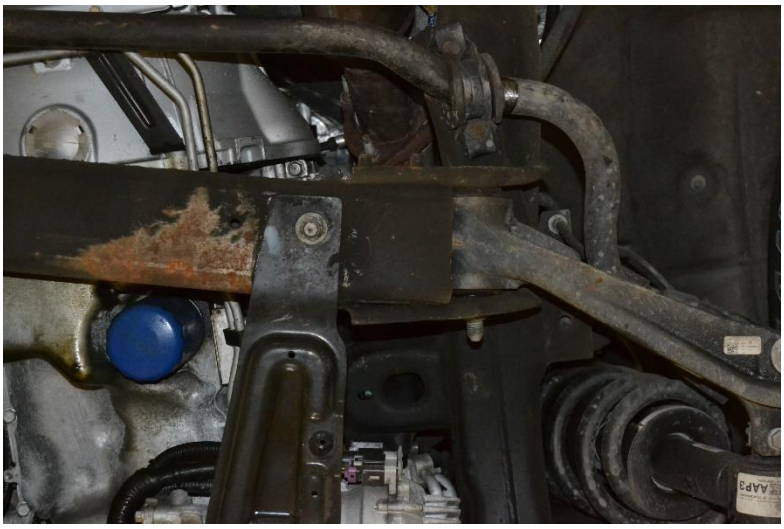


Figure 84. Undercarriage Damage, Test No. NCBR-2



Figure 85. Windshield Damage (Pre- and Post-Test), Test No. NCBR-2

Table 9. Maximum Occupant Compartment Intrusions by Location, Test No. NCBR-2

LOCATION	MAXIMUM INTRUSION in.	MASH 2016 ALLOWABLE INTRUSION in.
Toe Pan – Wheel Well	1.3	≤ 9
Floor Pan	0.5	≤ 12
A-Pillar	1.2	≤ 5
B-Pillar	1.4	≤ 5
A-Pillar (lateral)	1.2	≤ 3
B-Pillar (lateral)	1.4	≤ 3
Side Front Panel	1.6	≤ 12
Side Door (above seat)	1.6	≤ 9
Side Door (below seat)	0.5	≤ 12
Roof	0.2	≤ 4
Windshield	N/A	≤ 3
Side Window	Shattered due to contact with dummy's head	Test article did not cause window shatter
Dash	0.0	N/A[1]

N/A[1] – Not applicable

6.5 Occupant Risk

The calculated occupant impact velocities (OIVs) and maximum 0.010-sec average occupant ridedown accelerations (ORAs) in both the longitudinal and lateral directions, as determined from the accelerometer data, are shown in Table 10. Note that the OIVs and ORAs were within the suggested limits provided in MASH 2016. The calculated THIV, PHD, and ASI values are also shown in Table 10. Recorded data from the accelerometers and rate transducers are shown graphically in Appendix F.

Table 10. Summary of OIV, ORA, THIV, PHD, and ASI Values, Test No. NCBR-2

Evaluation Criteria		Transducer		MASH 2016 Limits
		SLICE-1 (primary)	SLICE-2	
OIV ft/s	Longitudinal	-21.49	-20.66	±40
	Lateral	27.89	26.20	±40
ORA g's	Longitudinal	-5.09	-5.06	±20.49
	Lateral	10.78	13.36	±20.49
MAX. ANGULAR DISPL. deg.	Roll	-9.3	-6.1	±75
	Pitch	3.0	2.4	±75
	Yaw	32.1	31.5	not required
THIV ft/s		36.41	34.48	not required
PHD g's		11.26	13.74	not required
ASI		1.91	1.84	not required

6.6 Barrier Loads

The longitudinal and lateral vehicle accelerations, as measured at the vehicle's c.g., were processed using an SAE CFC-60 filter and a 50-msec moving average. The 50-msec moving average vehicle accelerations were then combined with the uncoupled yaw angle versus time data in order to estimate the vehicular loading applied to the barrier system. The results of the barrier load estimate are shown in Figure 86. A peak load of 89.9 kip was noted at 0.052 s after impact, with a peak longitudinal wall force of approximately 30.6 kip. The resulting average overall estimated vehicle-barrier sliding friction coefficient was 0.237 measured over the first 0.1 s of impact. The vehicle exhibited a "tail slap" effect in which two separate peaks were observed, the first corresponding to the redirection of the front of the vehicle, and the second corresponding to the tail end of the vehicle contacting the barrier system. The initial redirection load was more than twice as large as the tail slap load.

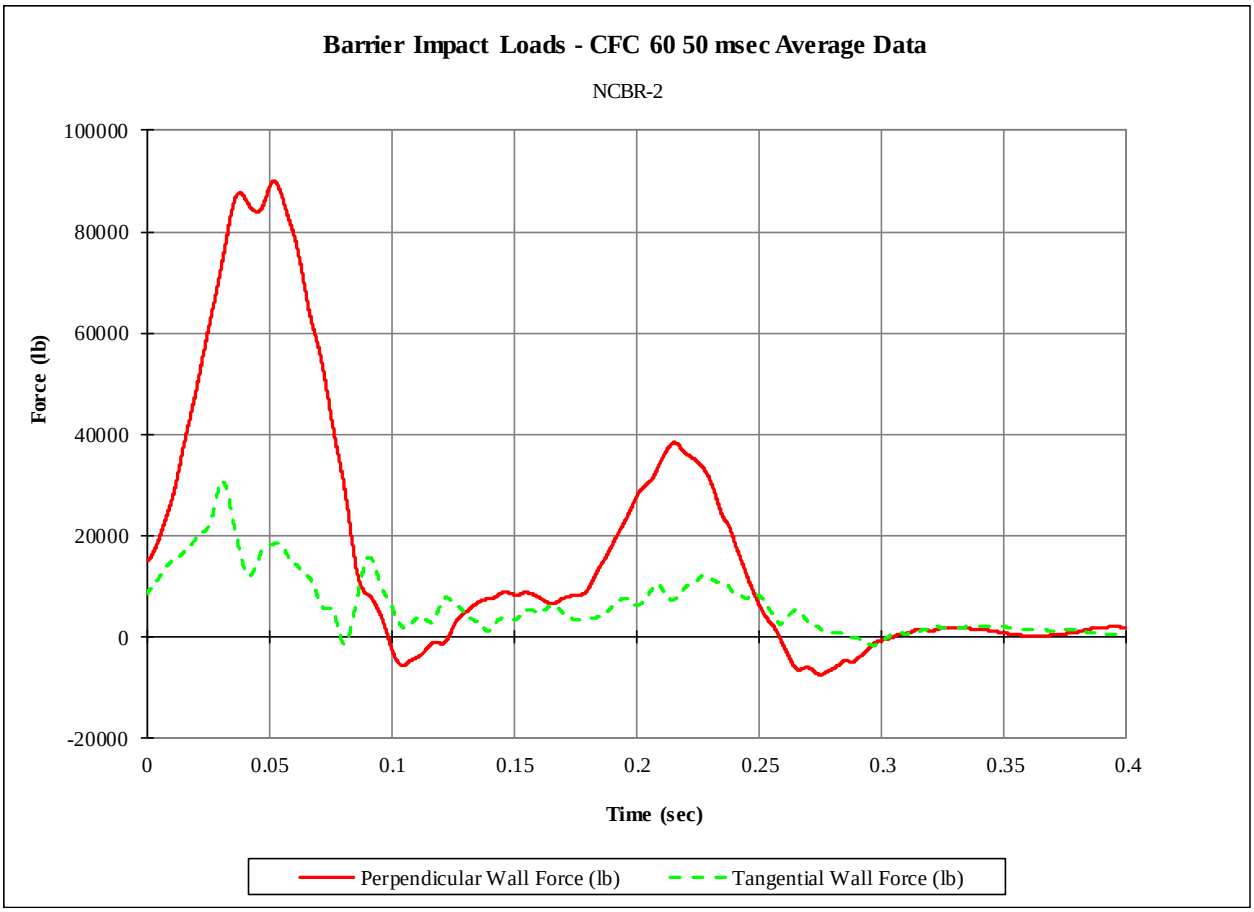


Figure 86. Estimated Barrier Impact and Friction Loads, Test No. NCBR-2

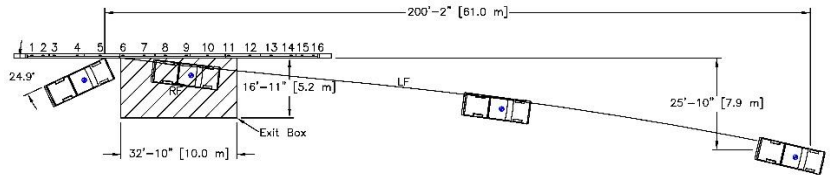
6.7 Discussion

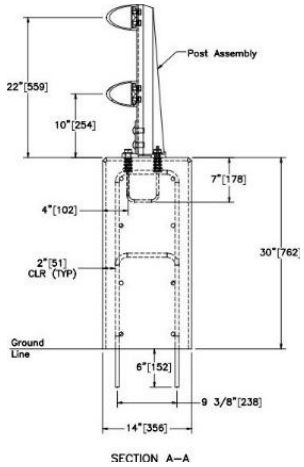
Analysis of the test results for test no. NCBR-2 showed that the system adequately contained and redirected the 2270P vehicle with minimal barrier damage and displacement. A summary of the test results and sequential photographs are shown in Figure 87. Detached elements, fragments, or other debris from the test article did not penetrate or show potential for penetrating the occupant compartment, or present an undue hazard to other traffic, pedestrians, or work-zone personnel. Deformations of, or intrusions into, the occupant compartment that could have caused serious injury did not occur. The test vehicle did not penetrate nor ride over the barrier and remained upright during and after impact. Vehicle roll, pitch, and yaw angular displacements, as shown in Appendix F, were deemed acceptable, because they did not adversely influence occupant risk nor cause rollover. After impact, the vehicle exited the barrier at an angle of 6.3 deg., and its trajectory did not violate the bounds of the exit box. Therefore, test no. NCBR-2 was determined to be acceptable according to the MASH 2016 safety performance criteria for test designation no. 3-11.

During the test, the dummy's head protruded out of the left-side window and extended into the ZOI but did not contact the system. This behavior is associated with an increased occupant risk. Further evaluation of the dummy movement is provided in Chapter 7.



0.000 sec 0.050 sec 0.100 sec 0.200 sec 0.300 sec





- Test Agency ..... MwRSF
- Test Number NCBR-2
- Date ..... June 11, 2019
- MASH 2016 Test Designation No. 3-11
- Test Article ..... NCDOT Two-Bar Metal Bridge Rail
- Total Length ..... 90 ft
- Key Component – Elliptical Aluminum Rail
  - Length ..... 26 ft – ½ in.
  - Width ..... 4 in.
  - Depth ..... 4¾ in.
- Key Component – Aluminum Post
  - Height ..... 23½ in.
  - Length ..... 5¾ in.
  - Width ..... 4¼ in.
  - Spacing ..... 78 in.
- Vehicle Make / Model ..... 2015 Chevrolet Silverado
  - Curb ..... 5,015 lb
  - Test Inertial ..... 5,018 lb
  - Gross Static ..... 5,183 lb
- Impact Conditions
  - Speed ..... 61.9 mph
  - Angle ..... 24.9 deg.
  - Impact Location ..... $61^{7}/_{8}$ in. upstream from post no. 6
- Impact Severity ..... 113.5 kip-ft > 106 kip-ft limit from MASH 2016
- Exit Conditions
  - Speed ..... 46.6 mph
  - Angle ..... 8.8 deg.
- Exit Box Criterion ..... Pass
- Vehicle Stability ..... Satisfactory
- Vehicle Stopping Distance ..... 200 ft – 2 in. downstream, 25 ft – 10 in. laterally in front
- Vehicle Damage ..... Moderate
  - VDS [10] 11-LFQ-4
  - CDC [11] 11-LFEW-3
  - Maximum Interior Deformation ..... 1.6 in.
- Test Article Damage ..... Minimal
- Maximum Test Article Deflections
  - Permanent Set ..... 0.7 in.
  - Dynamic ..... 0.8 in.
  - Working Width ..... 15.5 in.
- Transducer Data

Evaluation Criteria		Transducer		MASH 2016 Limit
		SLICE-1 (primary)	SLICE-2	
OIV ft/s	Longitudinal	-21.49	-20.66	±40
	Lateral	27.89	26.20	±40
ORA g's	Longitudinal	-5.09	-5.06	±20.49
	Lateral	10.78	13.36	±20.49
MAX ANGULAR DISP. deg.	Roll	-9.3	-6.1	±75
	Pitch	3.0	2.4	±75
	Yaw	32.1	31.5	not required
THIV – ft/s		36.42	34.48	not required
PHD – g's		11.26	13.74	not required
ASI		1.91	1.84	not required

Figure 87. Summary of Test Results and Sequential Photographs, Test No. NCBR-2

7 HEAD EJECTION ANALYSIS

During test nos. NCBR-1 and NCBR-2, the dummy shifted laterally during impact, resulting in head contact with the side window. For both tests, the window glass disengaged from the door panel and was ejected laterally into the barrier system. Subsequently, the dummy's head extended outside of the occupant compartment and toward the aluminum railing on top of the concrete parapet. It was noted that for MASH 2016 occupant risk evaluation criteria, no shattering of a side window from direct contact with a structural member of the test article should occur. By extension, this requirement is because direct contact between a test article and the side window is believed to place an occupant's head at significantly elevated risk of contacting the test article, increasing potential for serious injury, even if an impact does not violate any other MASH 2016 evaluation criteria. Thus, occupant head ejection out of the occupant compartment resulting in direct contact between the occupant's head and a test article or structurally-stiff element should also be considered a pass/fail test evaluation criterion. Based on this conservative interpretation and extension of MASH 2016, MwRSF and UNCC researchers evaluated high-speed video, onboard digital video, and dummy kinesthetics to determine if the dummy's head impacted the test article during the full-scale tests.

Available video views rendered head ejection extent difficult to measure. Overhead, upstream, and downstream views were partially obscured because of light reflection and shadows, dust and paint fragments from point of impact (POI), and test debris. Using available views, the lateral head extension was estimated to be approximately 2 in. for test no. NCBR-1 and 6 in. for test no. NCBR-2.

Onboard high-speed footage for test nos. NCBR-1 and NCBR-2 is shown in Figures 88 through 91. Onboard camera views of the occupant's head movement are shown in Figures 92 through 95. For test no. NCBR-1, the maximum head protrusion occurred at 0.109 s, and a close-up view of maximum head extension is shown in Figure 94. For test no. NCBR-2, the maximum head protrusion occurred at 0.142 s, and is shown in Figure 95.

Video analysis of the velocity profile and positioning of the dummy's head during both tests suggested that head contact did not occur. The velocity profiles, taken from onboard views, were smooth and lacked any abrupt transitions in speed or position, which would have indicated an impact. Vehicle positions at 0.109 sec for test no. NCBR-1 and 0.142 sec for test no. NCBR-2 are shown in Figure 96. Although significant head protrusion was visible in the overhead video, the protrusion did not appear to overlap the rail in either test. It was concluded that the dummy did not contact the test article in either of test nos. NCBR-1 or NCBR-2. Therefore, both tests were deemed to have successfully passed MASH 2016 evaluation criteria, using a stringent interpretation of the occupant risk criteria.



Figure 88. Onboard High-Speed Footage, Test No. NCBR-1



Figure 89. Onboard High-Speed Footage, Test No. NCBR-1



Figure 90. Onboard High-Speed Footage, Test No. NCBR-2

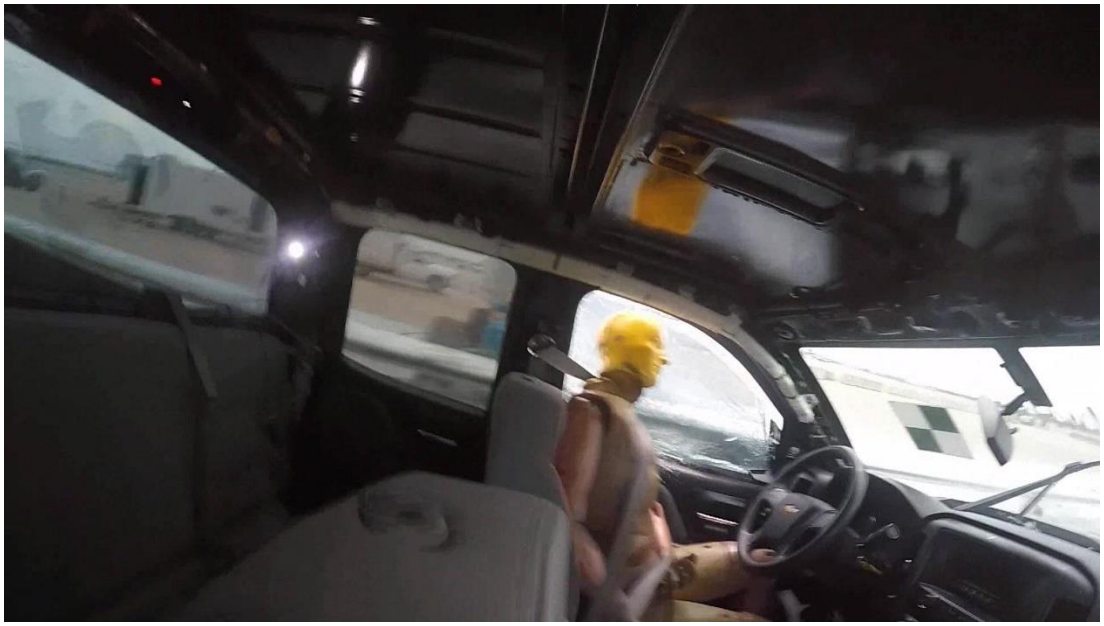


Figure 91. Onboard High-Speed Footage, Test No. NCBR-2



Figure 92. Occupant Head Movement, Test No. NCBR-1



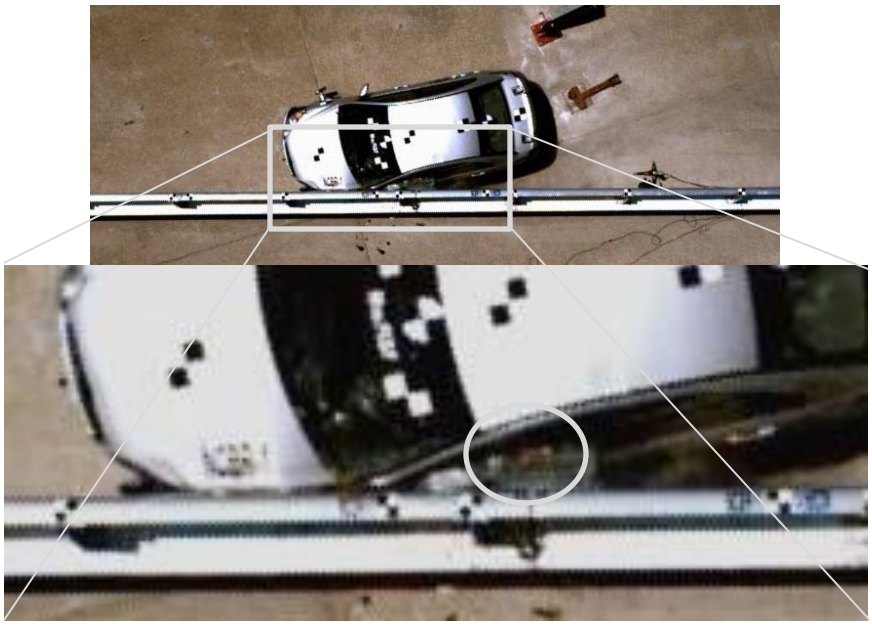
Figure 93. Occupant Head Movement, Test No. NCBR-2



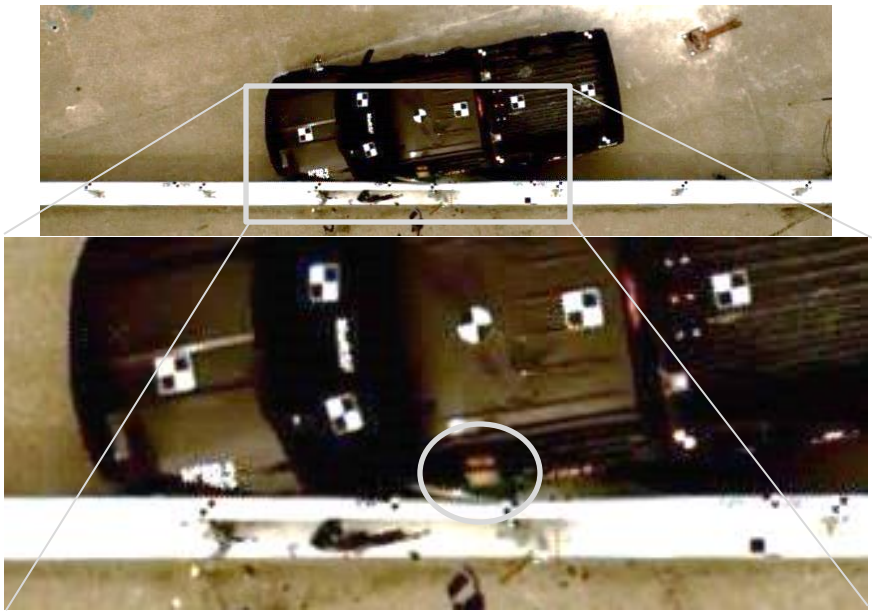
Figure 94. Maximum Occupant Head Protrusion, Test No. NCBR-1



Figure 95. Maximum Occupant Head Protrusion, Test No. NCBR-2



Test No. NCBR-1: 0.110 s



Test No. NCBR-2: 0.142 s

Figure 96. Vehicle Position and Dummy Head Protrusion at Maximum Dummy Movement, Test Nos. NCBR-1 and NCBR-2

8 SUMMARY AND CONCLUSIONS

In test no. NCBR-1, a 2,425-lb small car impacted the NCDOT two-bar metal rail system at 63.2 mph and an angle of 25.2 deg., resulting in an impact severity of 59.0 kip-ft and an estimated peak load of 57.7 kip on the system. Impact occurred 51.1 in. upstream from post no. 11, and the vehicle exited the system at 42.8 mph and an 8.5 deg. angle. The vehicle was successfully contained and smoothly redirected with minor damage to the barrier system and moderate damage to the vehicle. Windshield deformation was extreme, but not believed to violate MASH 2016 safety performance criteria, as it was measured several days after testing, allowing for settling to occur. All vehicle accelerations, ORAs, and OIVs fell within the recommended safety limits established in MASH 2016. Therefore, test no. NCBR-1 was successful according to the safety criteria of MASH 2016 test designation no. 3-10.

In test no. NCBR-2, a 5,018-lb quad cab pickup truck impacted the NCDOT two-bar metal rail system at 61.9 mph and a 24.9 deg. angle, resulting in an impact severity of 113.5 kip-ft and an estimated peak load of 89.9 kip on the system. Impact occurred $61^{7}/_{8}$ in. upstream from post no. 6, and the vehicle exited the system at 44.6 mph and an 8.8 deg. angle. The vehicle was successfully contained and smoothly redirected with minor damage to the barrier system and moderate damage to the vehicle. All vehicle accelerations, ORAs, and OIVs fell within the recommended safety limits established in MASH 2016. Therefore, test no. NCBR-2 was successful according to the safety criteria of MASH 2016 test designation no. 3-11. A summary of the test evaluations for test nos. NCBR-1 and NCBR-2 are shown in Table 8.

The bridge rail did not deflect, exhibit structural cracking, nor experience significant permanent set in the top-mounted aluminum rail. However, the bridge ends and upstream and downstream rail transitions were not evaluated in this project. At each end of the bridge rail, the longitudinal aluminum rails were terminated using ½-in. thick, L-shaped brackets bolted to the concrete parapet, and the rails were offset from the traffic-side face by 1 in. During both test nos. NCBR-1 and NCBR-2, contact was observed on the aluminum rail segments, indicating that vehicle components engaged the posts after extending over the top of the 30-in. tall concrete parapet. As a result, impacts near the downstream end of the bridge rail system could result in increased vehicle engagement with the vertical concrete buttress, which could contribute to increased occupant compartment crush. Further research may be required to evaluate the ends of the system. A MASH 2016-approved, TL-3 approach guardrail transition which is compatible and approved for use in combination with the end of the concrete buttresses is recommended.

Table 11. Summary of Safety Performance Evaluation

<table>
<tr><th>Evaluation Factors</th><th>Evaluation Criteria</th><th>Test No. NCBR-1</th><th>Test No. NCBR-2</th></tr>
<tr><td>Structural Adequacy</td><td>A. Test article should contain and redirect the vehicle or bring the vehicle to a controlled stop; the vehicle should not penetrate, underride, or override the installation, although controlled lateral deflection of the test article is acceptable.</td><td>S</td><td>S</td></tr>
<tr><td rowspan="4">Occupant Risk</td><td>D. 1. Detached elements, fragments, or other debris from the test article should not penetrate or show potential for penetrating the occupant compartment, or present an undue hazard to other traffic, pedestrians, or personnel in a work zone.</td><td>S</td><td>S</td></tr>
<tr><td>2. Deformations of, or intrusions into, the occupant compartment should not exceed limits set forth in Section 5.2.2 and Appendix E of MASH 2016.</td><td>S</td><td>S</td></tr>
<tr><td>F. The vehicle should remain upright during and after collision. The maximum roll and pitch angles are not to exceed 75 deg.</td><td>S</td><td>S</td></tr>
<tr><td>H. Occupant Impact Velocity (OIV) (see Appendix A, Section A5.2.2 of MASH 2016 for calculation procedure) should satisfy the following limits:
<table>
<tr><th colspan="3">Occupant Impact Velocity Limits</th></tr>
<tr><th>Component</th><th>Preferred</th><th>Maximum</th></tr>
<tr><td>Longitudinal and Lateral</td><td>30 ft/s</td><td>40 ft/s</td></tr>
</table></td><td>S</td><td>S</td></tr>
<tr><td>I. The Occupant Ridedown Acceleration (ORA) (see Appendix A, Section A5.2.2 of MASH 2016 for calculation procedure) should satisfy the following limits:
<table>
<tr><th colspan="3">Occupant Ridedown Acceleration Limits</th></tr>
<tr><th>Component</th><th>Preferred</th><th>Maximum</th></tr>
<tr><td>Longitudinal and Lateral</td><td>15.0 g’s</td><td>20.49 g’s</td></tr>
</table></td><td>S</td><td>S</td></tr>
<tr><td colspan="2">MASH 2016 Test Designation No.</td><td>3-10</td><td>3-11</td></tr>
<tr><td colspan="2">Final Evaluation (Pass or Fail)</td><td>Pass</td><td>Pass</td></tr>
</table>

S – Satisfactory U – Unsatisfactory NA - Not Applicable

9 MASH EVALUATION

The objective of this research was to evaluate the safety performance of NCDOT's two-bar metal bridge rail system. The system was tested at MASH 2016-compliant critical impact points selected by UNCC through simulation and verified by NCDOT. Test nos. NCBR-1 and NCBR-2 were conducted according to MASH 2016 test designation nos. 3-10 and 3-11, respectively. In both tests, the test vehicle was contained and smoothly redirected with minimal roll and pitch angular displacements. Damage to the system was minor and all ORA and OIV values were within MASH 2016 safety limits. The vehicle in test no. NCBR-1 experienced extreme windshield deformation, but this value was exaggerated due to settling in the time in between testing and measurement. No other occupant deformation limits were violated in either test.

Due to the success of test nos. NCBR-1 and NCBR-2, it was determined that impacts within the Length of Need (LON) of the two-bar bridge rail were crashworthy according to MASH 2016 TL-3 impact conditions.

10 REFERENCES

1. Ross, H.E., Sicking, D.L., Zimmer, R.A., and Michie, J.D., *NCHRP Report 350: Recommended Procedures for the Safety Performance Evaluation of Highway Features*, TRB, National Research Council, Washington, D.C., 1993.

2. *Manual for Assessing Safety Hardware, Second Edition*, American Association of State Highway and Transportation Officials (AASHTO), Washington, D.C., 2016.

3. *Manual for Assessing Safety Hardware*, American Association of State Highway and Transportation Officials (AASHTO), Washington, D.C., 2009.

4. *Structures Management Unit Manual: Chapter 6, Superstructures*, North Carolina Department of Transportation.

5. Hinch, J., Yang, T.L., and Owings, R., *Guidance Systems for Vehicle Testing*, ENSCO, Inc., Springfield, Virginia, 1986.

6. Singh, H., Ganesan, V., Davies, J., Paramasuwom, M., and Gradischnig, L., *Vehicle Interior and Restraints Modeling Development of Full Vehicle Finite Element Model Including Vehicle Interior and Occupant Restraints Systems For Occupant Safety Analysis Using THOR Dummies*, National Highway Traffic Safety Administration, May 2018.

7. MacInnis, D., Cliff, W., and Ising, K., *A Comparison of the Moment of Inertia Estimation Techniques for Vehicle Dynamics Simulation*, SAE Technical Paper Series – 970951, Society of Automotive Engineers, Inc., Warrendale, Pennsylvania, 1997.

8. *Center of Gravity Test Code* - SAE J874 March 1981, SAE Handbook Vol. 4, Society of Automotive Engineers, Inc., Warrendale, Pennsylvania, 1986.

9. Society of Automotive Engineers (SAE), *Instrumentation for Impact Test – Part 1 – Electronic Instrumentation*, SAE J211/1 MAR95, New York City, NY, July, 2007.

10. *Vehicle Damage Scale for Traffic Investigators*, Second Edition, Technical Bulletin No. 1, Traffic Accident Data (TAD) Project, National Safety Council, Chicago, Illinois, 1971.

11. *Collision Deformation Classification – Recommended Practice J224 March 1980*, Handbook Volume 4, Society of Automotive Engineers (SAE), Warrendale, Pennsylvania, 1985.

12. Gutierrez, D., Bielenberg, R.W., Faller, R.K., Reid, J.D., and Lechtenberg, K.A., *Development of MASH TL-3 Transition Between Guardrail and Portable Concrete Barriers*, Report No. TRP-03-300-14, Midwest Roadside Safety Facility, University of Nebraska–Lincoln, Lincoln, Nebraska, June 2014.

11 APPENDICES

Appendix A. NCDOT Standard Plans

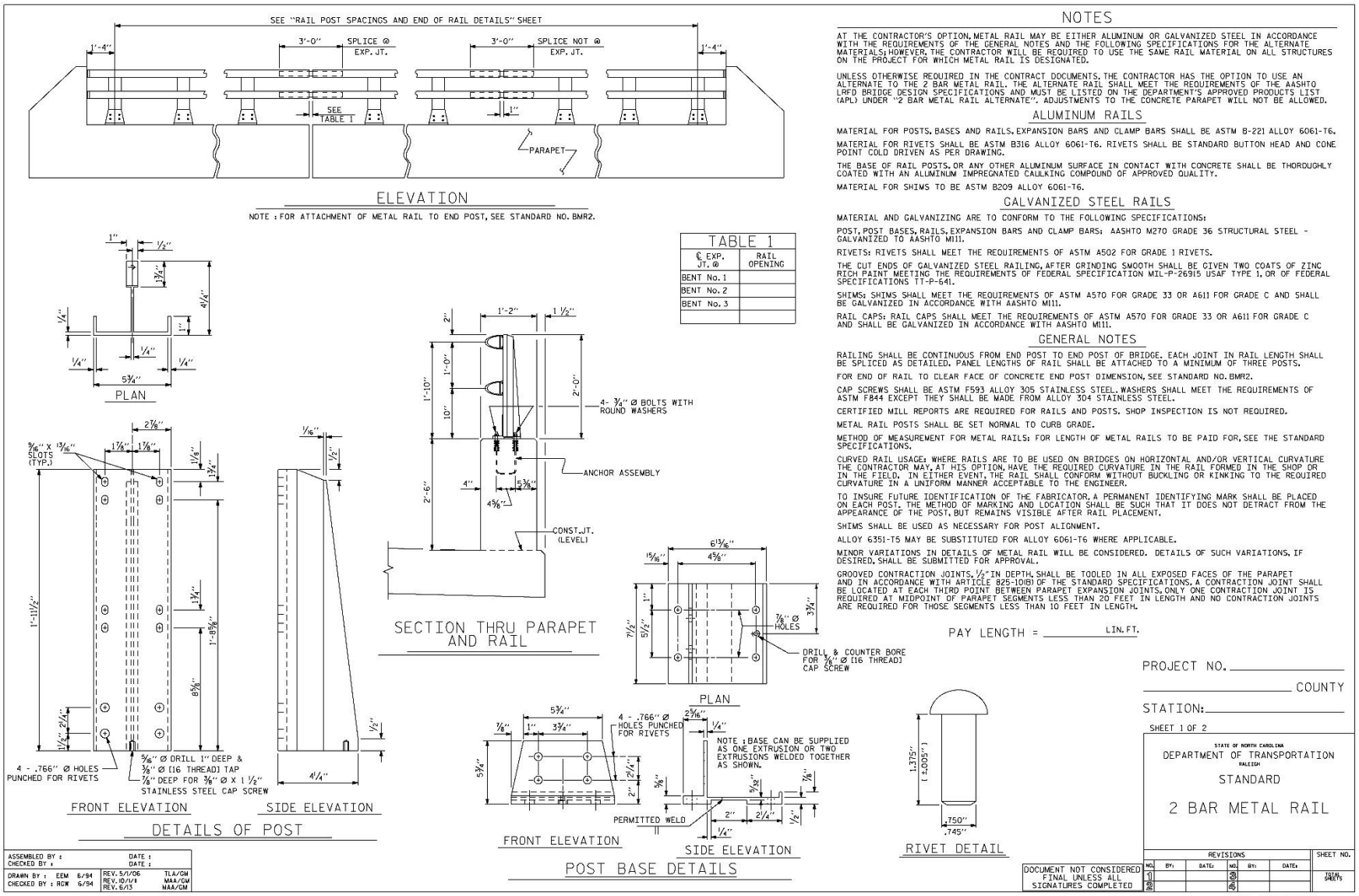


Figure A-1. NCDOT Design Standards of Two-Bar Metal Bridge Rail

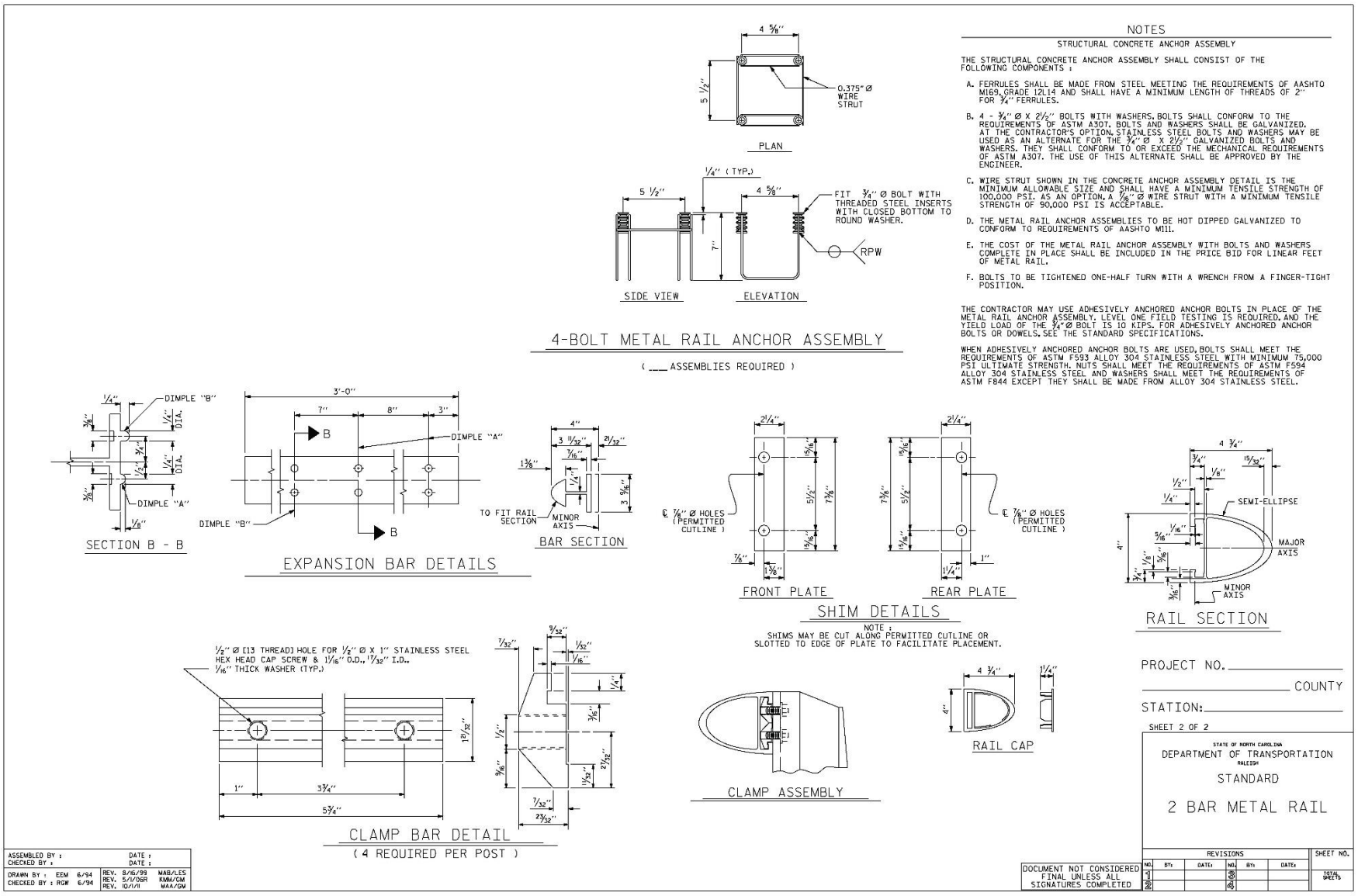


Figure A-2. NCDOT Design Standards of Two-Bar Metal Bridge Rail

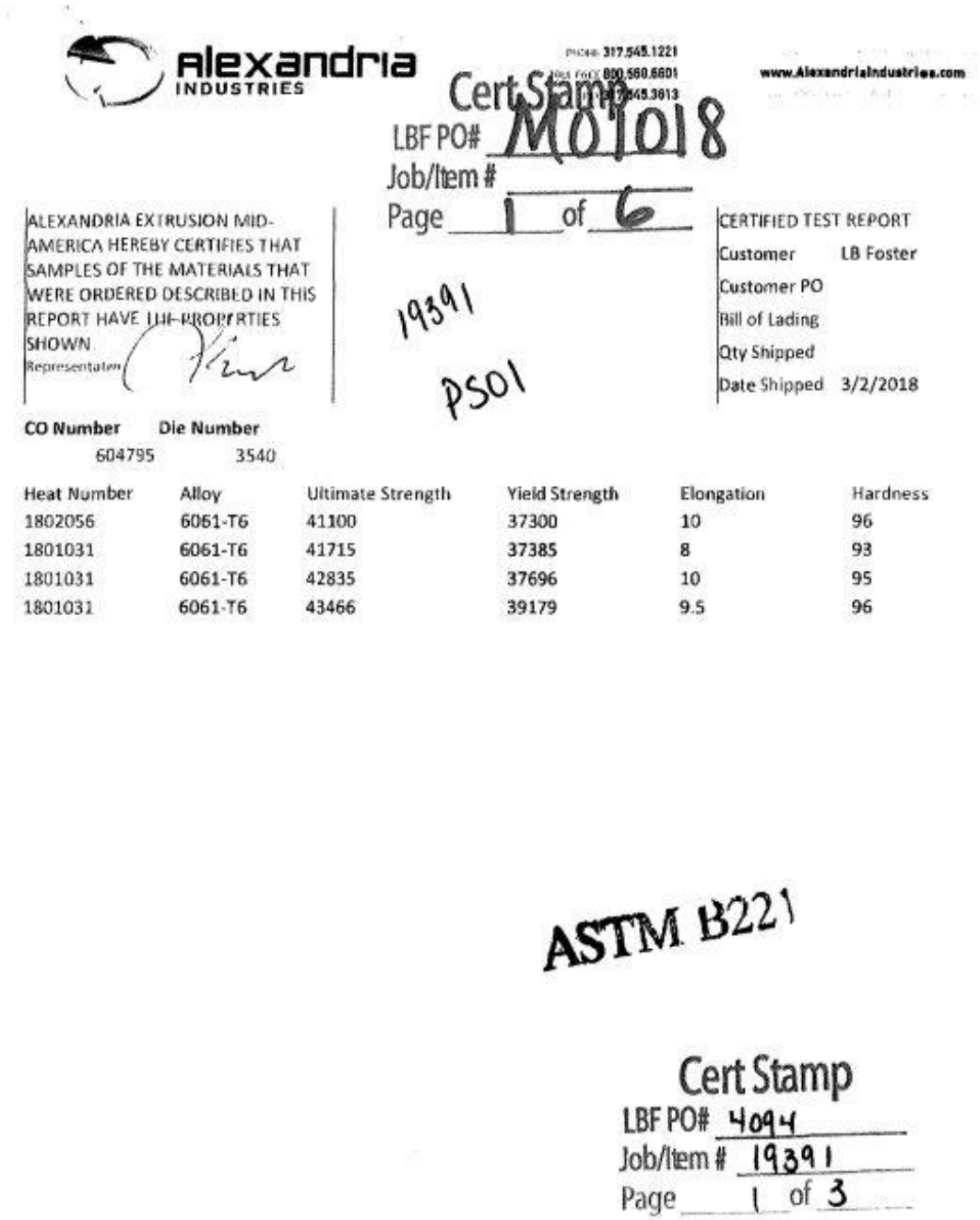
Appendix B. Material Specifications

Table B-1. Bill of Materials, Test Nos. NCBR-1 and NCBR-2

Item No.	Description	Material Specification	Certification
a1	5¾ in. x 4¼ in. x 23½ in. Long Post	ASTM B221 Alloy 6061-T6	H#1802056 or H#1801031 or H#1801065
a2	7½ in. x $3^{5}/_{16}$ x 5¾ in. Post Plate	ASTM B221 Alloy 6061-T6	H#1802056 or H#1801031 or H#1801065
a3	7½ in. x 3¼ in. x $^{7}/_{8}$ in. Post Plate	ASTM B221 Alloy 6061-T6	H#1802056 or H#1801031 or H#1801065
a4	5¾ in. x $1^{11}/_{16}$ in. x ¾ in. Clamp Bar	ASTM B221 Alloy 6061-T6	H#1802056 or H#1801031 or H#1801065
a5	¾ in. Threaded Ferrule	ASTM A108 Gr. 12L14	H#1820400
a6	$7^{3}/_{8}$ in. x 2¼ in. Front Shim	ASTM B209 Alloy 6061-T6	H#1802056 or H#1801031 or H#1801065
a7	$7^{3}/_{8}$ in. x 2¼ in. Rear Shim	ASTM B209 Alloy 6061-T6	H#1802056 or H#1801031 or H#1801065
b1	360 in. Long Elliptical Rail	ASTM B221 Alloy 6061-T6	H#1902024
b2	312½ in. Long Elliptical Rail	ASTM B221 Alloy 6061-T6	H#1902024
b3	11 in. x 4 in. x ½ in. Plate	ASTM A36	021137497
b4	4 in. x 4 in. x ½ in. Plate	ASTM A36	021137497
b5	4¼ in. x 4 in. x 1¼ in. Rail Cap	ASTM B221 Alloy 6061-T6	H#1802056 or H#1801031 or H#1801065
b6	36 in. x $3^{9}/_{16}$ in. x $3\ ^{5}/_{8}$ in. Expansion Bar	ASTM B221 Alloy 6061-T6	H#1802056 or H#1801031 or H#1801065
c1	Concrete	-	
c2	Concrete	-	
c3	Concrete	-	
c4	$^{3}/_{8}$ in. Dia. Wire Strut, 6¾ in. Long	Min. Tensile Strength = 100,000 psi	-
c5	$^{3}/_{8}$ in. Dia. Wire Strut, $15^{15}/_{16}$ in. Long Unbent	Min. Tensile Strength = 100,000 psi	-
c6	#5 Bar, 59½ in. Long Unbent	ASTM A615 Gr. 60	H#57177640
c7	#5 Bar, 355 in. Long	ASTM A615 Gr. 60	H#57177640

Table B-1. Bill of Materials, Test Nos. NCBR-1 and NCBR-2, Cont.

Item No.	Description	Material Specification	Certification
c8	#5 Bar, 356 in. Long	ASTM A615 Gr. 60	H#57177640
c9	#5 Bar, 36 in. Long	ASTM A615 Gr. 60	H#1810025501
c10	#5 Bar, 49½ in. Long Unbent	ASTM A615 Gr. 60	H#57177640
c11	#6 Bar, 22 in. Long	ASTM A615 Gr. 60	H#KN17101898
c12	#6 Bar, 40 in. Long	ASTM A615 Gr. 60	H#KN17101898
c13	#6 Bar, 43¼ in. Long	ASTM A615 Gr. 60	H#KN17101898
c14	#7 Bar, 31 in. Long	ASTM A615 Gr. 60	H#57165810
c15	#7 Bar, 36½ in. Long	ASTM A615 Gr. 60	H#57165810
c16	#7 Bar, 42 in. Long	ASTM A615 Gr. 60	H#57165810
c17	#7 Bar, 47½ in. Long	ASTM A615 Gr. 60	H#57165810
c18	#7 Bar, 52 in. Long	ASTM A615 Gr. 60	H#57165810
d1	¾ in. Dia., 1 $^{3}/_{8}$ in. Long Rivet	ASTM B316 Alloy 6061-T6	H#1801065
d2	¾ in. Dia., 6½ in. Long Hex Head Drill-In Anchor	ASTM A36	COC
d3	¾ in.-10 UNC, 2½ in. Long Hex Bolt	ASTM F3125 Gr. A325 Type I	Lot 798156
d4	$^{3}/_{8}$ in.-16 UNC, 1½ in. Long Cap Screw	ASTM F593 Alloy 305 Stainless Steel	H#205Y Certificate#60221G
d5	½ in.-13 UNC, 1¼ in. Long Hex Head Cap Screw	ASTM F593 Alloy 305 Stainless Steel	H#205Y Certificate#60221G
d6	½ in.-13 UNC, 1 in. Long Hex Head Cap Screw	ASTM F593 Alloy 305 Stainless Steel	H#205Y Certificate #60221G
e1	¾ in. Dia. Plain USS Washer	ASTM F436	H#281047
e2	¾ in. Dia. Plain SAE Washer	ASTM F436	H#A56620
e3	½ in. Dia. Plain SAE Washer	ASTM F844 Alloy 304 Stainless Steel	Coil 037VM5 H#7VM9
-	Ultrabond 1 Adhesive	ASTM C881 Type I, II, IV & V Gr. 3, Class A, B & C	Lot 1881003027



Alexandria INDUSTRIES

PHONE: 317.545.1221
FAX TOLL FREE: 800.560.6601
317.545.3913
www.AlexandriaIndustries.com

Cert Stamp
LBF PO# M01018
Job/Item #
Page 1 of 6

ALEXANDRIA EXTRUSION MID-AMERICA HEREBY CERTIFIES THAT SAMPLES OF THE MATERIALS THAT WERE ORDERED DESCRIBED IN THIS REPORT HAVE THE PROPERTIES SHOWN.
Representative

19391
PS01

CERTIFIED TEST REPORT
Customer LB Foster
Customer PO
Bill of Lading
Qty Shipped
Date Shipped 3/2/2018

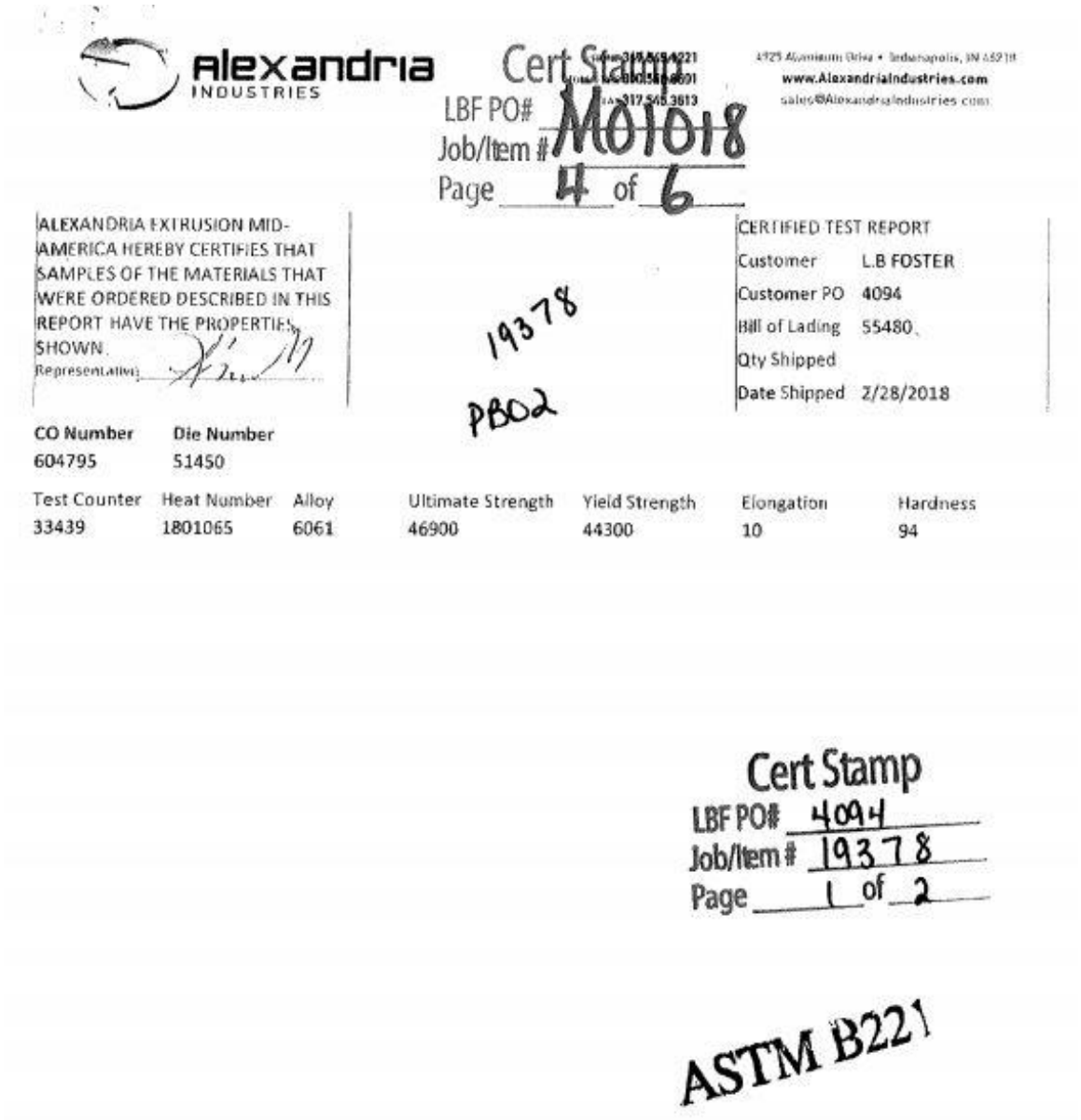
CO Number	Die Number
604795	3540

Heat Number	Alloy	Ultimate Strength	Yield Strength	Elongation	Hardness
1802056	6061-T6	41100	37300	10	96
1801031	6061-T6	41715	37385	8	93
1801031	6061-T6	42835	37696	10	95
1801031	6061-T6	43466	39179	9.5	96

ASTM B221

Cert Stamp
LBF PO# 4094
Job/Item # 19391
Page 1 of 3

Figure B-1. Aluminum Parts, Test Nos. NCBR-1 and NCBR-2



alexandria INDUSTRIES

4925 Aluminum Drive • Indianapolis, IN 46218
www.AlexandriaIndustries.com
sales@AlexandriaIndustries.com

Cert Stamp
LBF PO# M01018
Job/Item # 4 of 6
Page

ALEXANDRIA EXTRUSION MID-AMERICA HEREBY CERTIFIES THAT SAMPLES OF THE MATERIALS THAT WERE ORDERED DESCRIBED IN THIS REPORT HAVE THE PROPERTIES SHOWN.
Representative:

19378
PB02

CERTIFIED TEST REPORT

Customer	L.B FOSTER
Customer PO	4094
Bill of Lading	55480
Qty Shipped	
Date Shipped	2/28/2018

CO Number	Die Number
604795	51450

Test Counter	Heat Number	Alloy	Ultimate Strength	Yield Strength	Elongation	Hardness
33439	1801065	6061	46900	44300	10	94

Cert Stamp
LBF PO# 4094
Job/Item # 19378
Page 1 of 2

ASTM B221

Figure B-2. Additional Aluminum Parts, Test Nos. NCBR-1 and NCBR-2

MeadowBurke
A CRH COMPANY

Certificate of Origin

Sold to: L. B. FOSTER CO.
Shipped to: L. B. FOSTER CO.
BEDFROD, PA 15522

Purchase Order: 4578
MB Order Number: S480432

This document certifies that all products listed in the table below are manufactured by Meadow Burke, LLC in the United States, using steel manufactured in the United States from domestically produced billets.

Part Number	Description
MB432127303	GRD RL IN(4) 3/4" X 2.5" .02 FERRULES SPECIAL
	H=7" D=4-5/8" W=5-1/2" HDG RETAP

12-10-18

VP of Operations – Jason Tebeau — Date

VP of Engineering – Michael Recker

Meadow Burke, LLC

Cert Stamp
LBF PO# 4578
Job/Item # 31478
Page 1 of 3

Figure B-3. ¾ in. Threaded Ferrule, Test Nos. NCBR-1 and NCBR-2

ALEXANDRIA EXTRUSION MID-AM
4925 ALUMINUM DRIVE
INDIANAPOLIS, IN 46218
(317) 545-1221

Packing list number 408010 Page 2
3/28/19 14:50:29

Shipped from:
Company . . . : 6 ALEX EXT MID-AM Ship Date . . . : 3/28/19
Warehouse . . : 6 Shipment number : 19255

Ship to . : Midwest Roadside Safety Facility
4630 NW 36TH Street
LINCOLN NE 68524
United States of America

Carrier/pro number	Truck/trailer number	Gross weight	U/M
CPU		723.176	LB

Shipping instructions : CPU

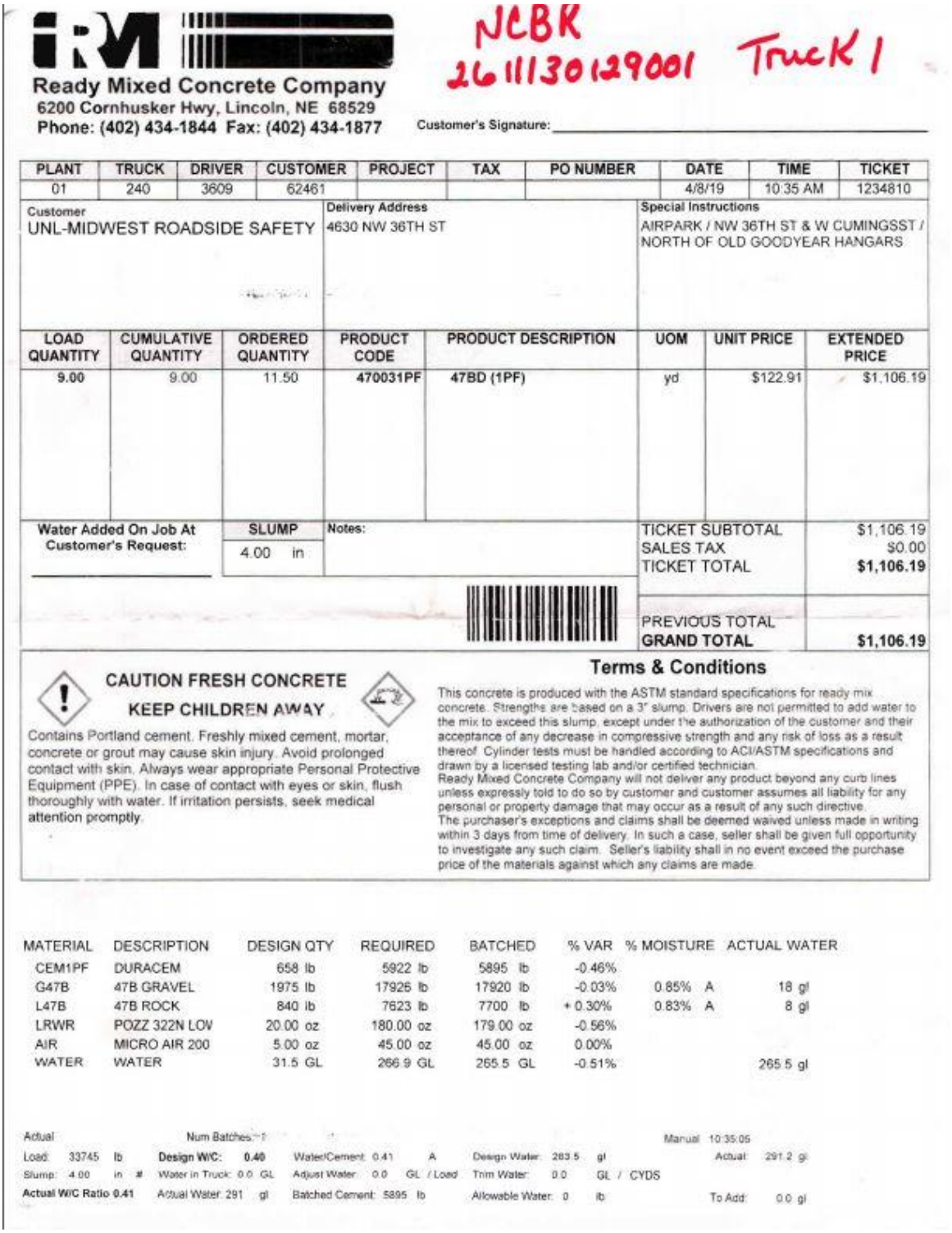
AR1164

ALL BUNDLES MUST BE
MARKED WITH PO 269157 AND
AR1164

Item number	Rel	Item description	Packed qty/ Backorder qty	U/M
00654034	1	BARRIER RAIL SEMI-EL	2.000	EA
654-30'		BARRIER RAIL SEMI-EL	.000	EA
00654209	1	BARRIER RAIL SEMI-EL	4.000	EA
654-26'-0 1/2"		BARRIER RAIL SEMI-EL	.000	EA

** End of list **

Figure B-4. Longitudinal Elliptical Rails, Test Nos. NCBR-1 and NCBR-2



Ready Mixed Concrete Company
6200 Cornhusker Hwy, Lincoln, NE 68529
Phone: (402) 434-1844 Fax: (402) 434-1877

NCBR
261113012900 1 Truck 1

Customer's Signature: _____

PLANT	TRUCK	DRIVER	CUSTOMER	PROJECT	TAX	PO NUMBER	DATE	TIME	TICKET
01	240	3609	62461				4/8/19	10:35 AM	1234810

Customer	Delivery Address	Special Instructions
UNL-MIDWEST ROADSIDE SAFETY	4630 NW 36TH ST	AIRPARK / NW 36TH ST & W CUMINGSST / NORTH OF OLD GOODYEAR HANGARS

LOAD QUANTITY	CUMULATIVE QUANTITY	ORDERED QUANTITY	PRODUCT CODE	PRODUCT DESCRIPTION	UOM	UNIT PRICE	EXTENDED PRICE
9.00	9.00	11.50	470031PF	47BD (1PF)	yd	$122.91	$1,106.19

Water Added On Job At Customer's Request:	SLUMP	Notes:		
	4.00 in		TICKET SUBTOTAL	$1,106.19
			SALES TAX	$0.00
			TICKET TOTAL	**$1,106.19**
			PREVIOUS TOTAL	
			GRAND TOTAL	**$1,106.19**

CAUTION FRESH CONCRETE
KEEP CHILDREN AWAY

Contains Portland cement. Freshly mixed cement, mortar, concrete or grout may cause skin injury. Avoid prolonged contact with skin. Always wear appropriate Personal Protective Equipment (PPE). In case of contact with eyes or skin, flush thoroughly with water. If irritation persists, seek medical attention promptly.

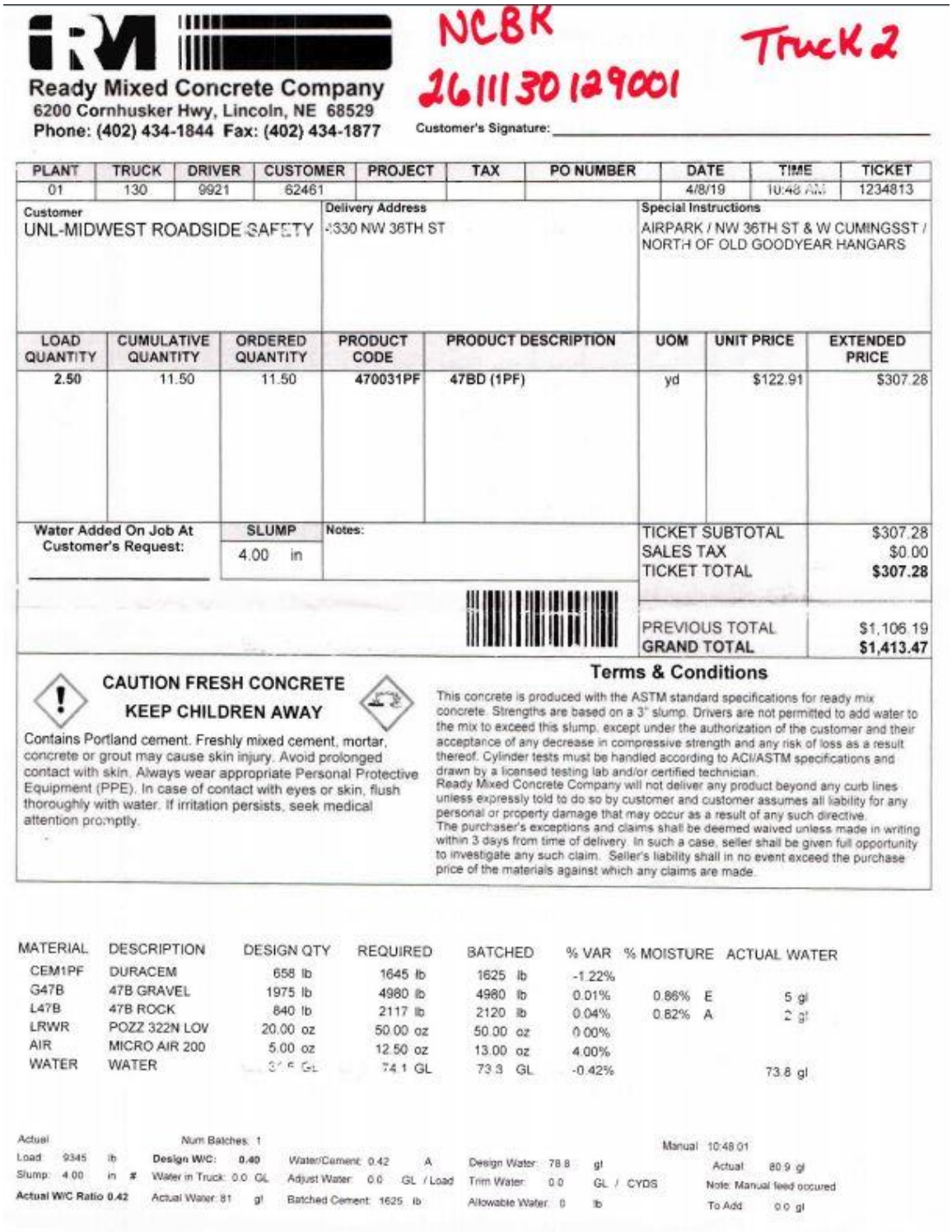
Terms & Conditions

This concrete is produced with the ASTM standard specifications for ready mix concrete. Strengths are based on a 3" slump. Drivers are not permitted to add water to the mix to exceed this slump, except under the authorization of the customer and their acceptance of any decrease in compressive strength and any risk of loss as a result thereof. Cylinder tests must be handled according to ACI/ASTM specifications and drawn by a licensed testing lab and/or certified technician.
Ready Mixed Concrete Company will not deliver any product beyond any curb lines unless expressly told to do so by customer and customer assumes all liability for any personal or property damage that may occur as a result of any such directive.
The purchaser's exceptions and claims shall be deemed waived unless made in writing within 3 days from time of delivery. In such a case, seller shall be given full opportunity to investigate any such claim. Seller's liability shall in no event exceed the purchase price of the materials against which any claims are made.

MATERIAL	DESCRIPTION	DESIGN QTY	REQUIRED	BATCHED	% VAR	% MOISTURE	ACTUAL WATER
CEM1PF	DURACEM	658 lb	5922 lb	5895 lb	-0.46%		
G47B	47B GRAVEL	1975 lb	17925 lb	17920 lb	-0.03%	0.85% A	18 gl
L47B	47B ROCK	840 lb	7623 lb	7700 lb	+0.30%	0.83% A	8 gl
LRWR	POZZ 322N LOW	20.00 oz	180.00 oz	179.00 oz	-0.56%		
AIR	MICRO AIR 200	5.00 oz	45.00 oz	45.00 oz	0.00%		
WATER	WATER	31.5 GL	266.9 GL	265.5 GL	-0.51%		265.5 gl

Actual — Num Batches: 1 — Manual 10:35:05
Load: 33745 lb — Design W/C: 0.40 — Water/Cement: 0.41 A — Design Water: 283.5 gl — Actual: 291.2 gl
Slump: 4.00 in # — Water in Truck: 0.0 GL — Adjust Water: 0.0 GL / Load — Trim Water: 0.0 GL / CYDS
Actual W/C Ratio 0.41 — Actual Water: 291 gl — Batched Cement: 5895 lb — Allowable Water: 0 lb — To Add: 0.0 gl

Figure B-5. Concrete, Test Nos. NCBR-1 and NCBR-2



Ready Mixed Concrete Company
6200 Cornhusker Hwy, Lincoln, NE 68529
Phone: (402) 434-1844 Fax: (402) 434-1877

NCBR
261130129001
Truck 2

Customer's Signature: _____

PLANT	TRUCK	DRIVER	CUSTOMER	PROJECT	TAX	PO NUMBER	DATE	TIME	TICKET
01	130	9921	62461				4/8/19	10:48 AM	1234813

Customer	Delivery Address	Special Instructions
UNL-MIDWEST ROADSIDE SAFETY	4330 NW 36TH ST	AIRPARK / NW 36TH ST & W CUMINGSST / NORTH OF OLD GOODYEAR HANGARS

LOAD QUANTITY	CUMULATIVE QUANTITY	ORDERED QUANTITY	PRODUCT CODE	PRODUCT DESCRIPTION	UOM	UNIT PRICE	EXTENDED PRICE
2.50	11.50	11.50	470031PF	47BD (1PF)	yd	$122.91	$307.28

Water Added On Job At Customer's Request: _____

SLUMP: 4.00 in

Notes:

TICKET SUBTOTAL	$307.28
SALES TAX	$0.00
TICKET TOTAL	**$307.28**
PREVIOUS TOTAL	$1,106.19
GRAND TOTAL	**$1,413.47**

CAUTION FRESH CONCRETE
KEEP CHILDREN AWAY

Contains Portland cement. Freshly mixed cement, mortar, concrete or grout may cause skin injury. Avoid prolonged contact with skin. Always wear appropriate Personal Protective Equipment (PPE). In case of contact with eyes or skin, flush thoroughly with water. If irritation persists, seek medical attention promptly.

Terms & Conditions

This concrete is produced with the ASTM standard specifications for ready mix concrete. Strengths are based on a 3" slump. Drivers are not permitted to add water to the mix to exceed this slump, except under the authorization of the customer and their acceptance of any decrease in compressive strength and any risk of loss as a result thereof. Cylinder tests must be handled according to ACI/ASTM specifications and drawn by a licensed testing lab and/or certified technician.
Ready Mixed Concrete Company will not deliver any product beyond any curb lines unless expressly told to do so by customer and customer assumes all liability for any personal or property damage that may occur as a result of any such directive.
The purchaser's exceptions and claims shall be deemed waived unless made in writing within 3 days from time of delivery. In such a case, seller shall be given full opportunity to investigate any such claim. Seller's liability shall in no event exceed the purchase price of the materials against which any claims are made.

MATERIAL	DESCRIPTION	DESIGN QTY	REQUIRED	BATCHED	% VAR	% MOISTURE	ACTUAL WATER
CEM1PF	DURACEM	658 lb	1645 lb	1625 lb	-1.22%		
G47B	47B GRAVEL	1975 lb	4980 lb	4980 lb	0.01%	0.86% E	5 gl
L47B	47B ROCK	840 lb	2117 lb	2120 lb	0.04%	0.82% A	2 gl
LRWR	POZZ 322N LOV	20.00 oz	50.00 oz	50.00 oz	0.00%		
AIR	MICRO AIR 200	5.00 oz	12.50 oz	13.00 oz	4.00%		
WATER	WATER	31.6 GL	74.1 GL	73.3 GL	-0.42%		73.8 gl

Actual
Load 9345 lb
Slump 4.00 in #
Actual W/C Ratio 0.42

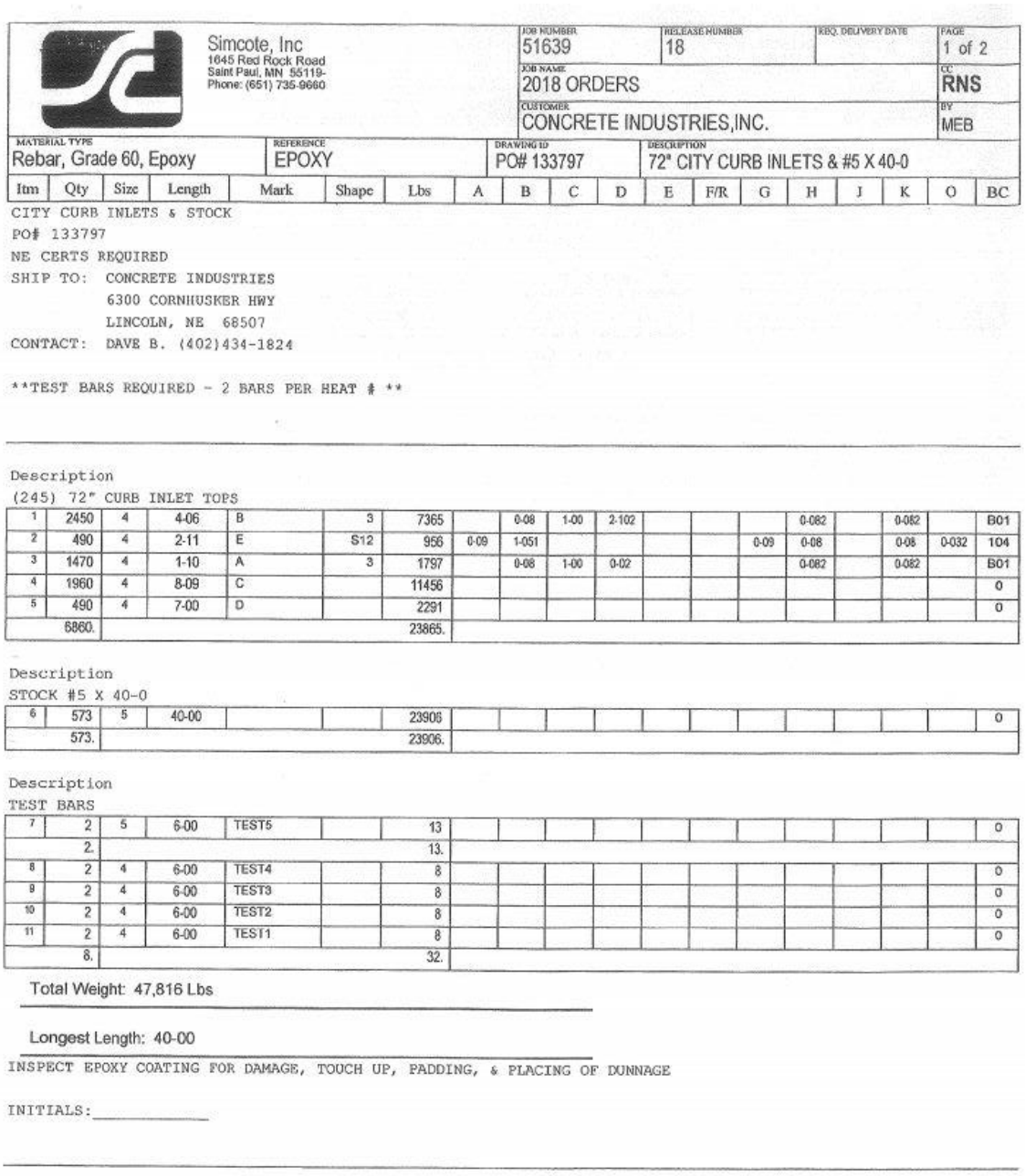
Num Batches: 1
Design W/C: 0.40
Water in Truck: 0.0 GL
Actual Water: 81 gl

Water/Cement: 0.42 A
Adjust Water: 0.0 GL / Load
Batched Cement: 1625 lb

Design Water: 78.8 gl
Trim Water: 0.0 GL / CYDS
Allowable Water: 0 lb

Manual 10:48:01
Actual 80.9 gl
Note: Manual feed occured
To Add 0.0 gl

Figure B-6. Concrete, Test Nos. NCBR-1 and NCBR-2



Simcote, Inc
1645 Red Rock Road
Saint Paul, MN 55119-
Phone: (651) 735-9660

JOB NUMBER	RELEASE NUMBER	REQ. DELIVERY DATE	PAGE
51639	18		1 of 2

JOB NAME: 2018 ORDERS
CC: RNS
CUSTOMER: CONCRETE INDUSTRIES,INC.
BY: MEB

MATERIAL TYPE	REFERENCE	DRAWING ID	DESCRIPTION
Rebar, Grade 60, Epoxy	EPOXY	PO# 133797	72" CITY CURB INLETS & #5 X 40-0

Itm	Qty	Size	Length	Mark	Shape	Lbs	A	B	C	D	E	F/R	G	H	J	K	O	BC
CITY CURB INLETS & STOCK																		
PO# 133797																		
NE CERTS REQUIRED																		
SHIP TO: CONCRETE INDUSTRIES																		
6300 CORNHUSKER HWY																		
LINCOLN, NE 68507																		
CONTACT: DAVE B. (402)434-1824																		
**TEST BARS REQUIRED - 2 BARS PER HEAT # **																		
Description																		
(245) 72" CURB INLET TOPS																		
1	2450	4	4-06	B	3	7365		0-08	1-00	2-102				0-082		0-082		B01
2	490	4	2-11	E	S12	956	0-09	1-051					0-09	0-08		0-08	0-032	104
3	1470	4	1-10	A	3	1797		0-08	1-00	0-02				0-082		0-082		B01
4	1960	4	8-09	C		11456												0
5	490	4	7-00	D		2291												0
	6860.					23865.												
Description																		
STOCK #5 X 40-0																		
6	573	5	40-00			23906												0
	573.					23906.												
Description																		
TEST BARS																		
7	2	5	6-00	TEST5		13												0
	2.					13.												
8	2	4	6-00	TEST4		8												0
9	2	4	6-00	TEST3		8												0
10	2	4	6-00	TEST2		8												0
11	2	4	6-00	TEST1		8												0
	8.					32.												

Total Weight: 47,816 Lbs

Longest Length: 40-00

INSPECT EPOXY COATING FOR DAMAGE, TOUCH UP, PADDING, & PLACING OF DUNNAGE

INITIALS:_____

Figure B-7. #5 Bar, Test Nos. NCBR-1 and NCBR-2

ABC COATING CO. OF ILLINOIS, INC.

1160 N. BOUDREAU ROAD
MANTENO, IL 60950
(708) 258-9633

AN ACUÑA CO.

DATE:	3/5/2018	CONTRACTOR:	Carroll Distributing
OUR JOB NO:	IL-8165	COUNTY:	
CUSTOMER:	Adelphia Metals, LLC	PROJECT NO:	SO# 222984
CUSTOMER PO NO:	822859/822844/5180	JOB NO:	2018 Stock

We certify that the following described bar material has been cleaned, coated with 3 M #413 or Nap-gard 7-2719, 7-2750 or Valspar 720A009 Powder inspected in accordance with and meets the specification requirements of the Iowa Department of Transportation and ASTM A775-17 AASHTO M284-06, ASTM D3963-01. Manufacturer's Certifications for the bar material and epoxy resin used are on file.

Mill	Lot/Heat	Powder	Size	Weight
Nucor GR 60	KN1810000601	3777133B	4/13	11,904
Nucor GR 60	KN1810025501	3804648	5/18	28,912
Nucor GR 60	KN1710201402	3649393	8/25	6,168
				45,984

Certifications for the listed material and resin are attached
STATE OF ILLINOIS)
COUNTY OF COOK)

OFFICIAL SEAL
FREDDIE ROCHA
NOTARY PUBLIC, STATE OF ILLINOIS
COOK COUNTY
MY COMMISSION EXPIRES 03/31/2018

Thomas Greenfield, Vice President
SUBSCRIBED AND SWORN BEFORE ME, a Notary Public in and for Cook County, Illinois, on this 5th day of March 2018

My commission expires 03-31-2018

Notary Public in and for Chicago, Illinois

CRSI MEMBER

Figure B-8. #5 Bar, 36 in. Long, Test Nos. NCBR-1 and NCBR-2

Simcote, Inc
1645 Red Rock Road
Saint Paul, MN 55119-
Phone: (651) 735-9660

JOB NUMBER	RELEASE NUMBER	REQ. DELIVERY DATE	PAGE
51639	16		1 of 2

JOB NAME: 2018 ORDERS — QC: QDM
CUSTOMER: CONCRETE INDUSTRIES,INC. — BY: Jud

MATERIAL TYPE	REFERENCE	DRAWING ID	DESCRIPTION
Rebar, Grade 60, Epoxy	EPOXY STOCK	PO# 133016	#3, 4, 5, & 6 STOCK STRAIGHT BAR

#3, 4 & 5 X 20' & #6 X 40' EPOXY STRAIGHT BAR
PO# 133016
NE CERTS REQUIRED
SHIP TO: CONCRETE INDUSTRIES
6300 CORNHUSKER HWY
LINCOLN, NE 68507
CONTACT: DAVE BORCHERS (402)434-1824

**TEST BARS REQUIRED - 2 BARS PER HEAT # **

Itm	Qty	Size	Length	Mark	Shape	Lbs	A	B	C	D	E	F/R	G	H	J	K	O	BC
1	256	6	40-00			15380												0
	256.					15380.												
2	1000	5	20-00			20860												0
	1000.					20860.												
3	600	4	20-00			8016												0
	600.					8016.												
4	500	3	20-00			3760												0
	500.					3760.												

Description
TEST BARS

5	2	6	6-00	TEST6		18												0
	2.					18.												
6	2	5	6-00	TEST5		13												0
	2.					13.												
7	2	4	6-00	TEST4		8												0
	2.					8.												
8	2	3	6-00	TEST3		5												0
	2.					5.												

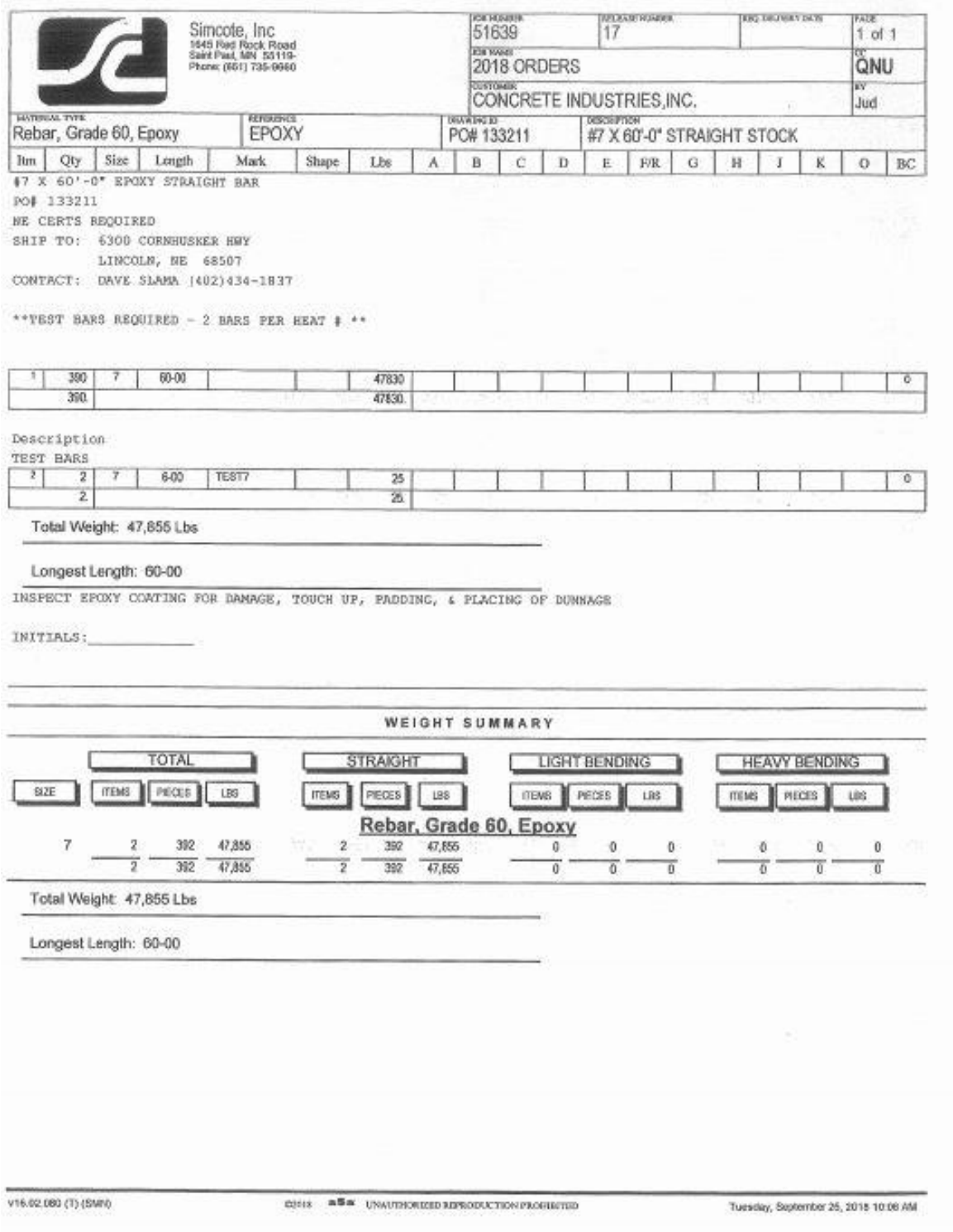
Total Weight: 48,060 Lbs

Longest Length: 40-00

INSPECT EPOXY COATING FOR DAMAGE, TOUCH UP, PADDING, & PLACING OF DUNNAGE

INITIALS:_____

Figure B-9. #6 Bar, Test Nos. NCBR-1 and NCBR-2



Simcote, Inc
1645 Red Rock Road
Saint Paul, MN 55119-
Phone: (651) 735-9960

JOB NUMBER	RELEASE NUMBER	REQ. DELIVERY DATE	PAGE
51639	17		1 of 1
JOB NAME			QC
2018 ORDERS			QNU
CUSTOMER			BY
CONCRETE INDUSTRIES,INC.			Jud

MATERIAL TYPE	REFERENCE	DRAWING ID	DESCRIPTION
Rebar, Grade 60, Epoxy	EPOXY	PO# 133211	#7 X 60'-0" STRAIGHT STOCK

Itm	Qty	Size	Length	Mark	Shape	Lbs	A	B	C	D	E	F/R	G	H	J	K	O	BC
#7 X 60'-0" EPOXY STRAIGHT BAR																		
PO# 133211																		
NE CERTS REQUIRED																		
SHIP TO: 6300 CORNHUSKER HWY																		
LINCOLN, NE 68507																		
CONTACT: DAVE SLAMA (402)434-1837																		
**TEST BARS REQUIRED - 2 BARS PER HEAT # **																		
1	390	7	60-00			47830												0
	390					47830												
Description																		
TEST BARS																		
2	2	7	6-00	TEST7		25												0
	2					25												

Total Weight: 47,855 Lbs

Longest Length: 60-00

INSPECT EPOXY COATING FOR DAMAGE, TOUCH UP, PADDING, & PLACING OF DUNNAGE

INITIALS:_____

WEIGHT SUMMARY

Rebar, Grade 60, Epoxy

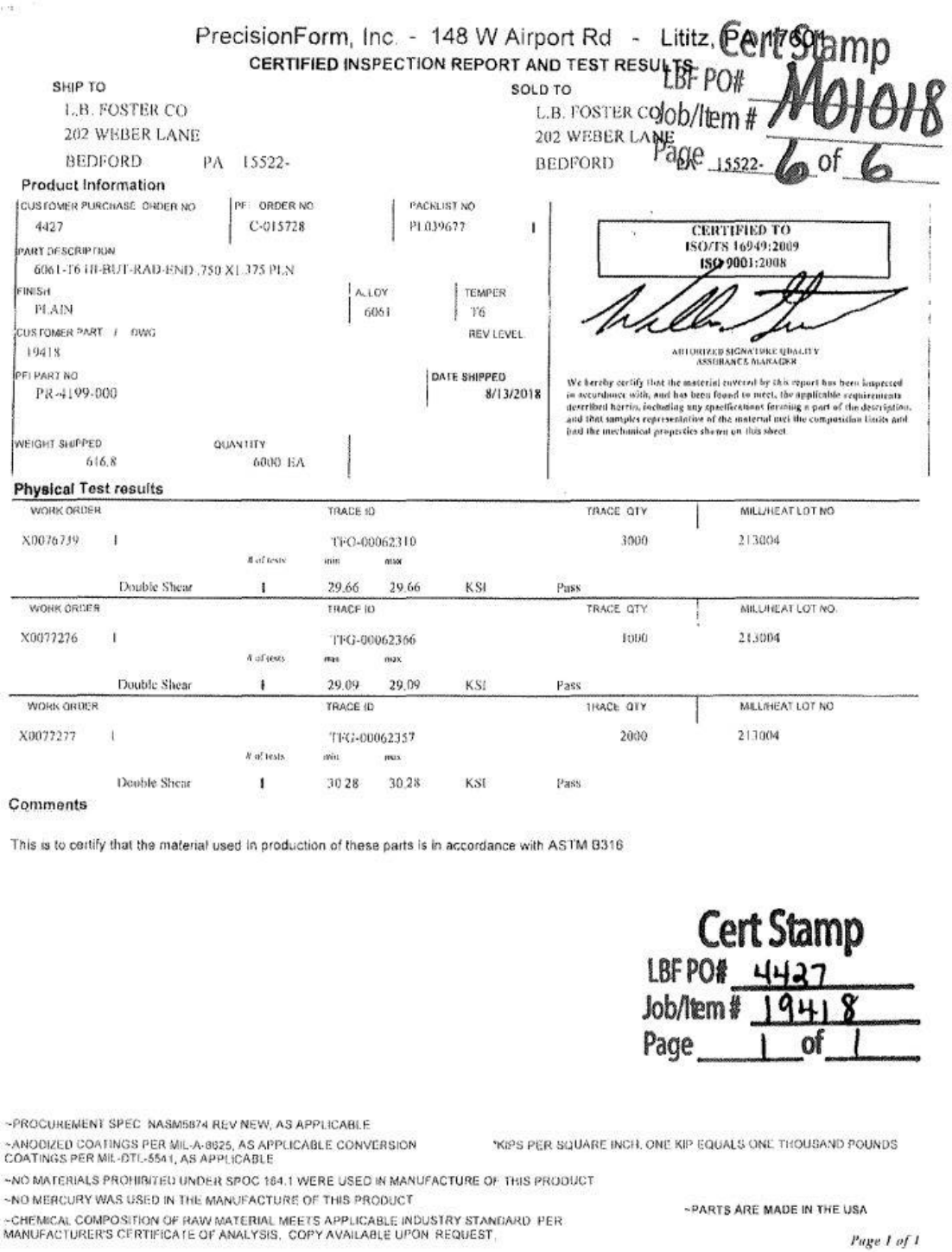
SIZE	TOTAL ITEMS	TOTAL PIECES	TOTAL LBS	STRAIGHT ITEMS	STRAIGHT PIECES	STRAIGHT LBS	LIGHT BENDING ITEMS	LIGHT BENDING PIECES	LIGHT BENDING LBS	HEAVY BENDING ITEMS	HEAVY BENDING PIECES	HEAVY BENDING LBS
7	2	392	47,855	2	392	47,855	0	0	0	0	0	0
	2	392	47,855	2	392	47,855	0	0	0	0	0	0

Total Weight: 47,855 Lbs

Longest Length: 60-00

V16.02.080 (T) (SWI) ©2018 aSa UNAUTHORIZED REPRODUCTION PROHIBITED Tuesday, September 25, 2018 10:06 AM

Figure B-10. #7 Bar, Test Nos. NCBR-1 and NCBR-2



PrecisionForm, Inc. - 148 W Airport Rd - Lititz, PA 17543

CERTIFIED INSPECTION REPORT AND TEST RESULTS

Cert Stamp
LBF PO# M01018
Job/Item #
Page 6 of 6

SHIP TO
L.B. FOSTER CO
202 WEBER LANE
BEDFORD PA 15522-

SOLD TO
L.B. FOSTER CO
202 WEBER LANE
BEDFORD PA 15522-

Product Information

CUSTOMER PURCHASE ORDER NO	PFI ORDER NO	PACKLIST NO
4427	C-015728	PL039677 1

PART DESCRIPTION: 6061-T6 HI-BUT-RAD-END .750 X1.375 PLN

FINISH	ALLOY	TEMPER	REV LEVEL
PLAIN	6061	T6	

CUSTOMER PART / DWG: 19418

PFI PART NO: PR-4199-000

DATE SHIPPED: 8/13/2018

WEIGHT SHIPPED	QUANTITY
616.8	6000 EA

CERTIFIED TO
ISO/TS 16949:2009
ISO 9001:2008

AUTHORIZED SIGNATURE QUALITY ASSURANCE MANAGER

We hereby certify that the material covered by this report has been inspected in accordance with, and has been found to meet, the applicable requirements described herein, including any specifications forming a part of the description, and that samples representative of the material met the composition limits and had the mechanical properties shown on this sheet.

Physical Test results

WORK ORDER			TRACE ID				TRACE QTY	MILL/HEAT LOT NO
X0076739	1		TPO-00062310				3000	213004
		# of tests	min	max				
	Double Shear	1	29.66	29.66	KSI	Pass		
WORK ORDER			TRACE ID				TRACE QTY	MILL/HEAT LOT NO
X0077276	1		TPG-00062366				1000	213004
		# of tests	min	max				
	Double Shear	1	29.09	29.09	KSI	Pass		
WORK ORDER			TRACE ID				TRACE QTY	MILL/HEAT LOT NO
X0077277	1		TPG-00062357				2000	213004
		# of tests	min	max				
	Double Shear	1	30.28	30.28	KSI	Pass		

Comments

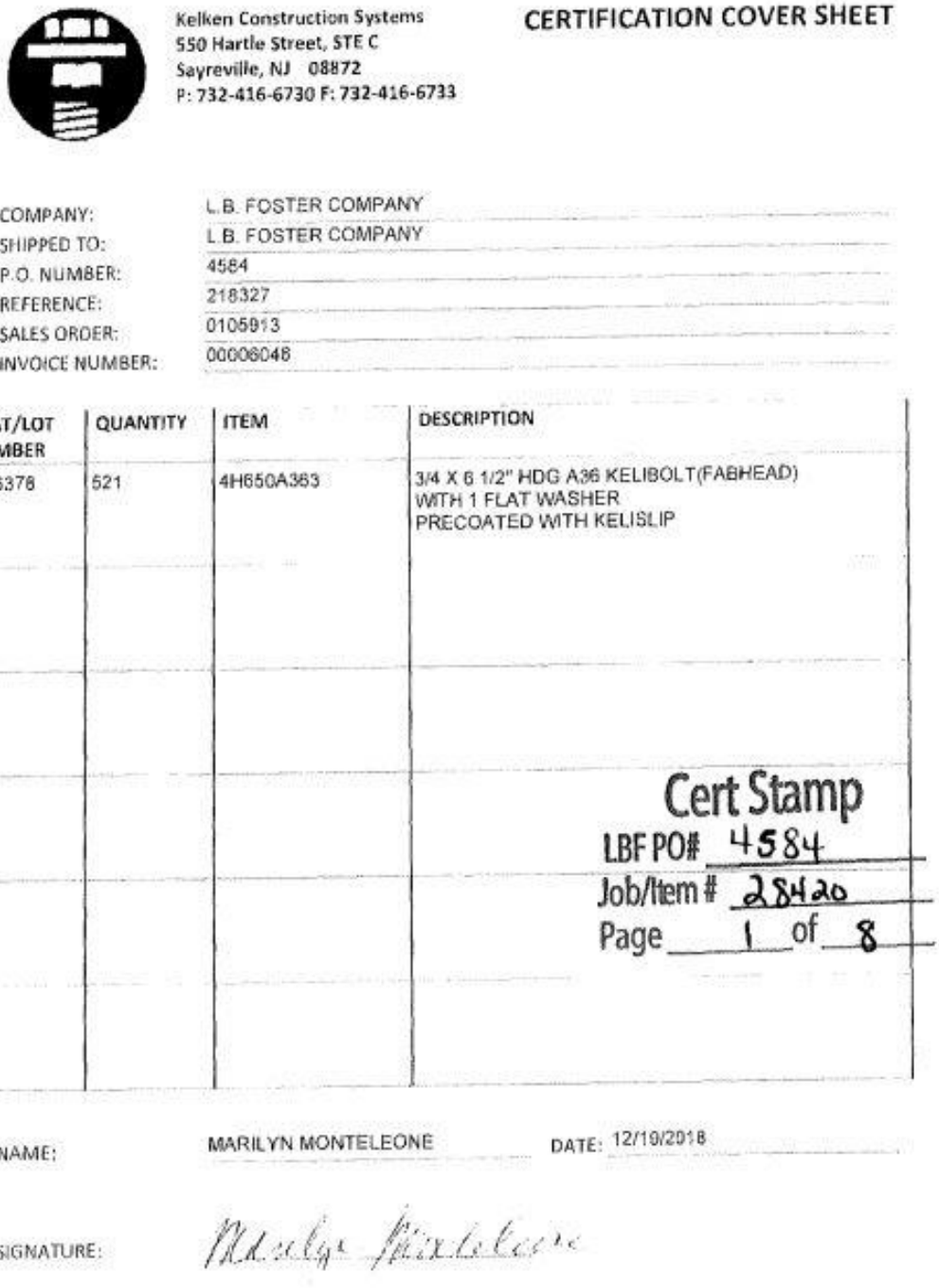
This is to certify that the material used in production of these parts is in accordance with ASTM B316

Cert Stamp
LBF PO# 4427
Job/Item # 19418
Page 1 of 1

~PROCUREMENT SPEC NASM5874 REV NEW, AS APPLICABLE
~ANODIZED COATINGS PER MIL-A-8625, AS APPLICABLE CONVERSION COATINGS PER MIL-DTL-5541, AS APPLICABLE
*KIPS PER SQUARE INCH. ONE KIP EQUALS ONE THOUSAND POUNDS
~NO MATERIALS PROHIBITED UNDER SPOC 164.1 WERE USED IN MANUFACTURE OF THIS PRODUCT
~NO MERCURY WAS USED IN THE MANUFACTURE OF THIS PRODUCT
~CHEMICAL COMPOSITION OF RAW MATERIAL MEETS APPLICABLE INDUSTRY STANDARD PER MANUFACTURER'S CERTIFICATE OF ANALYSIS. COPY AVAILABLE UPON REQUEST.
~PARTS ARE MADE IN THE USA

Page 1 of 1

Figure B-11. ¾ in.-Diameter, $1^{3}/_{8}$-in. Long Rivet, Test Nos. NCBR-1 and NCBR-2



Kelken Construction Systems
550 Hartle Street, STE C
Sayreville, NJ 08872
P: 732-416-6730 F: 732-416-6733

CERTIFICATION COVER SHEET

COMPANY: L.B. FOSTER COMPANY
SHIPPED TO: L.B. FOSTER COMPANY
P.O. NUMBER: 4584
REFERENCE: 218327
SALES ORDER: 0105913
INVOICE NUMBER: 00006048

HEAT/LOT NUMBER	QUANTITY	ITEM	DESCRIPTION
3076378	521	4H650A363	3/4 X 6 1/2" HDG A36 KELIBOLT(FABHEAD) WITH 1 FLAT WASHER PRECOATED WITH KELISLIP

Cert Stamp
LBF PO# 4584
Job/Item # 28420
Page 1 of 8

NAME: MARILYN MONTELEONE DATE: 12/19/2018

SIGNATURE:

Figure B-12. ¾-in. Diameter, 6½-in. Long Hex Head Drill-In Anchor, Test Nos. NCBR-1 and NCBR-2

32345

NUCOR
Nucor Steel Nebraska

Mill Certification
03/30/2018

MTR#: 45828
Lot #:10089087120
2911 E NUCOR ROAD
PO BOX 309
NORFOLK, NE 68701 US
402-644-0200
Fax: 402-644-0329

Sold To: FASTENER IN
PO BOX 6100
SAINT JOE, IN 46785-6100 US

Ship To: FASTENER IN2
6730 CR 60
SAINT JOE, IN 46785 US

Customer P.O	101303	Sales Order #	10089347 - 10.20
Product Group	Hot Roll - Engineered Bar	Product #	3099656
Grade	1030ML1	Lot #	10089087120
Size	0.7656"	Heat #	100890871
BOL #	BOL-143772	Load #	45828
Description	Hot Roll - Engineered Bar Round 49/64" 1030ML1 COIL 6200 lbs	Customer Part #	005012
Production Date	03/08/2018	Qty Shipped LBS	42335
Product Country Of Origin	United States	Qty Shipped EA	6
Original Item Description		Original Item Number	

I hereby certify that the material described herein has been manufactured in accordance with the specifications and standards listed above and that it satisfies these requirements.

Melt Country of Origin : United States — **Melting** Date: 03/02/2018

C (%)	Mn (%)	P (%)	S (%)	Si (%)	Ni (%)	Cr (%)	Mo (%)	Cu (%)	Ti (%)	V (%)	B (%)
0.41	0.88	0.008	0.012	0.23	0.06	0.09	0.01	0.12	0.001	0.003	0.000
Nb (%)	**N (PPM)**	**Sn (%)**	**Al (%)**	**Pb (%)**	**Ca (%)**						
0.002	**69**	**0.012**	**0.00**	**0.000**	**0.001**						

Reduction Ratio 96.33 : 1

Comments:
Coarse Grain Practice
Selenium,Tellurium,Lead,Bismuth or Boron were not intentionally added to this heat.
All manufacturing processes of the steel materials in this product, including melting, have been performed in the United States.
All products produced are weld free.
Mercury, in any form, has not been used in the production or testing of this material.
Test conform to ASTM A29-16, ASTM B416 and ASTM E1019-resulphurized grades or applicable customer requirements.
All material melted at Nucor Steel Nebraska is produced in an Electric Arc Furnace.
Strand Cast
ISO-17025 LAB accreditation cert available upon request.
Exporting Country-USA
Sales@nusene.com
California Proposition 65: This product contains chemicals known to the State of California to cause cancer, birth defects and other **reproductive** harm. The list of chemicals are available upon request. For more information, please call 402-644-0200.

Cert Stamp
LBF PO# 4214
Job/Item # 30150
Page 6 of 7

Chemistry Verification Checks

Part# 5012 Rn# 32345

	Checked By	Date
Receiving QA:	JP-1	4-2-18
Certifications QA:	JPS	4-2-18

Jim Hill

NBMG-10 January 1, 2012 — Jim Hill, Division Metallurgist — Page 1 of 1

Figure B-13. ¾ in.-10 UNC, 2½ in. Long Hex Bolt, Test Nos. NCBR-1 and NCBR-2



ROBBINS

BOX 3067150 1400 AIRPORT ROAD - FALL RIVER, MASSACHUSETTS 02722 508.675.2555 - FAX 508-677-0061

MANUFACTURERS OF STAINLESS STEEL, NON-FERROUS BOLTS, SCREWS, NUTS & SPECIAL COLD FORMED PARTS

CERTIFICATE OF COMPLIANCE - GENERAL

2/27/18

L.B. FOSTER COMPANY
C/O ACCOUNTS PAYABLE
202 REBER LANE
SEDFORD
PA 15522

CUSTOMER NO. 01604800
PURCHASE ORDER NO. 4008
LINE ITEM NO.
THREAD CLASS UNC 2A REPORT/CERTIFICATE NO. 60221G DATE OF MFG.: 2/23/18

COMPANY NO. 01 INVOICE NO.
ITEM NUMBER 50001312508AK
ITEM 1/2-13 X 1-1/4 HEX CAP 304
ROBBINS LOT NO. 156204 SHOP ORDER NO. C132257

MATERIAL 304L STAINLESS
HEAT/LOT NO. 205Y
QUANTITY SHIPPED 1,524

SPECIFICATION(S) INVOKED:

THIS REPORT MUST NOT BE REPRODUCED EXCEPT IN FULL, AND RELATES ONLY TO THE ITEM(S) TESTED.

MATERIAL	ASTM-F-593-09 304L	HEAD MARKINGS	F593C & R
MECH. PROP.	ASTM-F-593-09 GROUP 1 CW	COMMENTS	
DIMENSIONAL	ANSI B18.2.1		
NDT TESTING	N/A		
NDT ACCEPTANCE	N/A		

Cert Stamp
LBF PO# 4008
Job/Item # 22936
Page 3 of 3

THE UNDERSIGNED HEREBY CERTIFIES THAT:

ALL ITEMS FURNISHED IN THIS SHIPMENT ARE IN FULL COMPLIANCE WITH ALL PURCHASE ORDER AND SPECIFICATION REQUIREMENTS.

WHEN THE ABOVE CITED PURCHASE ORDER REQUIRES MATERIAL TEST REPORTS, THE UNDERSIGNED FURTHER CERTIFIES THAT:

THE TEST REPORTS SUPPLIED REPRESENT THE ACTUAL ATTRIBUTES OF THE ITEMS FURNISHED AND THE TEST RESULTS ARE IN FULL COMPLIANCE WITH ALL APPLICABLE SPECIFICATIONS AND PURCHASE ORDER REQUIREMENTS.

COMMONWEALTH OF MASS. COUNTY OF BRISTOL
SUBSCRIBED AND SWORN TO BEFORE ME
THIS 27th DAY OF Feb 20 18
NOTARY PUBLIC Mabel E. Monte
MY COMMISSION EXPIRES 06.18.2021

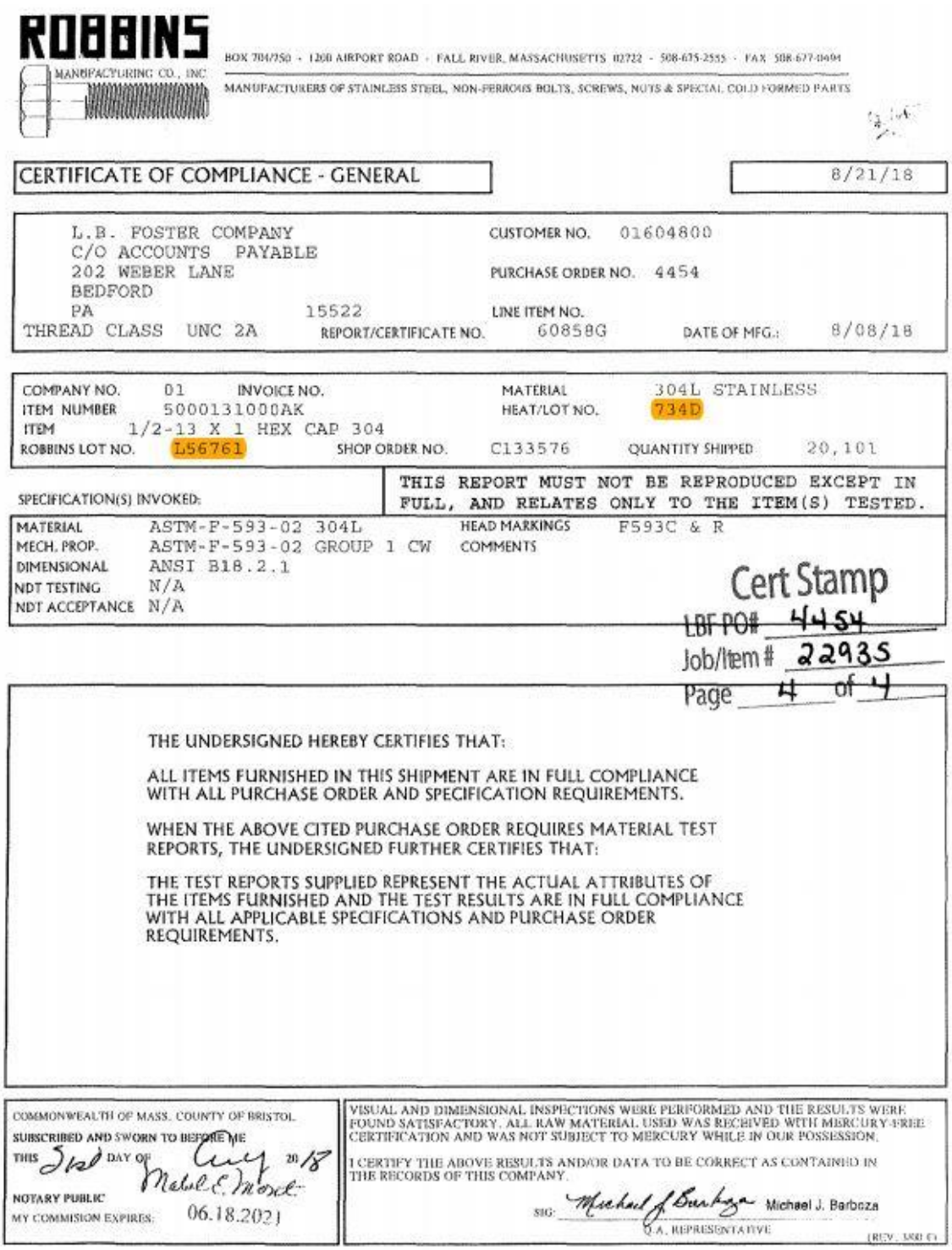
VISUAL AND DIMENSIONAL INSPECTIONS WERE PERFORMED AND THE RESULTS WERE FOUND SATISFACTORY. ALL RAW MATERIAL USED WAS RECEIVED WITH MERCURY-FREE CERTIFICATION AND WAS NOT SUBJECT TO MERCURY WHILE IN OUR POSSESSION

I CERTIFY THE ABOVE RESULTS AND/OR DATA TO BE CORRECT AS CONTAINED IN THE RECORDS OF THIS COMPANY

SIG
Q.A. REPRESENTATIVE

REV. 3/02/11

Figure B-14. ½ in.-13 UNC, 1¼ in. Long Hex Head Cap Screw, Test Nos. NCBR-1 and NCBR-2



ROBBINS MANUFACTURING CO., INC.
BOX 704/750 - 1200 AIRPORT ROAD - FALL RIVER, MASSACHUSETTS 02722 - 508-675-2555 - FAX 508-677-0494
MANUFACTURERS OF STAINLESS STEEL, NON-FERROUS BOLTS, SCREWS, NUTS & SPECIAL COLD FORMED PARTS

CERTIFICATE OF COMPLIANCE - GENERAL 8/21/18

L.B. FOSTER COMPANY
C/O ACCOUNTS PAYABLE
202 WEBER LANE
BEDFORD
PA 15522
CUSTOMER NO. 01604800
PURCHASE ORDER NO. 4454
LINE ITEM NO.
THREAD CLASS UNC 2A REPORT/CERTIFICATE NO. 60858G DATE OF MFG.: 8/08/18

COMPANY NO. 01 INVOICE NO.
ITEM NUMBER 5000131000AK
ITEM 1/2-13 X 1 HEX CAP 304
ROBBINS LOT NO. L56761 SHOP ORDER NO. C133576
MATERIAL 304L STAINLESS
HEAT/LOT NO. 734D
QUANTITY SHIPPED 20,101

SPECIFICATION(S) INVOKED:

THIS REPORT MUST NOT BE REPRODUCED EXCEPT IN FULL, AND RELATES ONLY TO THE ITEM(S) TESTED.

MATERIAL	ASTM-F-593-02 304L	HEAD MARKINGS	F593C & R
MECH. PROP.	ASTM-F-593-02 GROUP 1 CW	COMMENTS	
DIMENSIONAL	ANSI B18.2.1		
NDT TESTING	N/A		
NDT ACCEPTANCE	N/A		

Cert Stamp
LBF PO# 4454
Job/Item # 22935
Page 4 of 4

THE UNDERSIGNED HEREBY CERTIFIES THAT:

ALL ITEMS FURNISHED IN THIS SHIPMENT ARE IN FULL COMPLIANCE WITH ALL PURCHASE ORDER AND SPECIFICATION REQUIREMENTS.

WHEN THE ABOVE CITED PURCHASE ORDER REQUIRES MATERIAL TEST REPORTS, THE UNDERSIGNED FURTHER CERTIFIES THAT:

THE TEST REPORTS SUPPLIED REPRESENT THE ACTUAL ATTRIBUTES OF THE ITEMS FURNISHED AND THE TEST RESULTS ARE IN FULL COMPLIANCE WITH ALL APPLICABLE SPECIFICATIONS AND PURCHASE ORDER REQUIREMENTS.

COMMONWEALTH OF MASS. COUNTY OF BRISTOL
SUBSCRIBED AND SWORN TO BEFORE ME
THIS 3rd DAY OF July 2018
NOTARY PUBLIC Mabel E. Moore
MY COMMISION EXPIRES: 06.18.2021

VISUAL AND DIMENSIONAL INSPECTIONS WERE PERFORMED AND THE RESULTS WERE FOUND SATISFACTORY. ALL RAW MATERIAL USED WAS RECEIVED WITH MERCURY-FREE CERTIFICATION AND WAS NOT SUBJECT TO MERCURY WHILE IN OUR POSSESSION.

I CERTIFY THE ABOVE RESULTS AND/OR DATA TO BE CORRECT AS CONTAINED IN THE RECORDS OF THIS COMPANY.

SIG: Michael J. Barboza Michael J. Barboza
Q.A. REPRESENTATIVE

(REV. 3/01 C)

Figure B-15. ½ in.-13 UNC, 1 in. Long Hex Head Cap Screw, Test Nos. NCBR-1 and NCBR-2

AZZ GALVANIZING ROCKFORD

AUGUST 29, 2018

Technical Stamping
50600 E. Russell Schmidt
Chesterfield TWP, MI 48051

To Whom It May Concern:

This is to certify that the hot dip galvanizing of the following washers on your Purchase Order number 1638 conforms to specification ASTM A-153. The following sizes and lot numbers comply with the coating, workmanship, finish, and appearance requirements of ASTM F2329 specifications. The hot dip galvanizing is ROHS compliant. The galvanizing process was conducted in a temperature range of 830F to 855F.

PIECES	PART# & SIZE	LOT NUMBER	AVERAGE ZINC COATING IN MILS
3 14,174	#F0034 3/4" WASHER	0618-882	4.09

This certification in no way implies anything other than the quality of our hot dip galvanizing as it pertains to your order.

This product was galvanized in Rockford, IL USA

Yours very truly,

AZZ Galvanizing Rockford, IL

Peggy Doering

Peggy Doering
Office Manager

PD: bd

Cert Stamp
LBF PO# 4572
Job/Item # 14800
Page 5 of 5

Figure B-16. ¾ in. Dia. Plain Washers, Test Nos. NCBR-1 and NCBR-2

CertsNoe2_v1.0

PO Number None

Page 1

CMC STEEL TEXAS
1 STEEL MILL DRIVE
SEGUIN TX 78155-7510

CERTIFIED MILL TEST REPORT
For additional copies call
830-372-8771

We hereby certify that the test results presented here are accurate and conform to the reported grade specification

TOMMY HEWITT
Quality Assurance Manager

HEAT NO.:3076378 SECTION: ROUND .680 x 20'0" A36/52950 GRADE: ASTM A36-14/A529-14 Gr 50 ROLL DATE: 12/24/2017 MELT DATE: 12/08/2017 Cert. No.: 82374792 / 076378A901	S O L D T O	Unique Industries Inc 13488 Highway 25 Calera AL US 35040-5017 2056680490 2056680431	S H I P T O	Unique Industr Inc Highway 25 Calera AL US 35040-0000 2056680490 2056680431	Delivery#: 82374792 BOL#: 72461237 CUST PO#: 325046 CUST P/N: DLVRY LBS / HEAT: 17958.000 LB DLVRY PCS / HEAT: 727 EA		

Characteristic	Value	Characteristic	Value	Characteristic	Value
C	0.16%	Reduction of Area test 1	57%		
Mn	0.72%	Yield Strength test 2	53.2ksi		
P	0.011%	Tensile Strength test 2	76.5ksi		
S	0.030%	Elongation test 2	39%		
Si	0.23%	Elongation Gage Lgth test 2	2IN		
Cu	0.30%	Reduction of Area test 2	58%		
Cr	0.09%	BHN @ Surface test 1	156BHN		
Ni	0.08%				
Mo	0.028%				
V	0.003%				
Cb	0.001%				
Sn	0.012%				
Al	0.002%				
Carbon Eq F1554	0.30%				
Carbon Eq A529	0.37%				
Yield Strength test 1	52.4ksi				
Tensile Strength test 1	75.8ksi				
Elongation test 1	27%				
Elongation Gage Lgth test 1	8IN				

The Following is true of the material represented by this MTR:
- *Material is fully killed*
- *100% melted and rolled in the USA*
- *EN10204:2004 3.1 compliant*
- *Contains no weld repair*
- *Contains no Mercury contamination*
- *Manufactured in accordance with the latest version of the plant quality manual*
- *Meets the "Buy America" requirements of 23 CFR635.410*

REMARKS :

04/27/2018 17:14:13
Page 1 OF 1

Cert Stamp
BF PO# 4584
Job/Item # 28426
Page 2 of 8

Figure B-17. ½ in. Dia. Plain SAE Washer, Test Nos. NCBR-1 and NCBR-2

Appendix C. Vehicle Center of Gravity Determination

Date:	5/13/2019	Test Name:	NCBR-1	VIN:	kmhcn4ac1au467917
Year:	2010	Make:	Hyundai	Model:	Accent

Vehicle CG Determination

	Vehicle Equipment	Weight (lb)	Vertical CG (in.)	Vertical M (lb-in.)
+	Unballasted Car (Curb)	2505	22.761875	57018.497
+	Hub	19	10.6875	203.0625
+	Brake activation cylinder & frame	7	16.625	116.375
+	Pneumatic tank (Nitrogen)	30	13.75	412.5
+	Strobe/Brake Battery	5	20.25	101.25
+	Brake Receiver/Wires	6	43	258
+	CG Plate including DAQ	13	17.25	224.25
-	Battery	-31	27	-837
-	Oil	-8	11	-88
-	Interior	-82	24	-1968
-	Fuel	-21	15	-315
-	Coolant	-4	21	-84
-	Washer fluid	-1	18	-18
+	Water Ballast (In Fuel Tank)	0	0	0
+	Onboard Supplemental Battery	0	0	0
-	Spare Tire	-21	14.5	-304.5
				0
Note: (+) is added equipment to vehicle, (-) is removed equipment from vehicle				54719.434

Estimated Total Weight (lb): 2417

Vehicle Dimensions for C.G. Calculations

Wheel Base:	99.0	in.	Front Track Width:	57.875	in.
Roof Height:	57.625	in.	Rear Track Width:	57.25	in.

Center of Gravity	1100C MASH Targets	Test Inertial	Difference
Test Inertial Weight (lb)	2420 ± 55	2425	5.0
Longitudinal CG (in.)	39 ± 4	35.518	-3.482
Lateral CG (in.)	NA	0.154	NA
Vertical CG (in.)	NA	22.639	NA

Note: Long. CG is measured from front axle of test vehicle

Note: Lateral CG measured from centerline - positive to vehicle right (passenger) side

CURB WEIGHT (lb)

	Left	Right		
Front	823	773		
Rear	447	462		
FRONT	1596		lb	
REAR	909		lb	
TOTAL	2505		lb	

TEST INERTIAL WEIGHT (lb)

	Left	Right		
Front	778	777		
Rear	428	442		
FRONT	1555		lb	
REAR	870		lb	
TOTAL	2425		lb	

Figure C-1. Vehicle Mass Distribution, Test No. NCBR-1

Date:	6/11//2019	Test Name:	NCBR-2	VIN:	1GCRCPEH6FZ173614
Year:	2015	Make:	Chevrolet	Model:	Silverado

Vehicle CG Determination

	Vehicle Equipment	Weight (lb)	Vertical CG (in.)	Vertical M (lb-in.)
+	Unballasted Truck (Curb)	5015	27.8561	139698.34
+	Hub	31	14.5	449.5
+	Brake activation cylinder & frame	7	29 1/4	204.75
+	Pneumatic tank (Nitrogen)	31	26	806
+	Strobe/Brake Battery	5	26	130
+	Brake Receiver/Wires	6	54 1/4	325.5
+	CG Plate including DAQ	17	30	510
-	Battery	-40	41	-1640
-	Oil	-9	13	-117
-	Interior	-98	34 3/8	-3368.75
-	Fuel	-172	19 1/8	-3289.5
-	Coolant	-11	36 3/4	-404.25
-	Washer fluid	-10	35	-350
+	Water Ballast (In Fuel Tank)	0	0	0
+	Onboard Supplemental Battery	13	25 1/8	326.625
+	Boggie Plates in Bed	233	37 3/4	8795.75
				0
				142076.97

Note: (+) is added equipment to vehicle, (-) is removed equipment from vehicle

Estimated Total Weight (lb)	5018
Vertical CG Location (in.)	28.3135

Vehicle Dimensions for C.G. Calculations

Wheel Base: 144 in. Front Track Width: 68 in.
Rear Track Width: 67.5 in.

Center of Gravity	2270P MASH Targets	Test Inertial	Difference
Test Inertial Weight (lb)	5000 ± 110	5018	18.0
Longitudinal CG (in.)	63 ± 4	61.382224	-1.61778
Lateral CG (in.)	NA	0.3240335	NA
Vertical CG (in.)	28 or greater	28.31	0.31347

Note: Long. CG is measured from front axle of test vehicle

Note: Lateral CG measured from centerline - positive to vehicle right (passenger) side

CURB WEIGHT (lb.)

	Left	Right	
Front	1498	1433	
Rear	1026	1058	
FRONT	2931		lb
REAR	2084		lb
TOTAL	5015		lb

TEST INERTIAL WEIGHT (lb.)

	Left	Right	
Front	1433	1446	
Rear	1052	1087	
FRONT	2879		lb
REAR	2139		lb
TOTAL	5018		lb

Figure C-2. Vehicle Mass Distribution, Test No. NCBR-2

Appendix D. Vehicle Deformation Record

Date: 5/13/2019 Test Name: NCBR-1 VIN: kmhcn4ac1au467917
Year: 2010 Make: Hyundai Model: Accent

VEHICLE DEFORMATION
DRIVER SIDE FLOOR PAN - SET 1

	POINT	Pretest X (in.)	Pretest Y (in.)	Pretest Z (in.)	Posttest X (in.)	Posttest Y (in.)	Posttest Z (in.)	ΔX[A] (in.)	ΔY[A] (in.)	ΔZ[A] (in.)	Total Δ (in.)	Crush[B] (in.)	Directions for Crush[C]
TOE PAN - WHEEL WELL (X, Z)	1	64.0274	-11.5483	3.2591	64.1974	-10.3416	3.6540	-0.1700	1.2067	-0.3949	1.2810	0.0000	NA
	2	64.6351	-16.5250	3.1292	63.7302	-14.7847	2.6246	0.9049	1.7403	0.5046	2.0254	1.0361	X, Z
	3	64.8974	-21.7437	2.9131	63.8423	-19.9651	2.3591	1.0551	1.7786	0.5540	2.1409	1.1917	X, Z
	4	64.3931	-26.4336	1.3919	63.1575	-24.6474	1.0098	1.2356	1.7862	0.3821	2.2053	1.2933	X, Z
	5	61.7510	-31.4146	-1.1101	59.4663	-28.7906	-2.0034	2.2847	2.6240	0.8933	3.5921	2.4531	X, Z
	6	59.0730	-11.0782	3.5884	59.2986	-10.2164	3.6139	-0.2256	0.8618	-0.0255	0.8912	0.0000	NA
	7	60.2708	-16.4297	5.6631	59.6192	-14.7234	5.2611	0.6516	1.7063	0.4020	1.8702	0.7656	X, Z
	8	61.1665	-21.4484	5.1542	60.1708	-19.6748	4.8751	0.9957	1.7736	0.2791	2.0530	1.0341	X, Z
	9	61.9780	-26.8999	4.6677	60.9246	-25.1494	4.2631	1.0534	1.7505	0.4046	2.0827	1.1284	X, Z
	10	61.0537	-32.4899	1.9164	58.5324	-29.8840	1.0263	2.5213	2.6059	0.8901	3.7336	2.6738	X, Z
FLOOR PAN (Z)	11	53.2300	-10.9749	3.7162	53.4260	-10.7013	3.3939	-0.1960	0.2736	0.3223	0.4660	0.3223	Z
	12	55.1058	-15.9885	7.2470	54.0004	-15.1133	5.4782	1.1054	0.8752	1.7688	2.2620	1.7688	Z
	13	55.5284	-21.0545	7.2127	54.6932	-19.5202	7.1765	0.8352	1.5343	0.0362	1.7473	0.0362	Z
	14	55.5219	-27.1438	7.1926	55.0523	-25.5461	7.1084	0.4696	1.5977	0.0842	1.6674	0.0842	Z
	15	55.7073	-32.3551	7.1905	55.3910	-30.7451	6.9768	0.3163	1.6100	0.2137	1.6546	0.2137	Z
	16	48.3041	-10.9495	3.9244	48.4938	-10.6745	3.6553	-0.1897	0.2750	0.2691	0.4290	0.2691	Z
	17	48.8649	-15.2732	8.1615	48.4345	-15.7473	6.2476	0.4304	-0.4741	1.9139	2.0182	1.9139	Z
	18	49.1990	-20.7498	7.4283	48.4212	-19.5030	7.6493	0.7778	1.2468	-0.2210	1.4860	-0.2210	Z
	19	49.7707	-26.4426	7.6167	49.2818	-25.1902	7.8852	0.4889	1.2524	-0.2685	1.3710	-0.2685	Z
	20	50.2633	-32.1848	7.3800	49.9777	-30.8038	7.2975	0.2856	1.3810	0.0825	1.4126	0.0825	Z
	21	43.9165	-11.0497	4.2558	44.1234	-10.7755	3.9853	-0.2069	0.2742	0.2705	0.4372	0.2705	Z
	22	43.7170	-15.0540	8.2341	43.5988	-15.3588	6.9757	0.1182	-0.3048	1.2584	1.3002	1.2584	Z
	23	43.5466	-20.2315	7.6024	42.7523	-19.3082	7.9960	0.7943	0.9233	-0.3936	1.2800	-0.3936	Z
	24	44.4389	-26.1266	7.7253	44.0242	-25.1900	7.9113	0.4147	0.9366	-0.1860	1.0411	-0.1860	Z
	25	44.8518	-32.0431	7.5374	44.5744	-30.9144	7.6274	0.2774	1.1287	-0.0900	1.1658	-0.0900	Z
	26	38.1365	-10.6718	4.1612	38.3080	-10.4644	3.9909	-0.1715	0.2074	0.1703	0.3185	0.1703	Z
	27	38.5846	-14.5991	7.6906	38.4484	-14.2982	7.4967	0.1362	0.3009	0.1939	0.3830	0.1939	Z
	28	38.4376	-19.8256	7.6991	37.9346	-19.3825	7.8834	0.5030	0.4431	-0.1843	0.6952	-0.1843	Z
	29	42.4426	-21.9910	7.4207	38.0959	-25.2240	8.0212	4.3467	-3.2330	-0.6005	5.4504	-0.6005	Z
	30	42.9251	-26.2127	7.3468	38.1640	-29.5026	7.9888	4.7611	-3.2899	-0.6420	5.8227	-0.6420	Z

[A] Positive values denote deformation as inward toward the occupant compartment, negative values denote deformations outward away from the occupant compartment.
[B] Crush calculations that use multiple directional components will disregard components that are negative and only include positive values where the component is deforming inward toward the occupant compartment.
[C] Direction for Crush column denotes which directions are included in the crush calculations. If "NA" then no intrusion is recorded, and Crush will be 0.

Pretest Floor Pan	Posttest Floor Pan
	

Figure D-1. Occupant Compartment Deformation Data – Set 1, Test No. NCBR-1

Date: 5/13/2019 Test Name: NCBR-1 VIN: kmhcn4ac1au467917
Year: 2010 Make: Hyundai Model: Accent

VEHICLE DEFORMATION
DRIVER SIDE INTERIOR CRUSH - SET 1

	POINT	Pretest X (in.)	Pretest Y (in.)	Pretest Z (in.)	Posttest X (in.)	Posttest Y (in.)	Posttest Z (in.)	ΔX[A] (in.)	ΔY[A] (in.)	ΔZ[A] (in.)	Total Δ (in.)	Crush[B] (in.)	Directions for Crush[C]
DASH (X, Y, Z)	1	48.3238	-7.8324	-21.3445	48.6934	-6.4954	-21.8201	-0.3696	1.3370	-0.4756	1.4664	1.4664	X, Y, Z
	2	45.8878	-21.0222	-23.8189	46.2913	-19.7597	-24.3967	-0.4035	1.2625	-0.5778	1.4459	1.4459	X, Y, Z
	3	48.6044	-32.7687	-20.3852	49.0532	-31.3955	-20.8723	-0.4488	1.3732	-0.4871	1.5246	1.5246	X, Y, Z
	4	46.1260	-7.3155	-7.8768	46.3417	-6.2013	-8.2821	-0.2157	1.1142	-0.4053	1.2051	1.2051	X, Y, Z
	5	49.5810	-20.4721	-7.9093	49.8150	-19.1896	-8.3691	-0.2340	1.2825	-0.4598	1.3824	1.3824	X, Y, Z
	6	50.1209	-32.8981	-6.2997	49.7728	-31.4706	-6.6387	0.3481	1.4275	-0.3390	1.5079	1.5079	X, Y, Z
SIDE PANEL (Y)	7	53.5008	-34.3532	-1.4248	57.3967	-31.6191	-4.6482	-3.8959	2.7341	-3.2234	5.7484	2.7341	Y
	8	53.0566	-35.2060	2.5527	53.1255	-32.8226	2.2732	-0.0689	2.3834	-0.2795	2.4007	2.3834	Y
	9	57.9878	-34.9209	2.3493	58.0120	-32.0129	2.0861	-0.0242	2.9080	-0.2632	2.9200	2.9080	Y
IMPACT SIDE DOOR (Y)	10	45.8849	-35.5520	-16.8144	45.4089	-34.7546	-17.0097	0.4760	0.7974	-0.1953	0.9490	0.7974	Y
	11	36.7441	-35.4969	-17.5026	36.4055	-36.0685	-17.4648	0.3386	-0.5716	0.0378	0.6654	-0.5716	Y
	12	23.4699	-35.0620	-17.8750	23.1864	-36.9928	-17.6961	0.2835	-1.9308	0.1789	1.9597	-1.9308	Y
	13	42.8548	-35.7492	0.3252	42.7252	-35.2114	0.1346	0.1296	0.5378	-0.1906	0.5851	0.5378	Y
	14	36.7392	-35.5761	0.4717	36.6647	-35.7927	0.2877	0.0745	-0.2166	-0.1840	0.2938	-0.2166	Y
	15	27.6878	-35.2851	-0.0494	27.8023	-35.7695	-0.0665	-0.1145	-0.4844	-0.0171	0.4980	-0.4844	Y
ROOF - (Z)	16	32.6583	-7.8115	-36.6100	32.4933	-7.8914	-36.7103	0.1650	-0.0799	-0.1003	0.2090	-0.1003	Z
	17	32.6026	-12.0061	-36.4645	32.4894	-12.0717	-36.5983	0.1132	-0.0656	-0.1338	0.1871	-0.1338	Z
	18	31.8841	-17.4721	-36.2639	31.8570	-17.6244	-36.4221	0.0271	-0.1523	-0.1582	0.2213	-0.1582	Z
	19	31.4441	-22.3242	-35.9222	31.4076	-22.4147	-36.1395	0.0365	-0.0905	-0.2173	0.2382	-0.2173	Z
	20	30.7194	-27.0002	-35.4670	30.6927	-27.0954	-35.6907	0.0267	-0.0952	-0.2237	0.2446	-0.2237	Z
	21	29.0641	-7.7411	-38.5900	29.0553	-7.8807	-38.6921	0.0088	-0.1396	-0.1021	0.1732	-0.1021	Z
	22	28.6750	-12.0386	-38.5791	28.5624	-12.1592	-38.7228	0.1126	-0.1206	-0.1437	0.2188	-0.1437	Z
	23	28.2005	-17.1802	-38.4157	28.0912	-17.2486	-38.5588	0.1093	-0.0684	-0.1431	0.1926	-0.1431	Z
	24	27.6345	-22.1418	-38.1107	27.6281	-22.2806	-38.2296	0.0064	-0.1388	-0.1189	0.1829	-0.1189	Z
	25	26.8783	-26.6085	-37.7269	26.8762	-26.7872	-37.8142	0.0021	-0.1787	-0.0873	0.1989	-0.0873	Z
	26	25.1323	-7.8011	-39.1537	25.1308	-7.8983	-39.2351	0.0015	-0.0972	-0.0814	0.1268	-0.0814	Z
	27	24.8951	-12.0728	-39.1036	24.6865	-12.2473	-39.2200	0.2086	-0.1745	-0.1164	0.2958	-0.1164	Z
	28	24.3697	-17.0971	-38.9292	24.2862	-17.2384	-39.0247	0.0835	-0.1413	-0.0955	0.1899	-0.0955	Z
	29	23.8617	-22.0619	-38.6004	23.8728	-22.1855	-38.6750	-0.0111	-0.1236	-0.0746	0.1448	-0.0746	Z
	30	23.8026	-24.0776	-38.3837	23.4223	-24.3003	-38.4969	0.3803	-0.2227	-0.1132	0.4550	-0.1132	Z
A-PILLAR Maximum (X, Y, Z)	31	53.5472	-33.5715	-22.1561	53.7143	-32.5343	-22.6128	-0.1671	1.0372	-0.4567	1.1455	1.0372	Y
	32	49.4033	-32.7635	-25.0236	49.6958	-31.9488	-25.6378	-0.2925	0.8147	-0.6142	1.0614	0.8147	Y
	33	44.6571	-31.6196	-28.4963	45.0208	-31.1998	-29.0821	-0.3637	0.4198	-0.5858	0.8073	0.4198	Y
	34	41.6262	-30.8608	-30.3546	41.8181	-30.5637	-30.8675	-0.1919	0.2971	-0.5129	0.6230	0.2971	Y
	35	38.7291	-30.1760	-31.6508	38.8147	-29.9808	-32.1070	-0.0856	0.1952	-0.4562	0.5035	0.1952	Y
	36	35.1562	-29.3169	-33.5556	35.1852	-29.3084	-33.8720	-0.0290	0.0085	-0.3164	0.3178	0.0085	Y
A-PILLAR Lateral (Y)	31	53.5472	-33.5715	-22.1561	53.7143	-32.5343	-22.6128	-0.1671	1.0372	-0.4567	1.1455	1.0372	Y
	32	49.4033	-32.7635	-25.0236	49.6958	-31.9488	-25.6378	-0.2925	0.8147	-0.6142	1.0614	0.8147	Y
	33	44.6571	-31.6196	-28.4963	45.0208	-31.1998	-29.0821	-0.3637	0.4198	-0.5858	0.8073	0.4198	Y
	34	41.6262	-30.8608	-30.3546	41.8181	-30.5637	-30.8675	-0.1919	0.2971	-0.5129	0.6230	0.2971	Y
	35	38.7291	-30.1760	-31.6508	38.8147	-29.9808	-32.1070	-0.0856	0.1952	-0.4562	0.5035	0.1952	Y
	36	35.1562	-29.3169	-33.5556	35.1852	-29.3084	-33.8720	-0.0290	0.0085	-0.3164	0.3178	0.0085	Y
B-PILLAR Maximum (X, Y, Z)	37	13.2863	-28.0516	-34.3184	13.4028	-28.1925	-34.2184	-0.1165	-0.1409	0.1000	0.2084	0.1000	Z
	38	11.3043	-30.0839	-30.0338	11.4471	-30.1761	-29.8444	-0.1428	-0.0922	0.1894	0.2545	0.1894	Z
	39	15.1543	-31.0625	-27.8373	15.2340	-31.1552	-27.6123	-0.0797	-0.0927	0.2250	0.2561	0.2250	Z
	40	12.2434	-32.3109	-23.2984	12.3723	-32.3534	-22.9696	-0.1289	-0.0425	0.3288	0.3557	0.3288	Z
B-PILLAR Lateral (Y)	37	13.2863	-28.0516	-34.3184	13.4028	-28.1925	-34.2184	-0.1165	-0.1409	0.1000	0.2084	-0.1409	Y
	38	11.3043	-30.0839	-30.0338	11.4471	-30.1761	-29.8444	-0.1428	-0.0922	0.1894	0.2545	-0.0922	Y
	39	15.1543	-31.0625	-27.8373	15.2340	-31.1552	-27.6123	-0.0797	-0.0927	0.2250	0.2561	-0.0927	Y
	40	12.2434	-32.3109	-23.2984	12.3723	-32.3534	-22.9696	-0.1289	-0.0425	0.3288	0.3557	-0.0425	Y

[A] Positive values denote deformation as inward toward the occupant compartment, negative values denote deformations outward away from the occupant compartment.

[B] Crush calculations that use multiple directional components will disregard components that are negative and only include positive values where the component is deforming inward toward the occupant compartment.

[C] Direction for Crush column denotes which directions are included in the crush calculations. If "NA" then no intrusion is recorded, and Crush will be 0.

Figure D-2. Floor Pan Deformation Data – Set 1, Test No. NCBR-1

Date: 5/13/2019 Test Name: NCBR-1 VIN: kmhcn4ac1au467917
Year: 2010 Make: Hyundai Model: Accent

VEHICLE DEFORMATION
DRIVER SIDE INTERIOR CRUSH - SET 2

	POINT	Pretest X (in.)	Pretest Y (in.)	Pretest Z (in.)	Posttest X (in.)	Posttest Y (in.)	Posttest Z (in.)	ΔX[A] (in.)	ΔY[A] (in.)	ΔZ[A] (in.)	Total Δ (in.)	Crush[B] (in.)	Directions for Crush[C]
DASH (X, Y, Z)	1	48.4610	-7.5315	-21.2792	48.6934	-6.4954	-21.8201	-0.2324	1.0361	-0.5409	1.1917	1.1917	X, Y, Z
	2	46.1351	-20.7418	-23.7506	46.2913	-19.7597	-24.3967	-0.1562	0.9821	-0.6461	1.1859	1.1859	X, Y, Z
	3	48.9412	-32.4643	-20.3069	49.0532	-31.3955	-20.8723	-0.1120	1.0688	-0.5654	1.2143	1.2143	X, Y, Z
	4	46.2389	-7.0257	-7.8151	46.3417	-6.2013	-8.2821	-0.1028	0.8244	-0.4670	0.9530	0.9530	X, Y, Z
	5	49.7999	-20.1541	-7.8359	49.8150	-19.1896	-8.3691	-0.0151	0.9645	-0.5332	1.1022	1.1022	X, Y, Z
	6	50.4376	-32.5745	-6.2192	49.7728	-31.4706	-6.6387	0.6648	1.1039	-0.4195	1.3552	1.3552	X, Y, Z
SIDE PANEL (Y)	7	53.8219	-33.9999	-1.3385	57.3967	-31.6191	-4.6482	-3.5748	2.3808	-3.3097	5.4223	2.3808	Y
	8	53.3786	-34.8543	2.6388	53.1255	-32.8226	2.2732	0.2531	2.0317	-0.3656	2.0798	2.0317	Y
	9	58.3077	-34.5295	2.4426	58.0120	-32.0129	2.0861	0.2957	2.5166	-0.3565	2.5589	2.5166	Y
IMPACT SIDE DOOR (Y)	10	46.2389	-35.2677	-16.7388	45.4089	-34.7546	-17.0097	0.8300	0.5131	-0.2709	1.0127	0.5131	Y
	11	37.0990	-35.2867	-17.4407	36.4055	-36.0685	-17.4648	0.6935	-0.7818	-0.0241	1.0453	-0.7818	Y
	12	23.8223	-34.9590	-17.8332	23.1864	-36.9928	-17.6961	0.6359	-2.0338	0.1371	2.1353	-2.0338	Y
	13	43.1848	-35.4809	0.3963	42.7252	-35.2114	0.1346	0.4596	0.2695	-0.2617	0.5936	0.2695	Y
	14	37.0678	-35.3570	0.5337	36.6647	-35.7927	0.2877	0.4031	-0.4357	-0.2460	0.6425	-0.4357	Y
	15	28.0152	-35.1393	-0.0011	27.8023	-35.7695	-0.0665	0.2129	-0.6302	-0.0654	0.6684	-0.6302	Y
ROOF - (Z)	16	32.8186	-7.6445	-36.5681	32.4933	-7.8914	-36.7103	0.3253	-0.2469	-0.1422	0.4324	-0.1422	Z
	17	32.7966	-11.8393	-36.4206	32.4894	-12.0717	-36.5983	0.3072	-0.2324	-0.1777	0.4242	-0.1777	Z
	18	32.1219	-17.3108	-36.2183	31.8570	-17.6244	-36.4221	0.2649	-0.3136	-0.2038	0.4583	-0.2038	Z
	19	31.7205	-22.1662	-35.8748	31.4076	-22.4147	-36.1395	0.3129	-0.2485	-0.2647	0.4793	-0.2647	Z
	20	31.0328	-26.8477	-35.4184	30.6927	-27.0954	-35.6907	0.3401	-0.2477	-0.2723	0.5012	-0.2723	Z
	21	29.2270	-7.6041	-38.5536	29.0553	-7.8807	-38.6921	0.1717	-0.2766	-0.1385	0.3538	-0.1385	Z
	22	28.8725	-11.9046	-38.5410	28.5624	-12.1592	-38.7228	0.3101	-0.2546	-0.1818	0.4405	-0.1818	Z
	23	28.4393	-17.0497	-38.3758	28.0912	-17.2486	-38.5588	0.3481	-0.1989	-0.1830	0.4407	-0.1830	Z
	24	27.9128	-22.0156	-38.0691	27.6281	-22.2806	-38.2296	0.2847	-0.2650	-0.1605	0.4208	-0.1605	Z
	25	27.1921	-26.4881	-37.6842	26.8762	-26.7872	-37.8142	0.3159	-0.2991	-0.1300	0.4540	-0.1300	Z
	26	25.2966	-7.6960	-39.1230	25.1308	-7.8983	-39.2351	0.1658	-0.2023	-0.1121	0.2846	-0.1121	Z
	27	25.0939	-11.9695	-39.0711	24.6865	-12.2473	-39.2200	0.4074	-0.2778	-0.1489	0.5151	-0.1489	Z
	28	24.6087	-16.9978	-38.8950	24.2862	-17.2384	-39.0247	0.3225	-0.2406	-0.1297	0.4227	-0.1297	Z
	29	24.1403	-21.9664	-38.5645	23.8728	-22.1855	-38.6750	0.2675	-0.2191	-0.1105	0.3630	-0.1105	Z
	30	24.0971	-23.9824	-38.3468	23.4223	-24.3003	-38.4969	0.6748	-0.3179	-0.1501	0.7609	-0.1501	Z
A-PILLAR Maximum (X, Y, Z)	31	53.8930	-33.2281	-22.0700	53.7143	-32.5343	-22.6128	0.1787	0.6938	-0.5428	0.8988	0.7164	X, Y
	32	49.7470	-32.4549	-24.9442	49.6958	-31.9488	-25.6378	0.0512	0.5061	-0.6936	0.8601	0.5087	X, Y
	33	44.9969	-31.3511	-28.4245	45.0208	-31.1998	-29.0821	-0.0239	0.1513	-0.6576	0.6752	0.1513	Y
	34	41.9628	-30.6176	-30.2877	41.8181	-30.5637	-30.8675	0.1447	0.0539	-0.5798	0.6000	0.1544	X, Y
	35	39.0622	-29.9569	-31.5885	38.8147	-29.9808	-32.1070	0.2475	-0.0239	-0.5185	0.5750	0.2475	X
	36	35.4853	-29.1276	-33.4992	35.1852	-29.3084	-33.8720	0.3001	-0.1808	-0.3728	0.5116	0.3001	X
A-PILLAR Lateral (Y)	31	53.8930	-33.2281	-22.0700	53.7143	-32.5343	-22.6128	0.1787	0.6938	-0.5428	0.8988	0.6938	Y
	32	49.7470	-32.4549	-24.9442	49.6958	-31.9488	-25.6378	0.0512	0.5061	-0.6936	0.8601	0.5061	Y
	33	44.9969	-31.3511	-28.4245	45.0208	-31.1998	-29.0821	-0.0239	0.1513	-0.6576	0.6752	0.1513	Y
	34	41.9628	-30.6176	-30.2877	41.8181	-30.5637	-30.8675	0.1447	0.0539	-0.5798	0.6000	0.0539	Y
	35	39.0622	-29.9569	-31.5885	38.8147	-29.9808	-32.1070	0.2475	-0.0239	-0.5185	0.5750	-0.0239	Y
	36	35.4853	-29.1276	-33.4992	35.1852	-29.3084	-33.8720	0.3001	-0.1808	-0.3728	0.5116	-0.1808	Y
B-PILLAR Maximum (X, Y, Z)	37	13.6071	-28.0391	-34.2952	13.4028	-28.1925	-34.2184	0.2043	-0.1534	0.0768	0.2668	0.2183	X, Z
	38	11.6352	-30.0852	-30.0126	11.4471	-30.1761	-29.8444	0.1881	-0.0909	0.1682	0.2682	0.2523	X, Z
	39	15.4896	-31.0316	-27.8099	15.2340	-31.1552	-27.6123	0.2556	-0.1236	0.1976	0.3459	0.3231	X, Z
	40	12.5821	-32.3012	-23.2747	12.3723	-32.3534	-22.9696	0.2098	-0.0522	0.3051	0.3739	0.3703	X, Z
B-PILLAR Lateral (Y)	37	13.6071	-28.0391	-34.2952	13.4028	-28.1925	-34.2184	0.2043	-0.1534	0.0768	0.2668	-0.1534	Y
	38	11.6352	-30.0852	-30.0126	11.4471	-30.1761	-29.8444	0.1881	-0.0909	0.1682	0.2682	-0.0909	Y
	39	15.4896	-31.0316	-27.8099	15.2340	-31.1552	-27.6123	0.2556	-0.1236	0.1976	0.3459	-0.1236	Y
	40	12.5821	-32.3012	-23.2747	12.3723	-32.3534	-22.9696	0.2098	-0.0522	0.3051	0.3739	-0.0522	Y

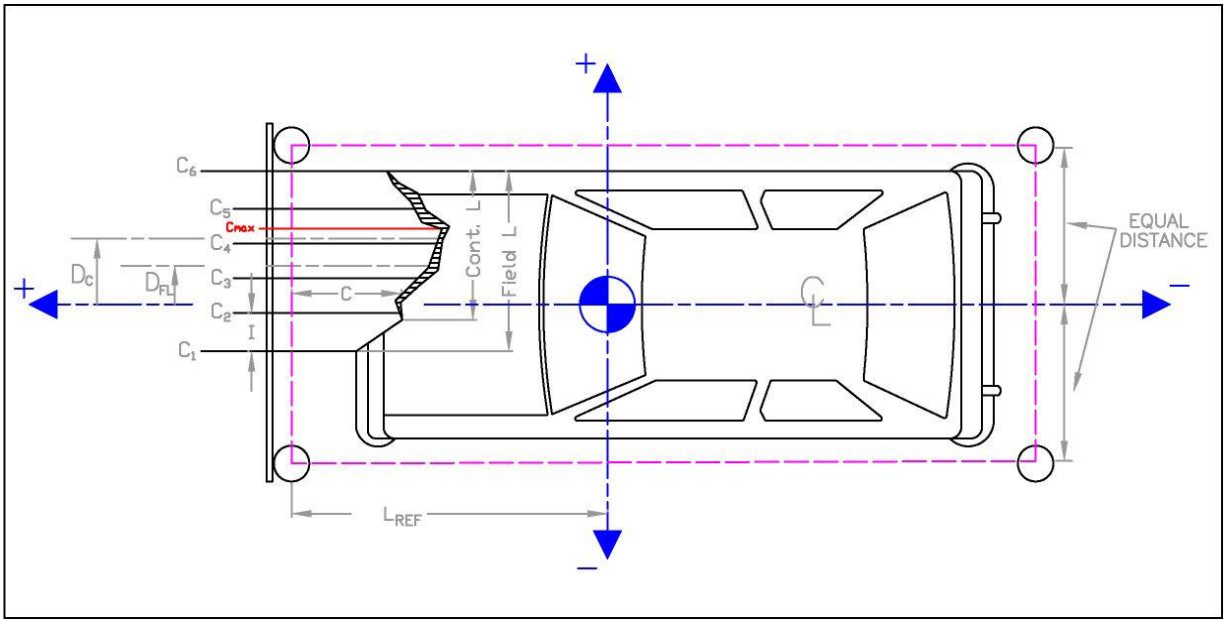
[A] Positive values denote deformation as inward toward the occupant compartment, negative values denote deformations outward away from the occupant compartment.

[B] Crush calculations that use multiple directional components will disregard components that are negative and only include positive values where the component is deforming inward toward the occupant compartment.

[C] Direction for Crush column denotes which directions are included in the crush calculations. If "NA" then no intrusion is recorded, and Crush will be 0.

Figure D-3. Occupant Compartment Deformation Data – Set 2, Test No. NCBR-1

Date:	5/13/2019	**Test Name:**	NCBR-1	**VIN:**	kmhcn4ac1au467917
Year:	2010	**Make:**	Hyundai	**Model:**	Accent



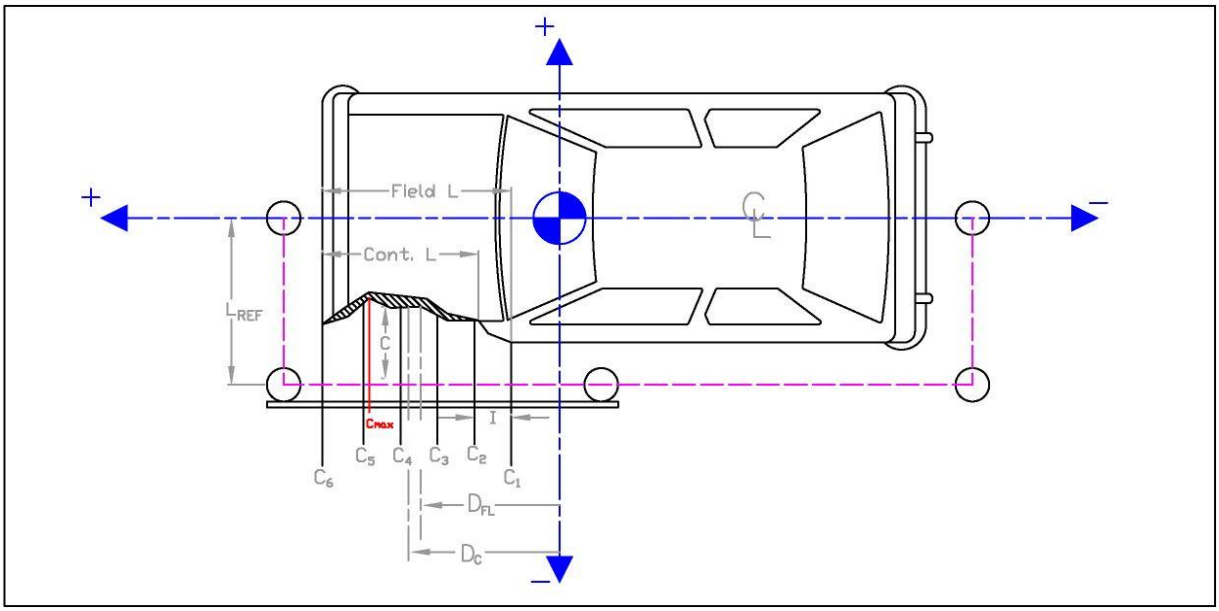
	in.	(mm)
Distance from C.G. to reference line - L_{REF}:	86	(2184)
Total Width of Vehicle:	66 7/8	(1699)
Width of contact and induced crush - Field L:	66 7/8	(1699)
Crush measurement spacing interval (L/5) - I:	13 3/8	(340)
Distance from center of vehicle to center of Field L - D_{FL}:	0	()
Width of Contact Damage:	15	(381)
Distance from center of vehicle to center of contact damage - D_C:	-22 3/4	-(578)

NOTE: Enter "NA" for crush measurement if distance can not be measured (i.e., side of vehicle has been pushed inward)
NOTE: All values must be filled out above before crush measurements are filled out.

	Crush Measurement		Lateral Location		Original Profile Measurement		Dist. Between Ref. Lines		Actual Crush	
	in.	(mm)	in.	(mm)	in.	(mm)	in.	(mm)	in.	(mm)
C_1	N/A	NA	-33 1/2	-(851)	20 1/4	(514)	15 3/4	(400)	NA	NA
C_2	20	(508)	-20 1/8	-(511)	5	(127)			- 3/4	-(19)
C_3	16 1/4	(413)	-6 3/4	-(171)	2 3/8	(60)			-1 7/8	-(48)
C_4	16	(406)	6 5/8	(168)	2 3/8	(60)			-2 1/8	-(54)
C_5	18 3/8	(467)	20	(508)	4 7/8	(124)			-2 1/4	-(57)
C_6	n/a	NA	33 3/8	(848)	19 7/8	(505)			NA	NA
C_{MAX}	23	(584)	-23 1/2	-(597)	6 3/8	(162)			7/8	(22)

Figure D-4. Exterior Vehicle Crush (NASS) - Front, Test No. NCBR-1

Date:	5/13/2019	**Test Name:**	NCBR-1	**VIN:**	kmhcn4ac1au467917
Year:	2010	**Make:**	Hyundai	**Model:**	Accent



	in.	(mm)
Distance from centerline to reference line - L_{REF}:	45	(1143)
Total Vehicle Length:	168 4/9	(4278)
Distance from vehicle c.g. to 1/2 of Vehicle total length:	-11 5/7	-(298)
Width of contact and induced crush - Field L:	168 4/9	(4278)
Crush measurement spacing interval (L/5) - I:	33 3/4	(857)
Distance from vehicle c.g. to center of Field L - D_{FL}:	-11 5/7	-(298)
Width of Contact Damage:	168 4/9	(4278)
Distance from vehicle c.g. to center of contact damage - D_C:	11 5/7	(298)

NOTE: Enter "NA" for crush measurement if distance can not be measured (i.e., front of vehicle has been pushed inward or tire has been removed)
NOTE: All values must be filled out above before crush measurements are filled out.

	Crush Measurement		Longitudinal Location		Original Profile Measurement		Dist. Between Ref. Lines		Actual Crush	
	in.	(mm)	in.	(mm)	in.	(mm)	in.	(mm)	in.	(mm)
C_1	18 1/2	(470)	-95 7/8	-(2435)	11 1/8	(283)	9	(229)	-1 5/8	-(41)
C_2	n/a	NA	-62 1/8	-(1578)	4	(102)			NA	NA
C_3	12	(305)	-28 3/8	-(721)	3 3/8	(86)			- 3/8	-(10)
C_4	12 3/4	(324)	5 3/8	(137)	3 1/4	(83)			1/2	(13)
C_5	n/a	NA	39 1/8	(994)	3 1/2	(89)			NA	NA
C_6	n/a	NA	72 7/8	(1851)	36	(914)			NA	NA
C_{MAX}	29 1/4	(743)	54	(1372)	5 1/2	(140)			14 3/4	(375)

Figure D-5. Exterior Vehicle Crush (NASS) - Side, Test No. NCBR-1

Date: 5/13/2019 Test Name: NCBR-1 VIN: kmhcn4ac1au467917
Year: 2010 Make: Hyundai Model: Accent

VEHICLE DEFORMATION
WINDSHIELD

	POINT	Vertical Reference Length[A]	Vertical Reference Side[B] (Top or Bottom)	Lateral Referece Length[C]	Lateral Reference Side[B] (Driver or Pass.)	Examplar Vehicle Measurement	Test Vehicle Measurment	Crush[D] (in.)
WINDSHIELD	1	5 3/4	Top	1 3/8	Driver	6 7/8	6 7/8	0
	2	1 3/4	Top	14	Driver	5 5/8	5 3/4	0.125
	3	6 3/4	Top	28	Driver	5 3/4	5 3/5	-0.15
	4	13 1/2	Top	5 1/2	Driver	6 1/4	9 3/8	3.125
	5	15	Top	21	Driver	5 1/4	8 1/4	3
	6	18 7/8	Top	2 1/4	Driver	7 1/8	7 1/4	0.125
	7	19 3/4	Top	14 1/4	Driver	5 1/2	10	4.5
	8	21 1/4	Top	17 1/8	Driver	5 1/8	10 1/8	5
	9	24	Top	3 1/8	Driver	6 7/8	7	0.125
	10	25 3/4	Top	15 1/2	Driver	5	8 1/4	3.25
	11	29 1/8	Top	24 1/8	Driver	5	6	1
	12	29 1/2	Top	31 1/2	Driver	4 7/8	5	0.125

[A] Length to vertical reference, typically the top or bottom of the windshield frame.
[B] Side of windshield frame, top, bottom, passenger, or driver, in which the reference was measured from.
[C] Length to lateral referene either the driver or passenger side windshield frame.
[D] Crush is the difference between the test vehcile and examplar vehicle that is the intrusion of the windshield deformation. The intrusion is perpendicular to the plane of the windshield which is a resultant of the X & Z directions.

Examplar Vehicle Description

Year: 2010 Make: Hyundai Model: Accent VIN: KMHCN4AC8BU608788

Windshield Deformation Notes:

The windshield deformation measurement were taken three days after the test and the windshield settled and deteriorated during this time. The values represented in these measurements do not reflect the test day values. It is likely the values were much less signifcant on the day of the test.





Figure D-6. Windshield Deformation, Test No. NCBR-1

Date: 6/11//2019 Test Name: NCBR-2 VIN: 1GCRCPEH6FZ173614
Year: 2015 Make: Chevrolet Model: Silverado

VEHICLE DEFORMATION
DRIVER SIDE INTERIOR CRUSH - SET 2

	POINT	Pretest X (in.)	Pretest Y (in.)	Pretest Z (in.)	Posttest X (in.)	Posttest Y (in.)	Posttest Z (in.)	ΔX[A] (in.)	ΔY[A] (in.)	ΔZ[A] (in.)	Total Δ (in.)	Crush[B] (in.)	Directions for Crush[C]
DASH (X, Y, Z)	1	55.2501	1.0252	-27.0936	55.3392	1.8708	-27.1193	-0.0891	-0.8456	-0.0257	0.8507	0.8507	X, Y, Z
	2	54.4103	-12.8645	-28.6392	54.3516	-11.9644	-29.1708	0.0587	0.9001	-0.5316	1.0470	1.0470	X, Y, Z
	3	54.4008	-29.0954	-26.7884	54.1430	-28.2785	-27.8652	0.2578	0.8169	-1.0768	1.3760	1.3760	X, Y, Z
	4	52.3038	1.4892	-16.5682	52.1158	2.0333	-16.6987	0.1880	-0.5441	-0.1305	0.5903	0.5903	X, Y, Z
	5	53.5830	-10.9189	-15.6419	53.2104	-10.3771	-16.1068	0.3726	0.5418	-0.4649	0.8053	0.8053	X, Y, Z
	6	52.4798	-29.3149	-15.3242	52.0496	-28.8210	-16.4757	0.4302	0.4939	-1.1515	1.3247	1.3247	X, Y, Z
SIDE PANEL (Y)	7	62.8151	-30.1859	-2.5010	62.2271	-28.6163	-3.2717	0.5880	1.5696	-0.7707	1.8448	1.5696	Y
	8	62.8769	-30.4575	1.5594	62.3305	-28.8729	0.9052	0.5464	1.5846	-0.6542	1.7993	1.5846	Y
	9	65.7132	-30.5027	2.0845	64.9462	-29.6573	1.3833	0.7670	0.8454	-0.7012	1.3397	0.8454	Y
IMPACT SIDE DOOR (Y)	10	28.1099	-30.9029	-20.7366	27.4268	-33.0617	-21.6000	0.6831	-2.1588	-0.8634	2.4233	-2.1588	Y
	11	40.7207	-31.6412	-20.0000	51.3589	-32.0855	-20.9713	-10.6382	-0.4443	-0.9713	10.6917	-0.4443	Y
	12	52.4889	-32.0649	-20.2124	27.7161	-30.5042	-0.9721	24.7728	1.5607	19.2403	31.4057	1.5607	Y
	13	28.1514	-31.0400	0.1349	41.7035	-31.4817	1.9557	-13.5521	-0.4417	1.8208	13.6810	-0.4417	Y
	14	42.3773	-31.9046	2.8951	50.6662	-31.9092	0.8253	-8.2889	-0.0046	-2.0698	8.5434	-0.0046	Y
	15	51.4193	-32.4455	1.6364	50.7002	-31.9055	0.8745	0.7191	0.5400	-0.7619	1.1786	0.5400	Y
ROOF - (Z)	16	48.8298	1.8323	-40.7430	49.1068	3.0193	-40.5743	-0.2770	-1.1870	0.1687	1.2305	0.1687	Z
	17	48.5125	-3.6603	-40.5928	48.7080	-2.5601	-40.6756	-0.1955	1.1002	-0.0828	1.1205	-0.0828	Z
	18	47.7721	-9.4783	-40.4618	47.9521	-8.2193	-40.7851	-0.1800	1.2590	-0.3233	1.3123	-0.3233	Z
	19	46.5598	-15.3907	-40.3241	46.7312	-14.2314	-40.8822	-0.1714	1.1593	-0.5581	1.2980	-0.5581	Z
	20	44.6083	-22.4867	-39.6231	44.7011	-21.2309	-40.5284	-0.0928	1.2558	-0.9053	1.5509	-0.9053	Z
	21	35.8812	2.4063	-45.0365	36.0437	3.7955	-44.9124	-0.1625	-1.3892	0.1241	1.4042	0.1241	Z
	22	35.9027	-1.6925	-45.0069	36.1695	-0.3276	-45.0471	-0.2668	1.3649	-0.0402	1.3913	-0.0402	Z
	23	35.1446	-7.6870	-44.9151	35.3680	-6.3126	-45.1948	-0.2234	1.3744	-0.2797	1.4203	-0.2797	Z
	24	34.9991	-14.1551	-44.5858	35.0952	-12.7480	-45.1237	-0.0961	1.4071	-0.5379	1.5095	-0.5379	Z
	25	34.1141	-20.6301	-44.0403	34.3312	-19.2077	-44.7954	-0.2171	1.4224	-0.7551	1.6250	-0.7551	Z
	26	23.8209	2.6692	-45.2462	24.1081	4.1513	-45.2206	-0.2872	-1.4821	0.0256	1.5099	0.0256	Z
	27	23.9674	-1.6014	-45.4793	24.1915	-0.1259	-45.6101	-0.2241	1.4755	-0.1308	1.4981	-0.1308	Z
	28	23.9821	-6.9333	-45.3496	24.2233	-5.4108	-45.6775	-0.2412	1.5225	-0.3279	1.5760	-0.3279	Z
	29	23.8083	-13.3864	-45.0622	23.9572	-11.8773	-45.5844	-0.1489	1.5091	-0.5222	1.6038	-0.5222	Z
	30	23.9543	-19.7926	-44.5101	24.1543	-18.2834	-45.2715	-0.2000	1.5092	-0.7614	1.7022	-0.7614	Z
A-PILLAR Maximum (X, Y, Z)	31	60.9411	-28.9676	-28.6246	60.7588	-28.1686	-29.3921	0.1823	0.7990	-0.7675	1.1228	0.8195	X, Y
	32	58.6922	-28.2467	-30.5574	58.5625	-27.4006	-31.4067	0.1297	0.8461	-0.8493	1.2058	0.8560	X, Y
	33	55.6269	-27.2601	-32.8968	55.5911	-26.3243	-33.7690	0.0358	0.9358	-0.8722	1.2797	0.9365	X, Y
	34	52.3517	-26.2625	-35.3927	52.3796	-25.2049	-36.2504	-0.0279	1.0576	-0.8577	1.3620	1.0576	Y
	35	49.3367	-25.2682	-37.1460	49.4750	-24.1724	-38.1381	-0.1383	1.0958	-0.9921	1.4846	1.0958	Y
	36	45.9482	-24.2197	-38.9812	46.0031	-23.0431	-39.9411	-0.0549	1.1766	-0.9599	1.5195	1.1766	Y
A-PILLAR Lateral (Y)	31	60.9411	-28.9676	-28.6246	60.7588	-28.1686	-29.3921	0.1823	0.7990	-0.7675	1.1228	0.7990	Y
	32	58.6922	-28.2467	-30.5574	58.5625	-27.4006	-31.4067	0.1297	0.8461	-0.8493	1.2058	0.8461	Y
	33	55.6269	-27.2601	-32.8968	55.5911	-26.3243	-33.7690	0.0358	0.9358	-0.8722	1.2797	0.9358	Y
	34	52.3517	-26.2625	-35.3927	52.3796	-25.2049	-36.2504	-0.0279	1.0576	-0.8577	1.3620	1.0576	Y
	35	49.3367	-25.2682	-37.1460	49.4750	-24.1724	-38.1381	-0.1383	1.0958	-0.9921	1.4846	1.0958	Y
	36	45.9482	-24.2197	-38.9812	46.0031	-23.0431	-39.9411	-0.0549	1.1766	-0.9599	1.5195	1.1766	Y
B-PILLAR Maximum (X, Y, Z)	37	16.4402	-23.2793	-40.2397	16.5729	-21.8820	-41.1058	-0.1327	1.3973	-0.8661	1.6493	1.3973	Y
	38	20.4870	-24.8650	-35.3611	20.5738	-23.6054	-36.2127	-0.0868	1.2596	-0.8516	1.5229	1.2596	Y
	39	17.4111	-26.3015	-30.6973	17.5832	-25.1478	-31.6876	-0.1721	1.1537	-0.9903	1.5301	1.1537	Y
	40	21.7709	-27.5253	-25.6436	21.8154	-26.5194	-26.6254	-0.0445	1.0059	-0.9818	1.4063	1.0059	Y
B-PILLAR Lateral (Y)	37	16.4402	-23.2793	-40.2397	16.5729	-21.8820	-41.1058	-0.1327	1.3973	-0.8661	1.6493	1.3973	Y
	38	20.4870	-24.8650	-35.3611	20.5738	-23.6054	-36.2127	-0.0868	1.2596	-0.8516	1.5229	1.2596	Y
	39	17.4111	-26.3015	-30.6973	17.5832	-25.1478	-31.6876	-0.1721	1.1537	-0.9903	1.5301	1.1537	Y
	40	21.7709	-27.5253	-25.6436	21.8154	-26.5194	-26.6254	-0.0445	1.0059	-0.9818	1.4063	1.0059	Y

[A] Positive values denote deformation as inward toward the occupant compartment, negative values denote deformations outward away from the occupant compartment.

[B] Crush calculations that use multiple directional components will disregard components that are negative and only include positive values where the component is deforming inward toward the occupant compartment.

[C] Direction for Crush column denotes which directions are included in the crush calculations. If "NA" then no intrusion is recorded, and Crush will be 0.

Figure D-7. Occupant Compartment Deformation Data – Set 1, Test No. NCBR-2

Date: 6/11//2019 Test Name: NCBR-2 VIN: 1GCRCPEH6FZ173614
Year: 2015 Make: Chevrolet Model: Silverado

VEHICLE DEFORMATION
DRIVER SIDE FLOOR PAN - SET 2

	POINT	Pretest X (in.)	Pretest Y (in.)	Pretest Z (in.)	Posttest X (in.)	Posttest Y (in.)	Posttest Z (in.)	ΔX[A] (in.)	ΔY[A] (in.)	ΔZ[A] (in.)	Total Δ (in.)	Crush[B] (in.)	Directions for Crush[C]
TOE PAN - WHEEL WELL (X, Z)	1	65.7826	-6.7257	1.9658	65.2176	-6.1431	2.1822	0.5650	0.5826	-0.2164	0.8399	0.5650	X
	2	67.2944	-12.0827	3.8956	66.6721	-10.9022	4.1189	0.6223	1.1805	-0.2233	1.3530	0.6223	X
	3	67.1760	-17.7259	4.7118	66.4678	-16.5001	4.8170	0.7082	1.2258	-0.1052	1.4196	0.7082	X
	4	66.8693	-23.0059	4.6670	65.8689	-21.7271	4.3436	1.0004	1.2788	0.3234	1.6555	1.0514	X, Z
	5	66.4526	-28.4145	4.6743	65.2647	-27.2452	4.1340	1.1879	1.1693	0.5403	1.7522	1.3050	X, Z
	6	61.8738	-6.1300	2.0986	61.2565	-5.6104	2.2749	0.6173	0.5196	-0.1763	0.8259	0.6173	X
	7	61.9620	-10.4525	5.8226	61.4424	-9.4999	6.1361	0.5196	0.9526	-0.3135	1.1295	0.5196	X
	8	61.7329	-17.2578	5.7325	61.3269	-16.1662	5.7489	0.4060	1.0916	-0.0164	1.1648	0.4060	X
	9	61.7157	-22.5748	5.5794	61.3362	-21.5553	5.4113	0.3795	1.0195	0.1681	1.1008	0.4151	X, Z
	10	61.1678	-28.7171	5.6615	60.8499	-27.5347	5.7910	0.3179	1.1824	-0.1295	1.2312	0.3179	X
FLOOR PAN (Z)	11	57.7543	-6.1302	2.6139	57.2132	-6.1565	2.6589	0.5411	-0.0263	-0.0450	0.5436	-0.0450	Z
	12	57.4014	-10.1253	5.8242	56.7406	-9.2719	6.2348	0.6608	0.8534	-0.4106	1.1548	-0.4106	Z
	13	57.5449	-16.8248	5.7356	57.1099	-15.8869	5.8257	0.4350	0.9379	-0.0901	1.0378	-0.0901	Z
	14	57.9708	-22.2480	5.5311	57.5942	-21.2730	5.4007	0.3766	0.9750	0.1304	1.0533	0.1304	Z
	15	57.4050	-27.9534	5.7129	57.1624	-26.9793	5.5990	0.2426	0.9741	0.1139	1.0103	0.1139	Z
	16	53.7852	-5.9175	2.9711	53.2015	-6.3335	2.7644	0.5837	-0.4160	0.2067	0.7460	0.2067	Z
	17	53.6126	-9.8724	5.8382	53.0299	-8.9538	6.3428	0.5827	0.9186	-0.5046	1.1992	-0.5046	Z
	18	53.4002	-16.2354	5.7261	52.9158	-15.4493	5.8941	0.4844	0.7861	-0.1680	0.9385	-0.1680	Z
	19	53.3403	-21.7337	5.7509	52.9399	-20.9099	5.6540	0.4004	0.8238	0.0969	0.9211	0.0969	Z
	20	52.9929	-27.6989	5.6228	52.6697	-26.7328	5.1903	0.3232	0.9661	0.4325	1.1067	0.4325	Z
	21	49.8679	-5.6045	3.2917	49.3528	-5.4406	3.2025	0.5151	0.1639	0.0892	0.5479	0.0892	Z
	22	49.7153	-9.4776	5.8337	49.1109	-8.6363	6.5108	0.6044	0.8413	-0.6771	1.2376	-0.6771	Z
	23	49.5921	-16.0232	5.7432	49.1120	-15.2128	5.9570	0.4801	0.8104	-0.2138	0.9659	-0.2138	Z
	24	49.3420	-21.5986	5.7846	48.9440	-20.8376	5.6941	0.3980	0.7610	0.0905	0.8635	0.0905	Z
	25	48.9220	-27.4278	5.6648	48.6344	-26.5834	5.1297	0.2876	0.8444	0.5351	1.0402	0.5351	Z
	26	45.8123	-5.2014	3.2632	45.5023	-5.2401	2.9382	0.3100	-0.0387	0.3250	0.4508	0.3250	Z
	27	45.0866	-9.0025	4.5605	44.6145	-8.5995	5.0186	0.4721	0.4030	-0.4581	0.7715	-0.4581	Z
	28	44.8299	-15.5699	4.6878	44.4236	-14.8021	4.8467	0.4063	0.7678	-0.1589	0.8831	-0.1589	Z
	29	44.6703	-21.2235	4.8297	44.2647	-20.3959	4.7187	0.4056	0.8276	0.1110	0.9283	0.1110	Z
	30	44.4349	-26.6620	4.8885	44.0832	-25.8000	4.4612	0.3517	0.8620	0.4273	1.0244	0.4273	Z

[A] Positive values denote deformation as inward toward the occupant compartment, negative values denote deformations outward away from the occupant compartment.
[B] Crush calculations that use multiple directional components will disregard components that are negative and only include positive values where the component is deforming inward toward the occupant compartment.
[C] Direction for Crush column denotes which directions are included in the crush calculations. If "NA" then no intrusion is recorded, and Crush will be 0.

Pretest Floor Pan	Posttest Floor Pan
	

Figure D-8. Floor Pan Deformation Data – Set 2, Test No. NCBR-2

Appendix E. Accelerometer and Rate Transducer Data Plots, Test No. NCBR-1

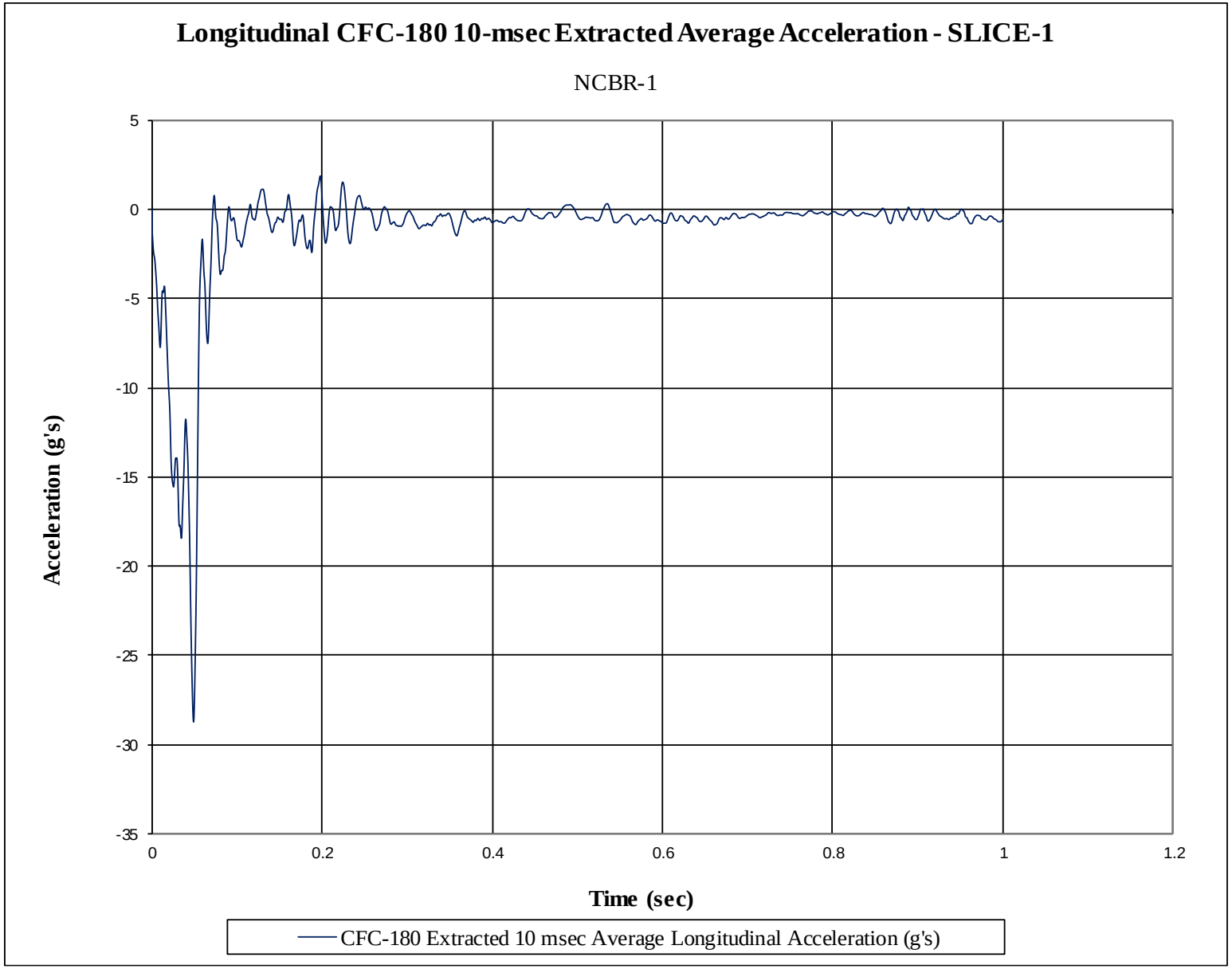


Figure E-1. 10-ms Average Longitudinal Deceleration (SLICE-1), Test No. NCBR-1

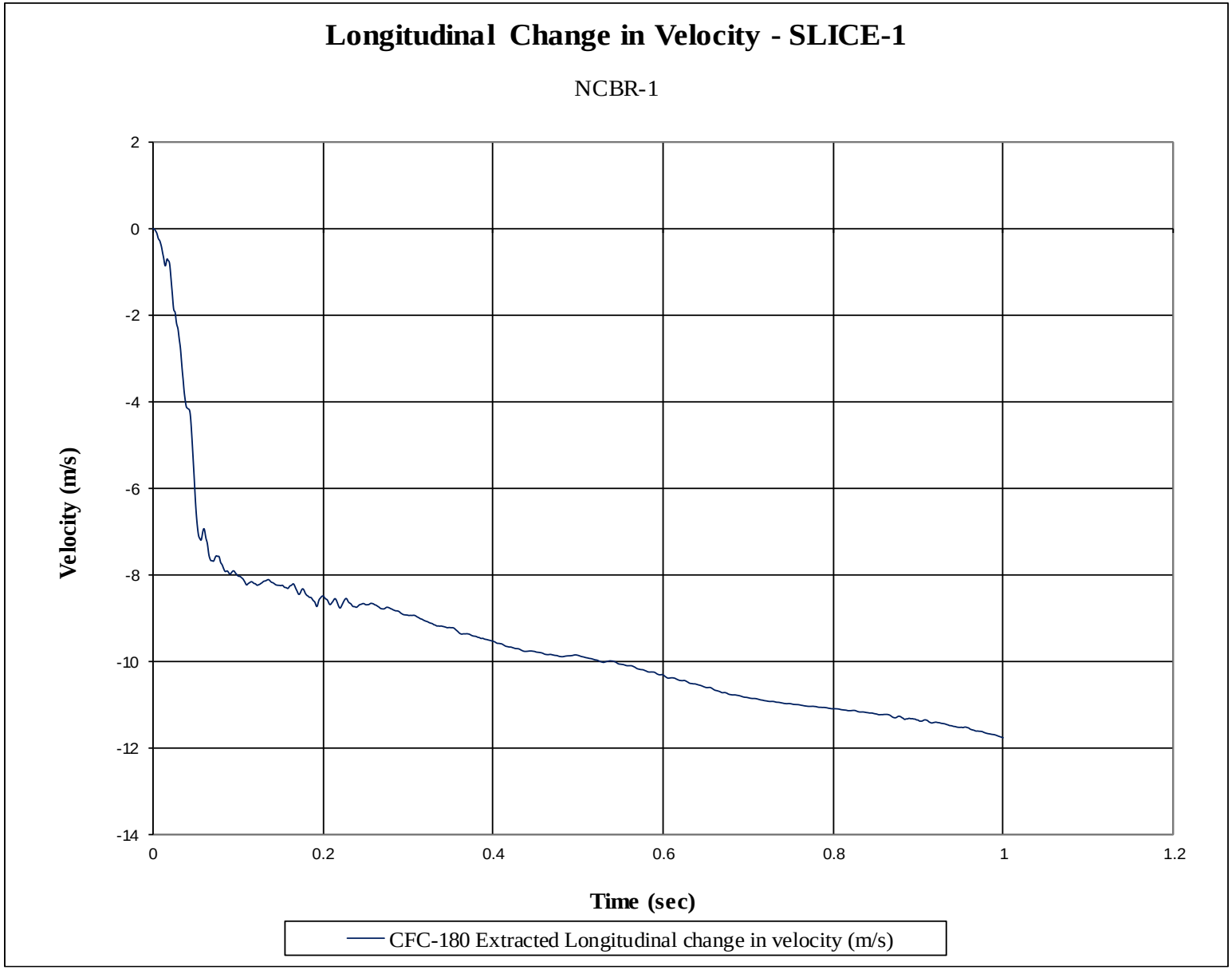


Figure E-2. Longitudinal Occupant Impact Velocity (SLICE-1), Test No. NCBR-1

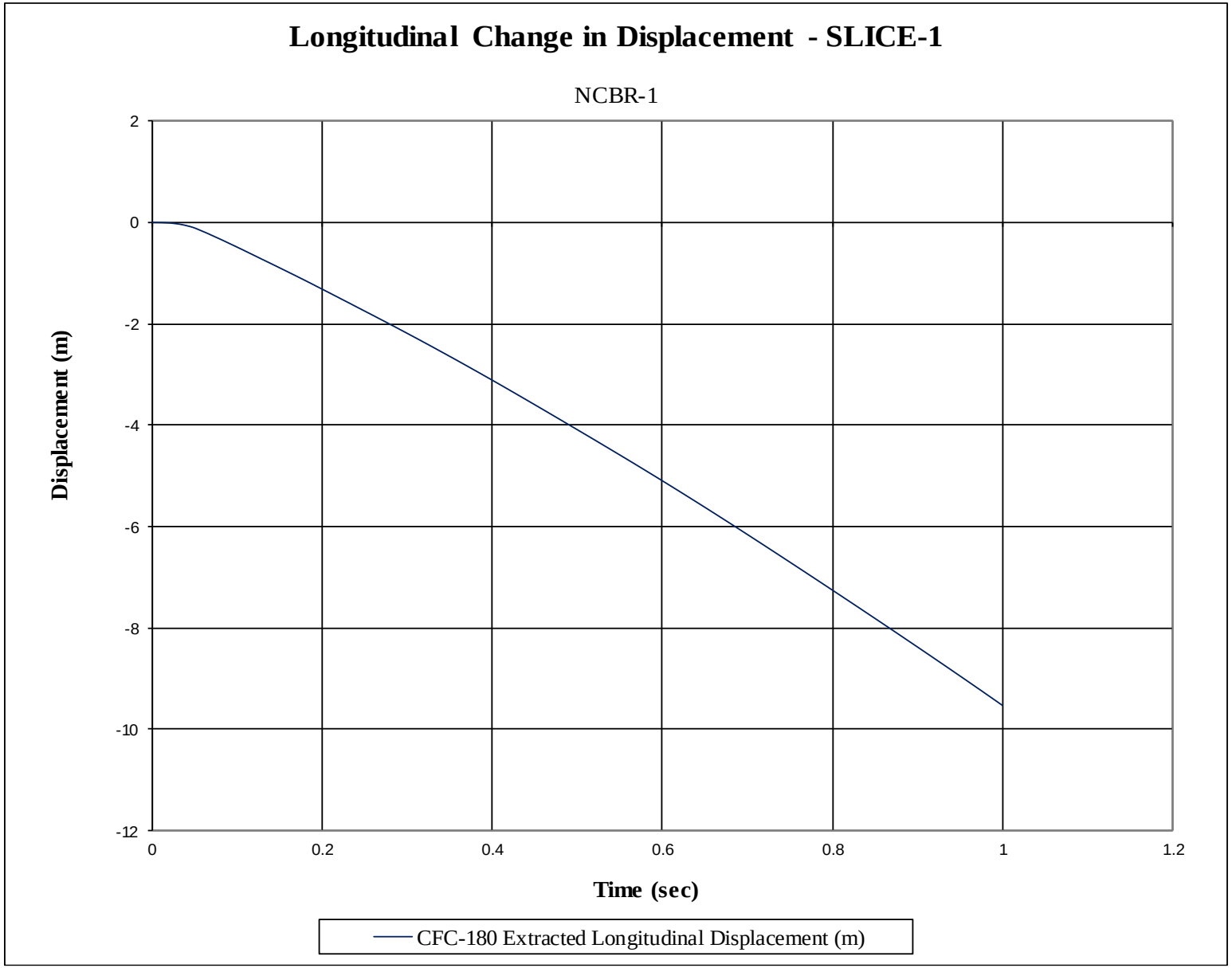


Figure E-3. Longitudinal Occupant Displacement (SLICE-1), Test No. NCBR-1

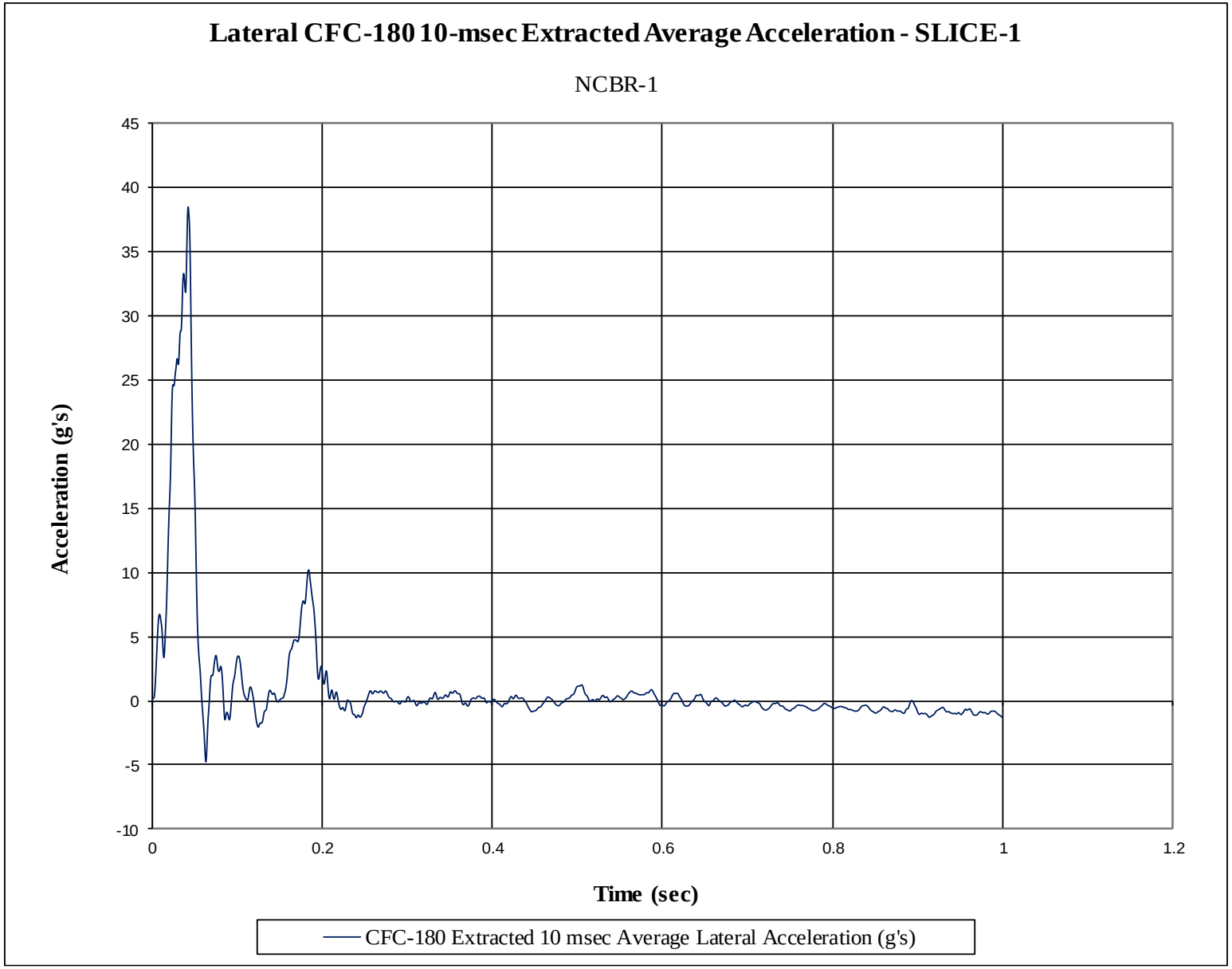


Figure E-4. 10-ms Average Lateral Deceleration (SLICE-1), Test No. NCBR-1

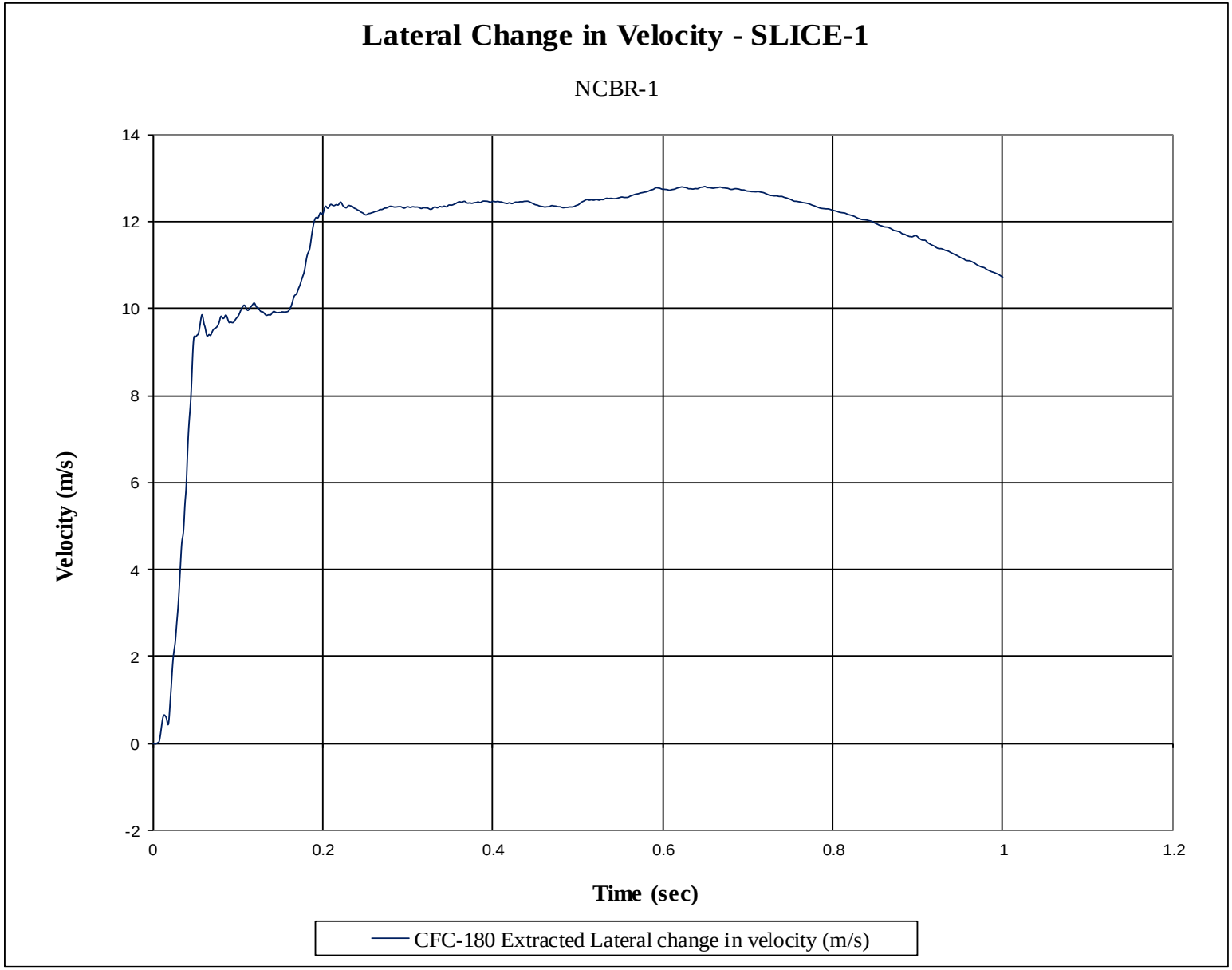


Figure E-5. Lateral Occupant Impact Velocity (SLICE-1), Test No. NCBR-1

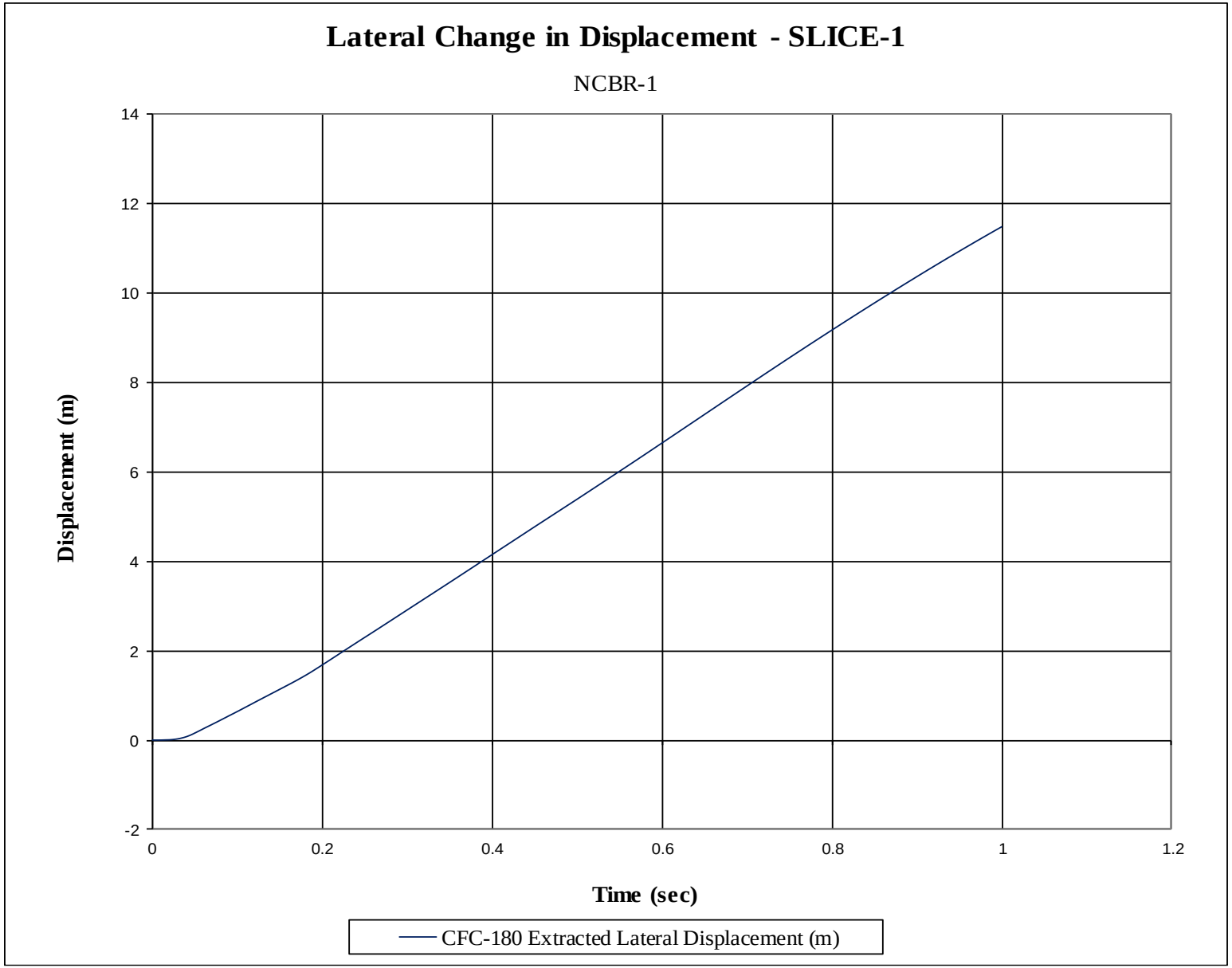


Figure E-6. Lateral Occupant Displacement (SLICE-1), Test No. NCBR-1

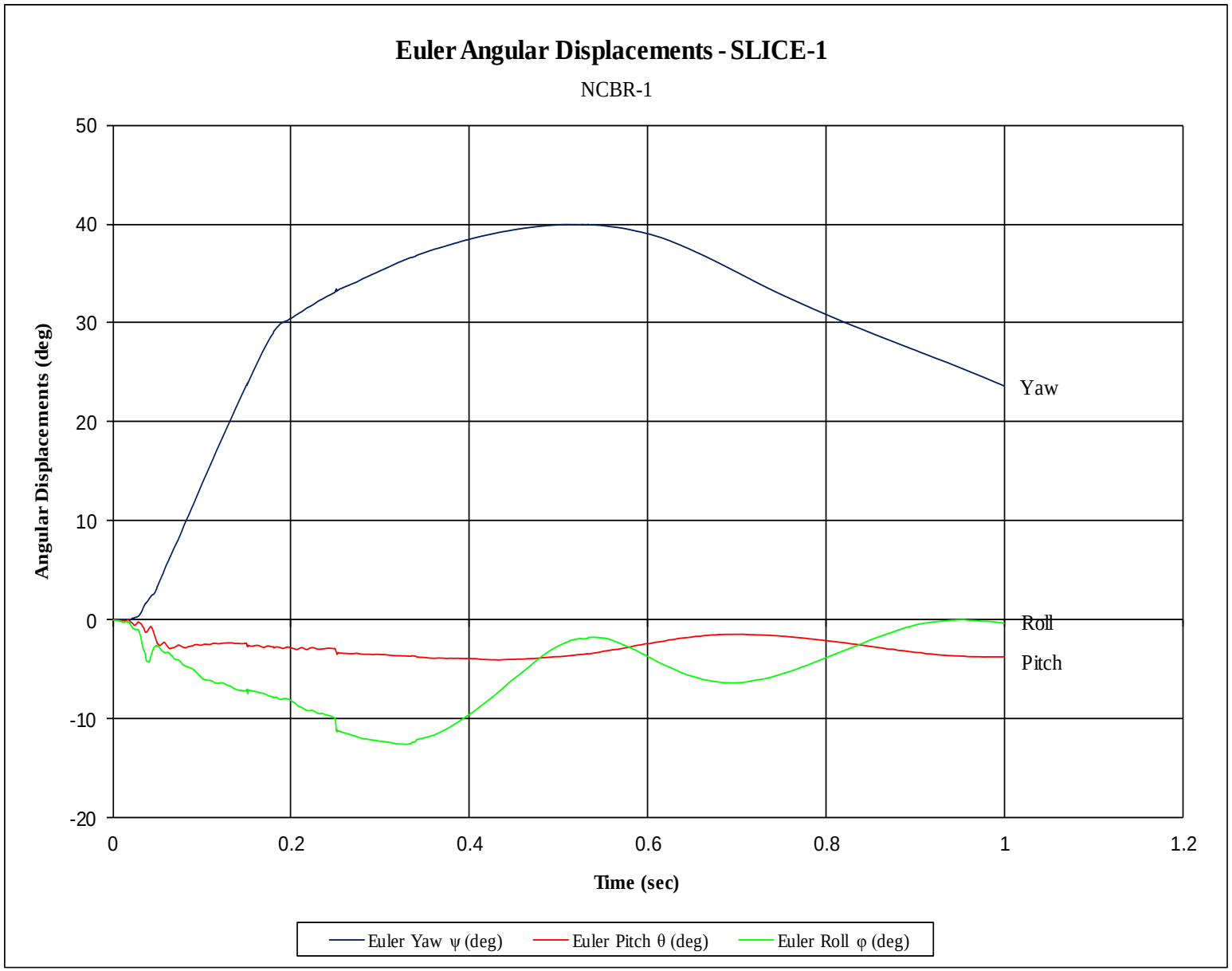


Figure E-7. Vehicle Angular Displacements (SLICE-1), Test No. NCBR-1

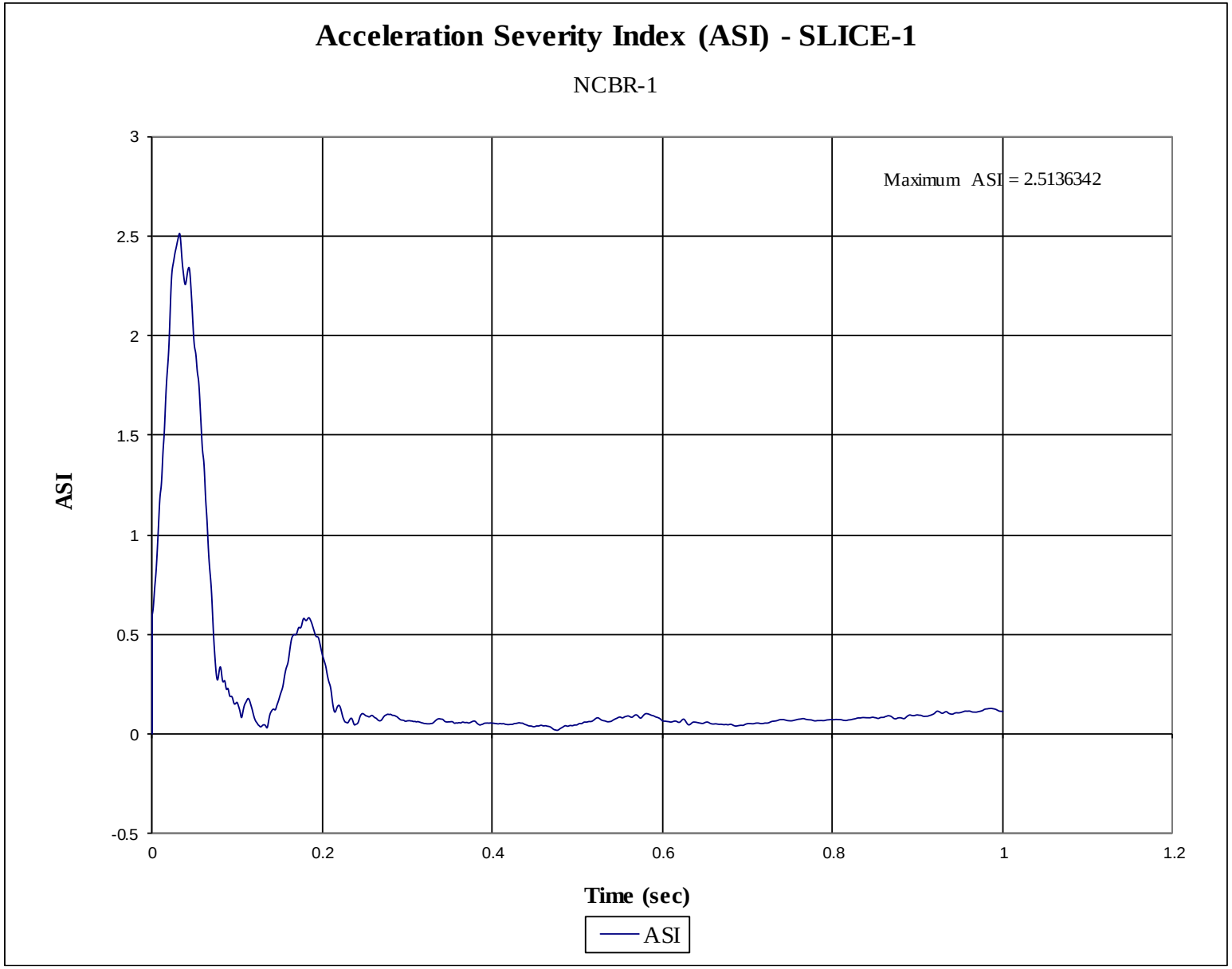


Figure E-8. Acceleration Severity Index (SLICE-1), Test No. NCBR-1

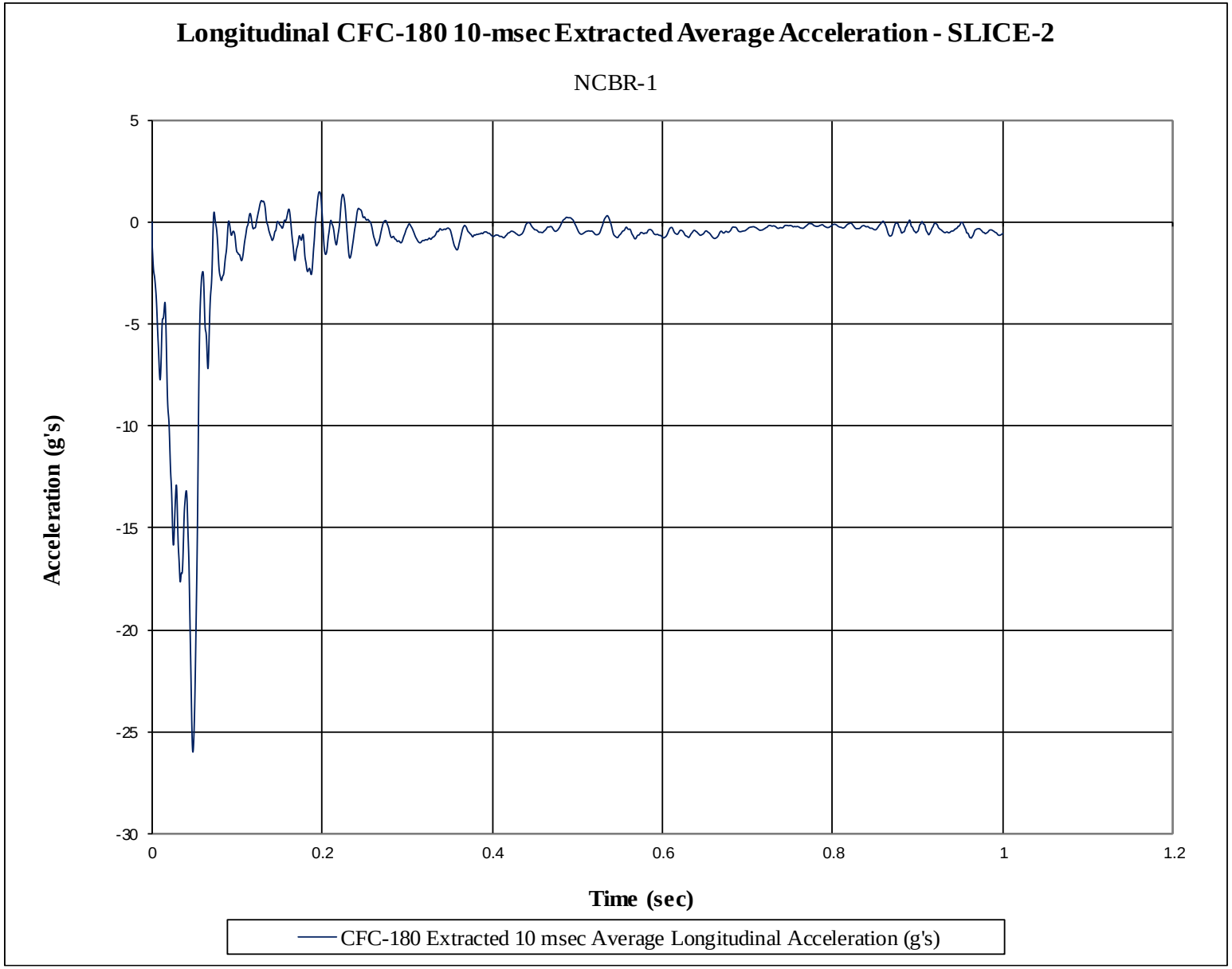


Figure E-9. 10-ms Average Longitudinal Deceleration (SLICE-2), Test No. NCBR-1

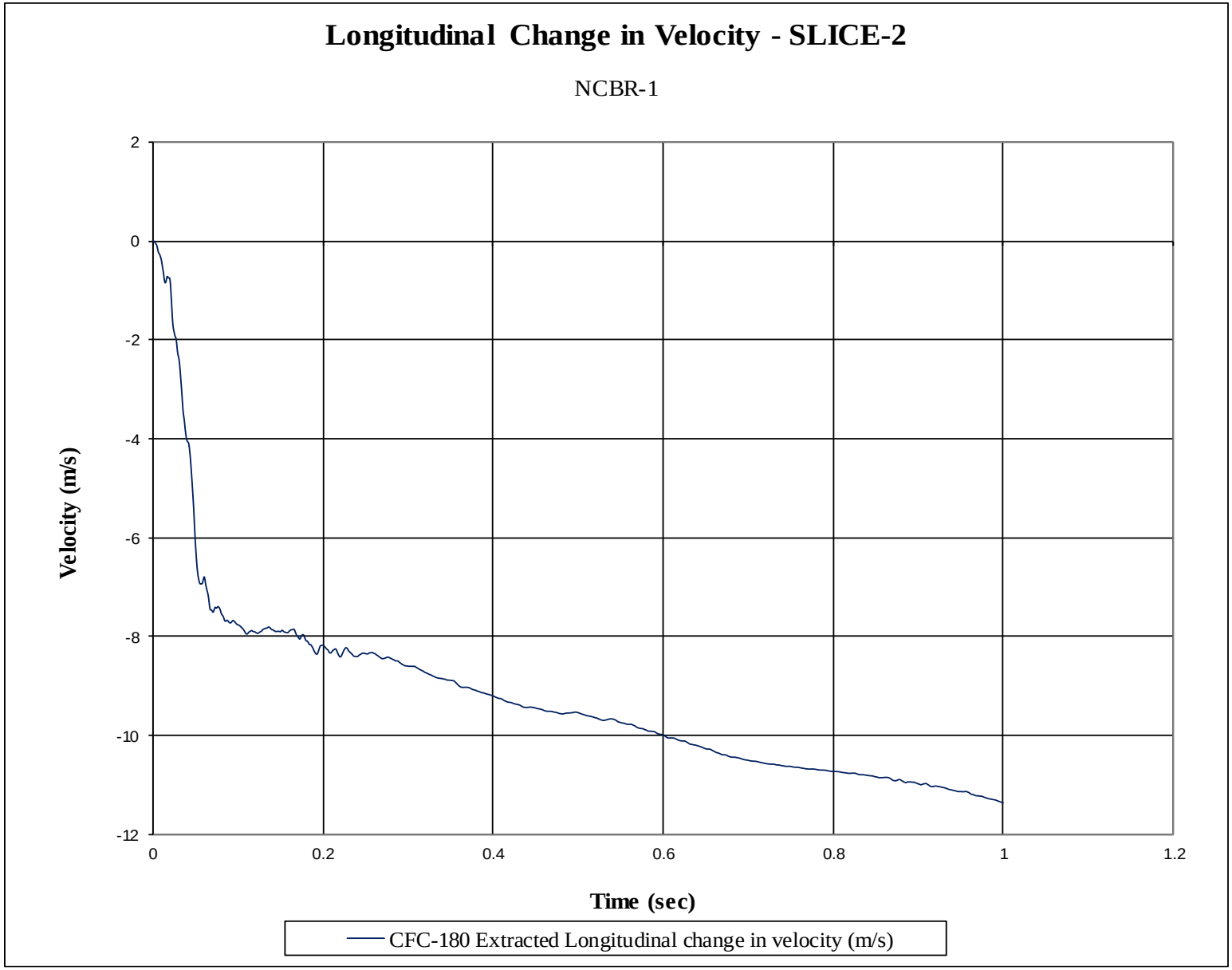


Figure E-10. Longitudinal Occupant Impact Velocity (SLICE-2), Test No. NCBR-1

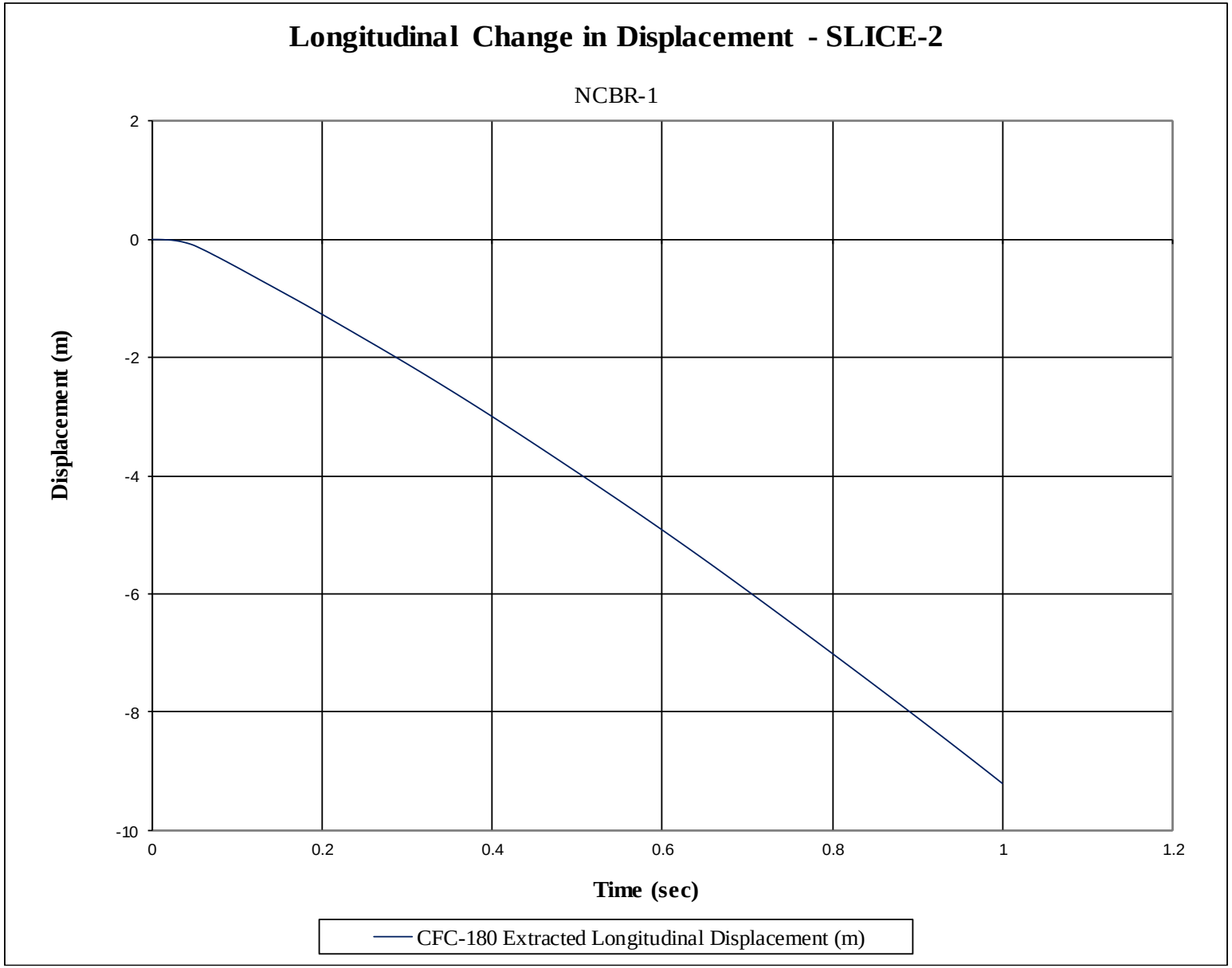


Figure E-11. Longitudinal Occupant Displacement (SLICE-2), Test No. NCBR-1

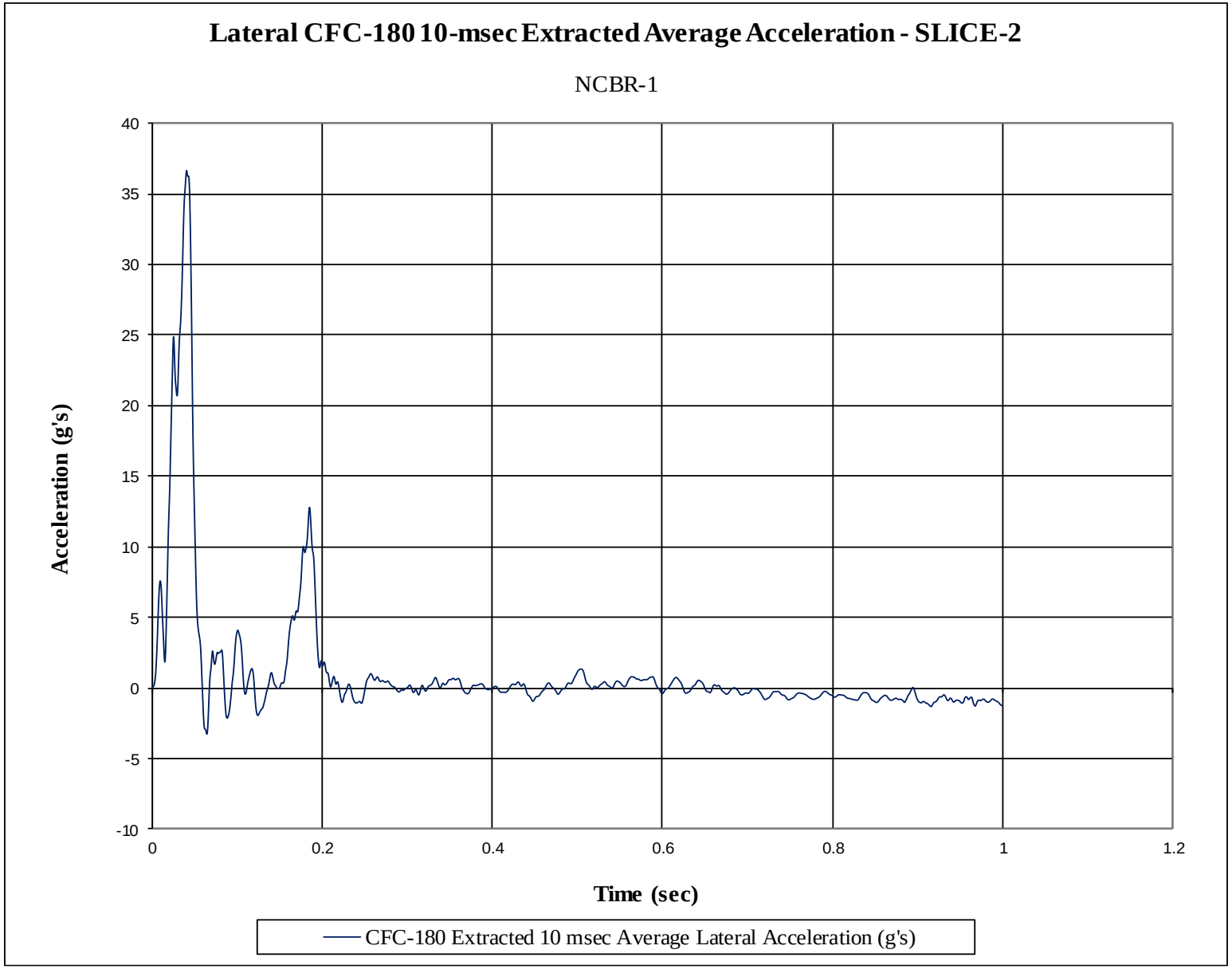


Figure E-12. 10-ms Average Lateral Deceleration (SLICE-2), Test No. NCBR-1

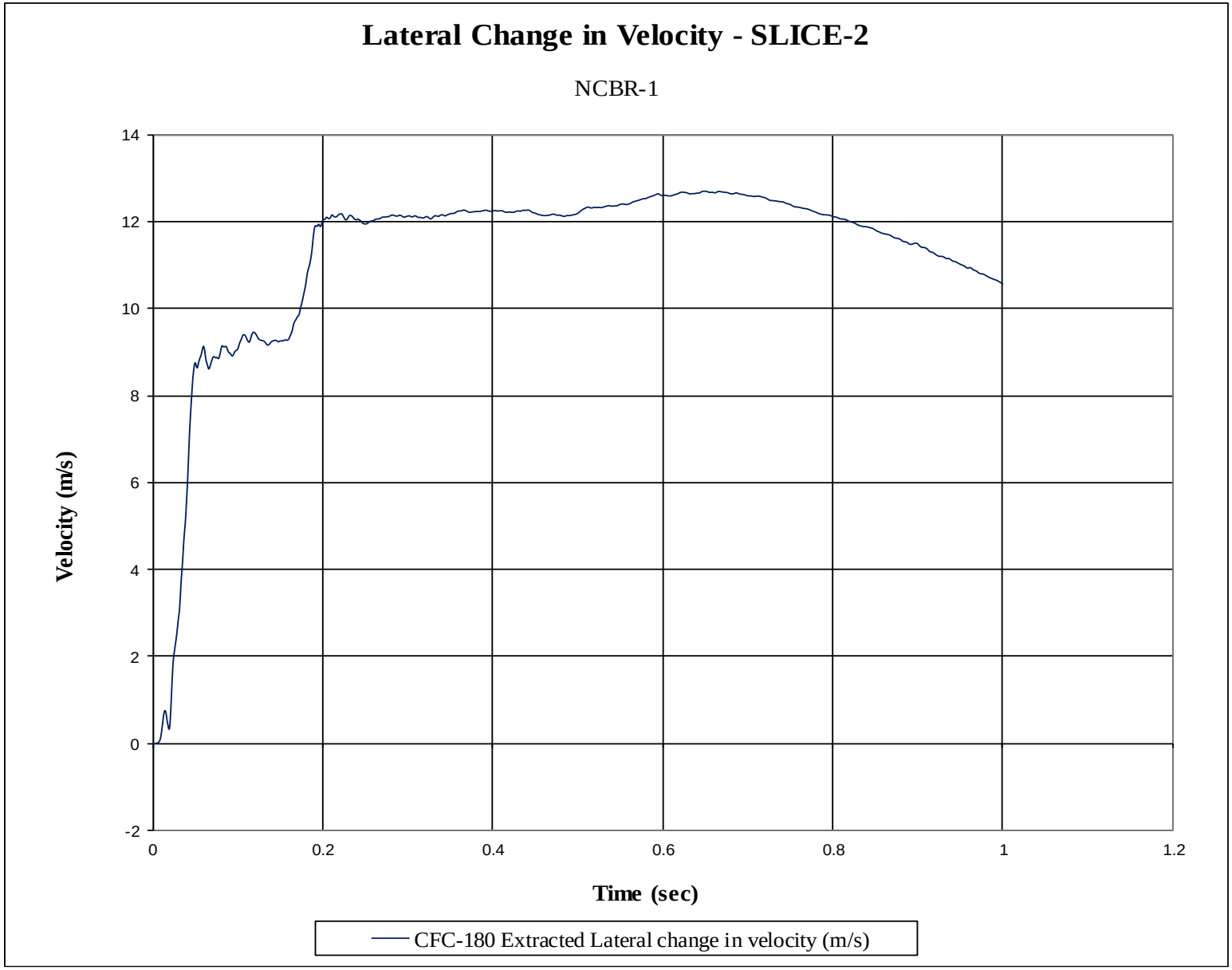


Figure E-13. Lateral Occupant Impact Velocity (SLICE-2), Test No. NCBR-1

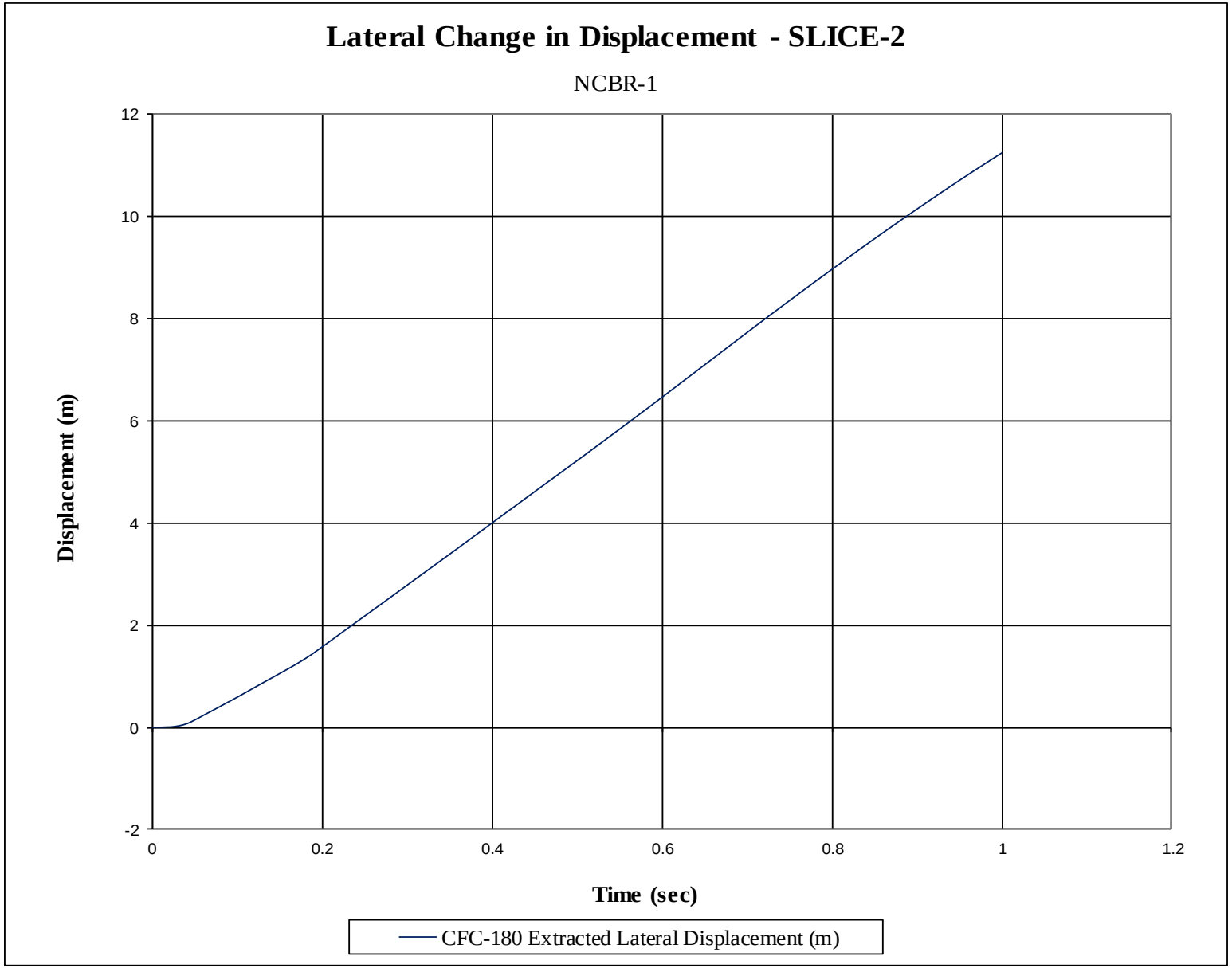


Figure E-14. Lateral Occupant Displacement (SLICE-2), Test No. NCBR-1

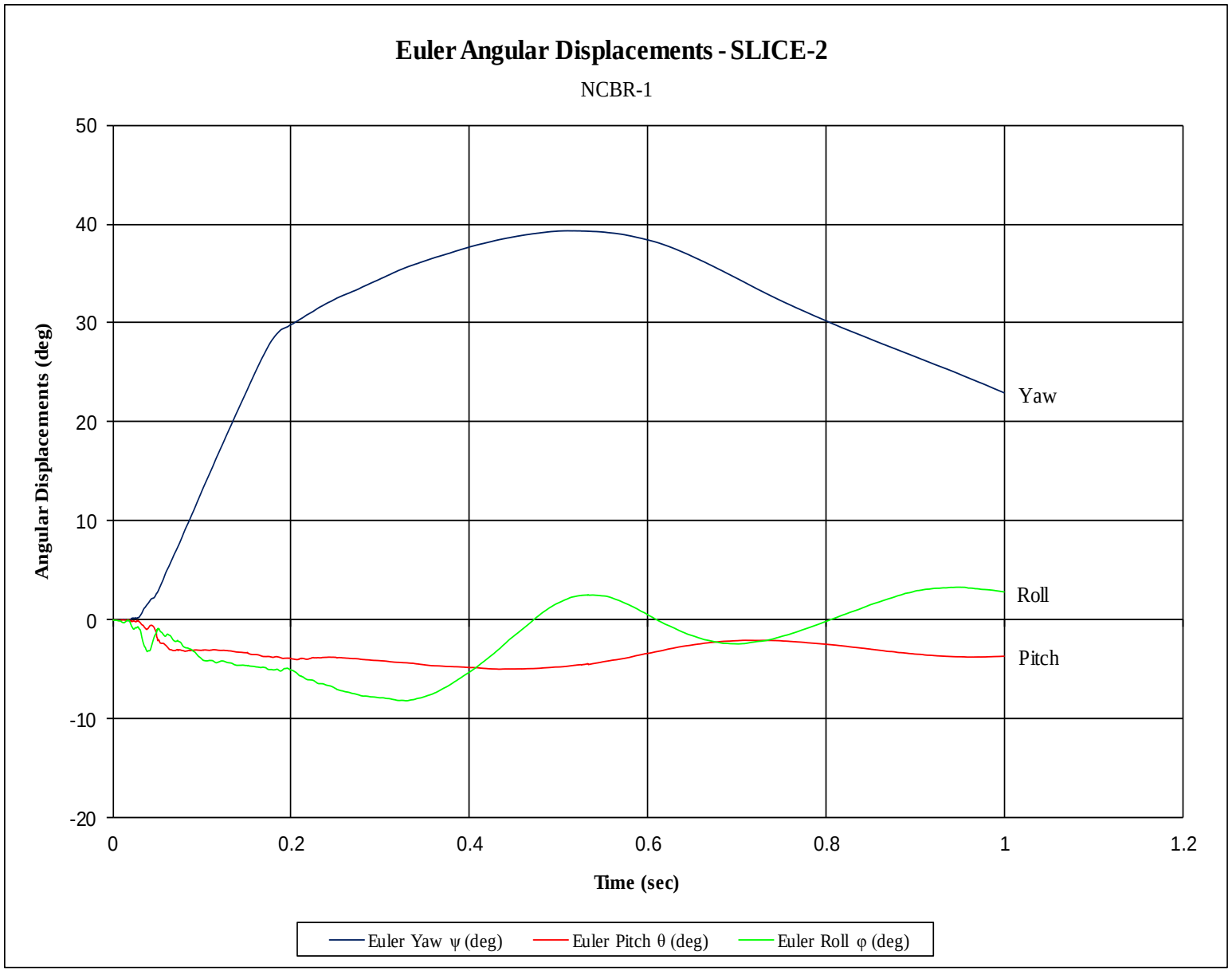


Figure E-15. Vehicle Angular Displacements (SLICE-2), Test No. NCBR-1

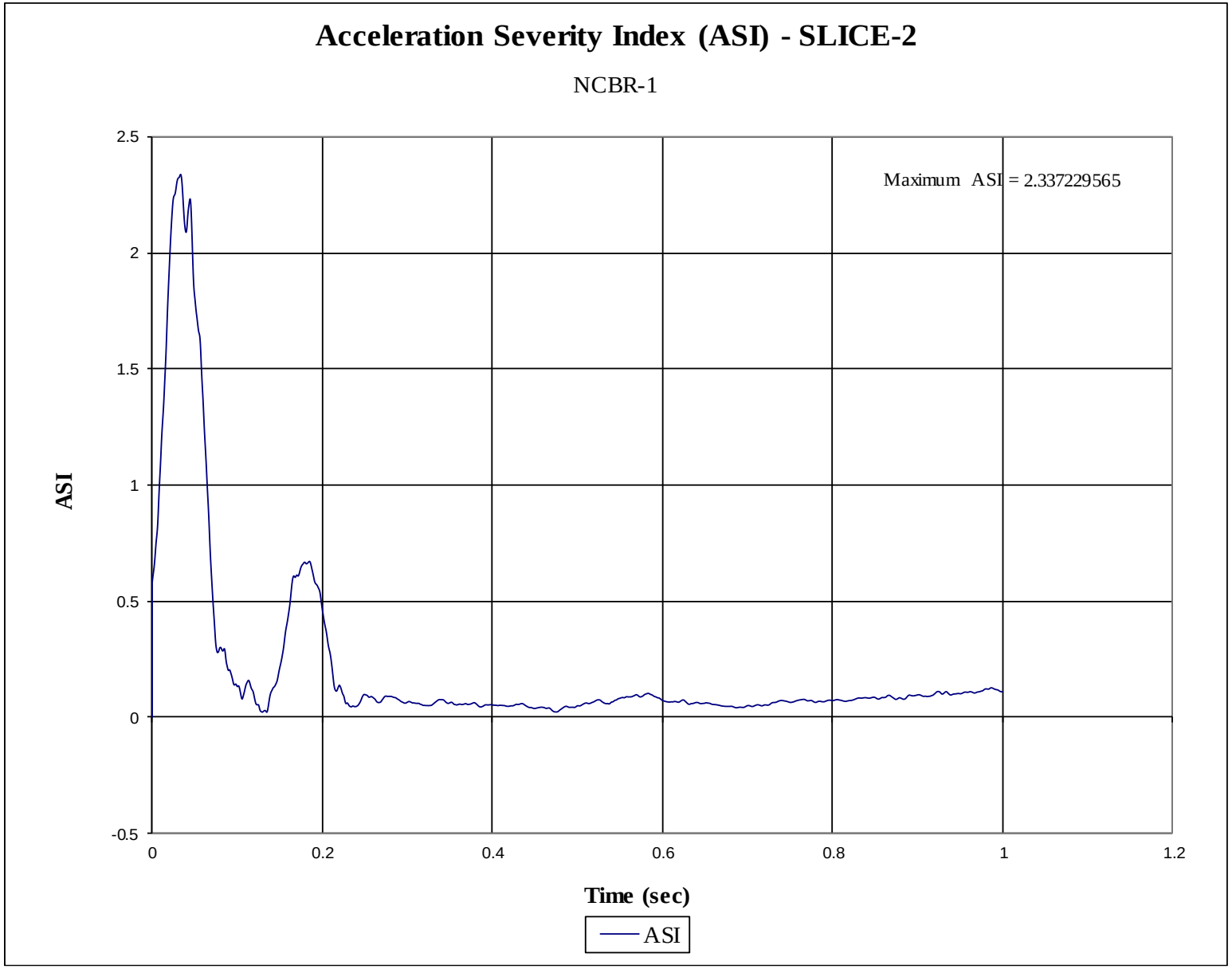


Figure E-16. Acceleration Severity Index (SLICE-2), Test No. NCBR-1

Appendix F. Accelerometer and Rate Transducer Data Plots, Test No. NCBR-2

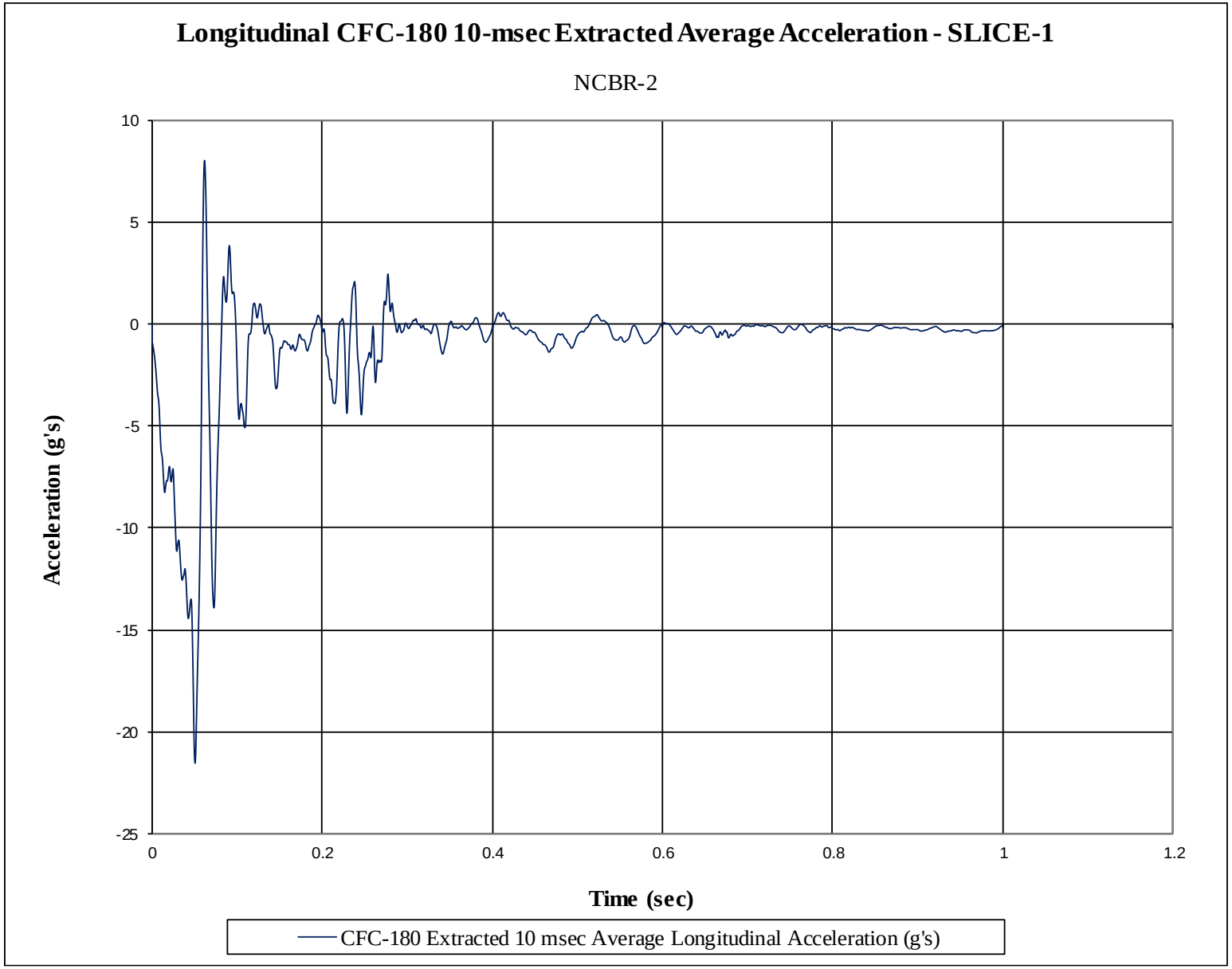


Figure F-1. 10-ms Average Longitudinal Deceleration (SLICE-1), Test No. NCBR-2

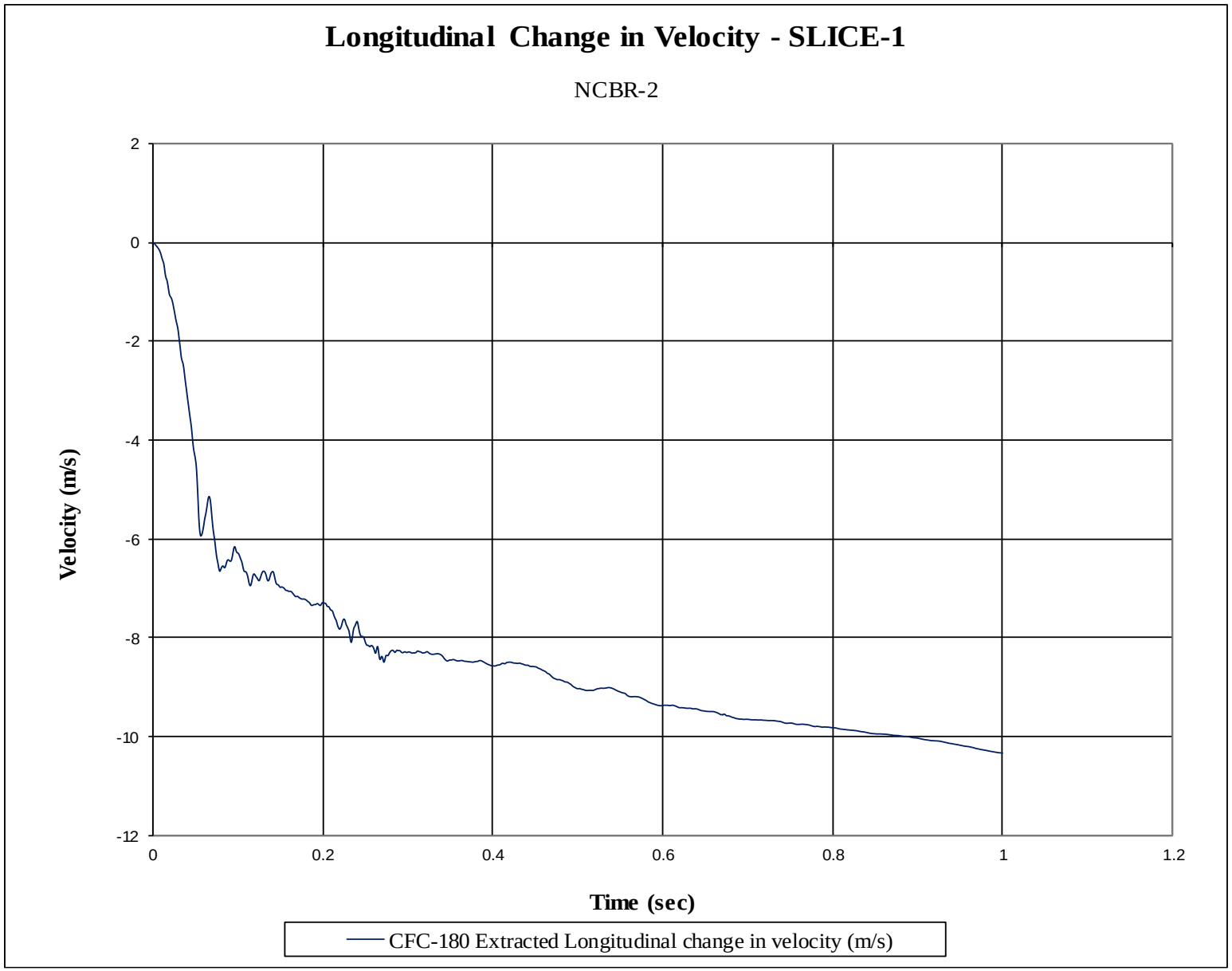


Figure F-2. Longitudinal Occupant Impact Velocity (SLICE-1), Test No. NCBR-2

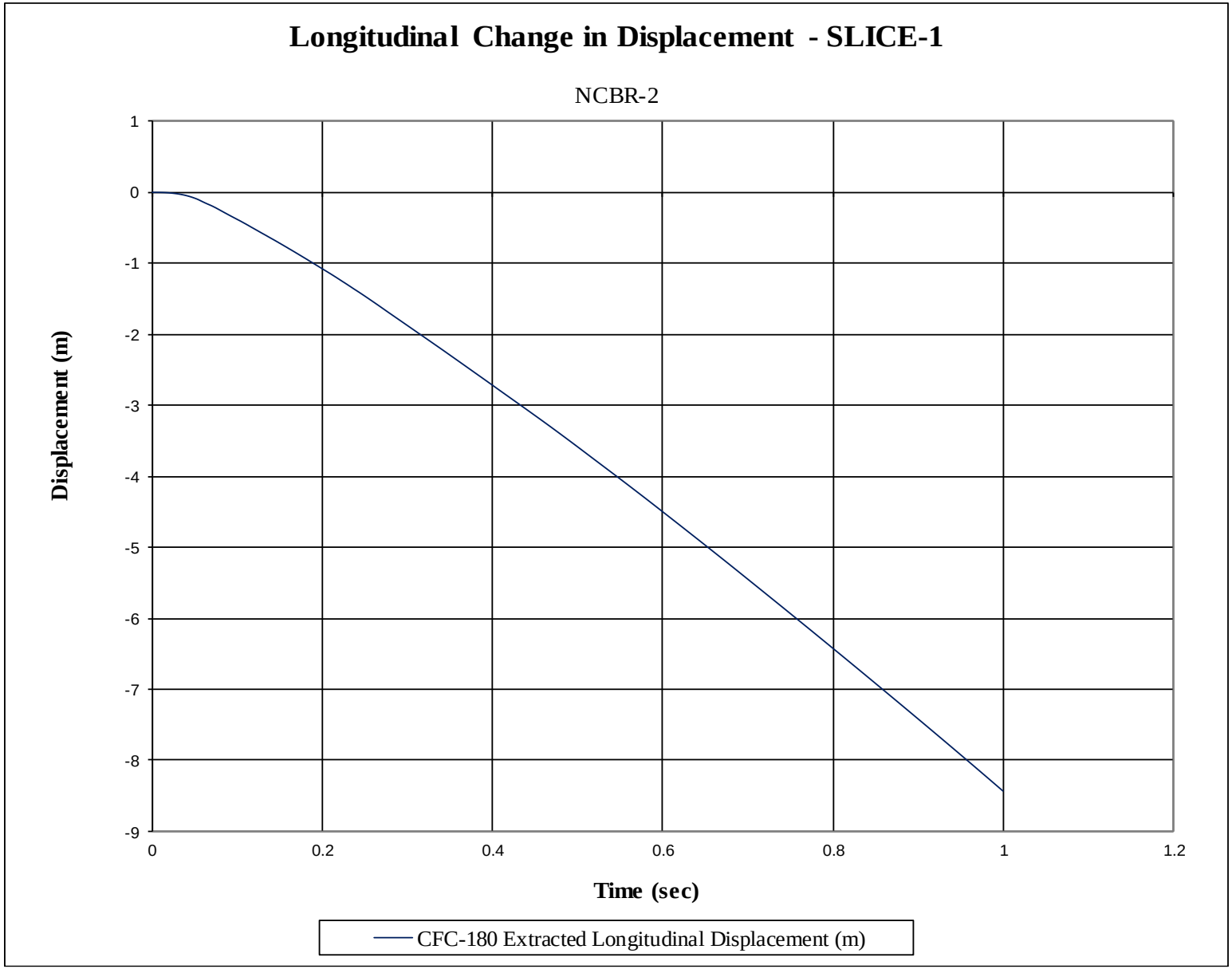


Figure F-3. Longitudinal Occupant Displacement (SLICE-1), Test No. NCBR-2

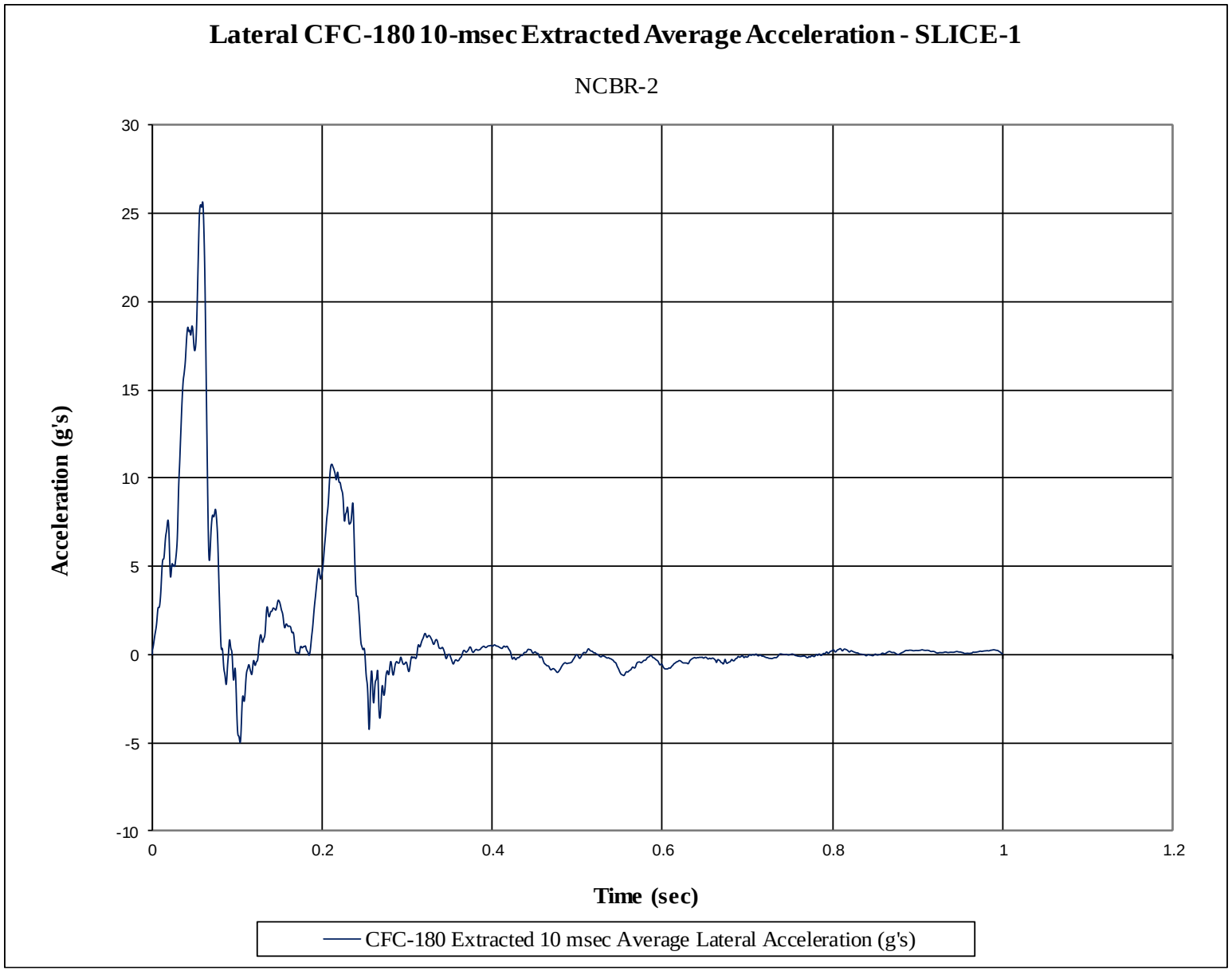


Figure F-4. 10-ms Average Lateral Deceleration (SLICE-1), Test No. NCBR-2

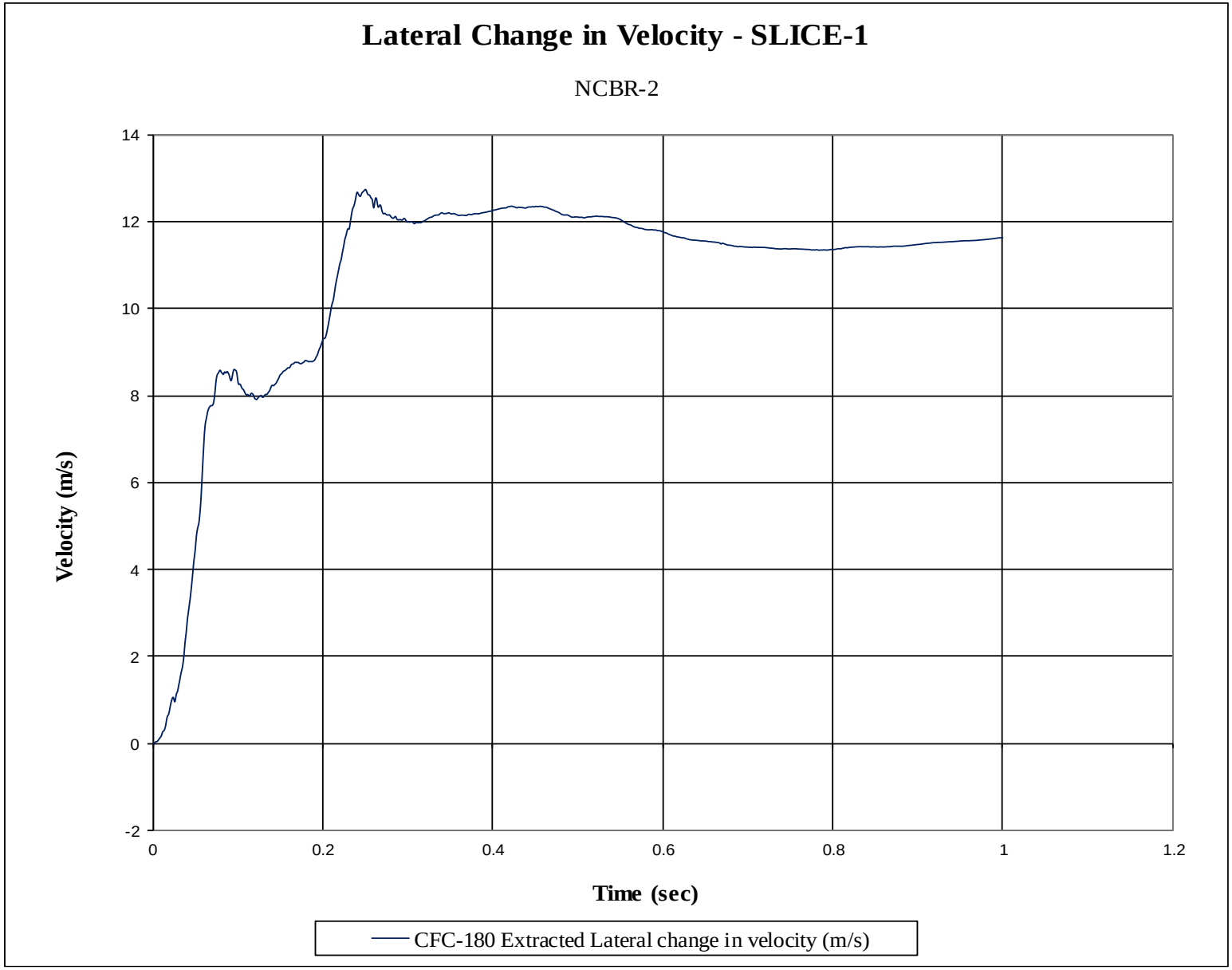


Figure F-5. Lateral Occupant Impact Velocity (SLICE-1), Test No. NCBR-2

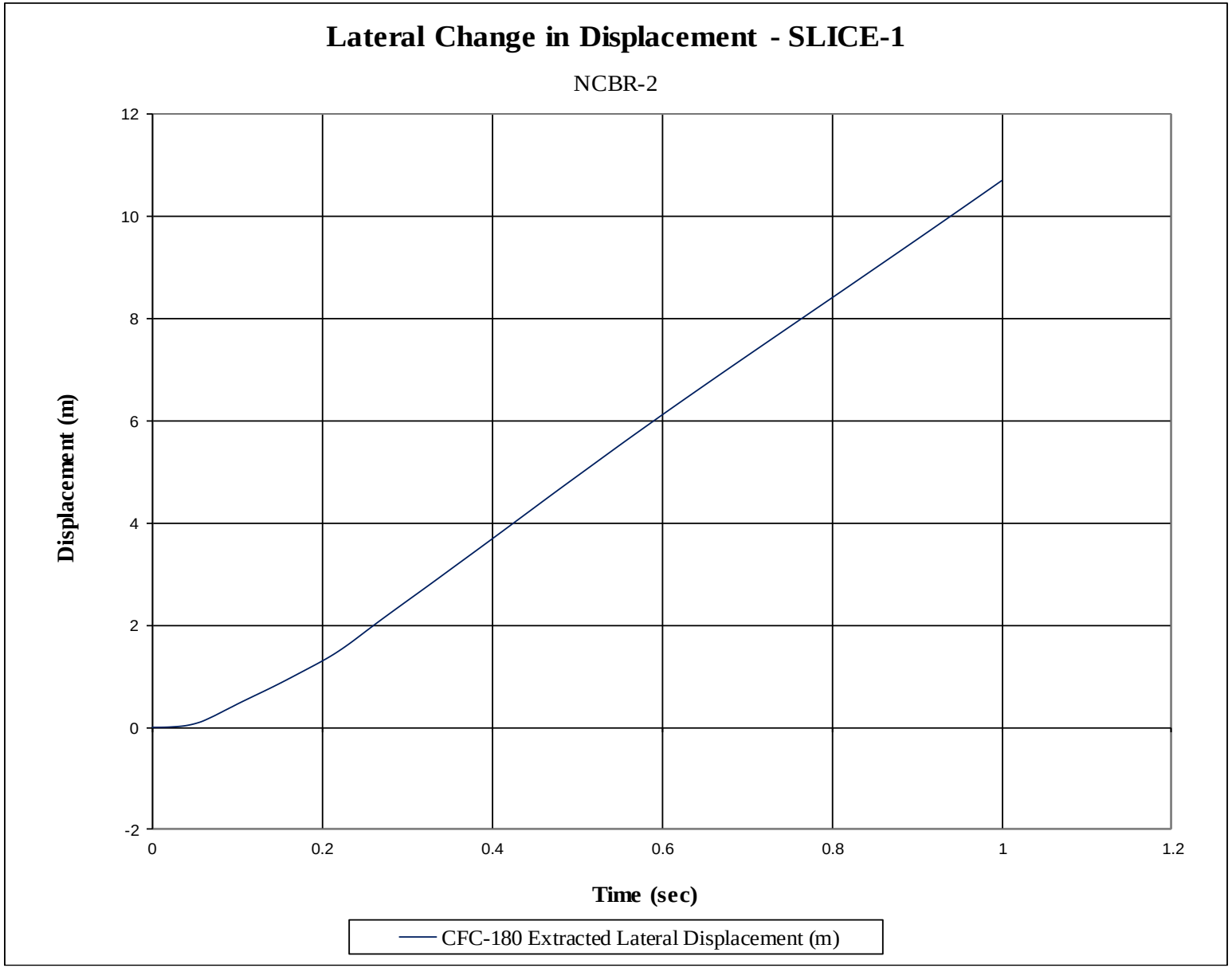


Figure F-6. Lateral Occupant Displacement (SLICE-1), Test No. NCBR-2

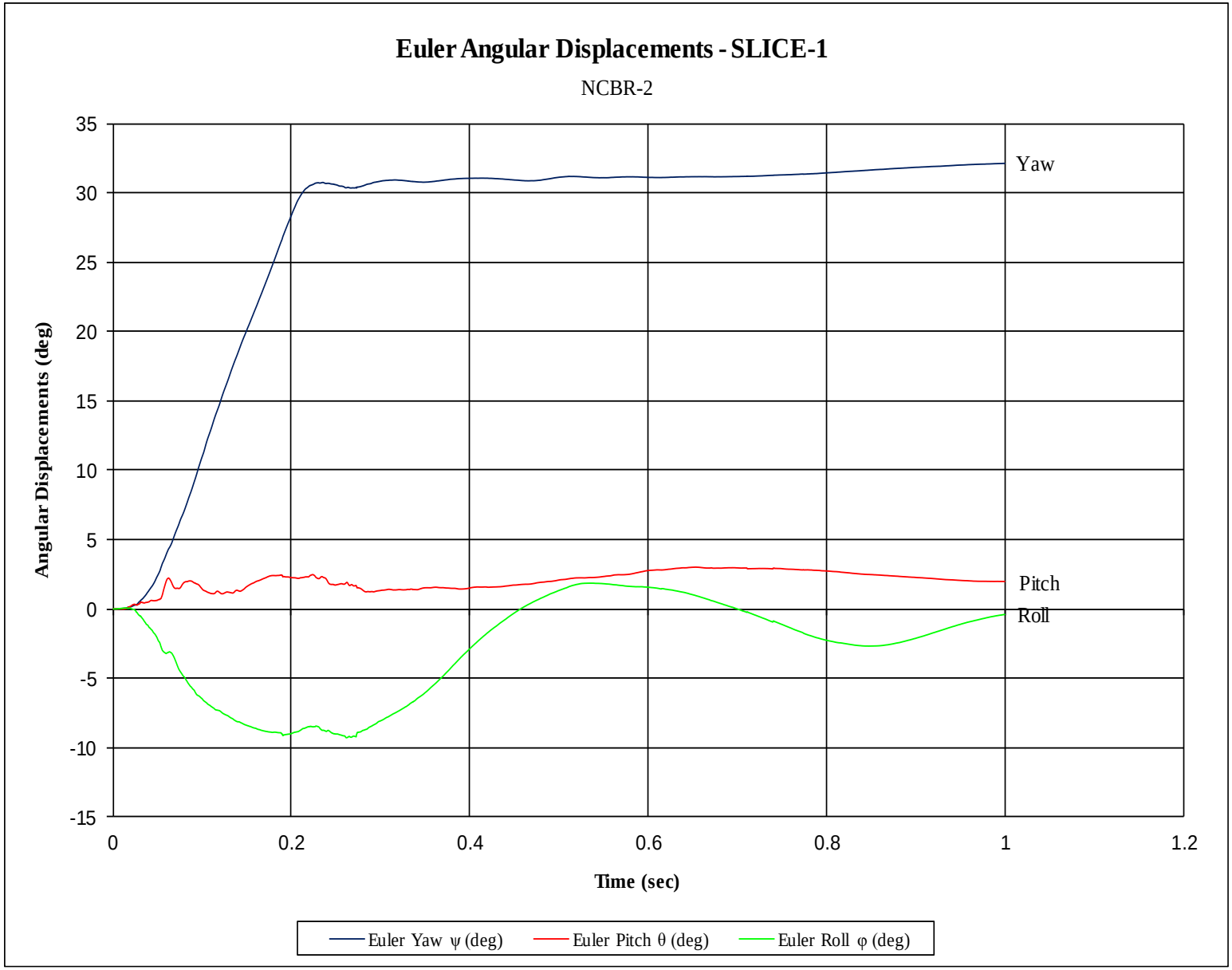


Figure F-7. Vehicle Angular Displacements (SLICE-1), Test No. NCBR-2

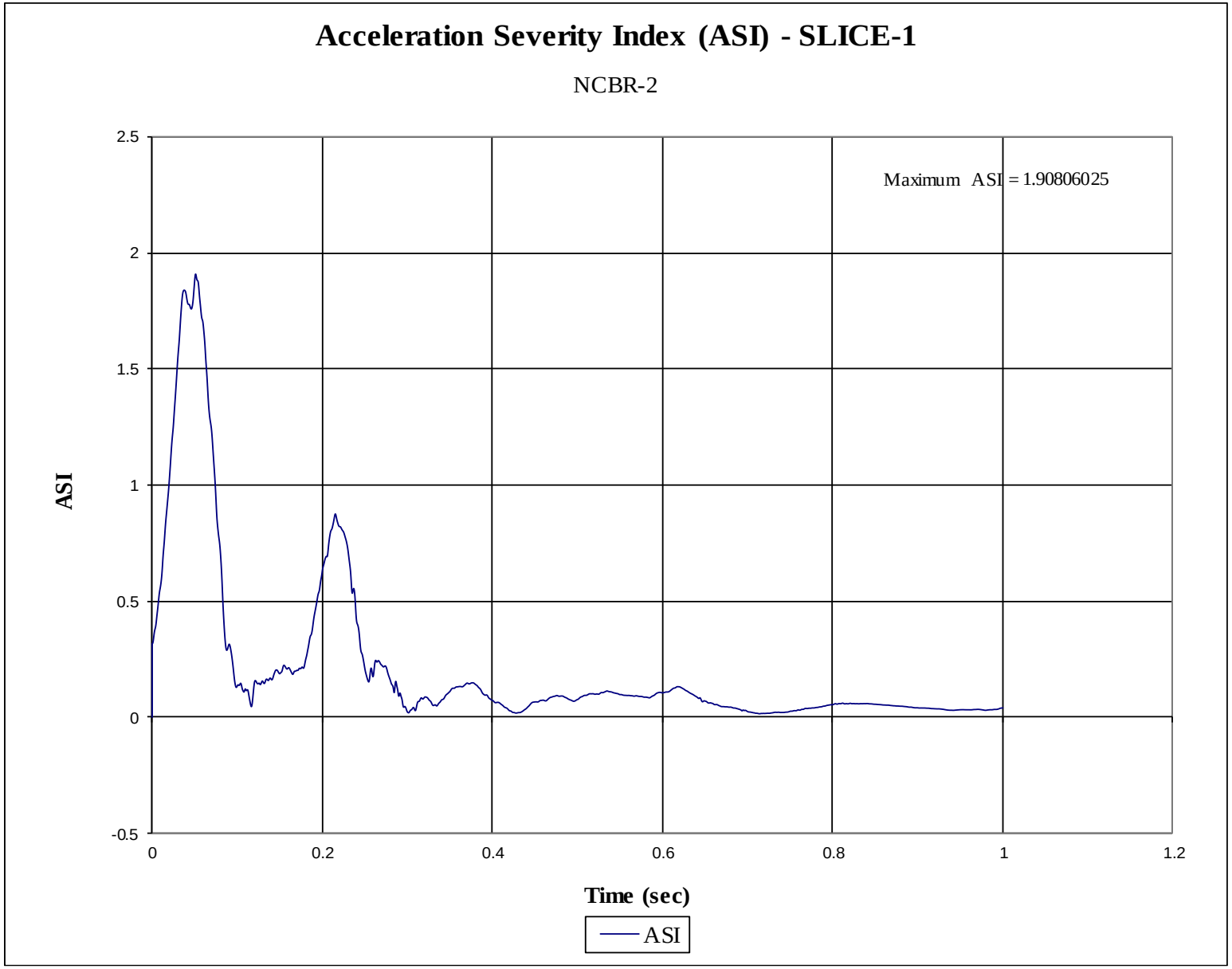


Figure F-8. Acceleration Severity Index (SLICE-1), Test No. NCBR-2

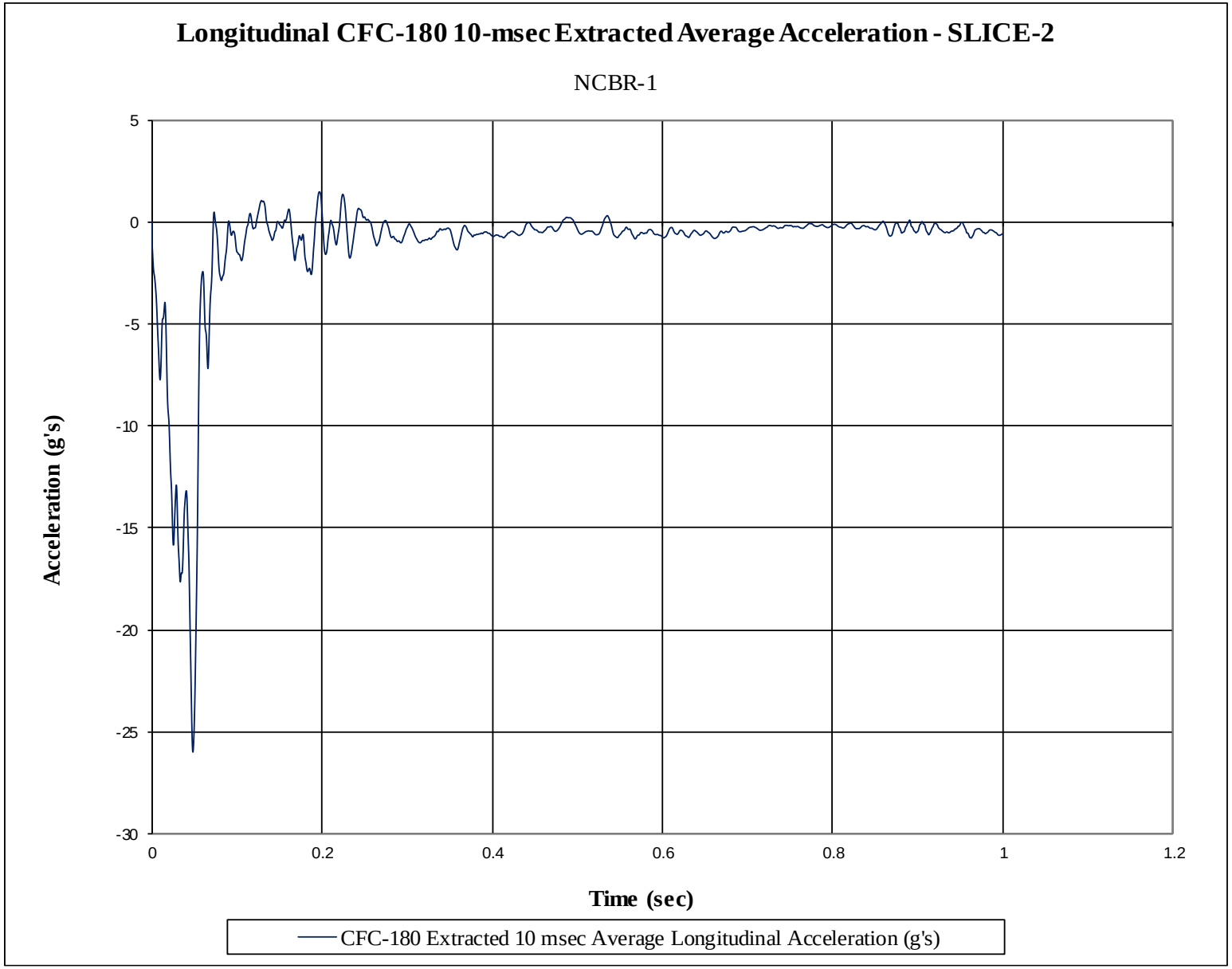


Figure F-9. 10-ms Average Longitudinal Deceleration (SLICE-2), Test No. NCBR-2

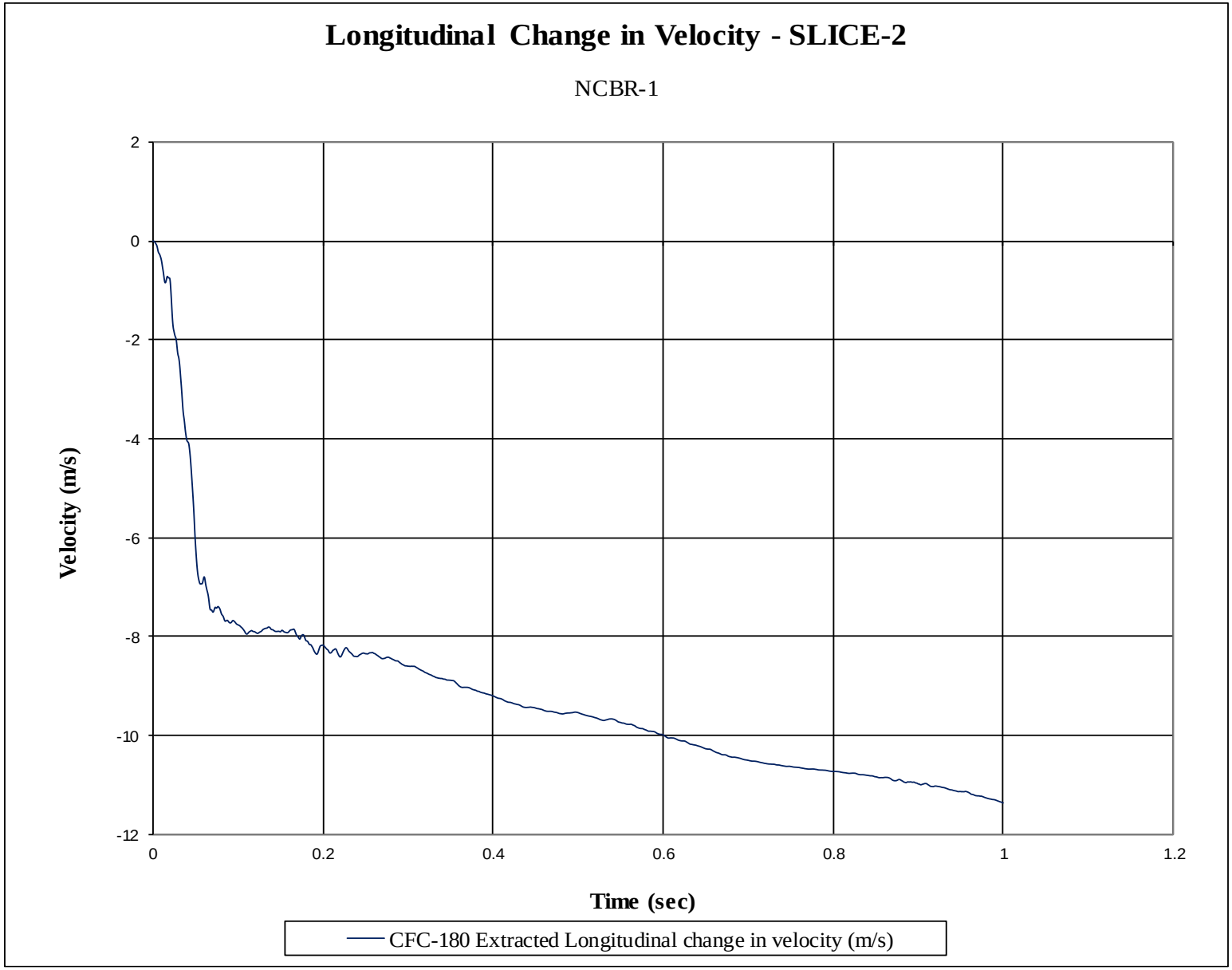


Figure F-10. Longitudinal Occupant Impact Velocity (SLICE-2), Test No. NCBR-2

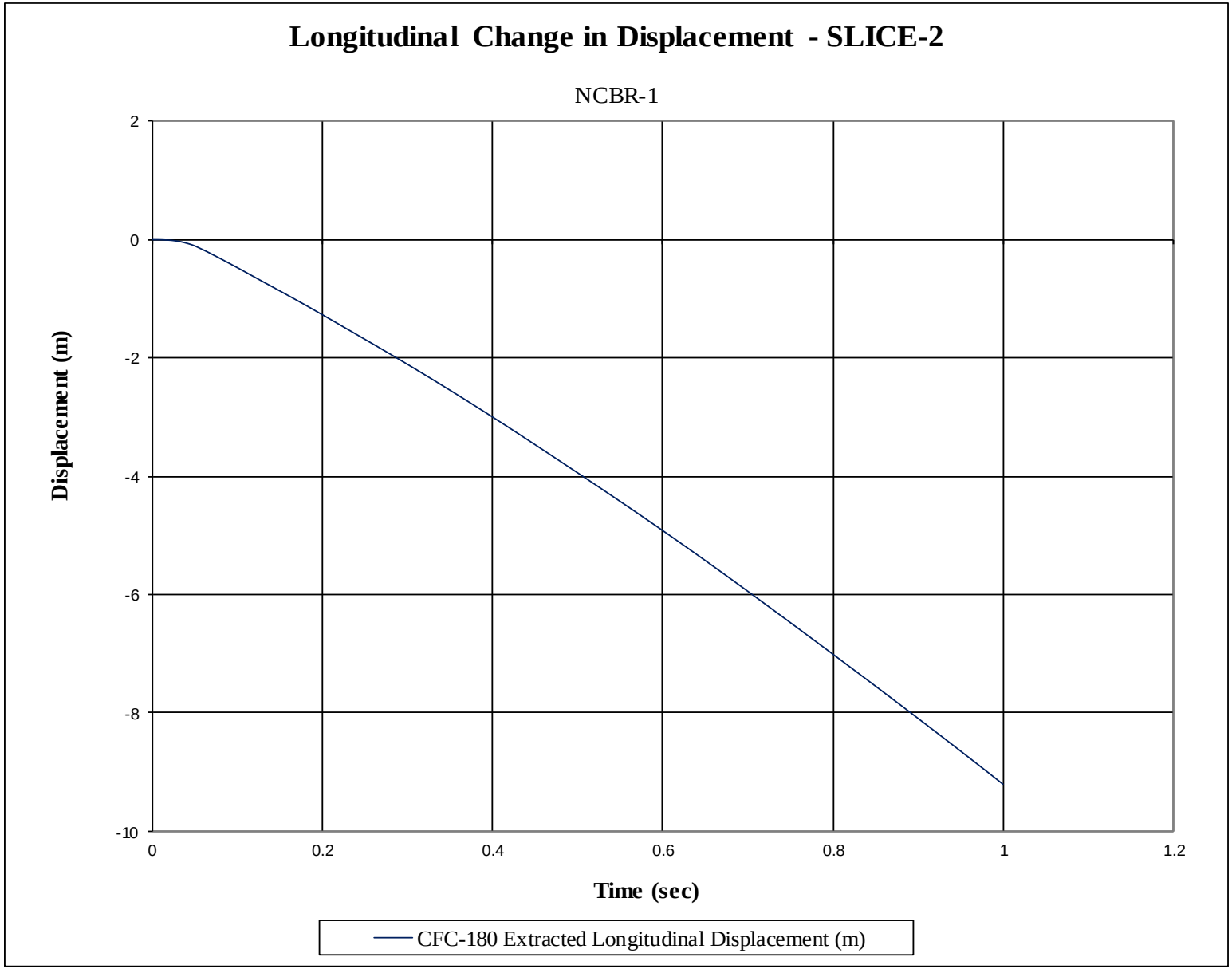


Figure F-11. Longitudinal Occupant Displacement (SLICE-2), Test No. NCBR-2

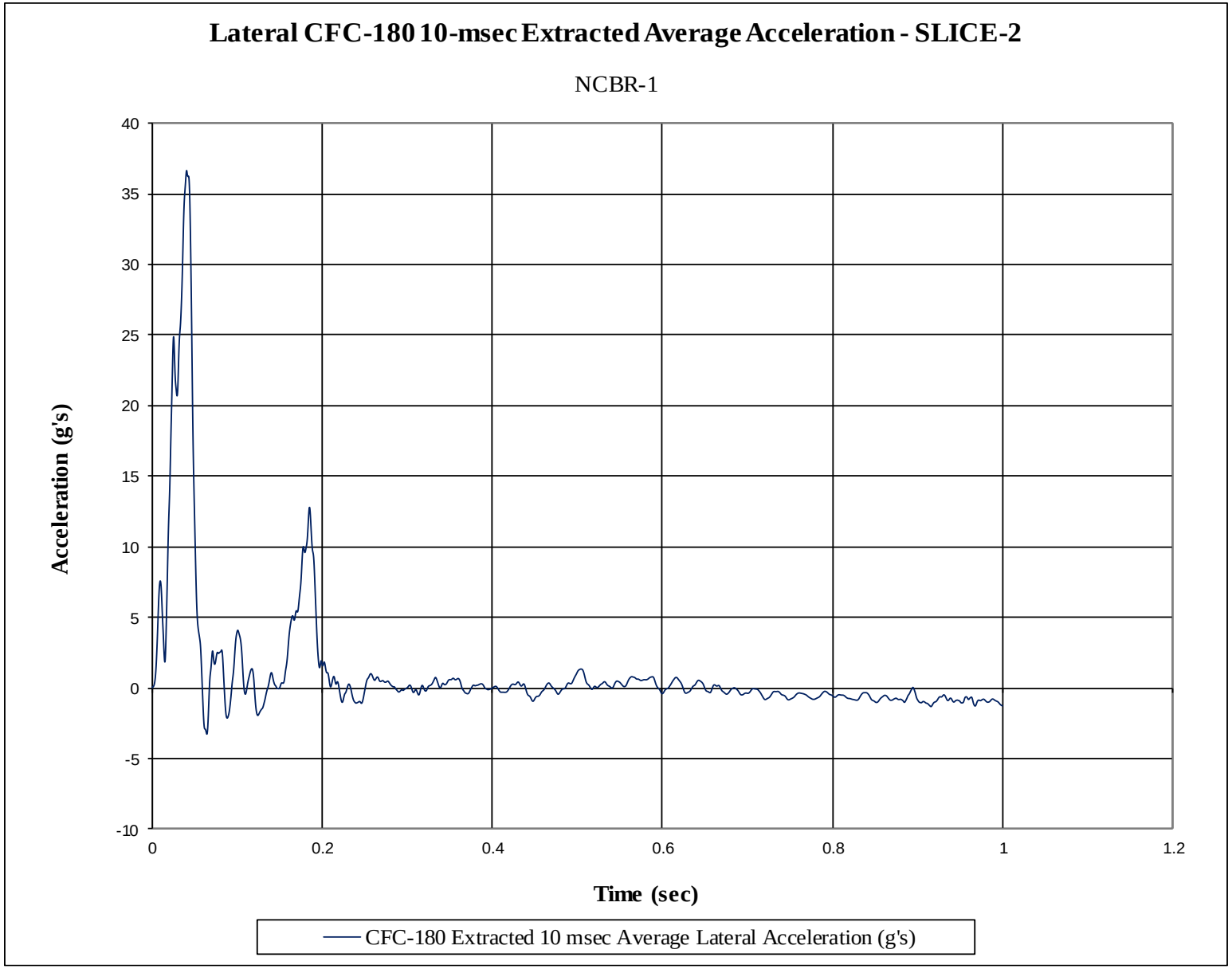


Figure F-12. 10-ms Average Lateral Deceleration (SLICE-2), Test No. NCBR-2

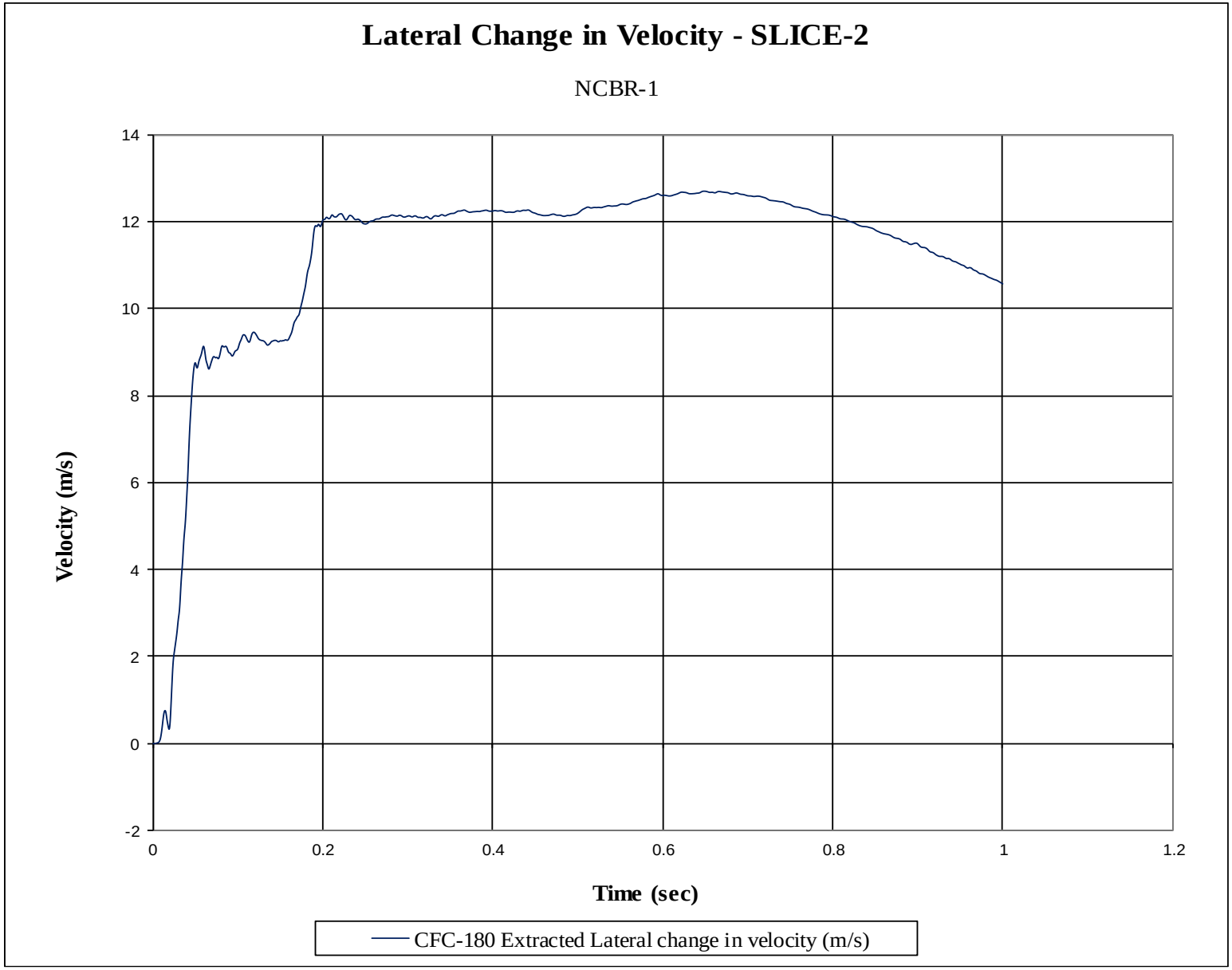


Figure F-13. Lateral Occupant Impact Velocity (SLICE-2), Test No. NCBR-2

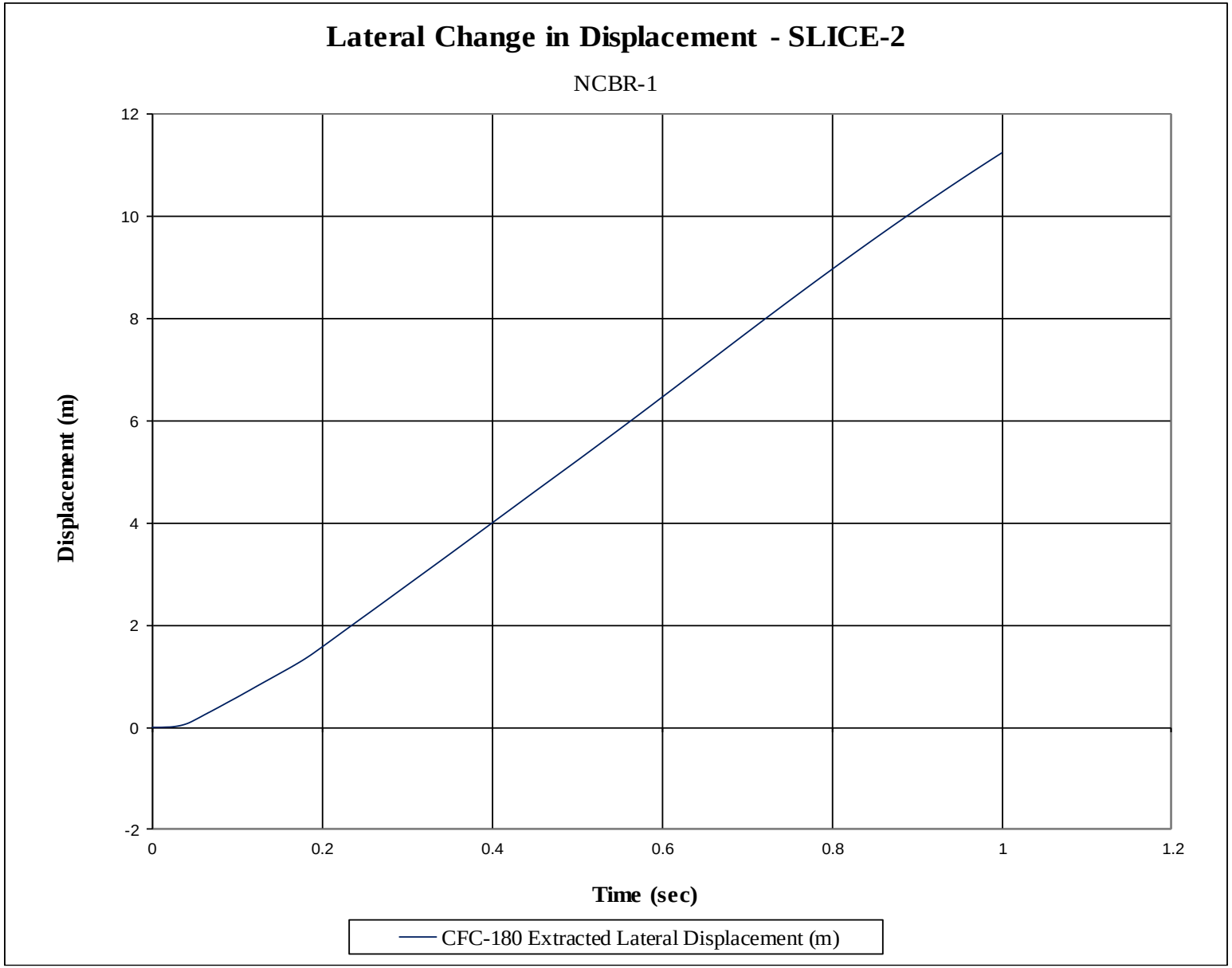


Figure F-14. Lateral Occupant Displacement (SLICE-2), Test No. NCBR-2

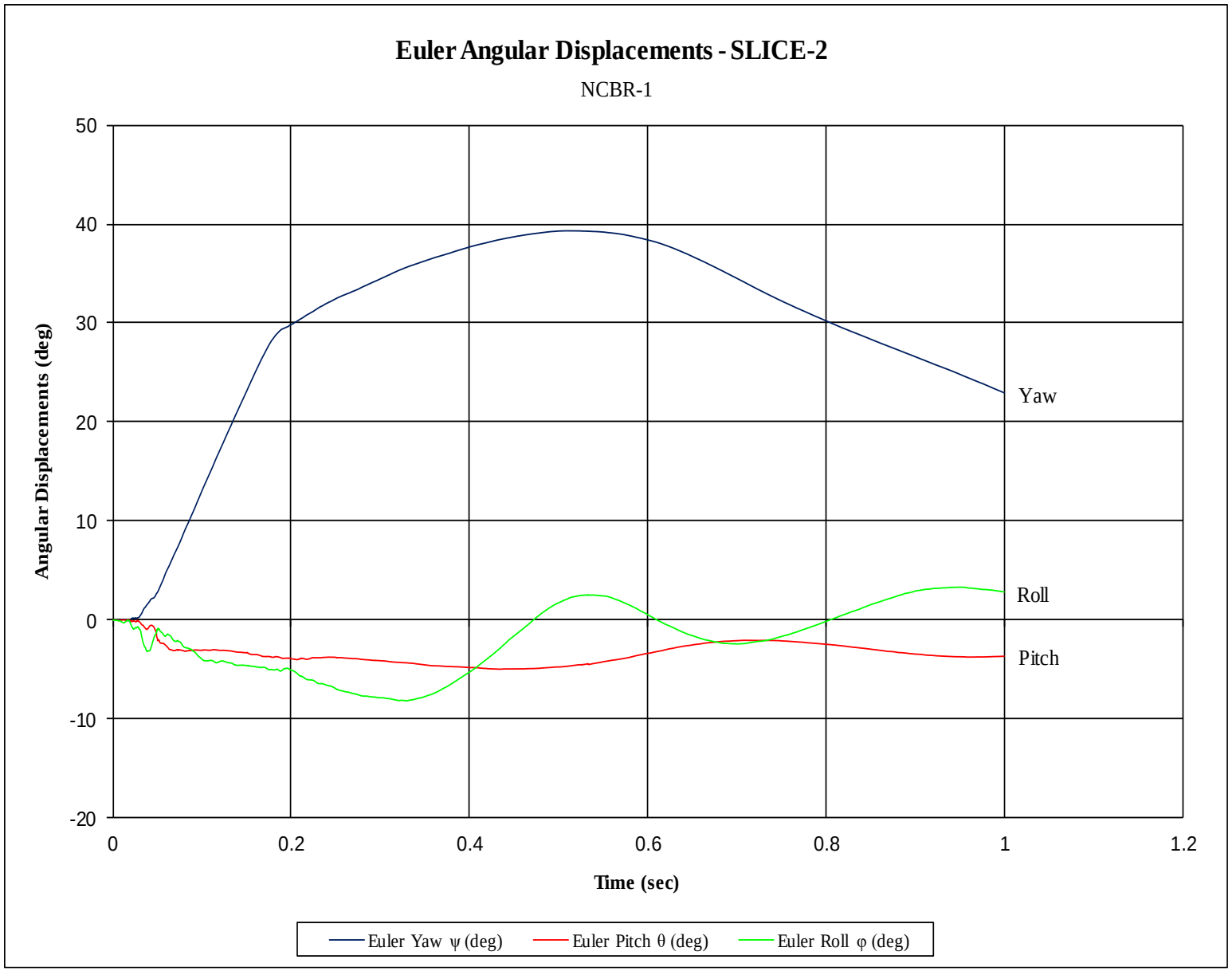


Figure F-15. Vehicle Angular Displacements (SLICE-2), Test No. NCBR-2

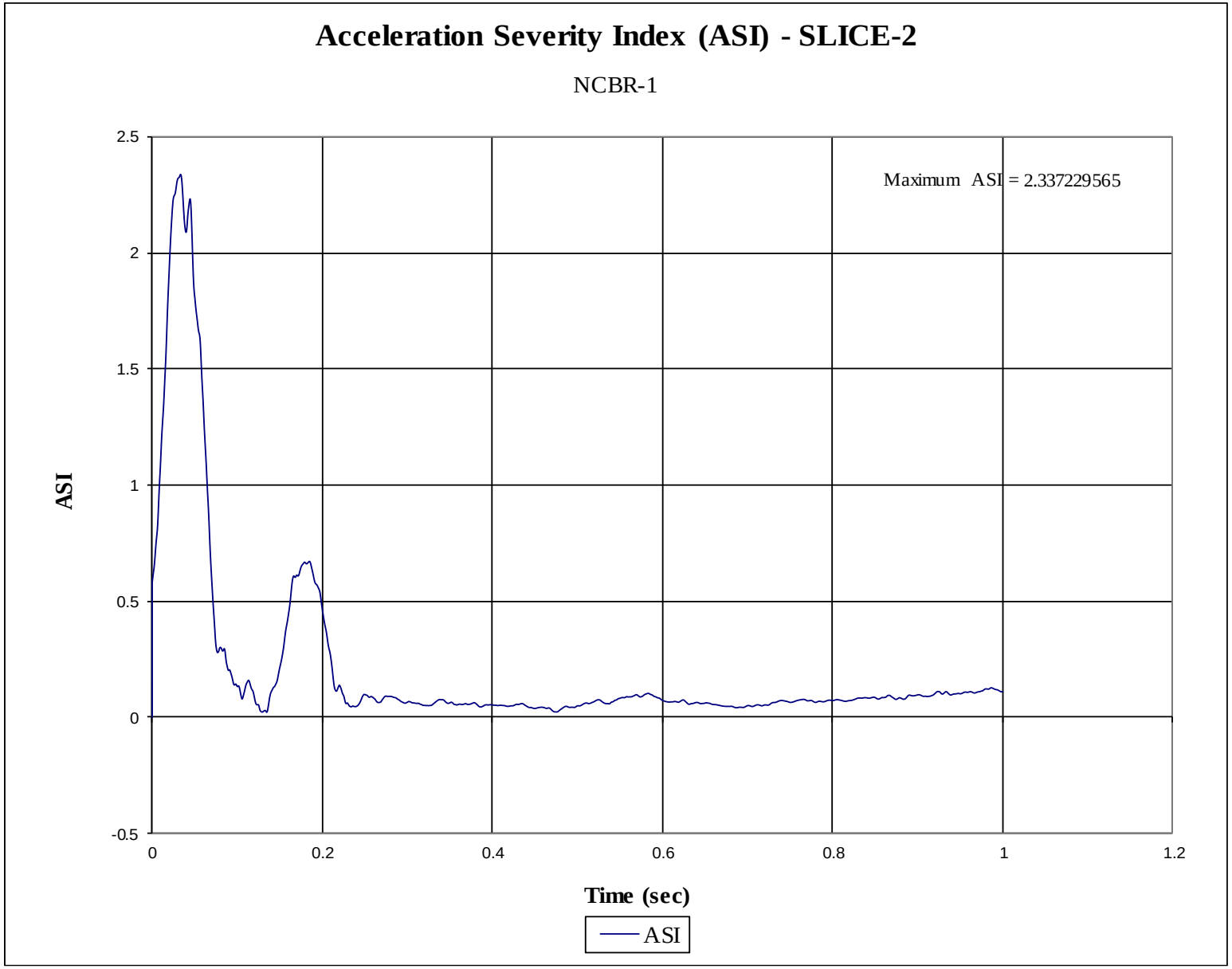


Figure F-16. Acceleration Severity Index (SLICE-2), Test No. NCBR-2

END OF DOCUMENT